Etude des dynamiques spatio-temporelles des interactions entre le microbiote et le métabolome de surface de la macroalgue Taonia atomaria par une approche multi-omiques

Benoît Paix

▶ **To cite this version:**

Benoît Paix. Etude des dynamiques spatio-temporelles des interactions entre le microbiote et le métabolome de surface de la macroalgue Taonia atomaria par une approche multi-omiques. Etudes de l'environnement. Université de Toulon, 2020. Français. NNT : 2020TOUL0012 . tel-03269975

HAL Id: tel-03269975
https://theses.hal.science/tel-03269975

Submitted on 24 Jun 2021

HAL is a multi-disciplinary open access archive for the deposit and dissemination of scientific research documents, whether they are published or not. The documents may come from teaching and research institutions in France or abroad, or from public or private research centers.

L'archive ouverte pluridisciplinaire **HAL**, est destinée au dépôt et à la diffusion de documents scientifiques de niveau recherche, publiés ou non, émanant des établissements d'enseignement et de recherche français ou étrangers, des laboratoires publics ou privés.

ÉCOLE DOCTORALE 548 – MER & SCIENCES

LABORATOIRE MATERIAUX POLYMERES INTERFACES ENVIRONNEMENT MARIN (MAPIEM)

THÈSE présentée par :

Benoît Paix

Soutenue le 17 Septembre 2020

Pour obtenir le grade de Docteur en Sciences de la Vie et de la Santé

Spécialité : Ecologie microbienne

Etude des dynamiques spatio-temporelles des interactions entre le microbiote et le métabolome de surface de la macroalgue *Taonia atomaria* par une approche multi-omiques

Thèse dirigée par Gérald Culioli et Jean-François Briand

JURY :

M^me^ Soizic Prado	Professeure des universités, Muséum national d'histoire naturelle	**Rapporteure**
M. Jean-François Ghiglione	Directeur de recherche CNRS, Sorbonne Université	**Rapporteur**
M^me^ Catherine Leblanc	Directrice de recherche CNRS, Sorbonne Université	**Examinatrice**
M^me^ Christine Ferrier-Pagès	Directrice de recherche, Centre Scientifique de Monaco	**Examinatrice**
M^me^ Marion Peirache	Référente Milieu Marin, Parc National de Port-Cros	**Invitée**
M. Gérald Culioli	Maître de conférences, HDR Université de Toulon	**Directeur de thèse**
M. Jean-François Briand	Maître de conférences, Université de Toulon	**Co-encadrant de thèse**

REMERCIEMENTS

Tout d'abord, je tiens à remercier le Pr. Jean-François Chailan, directeur du laboratoire MAPIEM, pour m'avoir permis de réaliser cette thèse au sein du laboratoire. Je remercie aussi la région sud Provence Alpes Côte d'Azur pour m'avoir attribué la bourse « Emplois Jeunes Doctorants ». Par ailleurs, je souhaite remercier le Parc National de Port-Cros (PNPC) dans le cadre de notre partenariat pour l'attribution de cette bourse.

Je remercie les membres du jury, le Pr. Soizic Prado, et le Dr. Jean-François Ghiglione, en tant que rapporteurs de cette thèse, le Dr. Catherine Leblanc et le Dr. Christine Ferrier-Pagès en tant qu'examinatrices, et le Dr. Marion Peirache en tant que membre invité. Merci à vous pour votre disponibilité et l'enthousiasme que vous avez manifesté en vue de l'évaluation de ce travail de thèse.

Je souhaite ensuite remercier mes deux encadrants de thèse, le Dr. Gérald Culioli et Dr. Jean-François Briand, pour m'avoir accompagné tout au long de cette aventure. Gérald et Jean-François, vous avez fait preuve d'un soutien immense au quotidien. Avec votre complicité et votre enthousiasme, j'ai su dès le début de cette thèse (même un peu avant …), que ce serait un réel plaisir de travailler avec vous deux, et je ne me suis pas trompé ! J'espère avoir profité au maximum de cet encadrement rigoureux que vous m'avez offert pendant ces quatre années passées avec vous.

Gérald, merci pour ta patience, et ta pédagogie. Pour le microbiologiste de formation que je suis, tu m'as rapidement transmis ta passion pour la métabolomique environnementale. Merci aussi pour tes encouragements et ta bonne humeur, qui étaient souvent une source importante de motivation pour cette thèse. Je sens que je n'ai pas encore fini d'entendre parler de tes blagues sur ma barbe, ou encore tes diverses anecdotes au volant de la voiture sur le chemin de nos prélèvements (tu pourras raconter celle des gendarmes à tes futurs doctorants).

Jeff, merci pour ton dynamisme et ta persévérance. Cela a été un plaisir de poursuivre mon apprentissage de l'écologie microbienne avec toi. Merci pour l'enthousiasme dont tu as su faire preuve après la découverte de chacun de nos résultats (je pense notamment à nos longs et riches échanges devant chacune des nouvelles NMDS obtenues). Merci aussi pour ton soutien, et la liberté que tu m'as accordée lors de la conception et la réalisation de nouvelles études que nous avions en tête au fur et à mesure de ces années de thèse.

Mes remerciements s'adressent ensuite aux membres des comités de suivi de thèse : le Dr. Jean-François Ghiglione, le Dr. Christophe Vieira et le Dr. Stéphane Greff. Merci à vous trois pour votre disponibilité, vos conseils avisés et les encouragements dont vous avez fait preuve à la suite de mes (longues) présentations.

Je tiens aussi à remercier les membres du PNPC, avec lesquels j'ai pu travailler au cours de cette thèse. Merci tout d'abord à l'ensemble du conseil scientifique du PNPC pour nous avoir permis de réaliser les prélèvements de *Taonia atomaria*, au sein de cette aire protégée. Merci à vous, Marion, pour ton soutien, ta disponibilité, ton écoute et pour avoir rendu possible ces prélèvements, et Rose-Abèle Viviani pour la gestion de ces prélèvements. Je pense aussi à l'ensemble des agents sur le terrain qui nous ont accompagné et aidé lors de ces échantillonnages : merci notamment à Isabelle Masinski, Gilles Esposito, Laurent Maxime et Etienne Baudin, cela a été un grand plaisir de pouvoir échanger avec vous. Merci aussi à Virginie Fernandez, pour l'accueil au sein de la maison du Parc, et pour l'organisation de nos différentes actions de vulgarisation sur Porquerolles qui se sont avérées très enrichissantes pour nous.

Avant de démarrer un tour des lieux de France et d'ailleurs, pour mentionner l'importance des diverses collaborations et échanges qui ont contribué à ces travaux de thèse, restons encore un peu dans le Var, en remerciant les collègues du MIO : le Dr. Benjamin Misson pour m'avoir formé à la cytométrie en flux, ainsi que le Dr. Cédric Garnier, le Dr. Nicolas Layglon, Sébastien d'Onofrio, Christophe Le Poupon, pour les analyses chimiques de l'eau. Merci notamment à vous deux, Ben et Nico pour vos remarques toujours pertinentes et votre intérêt porté à mon sujet.

Vient ensuite Marseille, où je souhaite remercier grandement le Dr. Stéphane Greff pour son aide pour les analyses à la plateforme MALLABAR. Steff, merci pour ta bonne humeur (toujours le sourire même quand le Q-ToF est en panne !), ta disponibilité, et ta sympathie. Merci aussi au Dr. Thierry Pérez, pour l'accueil toujours très chaleureux à la station, et l'intérêt porté à nos travaux. Enfin, mes pensées ne sauraient quitter Marseille sans remercier le Dr. Jean-Charles Martin pour les explications en métabolomique et en statistique, et surtout son humour toujours aussi efficace !

Direction Roscoff maintenant, pour remercier tout d'abord le Dr. Catherine Leblanc et le Dr. Philippe Potin grâce à qui le projet EMBRC a pu se réaliser. Un grand merci à vous deux pour votre disponibilité, j'ai énormément apprécié mon séjour à la station Biologique de Roscoff, dans le cadre de nos expériences en mésocosmes. Merci pour votre enthousiasme lors de ce projet, ainsi que le projet EC2CO porté sur la phylogénie et la biogéographie. Un grand merci à Gaëtan Schires, pour sa bonne humeur et pour l'aide apportée dans la construction de l'infrastructure pour les aquariums. J'ai beaucoup apprécié de pouvoir

participer à sa mise en place, qui j'espère sert et servira à beaucoup d'autres. Merci aussi à Cédric Leroux pour l'aide apportée à la plateforme de métabolomique METABOMER, et à Elodie Bourrigaud, pour l'aide technique apportée au sein du laboratoire d'accueil EMBRC. Un grand merci aussi au Dr. François Thomas et au Dr. Angélique Gobet pour les échanges que nous avons pu avoir, notamment au sujet des couples d'amorces ainsi qu'au Dr. Kevin Cascella, pour son aide et sa convivialité au cours de ce séjour Breton.

Continuons au nord, pour remercier le laboratoire de phycologie de Gand, avec en particulier le Dr. Olivier de Clerck et le Dr. Christophe Vieira, pour leur aide et l'enthousiasme porté au sujet de la phylogénie des algues *Taonia*. Merci Christophe pour ta motivation et ton implication dans le projet EC2CO, c'est toujours un plaisir de pouvoir échanger ensemble, malgré maintenant quelques fuseaux horaires qui nous séparent.

Retour maintenant au sud, à Villefranche-sur-Mer, ou j'ai eu le plaisir de travailler avec le Dr. Eva Ternon. Merci Eva, (quelques fuseaux horaires sont maintenant à considérer pour toi aussi), pour m'avoir accueilli ces quelques jours à l'observatoire de Villefranche-sur-Mer et pour l'enthousiasme que tu as porté dans le cadre de notre collaboration. Par la même occasion, un grand merci aussi au Dr. Olivier Thomas pour la participation dans ce projet ainsi que pour les échanges que l'on a pu avoir de manière plus générale et les conseils en métabolomique.

Enfin avant de revenir à Toulon, j'aimerais faire un détour à Banyuls, pour remercier le Dr. Raphaël Lami. Dans le cadre de cette thèse, merci Raphaël pour ton aide apportée lors des prélèvements à Banyuls et Cerbère, mais aussi un grand merci pour m'avoir initié et transmis ta passion pour l'écologie microbienne, il y maintenant un peu plus de 5 ans quand j'étais stagiaire.

Par un retour à Toulon, je voudrais remercier tous ceux qui m'ont aidé, et accompagné dans les moments de cette aventure empreinte d'une large dimension humaine. Ainsi je souhaite remercier les stagiaires qui ont travaillé avec nous, avec ferveur, pour annoter le métabolome de *Taonia*. Merci François, Nathan et Damien, pour votre implication et votre rigueur pour ce travail essentiel et tant nécessaire pour le reste de ma thèse. Je suis fier que vous ayez brillamment réussi vos stages, et vous souhaite plein de bonnes choses dans vos projets respectifs.

Merci aussi à Raphaëlle, Bruno, Marlène et Armand pour votre aide au laboratoire, que ce soit pour les commandes, les envois de colis, l'utilisation des appareillages, ou l'attention apportée à la sécurité ! Bruno merci en particulier pour ton aide à la RMN. Raphaëlle merci pour ton travail au microscope confocal et optique : toujours à la recherche de belles petites diatos !

Merci aussi à l'ensemble de l'équipe pédagogique avec laquelle j'ai pu travailler notamment au cœur de cette dernière année en tant qu'attaché temporaire d'enseignement et de recherche. Merci tout d'abord à toi Annick, pour ta bienveillance, les efforts et ta disponibilité à mon égard dans cette période d'enseignement. Merci aussi pour l'intérêt que tu as porté à mon sujet de thèse, lorsque je présentais mes travaux en réunion d'équipe entre deux bouchées de brioches dont tu as le secret. Un grand merci aussi à Natacha, pour l'organisation de mon service d'enseignement, ainsi qu'à Jean-Louis, Nadia et Sylvie pour votre disponibilité lors de la préparation de mes enseignements au sein de l'UFR.

Enfin il est temps de remercier tous les amis avec lesquels j'ai pu partager ces bons moments de joies et de rires, au cours de ces quatre années, que ce soit dans les labos, au bureau ou ailleurs (apéroplage, concerts, restos, cinés, festivals, bars, etc …). On va commencer par les ceux qui sont déjà Docteurs c'est la moindre des choses ! Merci Laurie, Clém, Sofyane, Damien, Thomas, Gabriela, Nadja, Ouassim, Richard, Alain, Mahmoud, Manar, Lina, Anthony, et Nesrine. Elisa, merci pour ton aide et ta bonne humeur apportée au bureau, avec Nicolas et Lua-Cecília, je vous souhaite plein de bonheur pour votre petite famille. Vitalys, ta danse de la boule je l'attends toujours. Cocleto, merci pour le conseil ultime, j'espère que tu n'es pas trop en manque de pastis la-bas ! Manu, le président, bientôt un nouveau mandat ? Laure, j'ai eu droit à plein de hashtags dans tes remerciements donc je te rends la pareille (#lareinedesmomentgenants,#arretedevolerlargentacitadelle,#taspasbientotfinisdembeterwiwi, #cestloooong), Wiwi, je tiens à m'excuser pour avoir été un mauvais shérif, j'espère que tes choix vestimentaires s'améliorent de jours en jours, on y croit !

Merci aussi à tous les futurs docteurs, vous me faites sentir un peu vieux maintenant, mais je vous aime quand même. Au MAPIEM, je pense notamment Elora, Nacer, Alexandre, Sigrid. Merci Nathan, le petiot ! C'est bientôt toi le doctorant vétéran de la bio. Si tu me demandes si « c'est une bonne ou mauvaise situation ça ? », je te répondrais que je ne crois pas qu'il y ait de bonne ou de mauvaise situation. Moi, si je devais résumer ma vie aujourd'hui, je dirais que c'est d'abord des rencontres. Des gens qui m'ont tendu la main peut-être à un moment où je ne pouvais pas, où j'étais seul chez moi **...** Aurélie, désolé je n'ai pas toujours été tendre avec toi, mais c'est pour ton bien, sache-le ! Cocleto a un super conseil à te donner, tu lui demanderas. J'espère que tu gardes toujours ton balai cassé en mon honneur. J'ai une pensée aussi pour le reste de la dream team du bâtiment X et tous les supers moments passés avec vous : Caro, Marion, Mélanie, Quentin, William (le pou !), Baptiste, Maxence, Anthony, Ahmad, Paul et Guillaume. Enfin, merci aux doctorants du R : Cyril, Gaël, Nico, Amanda, et Margaux.

Des remerciements qui me tiennent à cœur viennent ensuite à Sandro et Ali, l'homme du matin et celui du soir ! Merci pour votre aide, votre bonne humeur et les fous rires du quotidien au bureau, rien de mieux pour rester motiver !

Ensuite je souhaite remercier mes amis de longue date ! Merci Matthieu et Ysaline pour tout le soutien et l'attention que vous m'avez apportés durant toutes ces années, une grande aide. Matthieu, 12 ans d'amitiés et toujours plein de projets ensemble, j'ai hâte de pouvoir reprendre nos aventures ! Valou, Cindy, et Manon : les potes de Jussieu, vous me manquez ! Benjamin et Amélie, pareil, j'ai hâte de vous revoir malgré nos agendas de premier ministre. Une pensée aussi pour tous les amis de stage rencontrés à Banyuls !

Enfin, voici le moment de remercier la famille ! Tout d'abord, merci Maman, Papa, Amber, Guigui, Mariochka, Benoit et la plus belle, la plus adorable des petites nièces : Blanche ! (Oui je suis un tonton en admiration …). Un immense merci à vous, pour votre soutien sans faille depuis le début de mon cursus. Dans ces tous ces moments, votre amour et vos encouragements ont été essentiels pour moi. Maman, merci à toi pour m'avoir tant partagé et transmis ton engouement pour les sciences du vivant. Je sais d'ores et déjà où je vais ranger ce manuscrit de thèse ; au côté de l'exemplaire du tien que j'ai dans ma bibliothèque. Voilà une nouvelle source de motivation pour le terminer ! Un remerciement spécial pour toi, Papou, pour tes superbes aquarelles, qui illustrent parfaitement les différents sites de prélèvements qui m'ont été chers au cours de cette thèse. Je suis fier que tu aies ainsi contribué à ce manuscrit de thèse à ta façon. A toute la famille Itoux : Bernard, Laurence, cousinette, Bast, Lucie, Léo, Gaëlle et Sylvio ainsi qu'à la famille Picard : Jérôme, Maryannick, Manu, Camille, Pierre, Marion, Soph, Béa, Paulo, Basilou et le petit Anatole, un grand merci pour votre soutien et tout l'intérêt que vous avez porté pour ma thèse. Mounette, la matriarche, merci pour ta tendresse et la fierté dont tu me témoignes toujours à ta façon. Enfin, j'ai aussi une pensée pour Bibi ainsi qu'à toute la famille « du sud » pour l'accueil toujours très chaleureux au Beausset.

Isis, je sais que tu m'écoutes rigoler pendant que je tape ces mots et que tu meurs d'envie de les lire ! Merci du fond du cœur pour ton soutien sans faille, merci de partager tous ces moments au quotidien avec moi, merci pour toute la joie de vivre que tu m'apportes depuis maintenant un peu plus de deux ans.

A grand-papa et grand-maman,

Pour tout l'amour que vous m'avez apporté.

TABLE DES MATIERES

REMERCIEMENTS ---------- 3

TABLE DES MATIERES ----------10

TABLE DES ILLUSTRATIONS : FIGURES ----------19

TABLE DES ILLUSTRATIONS : TABLEAUX ----------27

LISTE DES ABREVIATIONS----------29

INTRODUCTION GENERALE ----------33

CHAPITRE I : ETAT DE L'ART----------37

1. L'holobionte, une unité fonctionnelle associant l'hôte et son microbiote ---------- 38

1.1. L'émergence du concept d'holobionte ---------- 38

1.2. La théorie de l'hologénome ---------- 41

1.3. Les holobiontes marins impliquant des microorganismes épiphytes ---------- 43

1.4. Le cas des macroalgues ---------- 47

2. Exemples de médiation chimique chez les macroalgues et leurs bactéries épiphytes ---------- 54

2.1. Le modèle *Delisea pulchra* ---------- 54

2.2. Le modèle *Ulva mutabilis* ---------- 56

2.3. Le modèle *Fucus vesiculosus* ---------- 58

2.4. L'induction de défenses oxydatives chez les algues *Gracilaria conferta* et *Laminaria digitata* ---------- 59

3. Les macroalgues holobiontes sous l'effet de perturbations environnementales ---------- 60

3.1. Hausse globale des températures et vagues de chaleurs marines ---------- 60

3.2. Acidification et effet combiné avec une augmentation de la température ---------- 62

3.3. Détérioration de la qualité de l'eau et effet de l'urbanisation côtière ---------- 63

3.4. Effets d'autres paramètres environnementaux : Exemple de l'intensité lumineuse et de la salinité--- 65

4. Le modèle *Taonia atomaria*---------- 66

4.1. Description morphologique et phylogénie du genre *Taonia* ---------- 66

4.2. Ecologie, répartition géographique et cycle de vie de *T. atomaria* ---------- 67

4.3. Production chimique chez *T. atomaria* et activités biologiques associées---------- 68

4.4. Critères liés au choix du modèle *T. atomaria* ---------- 72

5. Objectifs généraux de la thèse et méthodologies développées---------- 74

5.1. La complémentarité des approches -omiques pour aborder la complexité des systèmes holobiontes 75

5.2. L'approche par métabolomique pour élucider la production chimique à la surface de l'algue ---------- 77

5.3. L'approche métabarcoding complétée par la cytométrie en flux pour étudier le microbiote de surface 80

5.4. Objectifs et organisation de la thèse ---------- 82

CHAPITRE II : ETUDE PRELIMINAIRE ----------86

1. Avant-propos ---------- 87

2. Article: Temporal covariation of epibacterial community and surface metabolome in the Mediterranean seaweed holobiont *Taonia atomaria* ---------- 88

2.1. Summary ---------- 89

2.2. Introduction---------- 90

2.3. Results ---------- 92

2.3.1. Monitoring of the surface metabolome of T. atomaria---------- 92

2.3.2. 16S rDNA gene based analysis of epibiotic bacterial communities of T. atomaria ---------- 97

2.3.3. Multi-omics approach to assess temporal variations of T. atomaria----------101

2.4. Discussion ----------103

2.4.1. Diversity and composition of total and core microbiota associated with the surface of T. atomaria 103

2.4.2. Signalling cyclic dipeptides associated with the OMG BD1-7 clade ----------105

2.4.3. DMSP and proline betaine exhibited a key role within the correlation network ----------105

2.4.4. What about the role of the key network compounds DGTAs? ----------107

2.5. Experimental procedures----------108

2.5.1. Algal material----------108

2.5.2. Surface metabolome extraction, metabolomics analysis and data processing (See Supporting Information for more details) ----------108

2.5.3. MS/MS molecular networking and annotation of metabolites ---- 109
2.5.4. Epibacterial communities DNA Extraction, amplification and sequencing ---- 110
2.5.5. Metabarcoding data processing and statistical analysis ---- 110
2.5.6. Integration of metabolomic and metabarcoding dataset ---- 111
2.6. Acknowledgments ---- 112

3. Bilan du chapitre ---- 113

CHAPITRE III : ETUDE BIOGEOGRAPHIQUE ---- 114

1. Avant-propos ---- 115

2. Article: Host phylogeny and biogeography shape the surface microbiota and metabolome of the brown alga *Taonia* (Dictyotales) ---- 116
2.1. Abstract ---- 117
2.2. Introduction ---- 118
2.3. Material and Methods ---- 120
2.4. Results and discussion ---- 122
2.5. Conclusion ---- 129
2.6. Acknowledgments ---- 130

3. Bilan du chapitre ---- 131

CHAPITRE IV : ANNOTATION DU METABOLOME ---- 132

1. Avant-propos ---- 133

2. Article: Integration of LC/MS-based molecular networking and classical phytochemical approach allows in-depth annotation of the metabolome of non-model organisms - The case study of the brown seaweed *Taonia atomaria* ---- 134
2.1. Highlights ---- 135
2.2. Introduction ---- 136
2.3. Materials and methods ---- 138
2.3.1. Chemicals ---- 138
2.3.2. Algal material ---- 138
2.3.3. Isolation of chemical standards from T. atomaria ---- 138
2.3.4. Annotation of the metabolome of T. atomaria using molecular networking (MN) ---- 139

2.4. Results and discussion ----142
2.4.1. Isolation of chemical standards from T. atomaria: a “phytochemical approach” ----142
2.4.2. Annotation of the metabolome of T. atomaria using a restricted MN (MN-1) ----143
2.4.3. Further annotation of the metabolome of T. atomaria using less restricted MNs (MN-2 and MN-3) 152
2.4.4. Taxonomical and ecological significance of the annotated metabolites ----156
2.5. Conclusion ----158

3. Bilan du chapitre ----159

CHAPITRE V : ETUDE INTRA-THALLE---- 160

1. Avant-propos ----161

2. Article: A multi-omics analysis suggests links between the differentiated surface metabolome and epiphytic microbiota along the thallus of a Mediterranean seaweed holobiont ----162

2.1. Abstract ----163
2.2. Introduction----164
2.3. Materials and methods ----166
2.3.1. Sampling strategy ----166
2.3.2. Confocal laser scanning microscopy ----166
2.3.3. Quantitative flow cytometry analyses----167
2.3.4. DNA extraction, 16S rRNA gene amplification and sequencing ----167
2.3.5. 16S rRNA gene metabarcoding data processing and analysis----167
2.3.6. Extraction and samples preparation for metabolomics approaches ----168
2.3.7. Metabolomics data processing and analysis----169
2.3.8. Annotation strategy for metabolomics analysis ----170
2.3.9. Integration of surface metabolome and surface microbiota datasets----170
2.3.10. Statistical tests and cross validations ----170
2.4. Results ----171
2.4.1. Confocal laser scanning microscopy (CLSM) ----171
2.4.2. Quantification of epiphytic cells densities by flow cytometry ----171
2.4.3. Diversity and structure of bacterial communities ----172
2.4.4. Comparative metabolomics fingerprinting analysis ----178
2.4.5. Global annotation of metabolomes ----179
2.4.6. Variations of surface metabolites involved in the differentiation between thallus parts ---180

2.4.7. Integration of surface metabolome and surface microbiota datasets ---- 182
2.5. Discussion ---- 183
2.5.1. Specific microbiota selected at the algal surface ---- 183
2.5.2. Epibacterial communities differed from the basal to the apical algal parts ---- 183
2.5.3. Cross metabolomics and molecular networking allowed to attribute to algal metabolites the intra-thallus variations of the surface metabolome ---- 185
2.5.4. Algal growth could explain zonal variations of metabolome and microbiota ---- 186
2.5.5. Specific role of algal secondary metabolites on epibacterial communities ---- 188
2.6. Conclusions ---- 190
2.7. Acknowledgments ---- 190

3. Bilan du chapitre ---- 191

CHAPITRE VI : SUIVI SPATIO-TEMPOREL ---- 192

1. Avant-propos ---- 193

2. Article: A multi-omics approach deciphers how temperature and copper stress shape seaweed-microbiota interactions at the surface of *Taonia atomaria* on the NW Mediterranean coast ---- 194

2.1. Abstract ---- 195
2.2. Introduction ---- 196
2.3. Materials and methods ---- 198
2.3.1. Sampling strategy and biological material ---- 198
2.3.2. Chemical analysis of seawater ---- 198
2.3.3. Flow cytometry analyses ---- 198
2.3.4. DNA extraction, 16S rRNA gene amplification and high throughput sequencing ---- 199
2.3.5. 16S rRNA gene metabarcoding data processing and analysis ---- 199
2.3.6. Extraction of surface metabolome and UPLC-ESI-MS analyses ---- 199
2.3.7. Metabolomics data processing, annotation and statistical analyses ---- 200
2.3.8. Integration of metabolomics, metabarcoding, Tax4Fun and environmental datasets ---- 200
2.3.9. Statistical tests ---- 200
2.4. Results ---- 202
2.4.1. Environmental conditions and occurrence of T. atomaria ---- 202
2.4.2. Epibacterial community abundance ---- 202
2.4.3. Epibacterial diversity and community composition ---- 202
2.4.4. Predicted functional features of epibacterial community ---- 206

2.4.5. Surface metabolome profiling ---- 207
2.4.6. Surface compounds characterization and dynamics ---- 208
2.4.7. Multi-omics network analysis ---- 210
2.5. Discussion ---- 212
2.5.1. A winter, low diversified and host-specific pioneer community ---- 212
2.5.2. Temperature as a major temporal shaping factor ---- 213
2.5.3. Trace metal contamination plays locally a key role on the holobiont fitness ---- 215
2.6. Conclusion ---- 217
2.7. Declarations ---- 217
2.7.1. Ethics approval and consent to participate ---- 217
2.7.2. Consent for publication ---- 217
2.7.3. Availability of data and materials ---- 217
2.7.4. Competing interests ---- 217
2.7.5. Funding ---- 218
2.7.6. Authors' contributions ---- 218
2.7.7. Acknowledgements ---- 218

3. Bilan du chapitre ---- 219

CHAPITRE VII : ETUDE EN MESOCOSMES ---- 221

1. Avant-propos ---- 222

2. Article: Synergistic effects of temperature and light affect the relationship between *Taonia atomaria* and its epibacterial community: a mesocosm study ---- 223

2.1. Abstract ---- 224
2.2. Introduction ---- 225
2.3. Materials and methods ---- 227
2.3.1. Aquarium experimental device ---- 227
2.3.2. Sampling and biological material ---- 227
2.3.3. Mesocosms experiment ---- 228
2.3.4. Physicochemical parameters measurements ---- 229
2.3.5. Physiological assessment ---- 229
2.3.6. Flow cytometry analyses ---- 230
2.3.7. 16S rRNA gene metabarcoding analyses ---- 230
2.3.8. UHPLC metabolomics analyses ---- 231

2.3.9. Statistical tests ---- 232
2.4. Results ---- 232
2.4.1. Physicochemical parameters ---- 232
2.4.2. Physiological assessment ---- 233
2.4.3. Flow cytometry analyses ---- 233
2.4.4. Comparison of NOCHL and 515F-Y/926R primers ---- 233
2.4.5. Epibacterial community diversity ---- 233
2.4.6. Surface metabolome fingerprinting and VIP variations ---- 237
2.5. Discussion ---- 241
2.5.1. Effect of mesocosm conditioning on the holobiont system ---- 241
2.5.2. Short-term responses of algal surface microbiota and metabolome ---- 242
2.5.3. Effect of irradiance on surface microbiota: an indirect long-term effect mediated by the algal host? 243
2.5.4. Effect of temperature on the holobiont dynamics in a context of global warming and marine heatwaves 246
2.6. Conclusion ---- 249
2.7. Acknowledgments ---- 249

3. Bilan du chapitre ---- 250

CHAPITRE VIII : DISCUSSION GENERALE ---- 251

1. Rappels sur les objectifs de la thèse ---- 252

2. Bilan des approches utilisées ---- 253
2.1. L'annotation du métabolome ---- 253
2.2. Le choix de la méthode analytique pour la métabolomique ---- 256
2.3. Quelle est l'origine des métabolites de surface étudiés ? ---- 257
2.4. Le choix des amorces pour l'approche par metabarcoding ---- 258
2.5. Les approches multi-omiques pour le couplage de jeux de données hétérogènes ---- 262

3. Les communautés pionnières, cœurs et spécifiques à la surface de *Taonia* ---- 264
3.1. Les taxa pionniers sont aussi des taxa cœurs et spécifiques à l'algue ---- 264
3.2. Une dynamique associée à la maturation du biofilm et la croissance de l'algue. ---- 268

4. Impact de l'environnement sur la dynamique de l'holobionte ---- 270

4.1. La dynamique des Rhodobacteraceae : quels sont les liens avec le DMSP, la température et la luminosité ? ---- 270
4.2. Importance de la fucoxanthine en tant que photopigment antioxydant et antimicrobien ---- 274
4.3. Observation d'un phénomène de blanchissement chez *T. atomaria* : vers l'identification d'une éventuelle dysbiose médiée par l'augmentation de la température, l'abaissement des défenses chimiques de l'algue et la colonisation par des algues coralligènes ? ---- 277

5. Quid de la communauté microbienne eucaryote ? ---- 282

6. **Conceptualisation de la dynamique hôte-microbiote-environnement chez l'holobionte *T. atomaria* ---- 283**

CONCLUSION GENERALE ET PERSPECTIVES ---- 287

1. Conclusions ---- 288

2. Perspectives ---- 291

ANNEXE I : FOCUS SUR *OSTREOPSIS* CF. *OVATA* ---- 293

1. Avant-propos ---- 293

2. Article: Exploring the role of macroalgal surface metabolites on the settlement of the benthic dinoflagellate *Ostreopsis* cf. *ovata*. ---- 294

2.1. Abstract ---- 295
2.2. Introduction ---- 296
2.3. Materials and methods ---- 298
2.3.1. Microalgal cell abundance at the surface of the macroalgae ---- 298
2.3.2. Chemical extraction and analysis of macroalgal samples ---- 299
2.3.3. DNA extraction and amplification of the epiphytic communities ---- 299
2.3.4. 18S rRNA gene metabarcoding data processing and analysis ---- 299
2.3.5. Bioassays ---- 300
2.3.6. UHPLC-HRMS analysis of macroalgal extracts ---- 301
2.4. Results ---- 303
2.4.1. Assessment of the natural abundance of benthic microalgae using microscopy ---- 303
2.4.2. Diversity of epiphytic eukaryotes through 18S rRNA gene HTS ---- 304
2.4.3. Chemical analysis of macroalgal extracts ---- 305
2.4.4. Bioactivity of surface extracts (SEs) on O. cf. ovata ---- 311

2.5. Discussion ---------- 312
2.5.1. Potential control of the abundance of O. cf. ovata by the epiphytic community ---------- 312
2.5.2. Algal surface chemistry influences the growth of O. cf. ovata ---------- 315
2.6. Conclusion ---------- 317
2.7. Acknowledgments ---------- 317

ANNEXES ELECTRONIQUES ---------- 319

LISTE DES COMMUNICATIONS SCIENTIFIQUES ---------- 320

Publications acceptées (chapitres II, V et annexe I) ---------- 320

Publication soumise (chapitre VI) ---------- 320

Publications en préparations (chapitres III, IV et VII) ---------- 320

Communications orales ---------- 320

Communications par affiches ---------- 321

Autres présentations et actions de vulgarisations ---------- 321

REFERENCES BIBLIOGRAPHIQUES ---------- 322

TABLE DES ILLUSTRATIONS : FIGURES

CHAPITRE I : ETAT DE L'ART

Figure I.1. Exemples d'interactions possibles entre les coraux et leurs symbiontes (Peixoto et al., 2017) 40

Figure I.2. Schéma conceptuel représentant les différents génomes et leurs implications au sein de l'holobionte (Theis et al., 2016) 42

Figure I.3. Schéma représentant les différentes interfaces propices au développement de biofilms en milieu marin (Flemming and Wuertz, 2019) 44

Figure I.4. Les différentes étapes du cycle de vie d'un biofilm (Figure modifiée d'après Stoodley et al., 2002 et Monroe, 2007) 45

Figure I.5. Observations par microscopie à épifluorescence (A) et microscopie électronique à balayage (B) du biofilm à la surface de l'algue *Cladophora glomerata* (Zulkifly et al., 2012). 49

Figure I.6. Surface d'une macroalgue caractérisée par la présence de microorganismes et de molécules impliquées dans les interactions algue-microbiote (d'après Egan et al., 2013) 50

Figure I.7. Analyse multivariée (PCoA) montrant la spécificité de la β-diversité du microbiote épiphyte de huit kelps par rapport aux communautés bactériennes planctoniques et épilithiques de surfaces rocheuses (Lemay et al., 2018b). Les huit kelps étudiés sont : *Costaria costata*, *Alaria marginata*, *Pterygophora californica*, *Cymathaere triplicate*, *Laminaria setchellii*, *Nereocystis luetkeana*, *Saccharina groenlandica*, et *S. latissimi* 51

Figure I.8. (1) Exemples de furanones halogénées isolées de Delisea pulchra (d'après Manefield et al., 1999) agissant en tant qu'antagonistes d'HSLs. (2) Exemples d'HSLs impliquées dans les mécanismes du QS. 54

Figure I.9. L'algue *Delisea pulchra* récoltée sur les côtes australiennes (Bare Island, Sydney) présentant certaines zones médianes blanchies; l'une d'elles est signalée par une fleche (Fernandes et al., 2012). . 55

Figure I.10. Modèle proposé détaillant les interactions entre l'algue Ulva mutabilis et les bactéries impliquées dans sa morphogenèse (Kessler et al., 2018) 57

Figure I.11. Composés impliqués dans les interactions de l'holobionte Ulva mutabilis : DMSP (**I**) agissant en tant que chemo-attracteur de certaines souches productrices de facteurs de croissance pour l'algue, tels que la thallusine (**II**). 58

Figure I.12. L'algue *Taonia atomaria in* et *ex-situ*. Le thalle présente certaines caractéristiques-clés pour son identification morphologique telles que l'élargissement des frondes de la base vers le sommet, les

stries de poils horizontales et les extrémités apicales laciniées (http://www.seaweed.ie/descriptions/Taonia_atomaria.php) 67
Figure I.13. Principaux métabolites caractéristiques des algues brunes (**III** : β-carotène, **IV** : zéaxantine, **V** : violaxanthine, **VI** : fucoxanthine, **VII** : fucostérol et **VIII** :24-méthylènecholestérol) 69
Figure I.14. Structures chimiques des méroditerpènes isolés de *T. atomaria* 70
Figure I.15. Structures chimiques des sesquiterpènes isolés de *T. atomaria* 71
Figure I.16. Structure chimique du géranylgéranylglycérol isolé de *T. atomaria* 72
Figure I.17. Schéma expérimental proposé par Dittami et al., (2014) impliquant l'étude des génomes de l'algue et de son microbiote afin de déterminer leur complémentarité métabolique et d'identifier de potentiels processus de co-acclimatation au sein de l'holobionte 76
Figure I.18. Schéma conceptuel impliquant l'intégration conjointe des diverses approches -omiques associées d'une part à l'algue et, d'autre part, à son microbiote afin d'étudier l'intéractome de l'holobionte. 77
Figure I.19. Organisation des différents objectifs et questions de la thèse, associés à chaque chapitre .. 85

CHAPITRE II : ETUDE PRELIMINAIRE

Figure II.1. Seasonal structuring of the surface (A) metabolome (PCA) and (B) microbiota (PCoA) of *T. atomaria.* (C) showed the score plot of the multi-block PLS-DA (DIABLO analysis) built with the metabolomics and metabarcoding datasets. Ellipses are grouping replicates from each month with 70% of confidence for the PCA ordination (A), 90% for the PCoA ordination (B), and 85% for the DIABLO ordination (C). 93
Figure II.2. Molecular network of HRMS fragmentation data obtained from surface extracts of *T. atomaria* (collected monthly from February to July). 94
Figure II.3. Seasonal variations of some selected surface metabolites of *T. atomaria*. Individual metabolites obtained after UPLC-MS analysis were normalised by the sum, log10-transformed and mean-centred. A one-way ANOVA followed by post-hoc tests (HSD) allowed to show significant variations for relative concentrations of each metabolite during the year. 97
Figure II.4. Seasonal dynamics of diversity indexes. (A) show the chemodiversity measures calculated using Shannon index with the metabolomics dataset. (B, C and D) show the epibacterial alpha-diversity measures respectively calculated using Simpson, Shannon, and Chao1 indexes with the 16S metabarcoding dataset. A one-way ANOVA followed by post-hoc tests (HSD) allowed to show significant variations for the indexes during the year. 98

Figure II.5. Seasonal variations of the epibacterial communities on *T. atomaria* at the family level (A: total community, B: core community). A, B, C in sample names represent biological replicates. % in B are % of all the core sequences. 100
Figure II.6. Seasonal correlation network (multi-block PLS-DA) of the surface metabolome and the epibacterial communities of *T. atomaria.* Discriminant OTUs (orange circles and names) and metabolites (blue circles and names) are positively (green) or negatively (red) connected. Seasonal variation of their relative occurrence during the year was also represented inside the circles with pie charts. 102

CHAPITRE III : ETUDE BIOGEOGRAPHIQUE

Figure III. 1. Map with the location of the 19 sampling sites. From right to left: VILF: Villefranche-sur-Mer; ANTB: Cap d'Antibes; THEO: Théoule-sur-Mer; DRAM: Le Dramont; STMA: Sainte-Maxime; STCL; Saint-Clair; LLND: La Londe-les-Maures; PRQN: Porquerolles island (Northern coast); PRQS: Porquerolles island (Southern coast); CARQ: Carqueiranne; TAMR: Tamaris; BRUS: Le Brusc; BAND: Bandol; CASS: Cassis; MRSL: Marseille; AGD: Agde; BANY: Banyuls-sur-Mer; CERB: Cerbère; LOCQ: Locquirec. 120
Figure III.2. Bayesian phylogenetic tree of *Taonia* based on the concatenated alignment of cox3, psbA and rbcL datasets. Values at the nodes represent Bayesian (left) and maximum likelihood (right) support values. 123
Figure III.3. β-diversity and structure of prokaryotic communities at the surface of *Taonia* samples. The dendrogram corresponds to a UPGMA clustering based on Bray-Curtis distance and calculated at the OTU level. Histograms represent the relative abundances of the main families. * "Other" corresponds to unaffiliated families and those below 1%. 125
Figure III.4. Metabolomics fingerprinting of surface extracts of *Taonia* samples. The dendrogram corresponds to a Euclidian clustering based on the average method and calculated with all metabolites of the metabolomics dataset. The heatmap shows relative concentration of the 25 most discriminant metabolites according to both geographical areas (Mediterranean vs Atlantic sites). 126

CHAPITRE IV : ANNOTATION DU METABOLOME

Figure IV.1. Analytical workflow used in this study 142
Figure IV.2. Restrained MN (**MN-1**) built with MS/MS data of fractions obtained from the crude extract of the brown alga *Taonia atomaria.* Node colors were chosen according to their chemical classes (see color code below the network). Nodes with a diamond shape correspond to fragments ions, while those with a triangle shape are representing compounds with a distinct adduct from the rest of its cluster. Thickness of

an edge between two nodes was proportional to the cosine score (CS, from 0.851 to 0.995). Only clusters with at least three nodes were represented. The whole network also includes 39 clusters of two nodes, and 512 unbound nodes..... 144
Figure IV.3 Annotation of GGG derivatives in cluster **1F** and proposed MS/MS fragmentation pattern for the compounds MGGG (18:4) and MGGG (O-17:2) 149
Figure IV.4. Less restrained MN (**MN-3**) built with MS/MS data of fractions obtained from the crude extract of the brown alga *Taonia atomaria.* Node colors were chosen according to their chemical classes (see color code below the network). Nodes with a diamond shape correspond to fragments ions, while those with a triangle shape are representing compounds with a distinct adduct from the rest of its cluster. Nodes with a thick border correspond to newly annotated compounds via the MN enlargement. Thickness of an edge between two nodes was proportional to the cosine score (CS, from 0.701 to 0.995). Only clusters with at least three nodes were represented. The whole network also includes 37 clusters of two nodes, together with 326 unbound nodes. 153

CHAPITRE V : ETUDE INTRA-THALLE

Figure V.1. Variations of cells densities along the surface of *Taonia atomaria* and differences in α-diversity between algal parts, rocky biofilms and seawater collected in two Mediterranean sites (Carqueiranne and Tamaris). (**A**) Heterotrophic prokaryotes cell densities (cells.cm^{-2}) variations of the different parts [basal (B), median (M) and apical (A)] of the thallus surface of *T. atomaria* in Tamaris. (**B**) Variations of several α-diversity indexes of prokaryotic communities at the surface of thallus parts [basal (B), median (M) and apical (A)] of *T. atomaria*, in rocky biofilms (R) and in surrounding water (W). Boxplots correspond to whisker plots (n = 3) showing the lowest, median and highest values. p values and “a”, “b”, “c” indexes correspond to the results of one-way ANOVA analyses and post-hoc tests (HSD Tukey’s test), respectively. 172
Figure V.2. Structure and β-diversity of epibacterial communities at the surface of *T. atomaria*, in rocky biofilms and in seawater collected in two Mediterranean sites (Carqueiranne and Tamaris). NMDS plots based on weighted UniFrac distance for all samples (**A**) and algal samples only (B). Dashed lines grouped the different parts of a same individual thallus. (**C**) Relative percentages of each bacterial family across each group of samples (n = 3). Labels A, M, B, W and R corresponded to apical, median and basal algal parts, water samples and rocky biofilms, respectively. (*) “Others” correspond to unaffiliated families and/or families with a relative percentage below 1%. 174

Figure V.3. Co-occurrence network of OTUs from the 16S rDNA dataset of epibacterial communities at the surface of *T. atomaria*, in rocky biofilms and in seawater at Carqueiranne. Pie-chart inside each node revealed the distribution of each OTU across the different sample groups (Red: basal part, yellow: median part, green: apical part, grey: rocky biofilm, blue: seawater). Thickness of edges between each node was proportional to correlation or dissimilarity distances. The size of each node was proportional to the relative percentage of sequences of each OTU in all samples. 177

Figure V.4. PCA plots of GC-MS, LC-(-)-ESI-MS and LC-(+)-ESI-MS metabolomics analyses of surface and total extracts of *T. atomaria* (two sites: Carqueiranne and Tamaris; three algal parts: basal, median and apical) 179

Figure V.5. Normalised concentrations of selected surface metabolites (significant VIP features) detected by LC-(+)-ESI-MS and GC-MS across the different parts of the thalli of *T. atomaria*. Boxplots in red, yellow and green (labeled "B", "M" and "A") represented basal, median and apical algal parts, respectively. Boxplots corresponding to samples collected at Carqueiranne or Tamaris were labeled "C." and "T.", respectively. *p* values and "a", "b", "c" indexes correspond to the results of one-way ANOVA analyses and post-hoc tests (HSD Tukey's test), respectively. 181

Figure V.6. Weighted UniFrac distance-based redundancy analysis (db-RDA) plot constructed with the 16S rDNA dataset of epibacterial communities at the surface of *T. atomaria* and significant surface metabolites (VIPs) as explaining variables 182

CHAPITRE VI : SUIVI SPATIO-TEMPOREL

Figure VI.1. α-diversity metrics (Shannon and Chao1 indexes) for *T. atomaria*, rocky biofilms and seawater samples. A. Comparison between sample types for all samples, *p* values corresponded to the results of a one-way ANOVA with sample type as factor. B. Comparison between months within each sample type. C. Comparison between months within each site, for algal samples. B. and C. *p* values corresponded to the results of a one-way ANOVA with month as factor. 203

Figure VI.2. Structure and β-diversity of bacterial communities. (A) NMDS constructed with Bray-Curtis index showing β-diversity among seawater, rocky and algal samples. *p* value corresponded to the result of a one-way ANOVA with seawater, rocky and algal samples as factors. (B) db-RDA score plot showing environmental parameters as explaining variables of the β-diversity of algal samples. *p* value corresponded to the result of a two-way ANOVA using "Months" and "Sites" as factors. (C) Epibacterial community composition of *T. atomaria* at the family level. *: "Others" correspond to unaffiliated families and families below 1%. 205

Figure VI.3. Variations of predicted functions associated to the epibacterial communities of *T. atomaria*. *p* values corresponded to the results of a one-way ANOVA using "Month" as factor. 207
Figure VI.4. Diversity surface metabolome profiles assessed through LC-(+)-ESI-MS metabolomics. Score plots of (A) PCA, and PLS-DA constructed either with months (B) or sites (C) as supervised groups. *p* values corresponded to results of a two-way PERMANOVA using "Month" and "Site" as factors. 208
Figure VI.5. Normalized concentrations of significant and discriminant surface metabolites. (A) Discriminant metabolites according to temporal differences. *p* values corresponded to the results of a one-way ANOVA using "Month" as factor. (B) Discriminant metabolites according to spatial differences. *p* values corresponded to the results of a one-way ANOVA using "Site" as factor. 209
Figure VI.6. Spatiotemporal correlation network (multi-block sPLS-DA, DIABLO analysis) of the surface metabolome, epibacterial community, predicted functions and environmental variables. Using a sparse method, the network was constructed with an optimal number of variables according to the tuning procedure, which corresponded to a total of 29 metabolites, 28 OTUs, 6 predicted pathways and 3 environmental parameters with only positive correlations above 0.7 and negative correlations below -0.7. 211
Figure VI.7. Schéma bilan expliquant les effets des deux principaux facteurs environnementaux observés dans le cadre de l'étude spatio-temporelle : la température et la concentration en cuivre..... 220

CHAPITRE VII. ETUDE EN MESOCOSMES

Figure VII.1. Experimental design of the study. Each square representing an aquarium in this workflow, actually correspond to a triplicate of aquaria. 229
Figure VII.2. Multivariate analyses of surface microbiota and surface metabolomes including all samples of *T. atomaria*. (A) weighted UniFrac based NMDS plots showing β-diversity differences of epibacterial communities. (B) PCA score plots showing differences of surface metabolomes. 234
Figure VII.3. Weighted UniFrac based NMDS plots showing differences of β-diversity of epibacterial communities of *T. atomaria* samples collected at a specific sampling time: (A) t_1, (B) t_2, and (C) t_3. 235
Figure VII.4. Summary of significant variations of discriminant bacterial genera at the surface of *T. atomaria* samples collected at t_3 according to cross-conditions of temperature and irradiance. An arrow between two aquaria indicates a significant difference of relative abundance of a biomarker genus (Duncan's test and Benjamini-Hochberg *p*-value adjustment) between two conditions. ↗ and ↘ symbols after a genus name indicate whether a significant increase or decrease is respectively observed from the condition where the arrow starts to the condition where the arrow ends. 237

Figure VII.5. PCA score plots showing differences of surface metabolomes of *T. atomaria* depending on the sampling time: (A) t_1 samples, (B) t_2 samples, and (C) t_3 samples. 239
Figure VII.6. Summary of significant variations of discriminant surface metabolites of *T. atomaria* according to cross-conditions of temperature and irradiance at t_3. An arrow between two aquaria indicates a significant difference of the normalized concentrations of a chemical biomarker (ANOVA and Tukey's tests) between two conditions. ↗ and ↘ symbols after a compound name indicate whether a significant increase and decrease is respectively observed, from the condition where the arrow starts to the condition where the arrow ends. 240
Figure VII.7. Schéma bilan expliquant les effets de changements d'intensité lumineuse et de température, et les cinétiques associées, sur le microbiote et métabolome de surface 250

CHAPITRE VIII. DISCUSSION GENERALE

Figure VIII.1. Observations au microscope optique des tétrasporanges de *T. atomaria*. A et D : Coupes transversales de thalles présentant des tétraspores à leur surface. B : Coupe transversale d'un thalle présentant la germination du tétrasporange depuis la surface. C : Observation de tétrasporanges libres dans le milieu. Grossissements : A (× 100), B, C et D (× 400). E : Observation des différents stades de croissance des tétraspores de *T. atomaria* par Robinson, (1932)..... 261
Figure VIII.2. Dynamique des pourcentages relatifs des différents genres affiliés au Rhodobacteraceae observés à la surface de *T. atomaria* lors (A) des études spatio-temporelles (**chapitre VI**) et (B) en mésocosmes (**chapitre VII**). Les indices M1 à M6 correspondent aux mois allant de février à juillet. Les sites S1, S2, S3, S4 et S5 correspondent à Tamaris, Carqueiranne, Porquerolles côtes nord, Porquerolles côtes sud et La-Londe-les-Maures, respectivement. Les indices LT, AT, HT correspondent aux conditions de température faible, ambiante et forte. Les indices LI, AI, HI correspondent aux conditions d'intensité lumineuse faible, ambiante et forte. Les indices t-1 ; t0 ; t1 ; t2 et t3 correspondent aux échantillons de terrains, aux échantillons acclimatés, aux échantillons après 24h, 7 jours et 14 jours de conditionnement, respectivement..... 271
Figure VIII.3. Images 2D (**A**, **C**-**H**) et 3D (**B** et **I**) de thalles humides (**A**-**C**, **H** et **I**) et de thalles séchés (**D**-**G**) de *T. atomaria* obtenues par microscopie numérique (**A**-**F**) et par microscopie confocale (**H** et **I**) montrant des zones blanchies et/ou la présence d'algues coralligènes encroûtantes. Grossissements : **A** (×350), **B** et **C** (×140), **D** et **E** (x35), **F**, **H** et **I** (×200), et **G** (×50)..... 278
Figure VIII.4. Estimation de la proportion du thalle blanchie et colonisée par des macroalgues encroûtantes. 279

Figure VIII.5. Photographies des thalles séchés provenant du site S2 (Carqueiranne) (**A** et **B**) et du site S4 (côte sud de Porquerolles) (**C**) récoltées en Juillet. 280
Figure VIII.6. Premier cas de figure : l'environnement impacte la physiologie de l'algue et donc d'abord son métabolome 283
Figure VIII.7. Deuxième cas de figure : l'environnement impacte d'abord le microbiote..... 284
Figure VIII.8. Troisième cas de figure : l'environnement impacte simultanément l'algue et le microbiote 286

ANNEXE I : FOCUS SUR *OSTROPSIS* CF. *OVATA*

Figure AI.1. Cell density (cell cm^{-2}) of major diatoms and *O.* cf. *ovata* at the surface of the four macroalgae. Statistical significance was evaluated only for *O*. cf. *ovata* abundances using an ANOVA test (**p* = 0.0175) followed by a post-hoc Tukey's test. 303
Figure AI.2. Eukaryotic communities colonizing the surface of the four macroalgae and present in the surrounding seawater. Replicate samples of a same species were averaged (*n* = 3) and relative colonization to all sequences is given (%). Taxonomic affiliation corresponds to the Phylum and Class level. "Other" combines Classes that represent less than 2% of the total diversity. 305
Figure AI.3. PCA score plot obtained from LC-(+)-ESI-MS metabolomics analyses of both the total extracts (TEs) and surface extracts (SEs) of the four macroalgae. 306
Figure AI.4. PLS-DA score plot obtained from LC-(+)-ESI-MS metabolomics analyses of the surface extracts (SEs) of the four macroalgae. 307
Figure AI.5. Molecular network obtained from LC-(+)-ESI-MS/MS data of the SEs of the four macroalgal species. Only clusters with 3 or more nodes are represented. Nodes represent MS/MS spectra which are connected based on their spectral similarity. Colored nodes indicate biomarkers according to the four macroalgae (orange: *D*. dichotoma, green: *D. spiralis*, red: *T. atomaria*, no VIPs for *P. pavonica* were observed). The edge width is proportional to the cosine score. 309
Figure AI.6. (A) Growth rate (μ) of *O.* cf. *ovata* and (B) Maximum quantum yield of PSII (F_v/F_m) of dark-adapted samples of *O.* cf. *ovata* after exposure of 24h to macroalgal surface extracts (SEs) and blanks (*n* = 6 per condition). *p* values and a, b, c, d indexes correspond to results of the one-way ANOVA and Tukey's tests, respectively. 312

TABLE DES ILLUSTRATIONS : TABLEAUX

CHAPITRE I : ETAT DE L'ART

Tableau I.1. Récapitulatif des différentes études en mésocosmes portant sur l'effet de conditions climatiques futures (augmentation de température et acidification de l'eau) sur différentes macroalgues et leur microbiote de surface 63

CHAPITRE II : ETUDE PRELIMINAIRE

Table II.1. List of the biomarkers (VIP score ≥ 2) identified by LC−HRMS for the seasonal discrimination of the surface extracts of *T. atomaria*. [a] Constructor statistical match factor (comparison of theoretical and experimental isotopic patterns). [b] Abbreviations: DAG: diacylglycerol, DGTA: diacylglycerylhydroxymethyl-N,N,N-trimethyl-*β*-alanine, DMSP: dimethylsulfoniopropionate, Gln: glutamine, Ile: isoleucine, Leu: leucine, Phe: phenylalanine, Val: valine; [c] n.d.: not determined; [d] Not distinguishable from Gln-Ile. [e] Color code represents mean normalized concentrations values. 96

CHAPITRE VIII. DISCUSSION GENERALE

Tableau VIII.1. Tableau récapitulatif du nombre de métabolites identifiés par famille chimique en utilisant l'approche des réseaux moléculaires dans le cadre d'études sur les extraits de surface de *T. atomaria* 255

Tableau VIII.2. Comparaison du nombre de métabolites observés et annotés ainsi que des principales familles chimiques identifiées en fonction de trois méthodes d'analyses métabolomiques 256

Tableau VIII.3. Origine biosynthétique potentielle des principaux métabolites de surfaces déterminés comme étant des biomarqueurs 257

Tableau VIII.4. Liste des amorces codant l'ARN 16S utilisées pour l'étude des communautés procaryotiques à la surface de *T. atomaria* 258

Tableau VIII.5. Couverture in silico des amorces 775F/1103R et 515F-Y/926R d'après Pollet et al., (2018) 260

Tableau VIII.6. Liste des genres bactériens identifiés au cours des différentes études, comme étant les principaux contributeurs des communautés pionnières, cœurs ou spécifiques. n.d. : non déterminé ... 265

ANNEXE I : FOCUS SUR *OSTROPSIS* CF. *OVATA*

Table AI.1. Mean concentration (mg.cm^{-2}) of the SEs obtained from each macroalgal species given with the mean surface area measured for each species (*n* = 4). The concentration of the SEs tested in the bioassays is also given together with an estimation of the enrichment factors compared to natural concentrations. The enrichment factor was calculated as follow: $Enrichment\ factor = Concentration(testednatural)$. 299

Table AI.2. Putative annotation of the first 50 chemical markers (VIP score > 1.1) driving the distribution of the samples on the PLS-DA score plot obtained from LC-(+)-ESI-MS metabolomics analyses of the SEs of the four macroalgae. Identification of the compounds marked by * was confirmed with a chemical standard. Clusters "SL" corresponds to a self-loop (a metabolite only connected to itself). The colour code represents the mean concentration values obtained for each macroalga. 310

LISTE DES ABREVIATIONS

AAP	:	*Aerobic anoxygenic phototrophs*
ACC	:	*Algal core community*
ADN - *DNA*	:	Acide désoxyribonucléique - *Deoxyribonucleic acid*
ADNr - *rDNA*	:	ADN ribosomique - *ribosomal DNA*
AEC	:	*Algal enriched community*
AGD	:	Agde
AI	:	*Ambient irradiance*
AI-2	:	Auto-inducteur de type II
ANOVA	:	*Analysis of variance*
ANTB	:	Cap d'Antibes
ARN - *RNA*	:	Acide ribonucléique - *Ribonucleic acid*
ASW	:	*Artificial seawater*
AT	:	*Ambient temperature*
BAND	:	Bandol
BANY	:	Banyuls-sur-Mer
BI	:	*Bayesian inference*
BRUS	:	Le Brusc
CARQ	:	Carqueiranne
CASS	:	Cassis
CERB	:	Cerbère
CID	:	*Collision induced dissociation*
CLSM	:	*Confocal laser scanning microscopy*
COHESIONS	:	Couplage multi-omiques à l'échelle de l'holobionte : effet de la diversité spécifique des Phaeophyceae *Taonia* sur l'interaction hôte-microbiome à la surface
COI	:	*Cytochrome c oxidase subunit*
COSY	:	*Correlated spectroscopy*
cox3	:	*cytochrome c oxidase III*
DAG - DG	:	*Diacylglycerol*
DAPI	:	*4',6-diamidino-2-phenylindole*
db-RDA	:	*distance-based Redundancy Analysis*
DEPT	:	*Distortionless enhancement by polarization transfer*
DFG	:	*Diacylfarnesylglycerol*
DFuA	:	*Diacylglycerylfulvellic acid*
DGCC	:	*Diacylglyceryl-3-*O*-carboxy-(hydroxymethyl)-choline*
DGDG	:	*Digalactosyldiacylglycerol*
DGGE	:	*Denaturating gradient gel electrophoresis*
DGMG	:	*Digalactosyldiacylglycerol*

DGTA	:	*Diacylglycerylhydroxymethyltrimethyl-β -alanines*
DGTS	:	*Diacylglycerylhydroxymethyltrimethylhomoserine*
DIABLO	:	*Data integration analysis for biomarker discovery using latent variable approaches for 'Omics studies*
DIMS	:	*Direct-infusion mass spectrometry*
DmdA	:	*Dimethylsulfoniopropionate-dependent demethylase*
DMSO	:	*Dimethylsulfoxyde*
DMSP	:	*Dimethylsulfoniopropionate*
DOC	:	*Dissolved organic carbon*
DPASV	:	*Differential pulse anodic stripping voltammetry*
DRAM	:	Le Dramont
EC_2CO	:	Initiative structurante écosphère continentale et côtière
EC_{50}	:	*Half maximal effective concentration*
EDTA	:	*Ethylenediaminetetraacetic acid*
EMP	:	*Earth microbiome project*
EMPREINTES	:	Etude en mésocosmes de paramètres régulant l'interaction entre la macroalgue *Taonia atomaria* et son microbiome de surface
EPS	:	*Extracellular polymeric substances*
ESI	:	*Electrospray ionization*
FCM	:	*Flow cytometry*
FROGS	:	*Find, rapidly, Otus with Galaxy solution*
GC-MS	:	*Gas chromatography-mass spectrometry*
GGG	:	*Geranylgeranylglycerol*
GIEC	:	Groupe d'experts intergouvernemental sur l'évolution du climat
Gln	:	*Glutamine*
GMP	:	*Guanosine monophosphate*
GNPS	:	*Global natural product social molecular networking*
HI	:	High irradiance
HMBC	:	*Heteronuclear multiple bond correlation*
HMDB	:	*Human metabolome database*
HRMS	:	*High-resolution mass spectrometry*
HSD (Tukey's test)	:	*Honestly significant difference*
HSL	:	*Homoserine lactone*
HSQC	:	*Heteronuclear single quantum coherence spectroscopy*
HT	:	*High temperature*
Ile	:	*Isoleucine*
IR-TF	:	Spectroscopie infrarouge à transformée de Fourier
KEGG	:	*Kyoto encyclopedia of genes and genomes*
KO	:	*KEGG Orthology*
LC-MS	:	*Liquid chromatography-mass spectrometry*
LED	:	*Light-emitting diode*
LEfSe	:	*Linear discriminant analysis effect size*
Leu	:	*Leucine*

LI : *Low irradiance*
LLND : La Londe-les-Maures
LOCQ : Locquirec
LT : *Low temperature*
Lyso-PC : Lyso-*phosphatidylcholine*
MALDI : *Matrix assisted laser desorption ionization*
MCCV : *Mediterranean culture collection of Villefranche*
MC-PAM : *Multi-color pulse amplitude modulated*
MeOH : *Methanol*
MFG : *Monoacylfarnesylglycerol*
MFuA : *Monoacylglycerylfulvellic acid*
MG : *Monoacylglycerol*
MGDG : *Monogalactosyldiacylglycerol*
MGGG : *Monoacylgeranylgeranylglycerol*
MGGG-O : *Monoalkylgeranylgeranylglycerol*
MGMG : *Monogalactosylmonoacylglycerol*
MGTA - Lyso-*DGTA* : *Monoacylglycerylhydroxymethyltrimethyl*-β -*alanine*
MINT : *Multivariate integrative method*
ML : *Maximum likelihood*
MN : *Molecular network*
MoNA : *Massbank of North America*
MRC : *Marine Roseobacter clade*
MRSL : Marseille
MS : *Mass spectrometry*
NCBI : *National center for biotechnology information*
NGS : *Next generation sequencing*
NIST : *National institute of standards and technology*
NMDS : *Non-metric multidimensional scaling*
NOESY : *Nuclear overhauser spectroscopy*
NW : *North-west*
OL : *Ornithine lipid*
OTU : *Operational taxonomic units*
PAM : *Pulse amplitude modulation*
PANAM : *Phylogenetic analysis of next-generation amplicons*
PC : *Phosphatidylcholine*
PCA : *Principal component analysis*
PCR : *Polymerase chain reaction*
PE : *Phosphatidylethanolamine*
PERMANOVA : *Permutational analysis of variance*
PG : *Phosphatidylglycerol*
Phe : *Phenylalanine*
PICRUST : *Phylogenetic investigation of communities by reconstruction of unobserved states*

PLS-DA	:	*Partial least squares discriminant analysis*
PNPC	:	Parc national de Port-Cros
PRQN	:	*Porquerolles island (Northern coast)*
PRQS	:	*Porquerolles island (Southern coast)*
psbA	:	*photosystem II protein D1*
PSII	:	*Photosystem II*
Pyr-GC-MS	:	*Pyrolysis–gas chromatography–mass spectrometry*
q-PCR	:	*quantitative Polymerase chain reaction*
QS	:	*Quorum sensing*
QToF-MS	:	*Quadrupole-time of flight-mass spectrometry*
rbcL	:	*Ribulose-1,5-biphosphate carboxylase*
rCCA	:	*Regularized canonical-correlation analysis*
RMN - *NMR*	:	Résonance magnétique nucléaire - *Nuclear magnetic resonance*
ROS	:	*Reactive oxygen species*
RT	:	Retention time
SE	:	*Surface extracts*
SIMPER	:	*Similarity percentage*
SQDG	:	*Sulfoquinovosyldiacylglycerol*
SQMG	:	*Sulfoquinovosylmonoacyglycerols*
STCL	:	Saint-Clair
STMA	:	Sainte-Maxime
TAG - TG	:	*Triacylglycerol*
TAMR	:	Tamaris
TE	:	*Total extracts*
THEO	:	Théoule-sur-Mer
TN	:	*Total Nitrogen*
TRFLP	:	*Terminal restriction fragment length polymorphism*
UHPLC	:	*Ultra Performance Liquid Chromatography*
UPGMA	:	*Unweighted pair group method with arithmetic mean*
vHPO	:	*Vanadium haloperoxidases*
VILF	:	Villefranche-sur-Mer
VIP	:	*Variable importance in projection*

INTRODUCTION GENERALE

Vue sur le cap du Dramont

Dans un contexte de changement global, la biodiversité des écosystèmes marins côtiers se retrouve largement impactée sous l'effet notamment du réchauffement climatique, de l'acidification et de la pollution des mers et des océans (Bindoff et al., 2019; Collins et al., 2019). Les macroalgues sont des organismes particulièrement étudiés dans un tel contexte car non seulement elles s'avèrent sensibles à ces changements liés aux activités anthropogéniques (Wernberg et al., 2016; Bindoff et al., 2019), mais elles constituent aussi d'importantes ressources en termes d'habitat, de production primaire et de nutriments pour le reste de la biodiversité marine (Bruno et al., 2003; Schiel, 2006). Les macroalgues représentent en effet des espèces ingénieures de leurs écosystèmes (Jones et al., 1994) et elles sont par ailleurs connues pour interagir de manière étroite et complexe avec la composante biotique invisible de leur environnement que constituent les microorganismes (Egan et al., 2013; Hollants et al., 2013). La surface des macroalgues représente une niche microbienne à laquelle un certain nombre de microorganismes marins sont spécifiquement adaptés, que ce soient des bactéries, des microalgues, ou encore des fungi. Les interactions générées au niveau de cette zone d'échange constituent un élément majeur de l'histoire de vie des macroalgues, ce qui a conduit à étendre à leur propos le concept d'holobionte défini par l'association de l'hôte et de son microbiote en tant qu'unité fonctionnelle. La diversité des métabolites, spécialisés ou non, produits à la surface des macroalgues, ainsi que la présence de substancesés chimiques permettant de contrôler de manière plus ou moins sélective la diversité des épiphytes, conduisent à une augmentation des travaux menés en écologie chimique sur cette thématique de l'holobionte algal (Egan et al., 2013; Abdul Malik et al., 2019). De plus, l'importance et les effets des conditions environnementales sur ces interactions chimiques et leurs rôles dans la relation entre l'algue et son microbiote de surface restent encore largement inexplorés.

Cette thèse s'inscrit donc dans une vision intégrative suggérée par le concept d'holobionte, et se propose d'étudier les effets des paramètres environnementaux sur les relations entre la production chimique de surface et le microbiote épiphyte de l'algue brune *Taonia atomaria* (Dictyotaceae). *T. atomaria* est une espèce cosmopolite, très largement répandue en France, que ce soit sur les côtes atlantiques et méditerranéenne françaises. De précédents travaux menés au sein du laboratoire MAPIEM ont permis d'identifier des métabolites capables de réguler l'adhésion de certaines bactéries à la surface de cette macroalgue (Othmani et al., 2016a, 2016b) faisant de *T. atomaria* un modèle d'holobionte marin particulièrement adapté pour des études d'écologie chimique et d'écologie microbienne.

Dans le cadre de ces travaux, l'objectif était d'aborder de manière pluridisciplinaire l'analyse du microbiote et du métabolome de surface de l'algue. Pour conduire simultanément des démarches

d'écologie microbienne et chimique, le choix d'une approche de type multi-omiques a été effectué en couplant d'une part l'étude des communautés procaryotiques épiphytes (par séquençage de l'ADN codant l'ARN 16S) et d'autre part l'étude des métabolites de surface (principalement par LC-ESI-(+)-HRMS). L'intégration de ces deux jeux de données avec les données environnementales grâce à différentes approches statistiques multivariées s'est révélée être un outil innovant et exploratoire permettant de mettre en lumière des interactions entre variables environnementales, communautés bactériennes et métabolites de surface.

L'un des objectifs de cette thèse étant de considérer le rôle de l'environnement sur les interactions au sein de l'holobionte algal *T. atomaria*, cinq sites d'échantillonnage ont été choisis afin de pouvoir disposer de conditions environnementales contrastées. Ainsi, un partenariat avec le Parc National de Port-Cros (PNPC) a été établi pour cette thèse dans le cadre d'une bourse de doctorat financée par la région Sud. Ceci a permis d'intégrer des zones de collectes situées au sein du PNPC (deux sites au niveau de l'île de Porquerolles et un site à Carqueiranne) pour la mise en œuvre de plusieurs études *in situ*. La protection et la valorisation de la biodiversité étant l'un des objectifs principaux du PNPC, l'aire maritime située au cœur du parc (intégrant l'île de Porquerolles) est une zone particulièrement réglementée vis-à-vis des impacts anthropiques pouvant détériorer la qualité de l'eau. Cette aire protégée constitue une zone d'autant plus intéressante que les autres sites étudiés à proximité, dans les rades d'Hyères et de Toulon, sont soumis eux à de fortes pressions anthropiques. Cette dernière est notamment caractérisée par une importante contamination en éléments trace métalliques majoritairement liée aux activités historiques (activités militaires, sabordage de la flotte française durant la seconde guerre mondiale…) et économiques (utilisation de peintures antifouling comprenant des éléments organométalliques, …).

Trois projets de recherches ont partiellement contribué au financement de ces travaux de thèse. Il s'agit d'une part du projet « COHESIONS » (Couplage multi-Omiques à l'échelle de l'Holobionte : Effet de la diversité Spécifique des Phaeophyceae Taonia sur l'intéractION hôte-microbiome à la Surface), financé dans le cadre de l'appel à d'offre EC2CO 2019 et conduit en partenariat avec le laboratoire de Biologie Intégrative des Modèles Marins de la Station Biologique de Roscoff (C. Leblanc, P. Potin) et le laboratoire de Phycologie de Gand en Belgique (O. De Clerck, C. Vieira). Le second projet : « EMPREINTES » (Etude en Mésocosmes de Paramètres REgulant l'INTEraction entre la macroalgue *Taonia* atomaria et son microbiome de Surface) a été financé dans le cadre de l'appel à projet 2018 pour l'accès à EMBRC-France, et a été réalisé en partenariat avec le laboratoire de Biologie Intégrative des Modèles Marins de la Station Biologique de Roscoff (C. Leblanc, P. Potin). Le troisième projet (CMAPO) correspond à un projet financé

par le GdR Mediatec en 2017, en partenariat avec le Laboratoire d'Océanographie de Villefranche (E. Ternon) et l'Université de Galway (School of Chemistry and Ryan Institute, O. Thomas).

CHAPITRE I : ETAT DE L'ART

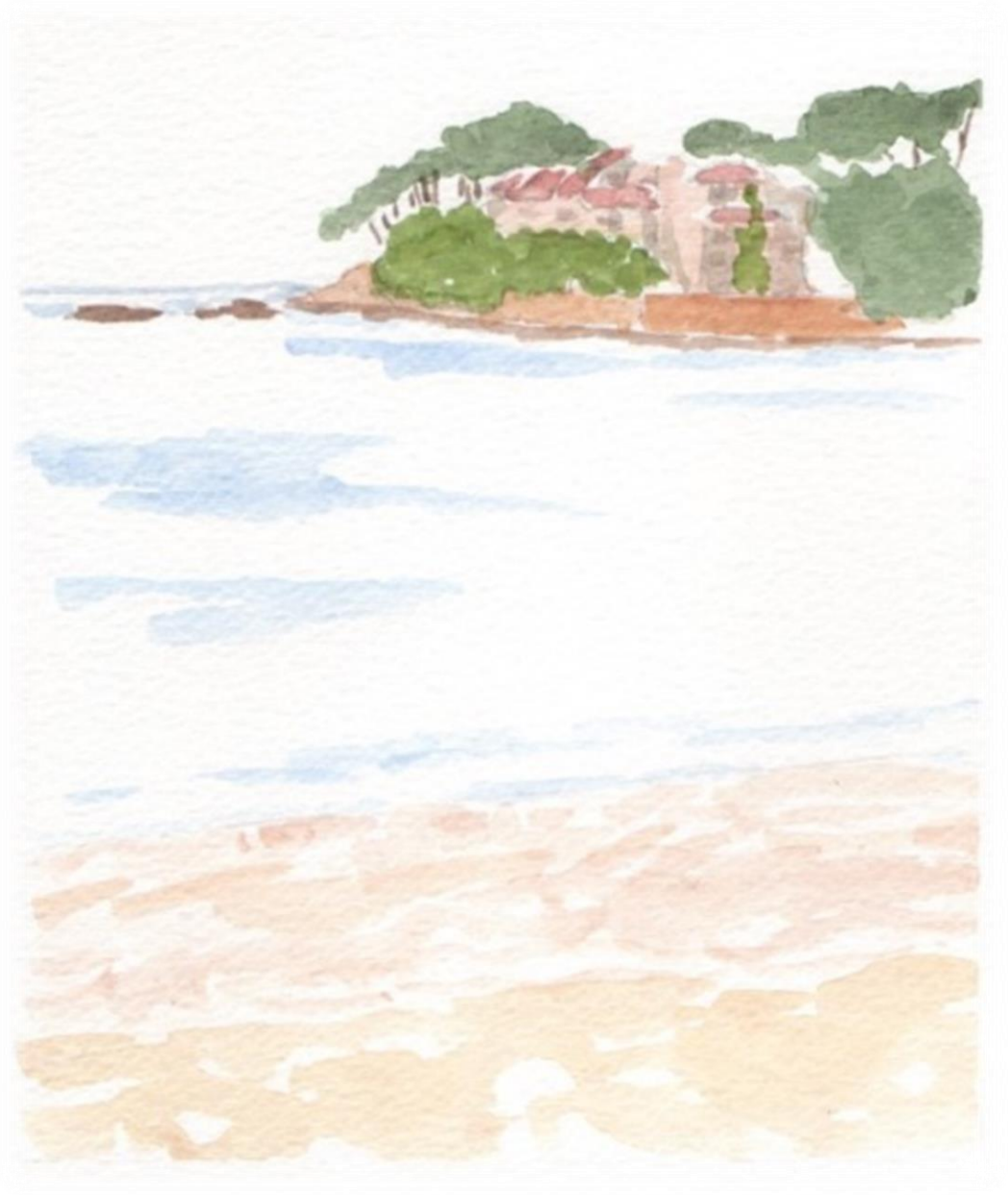

Plage de Renécros à Bandol.

1. L'holobionte, une unité fonctionnelle associant l'hôte et son microbiote

1.1. L'émergence du concept d'holobionte

Une très grande diversité de macroorganismes, tels que les animaux, les champignons, les plantes et les algues, sont reconnus pour vivre en association étroite avec les microorganismes (bactéries, archées et microeucaryotes) et les virus de leur environnement (Rosenberg and Zilber-Rosenberg, 2018). Ainsi, chacun de ces macroorganismes constitue une niche écologique pouvant héberger une communauté microbienne, également appelée microbiote, avec laquelle ils entretiennent des relations étroites et diverses. C'est au début des années 1990 que le terme « holobionte » est proposé pour définir une entité unique regroupant à la fois l'hôte et son microbiote associé (Margulis, 1990; Margulis and Fester, 1991; Theis et al., 2016). L'holobionte est un terme dérivé du grec provenant de « *holos* » et « *bios* » qui signifient respectivement « le tout » et « la vie ». Le concept d'holobionte s'intègre alors au sein d'une vision holistique de la biologie et de l'écologie, mettant en avant l'importance d'étudier les organismes et leur microbiote de manière conjointe afin de mieux comprendre la physiologie et l'évolution des organismes (Bordenstein and Theis, 2015). Bien que ce terme ait été proposé pour la première fois par Margulis, un tel concept émergeait déjà une quarantaine d'années plus tôt avec un lexique similaire (ex : « holobiosis ») ; concept initié par les travaux de Meyer-Abich, (1943) qui jusqu'à présent restaient peu cités (Baedke et al., 2020). Au début des années 2000, le concept d'holobionte a vu son intérêt grandir au sein de la communauté scientifique avec notamment les coraux comme modèles précurseurs (Rowan, 1998; Rohwer et al., 2002; Reshef et al., 2006). L'holobionte corallien est alors défini comme un ensemble constitué de l'animal corallien (Cnidaires de la classe des Anthozoaires), de ses microorganismes (bactéries, archées, fungi, et protistes) mais aussi de ses virus associés (Peixoto et al., 2017; van de Water et al., 2018). En établissant une symbiose [association étroite et durable de plusieurs espèces vivant ensemble] avec l'animal corallien, plusieurs espèces de dinoflagellés du genre *Symbiodinium* jouent un rôle particulièrement important au niveau de la physiologie de l'holobionte (Davy et al., 2012; Weber and Medina, 2012; van de Water et al., 2018). Les interactions symbiotiques entre le corail et ces microalgues sont notamment illustrées par un grand nombre de processus physiologiques dont :

(i) le transfert de produits de la photosynthèse de l'algue vers l'hôte,

(ii) l'amélioration de la calcification du corail grâce à la photosynthèse de l'algue permettant la précipitation du carbonate de calcium présent dans l'eau de mer,

(iii) la concentration par l'hôte de sources de carbone provenant de l'eau de mer, et ce à destination des symbiontes,

(iv) le recyclage par l'hôte des sources d'azote (sous forme d'acides aminés) utilisées par les symbiontes et nécessaires à la photosynthèse,

(v) la présence chez *Symbiodinium* de mécanismes permettant la réduction du stress oxydatif, à l'échelle de l'holobionte, lors de conditions de fortes intensités lumineuses,

(vi) l'existence de mécanismes de communication cellulaire permettant la reconnaissance et l'entrée de nouveaux symbiontes au sein de l'holobionte.

Bien que les interactions coraux-*Symbiodinium* aient été très largement étudiées avant même l'introduction de la notion d'holobionte, notamment à cause du phénomène de blanchissement des coraux (Muscatine and Porter, 1977; Brown, 1997), ce concept d'holobionte corallien a réellement émergé avec des études portant sur la communauté bactérienne associée (Bourne and Munn, 2005; Bourne et al., 2008, 2016; Hernandez-Agreda et al., 2018). Celles-ci ont ainsi révélé un grand nombre d'interactions entre les différents partenaires avec, par exemple, la mise en évidence de transferts horizontaux de gènes (Thompson et al., 2015; Peixoto et al., 2017). Il en va de même pour une grande diversité d'autres partenaires microbiens, tels que les fungi, les archées ou les virus, qui établissent des interactions étroites non seulement avec l'hôte mais également avec les autres symbiontes (**Figure I.1**, Peixoto et al., 2017).

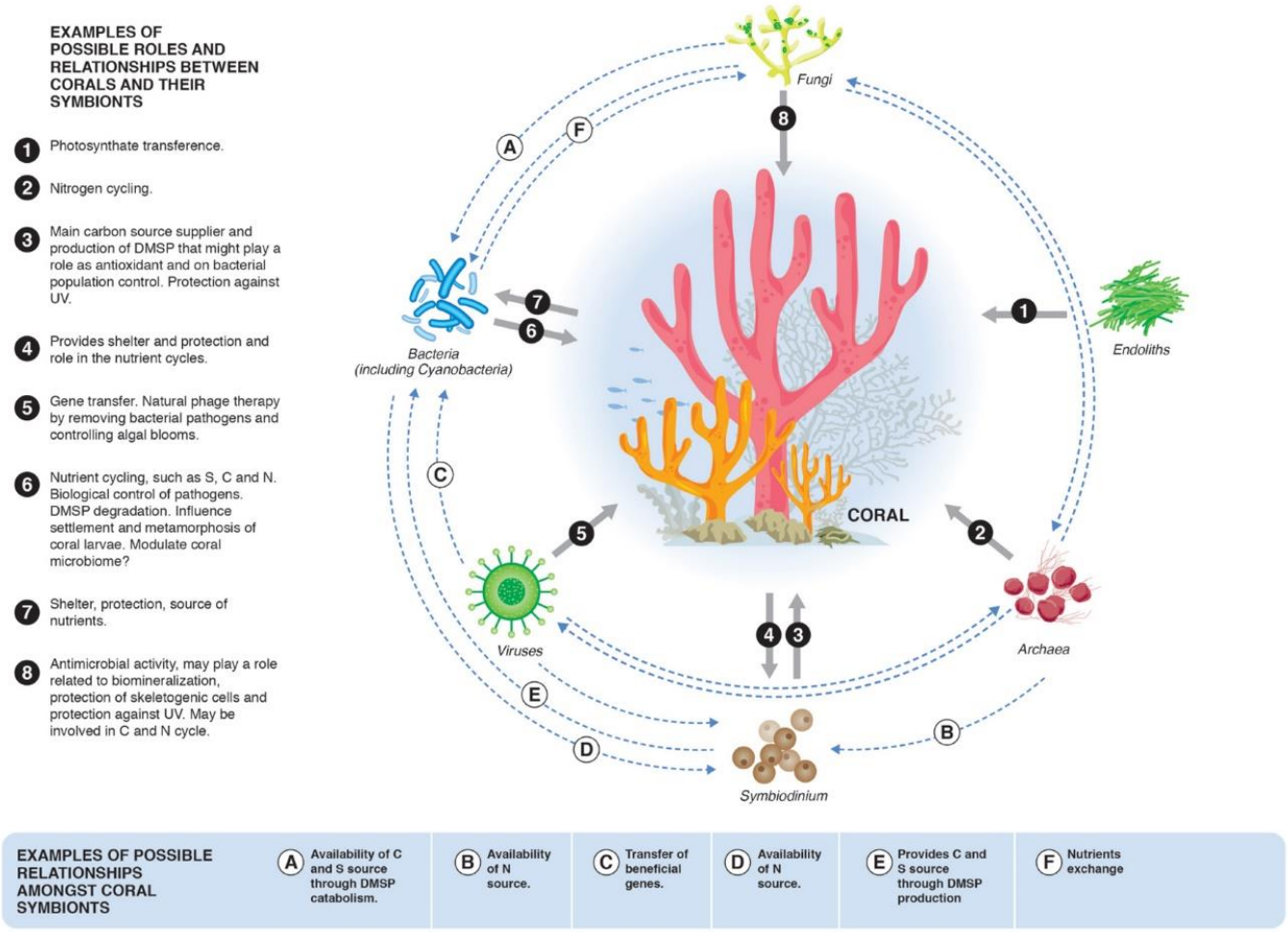

Figure I.1. Exemples d'interactions possibles entre les coraux et leurs symbiontes (Peixoto et al., 2017)

Ainsi, pour l'ensemble des modèles d'organismes pouvant être considérés comme des holobiontes, ce concept permet de prendre en compte une grande variété d'interactions entre l'hôte et ses microorganismes associés, avec par exemple des associations plus ou moins durables, pouvant impliquer des transferts verticaux ou horizontaux de microbiote et impliquant des effets bénéfiques, neutres ou néfastes pour les partenaires (Theis et al., 2016). L'holobionte constitue alors un concept ouvert, pouvant enrichir une grande diversité de situation, et qui s'adapte alors à différents niveau d'intégration entre le microbiote et son hôte (Catania et al., 2017). En définitive, le concept d'holobionte correspondrait à un degré plus ou moins important d'intégration de l'hôte et de son microbiote au sein d'une même unité fonctionnelle, génétique et spatiale (Bordenstein and Theis, 2015; Theis et al., 2016; Catania et al., 2017).

1.2.La théorie de l'hologénome

L'hologénome est défini comme l'ensemble des génomes de l'hôte et de son microbiote, donc de l'holobionte. Le terme hologénome a été proposé pour la première fois pour l'holobionte corallien, et a fait alors l'objet d'une théorie évolutive (Rosenberg et al., 2007). Alors que l'holobionte constitue une unité fonctionnelle du fait de l'association de l'hôte et de son microbiote, la théorie de l'hologénome soutient le fait que l'holobionte peut constituer une unité de sélection et souligne ainsi le rôle respectif de l'hôte et du microbiote au sein d'une coévolution globale (Zilber-Rosenberg and Rosenberg, 2008; Lloyd and Wade, 2019). Cette théorie se base sur des processus impliquant des liens entre les génomes du microbiote (microbiome) et les holobiontes. Ainsi, certains génomes issus du microbiote peuvent être transmis verticalement d'un hôte à la génération suivante. C'est par exemple le cas des bactéries du genre *Wolbachia* qui interagissent avec les systèmes reproducteurs des drosophiles (Moran et al., 2008). D'autre part, le microbiome s'adapte de manière plus rapide à la dynamique de l'environnement et peut alors permettre à l'hôte d'acquérir de manière plus rapide certains traits évolutifs face à différents stress environnementaux (Rosenberg and Zilber-Rosenberg, 2018). Ainsi, le génome du microbiote constituerait une composante sélectionnée au cours de l'histoire de vie de l'hôte qui se transmettrait d'une génération à une autre. Cette théorie vient donc ajouter un élément Lamarckien au sein d'une vision Darwinienne de la Théorie de l'Evolution puisque le microbiote constituerait alors un caractère à la fois héréditaire et acquis au sein de l'holobionte (Rosenberg et al., 2009).

Dans ce contexte, Theis et al., 2016 définissent trois catégories de symbiontes : (i) ceux dont les génomes sont impliqués directement dans des processus de coévolution avec l'hôte, et qui participent donc à l'établissement de son phénotype, (ii) ceux affectant le phénotype sans pour autant être impliqués dans des processus évolutifs en lien avec l'hôte, et enfin (iii) ceux dont le génome n'affecte pas le phénotype de l'hôte (**Figure I.2**)

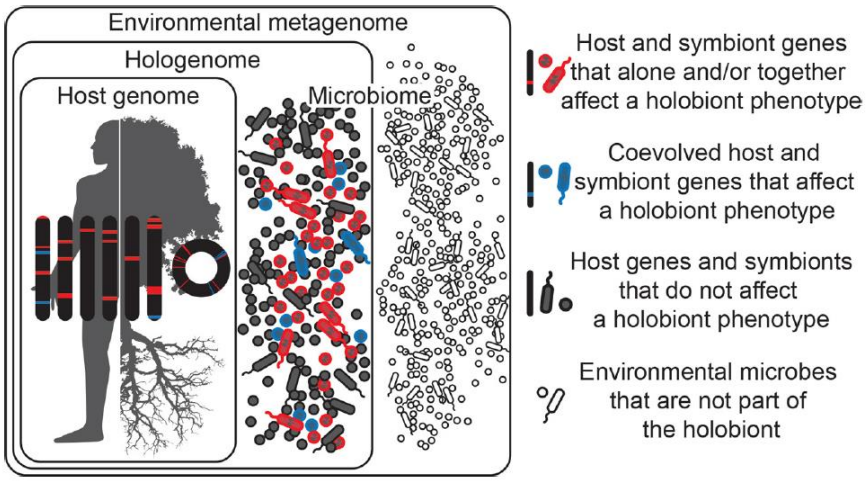

Figure I.2. Schéma conceptuel représentant les différents génomes et leurs implications au sein de l'holobionte (Theis et al., 2016)

Cependant, la part du microbiote impliquée dans l'évolution de l'holobionte en tant qu'unité de sélection est sujette à débat et la théorie de l'hologénome est souvent remise en question au sein de la communauté scientifique (Leggat et al., 2007; Moran and Sloan, 2015; Stencel and Wloch-Salamon, 2018). En effet, Stencel et Wloch-Salamon suggèrent par exemple que seule une faible part des symbiontes agit sur l'évolution globale de l'holobionte, tandis qu'une majeure partie du microbiote est constituée par des symbiontes co-acclimatés sans implication dans le processus évolutif de l'hôte. Les auteurs s'appuient notamment sur des modèles particuliers tels que certains pucerons (super-famille des Aphidoidea) connus pour leurs relations avec les bactéries endosymbiotiques du genre *Buchnera* (Baumann, 2005; Stencel and Wloch-Salamon, 2018). Dans le cadre de cette interaction symbiotique particulièrement étroite, les cellules du puceron hébergent ces bactéries spécifiques qui vont alors synthétiser des nutriments essentiels que le puceron ne peut pas trouver dans son alimentation. Des études ont notamment montré que ces symbiontes ont perdu un certain nombre de gènes au cours de leur coévolution avec le puceron et ne peuvent donc vivre qu'au sein des cellules de leur hôte (Gil et al., 2002; Baumann, 2005). Par ailleurs, ces *Buchnera* sont transmises d'une génération à une autre via le développement chez l'hôte de propagules spécialisés. L'association de ce genre bactérien avec le puceron peut donc être considérer comme une unité de sélection évolutive intégrant la théorie de l'hologénome. Ainsi Stencel et Whloch-Salamon suggèrent qu'une unité de sélection, telle que définie par la théorie de l'hologénome, n'est pas constituée nécessairement de l'ensemble du microbiote mais concerne uniquement certaines associations très spécifiques. L'holobionte constituerait alors une association caractérisée avant tout comme une unité de coopération et également, dans certains cas particuliers et de manière plus restrictive, comme une unité de sélection.

1.3.Les holobiontes marins impliquant des microorganismes épiphytes

Avec en moyenne 10^6 cellules par millilitre d'eau de mer, les bactéries représentent les organismes les plus abondants au sein des océans. En incluant également la présence d'autres microorganismes (tels que les archées et les microeucaryotes) ainsi que celle de virus, on peut alors considérer que les holobiontes marins vivent et évoluent dans un « océan de microbes » (Pita et al., 2018). Ces microorganismes jouent des rôles cruciaux au sein des écosystèmes marins que ce soit au niveau des cycles biogéochimiques mais également du fait de leurs interactions avec les macroorganismes. La richesse et l'abondance des microorganismes avec lesquels ils vivent, ainsi que les propriétés physico-chimiques du milieu aquatique, expliquent notamment les différences qui existent entre les holobiontes terrestres et aquatiques (Dittami et al., 2020). En effet, l'eau étant un vecteur induisant la diffusion d'une large gamme de molécules et de microorganismes, les milieux aquatiques favorisent les interactions chimiques entre micro- et macroorganismes et conduisent à une « connectivité chimique » plus importante (Dittami et al., 2020). Par ailleurs, le milieu marin est caractérisé par des changements rapides de conditions environnementales, que ce soit en termes de température, d'intensité lumineuse, ou de flux de carbone et de nutriments. Une adaptation rapide au sein de l'holobionte est alors possible grâce à l'importante plasticité des interactions microbiennes (Kinlan and Gaines, 2003; Martin-Platero et al., 2018) qui favorisent ainsi la résistance et la résilience de l'holobionte face à de telles perturbations. Cette plasticité est notamment favorisée par la présence d'une vaste diversité phylogénétique et fonctionnelle au sein du microbiome marin, diversité qui reste par ailleurs encore très largement inexplorée (Vargas et al., 2015; Thompson et al., 2017; Galand et al., 2018).

En outre, les milieux aquatiques se caractérisent également par la capacité des microorganismes à rapidement coloniser l'ensemble des surfaces immergées, résultant en la formation de biofilms. Défini comme étant un agrégat de microorganismes adhérés à une surface, le biofilm est notamment caractérisé par une structure tridimensionnelle intégrant les cellules au sein d'une matrice polymérique extracellulaire autoproduite (Costerton et al., 1987; Donlan, 2002). Les biofilms se développant sur toutes les surfaces immergées en milieu aquatique, ce mode de vie microbien spécifique est alors omniprésent au niveau des interfaces entre le milieu et les macroorganismes marins (Wahl et al., 2012; Flemming and Wuertz, 2019) (**Figure I.3**). La communauté microbienne des biofilms de l'holobionte joue un rôle crucial dans l'écologie de leur hôte (Harder, 2009; Wahl et al., 2012), et ce notamment chez les organismes sessiles (Wahl, 2009) tels que les éponges, les macrophytes et les coraux. Les densités des biofilms formés à la surface des macroorganismes sont variables en fonction des espèces avec, par exemple, des ordres de grandeurs :

- de 10^3 à 10^4 cellules par cm^2 pour le corail *Dendronephthya* sp. (Harder et al., 2003), les éponges *Haliclona cymaeformis* et *Callyspongia* sp. (Dobretsov et al., 2005), et certaines algues telles que *Caulerpa racemosa* (Dobretsov et al., 2006),

- allant jusqu'à 10^8 cellules par cm^2 pour d'autres macroalgues telles que *F. vesiculosus* (Wahl et al., 2010).

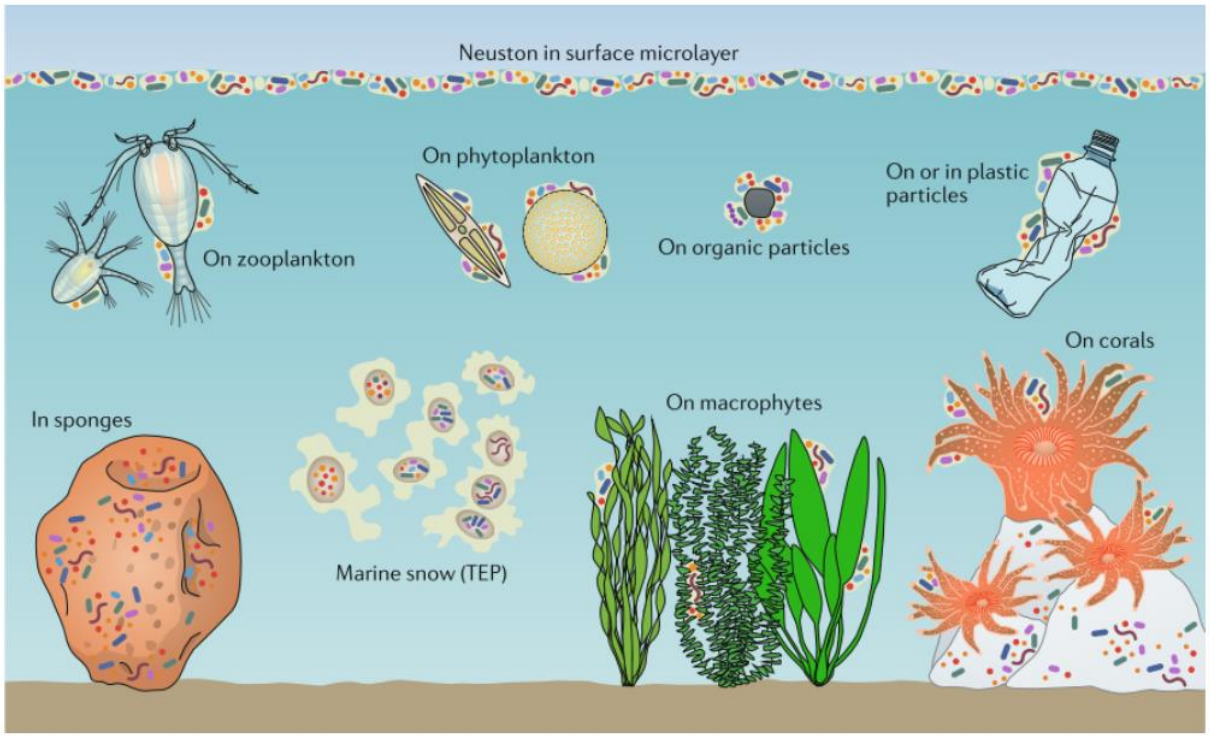

Figure I.3. Schéma représentant les différentes interfaces propices au développement de biofilms en milieu marin (Flemming and Wuertz, 2019)

La formation et l'évolution des biofilms s'effectuent généralement en cinq étapes comprenant : (i) le conditionnement biochimique de la surface, (ii) l'adhésion initiale de bactéries, (iii) la formation de microcolonies induisant l'irréversibilité de l'adhésion, (iv) la croissance du biofilm et sa maturation et enfin (v) la formation d'un biofilm secondaire avec la dispersion de certaines cellules (Stoodley et al., 2002; Monroe, 2007) (**Figure I.4**).

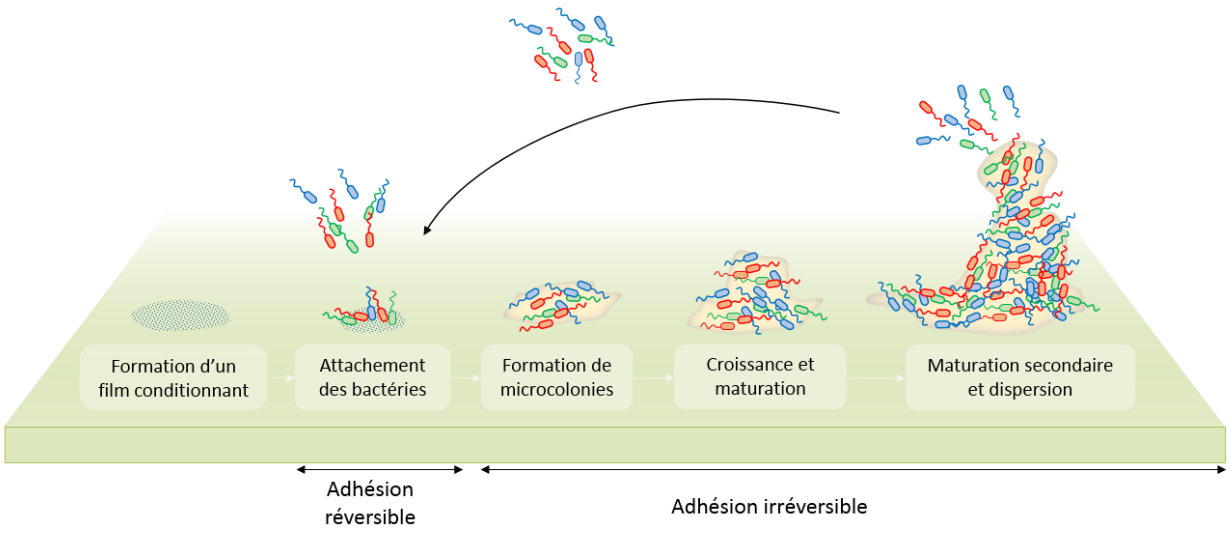

Figure I.4. Les différentes étapes du cycle de vie d'un biofilm (Figure modifiée d'après Stoodley et al., 2002 et Monroe, 2007)

Le conditionnement biochimique des surfaces constitue la première étape de la formation des biofilms. Cette étape initiale est caractérisée par l'adsorption de composés tels que des lipides, des polysaccharides, des protéines ou d'autres molécules organiques dissoutes constituant une source de nutriments pour les microorganismes (Loeb and Neihof, 1975; Wahl, 1989; Compère et al., 2001). Ce film biochimique va constituer une niche favorable à l'adhésion réversible de certains microorganismes. Cette deuxième étape fait notamment intervenir divers types de de mécanismes de reconnaissance physicochimique chez les bactéries impliquant les flagelles ou les pili de type I et IV (O'Toole and Kolter, 1998; Heydorn et al., 2002). Dans ce contexte, les propriétés physiques de la surface (rugosité, hydrophobicité…) jouent un rôle très important dans l'efficacité de l'adhésion bactérienne (Donlan, 2002; Dunne, 2002). La troisième étape implique l'irréversibilité de l'adhésion via l'établissement d'interactions fortes entre les bactéries et la surface. Au niveau des cellules bactériennes, cette étape met en jeu des appendices cellulaires tels que les fimbriae, les pili de type IV ou les flagelles (Dunne, 2002; Palmer et al., 2007). Les bactéries vont ensuite former des microcolonies et secréter une matrice exopolymérique constituée d'EPS (« *Extracellular Polymeric Substances* »), principalement des protéines et des polysaccharides. Cette matrice tridimensionnelle permet d'agréger les cellules entre-elles et de consolider la fixation (Flemming et al., 2016). En agissant tel un filtre capable de ralentir la diffusion de certaines molécules (fixation de nutriments, biosorption de biocides…), la matrice d'EPS confère aux microorganismes une meilleure protection vis-à-vis de certains stress environnementaux (Teitzel and Parsek, 2003; Harrison et al., 2005, 2006). L'étape suivante consiste en la croissance du biofilm qui s'effectue généralement via des processus de communications chimiques permettant une synchronisation des comportements cellulaires. Le

« *Quorum Sensing* » (QS) constitue l'un de ces modes d'interactions chimiques particulièrement étudiés chez les bactéries (Waters and Bassler, 2005; Lami, 2019). La libération de molécules de signalisation telles que les homosérine lactones (HSL) dépend notamment de la densité bactérienne et leur détection permet, une fois un seuil de densité cellulaire atteint, l'expression de gènes impliqués dans des fonctions telles que la maturation du biofilm, la motilité cellulaire, la bioluminescence ou encore l'expression de facteurs de virulence (Lami, 2019). Suite à la croissance du biofilm, sa maturation peut se poursuivre avec la colonisation par de nouveaux taxa microbiens, notamment eucaryotes, et l'acquisition de diverses conformations tridimensionnelles complexes (**Figure I.4**). Enfin, le détachement constitue l'étape finale de ce cycle et peut s'effectuer soit de manière passive, via l'érosion du biofilm généré par les forces physiques des mouvements d'eau, soit de manière active, avec notamment certains stress environnementaux pouvant induire le décrochage des cellules (Picioreanu et al., 2001). L'absence de nutriments ou d'oxygène, mais aussi les défenses chimiques de l'hôte dans le cadre de surfaces biotiques, constituent les principales conditions défavorables induisant un tel phénomène (O'Toole et al., 2000; Donlan, 2002; Wahl et al., 2012).

Wahl et al. (2012) présentent le biofilm à la surface des holobiontes marins tel une « seconde peau » pouvant moduler les interactions de l'hôte avec le reste de son environnement. Ainsi, le biofilm impacte de manière prépondérante l'accessibilité à certaines ressources telles que la lumière, le CO_2 ou encore les nutriments. Par exemple, une réduction de 50% de la luminosité naturelle, induite par un biofilm de quelques semaines, a été observée à la surface de l'algue *Fucus vesiculosus* (Wahl et al., 2010). En revanche, un biofilm d'une épaisseur suffisante pourrait aussi permettre de protéger l'hôte contre les radiations UV (Wahl, 2008). D'autre part, de nombreuses études ont montré que le microbiote de surface participait de manière active à la production de composés bioactifs permettant de défendre l'holobionte algal contre des pathogènes et des prédateurs (Flórez et al., 2015; Pita et al., 2018). Par exemple, certains symbiontes d'éponges sont connus pour leur production de polycétides caractérisés par de fortes activités cytotoxiques (Della Sala et al., 2014; Lackner et al., 2017). C'est notamment le cas des bactéries du genre *Candidatus* Entotheonella qui produisent une vaste diversité de polycétides dont la production était initialement attribuée à leur hôte, l'éponge *Theonella swinhoei* (Lackner et al., 2017). Parmi les nombreux exemples présents chez les éponges, on peut aussi citer le cas d'*Halichondria okadai* à partir de laquelle une bactérie du genre *Alteromonas* a été isolée et étudiée pour sa production en ubiquinones présentant un activité anti-adhésion vis-à-vis des larves de balanes de l'espèce *Amphibalanus amphitrite* (Kon-ya et al., 1995). De telles activités de défense chimique du microbiome de surface contre le recrutement de

larves d'invertébrés marins ont également été décrites pour des coraux (Dobretsov and Qian, 2004), des ascidies (Olguin-Uribe et al., 1997) ainsi que des macroalgues (Harder et al., 2004; Nasrolahi et al., 2012).

Depuis le début des années 2010, les macroalgues sont présentées comme des modèles particulièrement pertinents pour l'étude du concept d'holobionte (Barott et al., 2011; Egan et al., 2013) et elles constituent depuis les modèles d'holobiontes marins les plus étudiés pour leurs interactions avec leur microbiote de surface (Egan et al., 2013; Hollants et al., 2013). Une des raisons principales pourrait être que les macroalgues produisent à leur surface des métabolites jouant un rôle dans l'épibiose (le contrôle de la communauté épiphyte), que ce soit à l'échelle du micro ou du macrofouling (Harder, 2009; da Gama et al., 2014). Par ailleurs, l'abondance de matière première et la facilité de récolte des macroalgues constituent aussi des atouts méthodologiques en leur faveur.

1.4.Le cas des macroalgues

Les macroalgues sont des organismes eucaryotes multicellulaires photosynthétiques caractérisés par une absence de tissus spécialisés (Graham and Wilcox, 2000). Il s'agit d'un groupe paraphylétique majoritairement observés au sein de trois groupes distincts : les Chlorophyta, les Phaeophyceae et les Rhodophyta appelées communément respectivement algues vertes, brunes et rouges. Les approches phylogénétiques font continuellement évoluer ces classifications qui sont complexes, notamment parce que les capacités photosynthétiques des différents groupes d'algues sont liées à différentes endosymbioses (Boudouresque et al., 2011).

Les macroalgues constituent d'importantes ressources pour la biodiversité des environnement benthiques (Bruno et al., 2003; Schiel, 2006) et elles sont reconnues en tant qu'espèces « ingénieures » de leurs écosystèmes (Jones et al., 1994; Schiel, 2006). En effet, les macroalgues font partie des principaux producteurs primaires des écosystèmes côtiers et elles constituent ainsi des habitats pour une grande diversité d'organismes (Bertness et al., 1999; Mann, 2000; Schiel and Foster, 2006). Elles offrent notamment des refuges, permettant par exemple à des juvéniles de crabes et de poissons d'échapper à la prédation, et agissent alors en tant que « pouponnières » naturelles (Wilson et al., 1989, 2010; Shoji et al., 2009; Evans et al., 2014).

Les macroalgues peuvent être présentes en abondance dans certains écosystèmes, formant par exemple des forêts de kelps de *Macrocystis pyrifera* largement distribuées au niveau des côtes de l'océan Pacifique. D'autres espèces peuvent proliférer dans certaines conditions générant une forte eutrophisation du milieu ; c'est le cas notamment d'algues du genre *Ulva* pour lesquelles l'eutrophisation

est liée au lessivage des sols enrichis en engrais. Cependant, certains assemblages sont sensibles à des stress environnementaux pouvant générer un fort déclin de leur biodiversité, c'est notamment le cas des kelps du genre *Durvillaea* pour lesquelles une extinction locale a été observée après une vague de chaleur marine (voir partie 3.1) (Thomsen et al., 2019). En plus de l'augmentation de la température, la dégradation de la qualité de l'eau et la sédimentation peuvent être citées parmi les principaux facteurs de stress pour les algues (Tait and Schiel, 2011). Ainsi les cystoseires en Méditerranée peuvent constituer des modèles particulièrement pertinents pour l'évaluation de l'état des écosystèmes côtiers, et ce notamment en termes de qualité de l'eau (Blanfuné et al., 2016; Boudouresque et al., 2020).

En tant qu'holobionte, le bon état physiologique des macroalgues dépend aussi en grande partie de leur microbiote associé (Egan et al., 2014; Egan and Gardiner, 2016). A l'échelle du microbiote endophyte, il est proposé que la communauté bactérienne joue un rôle crucial en présentant par exemple des fonctions bénéfiques pour l'holobionte permettant la détoxification et/ou la fixation de l'azote au sein d'algues vertes présentant des siphons (ensemble de cellules ayant mis en communs leur cytoplasme après la perte du cloisonnement cellulaire) (Hollants et al., 2013). Une telle hypothèse a été notamment proposée chez les modèles *Bryospis* spp. de la côte Pacifique du Mexique (Hollants et al., 2011a, 2011b), ou *Caulerpa* spp., en Méditerranée (*C. racemosa*, *C. taxifolia*, *C. prolifera*) (Aires et al., 2013, 2015). Par ailleurs, les champignons constituent aussi des partenaires endophytes importants d'un point de vue fonctionnel au sein des macroalgues holobiontes, telles que *Ascophyllum nodosum*, *Pelvetia canaliculata*, *Laminaria digitata* et *Saccharina latissima*. En effet, la production métabolique de champignons isolés chez ces modèles serait impliquée dans la régulation de l'expression des auto-inducteurs de type 2 (AI-2) du QS chez les bactéries endophytes (Tourneroche et al., 2019).

Au niveau de la surface des macroalgues, l'abondance du microbiote épiphyte est souvent décrit avec des densités très variables en fonction des espèces, pouvant aller de 10^2 à 10^8 cellules par cm^{-2} (Wahl et al., 2012). De fortes fluctuations de densités bactériennes avec des extrêmes allant de 10^2 à 10^7 sont également observées au sein d'une même espèce, avec par exemple le cas de *Laminaria hyperborea* (Bengtsson et al., 2010). Un grand nombre d'analyses par microscopie à épifluorescence ou électronique ont conduit à observer des biofilms complexes à la surface des macroalgues. Ainsi, une étude portant sur la chlorophycée *Cladophora glomerata* a permis d'observer un biofilm présentant des structures tridimensionnelles en forme de « champignon » caractéristiques de biofilms matures (Zulkifly et al., 2012 ; **Figure I.5**).

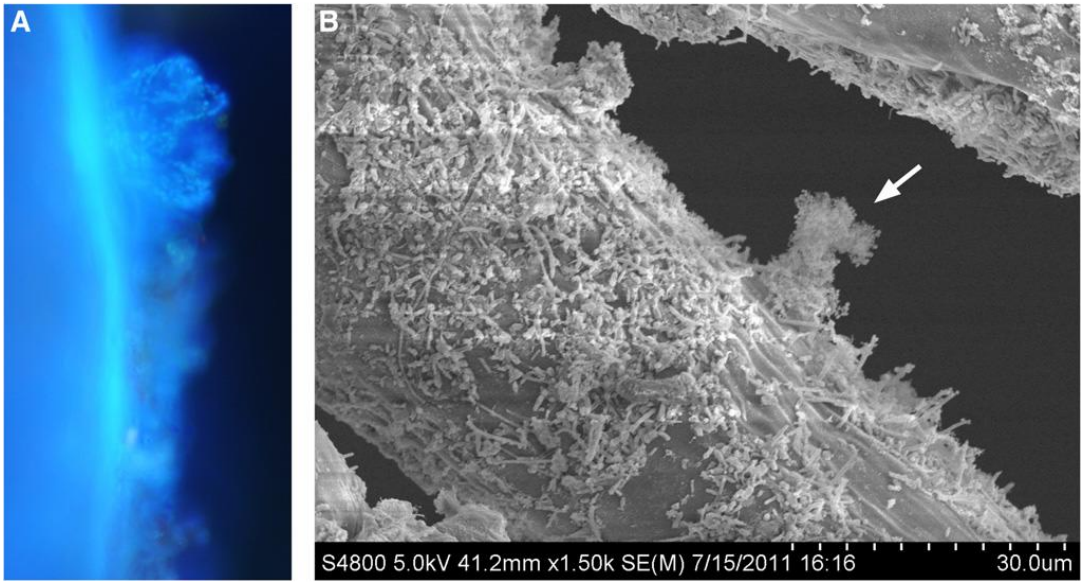

Figure I.5. Observations par microscopie à épifluorescence (A) et microscopie électronique à balayage (B) du biofilm à la surface de l'algue *Cladophora glomerata* (Zulkifly et al., 2012).

Les macroalgues sont très souvent caractérisées par une importante diversité de microorganismes à leur surface (Hollants et al., 2013) avec notamment la présence de bactéries, de protistes, de fungi, ainsi que de microalgues, telles que des diatomées et des dinoflagellés benthiques (Egan et al., 2013 ; **Figure I.6**). Parmi ces microorganismes, les bactéries constituent le groupe le plus abondant avec généralement des familles dominantes appartenant aux : (i) *α*-Proteobacteria, telles que les Hyphomonadaceae, les Rhodobacteraceae et les Sphingomonadaceae, (ii) *γ*-Proteobacteria, telles que les Alteromonadaceae et les Granulosicoccaceae, mais également (iii) Bacteroidetes, telles que les Flavobacteriaceae, les Saprospiraceae et les Cytophagaceae (Hollants et al., 2013; Lemay et al., 2018a, 2018b; Weigel and Pfister, 2019). Certaines de ces familles sont très diversifiées, avec par exemple les Rhodobacteraceae dont les taxa *Octadacabacter*, *Sulfitobacter*, *Roseobacter* et *Loktanella* sont particulièrement dominants, ou encore les Flavobacteriaceae avec les genres *Algitalea* et *Aquimarina* (Stratil et al., 2013; Kumar et al., 2016; Dogs et al., 2017). D'autres groupes taxonomiques s'avèrent spécifiquement dominants chez certains modèles, c'est le cas par exemple des Planctomycetes chez l'algue *Laminaria hyperborea* (Bengtsson and Øvreås, 2010).

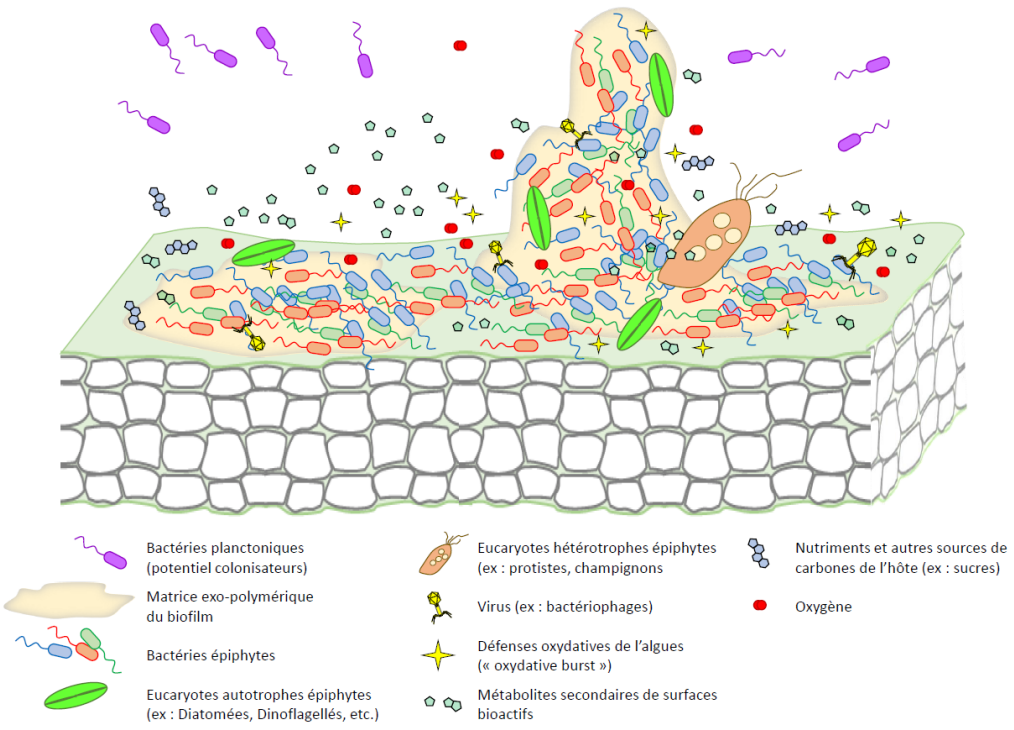

Figure I.6. Surface d'une macroalgue caractérisée par la présence de microorganismes et de molécules impliquées dans les interactions algue-microbiote (d'après Egan et al., 2013)

Pour certains modèles de macroalgues, la structure de la communauté des procaryotes épiphytes a fait l'objet de comparaisons avec celles de surfaces inertes et/ou des communautés planctoniques environnantes (Stratil et al., 2014; Mancuso et al., 2016; Chen and Parfrey, 2018; Lemay et al., 2018b, 2018a; Lin et al., 2018). Plus précisément, dans le cadre d'une étude portant sur huit kelps (**Figure I.7**) du nord-est de l'océan Pacifique (Colombie-Britannique, Canada) de fortes différences de diversité ont été observées entre des prélèvements réalisés sur les algues et ceux issus d'échantillons d'eau de mer et de biofilms à la surface de rochers prélevés à proximité (Lemay et al., 2018b) (**Figure I.7**). Au sein du même environnement, d'autres études (Chen and Parfrey, 2018; Lin et al., 2018) confirment aussi les différences avec la communauté planctonique pour les kelps *Nereocystis luktaneae* et *Mastocarpus pyrifera*. En mer Baltique, des différences de composition du microbiote épiphyte des macroalgues *Fucus vesiculosus* sont aussi observées par comparaison aux communautés épilithiques de substrats rocheux (Stratil et al., 2014). Enfin, des différences avec la communauté planctonique environnante ont aussi été observées pour *Cystoseira compressa* en mer Adriatique (Mancuso et al., 2016). Cependant, dans le cadre de cet axe de recherche portant sur la spécificité du microbiote épiphyte des macroalgues par rapport aux communautés épilithiques et planctoniques, l'ensemble de ces études ne permettent pas de généraliser qu'une telle spécificité est semblable pour l'ensemble des macroalgues au sein d'environnements plus

variés. Par ailleurs, la variabilité temporelle des communautés épiphytes de macroalgues par rapport à celle des communautés planctoniques et issues de substrats inertes est encore très largement inexplorée et la question de l'effet de l'environnement sur l'évolution d'une telle spécificité reste encore à élucider.

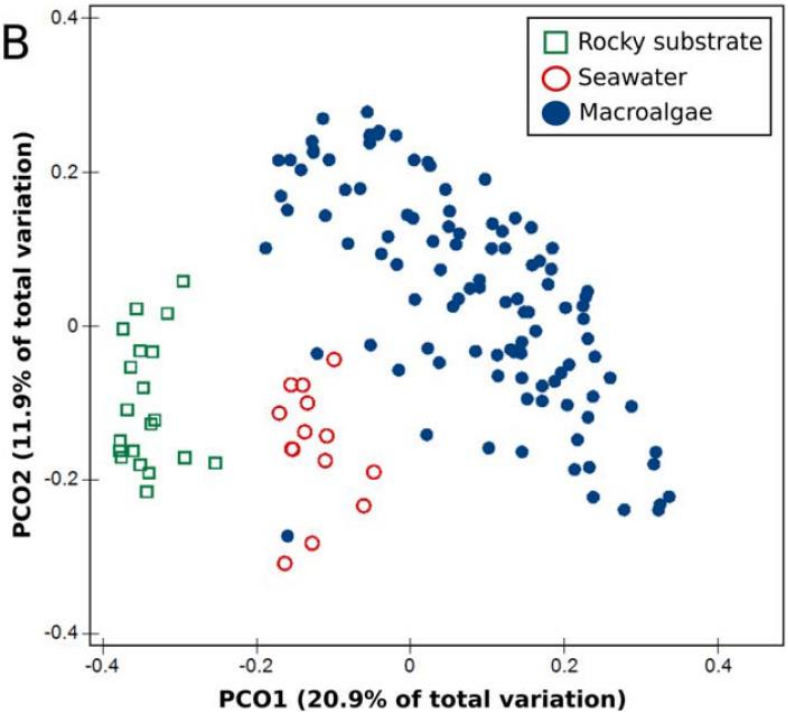

Figure I.7. Analyse multivariée (PCoA) montrant la spécificité de la *β*-diversité du microbiote épiphyte de huit kelps par rapport aux communautés bactériennes planctoniques et épilithiques de surfaces rocheuses (Lemay et al., 2018b). Les huit kelps étudiés sont : *Costaria costata*, *Alaria marginata*, *Pterygophora californica*, *Cymathaere triplicate*, *Laminaria setchellii*, *Nereocystis luetkeana*, *Saccharina groenlandica*, et *S. latissimi*

En mer Baltique, la spécificité du microbiote de surface a aussi été observée en fonction des espèces de macroalgues avec une discrimination en lien avec la phylogénie des hôtes qui a été observée pour les modèles *Fucus serratus*, *F. vesiculosus*, *Saccharina latissima*, *Ulva compressa*, *Delesseria sanguinea* et *Phycodrys rubens* (Lachnit et al., 2009). Cependant, la structure de la communauté peut être en même temps dépendante de différences associées à l'histoire de vie de l'hôte ou de paramètres environnementaux (voir les parties **2** et **3**) (Lachnit et al., 2011; Bondoso et al., 2017; Lemay et al., 2018b, 2018a; Morrissey et al., 2019).

Bien que peu étudiées, les propriétés physiques des macroalgues pourraient constituer des facteurs non négligeables afin d'expliquer la spécificité de leur microbiote. La morphologie globale du thalle fait notamment partie des hypothèses émises par Lemay et al. (2018) et ce facteur pourrait être lié aux différences de communautés observées entre les sporophytes et les gamétophytes des algues

Mastocarpus spp. du nord-ouest du Pacifique. Les conditions hydrodynamiques à micro-échelle pourraient ainsi différer en fonction de la morphologie et de la rigidité du thalle, influençant alors le cycle de vie du biofilm, notamment lors du processus d'adhésion. Des différences d'hydrophobicité de la surface, plutôt étudiées chez les plantes aquatiques (Yang et al., 2013a), pourraient également constituer un paramètre à étudier au niveau des macroalgues, puisque l'hydrophobicité est reconnue pour influencer l'efficacité de l'adhésion bactérienne lors des premiers stades de colonisation des surfaces inertes (Donlan, 2002; Dunne, 2002).

De nombreux composés chimiques observés à la surface des macroalgues sont décrits pour leurs effets sur les communautés épiphytes (Harder, 2009; da Gama et al., 2014). En premier lieu, la surface des macroalgues constitue un environnement riche en polysaccharides favorisant la colonisation et le développement de nombreux taxa bactériens spécialisés dans l'utilisation de ces sources spécifiques de carbone (Egan et al., 2013; Gobet et al., 2018). D'autre part, les macroalgues peuvent agir de manière active sur l'adhésion et le développement de certains microorganismes à leurs surfaces via divers modes d'actions par voie chimique tels que l'induction de stress oxydatifs, l'inhibition de l'adhésion ou encore l'inhibition du QS (Egan et al., 2013). L'exsudation de métabolites spécifiques à la surface de l'algue constitue alors un moyen de défense contre certains épiphytes ciblés, permettant ainsi de contrôler finement la colonisation de surface. De tels composés s'avèrent particulièrement importants afin de limiter le développement de bactéries pathogènes mais aussi pour éviter une trop forte pression de la part d'autres colonisateurs pouvant par exemple réduire l'activité photosynthétique de l'algue ou augmenter sa résistance hydrodynamique (Williams and Seed, 1992; Wahl et al., 2010). Les macroalgues peuvent aussi établir des interactions mutualistes avec certains symbiontes via l'expression de composés allélochimiques (Wichard and Beemelmanns, 2018; Ghaderiardakani et al., 2019), permettant par exemple le recrutement de taxa bénéfiques pour l'hôte (Kessler et al., 2018).

Certaines bactéries pouvant constituer des acteurs cruciaux de l'immunité de surface de l'algue, leur recrutement et leur maintien au sein du consortium épibactérien s'avèrent alors particulièrement important pour l'hôte. Le concept de « *microbial gardening* » a ainsi été développé chez les macroalgues (Saha and Weinberger, 2019) en montrant à l'aide de test d'activité que les métabolites de surface de l'algue *Agarophyton vermiculophyllum* permettaient (i) de réduire la colonisation de bactéries potentiellement pathogènes et (ii) d'attirer des souches bactériennes dites « protèctrices » empêchant le blanchissement de l'algue lié au développement de ces pathogènes.

Plusieurs exemples d'interactions entre des macroalgues et leurs bactéries épiphytes sont particulièrement développés dans la littérature. Certains modèles d'étude historiques tels que *Delisea pulchra*, *Ulva mutabilis*, *Fucus vesiculosus*, *Gracilaria conferta* et *Laminaria digitata* illustrent ainsi l'importance, la complexité et la diversité des échanges pouvant exister au sein de ces systèmes holobiontes. Ces exemples vont être présentés plus en détail dans la partie suivante.

2. Exemples de médiation chimique chez les macroalgues et leurs bactéries épiphytes

2.1. Le modèle *Delisea pulchra*

Delisea pulchra constitue historiquement le premier modèle d'algue pour lequel un intérêt particulier a été porté sur ses métabolites de défenses, et ce notamment en lien avec le phénomène de blanchissement et le développement de bactéries pathogènes opportunistes à sa surface. Cette rhodophycée (Classe : Florideophyceae, Famille : Bonnemaisoniaceae) est observée en milieu tempéré et subtropical, principalement le long des côtes sud et ouest de l'Australie (Womersley et al., 1996). Les premières études la concernant ont initialement porté sur la caractérisation d'une famille de métabolites bioactifs, les furanones halogénées (Pettus et al., 1977; de Nys et al., 1993, 1995). Ces molécules sont des analogues structuraux des homosérines lactones (HSLs) (**Figure I.8**), ces dernières constituant des acteurs majeurs impliqués dans les mécanismes du QS (Manefield et al., 1999; Harder et al., 2012).

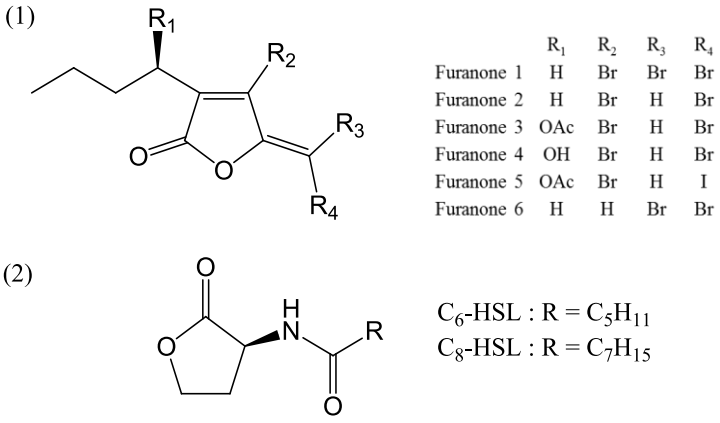

	R_1	R_2	R_3	R_4
Furanone 1	H	Br	Br	Br
Furanone 2	H	Br	H	Br
Furanone 3	OAc	Br	H	Br
Furanone 4	OH	Br	H	Br
Furanone 5	OAc	Br	H	I
Furanone 6	H	H	Br	Br

Figure I.8. (1) Exemples de furanones halogénées isolées de Delisea pulchra (d'après Manefield et al., 1999) agissant en tant qu'antagonistes d'HSLs. (2) Exemples d'HSLs impliquées dans les mécanismes du QS.

Ainsi, il a été démontré que les furanones halogénées bloquaient le mécanisme de QS en interférant spécifiquement dans la transcription des gènes médiée par les HSLs, et ce notamment au niveau de la protéine LuxR, un récepteur activé spécifiquement par les HSLs (Manefield et al., 1999, 2002). De manière générale, les tests d'activités et les observations *in situ* ont montré que l'activité des furanones halogénées était liée à une inhibition de l'attachement des bactéries (Maximilien et al., 1998). Par ailleurs, l'activité des furanones envers l'attachement de bactéries isolées à la surface de rochers s'est avérée plus importante que celle vis-à-vis de souches isolées à la surface de *D. pulchra*. De plus, des expériences de microscopie par épifluorescence et des analyses quantitatives ont permis de localiser ces métabolites spécialisés de l'algue au niveau des vésicules centrales des cellules glandulaires. Des concentrations

croissantes ont notamment été rapportées allant de la base vers les zones apicales de l'algue avec des valeurs moyennes de 100 ng.cm^{-2} pouvant atteindre localement jusqu'à 500 ng.cm^{-2} (Dworjanyn et al., 1999).

Un suivi *in situ* des populations de *D. pulchra* au cours de trois années successives au niveau des côtes est de l'Australie a permis d'observer un phénomène de blanchissement des thalles lors de la période estivale (**Figure I.9**). Ce phénomène se traduisant par des décolorations locales de la pigmentation rouge liées à la nécrose de cellules corticales des frondes de l'algue, est fortement corrélé à l'augmentation de la température de l'eau de mer (Campbell et al., 2011; Case et al., 2011). A l'échelle de l'hôte, le blanchissement se traduit par une diminution drastique de la valeur sélective (« *fitness* ») avec notamment une diminution de la croissance et de la fécondité de l'algue ainsi qu'un risque accru de prédation par les herbivores (Wright et al., 2000).

Figure I.9. L'algue *Delisea pulchra* récoltée sur les côtes australiennes (Bare Island, Sydney) présentant certaines zones médianes blanchies; l'une d'elles est signalée par une fleche (Fernandes et al., 2012).

Dans ce contexte, il a été observé que les algues blanchies étaient caractérisées par de plus faibles concentrations en furanones halogénées. Ainsi, le niveau de défense chimique de l'algue s'avèrerent négativement corrélé à l'augmentation de la température de l'eau. A l'échelle du microbiote de surface, des différences de structure ont été observées entre les algues blanchies et saines, laissant supposer le rôle potentiel des furanones halogénées dans la structuration de la communauté épibactérienne (Campbell et al., 2011). Les travaux de Case et al., 2011 ont par la suite mis en évidence la présence d'une bactérie pathogène (*Nautella* sp. R11) colonisant les spécimens de *D. pulchra* dépourvus de furanones halogénées dans des conditions de température élevée (24°C). Ainsi, ces conditions de température liées à l'absence de furanones halogénées conduisent à l'activation de facteurs de virulence et à la production

de molécules du QS chez *Nautella* sp. R11 (Case et al., 2011; Fernandes et al., 2011). Un certain nombre de ces facteurs de virulence sont communs à d'autre bactéries phytopathogènes, telle l'expression de protéines de nodulation inhibant l'expression de certaines défenses immunitaires innées chez les plantes (Marie et al., 2003; Bartsev et al., 2004; Fernandes et al., 2012). De manière intéressante, la colonisation de *Nautella* sp. R11 à la surface et l'activation de ses facteurs de virulence apparaissent dépendant de facteurs de régulation associés au QS (Fernandes et al., 2011, 2012; Gardiner et al., 2015). Ainsi, la régulation du QS par l'algue hôte, au moyen de l'expression d'antagonistes tels que les furanones halogénées constitue une facteur-clé impliqué dans la régulation des mécanismes associés au développement d'un mode de vie pathogène pour cette souche. Néanmoins, le phénomène de blanchissement de *D. pulchra* n'est pas lié à la présence de la seule souche *Nautella* sp. R11. Ainsi une seconde souche, *Phaeobacter gallaeciensis* LSS9, a aussi été identifiée comme ayant un rôle dans le phénomène de blanchissement (Fernandes et al., 2012; Zozaya-Valdés et al., 2015). De manière plus générale, de fortes différences fonctionnelles ont été observées au niveau de la communauté microbienne associée aux algues blanchies par rapport à celle d'algues saines, avec notamment un changement de communauté avant le blanchissement et en lien avec la diminution de la concentration en furanones halogénées (Fernandes et al., 2012). Des bactéries affiliées aux Rhodobacteraceae, Saprospiraceae et Flavobacteriaceae, ainsi que plus particulièrement aux genres *Alteromonas*, *Aquimarina* et *Agarivorans*, apparaissent plus abondantes dans les échantillons blanchis, suggérant ainsi qu'une grande diversité de bactéries sont impliquées dans le phénomène de blanchissement et constituent de fait un consortium de pathogènes opportunistes (Zozaya-Valdés et al., 2015, 2017; Kumar et al., 2016).

2.2.Le modèle *Ulva mutabilis*

Ulva mutabilis a particulièrement été étudié pour le rôle de son microbiote associé à sa morphogénèse et à son développement (Wichard et al., 2015; Kessler et al., 2018). Dans des conditions de cultures axéniques, le développement des gamètes d'*U. mutabilis* apparait perturbé avec une prolifération cellulaire de type « cal ». Ce phénotype est caractérisé par une formation anormale de la paroi cellulaire, l'absence de différentiation et une croissance ralentie. L'ajout de deux souches bactériennes isolées de *U. mutabilis* et affiliées aux genres *Roseovarius* (Rhodobacteraceae) et *Maribacter* (Flavobacteriaceae) dans le milieu de culture a permis de rétablir une morphogenèse normale de l'algue (Spoerner et al., 2012; Wichard and Beemelmanns, 2018).

La production de diméthylsulfoniopropionate (DMSP) par *U. mutabilis* a par la suite été étudiée et a montré que ce composé présente une activité chimioattractive pour la souche *Roseovarius* sp. MS2. Le

DMSP est donc considéré comme un facteur essentiel pour le recrutement de certaines souches bactériennes impliquées dans la morphogénèse de cette algue (Kessler et al., 2018) (**Figure I.10**). Par ailleurs, le catabolisme du DMSP par la souche *Roseovarius* sp. MS2 s'avère très rapide tandis que la souche *Maribacter* sp. MS6 ne semble pas dégrader cet osmolyte. Le modèle d'interaction propose qu'une fois recrutée à la surface de l'algue, la souche *Roseovarius* sp. MS2 utilise le glycérol présent à la surface de l'hôte comme source de carbone pour former un biofilm (**Figure I.10**). L'induction de la morphogenèse implique ensuite différents facteurs de promotion émis par les bactéries. La souche *Maribacter* sp. MS6, elle, induirait la formation du rhizoïde de l'algue (Kessler et al., 2018; Wichard and Beemelmanns, 2018).

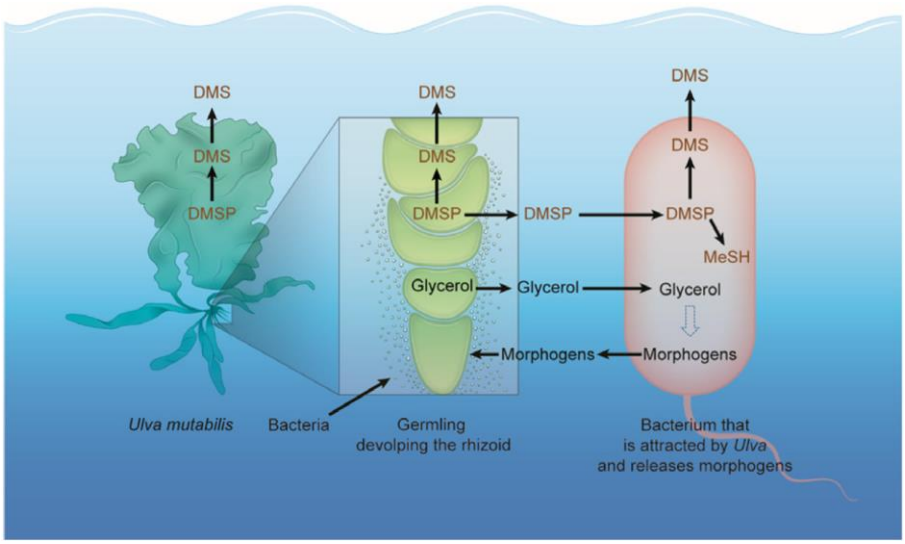

Figure I.10. Modèle proposé détaillant les interactions entre l'algue Ulva mutabilis et les bactéries impliquées dans sa morphogenèse (Kessler et al., 2018)

Récemment, les travaux d'Alsufyani et al., (2020) ont permis d'identifier la thallusine (**Figure I.11**) comme étant l'un des facteurs moléculaires-clés libéré par *Maribacter* sp. MS6 et induisant la formation du rhizoïde et de la paroi cellulaire d'*U. mutabilis*.

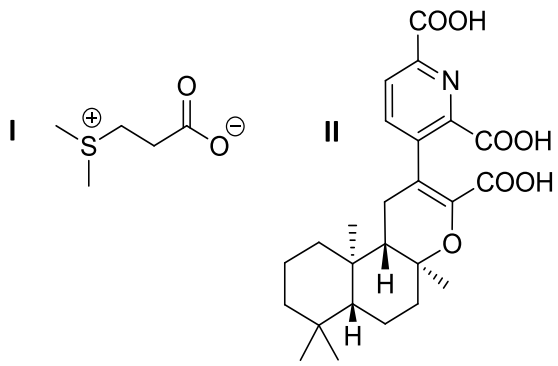

Figure I.11. Composés impliqués dans les interactions de l'holobionte Ulva mutabilis : DMSP (**I**) agissant en tant que chemo-attracteur de certaines souches productrices de facteurs de croissance pour l'algue, tels que la thallusine (**II**).

Ce modèle d'interaction simplifié peut impliquer d'autres combinaisons de souches bactériennes, (autre que le couple *Roseovarius* sp. MS2/*Maribacter* sp. MS6) qui seraient tout aussi susceptibles d'interagir avec l'algue pour assurer sa morphogenèse. Ainsi, il n'existerait pas dans l'environnement un seul couple spécifique de bactéries recrutées à la surface de l'algue pour assurer cette fonction, mais de tels échanges moléculaires pourraient être partagés avec tout une partie de la communauté bactérienne (Ghaderiardakani et al., 2017). En lien avec ces observations, les auteurs de cette étude soutiennent le « *competitive lottery model* » développé précédemment pour l'espèce *Ulva australis* par Burke et al., (2011a). Ce modèle propose que l'assemblage de la communauté épibactérienne à la surface des algues ne se fasse pas entièrement de manière déterministe mais implique aussi une part de hasard (Burke et al., 2011a). Ceci expliquerait pourquoi la spécificité d'une communauté bactérienne adaptée pour assurer la morphogenèse de l'algue *U. mutabilis* est susceptible de varier dans l'environnement (Ghaderiardakani et al., 2017).

2.3.Le modèle *Fucus vesiculosus*

L'algue brune *Fucus vesiculosus* constitue un modèle d'holobionte algal pour lequel l'effet de molécules présentes à sa surface a été évalué envers l'adhésion bactérienne. A l'aide d'un fractionnement bioguidé à partir d'extraits de surface de *F. vesiculosus*, la proline, le DMSP et la fucoxanthine ont été décrits comme étant les principaux métabolites impliqués dans la défense chimique de l'algue vis-à-vis de la colonisation épibactérienne (Lachnit et al., 2010; Saha et al., 2011, 2012; Lachnit et al., 2013; Rickert et al., 2015, 2016a).

Etant donné que la fucoxanthine est aussi produite par des microalgues pouvant potentiellement coloniser la surface de *F. vesiculosus*, des travaux ont montré que ce caroténoïde était majoritairement produit par l'algue elle-même (Saha et al., 2011). Des analyses plus approfondies menées par

spectroscopie Raman ont confirmé ces résultats en montrant un gradient de concentration de fucoxanthine (de la surface des cellules de l'algue vers le milieu environnant) au sein de la couche de diffusion de surface (« *diffusion boundary layer* ») de l'algue (Grosser et al., 2012). Des expériences *in situ* menées à l'aide d'un dispositif expérimental destiné à simuler la diffusion naturelle d'extraits ou de molécules à la surface d'une algue ont également montré qu'une fraction algale riche en fucoxanthine entrainait une diminution de 80% de la colonisation bactérienne alors qu'un extrait total de l'algue n'engendrait aucun effet significatif sur la structure de la communauté bactérienne à l'échelle du phylum ou de la classe (Lachnit et al., 2010, 2013).

2.4. L'induction de défenses oxydatives chez les algues *Gracilaria conferta* et *Laminaria digitata*

Des travaux portant sur *Gracilaria conferta* et *Laminaria digitata* ont permis d'observer des phénomènes de réponses immunitaires associées à la dégradation de leur paroi cellulaire. En effet, une réponse oxydative de l'hôte a été observée chez ces deux modèles en présence d'oligosaccharides mimant la dégradation de la paroi algale (ex : des oligoalginates tel que l'oligoguluronate) (Potin et al., 1999; Küpper et al., 2001; Weinberger, 2007; Thomas et al., 2014). La réponse immunitaire induite par des oligoguluronates est caractérisée par la libération de H_2O_2 à la surface de l'algue (Küpper et al., 2001, 2002a). Cette réponse oxydative (« *oxidative burst* ») non spécifique de l'algue favoriserait l'élimination de bactéries à sa surface, et notamment de celles dégradant sa paroi, tout en constituant également un moyen de se défendre vis-à-vis de la prédation exercée par les brouteurs herbivores (Leblanc et al., 2011; Thomas et al., 2014). Dans le cas de *L. digitata*, l'expression de gènes impliqués dans des fonctions de réponses oxydatives (ex : la glutathione-*S*-transferase), de production de métabolites antimicrobiens et de renforcement de la paroi cellulaire a été induite rapidement en présence d'oligoguluronates (Cosse et al., 2009). Par ailleurs, il a également été démontré que le métabolisme halogéné (et notamment celui de l'iode) était aussi très fortement régulé par l'ajout d'oligoguluronates (Cosse et al., 2009; La Barre et al., 2010). Enfin, ces mécanismes de défenses ont également été étudiés à l'échelle du thalle (Thomas et al., 2014) montrant qu'une induction locale de la réponse immunitaire par les oligoguluronates engendrait une réponse systémique, médiée par une communication intracellulaire le long des frondes, pour l'ensemble du thalle. Les mécanismes impliqués mettent notamment en jeu les activités d'halopéroxydases dépendantes du vanadium (vHPO) ainsi que la libération d'acides gras polyinsaturés par des phospholipases.

3. Les macroalgues holobiontes sous l'effet de perturbations environnementales

Sous l'effet des changements globaux induits par les activités humaines, les interactions étroites entre l'algue et son microbiote sont susceptibles d'être perturbées. Ceci est également vrai pour la majorité des holobiontes marins, avec pour effet une augmentation de l'apparition de maladies depuis ces 50 dernières années (Ward and Lafferty, 2004; van der Loos et al., 2019). Dans ce contexte, la dysbiose des holobiontes constitue un phénomène particulièrement décrit avec, comme principales conséquences, la modification du microbiote (lié notamment à la perte de symbiontes mutualistes) et/ou le développement de pathogènes susceptibles d'impacter négativement la physiologie de l'hôte (Egan and Gardiner, 2016). Afin d'améliorer notre compréhension de ces effets et de proposer des scénarios plausibles à plus long terme, la hausse de la température de l'eau et l'acidification des mers et océans comptent parmi les paramètres les plus étudiés (Webster et al., 2011; van der Loos et al., 2019). Bien qu'encore peu décrites dans la littérature, les interactions entre hôte et épiphytes sont de plus en plus étudiées afin de mieux comprendre comment elles vont affecter la résilience et la résistance globale de l'holobionte face aux évolutions environnementales.

3.1. Hausse globale des températures et vagues de chaleurs marines

La hausse globale de la température des océans de 4°C prévue d'ici 2080-2100 constitue une menace particulièrement importante pour les écosystèmes marins (Collins et al., 2013). Entre autres, cette hausse induirait une importante érosion de la biodiversité marine du fait de la perte d'espèces formant des habitats marins naturels tels que les récifs coralliens ou les forêts de kelps (Wernberg et al., 2016). L'étude de la résilience des macroalgues face à l'augmentation de la température constitue donc un sujet d'étude particulièrement pertinent dans le contexte actuel. En outre, la prise en considération de l'évolution des interactions entre l'hôte et son microbiote constitue un axe de recherche clé, notamment dans le cadre d'une possible diminution des défenses de l'algue et du développement de dysbioses. L'algue *Delisea pulchra*, (cf. partie 2.1) constitue ainsi un exemple privilégié pour illustrer ce type de scenario. En effet, l'augmentation de la température constituerait un facteur affectant doublement l'holobionte avec une baisse des défenses chimiques et le développement de souches bactériennes pathogènes appartenant principalement aux familles des Rhodobacteraceae (ex : *Nautella italica* R11 et *P. gallaeciensis* LSS9) et des Flavobacteriaceae (ex : *Aquimarina* sp.) (Case et al., 2011; Fernandes et al., 2011; Kumar et al., 2016). En prenant pour exemple ce modèle, et étant donné que les facteurs de virulence des pathogènes sont plus généralement activés sous l'effet de conditions environnementales changeantes, Egan et al., (2014) ont

suggéré que les conditions futures pourraient conduire à une augmentation globale du nombre de cas de maladies chez les macroalgues en lien avec une dysbiose bactérienne.

La température des océans apparait également comme un facteur majeur associé à des modifications de communauté épibactérienne chez d'autres modèles d'holobiontes algaux tels que *F. vesiculosus* (Stratil et al., 2013; Saha et al., 2014, 2020a) ou l'algue coralligène *Neogoniolithon fosliei* (Webster et al., 2011). Pour cette dernière, le phénomène de blanchissement a été observé en mésocosme à la suite d'une augmentation de la température (de 27°C à 32°C) qui a induit l'augmentation des Bacteroidetes et la réduction des *α*-Proteobacteria au niveau de la communauté associée. Au sein de cette dernière classe, une souche non identifiée fait partie des premières à être perdue lors de l'augmentation de température et bien que son rôle fonctionnel reste inexploré, il est suggéré qu'une telle perte pourrait impacter la santé de l'hôte. De plus, après un retour aux conditions de température initiales, l'activité photosynthétique de *N. fosliei* n'a pas été récupérée indiquant l'impact majeur d'un tel stress thermique sur la résilience de cette macroalgue.

Les vagues de chaleur marines (« *marine heatwaves* ») constituent des épisodes inhabituels d'augmentation de la température de surface des océans. Comme pour d'autres évènements climatiques extrêmes, tels que les inondations ou les tornades, les modèles de prévisions liés au changement climatique prévoient une augmentation de l'intensité, de la durée et de la fréquence de ces épisodes météorologiques. En 2006, la température d'eau de surface a atteint 28,5°C en mer Méditerranée sous l'effet d'une vague de chaleur causant une forte mortalité au niveau des herbiers de posidonies (Marbà and Duarte, 2010). De manière similaire, les vagues de chaleurs de 2017 et 2018 ont causé l'extinction des populations locales de *Durvillaea* spp. le long des côtes du sud de la Nouvelle-Zélande ; ces espèces ont été remplacées par des macroalgues invasives telles que *Undaria pinnatifida* (Thomsen et al., 2019). Les auteurs de cette étude ont émis l'hypothèse que l'effet du stress thermique chez les algues autochtones a constitué un facteur aggravant leur sensibilité face au développement de microorganismes pathogènes, et a ainsi induit une accélération de leur extinction locale.

A ce jour, une seule étude portant sur l'effet des vagues de chaleur marines sur des macrophytes a pris en considération le microbiote associé, et ce uniquement en termes de densité (Saha et al., 2020a). Cette étude menée sur la phanérogame *Zostera marina* et la macroalgue *F. vesiculosus* a permis de simuler en mésocosmes des vagues de chaleur successives montrant néanmoins un impact limité sur ces deux espèces. Dans le cas spécifique de *F. vesiculosus*, la forte variabilité des densités bactériennes observées

semble liée à la capacité de cette algue à s'adapter à des conditions environnementales extrêmement variables.

3.2.Acidification et effet combiné avec une augmentation de la température

L'acidification des océans constitue un deuxième facteur majeur du changement global avec pour principale cause l'augmentation de l'absorption du CO_2 atmosphérique émis par les activités anthropiques. Ces conséquences écologiques semblent particulièrement importantes et elles impactent, par exemple, les processus de calcification de divers organismes tels que les coraux, les mollusques, les échinodermes mais aussi les macroalgues coralligènes (Orr et al., 2005; Kroeker et al., 2013; Johnson et al., 2014). Deux études récentes en mésocosmes ont porté spécifiquement sur l'effet de l'acidification de l'eau sur des macroalgues holobiontes, l'algue coralligène *Sporolithon australe* et l'algue brune *Sargassum muticum*, en considérant leurs microbiomes de manière globale sans distinguer leurs composantes endo- et épiphytes (Aires et al., 2018; Cavalcanti et al., 2018). Aucune différence de structure de communauté des microbiotes n'est apparu entre les conditions contrôles et acidifiées, suggérant ainsi une certaine stabilité de l'holobionte. En revanche, d'autres études récentes, également réalisées en mésocosmes, portent de manière plus spécifique sur la composante épiphyte du microbiome d'autres modèles et incluent l'effet combiné ou non de la température en plus de celui de l'acidification (Mensch et al., 2016; Huggett et al., 2018; Minich et al., 2018; Roth-Schulze et al., 2018; Qiu et al., 2019). Pour ces études, quatre conditions ont été étudiées : (i) la température et le pH relevés *in situ*, (ii) l'augmentation de la température, (iii) l'augmentation du pH et (iv) une projection sur des conditions futures avec augmentation du pH et de la température. Ces conditions ont notamment été choisies en suivant les modèles de prévision du groupe d'experts intergouvernemental sur l'évolution du climat (GIEC) pour les années 2070-2110 avec des variations allant de +1.5 à +5°C et de -0.2 à -0.4 unités pH (Collins et al., 2013; Bindoff et al., 2019). Pour *Caulerpa taxifolia* (Roth-Schulze et al., 2018), l'effet combiné de l'augmentation de la température et de l'acidification apparait limité sur la β-diversité (**Tableau I.1**). En revanche, l'effet synergique du changement de ces deux paramètres impacte significativement la diversité épibactérienne pour les modèles *Ecklonia radiata*, *Macrocystis pyrifira*, *Fucus mytili* et *Amphiroa gracilis* (**Tableau I.1**). En outre, l'ensemble de ces travaux se sont aussi intéressés à l'effet de ces changements sur la physiologie de l'hôte, avec notamment certains paramètres physiologiques tels que la croissance, l'activité photosynthétique ou l'observation directe de potentielles pathologies. De manière générale, les résultats sont contrastés en fonction des modèles, avec un impact principalement de la température, de l'acidification, ou des deux combinés sur la β-diversité épibactérienne tandis que des effets sur un ou plusieurs des paramètres physiologiques sont également observés (**Tableau I.1**).

Reference	Algue modèle	Durée de l'expérience	Effet des conditions sur la β-diversité du microbiote épiphyte	Effet sur la croissance de l'hôte	Effet sur l'activité photosynthétique de l'hôte	Apparition de pathologies
Mensch et al., 2016	*Fucus mytili*	11 semaines	Effet fort de l'augmentation de température et plus faible de l'acidification.	Diminution de la croissance avec l'augmentation de température	Pas d'effet observé (ni sur le ratio C:N, ni sur la production de mannitol)	Non renseigné
Roth-Schulze et al., 2018	*Caulerpa taxifolia*	3 semaines	Pas d'effet de la température. Effet limité de l'acidification (uniquement à forte température avec l'augmentation de Planctomycetes)	Effet important et synergétique des deux paramètres dépendant du stade de croissance initial de l'algue	Pas d'effet observé sur l'activité du photosystème II	Non renseigné
Huggett et al., 2018	*Amphiroa gracilis*	3 semaines	Effet significatif indépendant et synergétique de la température et de l'acidification. Dominance de Bacteroidetes et Verrucomicrobia avec la température ; et de Planctomycetes avec l'acidification	Non renseigné	Pas d'effet significatif sur l'activité du photosystème II (malgré le blanchissement)	Apparition d'un phénomène de blanchissement lié à l'augmentation de la température mais réduit par l'acidification
Minich et al., 2018	*Macrocystis pyrifera*	4 semaines	Effets significatifs avec principalement l'effet de l'augmentation de la température et de combinaison des deux paramètres	Effet négatif de l'augmentation de température seule. Effet positif de la combinaison des deux conditions.	Non renseigné	Non renseigné
Qiu et al., 2019	*Ecklonia radiata*	2 semaines	Effet significatif des deux paramètres	Non renseigné	Diminution de l'activité photosynthétique liée au phénomène de boursouflement (acidification)	Apparition de boursouflements du thalle liée à l'acidification

Tableau I.1. Récapitulatif des différentes études en mésocosmes portant sur l'effet de conditions climatiques futures (augmentation de température et acidification de l'eau) sur différentes macroalgues et leur microbiote de surface

3.3. Détérioration de la qualité de l'eau et effet de l'urbanisation côtière

La détérioration de la qualité de l'eau via des pollutions d'origines anthropiques constitue des menaces supplémentaires pour l'ensemble des écosystèmes marins côtiers avec par exemple l'augmentation des déchets microplastiques, de la pollution en métaux traces, de l'eutrophisation des côtes, de la sédimentation ou encore de la contamination liée à des polluants persistants tels que certains hydrocarbures. Ces phénomènes impliquant la détérioration de la qualité des eaux marines ne sont au cœur que de rares études d'écologie microbienne dans le cadre d'holobiontes marins portant majoritairement sur les coraux (Hall et al., 2018; Bednarz et al., 2020; Lanctôt et al., 2020) et les éponges (Simister et al., 2012; Luter et al., 2014; Pineda et al., 2017). Dans le cas de macroalgues, l'effet de fortes concentrations en cuivre sur le microbiote des algues *Ulva* spp. et *Lessonia nigescens* (Phaeophyceae) a été étudié au niveau de certains sites contaminés de la côte chilienne (Hengst et al., 2010). Cette contamination n'a pas d'effet sur la β-diversité pour *L. nigescens* tandis que des différences significatives apparaissent pour le microbiote d'*Ulva* spp, avec une surreprésentation de certains taxa, en particulier des Verrucomicrobiae, dont le genre *Rubritaleae*, au niveau des sites contaminés. L'impact du cuivre sur la physiologie de ces deux algues n'a pas été abordé lors de cette étude. Cependant, l'effet de certains métaux traces tels que le cuivre ou le plomb est connu chez certaines macroalgues, avec notamment des phénomènes de photo-inhibition, d'induction de stress oxydatif, de diminution de la

croissance ou de réduction de l'allocation de ressources liées par exemple aux défenses antimicrobiennes (Küpper et al., 1996, 1998; Pinto et al., 2003; Connan and Stengel, 2011; Costa et al., 2016; Moenne et al., 2016).

D'autres perturbations d'origine anthropique généralement liées aux activités agricoles, telles que l'eutrophisation du littoral, impactent très fortement la diversité des écosystèmes côtiers. Bien que l'effet d'un enrichissement du milieu en nutriments n'ait pour le moment jamais été testé expérimentalement à l'échelle de macroalgues holobiontes, certaines études suggèrent que ce paramètre jouerait un rôle non négligeable dans les interactions au sein de l'holobionte (Wright et al., 2000; Barboza et al., 2019; Florez et al., 2019; Lachnit et al., 2019; Morrissey et al., 2019). Ainsi, l'hypothèse de l'influence négative des nutriments sur la production de furanones halogénées a été émise lors d'une étude biogéographique menée sur *D. pulchra* (Wright et al., 2000). Avec le modèle *F. vesiculosus*, une étude de terrain a analysé l'impact de l'enrichissement en nutriments sur la valeur sélective de l'algue, tout en considérant les épiphytes autotrophes (micro et macro-eucaryotes) grâce à l'analyse quantitative des pigments d'extraits de surface (telle que la chlorophylle a) permettant d'estimer leurs densités. Les résultats indiquent notamment qu'une plus forte densité d'épiphytes serait observée dans les zones géographiques caractérisées par : (i) un enrichissement en nutriments, (ii) une plus faible salinité et (iii) une forte irradiance (Barboza et al., 2019). Outre la salinité, une forte eutrophisation semble impacter le phénotype de *F. vesiculosus*, avec notamment des frondes moins nombreuses et plus petites, diminuer ses défenses antifouling et constituer des conditions favorables pour certains épiphytes (Barboza et al., 2019).

Une autre étude biogéographique portant sur des populations chiliennes de *Macrocystis pyrifera* s'est intéressée à l'effet de la concentration en nitrates sur la structure de leur communauté épibactérienne sur différents sites contrastés (Florez et al., 2019). Les sites du sud du Chili étaient caractérisés par une pollution constante en nitrates due à l'activité des fermes aquacoles tandis que ceux du nord montraient des fluctuations saisonnières en nutriments liés aux zones d'« *upwelling* » (Buschmann et al., 2006). Même si la génétique des populations et la température sont apparues comme les facteurs principaux expliquant les différences de diversité épibactérienne, la concentration en nitrates ainsi que la production chimique à la surface des algues pourraient également constituer des facteurs-clés pour la structuration du microbiote des populations localisées au nord. Des corrélations négatives entre la concentration en nitrates et certains genres bactériens prédominant chez les macroalgues, tels que *Granulosicoccus*, *Loktanella*, et *Sulfitobacter*, ont ainsi été observées.

Parmi d'autres effets anthropiques, des études ont montré des différences de structure du microbiote de l'algue brune *Ecklonia radiata* pour des spécimens provenant soit de récifs artificiels (piliers et digues), soit de substrats rocheux naturels (Marzinelli et al., 2018). Des taxa précédemment associés au blanchissement d'*E. radiata* s'avèrent majoritaires au niveau des structures artificielles. Néanmoins, la présence de récifs artificiels n'a pas exercé d'effet significatif sur l'activité photosynthétique des algues mais de telles structures pourraient diminuer l'ensoleillement, modifiant ainsi le microbiote de surface des algues et induisant alors un recrutement plus important de macroorganismes épiphytes (Marzinelli et al., 2015, 2018).

3.4. Effets d'autres paramètres environnementaux : Exemple de l'intensité lumineuse et de la salinité

Bien que l'effet des paramètres associés aux perturbations environnementales anthropiques constituent un axe de recherche prépondérant, d'autres effets environnementaux ont aussi été considérés du fait de leurs variations dans des écosystèmes particuliers (ex. : salinité en mer Baltique), de leur impact sur la physiologie de l'holobionte (ex. : lumière) ou de leur effet synergique avec ces perturbations.

A ce jour, seules deux études ont testé l'effet de différentes intensités lumineuses sur la physiologie de macroalgues dans le contexte de l'holobionte (Wahl et al., 2010; Saha et al., 2014). Wahl et al., (2010) ont proposé notamment que *F. vesiculosus* puisse être impactée négativement par le développement de biofilms matures agissant tels des filtres et réduisant ainsi jusqu'à 50% l'intensité lumineuse accessible pour l'algue. Les travaux de Saha et al., (2014), basés sur une étude en mésocosmes utilisant six conditions d'intensités lumineuses allant de l'exposition naturelle jusqu'à l'obscurité complète, ont montré que les variations de DMSP, de proline et de fucoxanthine en fonction de la luminosité étaient très limitées à la surface de l'algue et n'étaient que peu corrélées aux variations de la structure de la communauté épiphyte.

La salinité constitue un autre paramètre d'intérêt à étudier dans le contexte de l'holobionte algal ; ceci est notamment pertinent dans des écosystèmes spécifiques tels qu'en mer Baltique où un gradient de salinité est observé du nord au sud (Barboza et al., 2019). Dans le cadre d'une étude en mésocosmes, *F. vesiculosus* a été exposée à trois niveaux de salinité (5, 19 et 29 psu) pendant 14 jours montrant que ce paramètre constituait un facteur structurant de la communauté épibactérienne, bien que seulement 5% des OTUs soient significativement impliqués. Plus précisément, l'α-diversité était plus faible (à la fois en termes de richesse et d'équitabilité) et les différences de β-diversité étaient les plus importantes dans les conditions de faible salinité (Stratil et al., 2014). Des travaux similaires sur *Agarophyton vermicullophylum* se sont basés sur une gamme de salinité similaire (8,5, 16,5 et 25,5 psu) mais avec une durée d'effet plus

importante (5 mois). Des valeurs significativement plus importantes de richesse bactérienne ont été observées avec la salinité minimale tandis que de fortes différences de la β-diversité ont été relevées entre les différentes conditions de salinité, avec notamment un enrichissement en Cytophagia pour une faible salinité (Saha et al., 2020b). Pour ce paramètre également, l'effet sur la relation entre l'hôte et sa communauté épibactérienne reste donc encore largement inexploré.

4. Le modèle *Taonia atomaria*

4.1. Description morphologique et phylogénie du genre *Taonia*

Les algues du genre *Taonia* J. Agardh appartiennent à la classe des Phaeophyceae (algues brunes), l'ordre des Dictyotales et la famille des Dictyotaceae. Les Dictyotales constituent un groupe d'algues majeur au sein des écosystèmes côtiers européens, avec comme principale famille celle des Dictyotaceae caractérisée par une importante diversité, souvent cryptique, et illustrée notamment par certains genres tels que *Dictyota* (Clerck et al., 2006; Bittner et al., 2008; Tronholm et al., 2010b, 2010a). Les Dictyotaceae sont par ailleurs des algues particulièrement connues pour produire une grande diversité de terpènes témoignant d'activités écologiques variées (antimicrobienne, anti-appétante…) (Kelecom and Laneuville Teixeira, 1986; Vallim et al., 2005; Paula et al., 2011; Theophilus et al., 2020).

Le genre *Taonia* comprend actuellement six espèces acceptées taxonomiquement (Guiry and Guiry, 2020) : *Taonia abbottiana* Littler & Littler (décrite pour la première fois en Jamaïque), *T. atomaria* (Woodward) J. Agardh (Grande-Bretagne), *T. australasica* J. Agardh (Australie), *Taonia lacheana* Cormaci, Furnari & Pizzuto (Italie), *T. lennebackerae* Farlow ex. J. Agardh (Etats-Unis, Californie) et *T. pseudociliata* (J. V. Lamouroux) Nizamuddin & Godeh (Haïti). *T. atomaria* correspond à l'espèce-type de ce genre. L'espèce présente des thalles plats de couleur brun-olive qui s'élargissent de la base vers le sommet (Harvey, 1849) (**Figure I.12**). Les extrémités apicales se découpent de manière irrégulière : elles sont laciniées. Les thalles présentent des stries transversales liées à la présence de « touffes de poils » et du développement de tétrasporanges à proximité (Robinson, 1932). Les algues du genre *Taonia* possèdent généralement quatre couches de cellules, dont deux périphériques et deux médullaires, bien que pour *T. pseudociliata* les parties basales de l'algue soient caractérisées par six couches de cellules, allant potentiellement jusqu'à huit à proximité du crampon (Nizzamudin and Godeh, 1993). Les espèces de ce genre présentent toutes un crampon de type discoïde portant des rhizoïdes ramifiés. En ce qui concerne

plus particulièrement *T. atomaria*, la taille de ses thalles peut varier de 5 à 30 cm de long et de 1 à 4 cm de large.

Figure I.12. L'algue *Taonia atomaria in* et *ex-situ*. Le thalle présente certaines caractéristiques-clés pour son identification morphologique telles que l'élargissement des frondes de la base vers le sommet, les stries de poils horizontales et les extrémités apicales laciniées (http://www.seaweed.ie/descriptions/Taonia_atomaria.php)

4.2.Ecologie, répartition géographique et cycle de vie de *T. atomaria*

T. atomaria dont le spécimen-type a été prélevé à Great Yarmouth (côte sud-est de l'Angleterre) est très largement distribuée au niveau des côtes du nord-est de l'océan Atlantique, ainsi que sur l'ensemble du pourtour méditerranéen (Guiry and Guiry, 2020). Cette espèce est retrouvée majoritairement fixée à des substrats rocheux en mer Méditerranée, alors que, dans l'océan Atlantique, son substrat est principalement sablonneux ou composé de débris de coquillages. Il s'agit d'une algue annuelle principalement observée de février à juillet sur les côtes méditerranéennes françaises et plus tardivement, jusqu'en décembre, le long des côtes atlantiques. L'algue est présente dans les zones ensoleillées, protégées et peu profondes de l'étage infralittoral.

Avec l'observation de zones méristématiques situées sur les zones apicales des thalles, les travaux de Robinson, (1932) ont notamment permis de proposer certains mécanismes associés au mode de croissance de *T. atomaria*. La croissance, qui s'effectuerait donc de manière apicale, impliquerait par

ailleurs une production rythmique au niveau des zones apicales de « touffes de poils » transversales au thalle, expliquant ainsi la succession régulière de ces bandes. La croissance de l'algue serait marquée par une alternance entre la production de ces structures reproductrices associées à la présence de tétrasporanges et la croissance purement végétative de l'algue.

Le cycle de vie sexuée de *T. atomaria* témoigne d'un certain nombre de différences avec les espèces du genre *Dictyota*. Alors que pour ces dernières le cycle digénétique s'observe de manière clairement isomorphe avec une alternance entre la génération de gamétophytes et celle de sporophytes, pour *Taonia,* la génération de gamétophytes est très largement minoritaire par rapport à celle des sporophytes. Des observations font notamment état d'une quasi-absence de pied sexué sur la plupart des spécimens prélevés lors d'une étude menée le long des côtes françaises. Sans parvenir à cultiver l'espèce en laboratoire, Gaillard a ainsi proposé que ces différences observées chez *Taonia* étaient reliées à une adaptation du mode de reproduction et de l'alternance du cycle sexué en relation avec les conditions du milieu (Robinson, 1932; Gaillard, 1972).

4.3.Production chimique chez *T. atomaria* et activités biologiques associées

Les Phaeophyceae font partie des organismes marins qui ont été les plus étudiés initialement par les pionniers de la chimie des substances naturelles marines. Ces algues sont notamment caractérisées par la production spécifique de certains métabolites observés de manière récurrente au sein de ce groupe. Parmi ceux-ci, des caroténoïdes tels que le β-carotène, la zéaxanthine, la violaxanthine et la fucoxanthine (**Figure I.13**) ou encore des stérols tels que le fucostérol ou le 24-méthylènecholestérol (**Figure I.13**).

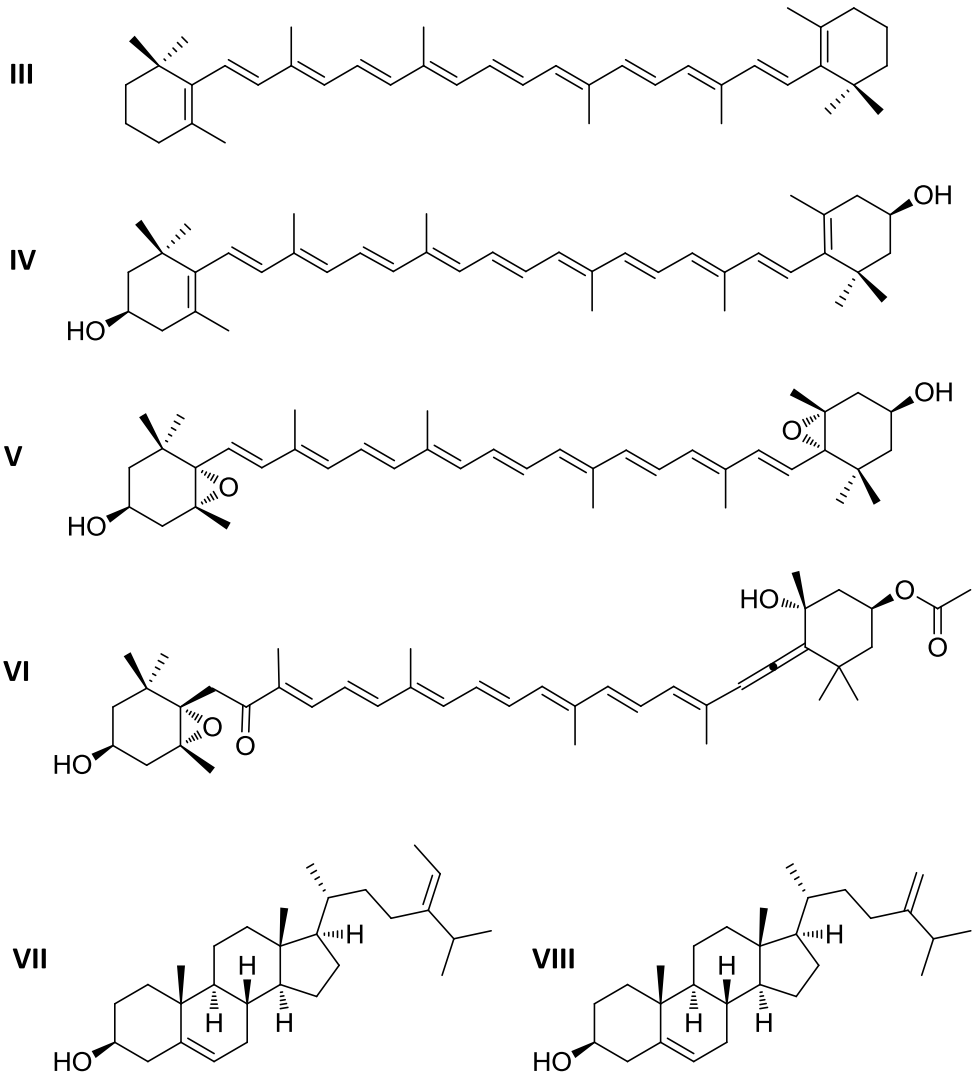

Figure I.13. Principaux métabolites caractéristiques des algues brunes (**III** : β-carotène, **IV** : zéaxantine, **V** : violaxanthine, **VI** : fucoxanthine, **VII** : fucostérol et **VIII** :24-méthylènecholestérol)

Une grande variété de lipides a été caractérisée à partir d'algues brunes incluant des acides gras libres et leurs dérivés (ex. : oxylipines), de nombreuses classes des glycérolipides et de glycérophospholipides ainsi que des aminolipides tels que les diacylglycérylhydroxyméthyl-*N,N,N*-triméthyl-β-alanines (DGTAs) (Ragonese et al., 2014; da Costa et al., 2019).

Parmi les métabolites plus spécifiques isolés chez les algues du genre *Taonia*, une grande majorité correspondent à des composés terpéniques tels que des méroditerpènes et des sesquiterpènes. Les méroditerpènes sont des composés à biogénèse mixte présentant un noyau hydroquinonique substitué par une chaine latérale diterpénique (Pellegrini et al., 1997). Cette chaine latérale peut être linéaire, comme dans le cas des composés **IX**-**XII** (Tziveleka et al., 2005), bicyclique, avec par exemple l'acide

atomarique (**XIII**) (González et al., 1974), tricyclique, tel que le taondiol (**XIV**) (González et al., 1971) ou encore tétracyclique, comme pour les atomarianones A et B (**XV** et **XVI**) (Abatis et al., 2005) (**Figure I.14**). La présence de ces composés au sein d'extraits de *Taonia* spp. est tout de même sujet à controverse car : (i) il n'est pas courant de trouver une algue ayant la capacité de biosynthétiser aussi bien des méroditerpènes et des sesquiterpènes et (ii) de nombreux méroditerpènes similaires ou identiques [ex. : taondiol et acide atomarique (Areche et al., 2009)] ont été isolés d'algues du genre *Stypopodium* qui sont morphologiquement et taxonomiquement proches de celles appartenant au genre *Taonia*.

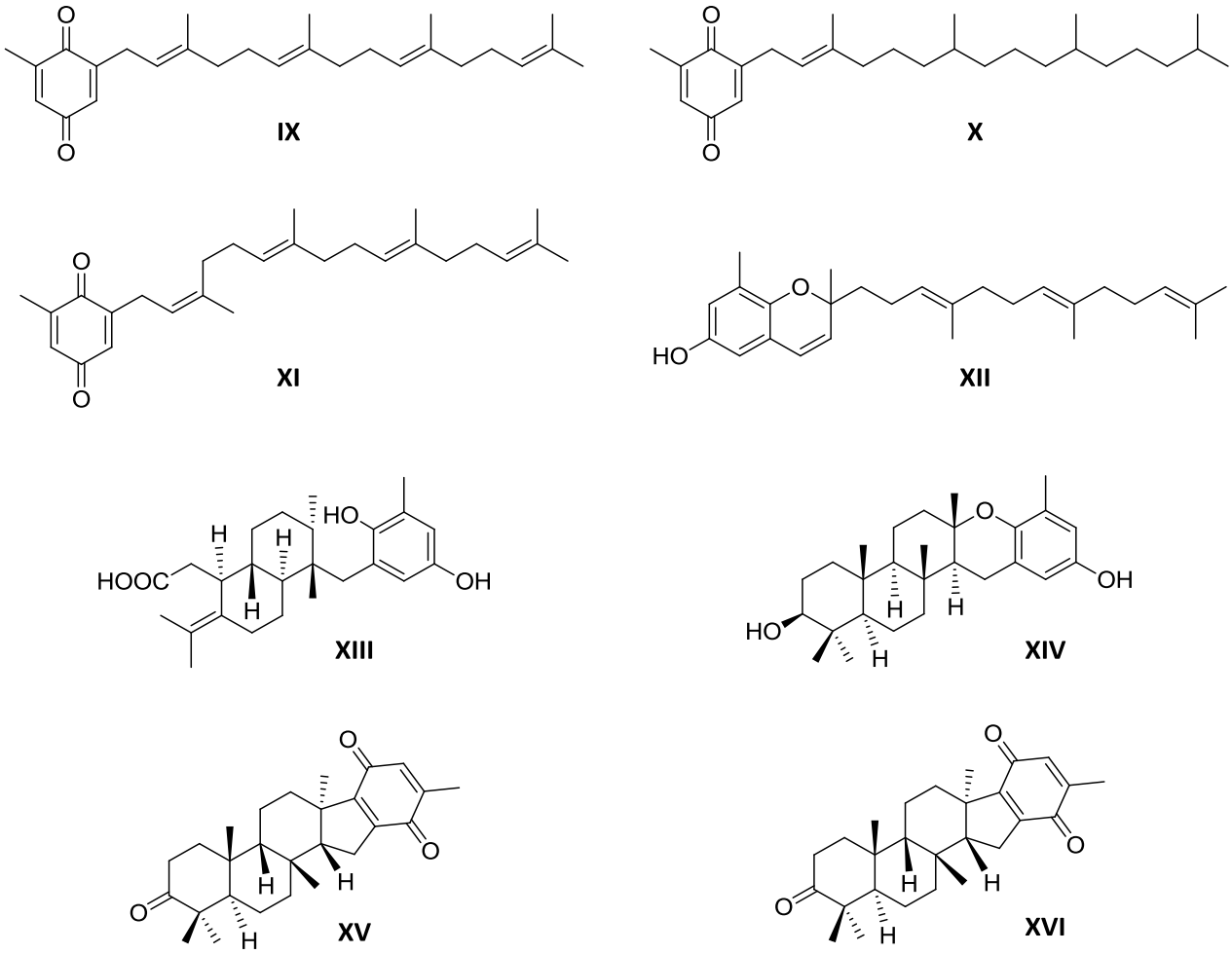

Figure I.14. Structures chimiques des méroditerpènes isolés de *T. atomaria*

Les sesquiterpènes sont des composés à trois unités isopréniques dont le squelette carboné peut être linéaire ou cyclique. Chez *T. atomaria*, l'ensemble des sesquiterpènes isolés sont cycliques mais présentent deux principaux types de squelette carboné (Figure I.15). Les sesquiterpènes les plus couramment isolés sont bicycliques et appartiennent à la famille des cadinanes (**XVII**-**XXVIII**), tels que le 4-cadinène (**XVII**), le cadina-4(14),5-diène et son épimère en C-10 (**XVIII** et **XIX**), le cubébol et le 4-*épi*-cubébol (**XX** et **XXI**) (De

Rosa et al., 1994). Les sesquiterpènes monocycliques de la famille des germacranes constituent le deuxième groupe majeur, avec notamment le germacrane D (**XXX**), le (1*S*, 5*E*, 7*S*) 1-acétoxygermacra-4(15),5,10(14)-triène (**XXXI**), ou encore le germacra-4(15),5,10(14)-trién-9-ol (**XXXII**). Plus rare, le squelette spiroaxane est seulement représenté par le (-)-gleenol (**XXIX**) et son stéréoisomère l'axenol (De Rosa et al., 1994; Othmani et al., 2016a, 2016b).

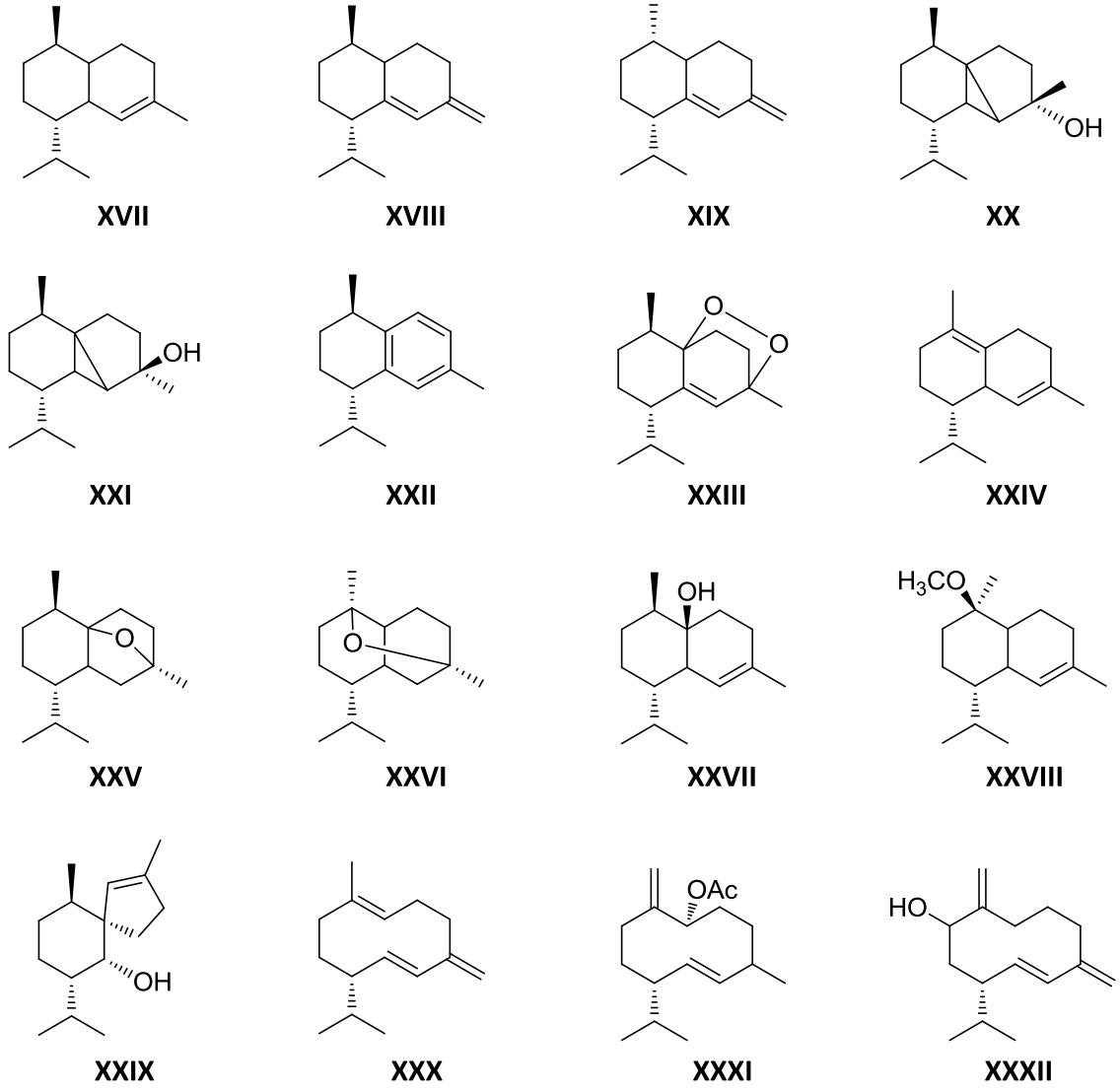

Figure I.15. Structures chimiques des sesquiterpènes isolés de *T. atomaria*

En plus de ces deux familles de dérivés terpéniques, le sn-3-*O*-(geranylgeranyl)glycérol (GGG) (**XXXIII**) (**Figure I.16**), dont la structure chimique est composée d'une chaine diterpénique linéaire liée à un groupement glycérol, constitue un composé majeur des extraits de *T. atomaria* (Tringali et al., 1995; Othmani et al., 2016a, 2016b).

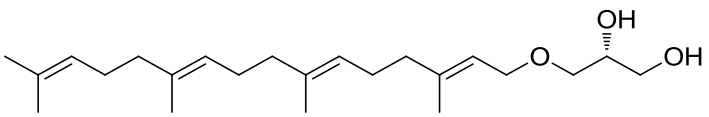

XXXIII

Figure I.16. Structure chimique du géranylgéranylglycérol isolé de *T. atomaria*

Parmi les métabolites isolés de *T. atomaria*, huit composés ont fait l'objet d'une étude approfondie de leur activité anti-adhésion vis-à-vis, d'une part, de souches isolées à la surface de *T. atomaria* (trois appartenant au genre *Pseudoalteromonas* et une au genre *Alteromonas*) et, d'autre part, de souches de références provenant de surfaces abiotiques (Othmani et al., 2016a). Ces composés sont six sesquiterpènes [(-)-gleenol (**XXIX**), (-)-*trans*-calaménène (**XXII**), méthoxy-*α*-cadinol (**XXVIII**), (1*S*, 5*E*, 7*S*)-1-acétoxygermacra-4(15),5,10(14)-triène (**XXXI**), germacra-4(15),5,10(14)-trién-9-ol (**XXXII**), 4-péroxymuurol-5-ène (**XXIII**)], le GGG (**XXXIII**) ainsi que l'acide (5*Z*, 8*Z*, 11*Z*, 14*Z*, 17*Z*)-eicosa-5,8,11,14,17-pentaénoïque. L'étude a montré que le gleenol (**XXIX**), qui constitue un composé majeur du métabolome de surface de *T. atomaria*, présentait une activité sélective avec une inhibition significative de l'adhésion des bactéries provenant de substrats artificiels (EC_{50} de l'ordre de 100 IM) mais aucune inhibition observée pour l'ensemble des souches isolées à la surface de *T. atomaria*. D'autres composés, tels que le GGG (**XXXIII**) ou le 4-péroxymuurol-5-ène (**XXIII**), présentaient des activités anti-adhésion plus importantes mais sans aucune sélectivité. Au cours d'une seconde étude, (Othmani et al., 2016b) ont aussi testé l'activité anti-adhésion de ces composés vis-à-vis de deux types de larves de balanes appartenant aux espèces *Amphibalanus amphitrite* et *Balanus perforatus*. Une activité anti-adhésion particulièrement importante du gleenol (**XXIX**) sur les larves des deux espèces de balanes a alors été démontrée. Ainsi, le gleenol (**XXIX**) constituerait un composé majoritaire de la surface de *T. atomaria* qui pourrait être impliqué dans le contrôle du micro et du macrofouling.

4.4.Critères liés au choix du modèle *T. atomaria*

Les critères de choix d'un modèle d'holobionte sont essentiels à la fois d'un point de vue méthodologique mais aussi en termes de représentativité (Krebs, 1975; Zallen, 1993; Lloyd and Wade, 2019). Les critères ayant permis de retenir l'algue *T. atomaria* comme modèle pour cette thèse sont les suivants :

(i) *T. atomaria* est très largement distribué le long des côtes françaises et notamment en mer Méditerranée. Certains sites à proximité du laboratoire sont caractérisés par une diversité

importante en Dictyotales, parmi lesquelles *T. atomaria* constitue l'une des espèces dominantes. Une telle distribution permet d'effectuer régulièrement des séries d'échantillonnages et de pouvoir disposer d'une large palette de sites d'échantillonnage.

(ii) Parmi cette grande diversité de Dictyotales, *T. atomaria* présente des caractéristiques morphologiques spécifiques, telles que des extrémités laciniées ou encore la présence de stries transversales, qui permettent une identification fiable des spécimens prélevés sur le terrain. Pour d'autres Dictyotaceae également très abondantes en mer Méditerranée, l'identification morphologique s'avère souvent plus ardue. C'est notamment le cas des algues appartenant au genre cryptique *Dictyota*, pour lesquelles l'identification à l'échelle de l'espèce requiert souvent une expertise morphologique et/ou phylogénétique approfondie (Tronholm et al., 2010a, 2010b).

(iii) Les thalles de l'algue présentent des frondes plates qui permettent d'estimer aisément les surfaces analysées via des logiciels de traitement d'images (ex. : ImageJ ou Mesurim Pro). Une estimation précise de la surface est nécessaire dans le cadre d'analyses quantitatives, comme par exemple l'estimation de la densité de cellules procaryotiques colonisant la surface de l'algue. Enfin, une surface plane permet aussi de faciliter le prélèvement du biofilm, que ce soit avec un scalpel ou un écouvillon.

(iv) Enfin, *T. atomaria* a déjà fait l'objet d'un certain nombre d'études phytochimiques au sein de notre laboratoire qui ont conduit à la purification et la caractérisation structurale d'une quinzaine de standards chimiques. D'une part, la purification de ces composés permet d'initier la constitution d'une banque de données et de faciliter l'annotation des métabolites d'intérêt lors d'une étude par métabolomique. D'autre part, la détermination de l'activité anti-adhésion de certains de ces composés vis-à-vis de différents types de souches bactériennes permet d'émettre des hypothèses quant au rôle potentiel du métabolome de surface de *T. atomaria* dans les interactions avec le microbiote associé à sa surface.

L'ensemble de ces critères font de *T. atomaria* un modèle d'holobionte particulièrement pertinent pour des études en écologie visant à étudier les interactions entre l'hôte algal et sa communauté épibactériennes.

5. Objectifs généraux de la thèse et méthodologies développées

L'écologie microbienne et l'écologie chimique constituent deux domaines scientifiques pluridisciplinaires et fortement complémentaires, permettant une compréhension fine des interactions complexes au sein de l'holobionte, mais aussi entre celui-ci et le reste de son environnement.

D'une part, l'écologie chimique marine constitue un axe de recherche relativement récent qui permet de comprendre l'écologie et l'évolution des populations marines via l'étude de produits naturels impliqués dans leurs interactions avec l'environnement. Les molécules de communications jouent notamment un rôle particulier puisqu'elles constituent des éléments majeurs caractérisant divers traits biologiques des organismes marins, tels que la croissance, la prédation, la fuite, la reproduction ou encore les défenses immunitaires (Hay, 2009). D'autre part, l'écologie microbienne marine vise à étudier la diversité et les fonctions associées aux bactéries, aux archées, aux microeucaryotes, mais aussi aux virus, qu'ils soient isolés ou non, afin d'appréhender leurs interactions au sein du milieu marin et leur importance écologique à plus large échelle.

Quelques études témoignent de l'importance de la complémentarité de ces deux approches pour la compréhension des macroalgues holobiontes (Saha et al., 2014, 2016; Parrot et al., 2019; Tourneroche et al., 2019). Les travaux de (Tait et al., 2005) et de (Wheeler et al., 2006) constituent par ailleurs des exemples supplémentaires soulignant l'importance d'une telle complémentarité. Dans le cadre de ces deux études, les auteurs ont pu démontrer que des molécules de communication du QS, produites par les bactéries au sein de biofilms, constituaient par ailleurs des messagers chimiques impliqués dans le recrutement des zoospores des algues *Ulva intestinalis*.

L'émergence des sciences –omiques, avec entre autres la métabolomiques en écologie chimique et la méta-génomique/metabarcoding en écologie microbienne, ont par ailleurs largement contribué à l'essor de ces deux domaines de recherche pour l'étude des holobiontes.

5.1. La complémentarité des approches -omiques pour aborder la complexité des systèmes holobiontes

Les récentes avancées en matière d'analyses à haut-débit et d'analyses statistiques multivariées ont permis le développement des approches dites « omiques » basées sur l'étude simultanée d'une grande diversité d'édifices moléculaires au sein d'échantillons biologiques variés.

La génomique, première des sciences omiques ayant vu le jour grâce à l'avancée des technologies de séquençage à haut-débit de l'ADN, s'intéresse à l'étude du génome d'un organisme. De manière similaire, la transcriptomique et la protéomique constituent des domaines propres respectivement à l'étude des transcrits et des protéines. Enfin, la métabolomique est la plus récente de ces sciences omiques, et vise à étudier l'ensemble des molécules non polymériques (métabolites) au sein d'échantillons biologiques. Ces quatre volets omiques sont généralement vus conceptuellement comme une « cascade », puisque la synthèse de métabolites dépend généralement de l'activité protéique, elle-même dépendant de la régulation des transcrits synthétisés à partir des génomes. Ainsi, ces approches sont intimement liées et leur intégration permet alors de reconstituer l'ensemble des mécanismes moléculaires impliqués, par exemple, dans les réponses d'un organisme modèle à des variations de son environnement.

Lorsque des échantillons sont constitués d'une communauté d'organismes, le préfixe méta- est alors utilisé. C'est notamment le cas d'un grand nombre d'études en écologie microbienne portant généralement sur l'ensemble d'une communauté microbienne, basée sur des approches indépendantes des méthodes de cultures. La métagénomique correspond ainsi à l'analyse de l'ensemble des génomes d'une communauté microbienne.

A ces sciences -omiques s'ajoutent un grand nombre de disciplines annexes basées sur les mêmes principes et visant à étudier de manière plus ciblée certaines molécules, avec par exemple l'épigénomique, la lipidomique, ou encore la glycomique. Enfin, l'intéractomique s'intéresse à des interactions moléculaires (ex. : protéines-protéines ou protéines-ADN) et nécessite généralement l'intégration de plusieurs jeux de données -omiques. L'étude des interactions chimiques entre la macroalgue hôte et son microbiote constitue un élément essentiel dans la compréhension du fonctionnement de l'holobionte. Ainsi, l'étude exhaustive de l'ensemble des mécanismes moléculaires impliqués dans ces interactions est particulièrement pertinent et les approches -omiques citées précédemment constituent des outils adaptés et originaux pour l'étude de ces holobiontes. Les analyses -omiques peuvent alors se combiner de diverses manières afin de répondre à des questions écologiques diverses. Dans ce contexte, Dittami et al., (2014) proposent notamment un schéma expérimental intégrant plusieurs analyses -omiques destinées à mieux

comprendre les processus de co-acclimation au sein de l'holobionte algal (**Figure I.17**). Cette méthodologie met notamment en avant la nécessité de reconstruire des réseaux métaboliques à partir des génomes du microbiote et de la macroalgue hôte, et ce afin de décrypter les processus impliquant leurs interactions potentielles (Burgunter-Delamare et al., 2020) et l'acclimatation de l'holobionte à divers stress environnementaux.

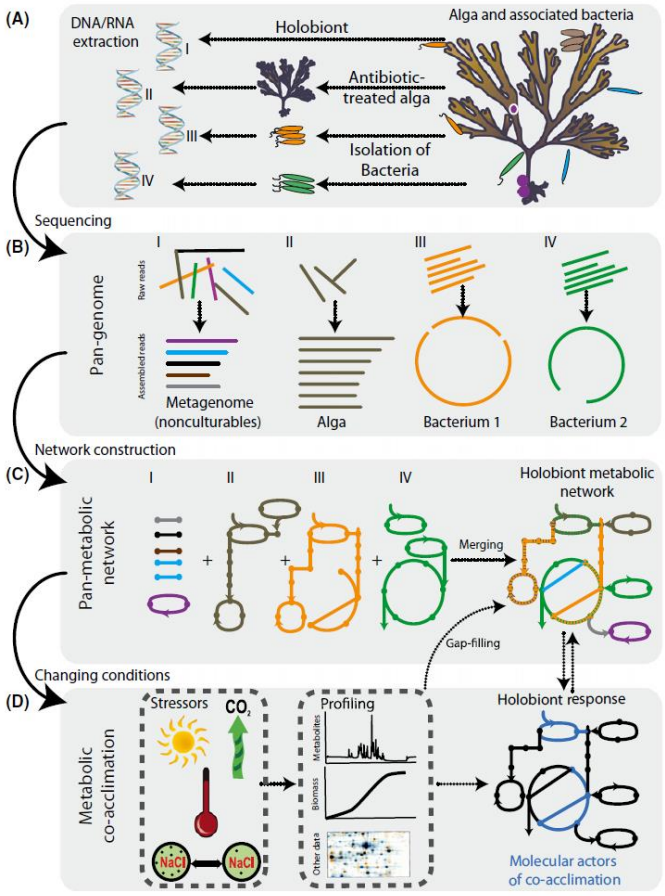

Figure I.17. Schéma expérimental proposé par Dittami et al., (2014) impliquant l'étude des génomes de l'algue et de son microbiote afin de déterminer leur complémentarité métabolique et d'identifier de potentiels processus de co-acclimatation au sein de l'holobionte

D'une manière conceptuelle, l'utilisation des sciences -omiques à l'échelle de l'holobionte peut donc s'effectuer à la fois au niveau de l'hôte et du microbiote. Idéalement, une étude multi-omiques pour caractériser l'ensemble des mécanismes moléculaires de l'holobionte viserait alors à réaliser des approches de génomique, transcriptomique, protéomique et métabolomique la fois pour l'hôte et pour le microbiote (**Figure I.18**). L'intégration de l'ensemble de ces jeux de données permettrait *in fine* une meilleure compréhension des mécanismes d'interactions moléculaires entre ces deux systèmes, résultant finalement en une analyse globale de type intéractomique.

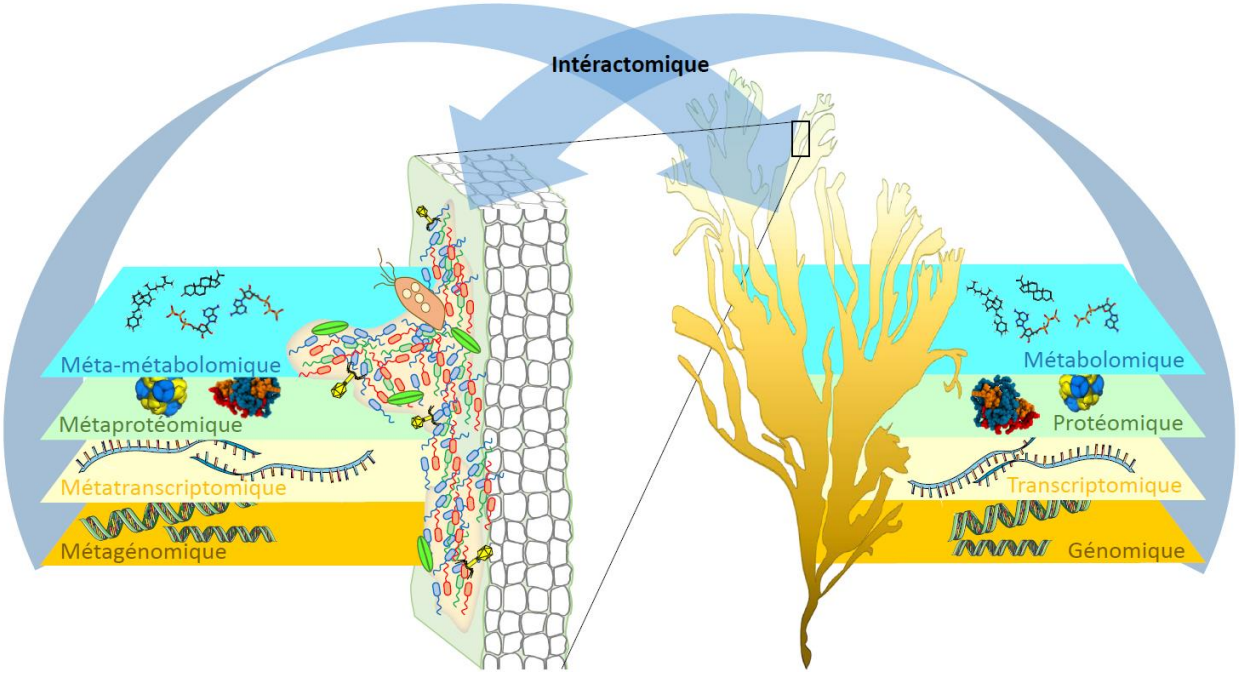

Figure I.18. Schéma conceptuel impliquant l'intégration conjointe des diverses approches -omiques associées d'une part à l'algue et, d'autre part, à son microbiote afin d'étudier l'intéractome de l'holobionte.

Dans l'optique d'intégrer plusieurs jeux de données au sein d'une analyse combinée destinée à améliorer la compréhension de l'ensemble de l'holobionte, deux approches vont être privilégiées dans le cadre de cette thèse :

(i) l'approche de metabarcoding qui constitue une méthode de métagénomique ciblée, par séquençage d'un marqueur génétique, permettant la caractérisation taxonomique et structurelle de l'ensemble de la communauté épiphyte,

(ii) l'approche métabolomique non-ciblée, ici focalisée sur l'étude du métabolome de surface, visant principalement à étudier l'ensemble des métabolites potentiellement impliqués dans les interactions entre l'algue et son microbiote.

5.2.L'approche par métabolomique pour élucider la production chimique à la surface de l'algue

La métabolomique environnementale constitue une science émergente dont l'ensemble des techniques d'analyse permettent d'améliorer la compréhension globale des interactions chimiques entre les organismes et leur environnement (Kuhlisch and Pohnert, 2015). En fonction des questions posées dans le cadre d'une étude en métabolomique, deux types d'approches peuvent être employées :

(i) la métabolomique non-ciblée, dont l'objectif est de fournir sans *a priori* une vision globale des différences métaboliques associées aux différentes conditions de l'étude,

(ii) la métabolomique ciblée, ayant pour but de se concentrer en particulier sur certains métabolites ou des familles spécifiques de métabolites d'intérêts. L'approche ciblée vise alors à développer de manière spécifique des méthodes d'extraction et d'analyse permettant d'optimiser l'étude de ces composés, et ce pour une compréhension plus fine de leurs rôles.

Dans ces deux cas, le choix des méthodologies d'extraction et d'analyse, et plus globalement l'ensemble du design expérimental, constituent des éléments cruciaux pour mener à bien une étude métabolomique visant à répondre aux questions posées.

Ainsi, la résonance magnétique nucléaire (RMN) qui constituait historiquement la technique analytique la plus utilisée en métabolomique présente l'avantage d'être une méthode non destructive, quantitative et particulièrement adaptée pour caractériser la structure chimique de certains métabolites d'intérêts. Par ailleurs, à l'inverse de certaines approches de spectrométrie de masse (*Mass Spectrometry*, MS), cette méthode s'affranchie des biais analytiques associés aux différences drastiques d'ionisation entre molécules.

Malgré ce biais, les plateformes analytiques basées sur une détection MS constituent des outils analytiques offrant une meilleure sensibilité que la RMN et permettant l'analyse, même à des concentrations très faibles, d'une très large gamme de métabolites au sein de matrices complexes (Dettmer et al., 2007; Verpoorte et al., 2008; Theodoridis et al., 2012). Un autre avantage des techniques MS réside aussi dans les temps d'analyses qui sont relativement courts. En outre, la détection MS peut être utilisée seule (*Direct Infusion Mass Spectrometry* : DIMS) ou couplée à diverses techniques chromatographiques permettant ainsi d'éviter la co-élution de certains composés et d'optimiser éventuellement les conditions d'analyses lors d'une approche ciblée. Ainsi, l'utilisation de la chromatographie en phase gazeuse (*Gas Chromatography-Mass spectrometry*, GC-MS) sera privilégiée lors de l'étude de composés volatils alors que la chromatographie en phase liquide (*Liquid Chromatography-Mass spectrometry*, LC-MS) permettra d'analyser un spectre plus large de composés mais avec une résolution analytique moindre. Dans le cadre des analyses chromatographiques, différents types de phases stationnaires peuvent être utilisés permettant d'optimiser la séparation en fonction du métabolome des organismes étudiés ou des métabolites ciblés. Enfin, les méthodes MS en tandem (MS^2 ou MS^n) permettent l'obtention d'ions fragments issus de la dissociation d'ions parents. Cette source d'information peut permettre d'élucider la structure de certains composés, via la reconstruction des voies

de fragmentations de la molécule. En outre, de récentes méthodes déréplicatives (telles que les réseaux moléculaires), ainsi que le partage de banques de données, contribuent au développement exponentiel des outils analytiques basés sur une détection MS en métabolomique (Wang et al., 2016).

Dans le cadre d'une étude portée sur les métabolites à la surface des macroalgues, diverses méthodes d'extraction ont été proposées pour cibler de manière spécifique cette partie du métabolome algal. La méthode dite de trempage constitue l'approche la plus courante. Les travaux de de Nys et al., (1998) ont initialement décrit cette méthodologie sur les Rhodophyceae *D. pulchra* et *Laurencia obtusa*. Deux paramètres essentiels permettent d'optimiser ce protocole d'extraction : le choix du solvant d'extraction et la durée d'immersion du thalle dans le solvant. Divers solvants [par ordre de polarité croissante : *n*-hexane, dichlorométhane (CH_2Cl_2), éther diéthylique et méthanol (MeOH)] ont été testés afin de vérifier s'ils induisaient ou non des lyses cellulaires à la surface de l'algue. Plusieurs temps de trempages ont alors été utilisés (10, 20, 30 et 60s) et les résultats ont montré que le *n*-hexane constituait le solvant le plus adapté pour préserver l'intégrité cellulaire, et ce jusqu'à 60s de trempage. Un tel protocole a ensuite été utilisé pour toutes les études portant sur le métabolome de surface de *D. pulchra* (Dworjanyn et al., 2006). Pour *F. vesiculosus*, un autre protocole basé sur un mélange *n*-hexane/MeOH (1 :1, v/v) pendant 10s a été adopté (Saha et al., 2011) tandis que, dans le cas de *G. vermiculophylla*, les algues ont été trempées dans un mélange CH_2Cl_2/*n*-hexane (1: 4, v / v) pendant 5s (Saha et al., 2016).

Enfin, les travaux d'Othmani et al., (2016a) ont conduit à l'optimisation d'un protocole similaire d'extraction du métabolome de surface dans le cas de *T. atomaria*. Différents systèmes de solvants [*n*-hexane, CH_2Cl_2, mélange CH_2Cl_2/MeOH (1: 1, v/v) et MeOH] et différents temps d'immersion (5, 15, 20, 30, et 60s et 24h) ont été testés. Pour chaque type de solvant, les extraits à 24h ont servi d'extraits totaux constituant ainsi un contrôle positif. Sur la base d'analyses LC-MS et GC-MS ainsi que de l'évaluation de l'intégrité de la membrane cellulaire par microscopie à épifluorescence après marquage au DAPI, les paramètres d'extraction optimisés conduisent à l'utilisation du MeOH avec un temps maximal d'immersion de 15s.

Dans le cadre de cette thèse, le choix d'un temps inférieur (5s) avec le même solvant (MeOH) a été fait pour l'ensemble des extractions du métabolome de surface afin d'assurer le minimum de biais expérimental lié à la présence potentielle de cellules lysées et d'assurer la meilleure reproductibilité analytique possible.

Bien que la méthode d'extraction par trempage soit la plus observée au sein de la littérature, des méthodes alternatives ont été proposées. Les métabolites de surface de thalle de *Dictyota* ont ainsi été

extraits en frottant un écouvillon à leur surface et en procédant alors à l'extraction des composés absorbés sur l'écouvillon pendant plusieurs heures à l'aide d'un mélange MeOH/CH_2Cl_2 (1 :1 ; v/v) (Schmitt et al., 1995). *F. vesiculosus* a également fait l'objet d'autres types d'extraction par simple contact avec des filtres GF/A (Brock et al., 2007) ou encore en plongeant des thalles dans de la silice C18 afin d'adsorber les composés situés au niveau de la couche de surface de l'algue (Cirri et al., 2016). Cependant, dans le cas de *T. atomaria* cette méthode d'extraction à l'aide d'un adsorbant n'a pas donné de résultats concluants en termes de détection de métabolites (Othmani et al., 2016a).

5.3. L'approche métabarcoding complétée par la cytométrie en flux pour étudier le microbiote de surface

Au cours des 25 dernières années, les analyses par séquençage de l'ADN codant l'ARN ribosomal ont permis de considérablement améliorer l'étude de la diversité taxonomique microbienne environnementale, qui était jusqu'alors très largement sous-estimée (Kyrpides, 2009). Ce constat est notamment illustré par le dogme énonçant qu'au sein des environnements marins et des sols, moins de 1% des bactéries sont cultivables dans les conditions standards de culture (Handelsman, 2004; Kyrpides, 2009). L'approche par séquençage de l'ADN constitue une méthode indépendante de la mise en culture (Olsen et al., 1986) et a ainsi permis de considérer une très grande diversité de microorganismes non ou difficilement cultivables. Les approches culturales restent néanmoins indispensables en écologie microbienne, puisqu'elles offrent d'importantes sources d'information sur la biologie des différents modèles isolés avec par exemple l'étude des phénotypes ou encore des mécanismes de régulation génétique par mutagenèse.

Parmi les marqueurs génétiques (aussi appelés gènes « barcodes ») couramment utilisés, celui codant la sous-unité 16S de l'ARN ribosomal constitue le plus usité pour l'étude globale de la diversité procaryotique. D'autres marqueurs s'avèrent particulièrement intéressants pour des analyses plus ciblées, tels le gène *rpoB* pour les Planctomycetes ou les *Vibrio* (Ki et al., 2009; Vos et al., 2012; Bondoso et al., 2013; Ogier et al., 2019). Pour l'étude de la communauté microbienne eucaryote, l'utilisation du gène codant l'ARN 18S est très courante (Vargas et al., 2015; Debroas et al., 2017) tandis que d'autre marqueurs plus spécifiques sont généralement utilisés pour cibler d'autres groupes taxonomiques, tels plusieurs régions de l'ITS (« *internal transcribed spacer* ») chez les fungi (Schoch et al., 2012) ou le gène *rbcL* pour les diatomées (Kermarrec et al., 2013; Rimet et al., 2019).

Initialement étudiée avec la méthode de clonage-séquençage Sanger, et éventuellement couplée en amont avec des méthodes d'empreintes telles que l'électrophorèse sur gel en gradient de dénaturation (DGGE) ou le polymorphisme de longueur de fragments de restriction terminaux (TRFLP), l'analyse de la diversité microbienne a par la suite gagné en résolution avec les avancées des nouvelles technologies de séquençage à haut débit (NGS), telles que les séquençages Roche 454, Ion Torrent ou encore Illumina MiSeq. Cette dernière méthode est d'ailleurs la plus utilisée actuellement. Cependant, ces approches de metabarcoding permettent uniquement d'étudier la structure de la communauté microbienne d'un point de vue taxonomique. De ce fait, le manque d'informations fonctionnelles lié à l'activité de la communauté constitue généralement un facteur qui limite l'interprétation des interactions des microorganismes entre eux ou avec leurs hôtes. Bien que des outils tels que PICRUSt (Langille et al., 2013), Tax4Fun (Aßhauer et al., 2015) ou encore FAPROTAX (Louca et al., 2016) permettent maintenant de fournir un certain nombre d'hypothèses de fonctions référencées au niveau des taxa identifiés, ces approches restent pour autant prédictives et peuvent souvent manquer de représentativité en fonction de la diversité étudiée.

La métagénomique, dont l'objectif est de séquencer l'ensemble des génomes d'une communauté microbienne (et cela indépendamment de la PCR), permet d'identifier un certain nombre de fonctions au sein de ces métagénomes. Des d'études menées sur les métagénomes du microbiote de *D. pulchra* ont notamment permis de déceler des fonctions caractéristiques du microbiote de spécimens blanchis : la présence de facteurs de virulence exprimés sous l'effet d'une augmentation de la température, des fonctions de réponse au stress oxydatif ou encore l'acquisition de nutriments ayant potentiellement un lien avec la pathogénicité (Fernandes et al., 2012; Zozaya-Valdés et al., 2017). Les travaux de Burke et al., (2011a) soulignent par ailleurs l'importance de ces analyses fonctionnelles pour caractériser la communauté microbienne algale. A travers l'étude des fonctions conservées dans l'ensemble des échantillons d'*Ulva australis* (« *functional core* »), les auteurs proposent que l'assemblage de la communauté s'effectuerait à l'échelle de certaines fonctions microbiennes partagées, plutôt qu'à une échelle spécifique d'un point de vue taxonomique. Bien que la métagénomique permette l'exploration d'un large panel de voies fonctionnelles pour l'ensemble d'une communauté microbienne, certaines limites comme le coût d'analyse par échantillon qui s'avère plus important que pour le métabarcoding, peut aussi constituer une limite supplémentaire, notamment dans le cadre de vastes séries d'échantillonnages.

Les approches de séquençage ne permettent cependant pas d'explorer l'aspect quantitatif de la communauté microbienne à la surface de l'algue et des méthodes telles que la microscopie confocale à

balayage laser, la PCR quantitative (qPCR) ciblant des marqueurs universels ou la cytométrie en flux constituent des outils d'analyses complémentaires permettant de pallier ce manque. Les travaux de Maximilien et al., (1998) font notamment état des premières analyses de la densité de bactéries à la surface d'algue avec un dénombrement effectué via l'utilisation d'un microscope électronique à balayage. D'autre approches plus adaptées ont depuis permis d'effectuer de manière similaire un tel dénombrement pour d'autres algues, en utilisant par exemple la microscopie a épifluorescence (Saha et al., 2014). Par ailleurs, bien que des analyses par cytométrie en flux n'aient jamais été effectuées sur des échantillons de microbiote prélevés à la surface de macroalgue, elles s'avèrent adaptées pour l'estimation de la densité de cellules au sein de biofilms formés sur des surfaces abiotiques (Camps et al., 2014; Pollet et al., 2018). Une telle approche pourrait être aisément adaptée à d'autres types de surfaces, notamment biotiques telles que celles des macroalgues.

5.4. Objectifs et organisation de la thèse

L'objectif général de la thèse est de comprendre comment varie la structure de la communauté bactérienne du microbiote de surface de *T. atomaria* en lien avec les variations de la production métabolique de surface de l'hôte et quelle est l'influence de l'environnement sur ces variations qui affectent et façonnent l'holobionte. Avec l'idée principale que le métabolome de surface de l'algue constitue un facteur-clé induisant, ou étant associé, à la structure de la communauté épibactérienne, le but est de mieux comprendre les liens unissant ces deux volets (bactéries/molécules) intrinsèquement liés l'un à l'autre. Cet objectif inclut par ailleurs la recherche d'une meilleure compréhension des paramètres, qu'ils soient biotiques ou abiotiques, associés aux variations du métabolome de surface et de la communautés épibactérienne de *T. atomaria.*

Ces objectifs trouvent leur source dans une étude multi-omiques (métabolomique/metabarcoding) préliminaire menée avec des échantillons issus d'une campagne de prélèvement de *T. atomaria* sur le site de Carqueiranne (Var, France) de février à juillet 2013 (Thèse A. Othmani). Cette étude a conduit à utiliser des analyses récentes d'acquisition de données et de coupler les informations issues du métabolome de surface et des communautés épibactériennes via l'intégration statistique des deux jeux de données (PLS-DA multi-blocs ; MixOmics) (Paix et al., 2019).

À la suite de cette étude préliminaire et des travaux précédents menés au sein du laboratoire MAPIEM sur *T. atomaria*, plusieurs questions scientifiques ont été identifiées et seront développées dans le cadre

de cette thèse. Ces questions sont résumées avec le schéma présenté **Figure I.19** et certaines d'entre elles ont été traitées au sein d'une même étude.

A un niveau plus global et sachant que les prélèvements précédents d'échantillons de *T. atomaria* se sont cantonnés à un seul site (Carqueiranne) de la région toulonnaise, il est intéressant d'analyser les variations du métabolome de surface et des communautés épibactériennes à une échelle géographique plus large en intégrant une étude phylogénétique de *T. atomaria* (totalité des côtes méditerranéennes françaises et côtes nord de la Bretagne).

↳ **Question 1 :** *La biogéographie et la phylogénie de l'hôte* T. atomaria *influencent-elles ses communautés et son métabolome de surface ?*

Afin de pouvoir discuter des interactions chimiques de surface entre l'hôte et la communauté bactérienne présente à sa surface, il est primordial d'identifier les métabolites d'intérêt du métabolome de surface. Il s'agit à l'heure actuelle de la difficulté majeure de la plupart des études menées en écologie chimique marine via des approches métabolomiques.

↳ **Question 2 :** *Comment annoter et optimiser l'annotation du métabolome d'un organisme (marin) non-modèle tel que* T. atomaria *?*

En outre, ayant préalablement fixé le protocole d'extraction du métabolome de surface de *T. atomaria* et ayant fait le choix d'une analyse métabolomique basée sur la MS, il s'avère néanmoins indispensable de sélectionner l'outil analytique le plus adapté à notre modèle et aux échantillons étudiés.

↳ **Question 3 :** *Quel est la plateforme analytique la plus adaptée pour obtenir la meilleure couverture du métabolome de surface de* T. atomaria *et l'information écologique la plus pertinente ?*

Les travaux préliminaires ayant porté sur l'étude de l'intégralité du thalle de *T. atomaria*, il est donc crucial de déterminer s'il existe des variations du métabolome et de la communauté bactérienne de surface à l'échelle d'un individu et si elles sont corrélées entre-elles.

↳ **Question 4 :** *Quelles sont les variations intra-thalles du métabolome et des communautés bactériennes à la surface de* T. atomaria *et quels sont leurs liens ?*

Les précédents travaux réalisés par notre équipe sur le modèle *T. atomaria* (Othmani et al., 2016a, 2016b) ont révélé la présence à la surface de cette algue de molécules déjà décrites pour leur effet sur les communautés bactériennes de surface et/ou ont permis de montrer pour certaines d'entre-elles des activités anti-adhésion marquées et quelquefois sélectives vis-à-vis d'un panel de souches bactériennes marines. Néanmoins, l'un des questionnements majeurs dans le contexte de ces travaux est de vérifier que l'hypothèse émise de la sélection de la communauté épibactérienne par l'hôte algal soit valide.

A un niveau plus local et en partenariat avec le Parc National de Ports Cros, l'un des objectifs principaux de cette thèse est d'étudier la spécificité des communautés épibactériennes de *T. atomaria* et d'identifier si des paramètres physico-chimiques peuvent structurer ces communautés et/ou impacter leur hôte via son métabolome de surface. Pour cela, une étude spatio-temporelle sur cinq sites de l'aire toulonnaise (incluant la Petite Rade très anthropisée et des sites sur l'ile de Porquerolles) a été menée sur un an.

↳ **Questions 5 et 6 :** *L'environnement influence-t-il les variations spatio-temporelles des communautés épibactériennes et du métabolome de surface de T. atomaria* ? *Quelle est la spécificité de la communauté bactérienne de surface de* T. atomaria *?*

En accord avec les résultats de l'étude préliminaire montrant une variation temporelle marquée au niveau du microbiote et du métabolome de surface de *T. atomaria* et en lien avec des scénarios futurs impliquant une élévation des températures et une augmentation d'épisodes météorologiques extrêmes, une étude expérimentale en mésocosmes a été mise en œuvre. Elle vise non seulement à observer l'impact respectif et combiné de la température et de l'intensité lumineuse (deux paramètres variant de manière similaire *in situ*) sur les variations du microbiote et du métabolome de surface de *T. atomaria*, mais également à étudier la cinétique des réponses respectives de ces deux composantes de l'holobionte à ses deux facteurs.

↳ **Question 7 :** *Quel est l'effet spécifique de variations de la température et de l'intensité lumineuse vis-à-vis du microbiote et du métabolome de surface de* T. atomaria *et quelles sont leurs cinétiques de réponse effectives ?*

Enfin une dernière étude présentée en annexe aborde les liens potentiels entre les métabolites de surface et les communautés eucaryotes épiphytes de quatre Dictyotaceae, dont *T. atomaria*, prélevées dans la baie de Villefranche-sur-Mer. L'objectif spécifique de ce travail est de déterminer si la colonisation de la surface de ces macroalgues par le dinoflagellé toxique *Ostreopsis* cf. *ovata*, dont les proliférations sont par ailleurs de plus en plus préoccupantes en mer Méditerranée, pouvait être influencée par la production métabolique des différentes Dictyotacées échantillonnées.

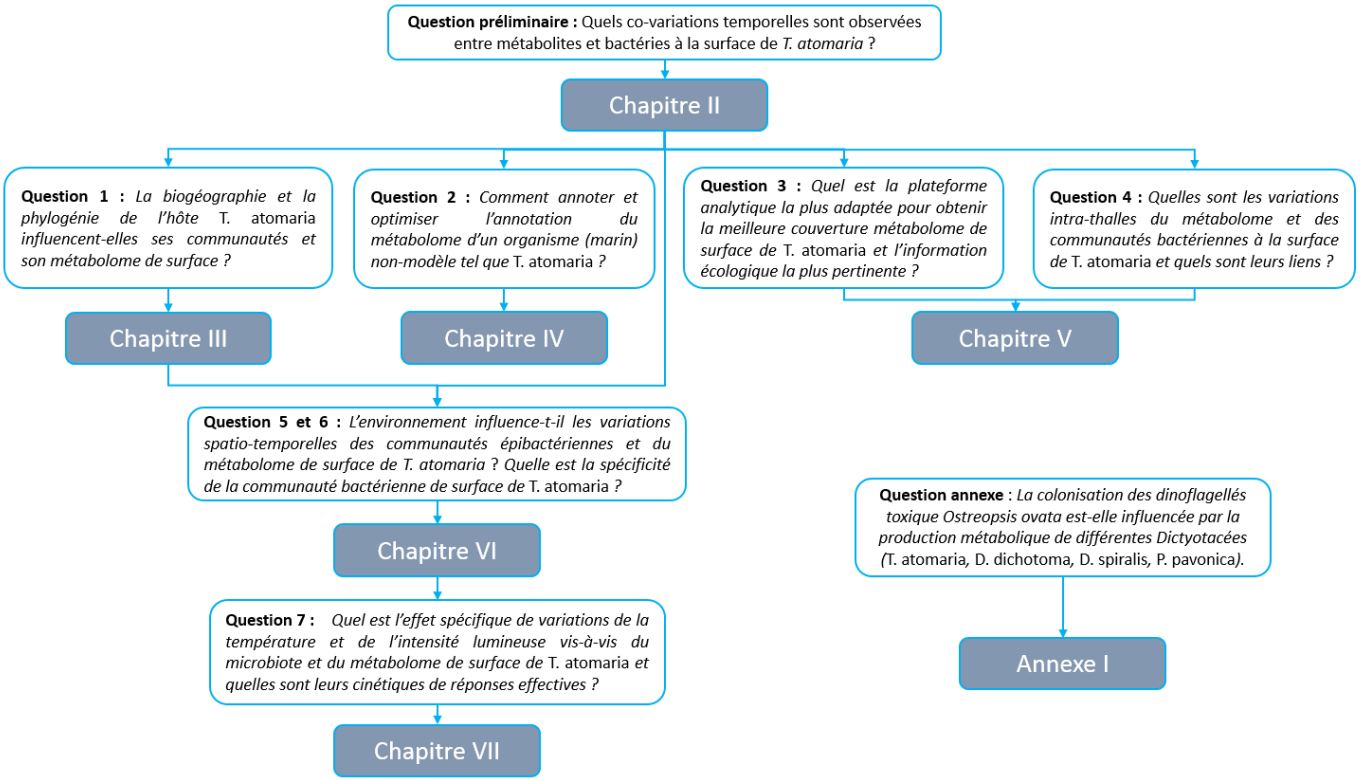

Figure I.19. Organisation des différents objectifs et questions de la thèse, associés à chaque chapitre

CHAPITRE II : ETUDE PRELIMINAIRE

Plage de Pins Penchés à Carqueiranne

1. Avant-propos

Cette première étude est une analyse préliminaire menée avec les échantillons issus d'une campagne de prélèvement de *T. atomaria* sur le site de Carqueiranne (Var, France) de février à juillet 2013 (Thèse A. Othmani). L'étude propose d'explorer les variations temporelles du microbiote et du métabolome à la surface de l'algue *T. atomaria*, via une approche multi-omiques intégrant les deux jeux de données multivariées obtenus par metabarcoding et métabolomique. Cette étude est présentée sous la forme d'un article de recherche publié dans la revue *Environmental Microbiology* [Paix et al., (2019). *Environ. Microbiol.* 21, 3346–3363. doi:10.1111/1462-2920.14617]. Les références bibliographiques citées dans cet article sont indexées en fin de manuscrit. La partie *Supplementary Information* de cet article est presentée dans l'annexe II du manuscrit (annexe électronique).

2. Article: Temporal covariation of epibacterial community and surface metabolome in the Mediterranean seaweed holobiont *Taonia atomaria*

Benoit Paix[1#], Ahlem Othmani[1#], Didier Debroas[2], Gérald Culioli[1]* and Jean-François Briand[1]*

[1] Université de Toulon, Laboratoire MAPIEM, EA 4323, Toulon, France.

[2] Université Clermont Auvergne, CNRS, Laboratoire Microorganismes: Génome et Environnement, UMR 6023, Clermont–Ferrand, France

[#] These authors contributed equally to this work

*Corresponding authors: J.-F. Briand (briand@univ-tln.fr) and G. Culioli (culioli@univ-tln.fr)

Running head:

Surface community and metabolome in *T. atomaria*

2.1.Summary

An integrative multi-omics approach allowed monthly variations for a year of the surface metabolome and the epibacterial community of the Mediterranean Phaeophyceae *Taonia atomaria* to be investigated. The LC-MS-based metabolomics and 16S rDNA metabarcoding datasets were integrated in a multivariate meta-omics analysis (multi-block PLS-DA from the MixOmic DIABLO analysis) showing a strong seasonal co-variation (Mantel test: $p < 0.01$). A network based on positive and negative correlations between the two datasets revealed two clusters of variables, one relative to the "spring period" and a second to the "summer period". The "spring period" cluster was mainly characterised by dipeptides positively correlated with a single bacterial taxon of the Alteromonadaceae family (BD1-7 clade). Moreover, "summer" dominant epibacterial taxa from the second cluster (including Erythrobacteraceae, Rhodospirillaceae, Oceanospirillaceae and Flammeovirgaceae) showed positive correlations with few metabolites known as macroalgal antifouling defences [e.g. dimethylsulphoniopropionate (DMSP) and proline] which exhibited a key role within the correlation network. Despite a core community that represents a significant part of the total epibacteria, changes in the microbiota structure associated with surface metabolome variations suggested that both environment and algal host shape the bacterial surface microbiota.

Keywords: Holobiont, Phaeophyceae, microbiota, surface metabolome, metabarcoding, metabolomics, multi-omics, biofilm, chemical communication

2.2.Introduction

The major ecological importance of marine macroalgae in coastal ecosystems no longer needs to be demonstrated, as these organisms play several crucial roles (e.g. oxygen production, source of food and energy, building and protective habitats). As for all immersed surfaces in seawater, seaweeds are colonised by microbial communities. Recently, several studies on the diversity and functions of algal surface-associated microbial communities led to a modification in the conceptual consideration of the relationships between these microbiomes and their basibionts. Diversified and species-specific bacterial communities have been described on seaweeds found in tropical coral reefs and the authors have proposed to apply the concept of holobionts to such biological systems. Primarily developed for corals (Rosenberg et al., 2007; Barott et al., 2011), the concept of the holobiont and hologenome have been rapidly extended to many multicellular eukaryotic hosts from plants to animals, including humans (Bordenstein and Theis, 2015). Recent advances in discussions of the concept of holobiont (Theis et al., 2016) confirmed the relevance applying it to seaweeds. Indeed, holobionts do not have to be restricted to special processes but should constitute “a wider vocabulary and framework for host biology in light of the microbiome”.

Few algal models have been studied to date and elucidation of host/microbiome relationships in the case of seaweeds remains to be unravelled (Egan et al., 2013; Hollants et al., 2013; Florez et al., 2017). However, the literature exhibits the crucial role that epibiotic bacterial communities may play in a wide range of ecological interactions, especially via chemicals (Wichard and Beemelmanns, 2018). In particular, the Rhodophyta *Delisea pulchra* has been intensively studied with respect to particular chemically-mediated interactions (i.e. quorum sensing modulation via the production of halogenated furanones) between the seaweed and its epibacterial community, including pathogens that can be involved in the temperature-dependent bleaching process (Fernandes et al., 2011; Harder et al., 2012; Zozaya-Valdés et al., 2017). More recently, the role of bacterial communities associated with the invasive Rhodophyta *Asparagopsis* spp. in southwestern Iberia (Aires et al., 2016), the Phaeophyceae *Lobophora* spp. which outcompete corals in New Caledonia (Vieira et al., 2016) or crustose coralline algal species that facilitate coral larval settlement (Sneed et al., 2015), has also been investigated. Among Phaeophyceae, kelp forests involving Laminariales species exhibit taxonomically diverse bacterial communities in time and space, without a clear relationship to environmental patterns (Michelou et al., 2013; Marzinelli et al., 2015; Lemay et al., 2018b). Considering the Phaeophyceae *Ecklonia radiata* in Australia, as for *D. pulchra*, bleaching has been identified as a stronger driver for bacterial communities than environmental parameters such as temperature or light (Marzinelli et al., 2015). The surface-associated bacterial

communities of the Phaeophyceae *Fucus vesiculosus* from the Western Baltic Sea shores have been found to vary seasonally and be algal species-specific (Lachnit et al., 2011). In addition, temperature and salinity shifts appear to modify the α-diversity as well as the composition of these bacterial communities (Stratil et al., 2013, 2014). Dimethylsulphoniopropionate (DMSP), proline and fucoxanthin, identified at the surface of *F. vesiculosus,* inhibit bacterial attachment (Saha et al., 2011, 2012) and mainly impact the abundance of surface communities (Lachnit et al., 2013). In addition, surface metabolites, including those mediating epibiotic bacterial communities, exhibit seasonal variations related to light and temperature (Saha et al., 2014; Rickert et al., 2016b).

Conversely, it has also been shown that high phylogenetic variability in bacterial species composition on the Chlorophyta *Ulva australis* was associated with a similar functional composition. These results suggest that the structure of bacterial communities may be addressed at the functional level (Burke et al., 2011a, 2011b). In accordance with these findings, different microbial communities have been shown to affect algal growth and development, and morphology of *Ulva intestinalis* and *U. mutabilis* (Spoerner et al., 2012; Grueneberg et al., 2016; Ghaderiardakani et al., 2017). The same research group has more recently demonstrated that DMSP produced by *U. mutabilis* may be used by bacterial strains involved in algal morphogenesis to detect the presence of the alga as a food source (glycerol boundary layer) (Kessler et al., 2018).

Taonia atomaria (Woodward) J. Agardh (family Dictyotaceae, class Phaeophyceae, phylum Ochrophyta) is an annual photophilic species of the infralittoral zone, located in calm areas, with a higher abundance in the early summer and very small numbers of individuals from late summer to late winter (Sala and Boudouresque, 1997). This intertidal seaweed, widely reported along the Mediterranean and North-Eastern Atlantic coasts, presents a flat thallus appropriate for surface microbiota investigations. In addition, *T. atomaria* has been previously shown to produce compounds with antifouling properties (Othmani et al., 2016b). Some of these active molecules, such as sn-3-*O*-(geranylgeranyl)glycerol or (-)-gleenol (Fig. SII.1), are exuded at its surface and could be involved in the selection of specific epibacterial communities (Othmani et al., 2016a).

Metabolomics, an emerging approach among the omics sciences, is defined as the qualitative and quantitative analysis of a wide range of metabolites in a biological sample at a specific time (Johnson et al., 2016). Its application to specifically determine seaweed surface metabolomes that can originate from both algae and surface microbiota may provide valuable information on their putative interactions.

The aim of this study was to further explore the temporal variations of both the surface metabolome and the epibacterial community of *T. atomaria* in a north-western Mediterranean shore. Thus, a multi-omics analysis was performed to deal with the underlying ecological question about the links between the surface microbiota and the metabolites found at the algal surface, including chemical compounds that could be involved in the defence mechanisms of the host. By coupling meta-omics approaches, new functional insights of biofilm communities can be unravelled, enabling an improved understanding of marine seaweed holobionts.

2.3.Results

2.3.1. Monitoring of the surface metabolome of T. atomaria

Thalli of *T. atomaria* were collected in triplicate at the same site from the infratidal zone, each month during the presence of alga from February to July. After the selective extraction of surface compounds using a previously reported specific protocol (Othmani et al., 2016a), the resulting samples were analysed by LC-MS (See chemical profiles in Fig S2). Treatment of the raw MS data with the XCMS package under R environment gave a primary dataset with 3,065 *m/z* features and, after data filtering, the final dataset was composed of 429 variables (Dataset S1). The PCA score plot for all samples displayed a homogeneous pattern of quality control (QC) samples and blanks, indicating the high stability and repeatability of the analytical instrument (Fig. SII.3). Taking into account only algal samples, a second PCA score plot was built which clearly indicated an unsupervised clustering of the chemical profiles of surface extracts of *T. atomaria* into three distinct groups: (i) “winter” (February and March), (ii) “spring” (April and May) and (iii) “summer” (June and July) samples (Permutational multivariate analysis of variance: PERMANOVA, $p < 0.05$). A separation between the “winter” cluster and the other two clusters was mainly observed on the first component (19.2% of the total variance), while the second component (15.9% of the total variance) allowed the discrimination between “spring” and “summer” samples (**Figure II.1A**).

A second step of this analysis was to build a supervised discriminative model using PLS-DA to determine which surface compounds were implicated in the discrimination between the three groups of samples. In such a model, the variable importance in projection (VIP) score values, commonly used for biomarker selection, indicated the importance of each *m/z* feature in the discrimination between specific sample classes (Fig. SII.4).

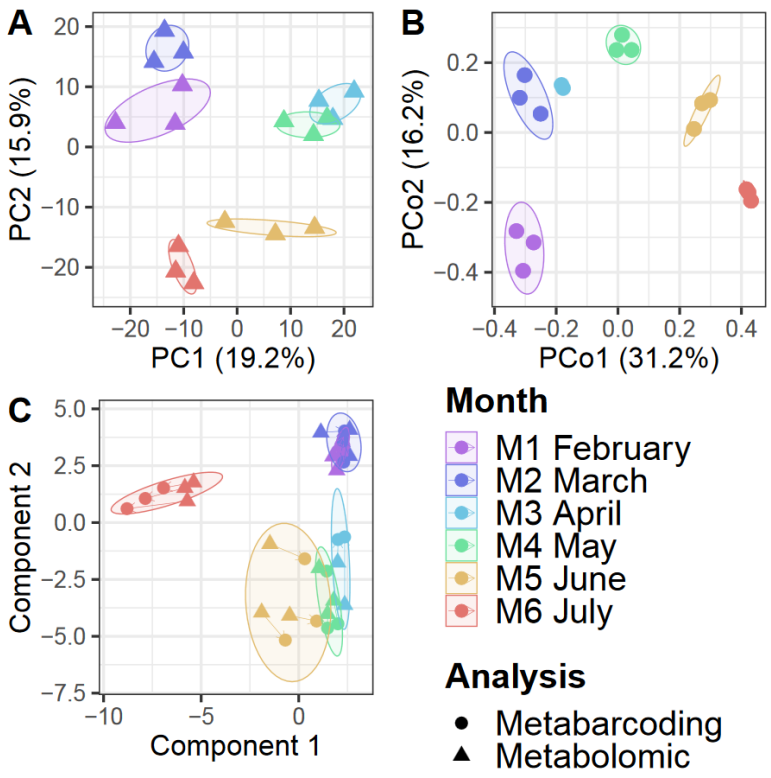

Figure II.1. Seasonal structuring of the surface (A) metabolome (PCA) and (B) microbiota (PCoA) of *T. atomaria.* (C) showed the score plot of the multi-block PLS-DA (DIABLO analysis) built with the metabolomics and metabarcoding datasets. Ellipses are grouping replicates from each month with 70% of confidence for the PCA ordination (A), 90% for the PCoA ordination (B), and 85% for the DIABLO ordination (C).

Focus was paid to those variables with a VIP score >2, corresponding to VIP with scores above the linear regression (Fig. SII.4B). For each VIP, a molecular formula was proposed based on accurate mass measurement, isotopic patterns and MS/MS data. In most of the cases, a putative identification was proposed (**Table II.1** and Fig. SII.5 to SII.22) and for three VIPs (DMSP, proline and proline betaine) the identification was strengthened by the comparison of the data with those of commercial standards. In relation to these results, organisation of the whole MS/MS dataset using the Global Natural Products Social (GNPS) molecular networking workflow allowed a global view of clusters containing VIPs (**Figure II.2**) (Wang et al., 2016). The main cluster (A) was composed of non-phosphorus betaine lipids identified as diacylglycerylhydroxymethyl-*N*,*N*,*N*-trimethyl-β-alanine (DGTA) derivatives on the basis of the diagnostic fragment ion (*m/z* 236.149, $C_{10}H_{22}NO_5$) for their polar group (Fig. SII.8, SII.10, SII.13 and SII.18). This class of lipids could be distinguished from the closely-related diacylglyceryl-*N*,*N*,*N*-trimethylhomoserines (DGTS) via the absence of a characteristic loss of *m/z* 87 (Roche and Leblond, 2010). This cluster could be divided in two groups constituted by mono- (*lyso*-DGTA) and diacyl (DGTA) derivatives, respectively. A second

cluster (C) was composed of dipeptides which were putatively characterised using their MS and MS/MS data, and these data were compared with online databases (Fig. SII.14, SII.17, SII.20 and SII.21).

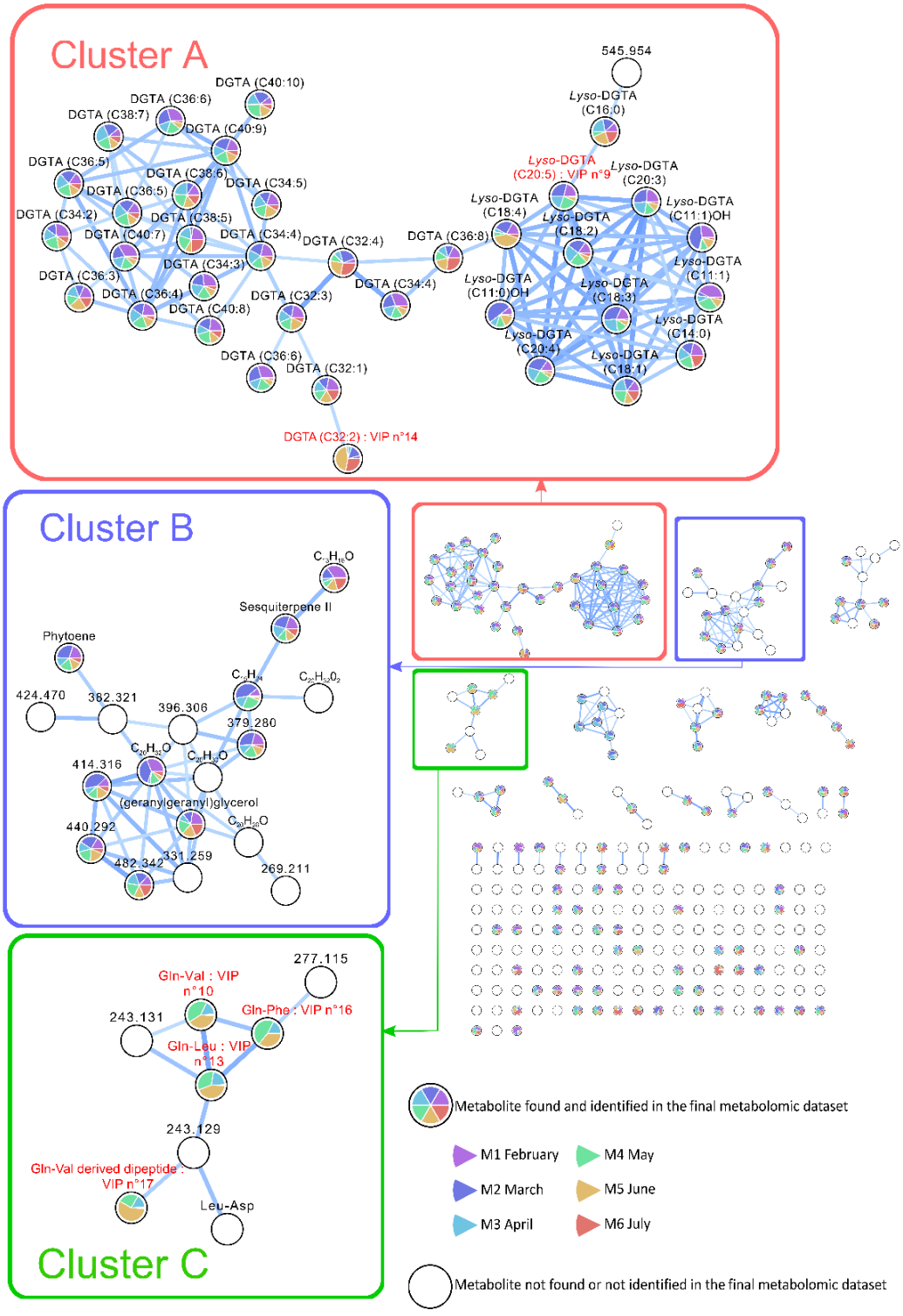

Figure II.2. Molecular network of HRMS fragmentation data obtained from surface extracts of *T. atomaria* (collected monthly from February to July).

More than half of the 19 VIPs (**Table II.1**) were amino acids or derivatives, such as dipeptides, and DGTAs. The main part of the VIPs (e.g. proline betaine, DMSP, ceramides and most of the DGTAs) was over-expressed in June and July samples while dipeptides were mostly produced in May and June samples. *Lyso*-DGTA (C20:5) was the only VIP to be more abundant in “spring” and “winter” samples than in “summer” ones.

VIP N°	*m/z*	RT (s)	VIP score	Formula	Mass error (ppm)	mσ[a]	MS/MS fragment ions (relative abundance in %)	Putative identification[b]	Feb.	Mar.	Apr.	May	Jun.	Jul.
1	144.1018	55	4.3	$C_7H_{14}NO_2$	0.5	4.5	144.1018 $[M + H]^+$ (100), 102.0548 $[C_4H_8NO_2]^+$ (2), 84.0807 $[C_5H_{10}N]^+$ (25), 58.0650 $[C_3H_8N]^+$ (19)	Proline betaine						
2	135.0473	53	3.2	$C_5H_{11}O_2S$	0.8	4.5	135.0473 $[M + H]^+$ (25), 73.0282 $[C_3H_5O_2]^+$ (100), 63.0261 $[C_2H_7S]^+$ (92), 61.0104 $[C_2H_5S]^+$ (4), 55.0177 $[C_3H_3O]^+$ (8)	DMSP						
3	538.5195	710	3.1	$C_{34}H_{68}NO_3$	-0.3	5.5	520.5096 $[M - H_2O + H]^+$ (2), 502.4972 $[M - 2\,H_2O + H]^+$ (1), 282.2794 $[M - H_2O - C_{16}H_{30}O + H]^+$ (21), 264.2687 $[M - 2\,H_2O - C_{16}H_{30}O + H]^+$ (100), 252.2688 $[C_{17}H_{34}N]^+$ (12)	Ceramide (dC18:1/C16:0)						
4	860.6397	700	3.1	$C_{54}H_{86}NO_7$	0.6	19.7	860.6397 $[M + H]^+$ (100), 550.4108 $[M - C_{22}H_{30}O + H]^+$ (13), 548.3949 $[M - C_{22}H_{32}O + H]^+$ (22), 546.3791 $[M - C_{22}H_{34}O + H]^+$ (13), 236.1506 $[C_{10}H_{22}NO_5]^+$ (5)	DGTA (C44:10)						
5	116.0706	51	2.9	$C_5H_{10}NO_2$	-0.3	3.4	116.0706 $[M + H]^+$ (2), 70.0652 $[M - HCO_2H + H]^+$ (100)	Proline						
6	856.6093	679	2.8	$C_{54}H_{82}NO_7$	-0.8	4.2	856.6093 $[M + H]^+$ (100), 546.3791 $[M - C_{22}H_{30}O + H]^+$ (67), 528.3690 $[M - C_{22}H_{30}O - H_2O + H]^+$ (11), 236.1491 $[M - 2\,C_{22}H_{30}O + H]^+$ (7)	DGTA (C22:6/C22:6)						
7	201.1637	689	2.8	$C_{15}H_{21}$	0.6	18.4	159.1167 $[C_{12}H_{15}]^+$ (29), 145.1012 $[C_{11}H_{13}]^+$ (100), 131.0856 $[C_{10}H_{11}]^+$ (9), 105.0697 $[C_8H_9]^+$ (10), 57.0697 $[C_4H_9]^+$ (7)	Sesquiterpene IV						
8	324.3260	649	2.8	$C_{21}H_{42}NO$	-2.0	3.4	324.3260 $[M + H]^+$ (100), 306.3157 $[M - H_2O + H]^+$ (5), 284.2947 $[C_{18}H_{38}NO]^+$ (20), 282.3161 $[C_{19}H_{40}N]^+$ (10), 110.0973 $[C_7H_{12}N]^+$ (18), 84.0808 $[C_5H_{10}N]^+$ (12)	$C_{21}H_{41}NO$						
9	520.3630	489	2.7	$C_{30}H_{50}NO_6$	-1.5	6.7	520.3630 $[M + H]^+$ (100), 236.1492 $[M - C_{20}H_{28}O + H]^+$ (4)	*Lyso*-DGTA (C20:5)						
10	246.1447	62	2.6	$C_{10}H_{20}N_3O_4$	1.0	1.5	228.1341 $[M - H_2O + H]^+$ (32), 183.1125 $[C_9H_{15}N_2O_2]^+$ (45), 138.0910 $[C_8H_{12}NO^+]^+$ (5), 118.0862 $[C_5H_{12}NO_2]^+$ (26), 101.0710 $[C_4H_9N_2O^+]^+$ (8), 84.0444 $[C_4H_6NO]^+$ (100), 83.0602 $[C_4H_7N_2]^+$ (60), 72.0807 $[C_4H_{10}N]^+$ (69)	Gln-Val						
11	741.6140	621	2.5	$C_{44}H_{86}O_6P$	2.2	9.4	601.5197 $[C_{39}H_{69}O_4]^+$ (100), 445.2961 $[C_{27}H_{41}O_5]^+$ (30), 339.2889 $[C_{21}H_{39}O_3]^+$ (39), 184.0735 $[C_5H_{11}O_4P + NH_4^+]^+$ (84)	n.d.[c]						
12	510.4886	694	2.5	$C_{32}H_{64}NO_3$	-0.9	11.2	492.4776 $[M - H_2O + H]^+$ (2), 474.4672 $[M - 2\,H_2O + H]^+$ (1), 282.2792 $[M - H_2O - C_{14}H_{26}O + H]^+$ (22), 264.2686 $[M - 2\,H_2O - C_{14}H_{26}O + H]^+$ (100), 252.2686 $[C_{17}H_{34}N]^+$ (15)	Ceramide (dC18:1/C14:0)						
13	260.1605	77	2.4	$C_{11}H_{22}N_3O_4$	-0.2	12.3	242.1498 $[M - H_2O + H]^+$ (29), 197.1283 $[C_{10}H_{17}N_2O_2]^+$ (27), 196.1449 $[C_{10}H_{18}N_3O]^+$ (16), 132.1016 $[C_6H_{14}NO_2^+]^+$ (20), 129.0659 $[C_5H_9N_2O_2]^+$ (11), 101.0709 $[C_4H_9N_2O]^+$ (8), 86.0964 $[C_5H_{12}N]^+$ (84), 84.0443 $[C_4H_6NO]^+$ (100), 83.0602 $[C_4H_7N_2]^+$ (59)	Gln-Leu[d]						
14	708.5776	695	2.4	$C_{42}H_{78}NO_7$	-0,5	11.1	708.5776 $[M + H]^+$ (100), 498.3782 $[M - C_{14}H_{26}O + H]^+$ (7), 472.3629 $[M - C_{16}H_{28}O + H]^+$ (21), 446.3474 $[M - C_{18}H_{30}O + H]^+$ (20), 236.1495 $[C_{10}H_{22}NO_5]^+$ (5)	DGTA (C32:2)						
15	583.4353	659	2.3	$C_{37}H_{59}O_5$	0.7	12.7	583.4353 $[M + H]^+$ (26), 565.4250 $[M - H_2O + H]^+$ (5), 335.2585 $[C_{21}H_{35}O_3]^+$ (100), 305.2111 $[C_{19}H_{29}O_3]^+$ (16), 261.2213 $[C_{18}H_{29}O]^+$ (13), 231.1743 $[C_{16}H_{23}O]^+$ (38), 81.0698 $[C_6H_9]^+$ (52)	DAG (C18:3/C16:4)						
16	294.1444	126	2.3	$C_{14}H_{20}N_3O_4$	-0.0	4.6	276.1350 $[M - H_2O + H]^+$ (28), 231.1120 $[C_{13}H_{15}N_2O_2]^+$ (19), 166.0865 $[C_9H_{12}NO_2]^+$ (57), 120.0807 $[C_8H_{10}N]^+$ (100), 101.0712 $[C_4H_9N_2O]^+$ (10), 84.0446 $[C_4H_6NO]^+$ (64), 83.0599 $[C_4H_7N_2]^+$ (63)	Gln-Phe						
17	229.1182	162	2.1	$C_{10}H_{17}N_2O_4$	0.4	2.9	183.1124 $[C_9H_{15}N_2O_2]^+$ (11), 118.0863 $[C_5H_{12}NO_2]^+$ (14), 84.0444 $[C_4H_6NO]^+$ (100), 72.0806 $[C_4H_{10}N]^+$ (78)	Gln-Val derived dipeptide						
18	331.0116	99	2.0	$C_{12}H_{11}O_9S$	0.7	9.6	251.0550 $[M - SO_3 + H]^+$ (57), 233.0451 $[M - SO_3 - H_2O + H]^+$ (70), 209.0445 $[C_{10}H_9O_5]^+$ (23), 205.0501 $[C_{11}H_9O_4]^+$ (23), 191.0333 $[C_{10}H_7O_4]^+$ (17), 165.0544 $[C_9H_8O_3]^+$ (50), 163.0395 $[C_9H_7O_3]^+$ (35), 139.0391 $[C_7H_7O_3]^+$ (100)	Difucol-*O*-sulfate						

Color code[e]: 3 / 2.5 / 0 / -2.5 / -5

Table II.1. List of the biomarkers (VIP score ≥ 2) identified by LC–HRMS for the seasonal discrimination of the surface extracts of *T. atomaria*. [a] Constructor statistical match factor (comparison of theoretical and experimental isotopic patterns). [b] Abbreviations: DAG: diacylglycerol, DGTA: diacylglycerylhydroxymethyl-N,N,N-trimethyl-*β*-alanine, DMSP: dimethylsulfoniopropionate, Gln: glutamine, Ile: isoleucine, Leu: leucine, Phe: phenylalanine, Val: valine; [c] n.d.: not determined; [d] Not distinguishable from Gln-Ile. [e] Color code represents mean normalized concentrations values.

In addition, attention was focused on annotated compounds [compounds previously detected at the surface of the thalli of *T. atomaria* (Othmani et al., 2016a) or already studied in previous ecological studies (e.g. fucoxanthin, mannitol)], in order to evaluate their temporal fluctuations (**Figure II.3**). The biosynthesis of fucoxanthin, geranylgeranylglycerol and sesquiterpenes I, II and V was fairly constant during the survey ($p > 0.05$), while those of mannitol showed a slight decline during summer ($p < 0.05$). Despite significant differences ($p < 0.05$), samples collected in winter and summer exhibited the highest amounts of sesquiterpene III. Finally, proline, DMSP and sesquiterpene IV were more present at the algal surface in summer than in the winter, with the highest production level being reached in June for proline (VIP n°1), in June and July for DMSP (VIP n°2) and in July for sesquiterpene IV (VIP n°7) ($p < 0.05$). Moreover, with the aim of determining how the richness of the chemical production of *T. atomaria* varied according to season, an estimate of the algal chemodiversity was determined using the Shannon index (Fig. 4A). The algal chemodiversity increased significantly from March to July ($p < 0.05$).

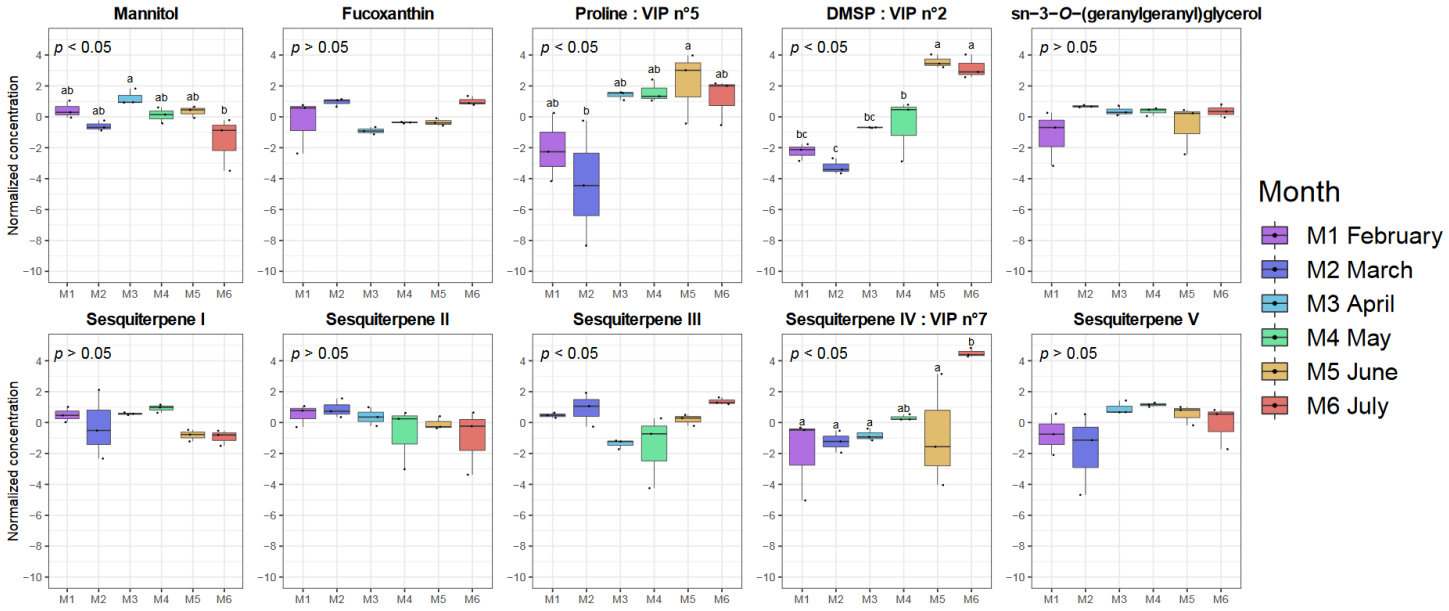

Figure II.3. Seasonal variations of some selected surface metabolites of *T. atomaria*. Individual metabolites obtained after UPLC-MS analysis were normalised by the sum, log10-transformed and mean-centred. A one-way ANOVA followed by post-hoc tests (HSD) allowed to show significant variations for relative concentrations of each metabolite during the year.

2.3.2. 16S rDNA gene based analysis of epibiotic bacterial communities of T. atomaria

The 16S rDNA gene was amplified and sequenced for three thalli replicates for each month from February to July. In total, 1 556 091 sequences and 63 494 OTUs were obtained with the Illumina MiSeq

sequencing. Samples were rarefied to the lowest number of sequences ie 11 469. One sample collected in April was removed from the analysis due to DNA contamination. α-diversity indexes indicated highly diversified communities with a significant trend observed for the Simpson index by decreasing from February to April before increasing from April to July ($p < 0.05$) (**Figure II.4B**, **4C** and **4D**).

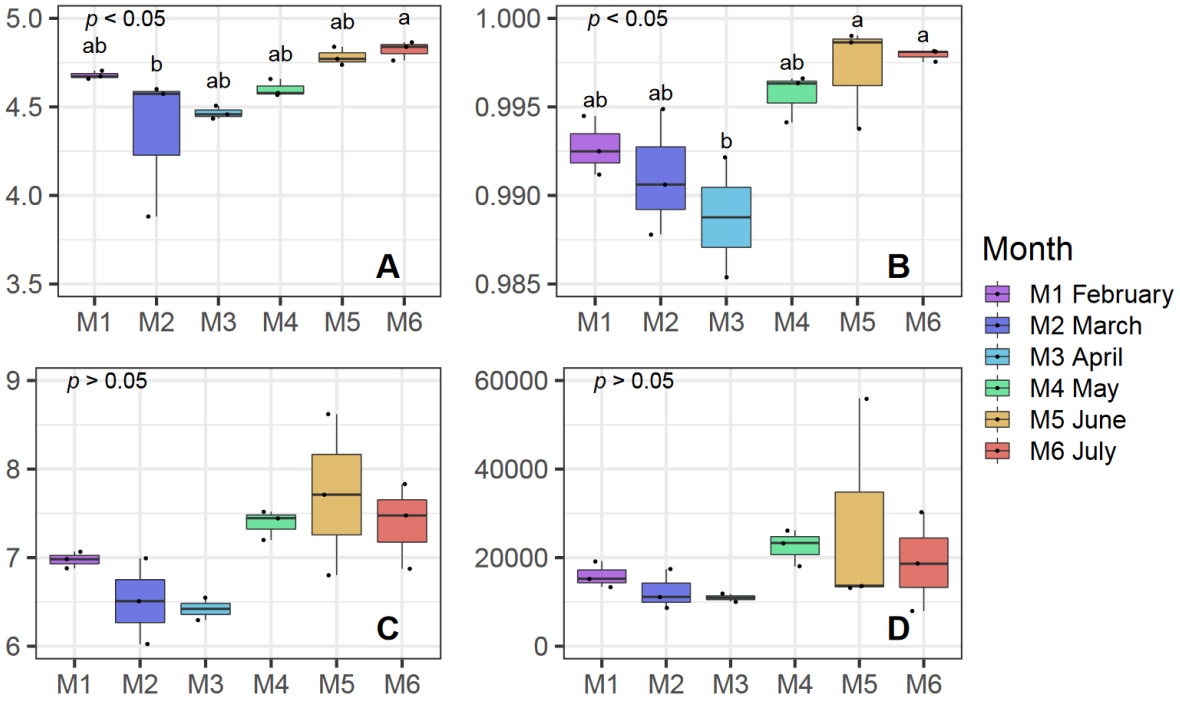

Figure II.4. Seasonal dynamics of diversity indexes. (A) show the chemodiversity measures calculated using Shannon index with the metabolomics dataset. (B, C and D) show the epibacterial alpha-diversity measures respectively calculated using Simpson, Shannon, and Chao1 indexes with the 16S metabarcoding dataset. A one-way ANOVA followed by post-hoc tests (HSD) allowed to show significant variations for the indexes during the year.

The PCoA based on Bray-Curtis dissimilarity distances (**Figure II.1B**) showed a high similarity between bacterial communities described from algal samples collected in the same month, together with a shift of these communities with time (PERMANOVA, $p < 0.05$). At the class level (Fig. SII.23), α- and γ-proteobacteria dominated the communities without significant seasonal change, except for a higher dominance of the α-proteobacteria in February (reaching 69% of the OTUs for the whole community) and an increase of the relative abundance of the *Cytophagia* (Bacteroidetes) in June and July. Flavobacteria, Sphingobacteria and unidentified Bacteroidetes, in addition to *Cytophagia*, accounted for 19 to 37% of the communities. Actinobacteria altogether never exceeded 12%, whereas β- and δ-proteobacteria showed high variations, sometimes reaching high percentages (such as 25% in June for β-proteobacteria). At the family level (**Figure II.5A**), the dominant taxa were Saprospiraceae (Bacteroidetes), Hyphomonadaceae (α-proteobacteria), Granulosicoccaceae (exclusively the genus *Granulosicoccus*) and Alteromonadaceae (γ-

proteobacteria), representing together between 33 and 56% of all sequences during the survey. Seasonal trends could be observed with the dominance, when the alga appeared in winter, of Saprospiraceae, Hyphomonadaceae, Rhodobacteraceae (mainly reported as unidentified) and Granulosicoccaceae, together with Vibrionaceae. The latter included at least 80% of *Vibrio* spp. with an increasing number of *Photobacterium* spp. in the spring and summer. Pseudoalteromonadaceae (exclusively *Pseudoalteromonas* spp.) could only be observed in March. During spring and summer, Alteromonadaceae (mainly the BD1-7 clade, which belongs to the oligotrophic marine γ-proteobacteria, OMG) clearly replaced Granulosicoccaceae as the dominant γ-proteobacteria, and an increase in Oceanospirillaceae was observed. α-proteobacteria appeared to diversify with the decrease in Hyphomonadaceae and Rhodobacteraceae that occurred concomitantly with the increase of Erythrobacteraceae (all the time around 70% of *Erythrobacter* spp.) and Rhodospirillaceae (mainly reported as unidentified taxa). Flammeovirgaceae also increased from May to July. Finally, among the Saprospiraceae, which remained constant during the survey, members of the genus *Lewinella* significantly increased while, on the contrary, *Aureispira* spp. decreased.

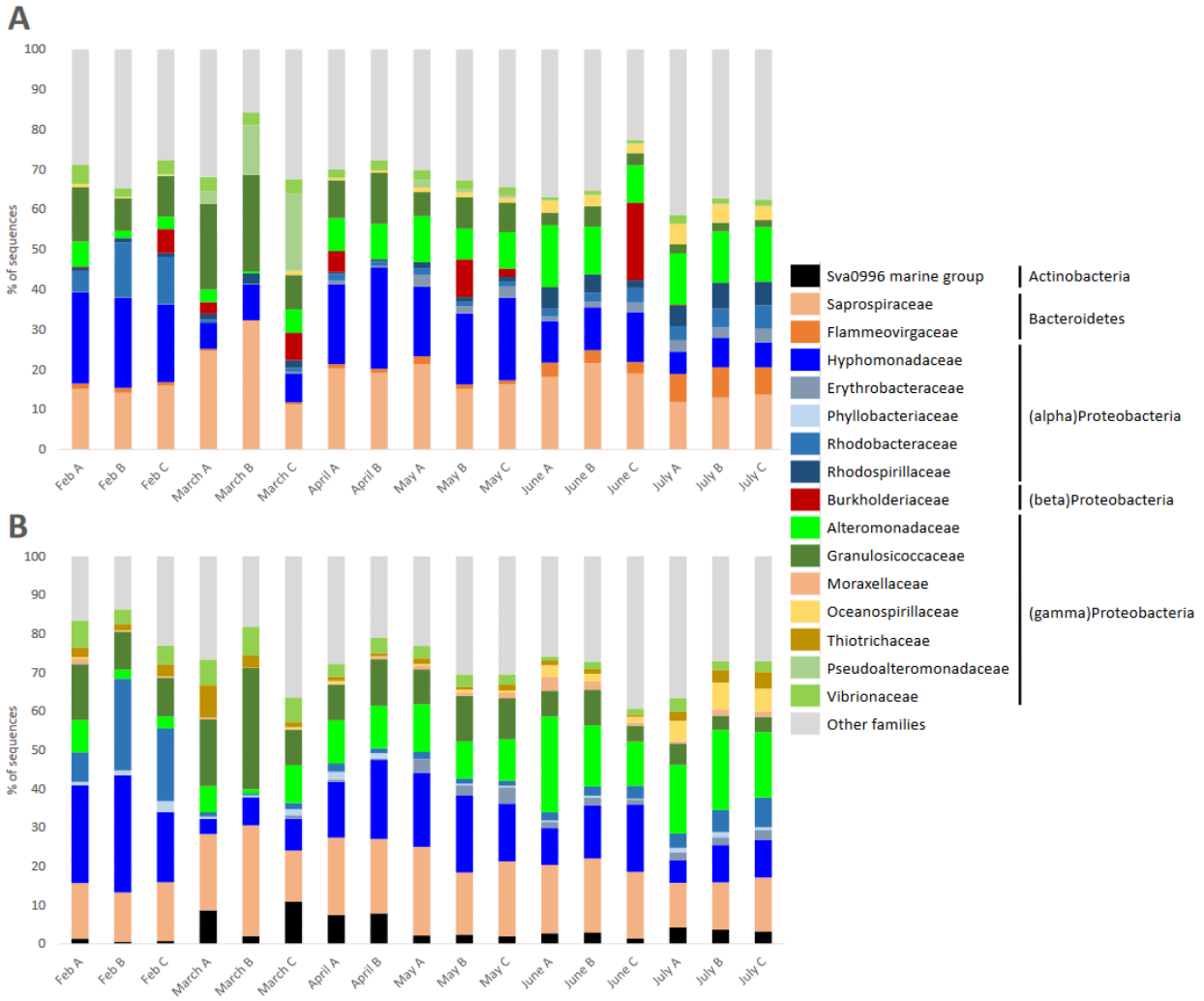

Figure II.5. Seasonal variations of the epibacterial communities on *T. atomaria* at the family level (A: total community, B: core community). A, B, C in sample names represent biological replicates. % in B are % of all the core sequences.

The core OTUs were defined as OTUs observed in at least one replicate each month. Thus, 1 544 OTUs, i.e. between 11 and 21% of the total OTUs per month, constituted the epibacterial core community of *T. atomaria* from February to July (Fig. SII.24). This core community corresponded to significantly higher percentages of sequences than OTUs for each sample, ranging from 27 to 53% ($p < 0.05$). As this percentages of sequences appeared quite high, this suggested that the core was not only composed by rare OTUs. In addition, a significant decrease in the percentage of the total core community sequences could be noticed from April to July ($p < 0.05$), without any significant variation in the percentage of OTUs. Similar trends as for the overall community could be noticed for the core community at the family level (Fig. 5B). In particular, the four dominant groups (>10%) remained the same (Saprospiraceae, Hyphomonadaceae, Granulosicoccaceae and Alteromonadaceae), together with the seasonal shift among γ-proteobacteria (and the replacement of Granulosicoccaceae by Alteromonadaceae), the significant

presence of Rhodobacteraceae only in February or the occurrence of Oceanospirillaceae and Erythrobacteraceae as the sub-dominant groups in the summer (1 to 10%). However, the Sva0996 marine group (Actinobacteria) and Moraxellaceae (γ-proteobacteria) specifically appeared in the core community as dominant and sub-dominant, respectively. The increase in Alteromonadaceae in the core community in spring and summer could be directly associated with the increase in members of the BD1-7 clade: they reached between 52 and 80% of the Alteromonadaceae in the core community, while they ranged between 22 and 46% in the overall community. Similarly, when identified, one genus clearly dominated each family in the core community (e.g. *Granulosicoccus* for Granulosicoccaceae, *Robiginitomaculum* for Hyphomonadaceae, *Erythrobacter* for Erythrobacteraceae, *Balneathrix* for Oceanospirillaceae, and *Thiothrix* for Thiotrichaceae).

2.3.3. Multi-omics approach to assess temporal variations of T. atomaria

A multi-block PLS-DA model was built using the MixOmic DIABLO analysis with the metabolomics and metabarcoding datasets. The resulting score plot (**Figure II.1C**) showed an initial strong seasonal co-variation between epibacterial communities and surface metabolites, with a correlation coefficient of 0.95 between the two datasets. This trend was confirmed by a Mantel test ($p < 0.01$). The second component progressively discriminated samples collected in February and March from those obtained in April and May. Samples from April to July were then progressively discriminated along the first component. Similar results can be observed on the heatmap of the relative abundance of a panel of highly relevant variables selected from the supervised multi-block PLS-DA model (Fig. SII.25). Three groups of samples were clearly distinct within the dendrogram: February and March, then April, May and June, and finally samples collected in July. The relative abundance of the selected variables on the heatmap representation showed then a continuous co-variation of surface metabolites and epibacterial OTUs from February to July.

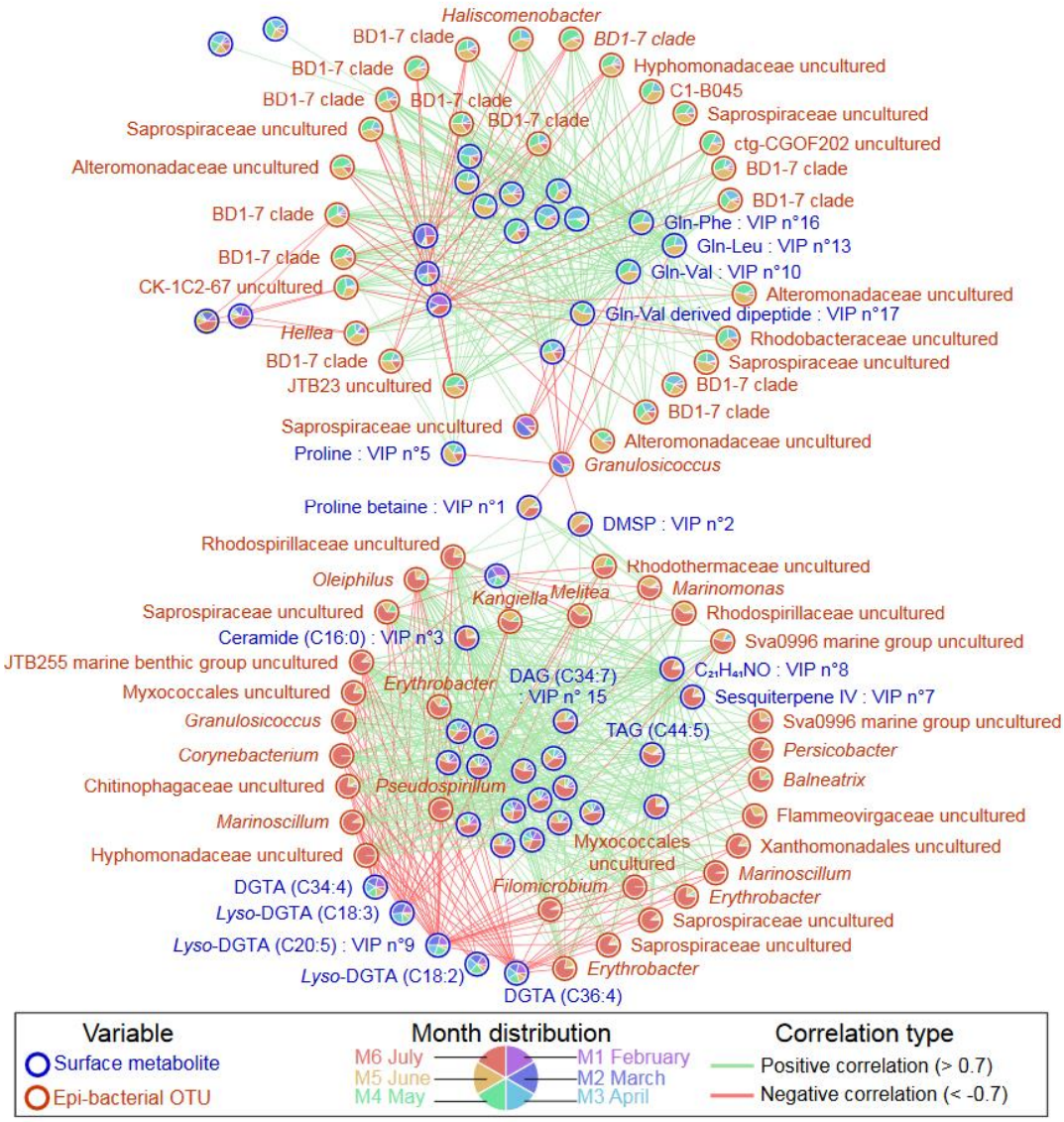

Figure II.6. Seasonal correlation network (multi-block PLS-DA) of the surface metabolome and the epibacterial communities of *T. atomaria.* Discriminant OTUs (orange circles and names) and metabolites (blue circles and names) are positively (green) or negatively (red) connected. Seasonal variation of their relative occurrence during the year was also represented inside the circles with pie charts.

Two clusters were observed on the correlation network built with the 108 most discriminant variables highlighted by the multi-block PLS-DA, among the surface metabolites and epibacterial OTUs datasets (**Figure II.6**). The first cluster, on top, showed mainly metabolites and epibacterial OTUs which were positively correlated due to their high relative abundance during the "spring period" (April, May and June). Interestingly, almost half of these OTUs were affiliated with the same group (BD1-7 clade, Alteromonadaceae), while annotated metabolites were proline and dipeptides. This cluster also showed a few unidentified metabolites that were negatively correlated to these specific OTUs. The second cluster,

on the bottom, revealed mainly positive correlations between several metabolites and OTUs which were both abundant during the "summer period" (June and July). The metabolites involved in such relationships were mostly non-polar lipids such as a ceramide, a di-(DAG) and a triacylglycerol (TAG) but also DMSP, proline betaine and sesquiterpene IV. Among the related OTUs, Erythrobacteraceae, Flammeovirgaceae, Oceanospirillaceae, and Rhodospirillaceae were the main families. Interestingly, several DGTAs and *lyso*-DGTAs were negatively correlated with these "summer epibacterial OTUs", showing lower relative concentrations during the "summer period".

2.4. Discussion

Holobionts put seaweed studies in the context of an integrated social unit as it was clearly observed that algal phenotypes are deeply affected by their complex surface-associated microbial communities. For example, bleaching of the Australian Rhodophyta *Delisea pulchra* (Fernandes et al., 2012; Zozaya-Valdés et al., 2017) or Ochrophyta kelps (Marzinelli et al., 2015) was associated with a shift in the algal epibacterial community structure associated with the lack of production of quorum sensing inhibitors (halogenated furanones) by the algal host. The Phaeophyceae *Ecklonia radiata* (kelp) maintains more specific microbial communities than those found its immediate surroundings but when the alga becomes stressed and bleaches, this specificity breaks down (Marzinelli et al., 2015). The cellular differentiation of Chlorophyceae (*Ulva* spp.) was shown to be associated to thalusin production by host associated bacteria (Matsuo et al., 2005). Within the framework of complex relationships, coral larvae may be able to use the observed differences in bacterial community composition on crustose coralline algal species to assess the suitability of these substrata for settlement and selectively settle on algal surfaces that bear beneficial bacteria (Sneed et al., 2015). This also indicates that host conditions could more strongly influence bacterial communities than geographical and environment-related parameters.

2.4.1. Diversity and composition of total and core microbiota associated with the surface of T. atomaria

This study aimed to identify the diversity and the composition of the epibacterial communities of the Dictyotaceae *T. atomaria* collected on the French Mediterranean coast and to unravel the seasonal variation of these microbiota in relation to those of surface metabolomes. Seaweeds and their surface-associated microbiota are considered as holobionts (Egan et al., 2013).

Highly diversified bacterial communities with the co-dominance of α-, γ-proteobacteria and Bacteroidetes colonised *T. atomaria* surfaces. The structure of these communities was similarto those of typical biofilms described on other seaweeds or artificial surfaces (Wahl et al., 2012; Dang and Lovell, 2016). A marked seasonal trait occurred in this colonisation process, which involved pioneer bacterial taxa (r-strategists especially among Rhodobacteraceae and Alteromonadaceae) followed by more adapted and seaweed-specific ones (K-strategists). Increasing seawater temperature and associated irradiation (data not shown) would be involved in the shaping of the epibacterial communities from February (winter) to July (summer). The concept of core community, still poorly studied in marine ecosystems, is related to the stable part of the bacterial community (Astudillo-García et al., 2017). The core is generally defined on the basis of a minimal percentage of occurrence in studied samples. Nevertheless, the choice of this abundance threshold is questionable. We consequently decided to define the core community not using an abundance threshold but as the set of OTUs identified all the months in at least one replicate whatever their abundance. Especially, this definition allowed to exclude OTUs not detected one specific month. Using this definition, the core community already included between 30 to 60% of the sequences. A more stringent definition would have increased this percentage and we assumed that one of the interest of the core concept is to focus on a more specific part of the microbial community. The core community of *T. atomaria* accounted for a large part of the whole set of sequences during the study, but this finding was not observed when considering OTUs. Thus few dominating abundant OTUs together with several transient low abundant OTUs seem to characterize the core community. The core community showed a similar composition as the overall community at the family level, but a lower diversity at the genus level. In addition, two original taxa (Sva0996 marine group and *Thiothrix* spp) emerged in the core community of *T. atomaria*. Members of Sva0996 marine group are gram-positive Actinobacteria that remain largely unknown. These bacteria were only sporadically noticed in various marine environments such as sediment surfaces of the Arctic ocean (Li et al., 2009), enriched bacterioplankton during phytoplankton blooms in the Sargasso Sea (Nelson et al., 2014) or associated with sponges (Verhoeven et al., 2017). *Thiothrix* spp. belong to the filamentous sulphur-oxidising bacteria, which have been mainly reported from activated-sludge wastewater treatment plants or as ectosymbionts of marine (Gillan and Dubilier, 2004) or freshwater (Flot et al., 2014) amphipods. However, the latter bacteria were also reported to form white-coloured films on portions of the surface of aquatic macrophytes located within the hydrothermal flow of vents of Yellowstone Lake (Konkol et al., 2010). *Thiothrix* spp., as a sulphide oxidiser, was thus suggested to be, in part, responsible for limitation of the toxicity associated with high sulphide concentrations. However, the poorly diversified dense mats dominated by *Thiothrix* spp. could also limit the

photosynthesis of the macrophytes. No mats were observed at the surface of *T. atomaria* and considering its sulphur metabolism, the occurrence of this taxa remained difficult to interpret.

2.4.2. Signalling cyclic dipeptides associated with the OMG BD1-7 clade

Multi-block analyses and correlation networks between the most discriminant metabolites and bacterial OTUs at the surface of *T. atomaria* in their respective seasonal clustering confirmed the similar seasonal dynamic, but mostly highlighted their putative interactions. The first cluster of the correlation network (Fig. 6) exhibited both OTUs and metabolites which were more abundant in the spring and positively correlated to each other. Most of the corresponding taxa were related to Alteromonadaceae, especially members of the BD1-7 clade which have been previously reported as pioneer bacteria on marine surfaces (Dang and Lovell, 2016; Pollet et al., 2018) and in nutrient-depleted environments (Spring et al., 2015). If already identified in the low nutrients containing Mediterranean Sea, the BD1-7 clade was not reported as a major taxon of biofilms formed on artificial substrates in the vicinity of the collection site (Briand et al., 2017), indicating a potential specific selection by *T. atomaria*. In addition, as a major component of the core community that represented a significant part of the total surface community, this clade should play a major ecological role. Most of the related metabolites identified at the surface of the alga were cyclic dipeptides: such compounds have been widely reported from bacteria and showed diverse biological activities (e.g. antimicrobial, antioxidant, antiviral or antitumor) (Huang et al., 2010). It was suggested that cyclic dipeptides could play a role in bacterial and trans-kingdom signalling (Ortiz-Castro et al., 2011).

2.4.3. DMSP and proline betaine exhibited a key role within the correlation network

On the correlation network built with discriminant variables of the surface metabolome and the microbiota of *T. atomaria* (Fig. 6), the link between the two clusters rests on the genus *Granulosicoccus.* The latter has been identified as a psychrotrophic taxon, widely reported from Antarctic coastal seawaters (Baek et al., 2014) and sediments (Wang et al., 2017), but also from the surface of an unidentified brown alga (Park et al., 2014) or the Mediterranean Chlorophyceae *Caulerpa* spp. (Rizzo et al., 2016). This major node of the network was negatively related to the two most important VIPs for the metabolite clustering, i.e. DMSP and proline betaine (*N*,*N*-dimethylproline, also known as stachydrine). Proline betaine and DMSP and, to a lesser extent, proline, were found to be the main discriminant surface metabolites for differentiation between months. The levels of these compounds constantly increased from February to June (**Table II.1** and **Figure II.3**). These low molecular mass molecules belong to a family of compounds that are collectively termed “compatible solutes” and accumulated to high intracellular concentrations in

a wide range of organisms (McNeil et al., 1999). In addition to their firmly established osmoprotective function, various physiological and ecological roles have been demonstrated for these compounds (e.g. stabilisation of proteins and membranes, protection of photosystem II, supply of carbon and nitrogen). More broadly, compatibles solutes have been shown to participate to the acclimation of organisms to a number of stresses. In the particular case of algae, proline and DMSP have been detected at the surface of the brown alga *Fucus vesiculosus* and it has been demonstrated that these compounds had antibacterial properties at natural concentrations (Saha et al., 2012). More particularly, DMSP content was high at 20°C and then decreased at 25°C, and was globally higher under dark conditions (Saha et al., 2014). In previous works dealing with total extracts of several macroalgae, it has been demonstrated that DMSP content increased with irradiance and decreased with temperature, with such variations being in accordance with the roles of DMSP as an antioxidant or cryoprotectant (Karsten et al., 1992; Lyons et al., 2010). More recently, a study has shown that DMSP released by the Chlorophyta *Ulva mutabilis* also acted as a chemoattractant for *Roseovarius* sp., a bacterium known to induce the morphogenesis of *Ulva* (Kessler et al., 2017). In the case of proline, the effect of temperature and light on its surface concentration on *F. vesiculosus* was shown to be limited (Saha et al., 2014), while an increase in proline levels was observed in the red alga *Gracilaria tenuistipitata* exposed to high temperatures (e.g. Chang and Lee, 1999)

In this study, DMSP, proline and proline betaine contents reached their maximal values in June and, to a lesser extent, in July when irradiance, sea temperature and fouling pressure were high. Their slight decrease in July coincided with the appearance of bleached portions on thalli of *T. atomaria*. This could thus explain such a trend which was previously reported for DMSP in the green alga *Codium fragile* (Lyons et al., 2010). Kessler et al., (2018) demonstrated that bacteria essential for *U*. *mutabilis* were able to catabolise algal DMSP into methanethiol and dimethylsuphide (DMS) faster than *de novo* production by the algal host in order to prevent the attraction of additional bacteria. Nevertheless, in the present work, algal samples collected *in situ* bore a complex bacterial community which certainly induced more complex chemically-based relationships that those described by an *in vitro* tripartite model. Moreover, it cannot be excluded that DMSP found in the samples was also produced by microorganisms associated at the surface of *T. atomaria*.

Interestingly, mannitol which has also been suspected to be implicated in algal response to stress (Dittami et al., 2011) remained constant from February to June and declined sharply in July (**Figure II.3**). This storage compound has previously been used as a proxy for energy availability in order to produce

chemical defences, and its production has been negatively correlated to microfouling colonisation (Rickert et al., 2015; Rickert et al., 2016b)

2.4.4. What about the role of the key network compounds DGTAs?

The second cluster at the bottom of the correlation network (**Figure II.6**) illustrated the higher diversity of summer surface microbiotea. Some of the taxa were major representatives of the core microbiota, e.g. *Balneathrix*, *Erythrobacter* and especially the Sva0996 marine group. *Erythrobacter* spp. are marine ubiquitous aerobic anoxygenic phototrophic bacteria, which have already been reported as the major taxa of biofilm communities on artificial surfaces (Briand et al., 2017; Oberbeckmann et al., 2018). As cyanobacteria failed to be identified in the surface community of *T. atomaria*, *Erythrobacter* spp. could be major actors of the primary production at the algal surface.

OTUs from this cluster were negatively correlated with several DGTAs. These non-phosphorus-containing betaine lipids were assumed to have similar functions to phospholipids and replaced this class of polar lipids in phosphorus-limited conditions (Dembitsky, 1996). Higher concentrations were recorded in winter or spring months, which could indicate their enrichment in young algae observed from February only. This finding was consistent with a recent study which showed that the total content of DGTAs in the Ochrophyta *Sargassum horneri* increased during the growth phase and decreased when the alga became mature (Zhang et al., 2018). On the contrary, positive correlations were reported between the OTUs from the second cluster and some lipid classes which were more produced in summer. These compounds were non-polar DAGs and TAGs, considered as energy and storage compounds, and ceramides. The occurrence of such lipids in the summer was not surprising as the accumulation of TAGs and their precursor DAGs in algae is known to occur under stress conditions, such as high light intensity, high salinity or N-deprivation (Liu and Benning, 2013). Among the wide range of biological roles, ceramides have also been characterised for their central role in response to biotic and abiotic stresses (Michaelson et al., 2016).

Unfortunately, several other metabolites which exhibited significant correlations with OTUs from the two clusters remained unidentified. This fact illustrated both the huge lack of molecular databases related to the marine organisms and the need to improve our knowledge on marine holobionts in order to better understand functions and roles associated with such complex living systems.

In conclusion, the meta-omics analysis performed here suggested that *T. atomaria* surface-associated microbiota was clearly specific and associated with key metabolites like DMSP, betaine or proline-betaine probably excreted by the host. In addition, despite a core community that represents a significant part of

the total epibacteria, changes occurred in the structure of the community. In association with the increase in seawater temperature, these changes were connected to surface metabolome variations, suggesting that both environment and algae shape the bacterial surface microbiota. In the near future, if environmental drivers should be determined, the major challenge will be to improve the identification of key metabolites that will allow us to further understand how the actors of *T. atomaria* holobiont interact.

2.5.Experimental procedures

2.5.1. Algal material

The collection of *Taonia atomaria* algal specimens was carried out by hand (1m depth) monthly during its occurrence period in the studied collection site (Carqueiranne, French Mediterranean coast, 43°5'12.41"N, 6°5'3.26"E) from February to July 2013. No thallus could be found in January or from August to December 2013. Following collection, three individual thalli were packed in 1L-plastic bags filled with ambient seawater and transported in an isotherm container to the laboratory. From the point of collection, algal samples were treated within 2h. Each month, three individual thalli of *T. atomaria* were collected as replicates. Each individual thallus was composed with several fronds and thus for each replicate one frond from a thallus was used for the metabolome extraction and another one from the same thallus was used for the DNA extraction.

2.5.2. Surface metabolome extraction, metabolomics analysis and data processing (See Supporting Information for more details)

The surface metabolome of samples of *T. atomaria* was obtained by a dipping method using methanol as an extraction solvent (Othmani et al., 2016a). A surface of approximately 10 to 12 cm^2 of one frond for each individual thallus was extracted for each month. It may be noted that, in the case of *T. atomaria*, the alternative solid phase extraction-based method previously described by Cirri et al. did not allow the detection of any compound by LC-MS (Cirri et al., 2016). The resulting surface extracts were concentrated under reduced pressure and stored at -20°C until analysis. Before injection, samples were solubilised in LC-MS grade methanol at a concentration of 10 $mg.ml^{-1}$. Analytical blanks were also prepared and all samples were randomly injected to avoid systematic errors following the same injection sequence as that used in Favre et al., (2017).

The metabolomic profiling was performed using a previously described experimental protocol (Favre et al., 2017), the sole difference being the elution gradient used. In the present study, the mobile phase gradient involved a binary programming of acidified acetonitrile (B) and water (A), containing each 0.1% of formic acid (v/v). The elution gradient started at 5% B, which was held for 2 min, then increased to 100% B (linear ramp) within 8 min and maintained for 4 min; it was then reduced to 5% B over 0.01 min and maintained for 1.99 min, for a total run time of 16 min.

Raw UPLC/MS data were analysed using DataAnalysis (version 4.3; Bruker Daltonics), converted into netCDF files and processed for peak finding, integration and alignment using the open source XCMS package (version 1.46.0, Smith et al., 2006) in the R 3.2.3 environment. The resulting variables list was further processed by the CAMERA package (version 1.26.0) (Kuhl et al., 2012) and three successive filtering steps (signal/noise ratio, coefficient of variation and coefficient of autocorrelation between variables in a same given "pcgroup") using an in-house script were run on R.

These variables were normalised by the sum, $\log_{10}$-transformed, mean-centred and analysed by principal component analysis (PCA) and partial least-square discriminant analysis (PLS-DA) using the MetaboAnalyst 3.5 online resource (http://www.metaboanalyst.ca). Analysed data from MetaboAnalyst were then exported and figures were generated in the R 3.2.3 environment using the "ggplot2" package. The seasonal clustering observed with PCA and PLS-DA scores plots were statistically tested respectively with PERMANOVA test (999 permutations) using the "Vegan" R package, and a permutation test using MetaboAnalyst webtool (Separation distance: B/W, 1000 permutations). The variation of each selected metabolite during each month was then statistically tested by one-way ANOVA followed by post-hoc test (HSD) using the "Agricolae" R package.

2.5.3. MS/MS molecular networking and annotation of metabolites

The MS/MS molecular network was generated on the GNPS online tool (https://gnps.ucsd.edu). Briefly, MS/MS data were clustered using default parameters for "medium data preset" with a precursor ion mass tolerance of 2 Da and a fragment ion mass tolerance of 0.5 Da. Data were analysed using Cytoscape (version 3.4.0), with nodes to represent *m/z* detected features and edges to represent the MS/MS spectral similarity between *m/z* features. Normalised concentrations for metabolites found commonly within the molecular network were imported into Cytoscape. By implementing these data, a pie chart was generated

into each node revealing the relative seasonal distribution of each metabolite. Transparency of edges connecting each node was proportional to the spectral similarity using a cosine score (CS).

In most metabolomics studies, and more particularly in the case of non-model organisms, the identification of VIPs and metabolome annotations are considered the limiting steps in the analytical workflow. In this study, annotation of the top discriminatory *m/z* features was undertaken using: (i) a thorough analysis of HRMS data and MS fragmentation patterns, (ii) the construction of a molecular network based on MS/MS experiments, and/or (iii) comparison of the MS and MS/MS data with free online databases (e.g. Metlin), including annotation tools such as MetFusion (Gerlich and Neumann, 2013), and with compounds that are commercially available or have already been isolated from *T. atomaria* or other algae by our research team (Viano et al., 2009; Othmani et al., 2016b). Using this methodology, eleven compounds were unambiguously annotated using chemical standards [4 commercial standards: DMSP, proline betaine, proline and mannitol; 7 natural compounds previously isolated in our laboratory (Othmani et al., 2016b)] and 33 *m/z* features were putatively identified through molecular networking, the analysis of HRMS/MS data and comparison with databases and chemical standards (Dataset S1). All commercial standards were purchased from Sigma-Aldrich or Cayman Chemicals.

2.5.4. Epibacterial communities DNA Extraction, amplification and sequencing

Each thallus was washed with PBS (phosphate buffered saline, pH 7.4). A sterile scalpel was used to scrape off the epiphytic bacteria, which were introduced into plastic Eppendorf tubes (2 mL). A surface of approximately 10 to 12 cm^2 of one frond from each three individual thalli was scrapped for each month. Extraction of the bacterial DNA was carried out using the PowerBiofilm DNA isolation Kits (Qiagen). For each DNA extract, the V5-V6 region of the 16S rDNA was targeted using 5' CAAACAGGATTAGATACCCTG 3' (775F) and 3'CGTTRCGGGACTTAACCCAACA 5' (1103R) following (Youssef et al., 2009). The amplicons were paired-end sequenced (2 × 250 bp) on an Illumina MiSeq plaform (RTL, Texas, US). Sequences assessed in this study have been submitted to NCBI under the accession number SUB4952404.

2.5.5. Metabarcoding data processing and statistical analysis

The MiSeq data were assembled with the vsearch tool (https://github.com/torognes/vsearch) and the sequences were cleaned as follows: sequences were removed if they presented ambiguous bases “N”, a length shorter than 200 bp, and had a mismatch in the forward and reverse primers. The putative

chimaeras were detected by vsearch. The remaining rRNA 16S sequences were clustered into “molecular species” (OTUs) at a 97% similarity threshold with vsearch (option cluster_small sorted by length) (Rognes et al., 2016). The representative sequence for each OTU was inserted into phylogenetic trees for taxonomic annotation. The seed OTUs were affiliated by similarity and phylogeny from reference sequences. These microbial references were extracted from the SSU SILVA database (Pruesse et al., 2007) according to the following criteria: length N 1200 bp, quality score N 75% and a pintail value N 50. After comparing the OTUs with the reference sequences using a similarity approach (vsearch tool), trees including OTUs with their closest references were built with FastTree (Price et al., 2010). The different taxonomic affiliations obtained were checked for inconsistency. This process was implemented using the pipeline PANAM (Phylogenetic Analysis of Next-generation AMplicons https://github.com/panammeb/PANAM2) and is described in more detail in (Taib et al., 2013).

Alpha-diversity metrics (Chao1, Shannon and Simpson indexes) were calculated using the Phyloseq R package and MicrobiomeAnalyst online tool (http://www.microbiomeanalyst.ca/) and tested statistically with a one-way ANOVA followed by a post-hoc test (HSD) using the Agricolae R package. Dissimilarity matrices using the Bray-Curtis distances were represented in a two-dimensional space by a Principal Coordinates Analysis (PCoA). The similarity difference observed between each month with the PCoA was then statistically tested with a PERMANOVA test (999 permutations), using the Vegan R package.

2.5.6. Integration of metabolomic and metabarcoding dataset

Correlation analysis between metabolomics and the metabarcoding dataset was performed using the multi-block analysis DIABLO (block.splsda function) from MixOmics R package (Lê Cao et al., 2009). Briefly, the aim of this multivariate analysis was to perform an N-block integration of different -omics datasets to identify the most correlated variables involved in the discrimination of each group of samples. Here, this multi-block analysis allowed the most correlated OTUs and metabolites involved in the discrimination of each month to be identified. To perform such an analysis, an optimal number of variables (49 metabolites and 59 OTUs), which were the most involved in the seasonal discrimination, was specifically selected using the tuning function (tune.block.splsda function). The level of correlation between the two selected datasets was checked using the correlation coefficient calculated by the DIABLO analysis and a Mantel test (“ade4” R package).

Based on this analysis, a correlation network showing only positive (> 0.7) and negative (< -0.7) correlations between the selected variables was built, and then imported and analysed with Cytoscape.

2.6.Acknowledgments

This work was supported by the Ministry of Higher Education and Scientific Research of Tunisia (A.O. PhD grant) and the French “Provence-Alpes-Côte d’Azur (PACA)” regional council (B.P. PhD grant). The authors are grateful to Dr S. Greff for his help during the acquisition of LC-MS profiles. LC-MS experiments were conducted on the regional platform MALLABAR funded by the Institute of Ecology and Environment (INEE) of the National Center for Scientific Research (CNRS) and the French PACA regional council.

3. Bilan du chapitre

Cette étude préliminaire montre une dynamique et une co-variation temporelle du microbiote et du métabolome de surface de *T. atomaria* à Carqueiranne (Nord-ouest de la mer Méditerranée) en 2013. L'analyse MixOmics DIABLO a en outre permis de construire un réseau de corrélation révélant deux clusters, le premier correspondant au printemps et le second à l'été, montrant plus précisément : (i) durant le printemps, un taxon spécifique de la famille des Alteromonadaceae (BD1-7 clade) corrélé à une série de dipeptides, et (ii) durant l'été, plusieurs taxa des familles des Erythrobacteraceae, des Rhodospirillaceae, des Oceanospirillaceae et des Flammeovirgaceae positivement corrélés à plusieurs métabolites connus pour leur implication dans les défenses antifouling de macroalgues (ex : DMSP, et proline). Bien que la communauté de coeur représente une part importante des bactéries épiphytes totales, leurs variations semblent dépendre à la fois des variables environnementales et de l'hôte algal.

CHAPITRE III : ETUDE BIOGEOGRAPHIQUE

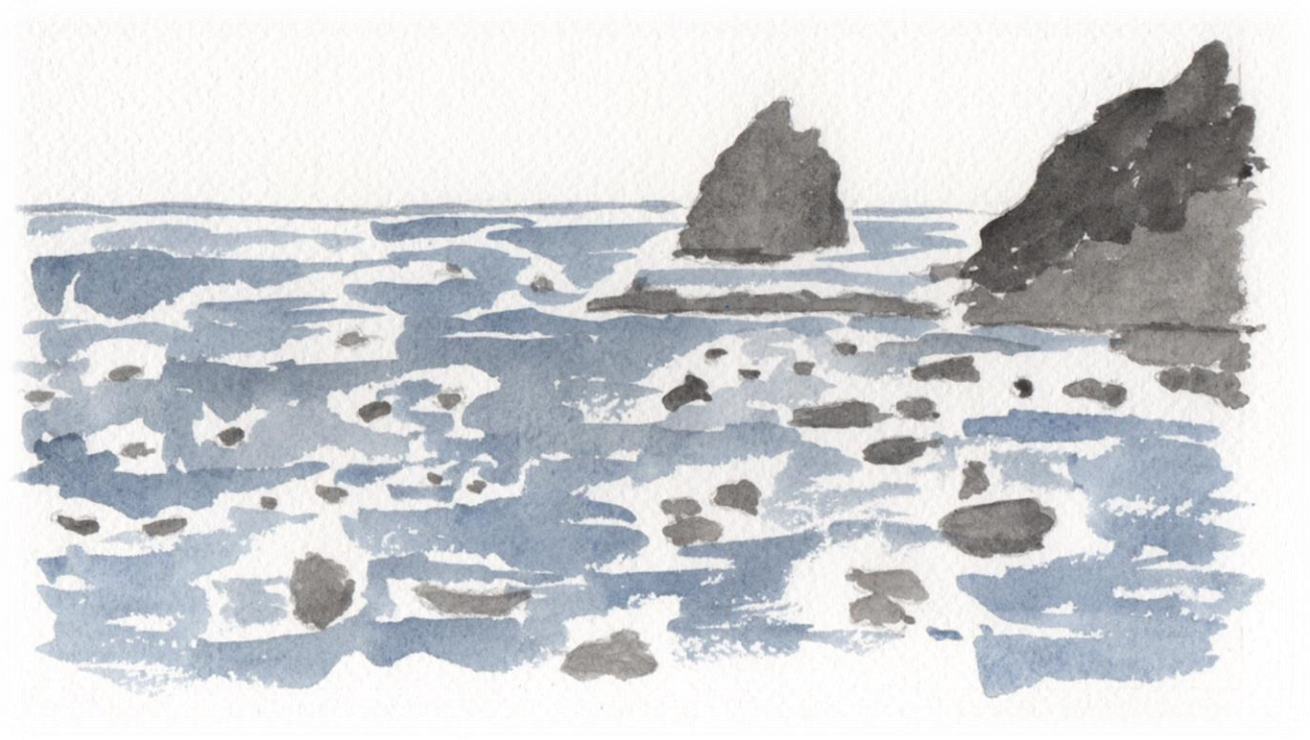

Plage des Falaises au Cap d'Agde

1. Avant-propos

A la suite de l'étude préliminaire menée sur un seul site (Carqueiranne, Var) de l'aire marine toulonnaise, ce chapitre s'intéresse aux variations du microbiote et du métabolome de surface de *T. atomaria* à une échelle géographique plus large (18 sites représentant la majeure partie des côtes méditerranéennes françaises et un site de la côte nord de la Bretagne). Ainsi, cette étude a pour objectif de déterminer dans quelle mesure la biogéographie et la phylogénie de l'hôte *T. atomaria* influencent ses communautés et son métabolome de surface. Cette étude est présentée sous la forme d'un article de recherche en préparation en vue d'une soumission dans *Journal of Applied Phycology*. Les références citées dans cet article sont indexées en fin de manuscrit. La partie *Supplementary Information* de cet article est presentée dans l'annexe III du manuscrit (annexe électronique).

2. Article: Host phylogeny and biogeography shape the surface microbiota and metabolome of the brown alga *Taonia* (Dictyotales)

Benoît Paix[1], Christophe Vieira[2], Philippe Potin[3], Catherine Leblanc[3], Olivier De Clerck[4], Jean-François Briand[1*], Gérald Culioli[1*]

[1] *Université de Toulon, Laboratoire MAPIEM, EA 4323, Toulon, France*

[2] *Kobe University Research Center for Inland Seas, Rokkodai, Kobe 657-8501, Japan*

[3] *Sorbonne Université, CNRS, Integrative Biology of Marine Models (LBI2M), Station Biologique de Roscoff (SBR), Roscoff, France*

[4] *Ghent University, Department of Biology, Phycology Research Group, Ghent, Belgium*

*corresponding authors : briand@univ-tln.fr, culioli@univ-tln.fr

2.1. Abstract

As holobiont systems, marine macroalgae and their microbiota constitute functional units displaying a large diversity of interactions. Main factors driving the assembly of epiphytic microbiota, and subsequent interactions with the host, are often associated to environmental differences but also host-taxonomy displaying specific chemical properties. Here, through a biogeographical study focusing on the brown algal genus *Taonia* (Dictyotaceae), we aimed to highlight the relative importance of the effects of environment, host taxonomy and surface metabolome on the epibacterial community of these seaweed-holobionts. Little is known on the phylogeny of this algal genus and this study constituted the first integrative analysis comparing algal specimens collected along the French Mediterranean and North Brittany coasts. Phylogenetic analysis based on the concatenated alignment of the *cox*3, *psb*A and *rbc*L genes indicated that specimens collected displayed two distinct clusters, one with specimens from the French Mediterranean coast only and the second with samples from Brittany. However, Mediterranean sub-clusters were clearly not related to geographical locations. For both metabarcoding and surface metabolome approaches, the main clustering pattern revealed clear differences between the Brittany and the Mediterranean thalli. Genetic and environmental differences observed between algae from different geographical areas could both explain such clustering. For example, environmental driver such as oxidative stress induced by higher irradiance might induce higher expression of fucoxanthin in Mediterranean sites, while higher eutrophication levels could explain the higher abundance of *Alteromonas* spp. on algal samples from Brittany coast.

2.2. Introduction

The concept of holobiont (i.e. the host-microbiota association), initially coined by Margulis and Fester, 1991 taking for model corals and their symbionts (e.g. *Symbiodinium* and associated bacteria), was later applied to other organisms [e.g., plants (Vandenkoornhuyse et al., 2015) or human (Kramer and Bressan, 2015)] including seaweeds (Egan et al., 2013). Knowing that the association between an host and its microbiota contributes to the overall stability of the holobiont system, this holistic view makes sense in seaweeds in the light of recent studies which demonstrated that epibacterial communities could impact the algal physiology through beneficial (e.g. morphogenesis or defense, Kessler et al., 2018; Saha and Weinberger, 2019) or detrimental processes (e.g. bleaching, Case et al., 2011; Kumar et al., 2016).

While the functions of the associated microbiota are still being explored in seaweed holobionts, a parallel line of research aims to determine to which extent the microbial assembly is specific to a host and which factors influence this community structure. A shift in the structure and/or the functions of the microbiota can occur at the algal surface in response to environmental drivers yet depending on the taxa (Hollants et al., 2013; Morrissey et al., 2019). However, the relative importance of both factors is often raised (Lachnit et al., 2009, 2011; Morrissey et al., 2019). For instance, variations in the microbiota of the green algae *Caulerpa prolifera* and *C. cylindrateca* (Bryopsidales, Chlorophyceae) were found to be: (i) host-specific, (ii) compartment-specific (e.g. rhizome, thalli), and (iii) influenced by the biogeography (Morrissey et al., 2019). While for some *Ulva* species (Ulvales, Chlorophyceae) biogeography and host-specificity also showed an effect on the bacterial assembly at the taxonomic scale, a large proportion of core functions were shared between *U. australis* (from Spain and Australia), *U. rigida* (Spain) and *U. ohnoi* (Australia) (Roth-Schulze et al., 2018).

In the first instance, the host surface chemistry could explain the specificity of the microbial community assembly associated to a given algal species (Hollants et al., 2013). Some surface metabolites act as chemical defenses displaying anti-adhesion activities (e.g., halogenated furanones; Manefield et al., 1999) while others show chemo-attracting properties allowing a specific microbial gardening (e.g., DMSP, Kessler et al., 2018; Wichard and Beemelmanns, 2018). Polysaccharides are also key biochemical components of algal surfaces and these biopolymers can be degraded by algal-specific associated bacterial taxa, such as *Zobellia galactanivorans,* which is hypothesized to form profitable and stable interactions with its algal host (Thomas et al., 2013; Barbeyron et al., 2016).

Moreover, biogeography implied differences in physicochemical parameters, such as temperature, irradiance, pH, salinity and anthropic pollutions, and thus could also explain variations observed in

microbial community assembly (Case et al., 2011; Saha et al., 2014, 2020b; Aires et al., 2018; Qiu et al., 2019). Environmental factors are notably known to shape the algal epiphytic microbiota but also the host condition leading in some cases to dysbiosis (Mensch et al., 2016; Zozaya-Valdés et al., 2016; Huggett et al., 2018; Minich et al., 2018; Paix et al., 2019). A continent-scale study conducted on *Ecklonia radiata* collected along Australian coasts highlighted that biogeographical differences of microbiota could be more strongly associated to host condition rather than to environmental variables (Marzinelli et al., 2015). While unexamined in this study, environmental differences among sampling sites may induce a differential expression of surface metabolites resulting in changes in host-microbiota interactions and consequently in the microbiota structure.

The Dictyotales represent an important brown algal order among the Phaeophyceae in terms of diversity, with 316 accepted species (Guiry and Guiry, 2020), and ecologically (Steen et al., *in review*; Vieira, 2020). The present study focuses on the genus *Taonia* J.Agardh (Dictyotales, Phaeophyceae) whose representative species are commonly observed along French Mediterranean and North Atlantic coasts. The genus *Taonia* currently comprises six taxonomically accepted species (Guiry and Guiry, 2020): *T. abbottiana* D.S.Littler & Littler (Jamaica), *T. atomaria* (Woodw.) J.Agardh (United Kingdom), *T. australasica* J.Agardh (Australia), *T. lacheana* Cormaci, G.Furnari & Pizzuto (Italy), *T. lennebackerae* Farl. ex J.Agardh (California), and *T. pseudociliata* (J.V.Lamour.) Nizam. & Godeh (Haiti). *Taonia atomaria*, the type species of the genus, is considered to show a cosmopolitan distribution (OBIS, 2020). However, this is not supported by molecular, nor morphological data and, to our knowledge, North Atlantic or English Channel populations of this species have never been compared with Mediterranean ones. *Taonia atomaria* has been already used as a holobiont model in previous studies on epibacterial communities and surface metabolites on Mediterranean sites (Othmani et al., 2016a; Paix et al., 2019, 2020)

Using barcoding and a multi-omics approach, coupling LC-MS-based metabolomics and 16S rRNA gene metabarcoding, the present study aims to: (1) determine if populations of *Taonia* spp. collected along the French Mediterranean and North Brittany coasts are conspecific; and (2) assess the role of the environment, the host taxonomy and the surface metabolome on the epiphytic microbial community assembly.

2.3. Material and Methods

Thalli of *Taonia* (Dictyotales, Phaeophyceae) individuals were collected by snorkeling in May and July 2018 at 18 sites along the French Mediterranean coast and one site on the French North Brittany coast (**Figure III. 1**, Table SIII.1). Temperature, pH, salinity, oxygen and turbidity were measured using two multiparameter probes: Hydrolab® DS5X (Hatch Hydromet, USA) for Mediterranean sites and YSI™ Professional Plus (YSI, USA) for the Brittany site. Triplicates of thalli (from three different individual) were collected at each site resulting in a total of 57 specimens, used for the four analyses: (1) barcoding of algal host, (2) metabolomics of algal surfaces, (3 and 4) metabarcoding and flow cytometry of epiphytic prokaryotic communities. On site, *Taonia* samples were dried in silica gel for (1), surface extracts were extracted as described in Paix et al., 2020, by dipping a frond during 5s in 5 mL of methanol for (2); epibacterial cells were collected by gently scraping squares of 1 cm^2 of two other fronds with a sterile scalpel as previously described in Paix et al., 2019, 2020 and conserved in a Tris-EDTA buffer for (3) and an in 4 mL of 1% glutaraldehyde filtered seawater solution for (4). Samples were kept at -20°C in a cool box and transported at lab within one hour. Surface extracts were conserved at -20°C and epibacterial cells at -80°C.

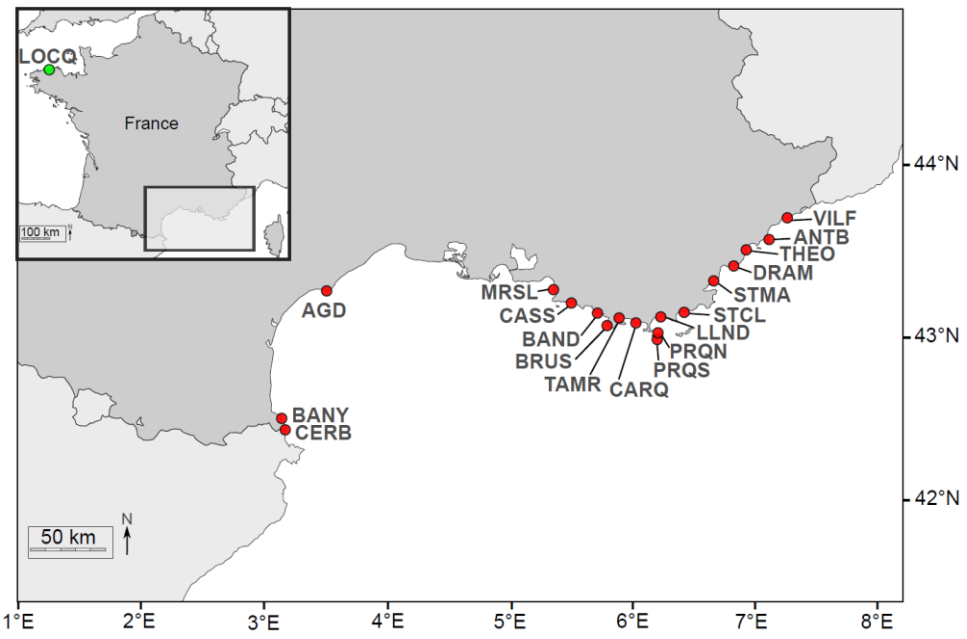

Figure III. 1. Map with the location of the 19 sampling sites. From right to left: VILF: Villefranche-sur-Mer; ANTB: Cap d'Antibes; THEO: Théoule-sur-Mer; DRAM: Le Dramont; STMA: Sainte-Maxime; STCL; Saint-Clair; LLND: La Londe-les-Maures; PRQN: Porquerolles island (Northern coast); PRQS: Porquerolles island (Southern coast); CARQ: Carqueiranne; TAMR: Tamaris; BRUS: Le Brusc; BAND: Bandol; CASS: Cassis; MRSL: Marseille; AGD: Agde; BANY: Banyuls-sur-Mer; CERB: Cerbère; LOCQ: Locquirec.

Total genomic DNA was extracted from *Taonia* tissue samples using a cetyltrimethylammonium bromide (CTAB) extraction method (Steen et al., 2015). Sequences were generated from the mitochondrial encoded cytochrome c oxidase III gene (*cox*3), the chloroplast encoded ribulose-1,5-biphosphate carboxylase (*rbc*L) and the photosystem II protein D1 (*psb*A) genes following Vieira et al. (2014). Sequences from the three genes were concatenated and aligned using MUSCLE v.3.5 (Edgar, 2004). Phylogenetic trees were reconstructed based on the concatenated alignment using Bayesian (BI) and maximum likelihood (ML) methods following (Vieira et al., 2014).

Metabolomics analyses were performed as described in Paix et al. (2019), by UHPLC-ESI-HRMS using a UPLC system (Dionex Ultimate 3000 rapid Separation; Thermo Fisher Scientific) equipped with an analytical core-shell reversed phase column (150 × 2.1 mm, 1.7 μm, Kinetex Phenyl-Hexyl; Phenomenex, Le Pecq, France) and coupled with a ESI-QToF Impact II mass spectrometer (Bruker Daltonics, Bremen, Germany) working in the positive ionization mode. Raw UPLC-MS data were processed for peak finding, integration and alignment using the open source XCMS package (Smith et al., 2006) in the R 3.2.3 environment. Data were filtered according to (Favre et al., 2017). The resulting data matrix was $\log_{10}$-transformed, mean-centered and analyzed using a hierarchical clustering dendrogram (Euclidean distance, mean method). PLS-DA analysis was performed to reveal the most discriminant metabolites involved in the differences between geographical areas. Metabolites were annotated as described in Paix et al. (2019).

Flow cytometry analyses were used to assess densities of prokaryotic heterotrophs at the surface of the algal samples. Cells were stained using SYBR green I (Invitrogen, Carlsbad, CA, USA) and enumerated using a BD Accuri C6 flow cytometer (BD Biosciences, San Jose, CA, USA) as previously described in Paix et al. (2020). Data were analyzed using ANOVA followed by an HSD Tukey's test.

Metabarcoding approaches were performed as previously described (Paix et al., 2020). Briefly, DNA extraction of algal biofilm samples was performed using the DNeasy PowerBiofilm kit (MoBio, Qiagen, Germantown, MD, USA). V4-V5 region of the 16S rRNA gene was amplified using the 515F-Y and 926R primers (Parada et al., 2016). Amplicons were sent to the GeT platform (Toulouse, France) for MiSeq Illumina sequencing (2 $\times$ 250 bp). 16S rRNA gene reads were processed using the FROGS workflow under the Galaxy environment (Escudié et al., 2018). Hierarchical clustering dendrogram was constructed using UPGMA method with Bray-Curtis distance. SIMPER analysis was conducted to reveal taxa which contribute the most to the overall dissimilarity between geographical areas. In this study, the core community was defined by keeping only OTUs occurring at least in one replicate of each site.

2.4. Results and discussion

Taonia atomaria forms rather dense cover on rocky shores along the Mediterranean coast, while specimens were observed on sandy substrates on the North Brittany coast. Samples from both locations differed morphologically with the Mediterranean specimens displaying small thalli (up to 8 cm long and 1 cm wide) characteristically branched and twisted, while the North Brittany specimens displayed larger thalli (up to 30 cm long and 4 cm wide) with fewer branches (Fig. SIII.1).

Phylogenetic results based on the concatenated alignment of the *cox*3, *psb*A and *rbc*L datasets indicated that the *Taonia* specimens collected in this study composed two distinct and well-supported genetic clusters in both analyses (ML and BI; **Figure III.2**). These genetic clusters reflect clear geographical differences. The first cluster (Cluster 1, **Figure III.2**) was composed of specimens from the French Mediterranean (mainland) coast only and the second one of specimens from North Brittany (Cluster 2, **Figure III.2**). Mediterranean sub-clusters were clearly not related to geographical locations. The literature reports the occurrence of two species from France (mainland): *T. atomaria* and *T. pseudociliata.* The two species were reported from the French Mediterranean coast, and only *T. atomaria* from Brittany. The species from North Brittany is morphologically closer to the description of *T. atomaria* than the species from the French Mediterranean coast. Admitting that the species identified from North Brittany corresponds to the genuine *T. atomaria* – originally described from the English Channel (Norfolk, UK) –, the species identified from the French Mediterranean coast could correspond to *T. pseudociliata*. However, no taxonomically confirmed sequence data are presently available from neither *T. atomaria* nor *T. pseudociliata* to check this assumption. Future taxonomic studies using molecular and morphological data are therefore needed to determine to which species correspond these two lineages identified from North Brittany and the French Mediterranean coast. Furthermore, it cannot be excluded that *T. lacheana* known so far only from Italy could also be present along the French Mediterranean coast and correspond to the species presently identified.

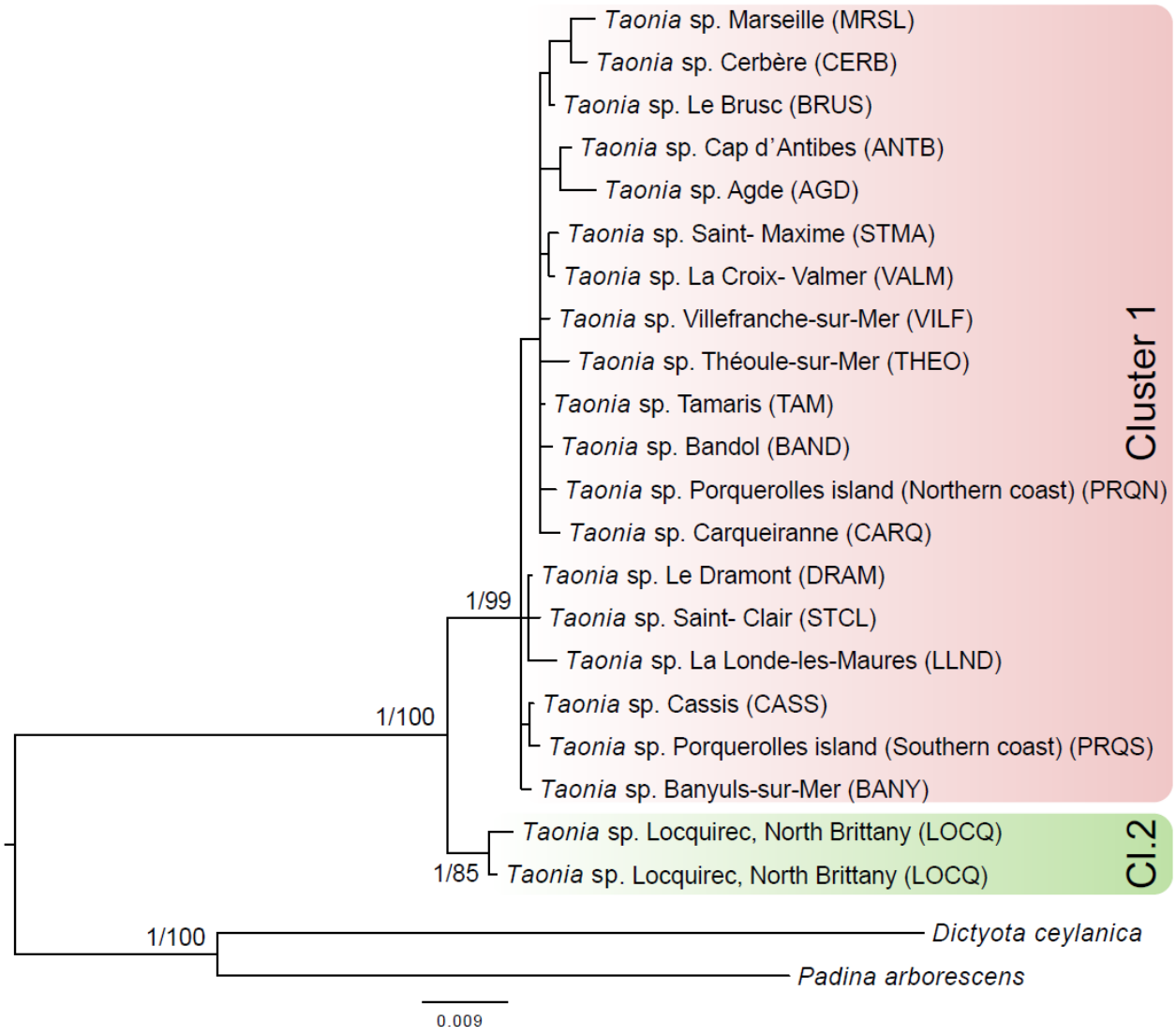

Figure III.2. Bayesian phylogenetic tree of *Taonia* based on the concatenated alignment of cox3, psbA and rbcL datasets. Values at the nodes represent Bayesian (left) and maximum likelihood (right) support values.

For both hierarchical dendrograms constructed with metabarcoding and surface metabolome datasets, the main clustering pattern revealed clear differences between the North Brittany samples (site LOCQ) on one hand, and the Mediterranean ones, on the other hand (**Figure III.3** and **Figure III.4**). In addition, Brittany samples exhibited a significant lower α-diversity compared to all Mediterranean ones (Fig. SIII.2). Considering Mediterranean sub-clusters of both metabolomics and metabarcoding analyses, they were not related to geographic areas. More interestingly, the clustering pattern (i.e. Brittany *vs* Mediterranean samples) appeared similar to the algal phylogenetic pattern described above. Two possible scenarios can be considered to explain such biogeographical features at the holobiont scale. On one hand, host-

phylogenetic differences observed between North Brittany and Mediterranean samples may involve physiological and functional differences, which could notably result in various selective pressures including the differential expression of surface metabolites involved in the selection of a specific microbiota. On the other hand, environmental differences between the English Channel and Mediterranean coasts could also constitute factors explaining such a clustering. Mediterranean conditions differ from those found on the English Channel coasts, notably with higher temperatures (21.9°C *vs* 18°C] and salinities (39.2 ppt *vs* 35.2 ppt). Besides, seawater on the North Brittany coast are mainly mesotrophic to eutrophic (Tappin and Millward, 2015) with substantial tidal regime, while those of the French Mediterranean coast are generally oligotrophic to mesotrophic, depending on the anthropic pressures (Béthoux et al., 1998; Thingstad et al., 2005), and non-tidal. Moreover, collection sites differed also in term of irradiance and substrate types since North Brittany samples were collected on a sandy zone at 3 to 5m depth (low tide) while Mediterranean ones were sampled on rocky substrates at 1 to 2m depth. Local Mediterranean specific conditions of wind, sea currents, pollutants and nature of rocky substrates, like volcanic stones close to Agde, may also provide dissimilar environmental conditions for the development of *T. atomaria* but appeared as less relevant factors.

The major epibacterial taxa observed for *Taonia* samples belonged to families Hyphomonadaceae, Rhodobacteraceae, and Sphingomonadaceae (Alpha-proteobacteria), Saprospiraceae and Flavobacteriaceae (Bacteroidetes), and Thiohalorhabdaceae (Gamma-proteobacteria) (**Figure III.3**). The mean percentage of sequences of core OTUs reached 65% of the total community. Conversely, a high level of intraspecies variability was observed for the core epibacterial OTUs of *Ulva* species including Australian and Spanish samples (Burke et al., 2011b, 2011a; Roth-Schulze et al., 2018), kelp species from different habitat types in US and Australian locations (Marzinelli et al., 2015; Weigel and Pfister, 2019) or *Caulerpa* species (Morrissey et al., 2019). The core community of *Taonia* was mainly affiliated to Hyphomonadaceae represented primarily by the genus *Litorimonas* (5.7% of sequences of all core OTUs), Thiohalorhabdaceae by the genus *Granulosicoccus* (9.5%), Saprospiraceae by the genera *Lewinella*, *Portibacter* and *Rubidimonas* (5.0, 3.8, and 3.6%), and Flavobacteriaceae by the genera *Algitalea*, *Tenacibaculum* and *Maribacter* (2.5, 2.1, and 2.0%). In addition, this core community appeared relatively high in comparison with a previous study focused on temporal variations of *T. atomaria* on a single Mediterranean site (CARQ) (Paix et al., 2019). It could indicate that temperature, that was proposed to drive temporal variations at CARQ, impacted more strongly epibacterial communities than salinity or nutrients that mainly differentiated Brittany from Mediterranean locations. However, several authors considered epibacterial recruitment as only partially deterministic and mentioned that environmental factors alone could not

explain epiphytic community structures (Burke et al., 2011a; Morrissey et al., 2019; Weigel and Pfister, 2019). Especially, functional aspects should have to be considered (Burke et al., 2011a; Marzinelli et al., 2015; Morrissey et al., 2019).

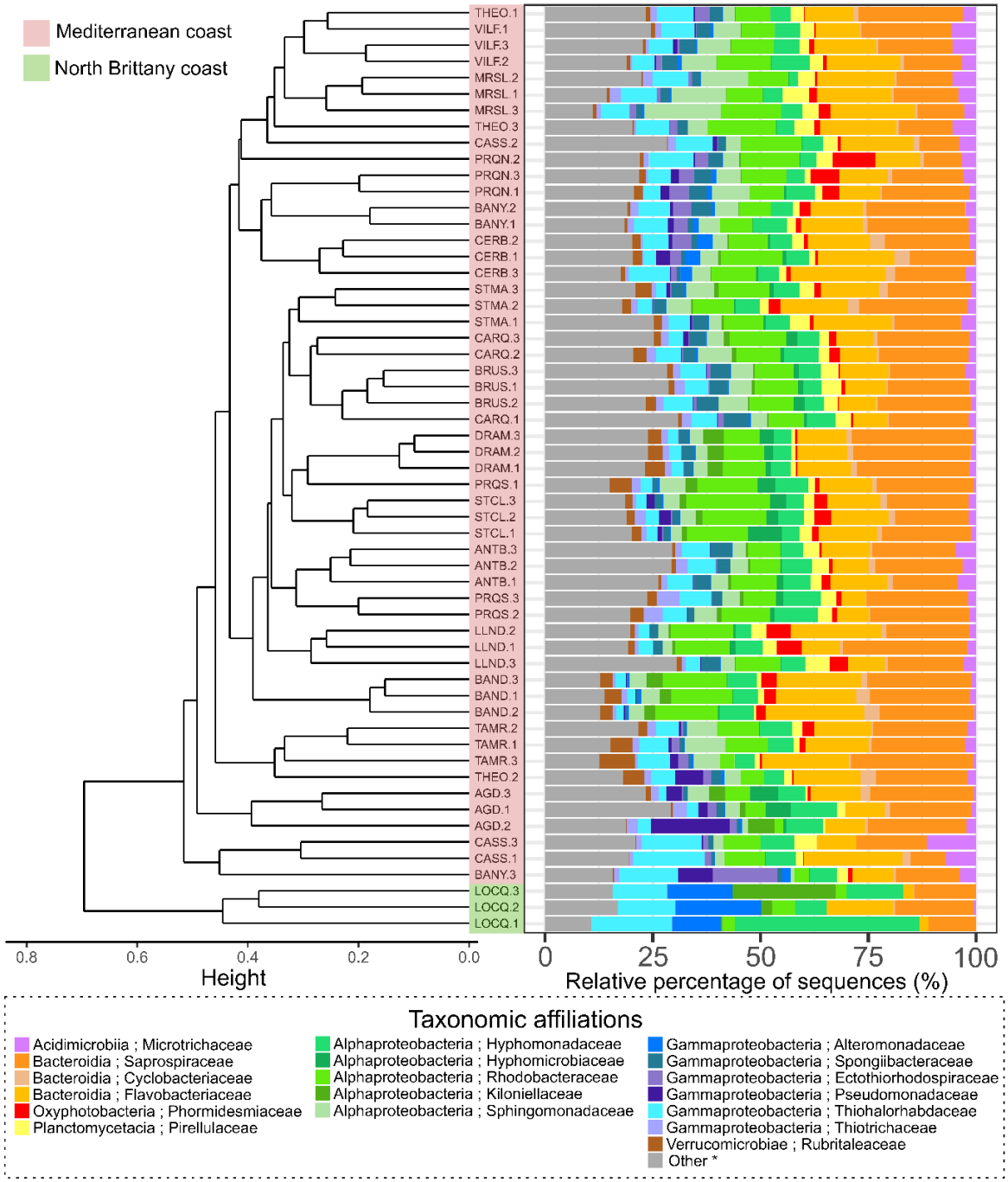

Figure III.3. β-diversity and structure of prokaryotic communities at the surface of *Taonia* samples. The dendrogram corresponds to a UPGMA clustering based on Bray-Curtis distance and calculated at the OTU level. Histograms represent the relative abundances of the main families. * "Other" corresponds to unaffiliated families and those below 1%.

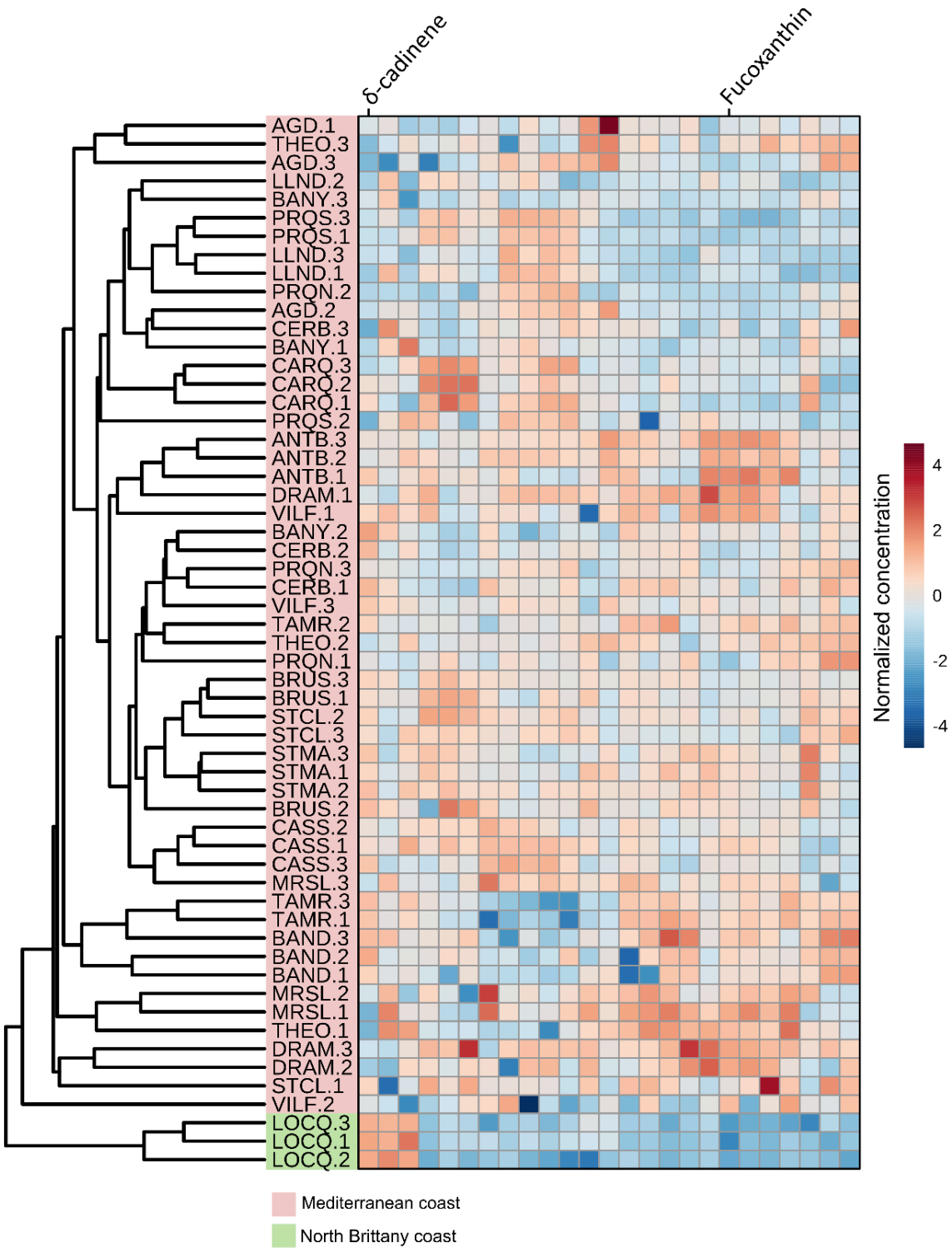

Figure III.4. Metabolomics fingerprinting of surface extracts of *Taonia* samples. The dendrogram corresponds to a Euclidian clustering based on the average method and calculated with all metabolites of the metabolomics dataset. The heatmap shows relative concentration of the 25 most discriminant metabolites according to both geographical areas (Mediterranean vs Atlantic sites).

Interestingly, among the core taxa the genus *Granulosicoccus* was already described as a major core and pioneer taxon identified in previous studies (Paix et al., 2019, 2020). In addition, predominant OTUs from the genus *Granulosicoccus* have been already encountered at the surface of many other algal models, such as *Laminaria hyperborea* (Bengtsson et al., 2012), *Fucus vesiculosus* (Lachnit et al., 2011), *Macrocystis pyrifera* (Weigel and Pfister, 2019), *Mastocarpus* spp. (Lemay et al., 2018), and *Ulva* spp. (Califano et al., 2020). In the case of *Mastocarpus* spp., this bacterial genus has been also found as a core taxon, common to both life history phases of the algal host (sporophytes *vs* gametophytes). For *L. hyperborea*, it has been suggested that *Granulosicoccus* spp. could be pioneer colonizers which benefit from a specific adaptation allowing a rapid attachment and development on young algal surfaces. For US kelp species, it was identified as the dominant genus (Weigel and Pfister, 2019). In accordance with these observations, we also suggested that OTUs among this genus may be especially adapted to the surface macroalgal niche in a large range of environmental conditions and host species.

When comparing all the samples, Gamma-proteobacteria showed higher percentages in North Brittany specimens of *Taonia* compared with Mediterranean ones, notably with the family Alteromonadaceae (**Figure III.3**). The SIMPER analysis (Table SIII.2) revealed *Litorimonas* (Hyphomonadaceae), *Granulosicoccus* (Thiohalorhabdaceae) and *Alteromonas* (Alteromonadaceae) as major significant genera involved in the dissimilarity between samples collected from these two geographical areas (6.5, 4.9, and 6%, respectively), with higher percentages at the surface of samples from North Brittany. In contrast, the genus *Croceitalea* (Flavobacteriaceae) appeared as a major taxon of Mediterranean samples and contributed significantly to 1.7% of the dissimilarity with samples from North Brittany.

Several species among the genus *Alteromonas* were notably described for their abilities to degrade algal polysaccharides (Akagawa-Matsushita et al., 1992). Some of them are also reported as r-strategists such as *Alteromonas macleodii* which was notably characterized by a quick growth within nutrient-enriched environments (Zemb et al., 2010; Romera-Castillo et al., 2011; Tada et al., 2011; Lawes et al., 2016). Consequently, the eutrophic status of the French North Brittany coast may constitute a favorable environment for the development of *Alteromonas* spp. on algae.

The PLS-DA analyses conducted with the LC-MS-based metabolomics dataset allowed to investigate the metabolites differentially expressed between Mediterranean samples and those from Brittany. Among surface metabolites, the two main discriminant ones were identified through their comparison with purified standards (Viano et al., 2009; Othmani et al., 2016b) and corresponded to fucoxanthin and a bicyclic sesquiterpene (*δ*-cadinene)(**Figure III.4** and SIII.3). Fucoxanthin (VIP score = 3.16) was observed in

significant higher concentrations in all Mediterranean sites compared to the Breton one (LOCQ) while the opposite tendency was observed for *δ*-cadinene (VIP score = 2.61, **Figure III.4** and SIII.3), characterized by significant higher concentrations at LOCQ compared with 5 Mediterranean sites (AGD, MRSL, PRQN, LLND and THEO). Fucoxanthin is a common photosynthetic pigment of brown algae and differences in its concentration can be linked to irradiance variations. Indeed, fucoxanthin content is known to increase with depth for many brown seaweeds. Such a pattern is explained as a photo-adaptation of the algae to lower light intensity and quality which occurs at greater depths in order to ensure an optimal photosynthetic activity (Ramus et al., 1977; Perez-Bermudez et al., 1981). Herein, on the contrary, fucoxanthin was observed in lower concentrations in Breton samples where algae were collected in rather deeper zones than Mediterranean ones. Consequently, in this case the differences of fucoxanthin production at the surface of *T. atomaria* might not result to a shading adaptation. However, fucoxanthin is also involved in the protection against several oxidative stresses. In particular, its radical scavenging activity constitutes a protection which allows to reduce damages caused by reactive oxygen species produced under high irradiance conditions (Mikami and Hosokawa, 2013). Through its oligo- to mesotrophic status and highly transparent waters, French Mediterranean seawaters are characterized by higher irradiance, in terms of both light intensities and length. Consequently, high irradiance may involve a photoprotective adaptation of Mediterranean *T. atomaria* individuals (Paix et al., *in prep.*). Besides, other factors resulting in an oxidative stress can also be implied in the differences observed in the fucoxanthin production. As an example, it could be interesting to take into account in further works the oxidative stress caused by copper in contaminated areas (Costa et al., 2016; Rodríguez et al., 2018).

Furthermore, previous studies conducted on *F. vesiculosus* and *Dictyota* sp. have shown that fucoxanthin acts as an antimicrobial compound at the algal surface by inhibiting the settlement of bacteria through bio-assays experiments (Saha et al., 2011; Viano et al., 2009). Besides, an *in situ* approach has also confirmed that a fraction of algal extracts containing fucoxanthin deposited at the surface of an experimental device significantly decreases the epibacterial colonization (Lachnit et al., 2013). However, heteroprokaryotic cells densities measured with cytometry analyses showed values ranging from 3×10^5 to 7×10^6 cells.cm^{-2} without any significant differences between Breton and Mediterranean samples, and neither between the Mediterranean sites. Moreover, when comparing cells densities and fucoxanthin concentrations, these two variables did not appear significantly correlated (Pearson correlation: r = 0.26, $p > 0.05$), suggesting no quantitative effect of fucoxanthin on the microbiota (Fig. SIII.2). Moreover, Shannon and Chao1 indexes were significantly higher for all Mediterranean samples compared to the Breton ones. Similarly, for both indexes, no significant correlation was observed with the fucoxanthin

concentration (Pearson correlation: r = 0.21, $p > 0.05$ for both indexes), suggesting also that fucoxanthin might not act as a major antimicrobial compound reducing the α-diversity at the surface of Mediterranean samples of *T. atomaria*.

The bicyclic sesquiterpene δ-cadinene was observed as a chemical biomarker of Atlantic samples. Terpenoids compounds were widely described among Dictyotales, such as cyclic diterpenes mainly found within the genus *Dictyota* (Kelecom and Laneuville Teixeira, 1986; Vallim et al., 2005; Paula et al., 2011). The main terpenoids isolated within the genus *Taonia* are geranylgeranylglycerol and cyclic sesquiterpenes (De Rosa et al., 1994; Tringali et al., 1995; Othmani et al., 2016b). Some of these compounds have been reported for their anti-adhesion activities against marine bacteria (Othmani et al., 2016a, 2016b). Moreover, the carbon skeletons of sesquiterpenes differ sharply between *Taonia* species: *T. lacheana* is characterized by aromadendrane sesquiterpenes (Tringali et al., 1995) while sesquiterpenoids with germacrane, cadinane and spiroaxane skeletons were observed in the extracts of *T. atomaria* (De Rosa et al., 1994; Othmani et al., 2016b; Jerković et al., 2019). Here, the presence of a cadinane sesquiterpene as a biomarker of Breton samples tended to confirm that these algal samples correspond to *T. atomaria* while their relative low abundance in Mediterranean samples may be consistent with phylogenetical differences. Neither on previous studies conducted at the site CARQ (Othmani et al., 2016a, 2016b; Paix et al., 2019), nor in this work, aromadendrane sesquiterpenes were observed while some cadinane and germacrane sesquiterpenoids were identified in these studies. This finding suggested that the Mediterranean thalli investigated in this study may also differ from *T. lacheana*.

Sesquiterpenes constitute a chemical class of natural products found in a large diversity of organisms (Blunt et al., 2007). These compounds often demonstrated antimicrobial activities such as bicyclic sesquiterpenes within floral organs of several plants (Junker and Tholl, 2013; Boachon et al., 2019) or halogenated sesquiterpenes from red algae of the genus *Laurencia* (Vairappan et al., 2008). In the case of *T. atomaria*, the spiroaxane sesquiterpene gleenol has been found to show specific anti-adhesion activities against a panel of marine bacteria at ecological relevant concentrations (Othmani et al., 2016a, 2016b). However, anti-adhesion activities of δ-cadinene have not been described in these latter studies and its effect on the selection of a specific microbiota at the surface of *T. atomaria* could be interesting to consider.

2.5. Conclusion

Focusing on the brown algal genus *Taonia*, we provide a growing body of elements that the host taxonomy, the environment and surface metabolomes need to be further considered in biogeographical

studies on seaweed holobionts. To our knowledge, this work constituted the first biogeographical study conducted at a large scale, which coupled these three complementary approaches. The genetic diversity within the genus *Taonia* was scarcely studied before and we revealed through phylogenetic analyses that algal samples from the French Mediterranean coast could constitute a distinct species from *Taonia* sp. encountered in the French North Brittany. Here, we brought evidence that genetical and environmental differences may both contribute to the specificity of metabolome and microbiome composition at the algal surface. More particularly, while differential expression of fucoxanthin at the surface could be more related to environmental adaptation, the case of *δ*-cadinene may rather result from phylogenetic differences. Such a contrasted metabolome at the surface of *T. atomaria* may consequently result in the selection of a specific microbiota while environmental differences could also constitute a major factor shaping directly the microbiota structure, notably when considering the *Alteromonas* enrichment in surface communities from Brittany.

2.6. Acknowledgments

This work was funded by the French “Sud Provence-Alpes-Côte d’Azur (Sud PACA)” regional council (PhD grant of B.P.) and the EC2CO project “COHESIONS”. The authors are grateful to Dr. M. Peirache, E. Baudin and L. Maxime (National Park of Port-Cros, Hyères-les-Palmiers, France) for the sampling at Porquerolles Island, to Dr R. Lami (Sorbonne University, LBBM, France) for the sampling at Banyuls-sur-Mer and Cerbère, to Dr. B. Misson (Toulon University, MIO, France) for his help with flow cytometry analyses, to Dr S. Greff (Aix-Marseille University, IMBE, France) for the acquisition of LC-MS profiles and to N. Carriot (Toulon University, MAPIEM, France) for his help for all sampling along the Mediterranean coasts and for the annotation of MS/MS data. LC-MS experiments were conducted on the regional platform MALLABAR funded by the Institute of Ecology and Environment (INEE) of the French National Centre for Scientific Research (CNRS) and the French Sud PACA regional council. This work was supported by Ghent University (BOF/01J04813) with infrastructure funded by European Marine Biological Resource Centre Belgium/Research Foundation - Flanders Project GOH3817N (to O.D.C.). CV is indebted to Ghent University – Special Research Fund for a grant as postdoctoral researcher.

3. Bilan du chapitre

Dans le cadre de cette étude biogéographique, les analyses phylogénétiques de spécimens de *Taonia* prélevés sur 20 sites couvrant l'ensemble de la côte méditerranéenne française et un site sur la côte nord de la Bretagne ont permis de révéler deux clusters distincts avec d'une part les échantillons méditerranéens et d'autre part ceux de Bretagne, suggérant ainsi deux espèces potentiellement distinctes. Des analyses de morphologie et de phylogénie plus détaillées seront néanmoins nécessaires pour valider cette hypothèse. De manière parallèle, les analyses du microbiote et du métabolome de surface des algues ont aussi montré des différences significatives entre les échantillons prélevés en mer Méditerranée et en Bretagne, bien que la similarité entre les communautés soit importante. Il est alors envisagé que la phylogénie mais aussi les différences de conditions environnementales puissent constituer deux facteurs non exclusifs expliquant de telles différences au niveau du microbiotes et du métabolome.

CHAPITRE IV : ANNOTATION DU METABOLOME

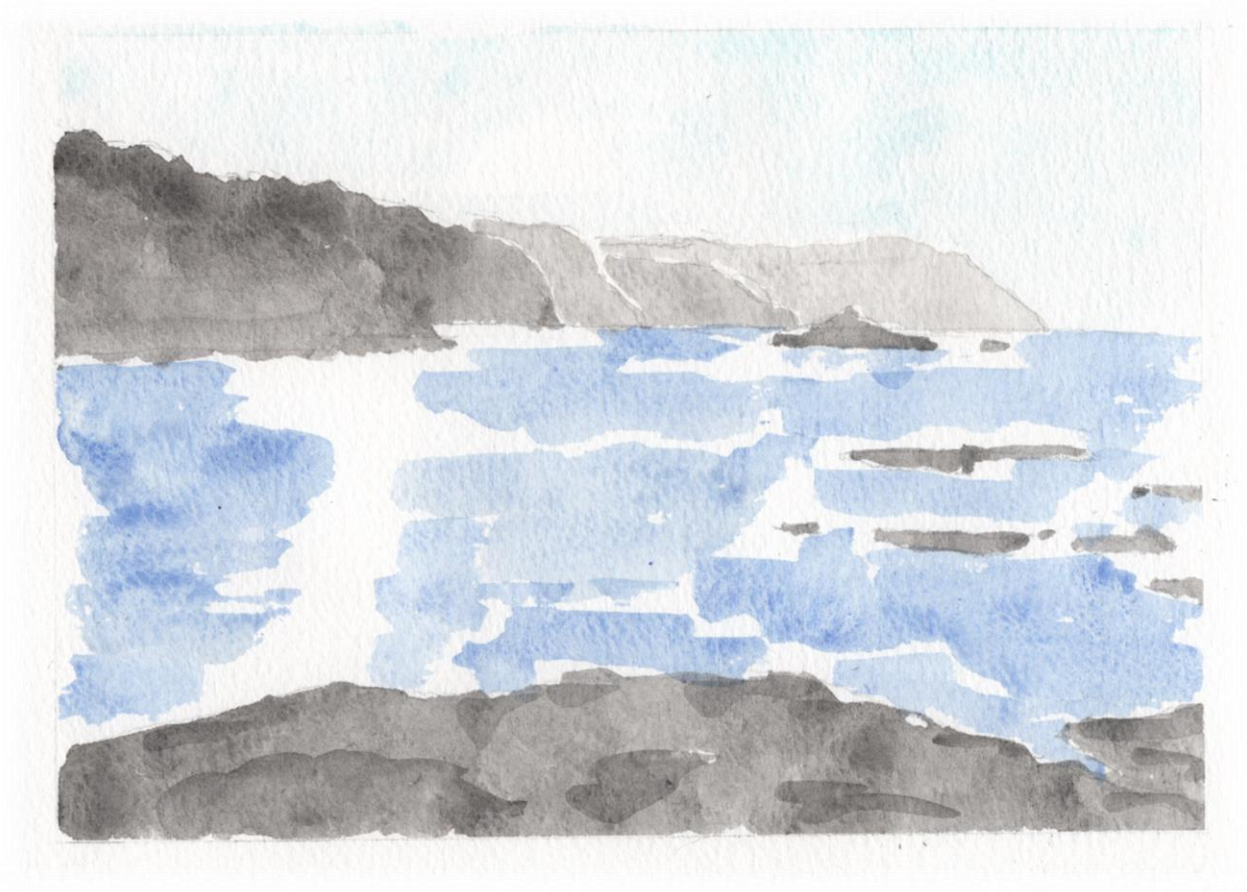

Le Brusc, vue depuis les promontoires rocheux de l'île du Petit Gaou

1. Avant-propos

L'annotation des métabolites de surface constitue une étape essentielle afin de pouvoir identifier d'éventuelles interactions chimiques à la surface entre *T. atomaria* et son microbiote. Elle représente généralement une difficulté majeure dans le cadre de travaux en écologie chimique marine menés par le biais d'approches métabolomiques. Ainsi, l'objectif de ce chapitre est de pouvoir annoter et optimiser l'annotation du métabolome d'un organisme (marin) non-modèle tel que *T. atomaria*. Cette étude est présentée sous la forme d'un article de recherche en préparation en vue d'une soumission dans la revue *Talanta*. Les références bibliographiques citées dans cet article sont indexées en fin de manuscrit. La partie *Supplementary Information* de cet article est presentée dans l'annexe IV du manuscrit (annexe électronique).

2. Article: Integration of LC/MS-based molecular networking and classical phytochemical approach allows in-depth annotation of the metabolome of non-model organisms - The case study of the brown seaweed *Taonia atomaria*

Nathan Carriot[a,1], Benoît Paix[a,1], Stéphane Greff[b], Bruno Viguier[a], Jean-François Briand[a], Gérald Culioli[a,*]

[a] Université de Toulon, MAPIEM, EA 4323, Toulon, France

[b] Aix Marseille Université, CNRS, IRD, Avignon Université, Institut Méditerranéen de Biodiversité et d'Ecologie marine et continentale (IMBE), Station marine d'Endoume, Marseille, France.

[1]These authors contributed equally to this work.

[*]Corresponding author.

E-mail address: culioli@univ-tln.fr (G. Culioli)

2.1. Highlights

- A new annotation method using MS/MS molecular networking was developed.
- A workflow coupling molecular networking and phytochemistry was described.
- Two new and one rare families of algal lipids were putatively described.
- 212 metabolites were annotated from the metabolome of the brown alga *T. atomaria*.

Keywords: Molecular networking; Metabolomics; Lipidomics; UHPLC-MS/MS; Macroalga; *Taonia atomaria*

2.2. Introduction

Marine chemical ecology is a recent field of research that aims to address the role of chemical communication in marine ecosystems. Indeed, the molecules expressed by marine organisms could have preponderant ecological functions related to foraging, defense or reproduction (Hay, 2009). This discipline is booming because it benefits from many recent technical advances including those of environmental metabolomics.

Metabolomics is the latest in the so-called "omics" sciences that brings together genomics, transcriptomics and proteomics (Tautenhahn et al., 2012). Ultimately, the aim is to decipher the metabolome, which represents the whole set of low-molecular-weight organic compounds present in an organism or more generally in a biological sample, and to evaluate its variations (Oliver et al., 1998). The metabolome is constituted by all quantifiable metabolites and appears to be higly complementary with other “omics” sciences for a global “systems biology” approach (Dittami et al., 2014; Monte et al., 2014).

Untargeted LC-MS-based metabolomic studies are currently the most common ones but metabolite identification is generally the limiting factor when interpreting the resulting data (Chaleckis et al., 2019). Indeed, the diversity of the metabolism is vast in nature (Vaniya and Fiehn, 2015) and metabolites implied in the discrimination between samples groups often remain unidentified. With an estimation of less than 2% of mass spectra which can be annotated from untargeted studies, the characterization of the chemical structures is the most challenging step of the metabolomic workflow (da Silva et al., 2015). Knowing that each LC-MS analysis generates a large number of spectra (Kind et al., 2012; Scheubert et al., 2017), spectral identification of each compound, one by one, using classical dereplication tools with reference databases such as NCBI, Metlin, NIST or MassBank, is way too time-consuming. Since few years, MS/MS molecular networking (MN) has been proposed as a new emerging tool to optimize this dereplication process (Yang et al., 2013b). Based on the idea that MS/MS fragmentation patterns are similar between molecules sharing a similar chemical structure, the Global Natural Products Social Molecular Networking (GNPS) Web-platform (http://gnps.ucsd.edu) allows to generate MNs where compounds are linked according to their molecular relatedness (Wang et al., 2016; Nothias et al., 2018). The resulting MNs show then diverse clusters composed by several *m/z* features (called nodes) characterized by their MS/MS data. The clusters generated in a MN could then gather metabolites belonging to a same chemical family or sharing closely related chemical structures.

In this study, the use in a first step of a restricted MN will allow to gather compounds having very similar chemical structures on order to facilitate their annotation. Indeed, to "unlock" clusters and identify all the

nodes in a cluster, two situations are expected: (i) if a compound is identified, all the nodes of a cluster are annotated using mass differences from this "seed node" (Duncan et al., 2015; Grim et al., 2019), (ii) if all the compounds remain unidentified, the annotation can be done by determining the common structural characteristics of the nodes thanks to the comparison of their MS/MS spectra. The enlargement of the MN is then considered in order to continue the annotation of the metabolome by using less restrictive parameters for the connection between nodes.

The selected model in this study was *Taonia atomaria*, a brown alga commonly reported along the Mediterranean and North-Eastern Atlantic coasts. To date, several types of chemical compounds, mainly sesquiterpenes (De Rosa et al., 1994; Tringali et al., 1995; Othmani et al., 2016a, 2016b), meroditerpenes (González et al., 1971, 1974; Pellegrini et al., 1997; Abatis et al., 2005; Tziveleka et al., 2005) and geranylgeranylglycerol (Amico et al., 1977; Tringali et al., 1995; Othmani et al., 2016b, 2016a), have been characterized from genus *Taonia* by classical natural products chemistry. Because of its morphology and distribution, this species represents a model of choice for the study in chemical ecology of the interactions between algae and their associated microbiota. For this reason, and in order to carry out metabolomic analyses for these purposes, our knowledge of the metabolome of this species needs to be improved.

The aim of the present study was to develop an optimal workflow dedicated to the annotation of a largely unexplored metabolome in the case of non-model species; in this case, *T. atomaria*. The proposed workflow was based on three successive steps: (i) a classical phytochemical approach permitting to isolate chemical standards which can then be used as seed nodes, initiating the “in-house” MS/MS database ; (ii) a GNPS networking approach with high restrictiveness allowing only the most structurally-related metabolites to cluster together and to enrich the database, and (iii) a GNPS networking approach with less restrictiveness allowing to gather other related metabolites in order to complete and finalize the database.

2.3. Materials and methods

2.3.1. Chemicals

Methanol (MeOH) and dichloromethane (CH_2Cl_2) used for the extraction of the algal material were of analytical grade, MeOH, CH_2Cl_2 and acetonitrile (ACN) used for Flash-chromatography and semi-preparative HPLC experiments were of HPLC grade, and ACN and MeOH used for UPLC experiments were of LC-MS grade. All these solvents were purchased from VWR (Fontenay-sous-Bois, France). Milli-Q water was generated by a Millipore ultrapure water system (Waters-Millipore Corporation, Milford, MA, USA). Formic acid of LC-MS grade (99%) used for UPLC analysis and deuterated chloroform and methanol (99,8%; $CDCl_3$ and CD_3OD, respectively) used for NMR experiments were purchased from Sigma-Aldrich (St Quentin-Fallavier, France).

2.3.2. Algal material

Thalli of the brown alga *Taonia atomaria* (Woodward) J. Agardh (family Dictyotaceae, class Phaeophyceae, phylum Ochrophyta) were collected by hand (1m depth) on the south eastern French Mediterranean coast (Tamaris; N 43°5'35.56, E 5°54'31.81) in February 2017. Algal samples were placed in plastic bags filled with surrounding seawater and transported within an hour to the laboratory in a cool box maintaining the seawater temperature.

2.3.3. Isolation of chemical standards from T. atomaria

2.3.3.1. Extraction of the algal material and fractionation of the crude extracts by Flash-chromatography

The collected algal samples were air-dried for 48h in the dark at room temperature, crushed and weighed. The dried algae (140g) were extracted using a mixture of MeOH/CH_2Cl_2 (1:1, v/v; 3 × 500 mL). The extracts were combined, filtered (filter paper), concentrated *in vacuo*, and weighted (25g; extraction yield: 17.9%, w/w).

A part of the resulting crude extracts was submitted to fractionation by flash chromatography (Spot Flash system; Armen Instruments, Saint Ave, France) on a reversed-phase column (SuperVarioFlash D40-RP18 model, 40-63 μm, 84g; Merck, Darmstadt, Germany). For fractionation, 4.7 g of these extracts were dissolved in 25 mL MeOH and mixed with 15g of reversed-phase silica gel (Sepra C18e, 50 μm; Phenomenex, Le Pecq, France), dried under reduced pressure and loaded on a guard column on the top of the column. The fractionation was monitored by UV detection at 205 nm. For the flow rate, a linear ramp was used from 2 to 32 mL/min during 2 min and then this final flow rate was maintained throughout

the entire experiment. The separation process was carried out using a ternary eluent system: H_2O (solvent A), MeOH (solvent B) and CH_2Cl_2 (solvent C). After an initial isocratic step with 90% of A and 10% of B from 0 to 3 min, a linear gradient up to 100% of B from 3 to 13 min, an isocratic step with 100% of B from 13 to 19 min, and a linear gradient up to 100% of C from 18 to 28 min, an isocratic step with 100% of C was finally used from 28 to 40 min. This process led to 39 fractions which were dried *in vacuo*, weighted and stored at -20°C (more details are given in Supporting Information, Table SIV.1).

2.3.3.2. Purification and structural characterization of chemical standards from T. atomaria

For a selection of fractions, an aliquot (5 to 10 mg) was solubilized in the appropriate deuterated solvent ($CDCl_3$ or CD_3OD) and analyzed by ^1H NMR on a 400 MHz Avance NMR spectrometer (Bruker BioSpin, Wissembourg, France) at room temperature.

Six fractions were selected based on the available quantities (m > 150 mg, see Table SIV.1) and the presence of NMR signals due to other compounds than common fatty acid derivatives. These fractions were then fractionated using a semi-preparative HPLC system (Prostar 210; Varian) equipped with a refractive index detector (Varian Prostar Model 350 RI) and a 50 μL injection loop. Purifications were done by iterative injections using various isocratic eluent conditions (mixtures of H_2O/ACN) at a flow rate of 3 mL/min on a reversed-phase C18 semi-preparative column (Purospher Star RP-18e, 5 μm, 10×250 mm; Merck) maintained at room temperature. This purification step yielded sub-fractions which were checked by ^1H NMR and allowed the obtention of eight pure compounds.

The chemical structure of pure compounds was determined through extensive 1D and 2D-NMR analysis (^{13}C, DEPT experiments, ^1H-^1H COSY, ^1H-^1H NOESY, HSQC and HMBC) and by comparison with data previously reported in the literature. The chemical shifts of the different spectra are fixed with respect to the residual signals of the solvent used: δ_H 7.26 and δ_C 77.16 for $CDCl_3$ and δ_H 3.31 and δ_C 49.00 for CD_3OD. All the purified compounds were analyzed by UPLC-ESI-QToF-MS/MS and these data [accurate mass, fragmentation pattern and retention time (RT)] were implemented in our in-house database.

2.3.4. Annotation of the metabolome of T. atomaria using molecular networking (MN)

2.3.4.1. UPLC-ESI-QToF-MS/MS analyses

For this analysis, sixteen selected fractions (see Table SIV.1) were solubilized in MeOH (5 mg/mL) and injected on a Dionex Ultimate 3000 Rapid Separation chromatographic system (Thermo Fisher Scientific, Sunnyvale, CA, USA) coupled via an ESI interface to a QToF Impact II mass spectrometer (Bruker Daltonics, Champs-sur-Marne, France). Chromatographic separations were performed on an analytical core-shell

reversed-phase column (150 × 2.1 mm, 1.7 μm, Kinetex Phenyl-Hexyl; Phenomenex) with a flow rate fixed at 0.5 mL/min. The column was maintained at 40°C, the injected sample volume was 5 μL and the autosampler temperature was kept at 4°C. An elution gradient involving a binary programming of acidified ACN and H_2O (0.1% of formic acid, v/v), was applied. The elution gradient started with 5% ACN and was kept for 2 min, then reached 100% ACN (linear ramp) in 10 min and was kept for 4 min; then came back to 5% ACN over 0.01 min and was maintained 2 min, for a total run time of 16 min.

The MS acquisition was performed in positive ionization and full scan range (*m/z* 50 to 1200 at a frequency of 2 Hz) modes. The following MS conditions were used: nebulizing gas (N_2) pressure: 0.4 bars, drying gas (N_2) flow: 4 L/min, drying temperature: 180°C, capillary voltage: 4.5 kV. The mass spectrometer was calibrated with a solution of formate/acetate forming clusters at the beginning of the sequence run and the same solution was automatically injected before each sample for internal mass calibration. MS/MS acquisition experiments were conducted by collision induced dissociation (CID) on each sample. Three major precursor ions were used and, after the acquisition of three MS/MS spectra per precursor ion, the corresponding *m/z* value was excluded from the precursor ion selection for 1 min.

2.3.4.2. MS/MS molecular networking using GNPS

Raw UPLC-MS/MS data were converted into ".mzXML" files using DataAnalysis software (version 4.3; Bruker Daltonics). The files corresponding to the sixteen fractions selected before (See Part 2.3.2.) were grouped into six folders corresponding to six polarity ranges. The Global Natural Products Social Molecular Networking online workflow (GNPS; http://gnps.ucsd.edu) was used to create MN of related compounds based on the similarity of their MS/MS fragmentation patterns (Wang et al., 2016). Three MNs (MN-1 to MN-3, from the most to the least restrictive) were then generated using various values of "*Minimum cosine score*", "*Minimum matched fragment ions*" and "*Network TopK*" (See Table SIV.2 for parameters details). Data from GNPS were imported into Cytoscape (version 3.7.0) using nodes to represent each spectrum (each *m/z* feature) and edges to represent the similarity of MS/MS fragmentation between two connected nodes (Wang et al., 2016). A specific color was attributed to each node according to the chemical family of the annotated metabolite or to the RT. Transparency of edges connecting each node was proportional to the spectral similarity using the cosine score as default parameter.

2.3.4.3. Metabolite annotation in the MNs

The strategy was to focus on clusters with the highest number of nodes. In such clusters, each node could be tentatively annotated by one or several of the following possibilities: (1) during the computational process dedicated to the construction of MNs on the GNPS platform, fragment similarity searches were

performed in several public databases (e.g. Massbank, HMDB, MoNA, Metlin…) for each *m/z* feature and the results were directly available into the MNs subsequently generated by Cytoscape, (2) MS data (accurate mass and fragmentation pattern) of a specific metabolite can also be compared with those found in other databases [e.g. PubChem (https://pubchem.ncbi.nlm.nih.gov), ChemSpider (www.chemspider.com), Lipidmaps (http://www.lipidmaps.org), CEU mass mediator (http://ceumass.eps.uspceu.es/) and/or Metlin (https://metlin.scripps.edu)] using various tools (e.g. MS-Finder) (Tautenhahn et al., 2012), (3) MS data and RT of the detected *m/z* features were compared with those of pure compounds isolated from *T. atomaria* (See Part 2.3.2.), and (4) in the case of absence of a hit in a database, the MS data of all the nodes in a same cluster were carefully analyzed to highlight specific common fragments or mass losses which could allow the identification of a specific chemical family in relation to the data available in the literature or through mass fragmentation pattern analysis.

In all these cases, once one *m/z* feature was annotated in a cluster, the main part of the corresponding cluster could be annotated from this seed node according to similarity of MS/MS spectra and to accurate masses differences between nodes.

2.4. Results and discussion

The metabolome of *T. atomaria* was investigated through an original workflow (**Figure IV.1**) including the analysis of its main chemical constituents by natural products chemistry and the building of several less and less unrestricted MNs coupled to database queries and MS/MS data analysis.

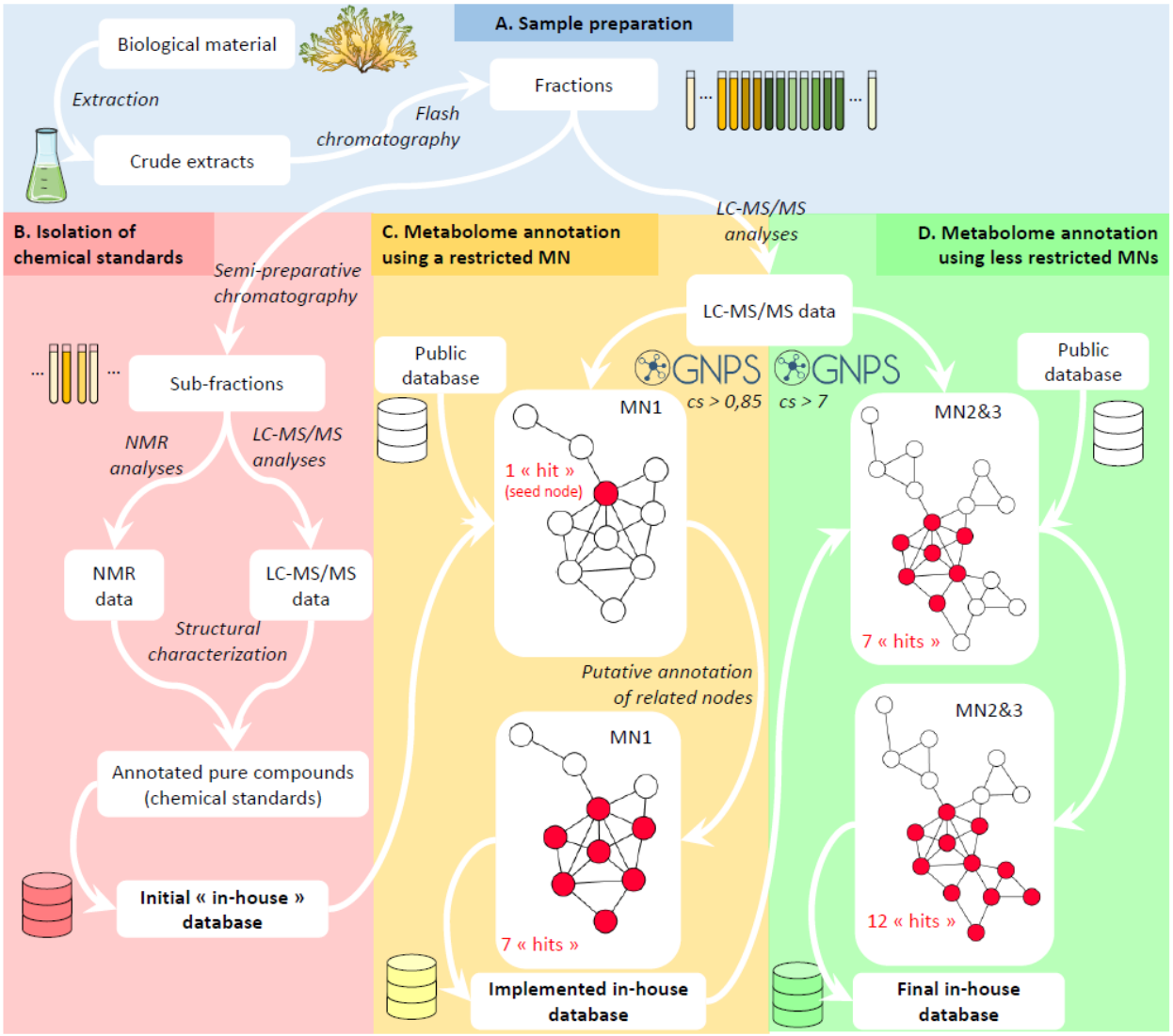

Figure IV.1. Analytical workflow used in this study

2.4.1. Isolation of chemical standards from T. atomaria: a "phytochemical approach"

Previous studies related to compounds isolated from extracts of the brown alga *T. atomaria* allowed the isolation and the structural characterization of GGG (Amico et al., 1977; Tringali et al., 1995; Othmani et al., 2016a, 2016b) and terpenes, with mainly germacrane and cadinane sesquiterpenoids (Amico et al., 1978; De Rosa et al., 1994; Tringali et al., 1995; Othmani et al., 2016b, 2016a; Jerković et al., 2019)

In this study, after the fractionation by flash-chromatography of the crude extracts of *T. atomaria* and the purification by semi-preparative HPLC of the main chemical components from a selection of fractions, eight metabolites were characterized. Seven of these compounds were already described from *T. atomaria*: cadina-4(14),5-diene, cubebol, 4-*epi*-cubebol, (+)-gleenol, germacra-4(15),5,10(14)-trien-9-ol, (1*S*, 5*E*, 7*S*) 1-acetoxygermacra-4(15),5,10(14)-triene and geranylgeranylglycerol (Table SIV.2). An additional compound was identified as dictyol A (Table SIV.2), a diterpene previously reported from the Phaeophyceae *Dictyota dichotoma* (Fattorusso et al., 1976) but described here for the first time from *T. atomaria*. As *Dictyota* spp. are morphologically and taxonomically close to *T. atomaria* and in order to avoid a possible contamination of the crude extracts studied here, the presence of this compound was confirmed by LC-MS/MS on specific crude extracts obtained within a single thallus of *T. atomaria*.

The MS data and RT of these eight compounds allowed to initiate the elaboration of an in-house database dedicated to this algal model.

2.4.2. Annotation of the metabolome of T. atomaria using a restricted MN (MN-1)

Three parameters were tested in this study, in order to obtained three distinct MNs with different level of restrictiveness. More precisely, the construction of a MN (named **MN-1**) with restrictive parameters (e.g. minimum cosine score > 0.85) allowed to obtain a simplified MN with very strong similarities between nodes in a same cluster, and permitted to start the annotation with a more confident perspective. Then, the use of less restive parameters (tested with **MN-2** and **MN-3**) allowed to continue the annotation and to test which set of parameters allowed the most specific clustering in relation to the different chemical families observed (i.e. : ideally one cluster for one family) (see **Part 2.4.3**).From **MN-1**, ten main clusters named **1A** to **1J** were obtained and carefully analyzed (**Figure IV.2**).

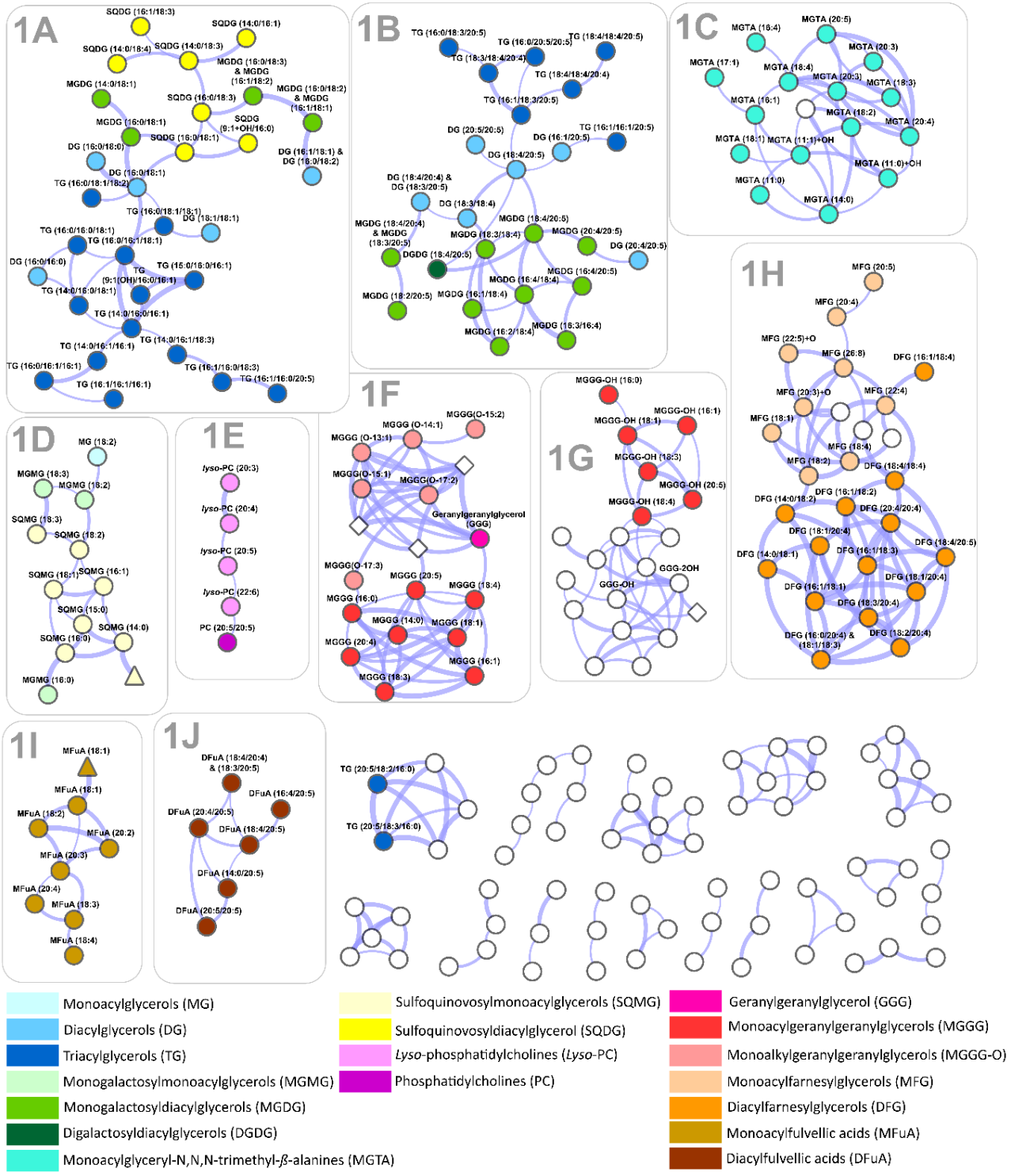

Figure IV.2. Restrained MN (**MN-1**) built with MS/MS data of fractions obtained from the crude extract of the brown alga *Taonia atomaria.* Node colors were chosen according to their chemical classes (see color code below the network). Nodes with a diamond shape correspond to fragments ions, while those with a triangle shape are representing compounds with a distinct adduct from the rest of its cluster. Thickness of an edge between two nodes was proportional to the cosine score (CS, from 0.851 to 0.995). Only clusters with at least three nodes were represented. The whole network also includes 39 clusters of two nodes, and 512 unbound nodes.

2.4.2.1. Annotation of known lipid classes: Clusters 1A to 1E

During the building process of **MN-1**, the only *m/z* feature matching within a database (MoNA) belonged to cluster **1A** and was identified as a triacylglycerol (TG). This feature with *m/z* 794.9208 $[C_{49}H_{96}NO_6]^+$ corresponding to the raw formula $C_{49}H_{95}NO_6$ was identified as TG (46:1) which ionized as a cationic adduct $[M + NH_4]^+$ (Samburova et al., 2013). The analysis of the MS/MS fragmentation pattern allowed its annotation as TG (14:0/16:0/16:1) since three groups of fragment ions were observed in the MS/MS spectrum of this compound: (i) diglyceride ions resulting of the loss of one fatty acid chain at *m/z* 549.4879 $[C_{35}H_{65}O_4]^+$ ($[M - C_{14:0} + H]^+$), *m/z* 523.4715 $[C_{33}H_{63}O_4]^+$ ($[M - C_{16:1} + H]^+$), and *m/z* 521.4560 $[C_{33}H_{61}O_4]^+$ ($[M - C_{16:0} + H]^+$), (ii) monoglyceride ions obtained after the loss of two fatty acids at *m/z* 313.2734 $[C_{19}H_{37}O_3]^+$ ($[M - C_{14:0} - C_{16:1} + H]^+$), *m/z* 311.2583 $[C_{19}H_{35}O_3]^+$ ($[M - C_{14:0} - C_{16:0} + H]^+$) and *m/z* 285.2420 $[C_{17}H_{33}O_3]^+$ ($[M - C_{16:0} - C_{16:1} + H]^+$), and (iii) acylium ions at *m/z* 239.2368 $[C_{16}H_{31}O]^+$, *m/z* 237.2214 $[C_{16}H_{29}O]^+$ and *m/z* 211.2058 $[C_{14}H_{27}O]^+$ (See Supporting information for MS/MS data and fragmentation pattern, Fig. SIV.1). Just using mass differences from this seed node (**Figure IV.2**), thirteen other TGs were readily detected in the neighboring nodes and their annotation was confirmed after examination of their MS/MS data. RT constitutes an essential parameter when analyzing lipids. In reversed phase chromatography, retention increases with the number of carbon atoms and decreases with insaturations, in a homologous series. In that respect, a RT-based representation of **MN-1** (See supporting information, Fig. SIV.2) confirmed that these nodes belong to the same lipid family. Interestingly, several nodes connected to TGs in the same cluster showed a lower retention: a similar MS/MS fragmentation pattern and lower molecular masses were then used to easily annotated these nodes as diacylglycerols (DGs). It's noteworthy that a TG which was connected to other TGs or DGs always bore with these nodes two common acyl chains [e.g. TG (14:0, 16:0, 16:1) and TG (15:0, 16:0, 16:1), TG (16:0/16:0/18:1) and DG (16:0/16:0) or TG (16:0/18:1/18:2) and DG (16:0/18:1)]. In cluster **1A**, a detailed analysis of the MS data of the remaining non-annotated nodes allowed to gather them in two subgroups. Some of these nodes showed a characteristic neutral loss of 261.05 Da which is typical of the loss of the polar sulfoquinovosyl group from the ammoniated adduct of sulfoquinovosyldiacylglycerols (SQDGs) (Popendorf et al., 2013). Seven of these lipids were then identified in cluster **1A** including, for example, SQDG (16:0/18:3) which was annotated using: (i) its cationic adduct at *m/z* 834.5396 $[C_{43}H_{80}NO_{12}S]^+$ ($[M + NH_4]^+$), (ii) fragment ions at *m/z* 573.4883 $[C_{37}H_{65}O_4]^+$ ($[M - C_6H_9O_7S - H_2O + H]^+$) and *m/z* 591.4988 $[[C_{37}H_{65}O_4]^+$ ($[M - C_6H_9O_7S + H]^+$) caused by the detachment of the polar head and generating neutral losses of *m/z* 261 and 243 Da, respectively, and (iii) two other fragment ions at *m/z* 335.2582 $[C_{21}H_{35}O_3]^+$ ($[M - C_6H_9O_7S - H_2O - C_{16:0} + H]^+$) and *m/z* 313.2739 $[C_{19}H_{37}O_3]^+$ ($[M - C_6H_9O_7S - H_2O - C_{18:3} + H]^+$) which allowed to defined the two acyl chains

as C16:0 and C18:3, respectively (See Supporting information for MS/MS data and fragmentation pattern, Fig. SIV.1). MS data of nodes of the second subgroup were characterized by a neutral loss of *m/z* 197.01 which allowed to annotate them as monogalactosyldiacylglycerols (MGDGs) (Isaac et al., 2007; Popendorf et al., 2013). For example, a feature at *m/z* 746.5770 $[C_{41}H_{80}NO_{10}]^+$ ($[M + NH_4]^+$) was identified as a MGDG (32:1) on the basis of the fragment ion at *m/z* 549.4874 $[C_{35}H_{65}O_4]^+$ ($[M -Gly - H_2O + H]^+$) which corresponded to a neutral loss of 197.01 Da. Its annotation as MGDG (14:0, 18:1) was fulfilled thanks to fragment ions at *m/z* 339.2890 $[C_{21}H_{39}O_3]^+$ ($[M - Gly - H_2O -C_{14:0} + H]^+$), and *m/z* 285.2420 $[C_{17}H_{33}O_3]^+$ ($[M - Gly - H_2O -C_{18:1} + H]^+$), and the two acylium ions at *m/z* 265.2524 $[C_{18}H_{33}O]^+$ and *m/z* 211.2054 $[C_{14}H_{27}O]^+$ (See Supporting information for MS/MS data and fragmentation pattern, Fig. SIV.1). Ultimately, all the nodes of cluster **1A** were annotated. The corresponding metabolites belonged to four lipid classes but the acyl chains of all these glycerolipids were mainly C16:0, C16:1 and C18:1.

Interestingly, seven nodes with characteristic RT of TGs were observed in cluster **1B** (See supporting information, Fig. SIV.2) and the detailed analysis of their MS data confirmed their annotation. As reported for cluster **1A**, the same approach allowed to annotate the other nodes as DGs and MGDGs. However, the MS data of one node matched with none of the chemical families previously defined in this molecular networking. This *m/z* feature produced an adduct ion at *m/z* 976.5977 $[C_{53}H_{86}NO_{15}]^+$ ($[M + NH_4]^+$) and its MS/MS spectrum showed fragment ions at *m/z* 617.4559 $[C_{41}H_{61}O_4]^+$ ($[M - 2 Gly - H_2O + H]^+$) and *m/z* 635.4668 $[C_{41}H_{63}O_5]^+$ ($[M - 2 Gly + H]^+$). These two fragment ions corresponding to neutral losses of 359 and 341 Da were characteristic of digalactosyldiacylglycerols (DGDGs) (Isaac et al., 2007; Popendorf et al., 2013). Further fragment ions attributed to monoglyceride ions at *m/z* 359.258 $[C_{23}H_{35}O_3]^+$ ($[M - 2 Gly - H_2O -C_{18:4} + H]^+$) and *m/z* 333.2423 $[C_{21}H_{33}O_3]^+$ ($[M - 2 Gly - H_2O -C_{20:5} + H]^+$), and to acylium ions at *m/z* 285.2213 $[C_{20}H_{29}O]^+$ and *m/z* 259.2056 $[C_{18}H_{27}O]^+$ allowed the annotation of this metabolite as DGDG (18:4/20:5) (See Supporting information for MS/MS data and proposed fragmentation pattern, Fig. SIV.3). It could be pointed out that glycerolipids of cluster **1B** were composed by longer FAs (eg. C18:4, C20:4 and C20:5) than those found in metabolites of cluster **1A**.

A third cluster (**1C**) consisted in nodes which showed a characteristic MS/MS fragment ion at *m/z* 236 corresponding to the raw formula $[C_{10}H_{22}NO_5]^+$. A comparison of these MS data with those from the literature indicated that this fragment ion is typical of mono- and diacylglycerylhydroxymethyl-*N*,*N*,*N*-trimethyl-*ß*-alanines (MGTAs and DGTAs) (Kind et al., 2012). This class of betaine lipids has already been observed in *T. atomaria* (Paix et al., 2019, 2020) and such glycerolipids can be differentiated from the very similar mono- and diacylglyceryl-*N*,*N*,*N*-trimethylhomoserines (MGTSs and DGTSs) via the absence of a

characteristic mass loss of *m/z* 87 (Roche and Leblond, 2010). Fifteen MGTAs were identified in cluster **1C** using the MGTA (14:0) (*m/z* 446.3481, $[C_{24}H_{48}NO_6]^+$) as a seed node. This MGTA showed a characteristic MS fragmentation pathway with: (i) a fragment ion at *m/z* 428.3386 $[C_{24}H_{46}NO_5]^+$ ($[M - H_2O + H]^+$) resulting from the loss of water from the molecular ion, (ii) a fragment ion at *m/z* 285.2437 $[C_{17}H_{33}O_3]^+$ ($[M – C_7H_{15}NO_3]^+$ resulting from the loss of the hydroxymethyl-*N*,*N*,*N*-trimethyl-*ß*-alanine group, and (iii) several ions, including the characteristic fragment ion at *m/z* 236.1491 $[C_{10}H_{22}NO_5]^+$ resulting from the loss of the acyl chain, obtained by successive fragmentations of the polar head group, such as at *m/z* 218.1401 $[C_{10}H_{20}NO_4]^+$ (loss of water), *m/z* 162.1125 $[C_7H_{16}NO_3]^+$ (loss of glycerol) and *m/z* 144.1018 (loss of glycerol and water) (See Supporting information for MS/MS data and proposed fragmentation pattern, Fig. SIV.4). These last fragment ions observed in all the MS/MS spectra of the nodes found in cluster **1C** were thus characteristic of MGTAs (but also of DGTAs) and allowed to group these lipids within a single cluster.

A fourth cluster (**1D**) gathered nodes among which some showed a characteristic neutral loss of 261 Da on their MS/MS spectra. Based on the annotation previously carried out for the SQDGs and considering their MS and MS/MS data, the compounds of this cluster were annotated as sulfoquinovosylmonoacylglycerols (SQMGs). For example, SQMG (18:1) was identified through the adduct ion at *m/z* 600.3411 $[C_{27}H_{54}NO_{11}S]^+$ ($[M + NH_4]^+$), the characteristic fragment ions at *m/z* 339.2895 $[C_{21}H_{39}O_3]^+$ ($[M – C_6H_9O_7S -H_2O + H]^+$) and *m/z* 357.3007 $[C_{21}H_{41}O_4]^+$ ($[M – C_6H_9O_7S + H]^+$), which corresponded to the loss of the sulfoquinovosyl group (neutral losses of 261 and 243 Da, respectively, from the ammoniated adduct), and the acylium ion at *m/z* 265.2532 $[C_{18}H_{33}O]^+$ (See Supporting information for MS/MS data and proposed fragmentation pattern, Fig. SIV.5). Six other SQMGs were identified in cluster **1D** together with several structurally related lipids: three monogalactosylmonoacylglycerols (MGMGs) and a monoacylglycerol (MG). It can be noticed that in this restrictive MN the SQMGs appeared in a separate cluster than the SQDGs (only found in cluster **1A**) showing that the fragment ions due to the acyl chains were in this context more important for the gathering than those of the sulfoquinovosyl part.

A further cluster (**1E**) was composed by five compounds belonging to a known lipid family. All these compounds showed in their MS/MS spectrum a characteristic fragment ion at *m/z* 184 which corresponded to the head polar group of phosphatidylcholines (PCs) (Suárez-García et al., 2017). As an example, the node with *m/z* 542.3240 $[C_{28}H_{49}NO_7P]^+$ ($[M + H]^+$) was annotated as *lyso*-PC (20:5) using the typical fragment ion of the polar head at *m/z* 184.0734 $[C_5H_{15}NO_4P]^+$, but also those due to its subsequent fragmentation at *m/z* 104.1074 $[C_5H_{14}NO]^+$ and *m/z* 86.0967 $[C_5H_{12}N]^+$, while the acyl chain wad deduced from the molecular formula and the fragment ions at *m/z* 359.2577 $[C_{23}H_{35}O_3]^+$ ($[M - C_5H_{15}NO_4P + H]^+$),

m/z 258.1102 $[C_8H_{21}NO_6P]^+$ ($[M - C_{20:5} + H]^+$) and *m/z* 285.2220 $[C_{20}H_{29}O]^+$ (See Supporting information for MS/MS data and proposed fragmentation pattern, Fig. SIV.6). Thus, using further fragment ions, such as acylium ions, it was possible to identify the five other nodes as four *lyso*-PCs and a PC.

2.4.2.2. Putative annotation of new lipid classes: Clusters 1F to 1J

a) Geranylgeranylglycerol derivatives (Clusters **1F** and **1G**)

Geranylgeranylglycerol (GGG), previously isolated using the "phytochemical approach", was identified in cluster **1F** using the experimental data (RT, MS and MS/MS data) obtained from the chemical standard. In this situation, this known metabolite served as a seed node to annotate the rest of this cluster as no other metabolites matched with a hit. Thanks to the MS fragmentation of the precursor adduct ion of GGG at *m/z* 382.3290 $[C_{23}H_{44}NO_3]^+$ ($[M + NH_4]^+$), many of the resulting fragment ions observed on the MS/MS spectrum of GGG were also found in the MS/MS spectra of the other compounds of this cluster (**Figure IV.3**). More particularly, the characteristic fragment ion at *m/z* 273.257 $[C_{20}H_{33}]^+$ corresponding to the geranylgeranyl (GG) moiety was observed for all nodes of the cluster **1F**. After a detailed analysis of their MS/MS data, most of the nodes of this cluster have been putatively annotated as belonging to a new class of glycerolipids, monoradylgeranylgeranylglycerols (MGGGs), which could be divided in two main groups, namely monoacyl and monoalkyl derivatives of GGG. Eight monoacyl derivatives were then identified by first using the high similarity (CS = 0.896) between the MS/MS data of GGG and those of the node at *m/z* 640.5291 5291 $[C_{41}H_{70}NO_4]^+$ ($[M + NH_4]^+$) (See **Figure IV.3**). For this particular node, in addition to the characteristic ion fragment of the GG moiety at *m/z* 273.2570 $[C_{20}H_{33}]^+$, a fragment ion at *m/z* 351.2532 $[C_{21}H_{35}O_4]^+$ ($[M - GG + H]^+$) resulting from the loss of the GG part and an acylium ion at *m/z* 259.2058 $[C_{18}H_{27}O]^+$ together with its dehydrated counterpart at *m/z* 241.1953 $[C_{18}H_{25}]^+$ were also observed allowing its annotation as MGGG (18:4) (See **Figure IV.3**). Seven other nodes of the cluster with acyl chains varying from C16 to C20 with various insaturations levels were then easily identified in the same way. In the same cluster, six other nodes showed molecular formulae lacking one oxygen atom which were inconsistent with a substitution of GGG by an acyl chain but in accordance with the occurrence of an ether-linked chain. For example, in addition to characteristic fragment ions of the GG chain, MGGG (O-17:2) was characterized by an adduct ion at *m/z* 616.5651 $[C_{40}H_{74}NO_3]^+$ ($[M + NH_4]^+$), a fragment ion at m/z 327.2897 $[C_{20}H_{39}O_3]^+$ ($[M - GG + H]^+$) resulting of the loss of the GG moiety, and two fragment ions specific to the alkyl chain at *m/z* 252.2680 $[C_{17}H_{34}N]^+$ ($[C_{17}H_{30} + NH_4]^+$) and *m/z* 235.2417 $[C_{17}H_{31}]^+$ (See **Figure IV.3**). Five other nodes with a similar fragmentation pattern were putatively annotated as monoalkyl derivatives of GGG in cluster **1F**.

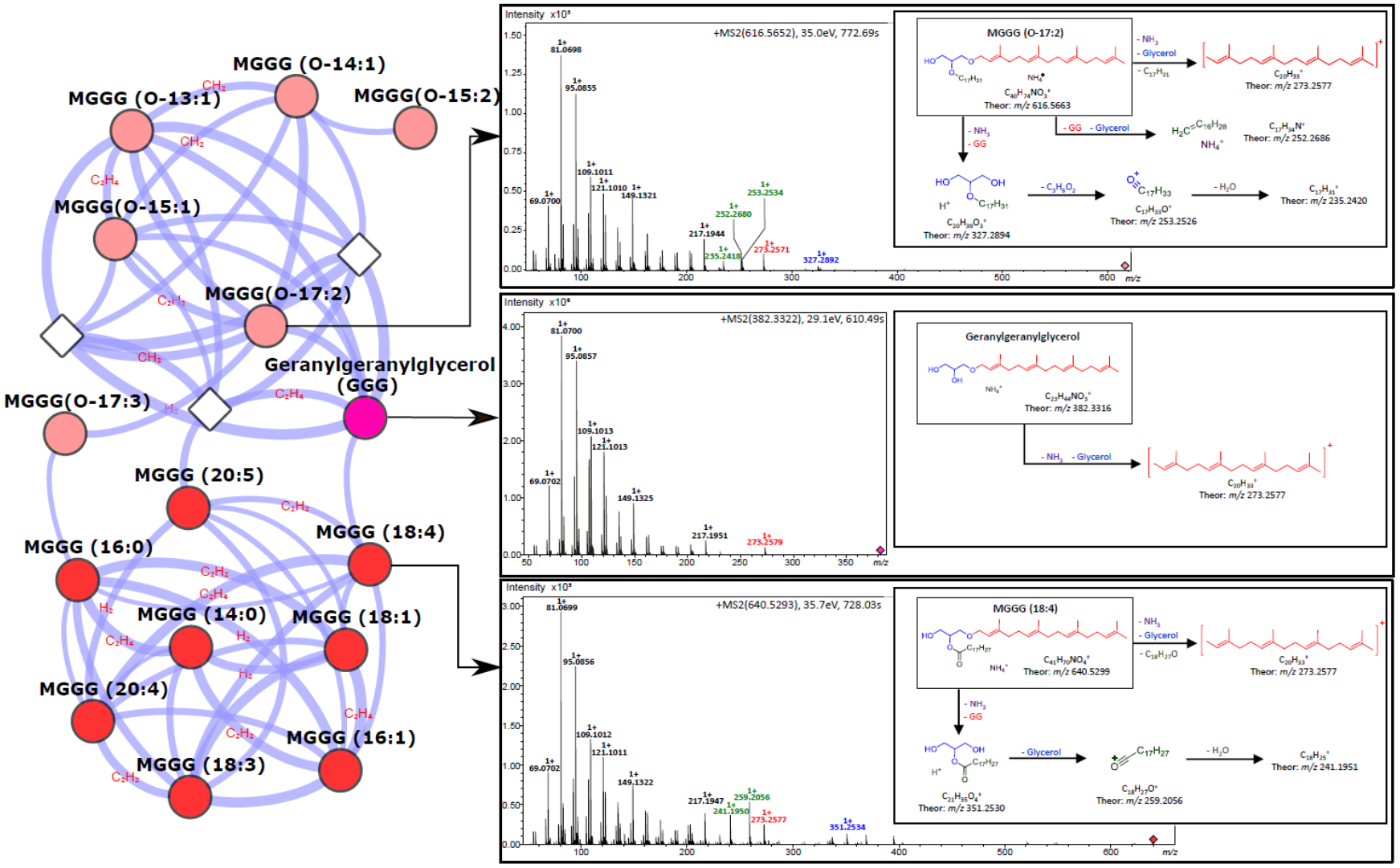

Figure IV.3 Annotation of GGG derivatives in cluster **1F** and proposed MS/MS fragmentation pattern for the compounds MGGG (18:4) and MGGG (O-17:2)

Another cluster (**1G**) was composed of *m/z* features which showed a similar fragmentation pattern than those of cluster **1F**, the main differences in their MS/MS data being a greater number of oxygen atoms in their molecular formulae and a characteristic ion fragment at m/z 271.2427 $[C_{20}H_{31}]^+$. An in-depth analysis of the MS/MS spectra of these nodes allowed to putatively annotate them as GGG derivatives bearing an oxidized GG side chain. More particularly, the node at *m/z* 398.3275 $[C_{23}H_{44}NO_4]^+$ was characterized using the fragment ions at *m/z* 289.2532 $[C_{20}H_{33}O]^+$ ($[M – glycerol + H]^+$) and *m/z* 271 $[C_{20}H_{31}]^+$ ($[M – glycerol - H_2O + H]^+$) as an analog of GGG with one hydroxyl group on the GG chain (named here GGGOH). Through their characteristic MS/MS fragmentation pattern, six other nodes of cluster **1G** were easily identified as monoacyl derivatives of GGGOH. For example, among these derivatives MGGGOH (18:4) was characterized through the adduct ion at *m/z* 656.5239 $[C_{41}H_{70}NO_5]^+$ $[M + NH_4]^+$, the characteristic fragment ions at *m/z* 351.2530 $[C_{21}H_{35}O_4]^+$ $[M – GGGOH + H]^+$ and *m/z* 289.2528 $[C_{20}H_{33}O]^+$ $[M - Glycerol – C_{18:4} + H]+$ and their respective dehydrated counterparts at *m/z* 333.2426 $[C_{21}H_{33}O_3]^+$ and *m/z* 271.2419 $[C_{20}H_{31}]^+$.

b) Farnesylglycerol derivatives (Cluster **1H**)

Cluster (**1H**) was composed by nodes showing a characteristic ion fragment at *m/z* 205.195 $[C_{15}H_{25}]^+$ which matched with the occurrence of a farnesyl (i.e. C_{15}-terpenoid) side chain. This putative assumption was strengthened by the strong similarity of the MS/MS fragmentation pattern of this ion with that of farnesol found in online databases (e.g. Metlin).

A detailed analysis of the MS/MS data of the nodes of cluster **1H** allowed to putatively annotate them as mono- and diacyl derivatives of farnesylglycerol (MFGs and DFGs, respectively). For example, the node at *m/z* 578.5142 $[C_{36}H_{68}NO_4]^+$ ($M + NH_4]^+$) was characterized as MFG (18:1) through: (i) a fragment ion at *m/z* 357.3005 $[C_{21}H_{41}O_4]^+$ ($[M – C_{15}H_{25} + H]^+$) resulting from the loss of the farnesyl part and the corresponding dehydrated ion at *m/z* 339.2893 $[C_{21}H_{39}O_3]^+$ ($[M – C_{15}H_{25} – H_2O + H]^+$), (ii) the characteristic ion fragment of the farnesyl chain at *m/z* 205.1949 $[C_{15}H_{25}]^+$ ($[M - Glycerol – C_{18:1} + H]^+$) and (iii) an acylium ion at *m/z* 283.2624 $[C_{18}H_{35}O_2]^+$ and its dehydrated counterpart at *m/z* 265.2517 $[C_{18}H_{33}O]^+$ (See Supporting information for MS/MS data and proposed fragmentation pattern, Fig. SIV.7). A similar MS fragmentation was also observed for five other nodes while two other nodes showed the occurrence of oxygenated acyl chains.

In the same cluster (**1H**), 14 other nodes showing higher molecular masses and retention times were annotated as DFGs. Thus, DFG (18:1/16:1) was putatively identified on the basis of the adduct ion at *m/z* 814.7280 $[C_{52}H_{96}NO_5]^+$ ($[M + NH_4]^+$) and the characteristic fragment ions at *m/z* 593.5096 $[C_{37}H_{69}O_5]^+$

([M - $C_{15}H_{25}$ +H]$^+$), *m/z* 575.5033 [$C_{37}H_{67}O_4$]$^+$ ([M - $C_{15}H_{25}$ – H_2O +H]$^+$), *m/z* 339.2889 [$C_{21}H_{39}O_3$]$^+$ ([M - $C_{15}H_{25}$ – H_2O -$C_{16:1}$ +H]$^+$) and *m/z* 311.2579 [$C_{19}H_{35}O_3$]$^+$ ([M - $C_{15}H_{25}$ – H_2O -$C_{18:1}$ +H]$^+$) due to the respective losses of the farnesyl chain, a molecule of water and one acyl chain (See Supporting information for MS/MS data and proposed fragmentation pattern, Fig. SIV.7).

c) Fulvellic acid derivatives (Clusters **1I** and **1J**)

Two other clusters (**1I** and **1J**) were composed by nodes which showed molecular formulae and MS/MS fragmentation pattern, more particularly the characteristic fragment ion at *m/z* 85.028 [$C_4H_5O_2$]$^+$, corresponding to those of mono- and diacylglycerols substituted by a $C_4H_5O_2$ additional chemical group. These findings were in accordance with the chemical structure of fulvellic acid derivatives (i.e. acylglycerols bearing a methacrylic acid moiety) which have been previously described from Japanese samples of the brown alga *Sargassum fulvellum* (Kusumi et al., 1981). Thus, we proposed to putatively annotate these compounds as fulvellic acid derivatives even if the lack of MS/MS data in the literature did not allow their unambiguous characterization.

In more detail, the seven nodes of cluster **1I** were described as monoacyl fulvellic acid derivatives (MFuAs) based on their MS/MS fragmentation. For example, MFuA (20:4) was characterized through the adduct ion at *m/z* 480.3318 [$C_{27}H_{46}NO_6$]$^+$ ([M + NH_4]$^+$) and the following ion fragments found on its MS/MS spectrum such as: (i) the ion at *m/z* 445.2942 [$C_{27}H_{41}O_5$]$^+$ ([M - H_2O + H]$^+$) resulting of a loss of water, (ii) the ion at *m/z* 361.2734 [$C_{23}H_{37}O_3$]$^+$ ([M - H_2O - $C_4H_5O_2$ + H]$^+$) due to the subsequent loss of the methacrylic acid part, (iii) the acylium ion at *m/z* 287.2366 [$C_{20}H_{31}O$]$^+$ and (iv) the characteristic fragment ion of the methacrylic acid moiety at *m/z* 85.0283 [$C_4H_5O_2$]$^+$ (See Supporting information for MS/MS data and proposed fragmentation pattern, Fig. SIV.8).

Concerning the six nodes of cluster **1J**, their RT, molecular formulae and MS/MS data were in accordance with their putative annotation as diacyl fulvellic acid derivatives (DFuAs). As an example, DFuA (20:4/20:5) was characterized on the basis of the adduct ion at *m/z* 764.5456 [$C_{47}H_{74}NO_7$]$^+$ ([M + NH_4]$^+$), the fragment ions characteristic of the presence of the fulvellic acid part at *m/z* 645.4883 [$C_{43}H_{65}O_4$]$^+$ ([M - H_2O - $C_4H_5O_2$ + H]$^+$) and at *m/z* 85.0286 [$C_4H_5O_2$]$^+$, the fragment ions due to the loss of an acyl chain at *m/z* 445.2950 [$C_{27}H_{41}O_5$]$^+$ ([M - H_2O – $C_{20:5}$ + H]$^+$) and *m/z* 443.2797 [$C_{27}H_{39}O_5$]$^+$ ([M - H_2O – $C_{20:4}$ + H]$^+$), and the acylium ions at *m/z* 287.2372 [$C_{20}H_{31}O$]$^+$ and *m/z* 285.2214 [$C_{20}H_{29}O$]$^+$.

3.2.3. Assessment of the annotation carried out using the restricted MN-1

This MN approach allowed to quickly identify chemically related compounds gathered in a same cluster because these metabolites showed common MS fragment ions and/or similar MS/MS fragmentation

patterns. Indeed, as soon as a metabolite was annotated (seed node), the chances of annotating the whole cluster were very strong. In the case of **MN-1**, nearly 90% of the metabolites belonging to a cluster where a seed node has been identified were annotated. Nevertheless, it should be pointed out that to isobaric molecules [e.g. DG (16:1/18:1) & DG (16:0/18:2)] constituted one limitation of this type of approach as they are commonly detected in a same node.

Finally, the careful analysis of **MN-1** led to the annotation of 148 metabolites distributed in twenty chemical classes (**Figure IV.2** and **Table IV.1**). Even if the nodes belonging to the major clusters were annotated, certain compounds and/or clusters are still to be determined. Then, the use of less restricted MNs would allow to include unbound metabolites within a cluster which could facilitate their identification (**Figure IV.1**).

2.4.3. Further annotation of the metabolome of T. atomaria using less restricted MNs (MN-2 and MN-3)

The previous MN (MN-1) was based on restricted parameters that only permitted to highlight strong similarities between the MS/MS spectra of metabolites within a same cluster. In order to further enrich the chemical database of T. atomaria, the metabolites previously identified by the phytochemical approach and the analysis of MN-1 were incorporated into a less restricted network (**MN-2**) (Fig. SIV.9, CS threshold : 0.8) and then an even less restricted one (**MN-3**) (**Figure IV.4**, CS threshold : 0.7). Reducing this restriction allowed certain unbound metabolites to be gathered in clusters containing known compounds. Their annotation became easier by highlighting fragment ions and MS/MS fragmentation pathways which were common with previously identified nodes.

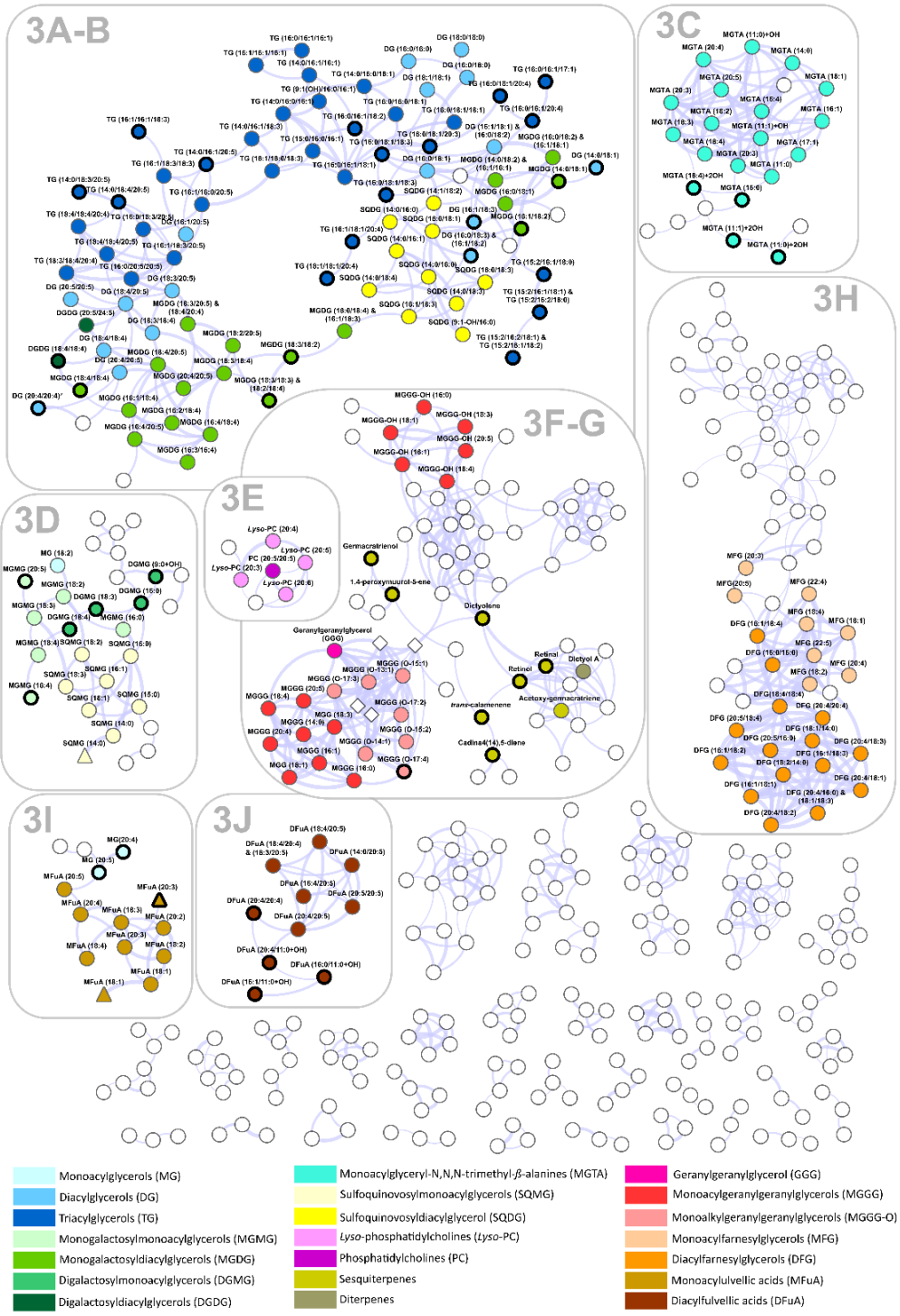

Figure IV.4. Less restrained MN (**MN-3**) built with MS/MS data of fractions obtained from the crude extract of the brown alga *Taonia atomaria*. Node colors were chosen according to their chemical classes (see color code below the network). Nodes with a diamond shape correspond to fragments ions, while those with a triangle shape are representing compounds with a distinct adduct from the rest of its cluster. Nodes with a thick border correspond to newly annotated compounds via the MN enlargement. Thickness of an edge between two nodes was proportional to the cosine score (CS, from 0.701 to 0.995). Only clusters with at least three nodes were represented. The whole network also includes 37 clusters of two nodes, together with 326 unbound nodes.

Moreover, the use of less restricted MNs allowed the gathering of nodes belonging to close chemical classes in a same cluster. Thus, MN enlargement (**MN-2 and 3**) brought together two clusters (**1A** and **1B**) which were separated in **MN-1** in a single cluster (**2A-B** and **3A-B**, respectively) which showed the gathered several classes of structurally related lipids (DGs, TGs, MGDGs and SQDGs). In the same way, the two clusters **1F** and **1G** comprising various GGG derivatives grouped together in **MN-3** (**3F-G**). Moreover, several terpenes, some of which have been identified in the phytochemical approach, namely dictyol A, (1*S*, 5*E*, 7*S*) 1-acetoxygermacra-4(15),5,10(14)-triene and germacra-4(15),5,10(14)-trien-9-ol, which appeared previously in **MN-1** as unbound nodes, were found clustered with the MGGGs in **MN-2** (cluster **2G**) and in **MN-3**(cluster **3F-G**). These clusters also allowed to confirm the annotation of other terpenes, such as retinol, retinal, and dictyolene identified through online databases and *trans*-calamenene and 1,4-peroxymuurol-5-ene already isolated by our group from this algal species and referenced in our in-house database, which appeared as unbound nodes in **MN-1**. This strategy made it possible to annotate 59 additional metabolites very easily and to further enrich the database. Finally, a total of **212 metabolites** (**Table IV.1**) were putatively identified within the metabolome of *T. atomaria* metabolome using the workflow described in this study.

Chemical family	Abbreviation	Color codes in MN-1, 2 and 3	Characteristic fragment	Characteristic mass loss	Number of m/z features annotated in MN-1	Number of m/z features anotated with less restricted MNs (MN-2 and 3)
Monoacylglycerols	MG		-	-	0	2
Diacylglycerols	DG		-	-	13	20
Triacylglycerols	TG		-	-	21	38
Monogalactosylmonoacylglycerols	MGMG		-	197.01	4	6
Monogalactosyldiacylglycerols	MGDG		-	197.01	17	25
Digalactosyldiacylglycerols	DGMG			374.14	0	4
Digalactosyldiacylglycerols	DGDG		-	374.14	1	2
Sulfoquinovosyldiacylglycerols	SQDG		-	261.05	7	11
Sulfoquinovosylmonoacyglycerols	SQMG		-	261.05	7	7
Monoacylglycerylhydroxymethyltrimethyl-β–alanines	MGTA		*m/z* 236.15 $[C_{10}H_{22}NO_5]^+$	-	15	19
Lyso-Phosphatidylcholines	*Lyso*-PC		*m/z* 184.07 $[C_5H_{14}NO_4P]^+$	-	4	4
Phosphatidylcholines	PC		*m/z* 184.07 $[C_5H_{14}NO_4P]^+$	-	1	1
Monoacylglycerylfulvellic acids	MFuA		*m/z* 141.05 $[C_7H_9O_3]^+$; *m/z* 85.03 $[C_4H_5O_2]^+$		8	8
Diacylglycerylfulvellic acids	DFuA		*m/z* 141.05 $[C_7H_9O_3]^+$; *m/z* 85.03 $[C_4H_5O_2]^+$	-	7	12
Monoacylgeranylgeranylglycerols	MGGG		*m/z* 273.26 $[C_{20}H_{33}]^+$	-	14	14
Monoalkylgeranylgeranylglycerols	MGGG-O		*m/z* 273.26 $[C_{20}H_{33}]^+$	-	5	6
Monoacylfarnesylglycerols	MFG		*m/z* 205.20 $[C_{15}H_{25}]^+$	-	8	8
Diacylfarnesylglycerols	DFG		*m/z* 205.20 $[C_{15}H_{25}]^+$		15	15
Diterpenes (and GGG)	-		-	-	1	4
Sesquiterpenes	-		-	-	0	6
Total					148	212

Table IV.1. Summary of the metabolome annotation

2.4.4. Taxonomical and ecological significance of the annotated metabolites

In line with previous observations on *T. atomaria* from the French Mediterranean coasts (Othmani et al., 2016a, 2016b; Paix et al., 2019, 2020), no meroditerpenes were observed here either with the phytochemical approach or using MNs. In these previous studies and in the present one, the main isolated terpenes were GGG and sesquiterpenes with cadinane, germacrane or spiroaxane carbon skeletons. The same trend was also observed for specimens of *T. atomaria* collected in the Adriatic Sea (Croatia) (De Rosa et al., 1994; Jerković et al., 2019), or for samples of *Taonia pseudociliata* from the Gulf of Catania (Italy, Sicily) (previously identified as *Dilophus fasciola*, Amico et al., 1977, 1978; Tringali et al., 1995) and no meroditerpenes were reported either in these studies.

However, diverse meroditerpenes were identified in previous works focusing on algal species reported as *Taonia atomaria* from Canary Islands (e.g. taondiol and atomaric acid) (González et al., 1971, 1974), or from the Aegean Sea (e.g. taondiol, atomaric acid, sargaquinone, and atomarianones A and B) (Abatis et al., 2005; Tziveleka et al., 2005; Nahas et al., 2007). In these studies, which did not report any sesquiterpenes or GGG, such chemical composition appeared to be strikingly close to those of *Stypopodium* species widely reported for their meroditerpenes production (Gerwick and Fenical, 1981; Rovirosa et al., 1992; Gil et al., 1995; Wessels et al., 1999; Sabry et al., 2005). For instance, atomaric acid and taondiol have been previously isolated from *Stypopodium zonale* (Soares et al., 2003) while *epi*-taondiol and sargaquinone were described from *Stypopodium flabelliforme* (Areche et al., 2009). *Stypopodium* and *Taonia* are morphologically and phylogenetically close genera among the Dictyotaceae family (Paula et al., 2011) and, as suggested by (Soares et al., 2003), the hypothesis of a botanical misidentification of *Stypopodium* spp. samples as *T. atomaria* could a plausible scenario to consider. However, more thorough chemotaxonomic studies are necessary to confirm this hypothesis and an integrative approach coupling morphological, phylogenetic and metabolomics analyses could provide the information needed to clarify this situation.

In an ecological point of view, sesquiterpenes and GGG produced by *T. atomaria* have demonstrated anti-adhesion activities against several epiphytes including diverse bacterial strains (Othmani et al., 2016a, 2016b) and barnacle larvae (Othmani et al., 2016b), with gleenol and GGG showing the strongest activities. Through a specific extraction procedure developed for this seaweed (Othmani et al., 2016a), these two compounds were also characterized as main components of the surface metabolome of *T. atomaria* (Othmani et al., 2016a; Paix et al., 2019, 2020). These studies brought evidence that these chemical compounds may be implied in the regulation of the epibiosis at the algal surface. In line with the optimal

defense theory, which assume that chemical resources are allocated within the organism to maximize the plant fitness (McKey, 1979), sesquiterpenes have been observed mainly at apical parts where the meristems are located, which may allow to protect such parts involved in the algal growth against diverse fouling organisms (Paix et al., 2020). The biosynthetic pathway and mechanisms allowing the expression by *T. atomaria* of such compounds at its surface remain uncertain and not documented, implying the need to improve the annotation of its metabolome.

In this study, we also putatively annotated two new lipid classes, GGG and FG derivatives, which are likely to play an important role in the biogenesis and storage of GGG and sesquiterpenes, respectively, since glycerides are generally known for their fundamental storage role. More precisely, GGG derivatives could act as a lipid form of storage for GGG; while mono- and di-FG, harboring a farnesyl chain, could be used by the alga as storage compounds for biosynthetic precursors of sesquiterpenes.

Concerning the fulvellic acid derivatives, their description remains uncertain because they have only been described from the Japanese alga *Sargassum fulvellum* (Kusumi et al., 1981), but their presence, in addition to those of all the other lipid families described here, shows that *T. atomaria*, and more broadly marine macroalgae, constitute an immeasurable source of still untapped lipid derivatives.

2.5. Conclusion

An efficient method dedicated to the annotation of the metabolome of a non-model organism, the brown alga *T. atomaria*, has been developed by coupling two types of approaches, one based on a classical study of the organic extracts of this alga by natural products chemistry and the other, more recent, highlighting the power of annotation of MNs built with fractions of these extracts. Following the elaboration of a first very restricted MN (i.e. implying a very high similarity between the MS/MS data of the metabolites within a same cluster), the annotation was carried out using either seed nodes (i.e. metabolite identified through the interrogation of online databases or isolated standards during the phytochemical analysis of the alga) or by analyzing the similarities and/or interpreting the MS/MS data of the nodes belonging to a same cluster. This first step allowed to annotate more than 150 compounds in the ten main clusters of the restricted MN (**MN-1**) and to putatively characterize two new lipid classes including a geranylgeranyl or a farnesyl part together with a rare class of acylglycerols bearing a methacrylic acid moiety (fulvellic acid derivatives). The implementation, in a second phase, of less constrained MNs allowed to enlarge the size of the clusters and to annotate 63 additional metabolites.

The use of such a method, which is simple to implement, could allow to broaden our knowledge of the metabolome of species, particularly marine ones, which are still little studied to date. Such a method could thus be an indispensable tool for the study of these organisms by environmental metabolomics for taxonomic or ecological purposes.

3. Bilan du chapitre

L'annotation du métabolome de *T. atomaria* s'est basée sur la complémentarité de deux approches méthodologiques, avec

(i) d'une part, l'approche phytochimique (approche utlisée de façon courante en chimie des substances naturelles) permettant de purifier par chromatographie semi-préparative puis de caractériser la structure chimique des composés isolés par spectroscopies (RMN, MS…). Avec principalement la caractérisation d'une dizaine de composés -dont des sesquiterpènes et le GGG- dans les extraits de *T. atomaria*, cette première étape a permis d'initier une base de données interne prenant en compte les données MS, MS/MS et les temps de rétention des composés isolés.

(ii) d'autre part, l'approche utilisant les réseaux moléculaire construits sur la base des données MS/MS, permettant de regrouper les composés présentant des schéma de fragmentation similaires en MS et donc une forte analogie structurale. Avec l'objectif d'identifier des nœuds « *seeds* » notamment grâce à l'approche phytochimique ou les banques de données publiques, cette étape a permis alors d'accélérer le processus de déréplication en annotant plus de 200 molécules du métabolome de *T. atomaria*.

CHAPITRE V : ETUDE INTRA-THALLE

Anse de Magaud à Toulon

1. Avant-propos

Ayant fait le choix d'une analyse métabolomique basée sur une détection par spectrométrie de masse (MS), il s'avère néanmoins indispensable de sélectionner la plateforme analytique la plus adaptée à notre modèle biologique et aux échantillons étudiés. Ainsi, le premier objectif de ce chapitre est de sélectionner un protocole d'analyse chimique le plus à même de conduire à la meilleure couverture possible du métabolome de surface de *T. atomaria* et à l'information écologique la plus pertinente. Par ailleurs, les précédents travaux ayant porté sur l'étude de l'intégralité du thalle de *T. atomaria*, il est nécessaire de déterminer s'il existe des variations du métabolome et de la communauté bactérienne de surface à l'échelle d'un individu. Outre son intérêt propre, cette étude a pour vocation de valider la représentativité de la zone du thalle à échantillonner. Ainsi, le second objectif de ce chapitre est de déterminer quelles sont les variations intra-thalles du métabolome et des communautés bactériennes à la surface de *T. atomaria*, quels sont leurs liens, et quels facteurs pourraient expliquer ces variations potentielles.

Cette étude est présentée sous la forme d'un article de recherche publié dans la revue *Frontiers in Microbiology* [Paix et al., (2020). *Front. Microbiol.* 11, 494. doi:10.3389/fmicb.2020.00494]. Les références bibliographiques citées dans cet article sont indexées en fin de manuscrit. La partie *Supplementary Information* de cet article est presentée dans l'annexe V du manuscrit (annexe électronique).

2. Article: A multi-omics analysis suggests links between the differentiated surface metabolome and epiphytic microbiota along the thallus of a Mediterranean seaweed holobiont

Benoît Paix[1], Nathan Carriot[1], Raphaëlle Barry-Martinet[1], Stéphane Greff[2], Benjamin Misson[3], Jean-François Briand[1,*] and Gérald Culioli[1,*]

[1]Université de Toulon, MAPIEM, EA 4323, Toulon, France.

[2]Aix Marseille Université, CNRS, IRD, Avignon Université, Institut Méditerranéen de Biodiversité et d'Ecologie marine et continentale (IMBE). Station marine d'Endoume, Marseille, France.

[3]Université de Toulon, Aix Marseille Université, CNRS, IRD, Mediterranean Institute of Oceanography (MIO), UM110, France.

[*]Corresponding authors: J.-F. Briand (briand@univ-tln.fr) and G. Culioli (culioli@univ-tln.fr)

Running head: Microbiota & Metabolome along the Surface of Algal Thallus

2.1. Abstract

Marine macroalgae constitute an important living resource in marine ecosystems and complex ecological interactions occur at their surfaces with microbial communities. In this context, the present study aimed to investigate how the surface metabolome of the algal holobiont *Taonia atomaria* could drive epiphytic microbiota variations at the thallus scale. First, a clear discrimination was observed between algal surface, planktonic and rocky prokaryotic communities. These data strengthened the hypothesis of an active role of the algal host in the selection of epiphytic communities. Moreover, significant higher epibacterial density and α-diversity were found at the basal algal parts compared to the apical ones, suggesting a maturation gradient of the community along the thallus. In parallel, a multiplatform mass spectrometry-based metabolomics study, using molecular networking to annotate relevant metabolites, highlighted a clear chemical differentiation at the algal surface along the thallus with similar clustering as for microbial communities. In that respect, higher amounts of sesquiterpenes, phosphatidylcholines (PCs), and diacylglycerylhydroxymethyl-*N*,*N*,*N*-trimethyl-β-alanines (DGTAs) were observed at the apical regions while dimethylsulfoniopropionate (DMSP) and carotenoids were predominantly found at the basal parts of the thalli. A weighted UniFrac distance-based redundancy analysis linking the metabolomics and metabarcoding datasets indicated that these surface compounds, presumably of algal origin, may drive the zonal variability of the epibacterial communities. As only few studies were focused on microbiota and metabolome variation along a single algal thallus, these results improved our understanding about seaweed holobionts. Through this multi-omics approach at the thallus scale, we suggested a plausible scenario where the chemical production at the surface of *T. atomaria*, mainly induced by the algal physiology, could explain the specificity and the variations of the surface microbiota along the thallus.

Keywords: Seaweed surface; Holobiont; Microbial community; Metabolomics; Multi-omics analysis.

2.2. Introduction

Marine macroalgae are major contributors of marine coastal biodiversity and considered as engineers in such ecosystems. They form natural habitats acting as ecological niches for surrounding organisms, in particular for many epiphytic life-forms found at their surfaces (Wahl et al., 2012). With surface densities recorded from 10^2 to 10^7 cells.cm^{-2} across different seaweeds, epiphytic bacteria are the main contributors to the microbial communities associated with algal surfaces (Bengtsson and Øvreås, 2010; Hollants et al., 2013).

Several studies have already highlighted the importance of inter-kingdom interactions, which can be essential for the physiology of all partners (Wichard et al., 2015). In that respect, some bacterial strains have been shown to be involved in the morphogenesis of the green alga *Ulva mutabilis*. This seaweed releases dimethylsulfoniopropionate (DMSP) into the surrounding waters which acts as a chemoattractant food source signal for the *Roseovarius* sp. MS2 strain. Once the signal is detected, the bacterial cells use the glycerol boundary layer as carbon source and promote the morphogenesis of two *Ulva* spp. (Kessler et al., 2018; Wichard and Beemelmanns, 2018). Conversely, several other studies have demonstrated the detrimental effect of some epiphytic bacteria which can negatively affect the host fitness. In the case of the red seaweed *Delisea pulchra*, the occurrence of pathogenic bacteria causing thallus bleaching was linked with a decrease of the algal chemical defences (halogenated furanones acting as quorum sensing inhibitors) observed during the summer period (Wright et al., 2000; Campbell et al., 2011; Case et al., 2011). Epiphytes associated to macroalgae can even show evolutionary adaptation to macroalgal niches through, for example, their ability to degrade algal cell walls (Gobet et al., 2018). The close interactions between seaweeds and their surface-associated microbiota lead to consider these biological systems as holobionts (Egan et al., 2013).

With the increasing number of studies and models showing such interactions, it has been shown that the chemical production at the surface of algae may represent one of the main parameter driving the dynamic of epiphytic microbial communities (Nylund et al., 2010; Lachnit et al., 2013; Saha et al., 2014). In addition, environmental parameters also seem to be involved in the shaping of surface microbiota of seaweed holobionts such as *Fucus vesiculosus, Ecklonia radiata*, *Caulerpa prolifera*, *Caulerpa cylindracea*, *Macrocystis pyrifera*, *Delisea pulchra,* and *Sargassum muticum* (Stratil et al., 2013, 2014; Marzinelli et al., 2015, 2018; Zozaya-Valdés et al., 2016; Aires et al., 2018; Minich et al., 2018; Morrissey et al., 2019; Qiu et al., 2019). Nevertheless, while the microbial communities associated with the surface of algae are

increasingly studied, the chemical composition of the surface of the algal hosts and the variations of the metabolic production at the thallus scale have been only rarely investigated to date.

In this context, the aim of this study was to evaluate to what extent metabolites produced by an algal holobiont at its own surface could lead to changes in the epiphytic microbiota community at the thallus scale. To our knowledge, this study was the first to couple intra-thallus variations of the surface metabolome of an algal host, thus taking into account physiological differentiations such as algal growth, and those of its epiphytic communities. The seaweed holobiont model selected for this study, *Taonia atomaria* (Woodward) J. Agardh, is an annual photophilic marine Phaeophyceae widely reported along the Mediterranean and Northwestern Atlantic coasts. This intertidal seaweed is commonly found from February to July on infralittoral rocky habitats of the French Mediterranean coasts (Sala & Boudouresque, 1997). Several compounds isolated from extracts of *T. atomaria*, and more specifically expressed at its surface, have been previously shown to display anti-adhesion properties and thus could be involved in the selection of specific epibacterial communities (Othmani et al., 2016a, 2016b). More recently, a clear temporal co-variation of the structure of the epibacterial communities and surface metabolites has been highlighted for *T. atomaria* collected on the French Mediterranean coasts (Paix et al., 2019).

In the present study, metabarcoding and flow cytometry were performed to determine whether prokaryotic communities found at the surface of *T. atomaria* were specific and whether they varied at the thallus scale. Thus, the specificity of surface prokaryotic communities was evaluated using, in addition to algal samples, surrounding water and biofilms formed on nearby small rocks. Intra-thallus variability was assessed dividing each thallus into three parts from the base to the apex. Then, at the same thallus scale, we studied in parallel the variations of the endometabolome and surface metabolome of the alga using a multi-platform mass spectrometry-based metabolomics approach [LC-ESI-(+)-MS, LC-ESI-(-)-MS and GC-MS], with the aim of increasing the annotation of relevant metabolites through the use of molecular networking. The use of a specific analytical methodology previously validated on this algal model allowing the extraction and the annotation of a wide range of surface molecules (Othmani et al., 2016a; Paix et al., 2019), as well as the ability to compare the endometabolome and surface metabolome of *T. atomaria,* was of crucial interest to gain insight the biological origin of the compounds implied in the intra-thallus differentiation of the surface extracts. In light of these results, a UniFrac distance-based redundancy analysis coupling the resulting multi-omics datasets was conducted to understand to what extent the intra-thallus variations of algal surface metabolites could shape the epiphytic microbiota of *T. atomaria*. To test

whether the potential variations along the thalli were not restricted to a specific geographical area, this study was conducted on two sampling sites on the South-Eastern French Mediterranean coasts.

2.3. Materials and methods

2.3.1. Sampling strategy

The sampling was performed on June 2017 by scuba diving at two sites located along the French Mediterranean coasts: Tamaris (La Seyne-sur-Mer; 43°5'35.56''N, 5°54'31.81''E) and Carqueiranne (43°5'12.41"N, 6°5'3.26"E). Thalli of *T. atomaria* (Woodward) J. Agardh (Class: Phaeophyceae, order: Dictyotales, family: Dictyotaceae) were collected by carefully detaching holdfasts from rocky substrates (1m depth). Algal samples were stored in sterile bags filled with surrounding seawater. For both sampling sites, different individuals harvested on the same rocky substrate were considered as biological replicates. In addition to seaweed samples, triplicates of rocks (type of substrates chosen haphazardly) and surrounding seawater (5L) were also collected. From the point of collection, samples were transported in a cool box maintaining the seawater temperature and treated at lab within one hour as previously described (Paix et al., 2019).

The global analytical workflow used in this study was described in Fig. SV.1. More precisely, once at lab, only thalli measuring 9 ± 0.5 cm length were considered. To ensure multi-omics cross-comparison, metabarcoding and metabolomics analyses were performed for each replicate on different fronds from the same thallus. Distinct thalli were used for cytometry and confocal microscopy. For each thallus, fronds were divided into three parts of equal length (3 ± 0.2 cm), defined as basal, median and apical parts (Fig. SV.2A and SV.2B). These parts were separated with a sterile scalpel and photographed to estimate their surface with the Mesurim pro software (v. 3.4). Before flow cytometry and molecular approaches, microbiota of *T. atomaria* were sampled by scraping the surface of the three parts of each replicate of thalli (n = 3) with a sterile scalpel as previously described (Paix et al., 2019). Biofilms on rocks were sampled using the same methodology and seawater samples (5L) were filtered on 0.2 μm filters (Millipore-Merck, Darmstadt, Germany).

2.3.2. Confocal laser scanning microscopy

Triplicates of thalli of *T. atomaria* were fixed during 30 min in a 3.7% formaldehyde solution, then washed three times with artificial seawater (ASW). Squares of basal, median and apical parts were dissected in each pre-fixed thallus and stained individually in a 24-well plate. Staining was performed in

the dark, with DAPI (4 μg.mL^{-1}; Sigma-Aldrich-Merck, Darmstadt, Germany) for 20 min at room temperature. After three washes in ASW, squares were mounted on microscope slices with one drop of ProLong Diamond Antifade (ThermoFisher Scientific, Waltham, MA, USA) and incubated for 24h at room temperature in the dark. Confocal images were acquired with a 20X/0.75NA objective on a Zeiss Confocal LSM 510 Meta. Individual tracks were set as follow: laser 405 nm - BP 405-480 IR; laser 488 nm - LP 650, to respectively acquire DAPI and chlorophyll signals.

2.3.3. Quantitative flow cytometry analyses

Flow cytometry analyses were used to assess the epiphytic heterotroph densities at the surface of the algal samples. Analyses were conducted only for samples of *T. atomaria* collected in Tamaris, since not enough algal replicates were available at Carqueiranne. Replicates of samples (n = 3) were fixed in 4 mL of 1% glutaraldehyde-sterile filtered seawater solution and directly conserved at -80°C until analysis. Aggregated cells were dissociated according to Pollet et al. (2018) with an optimised sonication time of 2 min. Heterotrophic prokaryotes were stained using SYBR green I (Invitrogen, Carlsbad, CA, USA) and enumerated using a BD Accuri C6 flow cytometer (BD Biosciences, San Jose, CA, USA) as previously described (Pollet et al., 2018, Fig. SV.3). Results were expressed as densities of cells per cm^2 using the measured surface of each thallus part.

2.3.4. DNA extraction, 16S rRNA gene amplification and sequencing

DNA extraction of biofilm samples was performed using the DNeasy PowerBiofilm kit (MoBio, Qiagen, Germantown, MD, USA) and samples were conserved at -80°C. DNA extraction of filtered seawater samples was performed using the SA-Gen method described in Vasselon et al. (2017). After DNA extraction, the V4-V5 region of 16S rRNA gene was amplified using 515F-Y and 926R primers (Parada et al., 2016), following the PCR protocol from Pollet et al., (2018). Amplicons were sent to GeT Platform (Toulouse, France) for MiSeq Illumina sequencing (2 $\times$ 250 bp).

2.3.5. 16S rRNA gene metabarcoding data processing and analysis

16S rRNA gene reads were processed using the FROGS workflow under Galaxy environment (Escudié et al., 2018). Sequences were quality filtered by removing those for which primers sequences were not present. The primer search accepts 10% of differences. Primers sequences were then removed in the remaining sequence using “cutadapt”. Then, merged sequences with length below 300 pb and above 500 pb were removed. Clustering step was performed using SWARM with a clustering aggregation distance set to 3 (Mahé et al., 2014). Chimeric sequences were removed *de novo* using VSEARCH (Rognes et al., 2016). Rare OTUs representing less than 0.005% of all sequences were removed. OTUs were affiliated with

the silva132 16S rRNA gene database. The final matrix was obtained by removing all sequences affiliated to 16S rRNA gene from chloroplasts and mitochondria, and by performing a rarefaction to the minimum library size using the "phyloseq" R package (McMurdie and Holmes, 2013). Mean percentages of sequences affiliated to chloroplasts and mitochondria were 36.3 and 1.2 %, respectively. α-diversity was estimated using the number of OTUs, Chao1 and Shannon indexes. β-diversity was analysed with a non-metric multidimensional scaling (NMDS), using weighted UniFrac distances, allowing to consider phylogenetic distances between OTUs. These analyses were performed using the "phyloseq" R package and graphical outputs were generated using the "ggplot2" R package. Discriminant analyses were performed to determine specific taxa of each group of samples for both sampling sites, using the LEfSe algorithm in the Galaxy environment with a LDA threshold set to 4. SIMPER analyses were performed with the "vegan" R package to identify the relative contribution of the most relevant prokaryotic genera involved in the dissimilarities between: (i) seawater and algal samples, (ii) rocky biofilms and algal samples, and (iii) basal and apical zones of the thalli. Co-occurrence networks (OTUs-OTUs) were built using the Cytoscape App CoNet (Faust and Raes, 2016). Data were processed using Pearson and Spearman correlation, with Bray-Curtis and Kullback-Leiber dissimilarity distances, and using a threshold of 200 edges. Venn diagrams were used to identify the relative percentage of sequences shared between the different groups of samples and were generated using the Venn webtool (http://bioinformatics.psb.ugent.be/webtools/Venn/). An OTU was considered as common to different groups of samples when it was found at least in one triplicate of each group of samples.

2.3.6. Extraction and samples preparation for metabolomics approaches

Extraction of surface metabolomes (surface extracts) was performed by dipping each algal part in 5 mL of liquid chromatography-mass spectrometry (LC-MS) grade methanol (MeOH; VWR, Fontenay-sous-Bois, France) during 5s, according to Othmani et al., (2016a) and (Paix et al., 2019). This protocol has been previously developed in order to preserve the integrity of the outer membrane cell of *T. atomaria*. Three algal replicates were used for Carqueiranne (n = 3) and five for Tamaris (n = 5). For this extraction step, particular care was taken to prevent any contact between the solvent and cut ends of thalli to prevent any release of intracellular metabolites (Fig. SV.2A). The algal endometabolomes (total extracts) were then obtained by dipping the thallus parts previously used for the extraction of surface metabolomes in 5 mL of MeOH during 24h in the dark (See Fig. SV.2A). Six experimental blanks for each type of extracts were also prepared during this procedure. The resulting surface and total extracts were dried under N_2 flow and stored in 8 mL vials at -20°C under inert atmosphere (Argon) until analysis.

Samples were prepared by solubilising the resulting extracts in 1 mL of MeOH for LC-MS analyses and 1 mL of dichloromethane (CH_2Cl_2) for GC-MS analyses. Ten quality control samples (QCs) were prepared by mixing all the samples at equimolar concentrations. Additionally, two experimental blanks (only MeOH or CH_2Cl_2) were also prepared. Samples and experimental blanks were randomly injected and a QC was injected every five samples. Analytical blanks were injected at the beginning and at the end of the injection sequence.

The LC-ESI-MS analyses were performed on a UHPLC-HRMS system (Dionex Ultimate 3000 Rapid Separation; Thermo Fisher Scientific) coupled with a QToF Impact II mass spectrometer (Bruker Daltonics, Bremen, Germany) in positive and negative ionisation modes. The separations were carried out with an analytical core-shell reversed-phase column (150 × 2.1 mm, 1.7 μm, Kinetex Phenyl-Hexyl; Phenomenex, Le Pecq, France). More details are given in supplementary information.

The GC-MS analyses were performed on a 7890B GC system equipped with a 7693 autosampler and coupled to a 5977A MSD mass selective detector (Agilent Technologies, Palo Alto, CA, USA) using to the same methodology described in (Gaubert et al., 2019), as detailed in supplementary information.

2.3.7. Metabolomics data processing and analysis

LC-MS raw data obtained in positive and in negative modes were respectively converted into netCDF files using DataAnalysis (v. 4.3; Bruker, Germany) and processed with XCMS using Workflow4Metabolomics (W4M) under the Galaxy environment (https://workflow4metabolomics.org/; Giacomoni et al., 2015). GC-MS raw data were converted into netCDF files using MSD ChemStation (v. F.01.00.1903) and were processed with the R package “eRah” (Domingo-Almenara et al., 2016). Parameters used for peak picking, alignment of peaks and gap filling are listed in Table SV.1. Following each workflow, the three data matrices were submitted to three filtering steps using an in-house script on R. Each step of the script consisted in removing successively experimental and analytical bias according to signal/noise ratio (using blanks), coefficient of variation (using QCs), and coefficient of correlation (using samples). After filtration of the three data matrices, a chemodiversity estimation was calculated using the Shannon index. For multivariate analyses, the three resulting data matrices were analysed using the Metaboanalyst 3.5 online webtool (https://www.metaboanalyst.ca/ ; Chong et al., 2018). These data were log10-transformed, mean-centred and normalised using the sum of the chromatographic peak areas. This method of normalisation was found to be identical to that based on the algal surface areas, since a proportional relationship was observed between the sum of the chromatographic peak areas and the algal surfaces (linear regression: R2 > 0.9, see Table SV.2). The same results, in terms of significance for ANOVA,

post-hoc tests and VIP ranks, were observed using both normalisation methods. Data were then analysed using principal component analysis (PCA), followed by partial least-square discriminant analysis (PLS-DA) allowing to reveal features discriminating samples between each part of the thalli for both sites. These VIP (Variable Importance in Projection) features were selected according to their VIP score (> 2) and their significance, and particular attention was paid to their annotation.

2.3.8. Annotation strategy for metabolomics analysis

For LC-ESI-MS data, the methodology of annotation described in (Paix et al., 2019) was applied and is detailed in supplementary information. In brief, isolated compounds and commercial standards were used, together with public databases, for the annotation of selected MS/MS spectra. Moreover, molecular networks were used through the GNPS platform (https://gnps.ucsd.edu/) to facilitate the dereplication procedure by comparing MS/MS spectra obtained in both positive and negative modes. For GC-MS, purified standards, Wiley 2008 and NIST 2011 databases together with the calculation of the Van den Dool and Kratz retention indices were used to annotate the dataset (van Den Dool and Kratz, 1963).

2.3.9. Integration of surface metabolome and surface microbiota datasets

Metabolites were used as explaining factors to investigate whether they could explain the variations of the structure of microbiota communities along thalli. A distance-based redundancy analysis (db-RDA) was conducted with the weighted UniFrac distance matrix from the 16S rRNA gene dataset and normalised concentrations of significant, discriminant and annotated surface compounds. This analysis was performed using the "phyloseq" and "vegan" R packages with the *capscale()* function using the methodology described by Shankar et al., (2017). Since for each replicate the same thallus was used for both metabarcoding and metabolomics analyses, the correspondence between each replicate and between both analyses was considered in the correlation between both datasets.

2.3.10. Statistical tests and cross validations

One-way ANOVA followed by HSD Tukey's tests were used to evaluate the significance of density, diversity and specific metabolites across the different groups of samples (geographical sites and thallus parts). One-way ANOVA followed by HSD Tukey's tests were performed using respectively the *aov()* and *HSD.test()* functions from the "ade4" and "agricolae" R packages (Dray and Dufour, 2007; Mendiburu, 2019). Following NMDS and PCA, discriminations between the different groups of samples were statistically tested with a PERMANOVA and a multivariate pairwise test using the *adonis()* and *pairwise.perm.manova()* functions with the "vegan" and "RVAideMemoire" packages, respectively. Multivariate pairwise tests were conducted with weighted UniFrac and Euclidean distances for

metabolomics and metabarcoding datasets, respectively. PLS-DA were subjected to cross-validations using the MetaboAnalyst tool. db-RDA model for datasets integration was statistically tested using the *anova.cca()* function.

2.4. Results

2.4.1. Confocal laser scanning microscopy (CLSM)

CLSM images only allowed to have a global visualization of the seaweed surface coverage without any ambition to identify or quantify organisms. These images were analysed regarding individuals and merged channels (red: chlorophyll auto-fluorescence, grey: DAPI staining) (Fig. SV4). Chlorophyll emission showed several diatom-like structures. With DAPI staining, a relatively high density of filamentous structures, assigned to filamentous bacterial cells according to their size (50 to 100 μm of length and 2 μm of diameter), was observed. Those filaments did not reveal any overlapping signal with chlorophyll auto-fluorescence, supporting the fact that they could be whether heterotrophic filamentous bacteria or fungi hyphae. Interestingly, these structures were mainly attached at the interface between algal cells. Finally, when comparing the different thallus parts, no clear pattern of surface colonisation could be determined, as both diatom-like and filamentous bacteria-like structures were mainly observed indiscriminately on all algal samples.

2.4.2. Quantification of epiphytic cells densities by flow cytometry

Flow cytometry analyses were only performed on thalli collected in Tamaris and showed significant higher densities of heterotrophic prokaryotes at the basal algal parts (**Figure V.1A**, $p = 0.02$). Density of epiphytic heterotrophic prokaryotes increased by an average of 189% from the apical/median parts (0.39×10^6 cells.cm^{-2}) to the basal ones (1.12×10^6 cells.cm^{-2}). No significant difference was observed between the median and the apical parts (post-hoc test).

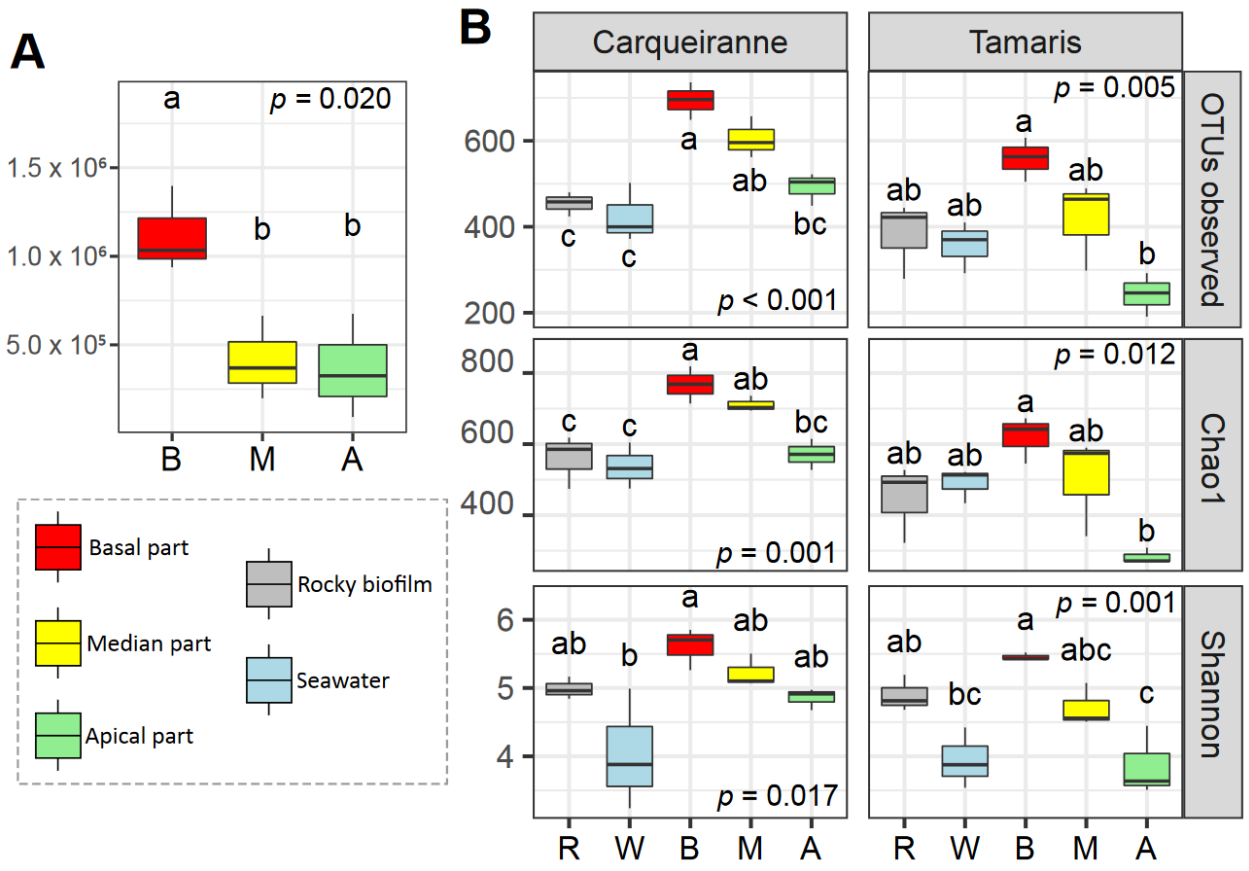

Figure V.1. Variations of cells densities along the surface of *Taonia atomaria* and differences in α-diversity between algal parts, rocky biofilms and seawater collected in two Mediterranean sites (Carqueiranne and Tamaris). (**A**) Heterotrophic prokaryotes cell densities (cells.cm^{-2}) variations of the different parts [basal (B), median (M) and apical (A)] of the thallus surface of *T. atomaria* in Tamaris. (**B**) Variations of several α-diversity indexes of prokaryotic communities at the surface of thallus parts [basal (B), median (M) and apical (A)] of *T. atomaria*, in rocky biofilms (R) and in surrounding water (W). Boxplots correspond to whisker plots (n = 3) showing the lowest, median and highest values. p values and "a", "b", "c" indexes correspond to the results of one-way ANOVA analyses and post-hoc tests (HSD Tukey's test), respectively.

2.4.3. Diversity and structure of bacterial communities

Rarefaction curves reached a plateau indicating a good coverage of the global diversity for all samples (Fig. SV.5). Normalisation was performed at the smallest sequenced samples, i.e. 6939 sequences.

α-diversity was measured using the number of OTUs, Chao1 and Shannon indexes (**Figure V.1B**). When considering the different parts of *T. atomaria* collected in Tamaris, all indexes showed significant higher values for the basal parts in comparison with the apical ones ($p < 0.05$). No significant difference could be observed between the median parts and the two other algal parts. For samples collected in Carqueiranne, the same significant trend was only observed for the richness indexes (number of OTUs and Chao1). Water

samples showed a lower α-diversity than that of basal parts for the Shannon index at both sites and the richness indexes only at Carqueiranne ($p < 0.05$). Biofilm samples collected on rocky substrates showed significant lower richness indexes compared to those of the basal and median parts of algal thalli collected in Carqueiranne ($p < 0.05$).

β-diversity was analysed using weighted UniFrac distance. The resulting NMDS plot (**Figure V.2A**) showed a distinct clustering pattern between prokaryotic communities from surrounding seawater, biofilms on rocky substrates and biofilms on *T. atomaria* surface (Tables SV.3 and SV.4). Despite the rationale was not to compare both sites, the corresponding samples appeared as two separate groups (Tables SV.3 and SV.4). When focusing on algal samples (**Figure V.2B**), the basal and apical zones were significantly discriminated but both did not appear significantly different from the median parts (Tables SV.3 and SV.4). Thalli from Tamaris showed a higher dissimilarity between parts comparing to those collected in Carqueiranne. A lower dissimilarity was observed between the basal parts and the other algal parts at both sites. For both sites, weighted UniFrac distances between biofilms formed on rocky substrates and basal parts were significantly lower than those between biofilms on rocky substrates and apical parts (Fig. SV.6).

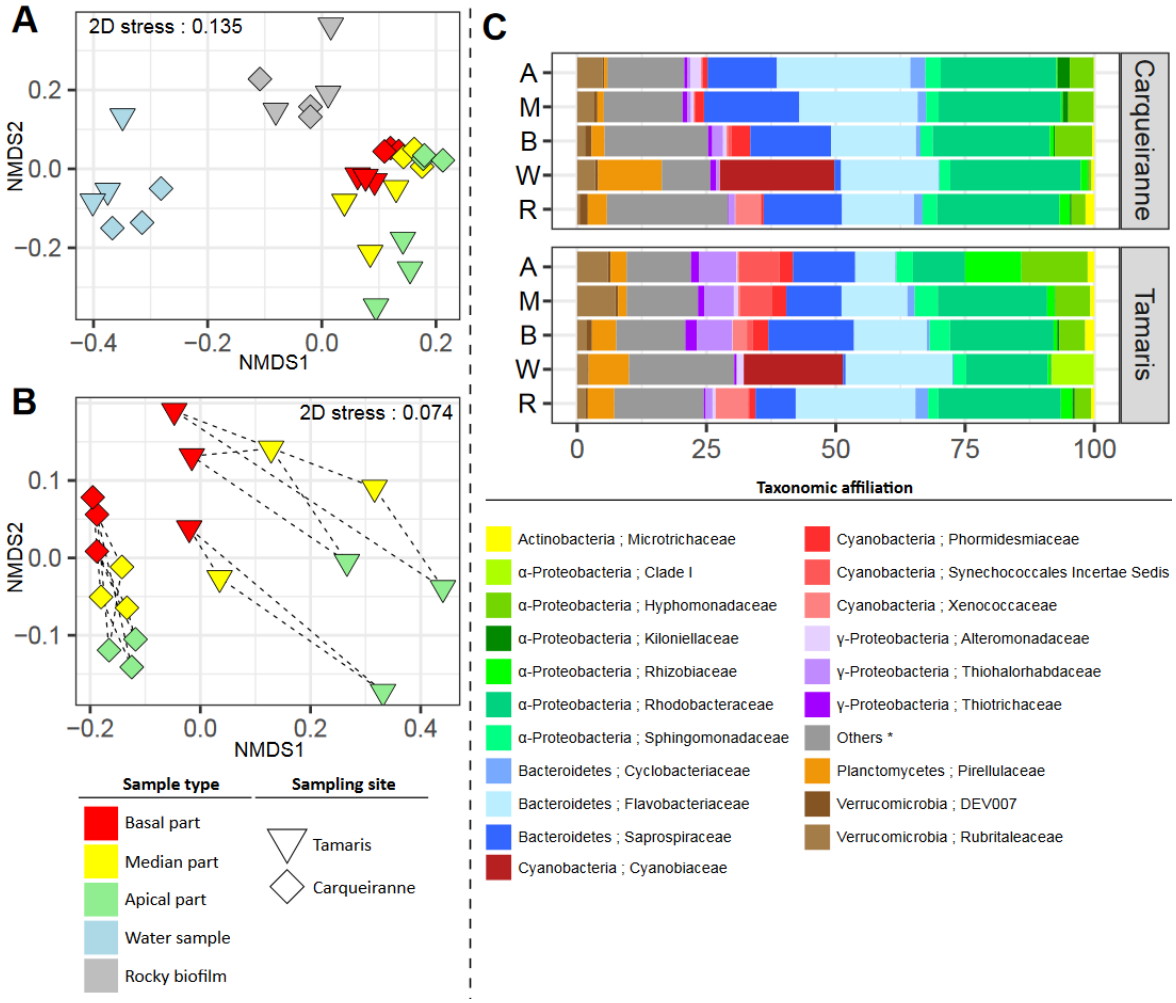

Figure V.2. Structure and β-diversity of epibacterial communities at the surface of *T. atomaria*, in rocky biofilms and in seawater collected in two Mediterranean sites (Carqueiranne and Tamaris). NMDS plots based on weighted UniFrac distance for all samples (**A**) and algal samples only (B). Dashed lines grouped the different parts of a same individual thallus. (**C**) Relative percentages of each bacterial family across each group of samples (n = 3). Labels A, M, B, W and R corresponded to apical, median and basal algal parts, water samples and rocky biofilms, respectively. (*) "Others" correspond to unaffiliated families and/or families with a relative percentage below 1%.

Bacterial community structure in water samples was clearly distinct from that of other samples with several discriminant orders, such as Synechococcales, Myxococcales, and Cellvibrionales for Tamaris, and Pirellulales for Carqueiranne (Fig. SV.7 and SV.8). More particularly for the Synechococcales, the dominance of Cyanobiaceae clearly appeared at both sites (**Figure V.2C**). The main representing genus, *Synechoccocus*, contributed to 11 and 9% of the overall dissimilarities with algal samples from Carqueiranne and Tamaris, respectively (Tables SV.5 and SV.6). At Carqueiranne, *Polaribacter* (Flavobacteriaceae) showed significant higher percentages in water samples and contributed to 4% of the dissimilarity between water and algal samples at this site (Table SV.5). At Tamaris, the SAR11 Clade Ia was significantly present in water samples and contributed to 4% of the dissimilarity with algal samples (Table

SV.6). With a dominance of Saprospiraceae (8 to 19% of sequences), Rhodobacteraceae (10 to 24% of sequences) and Flavobacteriaceae (from 8 to 26% of sequences), Proteobacteria (mainly *α*-Proteobacteria) and Bacteroidetes were the two main phyla observed in epiphytic algal and rocky communities (**Figure V.2C**). In particular, an unidentified genus from the Saprospiraceae was predominantly found on algal samples and contributed significantly (3%) to the dissimilarity with water samples at both sites (Tables SV.5 and SV.6).

The genera *Algitalea* (Flavobacteriaceae) at Carqueiranne and *Granulosicoccus* (Thiohalorhabdaceae) at Tamaris were observed in significant higher abundance on algal samples compared with rocky samples. These genera contributed to 3 and 5% of the dissimilarity between both sample groups, respectively (Tables SV.7 and SV.8). The Nostocales, and more precisely the Xenococcaceae family with the genus *Pleurocapsa*, were found as biomarkers of rocky biofilms at Tamaris (Fig. SV.7). *Pleurocapsa* notably contributed to 2% of the dissimilarity between rocky and algal samples from Tamaris (Table SV.8).

Differences between algal parts were mainly due to genera among Rhodobacteraceae (*Loktanella*), Rubritaleaceae (*Rubritalea*) and especially Flavobacteriaceae (*Algitalea* and *Croceitalea*) which were found with higher percentages in the apical parts at Carqueiranne (Table SV.9, **Figure V.2C**). The families Kiloniellaceae, Alteromonadaceae and Rubritaleaceae were identified as biomarkers of the apical parts (Fig. SV8). More precisely, the genus *Rubritalea* represented 2% of the dissimilarity with the basal parts as mentioned above. Differences among the algal parts were mainly based on taxa belonging to the *α*-Proteobacteria for Tamaris samples. Higher percentages of Rhizobiaceae and Hyphomonadaceae families were observed in apical parts (**Figure V.2C** and SV.7). In particular, *Nitratireductor* (Rhizobiaceae) and *Litorimonas* (Hyphomonadaceae) were key genera which contributed to 5% of the dissimilarity between the apical and basal parts (Table SV.10). In contrast, the basal parts showed higher relative percentages of several families such as Saprospiraceae (**Figure V.2C**), notably several discriminant genera such as *Lewinella* and *Portibacter* (Fig. SV.7 and Table SV.10). Moreover, *Algitalea* was also observed as the main discriminant genus of the basal parts of Tamaris samples (Fig. SV.7) contributing to 4 and 2% of the dissimilarity with apical parts for Carqueiranne and Tamaris, respectively (Table SV.10). Finally, it can be noticed that no sequences affiliated to Archaea were observed for algal samples in contrast with water and rocky samples for which the only detected OTU was below 0.06% of sequences and was affiliated to Nitrosopumilaceae (Thaumarchaeota).

A co-occurrence network was built at the OTU level for each site using water, rocky and *T. atomaria* samples. For both networks, a high number of OTUs co-occurred in basal and median algal parts, and rocky

biofilms. At Carqueiranne, a first cluster (cluster A, **Figure V.3**) showed not only OTUs mainly present in rocky biofilms but also OTUs co-occurring in rocky biofilms and basal or median algal parts. These OTUs were mainly affiliated to the genera *Octadecabacter*, *Ruegeria*, *Loktanella*, and *Granulosicoccus*. Cluster A showed several links with cluster B which exhibited OTUs, mainly affiliated to *Erythrobacter*, *Granulocicoccus* and *Algimonas*, with a high specificity for basal and median algal parts. Cluster C was composed by OTUs highly specific of median and apical parts: they were mainly affiliated to the genera *Loktanella*, *Ruegeria*, *Algitalea*, *Croceitalea* and *Aquamarina*. Cluster D included OTUs mostly occurring in water samples, with the predominance of several genera such as *Synechoccocus*, *Polaribacter* and *Planktomarina*. For Tamaris samples, a similar clustering pattern was also observed (Fig. SV.9). In this network, no OTUs co-occurring mainly in apical algal parts and rocky biofilms were found. Cluster A was composed by OTUs mainly found in rocky biofilms or which co-occurred in rocky biofilms, and in water samples and/or on basal algal parts. Similarly, this cluster was connected to cluster B which showed OTUs mainly found on basal and median parts of the thalli. Cluster B was also connected to the cluster C which was composed of OTUs dominant in apical algal parts. Finally, cluster D displayed OTUs mainly found in water samples, with the predominance of the genera *Polaribacter* and *Planktomarina*.

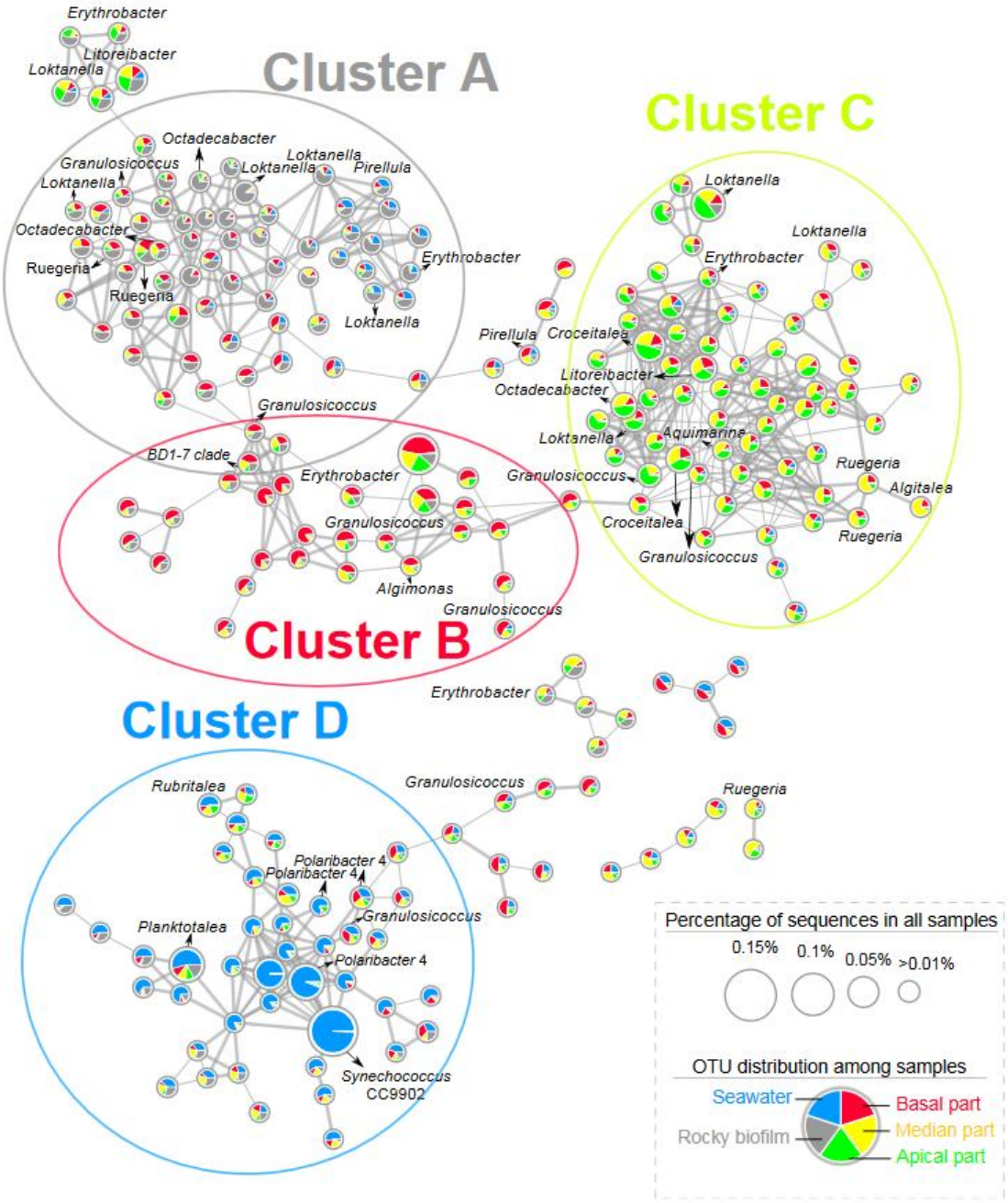

Figure V.3. Co-occurrence network of OTUs from the 16S rDNA dataset of epibacterial communities at the surface of *T. atomaria*, in rocky biofilms and in seawater at Carqueiranne. Pie-chart inside each node revealed the distribution of each OTU across the different sample groups (Red: basal part, yellow: median part, green: apical part, grey: rocky biofilm, blue: seawater). Thickness of edges between each node was proportional to correlation or dissimilarity distances. The size of each node was proportional to the relative percentage of sequences of each OTU in all samples.

Venn diagrams (Fig. SV.10) showed also a higher percentage of common OTUs between algal samples and rocky biofilms rather than between algal and water samples (Carqueiranne: 58.4% *vs* 50.8%,

respectively; Tamaris: 47.1% *vs* 41.0%, respectively). The algal parts sharing the highest percentages of sequences with only rocky biofilms were the basal ones (Carqueiranne: 3.5%, Tamaris: 2.7%).

2.4.4. Comparative metabolomics fingerprinting analysis

After extraction and filtering of the raw chromatographic data obtained from all algal samples (total and surface extracts), three data matrices were obtained with 433, 135 and 261 *m/z* features for the LC-(+)-ESI-MS, LC-(-)-ESI-MS and GC-MS analyses, respectively. Chemodiversity estimation of surface extracts calculated with the Shannon index showed in some instances higher values at the apical parts (Fig. SV.11). More precisely, for LC-(+)-ESI-MS analyses of samples collected at Carqueiranne and for LC-(-)-ESI-MS and GC-MS analyses of samples from Tamaris, the resulting surface metabolomes from apical parts showed the highest chemodiversity. Furthermore, LC-(+)-ESI-MS was the analytical approach which revealed the larger chemodiversity in all sample groups.

For total extracts, the resulting PCA plots, but also to a higher extent PLS-DA plots, showed a significant discrimination according to the sampling sites on the first component, while samples were discriminated according to the thallus parts on the second component (**Figure V.4A-C**, and SV.12A-C, Table SV.11). The zonal discrimination was observed linearly from the basal to the median and then to the apical algal parts with all analyses (**Figure V.4** and SV12), excepted for the PCA plot built with the LC-(-)-ESI-MS data (**Figure V.4B**). This observation indicated a continuous global shift of the total metabolome composition along the thalli. For GC-MS and LC-(+)-ESI-MS analyses, pairwise tests revealed that the basal parts were significantly different from the apical and median ones (Table SV.12).

For surface extracts, LC-(+)-ESI-MS analysis also showed a clear discrimination according to both sampling sites and zonal distribution, with a high proximity between the chemical composition of the basal parts from both sites (**Figure V.4F** and S12F). In this case, pairwise tests also revealed that the basal parts were significantly different from the apical and median ones (Tables SV.11 and SV.12). In the case of LC-(-)-ESI-MS data, the discrimination between the samples appeared less evident but can still be observed between sites on the first component and, only in the case of algal samples from Tamaris, between thallus parts on the second component (**Figure V.4E** and S12E). Significant differences were still observed with the pairwise analysis between both sites and between the algal parts (Tables SV.11 and SV.12). GC-MS analysis showed a higher variability between replicates and no discrimination can be clearly observed from multivariate plots (**Figure V.4D** and SV.12D). In this case, only the apical parts were significantly different from the other parts (Tables SV.11 and SV.12).

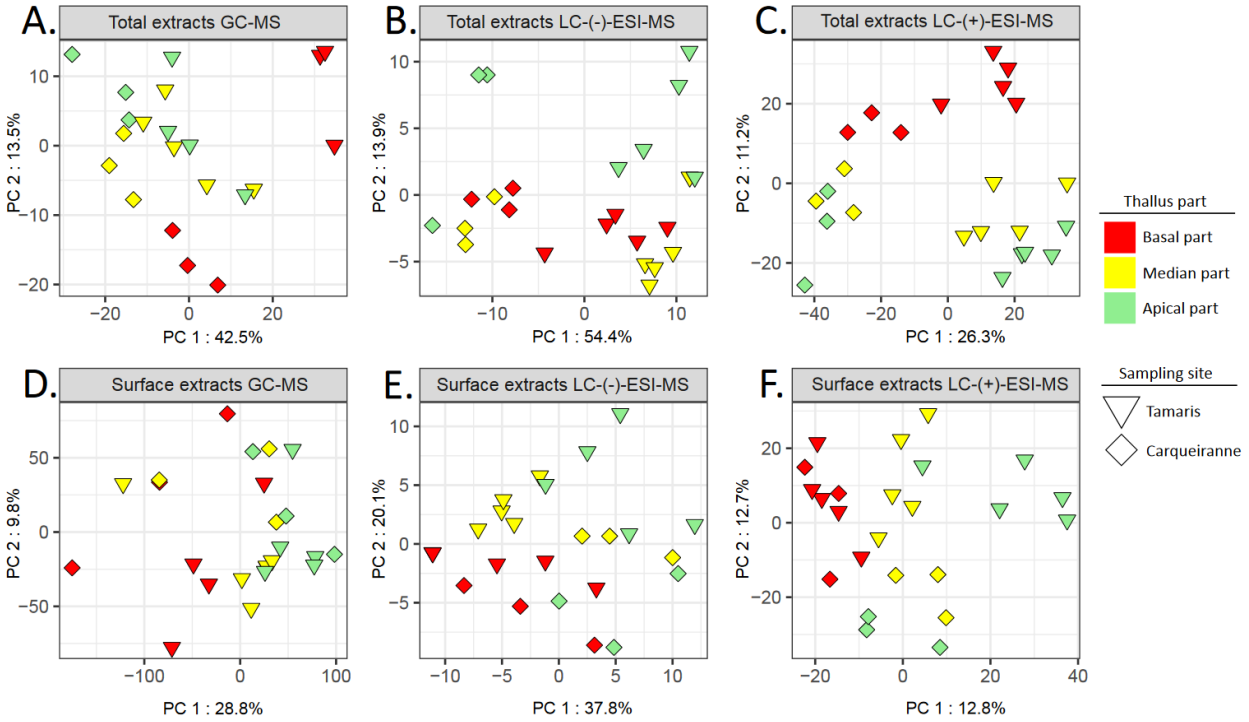

Figure V.4. PCA plots of GC-MS, LC-(-)-ESI-MS and LC-(+)-ESI-MS metabolomics analyses of surface and total extracts of *T. atomaria* (two sites: Carqueiranne and Tamaris; three algal parts: basal, median and apical)

Finally, it can be noted that for all PLS-DA analysis (except for surface extracts analysed by GC-MS), cross validations strengthened these results showing differences between algal parts ($R^2 > 0.8$ for all, Table SV.13).

2.4.5. Global annotation of metabolomes

The 25 major metabolites from the GC-MS dataset were attributed to sesquiterpenes. Among them, 17 were annotated by comparing their MS spectra and retention indexes with those found in databases (Table SV.14). More specifically, gleenol was identified through the comparison of the experimental data with those obtained with a purified standard (Othmani et al., 2016b).

For the LC-MS datasets, a MS/MS molecular network was built for each mode (positive and negative) using the GNPS platform with both extract types. For the LC-(+)-ESI-MS/MS network (Fig. SV.13), clusters A and E gathered lipids including mainly diacylglycerylhydroxymethyl-*N*,*N*,*N*-trimethyl-β-alanines (DGTAs) and phosphatidylcholines (PCs), but also sulfoquinovosyldiacylglycerols (SQDGs), diacylglycerols (DGs), and monogalactosyl-diacylglycerols (MGDGs). For some of them, these lipid families were characterised through specific fragment ions, such as *m/z* 236.1494 $[C_{10}H_{22}NO_5]^+$ for DGTAs and *m/z* 184.0722 $[C_5H_{15}NO_4P]^+$ for PCs. DGTAs were distinguished from their structural isomers diacylgycerol-*N*-

trimethylhomoserines (DGTSs) based on the absence of a characteristic loss of *m/z* 87 (Roche & Leblond, 2010), even if it is matter of controversy (Li et al., 2017). Clusters B and F consisted of terpenoids, including several sesquiterpenes and geranylgeranylglycerol (GGG) previously purified from *T. atomaria* (Othmani et al., 2016a, 2016b). In cluster B, several compounds were putatively annotated as GGG derivatives on the basis of their MS/MS fragmentation pattern. Cluster C was constituted by *lyso*-DGTAs identified, as in the case of DGTAs, through the characteristic fragment ion at *m/z* 236.1494. Finally, Cluster D was found to contain pheophytin A and derivatives.

The LC-(-)-ESI-MS/MS-based molecular network (Fig. SV.14) mainly showed the occurrence of phospholipids and sulfolipids. Cluster A gathered phosphatidylethanolamines (PEs) annotated on the basis of their characteristic fragment ion at *m/z* 140.0119 $[C_2H_7NO_4P]^-$. A second cluster (cluster B) gathered sulfoquinovosyldiacylglycerols (SQDGs) and sulfoquinovosylmonoacylglycerols (SQMGs) elucidated with the help of the typical fragment ion at *m/z* 225.0070 $[C_6H_9O_7S]^-$.

Finally, by using molecular networking for both LC-ESI-MS/MS methods, a total of 82 lipids were putatively annotated including 32 DGTAs /*lyso*-DGTAs, 25 SQDG/SQMGs, 9 *lyso*-PEs, 7 DGs, 5 PCs/*lyso*-PC, 2 GGG derivatives, 2 MGDGs.

2.4.6. Variations of surface metabolites involved in the differentiation between thallus parts

Among the major compounds detected by GC-MS, sesquiterpenes were mainly found at the surface of the apical parts (Fig. SV.15). As example, γ-muurolene for both sites, *cis*-cadina-1,4-diene for Carqueiranne samples and β-cubebene for Tamaris samples, were predominantly found on the apical parts (**Figure V.5**).

For the LC-(+)-ESI-MS analysis, attention was focused on several surface metabolites determined from the PLS-DA according to their statistical significance and VIP score. Among the 31 VIPs characterised in the resulting dataset, 6 were annotated as DGTAs (or *lyso*-DGTAs, Tables SV.15 and SV.16). In comparison to the basal parts, these lipids were found in higher amounts on the apical ones at both sites [e.g. *lyso*-DGTA (C20:3), *lyso*-DGTA (C16:0) and DGTA (C30:1) for Tamaris samples; $p < 0.05$] (**Figure V.5** and SV16). No significant differences were observed with the post-hoc test between the median parts and the two other algal parts. For Carqueiranne samples, among the 15 VIP features characterised, 5 were annotated as PCs through the analysis of their MS and MS/MS data (Table SV.13). PCs were mainly produced on the apical parts [e.g. PC (C31:1) and PC (C39:5) for Carqueiranne and Tamaris samples, respectively; $p < 0.05$] (**Figure V.5** and S16). Unfortunately, several VIPs remained unidentified even if a chemical formula was proposed (Tables SV.15 and SV.16). Among them, two compounds ($C_{29}H_{40}$ and $C_{17}H_{22}O_5$) were found in significant

lower amounts on the basal parts in comparison to the median ones at Carqueiranne, and to the apical parts at Tamaris (**Figure V.5** and SV.16). In contrast, only few metabolites were found in lower quantities at the apical parts, including for Tamaris, a diacylglycerol [DG (C34:1)], DMSP, and a putative *apo*-carotenoid ($C_{30}H_{40}O_2$) ($p < 0.05$, **Figure V.5**). For the LC-(-)-ESI-MS method, neither PEs, SQMGs, nor SQDGs identified in the dataset (Fig. SV.17) were found among the most discriminant (VIP scores < 2) and significant features.

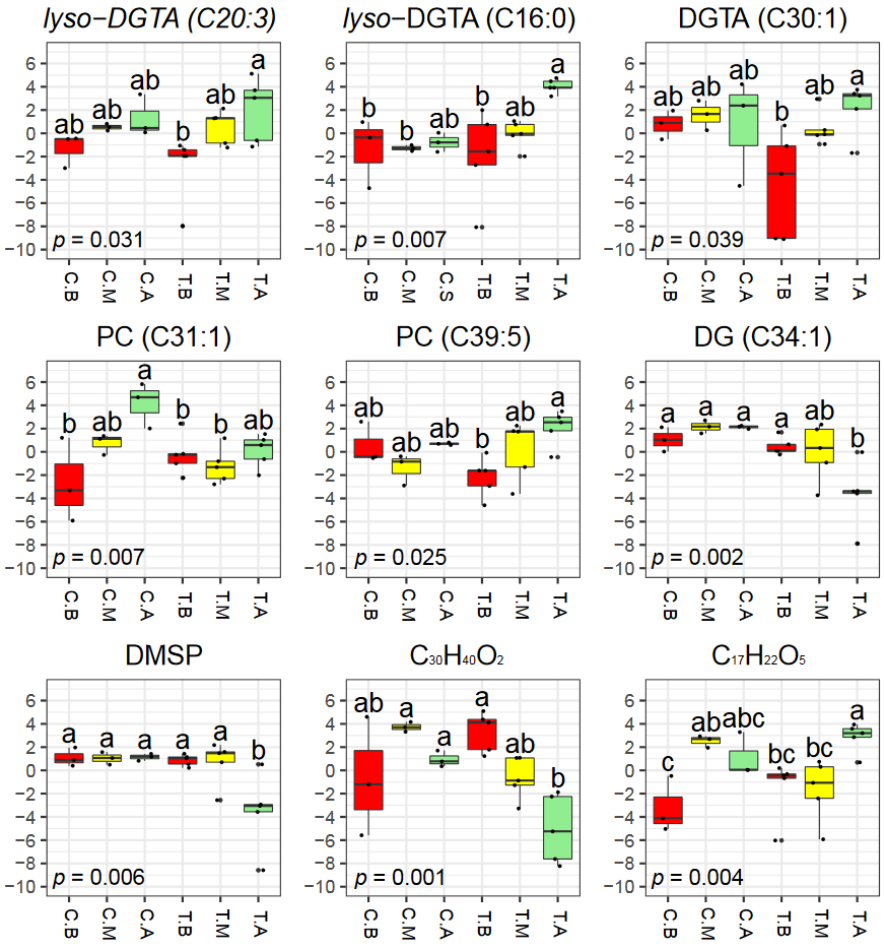

Figure V.5. Normalised concentrations of selected surface metabolites (significant VIP features) detected by LC-(+)-ESI-MS and GC-MS across the different parts of the thalli of *T. atomaria*. Boxplots in red, yellow and green (labeled "B", "M" and "A") represented basal, median and apical algal parts, respectively. Boxplots corresponding to samples collected at Carqueiranne or Tamaris were labeled "C." and "T.", respectively. *p* values and "a", "b", "c" indexes correspond to the results of one-way ANOVA analyses and post-hoc tests (HSD Tukey's test), respectively.

Finally, while the majority of PCs, DGTAs and sesquiterpenes were found in significant higher amounts at the apical parts of surface extracts, the same trends were not significantly observed, for their majority, in the case of total extracts (Fig. SV15 and SV16).

2.4.7. Integration of surface metabolome and surface microbiota datasets

A distance-based redundancy analysis (db-RDA) was performed using weighted UniFrac distance matrix from 16S rRNA gene sequencing dataset and normalised concentrations of surface metabolites of interest as explaining variables. Surface compounds were selected according to their statistical significance and VIP score (> 2). Nevertheless, in some cases, redundancy was observed between metabolites of the same chemical family (e.g. DGTAs, PCs or sesquiterpenes). Thus, only a limited number of compounds were selected and considered as representative of their respective chemical class (**Figure V.6**, permutation test: p = 0.042).

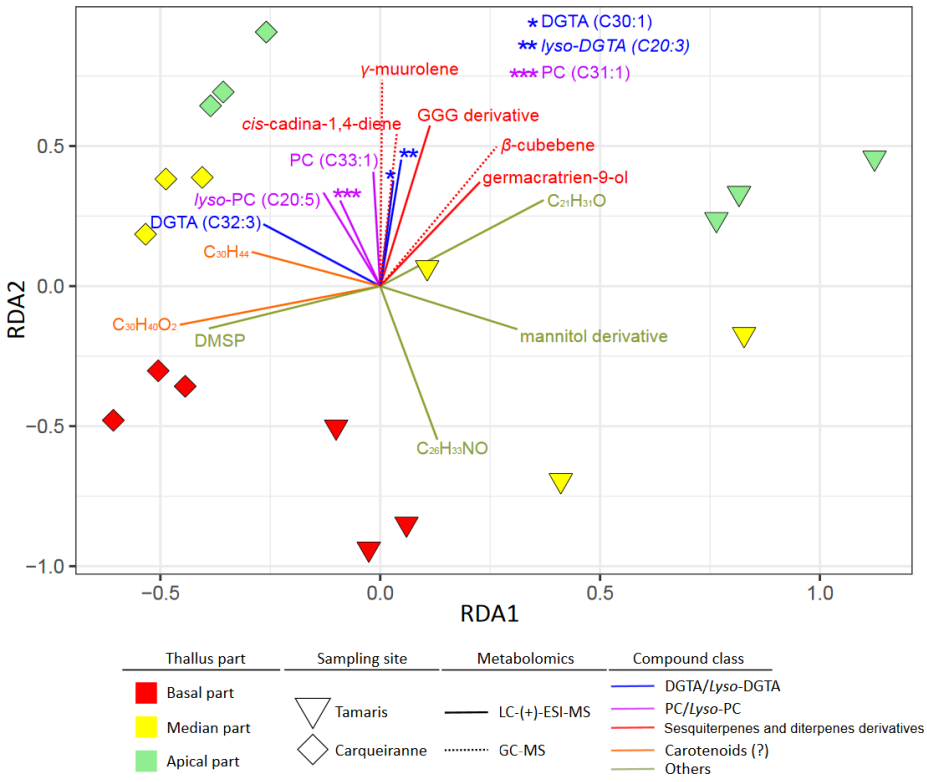

Figure V.6. Weighted UniFrac distance-based redundancy analysis (db-RDA) plot constructed with the 16S rDNA dataset of epibacterial communities at the surface of *T. atomaria* and significant surface metabolites (VIPs) as explaining variables

Several groups of metabolites, discriminated on the second RDA axis, could be viewed as factors directly or indirectly correlated with specific microbiota from the apical parts whatever the site. Among these metabolites, some (*lyso*-)DGTAs and (*lyso*-)PCs but also several sesquiterpenes, such as *β*-cubebene, *γ*-muurolene, *cis*-cadina-1,4-diene and germacratrien-9-ol, appeared as potential specific drivers of the apical microbiota. Only an unidentified compound ($C_{26}H_{33}NO$) seemed to be more specifically linked with basal communities of Tamaris samples. While DMSP, putative *apo*-carotenoids ($C_{30}H_{40}O_2$ and $C_{30}H_{44}$) and

a putative mannitol derivative, appeared discriminant along thalli from Tamaris (**Figure V.5**), these metabolites were also involved in the chemical differentiation between both sites.

2.5. Discussion

Seaweed surface microbiota is increasingly studied in the holobiont context but thalli are generally considered as a whole. However, we assumed that a physiological differentiation occurred along the thallus of *T. atomaria* since meristematic cells are located in the apical part which is consequently the zone where growth happens (Robinson, 1932). Thus, one specific aim of this study was to investigate if the growth of the alga could influence the surface-associated microbiota at the thallus scale.

2.5.1. Specific microbiota selected at the algal surface

The algal epibacterial community structure was compared to communities from seawater and rocky biofilms to assess the host-specificity. Similarly to Canadian kelps and *Mastocarpus* spp. (Lemay et al., 2018a, 2018b), a clear discrimination was observed between overall algal, planktonic, and rocky communities. Dissimilarities between seawater and biofilms underlined the specificity of the ecological niche that represents the life at a surface (Flemming et al., 2016), including algal surface (Sneed et al., 2015; Lemay et al., 2018b). The specificity of algal surface microbiota with respect to that found on rocky biofilms in similar environmental conditions strengthens the hypothesis of an active role of the algal host in the selection of epiphytic communities. Moreover, the main bacterial taxon involved in the dissimilarity with rocky biofilms, *Algitalea*, has been previously described from the surface of the Chlorophyta *Ulva pertusa*, as a new genus (Yoon et al., 2015). It can be noticed that the specificity is all the higher as rocks sampled were collected at both sites and corresponded to diversified mineral substrates with various physico-chemical properties (e.g. roughness) and probably various times of immersion. Interestingly, no Archaea were identified for algal samples when rocky biofilms exhibited low relative abundances (<0.1%), in the same range as for biofilms formed on artificial surfaces (Pollet et al., 2018; Catão et al., 2019).

2.5.2. Epibacterial communities differed from the basal to the apical algal parts

Epibacterial cells were found in significant higher densities at the basal parts of *T. atomaria* collected at Tamaris. A similar tendency has been previously observed at the surface of *Ulva australis* and *Delisea pulchra* with densities from 10^6 cell.cm^{-1} at the distal parts to more than 10^7 cells.cm^{-1} at the basal parts (Maximilien et al., 1998; Tujula, 2006). In the case of *T. atomaria*, a lower order of magnitude was observed, ranging from 10^5 to 10^6 cell.cm^{-1}. Such inter-species differences could be explained by the host-specificity or local environmental conditions.

We tried to visualize surface microbiota of algal parts through a CLSM approach. Images revealed the presence of diatoms, but also probably of fungi hyphae or heterotrophic filamentous bacteria. When comparing this information with the 16S rRNA gene metabarcoding dataset, the major taxa of heterotrophic filamentous bacteria found were Thiothricaceae, and more particularly *Leucothrix* spp., which have been already reported as seaweed epiphytes (Bland and Brock, 1973).

α-diversity metrics decreased from the basal to the apical parts of *T. atomaria* at both sites. Similar results have been previously reported for the Phaeophyceae *Sargassum muticum* for which the α-diversity of the bacterial communities is significantly higher at the holdfast in comparison to the tips (Serebryakova et al., 2018). By contrast, no significant differences have been determined for *Fucus vesiculosus* when comparing tips, thallus and the whole seaweed (Parrot et al., 2019).

β-diversity analyses revealed both site and "thallus-part" specificities of the community structure, which suggested that microbiota structure differed significantly depending on the geographical area but also, at a smaller scale, along the thallus. Even if no environmental characterisation was performed for this study, Tamaris is located within the Toulon bay, and exhibited a higher level of anthropization compared to Carqueiranne (e.g. trace metals, Coclet et al., 2019). A more thorough study should be carried out to test if environmental parameters could explain the differences observed between both sites, whatever the thallus part.

Along thalli from both sites, two Bacteroidetes families constituted key taxa of surface associated communities with global constant proportions. However, some unknown Saprospiraceae genera were mainly associated to the basal parts at both sites whereas Flavobacteriaceae genera (*Algitalea*, *Croceitalea* and *Winogradskyella*) belonged to the pioneer communities found on the apical parts of *Taonia*. At the apical parts of samples from Tamaris, a higher percentage of Hyphomonadaceae, and more particularly the genus *Litorimonas*, was observed in comparison to other algal parts. In the case of *Fucus vesiculosus*, the family Hyphomonadaceae has been also observed with a higher relative abundance on the tips (Parrot et al., 2019). Hyphomonadaceae have been also reported to produce a polar holdfast structure which facilitates surface colonisation (Dang and Lovell, 2016). Therefore, Hyphomonadaceae could represent a pioneer family able to colonise the youngest parts of the thalli. This result was strengthened by observations we have made in a previous temporal study when Hyphomonadaceae have been observed as one of the main family in February and March, the early period of occurrence of *T. atomaria* in the French Mediterranean coasts (Paix et al., 2019).

The similarity of structure with rocky biofilms, which were not the substrates where algal thalli were settled, decreased from the basal to the apical parts. However, rocky biofilms probably included communities with dissimilar ages and surface natures which prevent to go further on if the relative specificity of the different parts of the thalli differs. The higher abundance and α-diversity at basal compared to apical zones could be explained by the maturation of the biofilm (potentially including EPS production). In addition, maturation was reputed to improve the ability of biofilms to limit the influence of environmental pressures (Flemming et al., 2016) which could explain the higher similarity of the basal communities at both sites.

2.5.3. Cross metabolomics and molecular networking allowed to attribute to algal metabolites the intra-thallus variations of the surface metabolome

A multiple platform metabolomics approach combining LC-(+)-ESI-MS, LC-(-)-ESI-MS and GC-MS analyses offered a comprehensive coverage of the total and surface metabolomes of *T. atomaria*. While both LC-ESI-MS methods gave a good coverage of the lipidome, the complementary GC-MS approach allowed a better view of the surface "volatilome" of the seaweed since a higher range of sesquiterpenes were identified. Moreover, the ability of the dipping method used here to extract a large part of the surface metabolome of *T. atomaria* was validated by the fact that during this study, but also in a previous work (Paix et al., 2019), polar compounds (e.g. DMSP, mannitol or dipeptides) have been also detected in addition to lipophilic compounds more logically expected (e.g. fatty acid derivatives and terpenes). To date, only few studies have been used to decipher the chemical production of macroalgae by metabolomics. Unfortunately, in most of them, only a few number of metabolites were identified.

The annotation of large metabolomics datasets is often considered as the most challenging step in metabolomics studies. The recent development of molecular networking as an annotation tool allowed a more powerful identification of metabolites for non-model organisms (Wang et al., 2016). In the specific case of macroalgae which are known to produce a wide range of lipids, such an analytical tool seems particularly adapted as these compounds show similar MS/MS fragmentation pattern and could be thus gathered in clusters facilitating their annotation (Paix et al., 2019; Parrot et al., 2019).

In the context of this study, the main families of surface compounds implied in the intra-thallus variations were DGTAs, terpenes and PCs (Tables SV.14 and SV.15). Among these compounds, DGTAs are known to be mainly produced by eukaryotic organisms, and more particularly by Ochrophyta, while the occurrence of DGTAs in bacteria has been only scarcely reported in the literature (Dembitsky, 1996; López-Lara et al., 2003). Concerning terpenes found at the algal surface, the main part of them have been already

isolated in relatively high amounts from the total extracts of *T. atomaria* (Othmani et al., 2016b) and are typical of the family Dictyotaceae (e.g. cyclic sesquiterpenes and geranylgeranylglycerol). Conversely, few of these compounds have been described to date from prokaryotes. The case of PCs was more controversial because, even if such compounds are considered as one of the main membrane phospholipids in eukaryotes, it has been shown recently that some bacteria can also biosynthesize PCs (Sohlenkamp and Geiger, 2016). Moreover, typical bacterial membrane lipids such as PEs, phosphatidylglycerols (PGs) or the more specific ornithine lipids (OLs) were not detected and/or not implied in the intra-thallus chemical discrimination of the surface extracts. All these reasons led us to believe that the chemical production of the algal host was predominant in the surface metabolome and that, in the case of *T. atomaria*, it was heavily involved in the differences observed at the thallus scale. Nevertheless, we are also aware of the limitation of our method because it did not allow us to characterise all the components of the phycosphere, in particular higher-molecular-weight molecules such as polysaccharides, proteins or nucleic acids.

2.5.4. Algal growth could explain zonal variations of metabolome and microbiota

With a clear discrimination between sites and thallus parts, the surface metabolomes [more particularly those analysed by LC-(+)-ESI-MS] showed a similar clustering pattern than that observed for the microbial β-diversity. As it has been already reported in the case of temporal variations of the same holobiont model (Paix et al., 2019), this similar trend suggested that a high number of co-variations occurred between surface metabolites and epibacterial OTUs.

Nevertheless, while the α-diversity of prokaryotic communities decreased from the basal to the apical parts, the opposite tendency was observed for the chemodiversity of surface compounds. It appeared that surface of the apical parts is composed by a more diverse range of chemical families than the older algal parts (base and median parts).

Annotation allowed to confirm that trend since higher amounts of PCs, DGTAs and sesquiterpenes were specifically found on apical parts. Similarly, DGTAs (and/or DGTS) have been also identified as the main components of the surface lipidome of *F. vesiculosus*, one of these betaine lipids being also found in higher concentrations in the upper part of the thallus (Parrot et al., 2019). DGTAs have been previously found to be mainly expressed during the early period of occurrence of *T. atomaria* (February and March; (Paix et al., 2019). These results could indicate that these betaine lipids are produced in higher relative concentrations at the membrane of cells during their early stage. Therefore, among factors which could explain the difference of metabolome at the thallus scale, growth of the seaweed must be taken into

account. In a recent study, the total content of DGTAs of the Ochrophyta *Sargassum honeri* has been found to first increase during the early growth phase of the sporophytes, and then to decrease later when the alga reaches its mature stage (Zhang et al., 2018). Moreover, the lipid content of the Rhodophyta *Porphyra dioica* has been investigated and specific profiles of betaine lipids and phospholipids have been reported depending of the life stages (gametophytes or sporophytes), indicating the importance of the variations of the membrane lipidome during the whole life cycle of the seaweed (da Costa et al., 2018).

In the case of *T. atomaria*, it has been shown that growth takes place at the level of meristems which are located at the apex (Robinson, 1932). Thus, cell membranes from the apical part of the seaweed could be characterised by a chemical composition specific to the early stages of growth, including potentially PCs and DGTAs. This specificity of apical membranes could induce the selection of specific epibacterial communities and could be a realistic assumption to explain why the epibacterial community differed significantly by its abundance and/or structure along the thallus.

The presence of reproductive structures could also play a key role in the zonal profiling of the surface metabolome. The development of *T. atomaria* from British coasts has been previously studied and characterised by the production of “hairs bands” and tetrasporangia at the apical parts of the thallus (Robinson, 1932). These reproductive structures were also reported in this study at the surface of the apical parts and, in less cases, on the median parts (data no shown). This observation could also explain the metabolome differences reported along the thallus, with specific families of compounds produced in higher concentrations at the apical parts. The presence of “hairs bands” and tetrasporangia at apical parts could also modify the size and the morphology of the surface at a micro-scale and thus could directly impact the adhesion efficiency of specific microbial communities. Thus, differentiated textures at the algal surface, as reported for aquatic plants (Yang et al., 2013a), could be involved in such a dissimilar colonisation.

In the case of the seaweed *Mastocarpus* spp, a recent study has also highlighted the importance of the host life-cycle on microbial associated communities (Lemay et al., 2018a). In connection with our study, the sexual and even the growth state of the algal host could be considered as key factors when studying seaweed microbial communities.

Moreover, the meristematic growth of the alga implies that the apical parts are younger than the rest of the thallus. Conversely, the basal zones constitute the first parts of the young sporophytes and then would be subjected to a longer period of exposure to planktonic microbial communities. The basal zones consequently experienced microbial communities’ succession together with biofilm maturation including

EPS secretion, which could explain a higher microbial density and diversity. Moreover, especially for mature thalli, the apical parts suffer from higher amplitudes of movement in the seawater and consequently shear stress could perhaps also impact the colonisation process at their surface.

2.5.5. Specific role of algal secondary metabolites on epibacterial communities

DMSP has been already studied in the case of several other seaweed-holobiont models and showed interesting key ecological roles involved in the bacterial-seaweed interactions such as anti-adhesion properties for *Fucus vesiculosus* (Saha et al., 2011, 2012) or microbial gardening for the morphogenesis of *Ulva mutabilis* (Wichard and Beemelmanns, 2018). Additionally, DMSP has also showed other functions such as cryoprotection, defence against herbivory, and antioxidant properties (Karsten et al., 1992; Sunda et al., 2002; Lyons et al., 2010). In this study, DMSP was found in lower concentrations at the apical parts in comparison of basal ones for samples collected at Tamaris. Previously, DMSP has been reported in significant lower amounts at the surface of *T. atomaria* during the winter period (early period of occurrence on the sampling site) compared to the spring and summer periods (Paix et al., 2019). Considering that the apical parts are younger than the basal ones, DMSP could be viewed as a metabolite expressed by the alga after the early period of occurrence of the sporophytes or produced by some microorganisms (e.g. diatoms) found in mature biofilms. However, clear causalities links remain difficult to assume, and the role of this metabolite needs to be more specifically investigated in *T. atomaria*. Besides, several bacterial taxa from the *Roseobacter* clade (Rhodobacteraceae) are well known for their catabolism associated to DMSP with several enzymes, such as DddD and DddP, involved in the cleavage of DMSP into dimethyl sufide (DMS) (Curson et al., 2011). A focus on these enzymatic pathways, together with a precise quantification of DMSP at the algal surface would constitute a complementary perspective to allow further hypothesis on the role of this compound on the zonal specificity of the epibiota of *T. atomaria*.

In Othmani et al., 2016, two sesquiterpenes (gleenol and *trans*-calamenene) have been described for their anti-adhesion activities against several bacterial strains at relevant natural concentrations. In the present work, all sesquiterpenes detected, including gleenol and *trans*-calamenene, were detected with increasing concentrations from the basal to the apical algal parts. Sesquiterpenes are well-known, in the case of terrestrial plants, as volatile organic compounds particularly present in reproductive organs and playing a role in the plant growth, but also in their chemical defence against microbial pathogens (Junker and Tholl, 2013; Boachon et al., 2019). More broadly, the optimal defence theory assumes that the level of defences varies among organism parts as the resources are allocated in order to have the best

benefit/cost ratio in terms of fitness (McKey, 1979). In that way, higher concentrations of defence sesquiterpenes could be specifically produced at the surface of the apical parts which are the more valuable for the algal fitness, and thus these compounds could be involved in the selection of specific epibacterial communities. Since the apical parts are constituted by meristematic cells, together with reproductive structures (tetrasporangia and “hair bands”), sesquiterpenes could be exuded at the surface as defence compounds to protect these specific types of differentiated cells.

2.6. Conclusions

Only few studies were focused on microbiota variations at the scale of a single algal individual. Thus, factors explaining the variations of epiphytic microbiota still need to be more investigated to better understand the ecology and physiology of seaweed holobionts. This study is the first one which confirmed that surface microbiota of a seaweed displayed host-specificity and differed significantly and gradually from the basal to the apical parts in abundance, α-diversity and structure in relation with a similarly differentiated surface metabolome. Based on these main results, this study suggested a plausible scenario where the algal physiology along the thallus surface could explain such variations. In addition, with a complementary metabolomics approach, the meristematic growth was proposed to involve several lipids, such as DGTAs and PCs, but also chemical defences with several sesquiterpenes acting in the selection of microbial communities.

2.7. Acknowledgments

This work was supported by the “Sud Provence-Alpes-Côte d’Azur” regional council (B.P. PhD grant). The authors are grateful to B. Viguier and E. Catão (University of Toulon, MAPIEM) for their help during the acquisition of GC-MS profiles and the data processing of 16S rRNA gene reads, respectively. We are grateful to J.-C. Martin (Aix-Marseille University, C2VN) for in-house scripts allowing metabolomics data filtering. LC-MS experiments were conducted on the regional platform MALLABAR funded by the Institute of Ecology and Environment (INEE) of the French National Center for Scientific Research (CNRS) and the Sud-PACA regional council. GC-MS experiments were conducted at the IMBE Support Service on Chemical Ecology and Metabolomics funded by the CNRS, the “Sud Provence-Alpes-Côte d’Azur” regional council, the TOTAL Foundation and the French National Research Agency (ANR).

3. Bilan du chapitre

Cette étude portant sur les variations du métabolome et du microbiote de surface le long du thalle de *T. atomaria* a permis dans un premier temps de comparer trois approches analytiques demétabolomique mises en œuvre par MS [LC-(+)-ESI-MS, LC-(-)-ESI-MS et GC-MS]. Ces trois s'approches s'avèrent complémentaires pour étudier le métabolome de l'algue, avec notamment les deux approches LC-ESI-MS permettant une couverture globale du lipidome tandis que la GC-MS s'avère particulièrement adaptée pour l'analyse et l'identification des sesquiterpènes. En comparant ces trois approches, celle menée par LC-(+)-ESI-MS couvre la plus grande fenêtre de composés, que ce soit en termes de nombre de molécules identifiées et de diversité chimique. Par ailleurs, en regardant outre les résultats de cette étude ceux présentés au niveau des **chapitres II et III**, il apparait que cette méthodologie permet l'analyse simultanée d'un certains nombres de composés particulièrement pertinents d'un point de vue écologique, tels que la fucoxanthine, le gleenol, le DMSP, la proline, la proline bétaine ou encore les DGTAs.

Le deuxième objectif portant sur les variations intra-thalles du microbiote et du métabolome de surface a permis de mettre en évidence une différenciation graduelle allant de la base jusqu'à la zone apicale de *T. atomaria*. La croissance de l'algue apparait comme le facteur principal pouvant expliquer les différences de microbiote et de métabolome à une telle échelle, avec notamment la présence de taxa pionniers et de métabolites impliqués dans la croissance et dans la défense au niveau des zones méristématiques (zones apicales), tandis qu'un microbiote plus dense, moins spécifique et plus diversifié apparait au niveau des zones plus matures de l'algue (zones basales).

CHAPITRE VI : SUIVI SPATIO-TEMPOREL

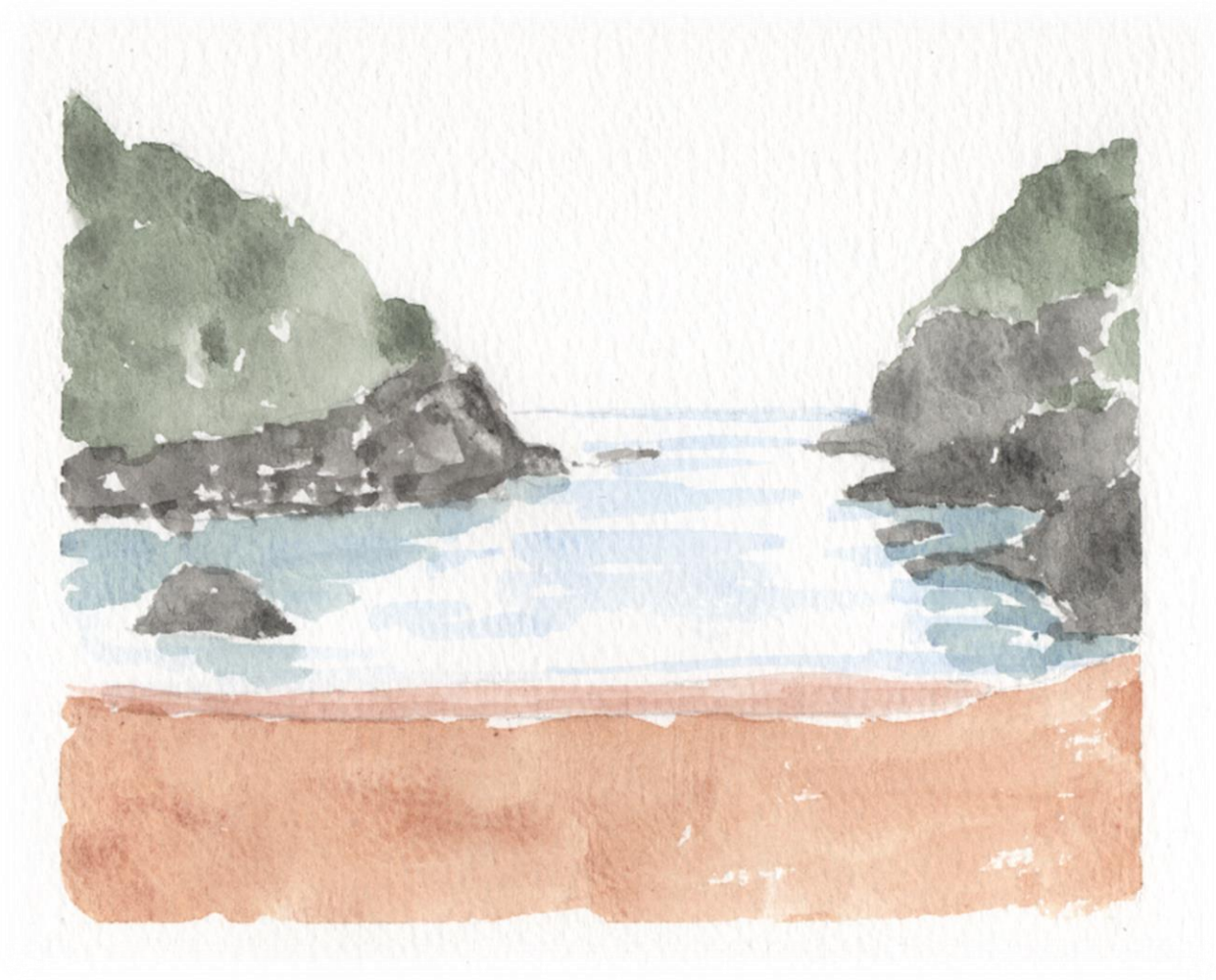

Calanque du Bregançonnet sur l'île de Porquerolles

1. Avant-propos

En partenariat avec le Parc National de Ports Cros, l'un des objectifs principaux de cette thèse est d'étudier l'influence de l'environnement sur les variations du microbiote et du métabolome de surface de *T. atomaria*. La variabilité spatio-temporelle de la structure des communautés épiphytes ainsi que celle de l'hôte, via son métabolome de surface, a été étudiée sur cinq sites de l'aire toulonnaise (incluant la Petite Rade de Toulon très anthropisée et deux sites sur l'île de Porquerolles) afin d'identifier l'influence des paramètres environnementaux. Au cours de ce suivi spatio-temporel, il a été également question de valider l'hypothèse d'une sélection spécifique de la communauté procaryote épiphyte de l'algue par comparaison avec celle de substrats inertes, tels que des surfaces rocheuses, et celle planctonique de l'eau de mer environnante.

Cette étude est présentée sous la forme d'un article de recherche soumis dans la revue *Microbiome*. Les références bibliographiques citées dans cet article sont indexées en fin de manuscrit. La partie *Supplementary Information* de cet article est presentée dans l'annexe VI du manuscrit (annexe électronique).

2. Article: A multi-omics approach deciphers how temperature and copper stress shape seaweed-microbiota interactions at the surface of *Taonia atomaria* on the NW Mediterranean coast

Benoit Paix[1], Nicolas Layglon[2], Christophe Le Poupon[2], Sébastien D'Onofrio[2], Benjamin Misson[2], Cédric Garnier[2], Gérald Culioli[1*] and Jean-François Briand[1*]

[1]*Université de Toulon, Laboratoire MAPIEM, EA 4323, Toulon, France*

[2]*Université de Toulon, Aix Marseille Université, CNRS, IRD, Mediterranean Institute of Oceanography (MIO), UM110, France*

*corresponding authors : briand@univ-tln.fr, culioli@univ-tln.fr

2.1. Abstract

Background: Although considered as holobionts, macroalgae and their surface microbiota share intimate interactions that are still poorly understood. Especially, how environmental parameters influence the interactions between the host and its surface-associated microbiota constitutes a research field where studies are lacking. Within this context, we first investigated the specificity of epibacterial communities associated to the brown seaweed *Taonia atomaria* from five locations in the North-Western Mediterranean coast and then, we intended to decipher the impact of local environmental parameters on the holobiont dynamics through a multi-omics approach combining metabarcoding and untargeted LC-MS-based metabolomics.

Results: Epibacterial communities of *T. atomaria* exhibited a high specificity whatever the five environmentally contrasted collecting sites investigated on the NW Mediterranean coast. By integrating metabarcoding and metabolomics analyses, the holobiont dynamics was found to vary as a whole. During the occurrence period of *T. atomaria*, epibacterial densities and α-diversity increased while the relative proportion of core communities decreased. Pioneer bacterial colonizers constituted a large part of the specific and core taxa and displayed potential functional features involved in adhesion, biofilm formation and adaptation to the epiphytic lifestyle. Then, the concomitant increase of temperature and several algal compounds, especially DMSP, could explain the bacterial diversification, especially with *Roseobacter* taxa specialized in the catabolism of this metabolite. Copper concentration constituted a second factor shaping the holobiont system. The resulting oxidative stress caused an adaptation of the algal surface metabolome with a higher expression of carotenoids, which could have, in turn result in the selection of particular epibacterial taxa.

Conclusion: We showed that associated epibacterial communities were highly specific to the algal host and that the holobiont dynamics varied as a whole. Especially, the temperature increase and trace metal contaminations constituted major direct and/or indirect environmental factors shaping seaweed-epibacterial interactions. In a context of global change, this study brought new insights on the dynamics of a Mediterranean holobiont submitted to heavy anthropic pressures.

Keywords: holobiont, surface metabolome, surface microbiota, temperature, copper-stress, chemical interactions, multi-omics, metabarcoding, metabolomics.

2.2. Introduction

In the marine environment, seaweed surfaces constitute niches for a large diversity of epiphytic organisms among which bacteria represent a major biological compartment (Wahl et al., 2012; Egan et al., 2013; Hollants et al., 2013). Macroalgal epibacterial communities show a high specificity to their host (Lachnit et al., 2011; Aires et al., 2016; Roth-Schulze et al., 2018; Morrissey et al., 2019) and chemical mediation appears to be involved in their relationships at the surface (Goecke et al., 2010; Wichard and Beemelmanns, 2018). Positive interactions have been demonstrated for the *Chlorophyta Ulva mutabilis* which releases a chemo-attracting signal (dimethylsulfoniopropionate, DMSP) for the *Roseovarius* sp. MS2 bacterial strain, which then uses the glycerol boundary layer as a carbon source and promotes the morphogenesis of the algal host (Kessler et al., 2018; Wichard and Beemelmanns, 2018). Negative interactions, like chemical defenses against epibacterial pathogens, were also observed. (Maximilien et al., 1998; Manefield et al., 1999). These results support that the algal host, mainly through the chemical production at its surface, could be strongly involved in the selection of a specific epiphytic microbiota that plays in turn major roles in the fitness of the alga. Considering intimate interactions between both, macroalgae and their surface microbiota may thus be considered together as a holobiont system (Egan et al., 2013; Longford et al., 2019; Paix et al., 2019).

However, little is known about the effect of environmental parameters on the relationships within the algal holobiont(Stratil et al., 2014; Dittami et al., 2016; Coelho-Souza et al., 2017). The production of halogenated furanones in *D. pulchra* decreases when the seawater temperature increases (Wright et al., 2000; Campbell et al., 2011) and this finding is linked to the occurrence of two bacterial pathogenic strains causing thalli bleaching (Case et al., 2011; Zozaya-Valdés et al., 2016, 2017) and subsequently an increased colonization of the algal surface (Campbell et al., 2014). For the *Phaeophyceae Fucus vesiculosus*, light and temperature are the main factors explaining a global temporal shift of the surface metabolome (da Costa et al., 2018; Rickert et al., 2015, 2016b). Moreover, a shift of its epiphytic bacterial community structure has been observed through experimental approaches using different temperature or salinity conditions (Stratil et al., 2013, 2014). Overall, concerns have been raised for seaweeds fitness due to the modification of their microbiota structure that can lead to dysbiosis under the effect of anticipated climate conditions, especially ocean temperature and acidification increases (Egan et al., 2014; Mensch et al., 2016; Aires et al., 2018; Huggett et al., 2018; Minich et al., 2018; Qiu et al., 2019; van der Loos et al., 2019). Global change, together with the increase of other anthropic pressures such as plastic pollution, trace metals contaminations or eutrophication (Coll et al., 2010; Lejeusne et al., 2010), particularly threatens the Mediterranean Sea which is considered a hot-spot of marine biodiversity (Coll et al., 2010).

In this context, the host studied here was the Phaeophyceae *Taonia atomaria* (Woodward) J. Agardh which is widely distributed on the North Western Atlantic and Mediterranean coasts. Some metabolites have been previously characterized at its surface and they showed anti-adhesion properties against marine bacteria, supporting the hypothesis of a chemical selection of the epibacterial community (Othmani et al., 2016b, 2016a). This consideration has been strengthened by the strong temporal co-variations observed between the epibacterial community and the surface metabolome of *T. atomaria* at a single site along the NW Mediterranean coast (Paix et al., 2019). Nevertheless, an investigation of environmental drivers that could control the holobiont dynamics appears necessary.

In this study, we hypothesized that the selection of specific epibacterial communities could be the result of both the effect of the chemical production at the algal surface and environmental factors. Thus, a spatiotemporal multi-omics monitoring of the epiphytic microbiota and the algal surface metabolome, associated to the analysis of environmental parameters, was achieved during the annual occurrence of *T. atomaria* at five environmentally different collecting sites along the French NW Mediterranean coast.

2.3. Materials and methods

2.3.1. Sampling strategy and biological material

Sampling was performed monthly (~1m depth) on rocky substrates during the occurrence period of *T. atomaria* in 2017 (February to July) at five sites named S1 to S5 (Fig. SVI.1) on the French Mediterranean coast. These sites were chosen considering the presence of *T. atomaria* and for their different environmental conditions, in terms of seawater quality, wind and currents (Fig. SVI.1). S1 was inside the Toulon Bay which is a highly anthropized area due to intensive military and commercial harbor activities (Coclet et al., 2019). S3 and S4 were located at Porquerolles Island in the marine preserved area of the Port-Cros National Park. S2 (a previously studied site (Paix et al., 2019; Othmani et al., 2016b, 2016a; Paix et al., 2020)) and S5 were chosen to represent shores in the Gulf of Giens and the Bay of Hyères Islands, respectively. The latter is closed to where a coastal river flows into the bay, but with an erratic functioning associated to massive rainfall. In addition, S3 and S5 were characterized by sandy bottom compared to rocky shores for the other collecting sites. For each sampling, three thalli of *T. atomaria* were collected as replicates for metabolomics, flow cytometry and metabarcoding, together with one neighboring rock and 5L of surrounding seawater for metabarcoding. Temperature, pH, salinity and oxygen were measured using a multiparameter probe (Hydrolab® DS5X, Hatch Hydromet, USA) and surrounding seawater was also sampled for nutrients, total nitrogen (TN), dissolved organic carbon (DOC) and trace metals analyses (SI).

Thalli were transported to the laboratory as described in (Paix et al., 2019). For each triplicate, one frond was used for flow cytometry, a second for DNA extraction and sequencing, and a third for metabolomics.

2.3.2. Chemical analysis of seawater

Nutrients (NO^{3-}, PO_4^{3-} and $Si[OH]_4$) were analyzed using standard colorimetric methods and DOC and TN with a TOC-VCSH analyzer (Shimadzu, Noisiel, France) (Coclet et al., 2019). Dissolved and total concentrations of trace metals (lead, zinc, cadmium and copper) were obtained by differential pulse anodic stripping voltammetry (DPASV) (See SI).

2.3.3. Flow cytometry analyses

Heteroprokaryotic cells densities at the thalli surfaces and their abundance in seawater samples were obtained after sampling, fixation, extraction and staining as detailed in SI (see Supplementary information for Material and Methods). Analyses were performed with a BD Acuri C6 flow cytometer (BD Biosciences,

San Jose, CA, USA). Densities at the algal surface were expressed using the measured surface of each frond (Fig. SVI.2 and SI).

2.3.4. DNA extraction, 16S rRNA gene amplification and high throughput sequencing

Epiphytic cells were collected from algal samples and rocks by gently scraping the surface with sterile scalpels (Paix et al., 2019). Seawater (5L) was filtered using 0.2 μm Millipore filters. DNA from algal and rocky surfaces was extracted using the DNeasy PowerBiofilm Kit (Qiagen, Courtaboeuf, France) according to the manufacturer's instructions. DNA from filtered seawater was extracted using the SA-Gen protocol (Vasselon et al., 2017). For all samples, the V4-V5 region of 16S rRNA gene was targeted and amplified using 515F-Y/926R primers (Parada et al., 2016). Amplicons were sent to Genoscreen platform (Lille, France) for Illumina MiSeq 2 × 250 pb paired-end sequencing.

2.3.5. 16S rRNA gene metabarcoding data processing and analysis

16S rRNA gene reads were processed using the FROGS workflow (Escudié et al., 2018) (details in SI). α-diversity measures were estimated using Chao1 and Shannon indexes. β-diversity was analyzed with a non-metric multidimensional scaling (NMDS) and distance base redundancy analysis (db-RDA) using Bray-Curtis distance with "phyloseq" and "vegan" packages, respectively (McMurdie and Holmes, 2013; Oksanen et al., 2019). The use of environmental constraints for db-RDA is detailed in SI. LEfSe analyses were performed to reveal specific taxa using the online tool from the Galaxy environment. SIMPER analyses were performed at the genus level with the "vegan" package to identify which genera are contributing the most to the dissimilarity between samples. The algal core community (ACC) of each algal sample was defined as the community spatially and temporally stable in terms of composition, and thus by keeping only OTUs occurring at least in one of each replicate. This definition was used according to (Paix et al., 2019) and prevent to fix an arbitrary percentage. The algal enriched community (AEC) was defined by keeping only OTUs with an average relative abundance 10 times higher for algal samples compared to seawater and rocky samples. Predicted functions associated to bacterial communities were determined with Tax4Fun (Aßhauer et al., 2015) as described in SI and analyzed using principal component analysis (PCA).

2.3.6. Extraction of surface metabolome and UPLC-ESI-MS analyses

The surface metabolome was extracted in the laboratory by dipping each frond in 5 mL of LC-MS grade methanol (Carlo Erba, Peypin, France) during 5s according to (Othmani et al., 2016a) and subsequent sample preparation is detailed in SI. Analyses were performed on a UHPLC-ESI-HRMS system (Dionex Ultimate 3000 rapid Separation; ThermoFisher Scientific, Illkirch, France) with an analytical core-shell reversed phase column (150 × 2.1 mm, 1.7 μm, Kinetex Phenylhexyl; Phenomenex, Le Pecq, France)

coupled with a QToF Impact II mass spectrometer (Bruker Daltonics, Bremen, Germany) in positive mode (details in SI).

2.3.7. Metabolomics data processing, annotation and statistical analyses

Raw UPLC-MS data were converted into netCDF files using DataAnalysis software (version 4.3, Bruker Daltonics) and processed for peak finding, integration and alignment using the XCMS package (Smith et al., 2006) (details in SI). Data were filtered according to (Favre et al., 2017) by considering signal/noise ratio, coefficient of variation and correlation. The resulting data matrix was $\log_{10}$-transformed, mean-centered, normalized using the sum of the chromatographic peak areas as described in (Paix et al., 2020)and analyzed using PCA followed by partial least-square discriminant analysis (PLS-DA) allowing to reveal discriminant features according to sampling months or sites. The most discriminant features were selected according to their significance and their variable importance in projection (VIP) scores to pay attention on their annotation.

The annotation step was performed as described in (Paix et al., 2019, 2020). In brief, annotation was assessed by comparison of *m/z* value, retention time and MS/MS spectra with those of our in-house database (purified compounds and commercial standards listed in SI), and public databases (e.g. MetLin, LipidMaps). To confirm our annotation, elucidation of the fragmentation pathways was performed and, when possible, compared to the literature. The whole dereplication procedure was facilitated using molecular networking (GNPS platform; details in SI).

2.3.8. Integration of metabolomics, metabarcoding, Tax4Fun and environmental datasets

Environmental parameters, 16S rRNA gene metabarcoding, functional predictions, and surface metabolomics datasets were analyzed together into a global integrative approach to assess the correlations existing between each group of variables. To perform this analysis, the DIABLO approach using mixOmics R package (Lê Cao et al., 2009) was used with the *block.splsda()* function, allowing to build a correlation network with the most correlated and discriminant features of each dataset (details in SI).

2.3.9. Statistical tests

ANOVA followed by HSD Tukey's tests were used to evaluate the significance of variables (diversity metrics, predicted functions and metabolites) across the different groups of samples with "ade4" and "agricolae" R packages (Dray and Dufour, 2007; Mendiburu, 2019). After NMDS and PCA, differences between groups were statistically checked with two-way PERMANOVA tests combining "Site" and "Month" factors, followed by multivariate pairwise tests using "vegan" and "RVAideMemoire" packages,

respectively (Oksanen et al., 2019; Hervé, 2020). The db-RDA model was statistically validated as described in SI. PLS-DA were subjected to cross-validations tests calculated with the 6 first components, using the MetaboAnalyst tool (Chong et al., 2019).

2.4. Results

2.4.1. Environmental conditions and occurrence of T. atomaria

Sporophytes of *T. atomaria* were observed from February to May at S3 and S5 and from February to July at S2 and S4. According to thallus observations and length measures (Fig. SVI.3), only one generation of sporophytes was observed for all sites excepted at S1, where a first generation was observed from February to April followed by a second one from May to June.

From February to July, an increase of seawater temperature from 13 to 22°C was observed for all sites, together with stable salinity and pH around 38 and 8, respectively (Table SVI.1). No clear difference was noticed considering nutrients and DOC neither between sites nor time, except phosphates decreasing from February to June. Concentrations were those of mesotrophic systems (Table SV.1). S1 was characterized by high concentrations of copper, lead, and zinc for both total and dissolved fractions, with values going up to 63.2, 15.2, 109.2 and 37.5, 1.7, 61.0 nM, respectively (Table SVI.1). S5 was also characterized by a specific metal trace contamination with relative high concentrations of lead, zinc and cadmium, especially for April with 1.7, 78.2, and 0.2 nM for the dissolved fraction (Table SVI.1).

2.4.2. Epibacterial community abundance

When considering all sites together (Fig. SVI.5A), densities for the two first sampling months (February and March) appeared to be significantly lower compared to the following ones (from April to July). From February to July, densities were ranging from 10^3 up to 10^6 cells.cm^{-1}. When considering all sites independently (Fig. SVI.4A), the temporal increase tendency was observed for all sites (not significant for S5). In addition to temporal differences, sampling sites appeared also to differ (ANOVA: $p < 0.001$), with higher densities for S2 compared to S5. For seawater samples, no significant variation of cell abundance was observed neither across the different sampling months and nor the sites (Fig. SVI.4B).

2.4.3. Epibacterial diversity and community composition

Overall, Shannon indexes showed significant higher values for rocky biofilms in comparison to algal and seawater samples, while Chao1 indexes did not appear significantly different (**Figure VI.1A**). For both indexes, a temporal increase was the major tendency for algal samples, while no difference was observed according to sites (**Figure VI.1B** and SVI.5B). However, S1 showed a lower value in May, depicting two periods of α-diversity increase (**Figure VI.1C**). For rocky samples, both indexes did not show any significant difference whatever the month or site. For seawater samples, only the Chao1 index significantly decrease from February to July (**Figure VI.1B**).

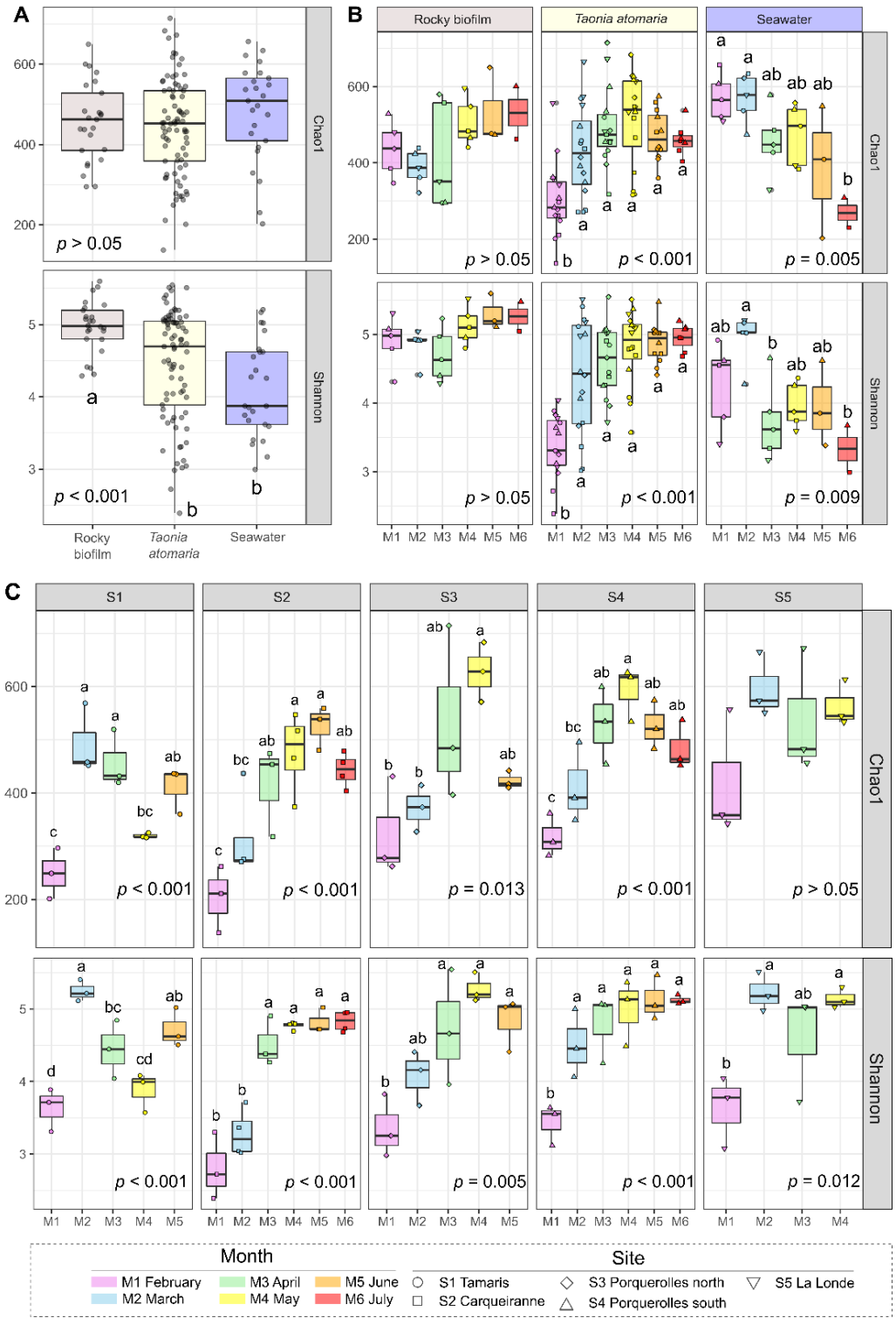

Figure VI.1. *α*-diversity metrics (Shannon and Chao1 indexes) for *T. atomaria*, rocky biofilms and seawater samples. A. Comparison between sample types for all samples, *p* values corresponded to the results of a one-way ANOVA with sample type as factor. B. Comparison between months within each sample type. C. Comparison between months within each site, for algal samples. B. and C. *p* values corresponded to the results of a one-way ANOVA with month as factor.

ß-diversity was analyzed through NMDS analysis with a Bray-Curtis distance matrix, at first with all samples. The NMDS showed a clear significant discrimination between communities from seawater, rocky and *T. atomaria* samples (**Figure VI.2A**, Table SVI.2). When focused on *T. atomaria*, the NMDS (Fig. SVI.6) showed first a temporal shift on the first axis with significant differences observed between each month (Table SVI.3). Then, differences between sites were observed on the second axis, with mainly S1 which appeared as the most discriminated site (Fig. SVI.6). All the sites were significantly different from each other, excepted S3 and S4 (Table SVI.3). The db-RDA showed a similar clustering pattern as the NMDS (**Figure VI.2B**), with differences along the first axis mainly explained by the continuous increase of temperature, together with a decrease of PO_4^{3-}, from February to July (Table SVI.1). Differences between communities observed at S1 and those from the other sites seemed to be explained by higher copper and, to a lesser extent, lead concentrations (**Figure VI.2B**). Singularly at S1, considering both NMDS and db-RDA analyses, May communities appeared located close to February and March ones, in relation to the second algal generation specifically observed at this site (**Figure VI.2B** and SVI.6). With the NMDS constructed only with rocky samples, no significant clustering appeared neither between months nor sites (Fig. SVI.7A, Table SVI.4), and no significant effect of trace metals has been observed using a db-RDA model (PERMANOVA: $p > 0.05$). For seawater samples, significant clustering only appeared between months whatever the site (Fig. SVI.7B, Table SVI.5).

The structure of prokaryotic communities differed significantly between algal surface and seawater mainly by the dominance in seawater of specific genera such as *Synechococcus*, *Litorimicrobium*, an unknown genus of *Pirellulaceae*, and *Planktotalea* contributing to 6.8, 2.8, 2.3, and 1.5% of the total dissimilarity, respectively (Table SVI.6). Several discriminant taxa found in a higher abundance in rocky samples were identified as belonging to the genera *Maritimimonas* and *Lewinella* and the family *Xenococcaceae*, mainly represented by the genus *Pleurocapsa* (Fig. SVI.8). These three genera, together with the genera *Loktanella* and *Aquimarina*, contributed for 1.5, 1.2, 0.8, 1.9 and 1.2% of the total dissimilarity within algal samples, respectively (Table SVI.7). In contrast, several taxa were specific to algal samples, including *Litorimonas*, *Granulosicoccus*, *Rubidimonas*, *Algitalea*, and *Nitratireductor* at the genus level, and *Hyphomonadaceae*, *Thiohalorhabdaceae*, and *Saprospiraceae* at the family level (Fig. SVI.8).

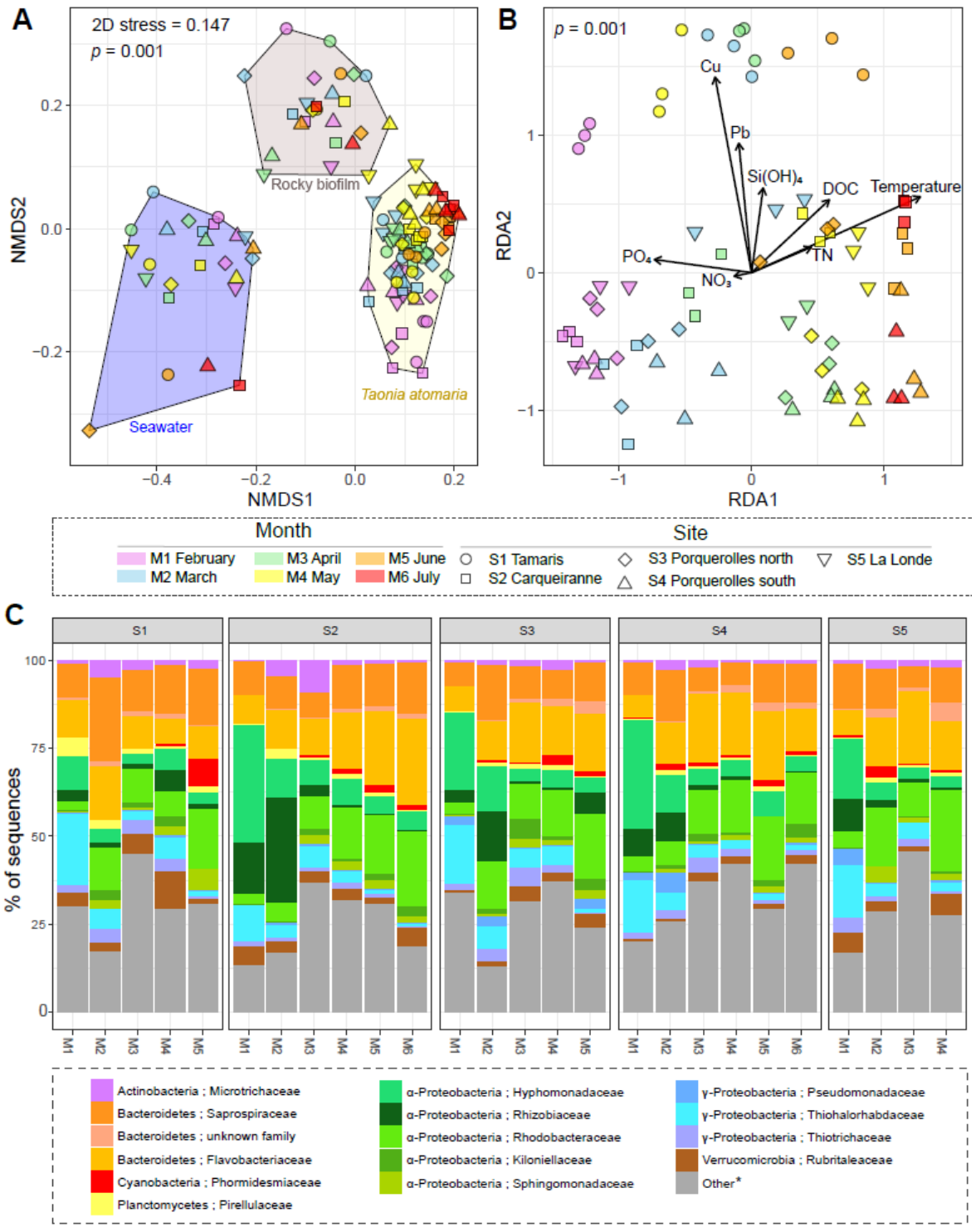

Figure VI.2. Structure and β-diversity of bacterial communities. (A) NMDS constructed with Bray-Curtis index showing β-diversity among seawater, rocky and algal samples. *p* value corresponded to the result of a one-way ANOVA with seawater, rocky and algal samples as factors. (B) db-RDA score plot showing environmental parameters as explaining variables of the β-diversity of algal samples. *p* value corresponded to the result of a two-way ANOVA using "Months" and "Sites" as factors. (C) Epibacterial community composition of *T. atomaria* at the family level. *: "Others" correspond to unaffiliated families and families below 1%.

Among algal samples, a clear temporal shift appeared whatever the site with the main occurrence of specific families, such as *Hyphonomonadaceae* and *Thiohalorhabdaceae*, in February (**Figure VI.3C**). These two families, mainly represented by the genera *Litorimonas* and *Granulosicococcus*, respectively, appeared as biomarkers of this month whatever the site (Fig. SVI.9). From February to July, the average relative proportions of these families decreased from 22.5 to 4.8% and from 15.4 to 1%, respectively. In contrast, a continuous temporal increase was observed for the families *Rhodobacteraceae* and *Flavobacteriaceae* (from 3.5 to 18% and 7.8 to 18.3%, respectively). Through the LEfSe analysis, these two families were also specific taxa of July (Fig. SVI.9). Since the temporal discrimination was preponderant in the clustering of the whole set of algal samples, discriminant analyses according to sites were conducted, firstly with all months, and then month by month (not shown). Whatever the month, several taxa were found as site biomarkers such as *Rubritaea*, *Roseibacillus*, *Ornithococcus*, *Clostridiales* and *Micrococcales* for S1, *Ekhidna* for S2, *Persicirhabdus* and *Cellvibrionaceae* for S3, *Vibrionales* for S4 and Nostocaceae for S5 (Fig. SVI.10). Considering each month independently, *Rubritalea* appeared recurrently discriminant for S1, from April to June (LDA > 3.5).

Both relative percentages of OTUs and sequences of the ACC showed a significant decrease mainly from February to May (Fig. SVI.5C and SVI.11A). Percentages of OTUs and sequences of the AEC showed a similar tendency to the ACC with a significant decrease observed from February to March (Fig. SVI.5D and SVI.11B). As for the total community, *Hyphomonadacaceae* and *Thiohalorhabdaceae* were found as the major families of the early ACC and AEC, and appeared to decline from February to April, while *Rhodobacteraceae* and *Flavobacteriaceae* increased after February (Fig. SVI.11).

2.4.4. Predicted functional features of epibacterial community

KEGG profiles predicted by the Tax4Fun analysis, were firstly analyzed at the KO level using a PCA with all samples and then only algal samples (Fig. SVI.12). This first analysis revealed that algal, rocky and seawater samples showed significant differences of functional profiles (Table SVI.8). For algal samples only, the PCA (Fig. SVI.13) showed a significant difference between February and the other months (Table SVI.9) while no significant differences were observed between sites.

At the KEGG pathway level, bacterial chemotaxis, biofilm formation (described for *E. coli*, *P. aeruginosa* and *V. cholerae*), flagellar assembly, secretion system, and lipopolysaccharide biosynthesis were functional features showing higher average percentages in February, followed by significant decrease tendencies the other months of the monitoring (**Figure VI.3** and S14). In contrast, metabolic pathways associated to

cysteine/methionine and arginine/proline metabolisms were found to significantly increase during the monitoring period (**Figure VI.3** and S14).

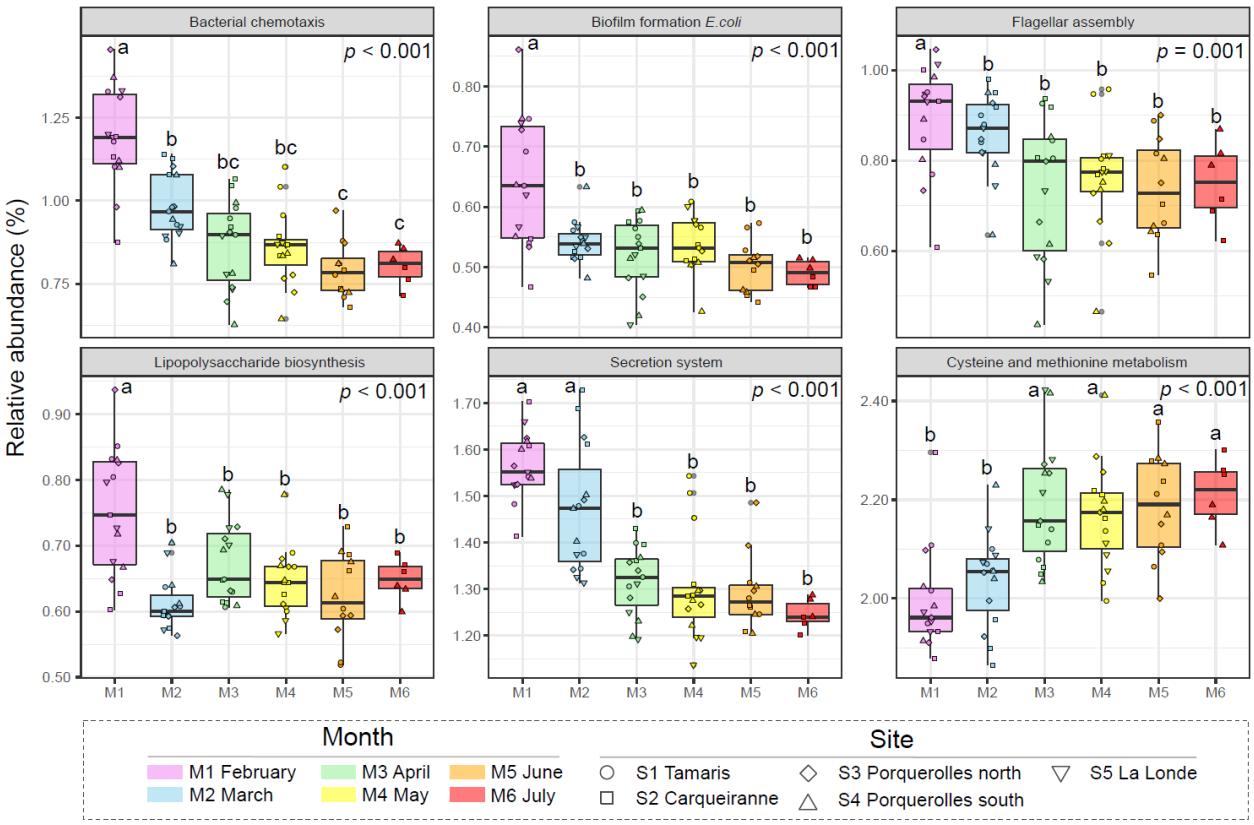

Figure VI.3. Variations of predicted functions associated to the epibacterial communities of *T. atomaria*. *p* values corresponded to the results of a one-way ANOVA using "Month" as factor.

2.4.5. Surface metabolome profiling

The surface metabolomics dataset (422 *m/z* features) was first analyzed by PCA (**Figure VI.4A**) and showed a clear temporal shift according to each month (Table SVI.10). Statistical differences between sites were observed, excepted between S2 and S4 (Table SVI.10). Component 1 (23% of the total variance) showed a metabolomic shift from May to July whereas component 2 (11% of the total variance) mainly explained the metabolomic shift from February to May. Two PLS-DA models were constructed using either months or sites as supervised groups. The PLS-DA model discriminating months (**Figure VI.4B**) showed a score plot highly similar to the pattern obtained with the PCA. The second PLS-DA model discriminating sites showed a clear difference between S1 and the other sampling sites (**Figure VI.4C**).

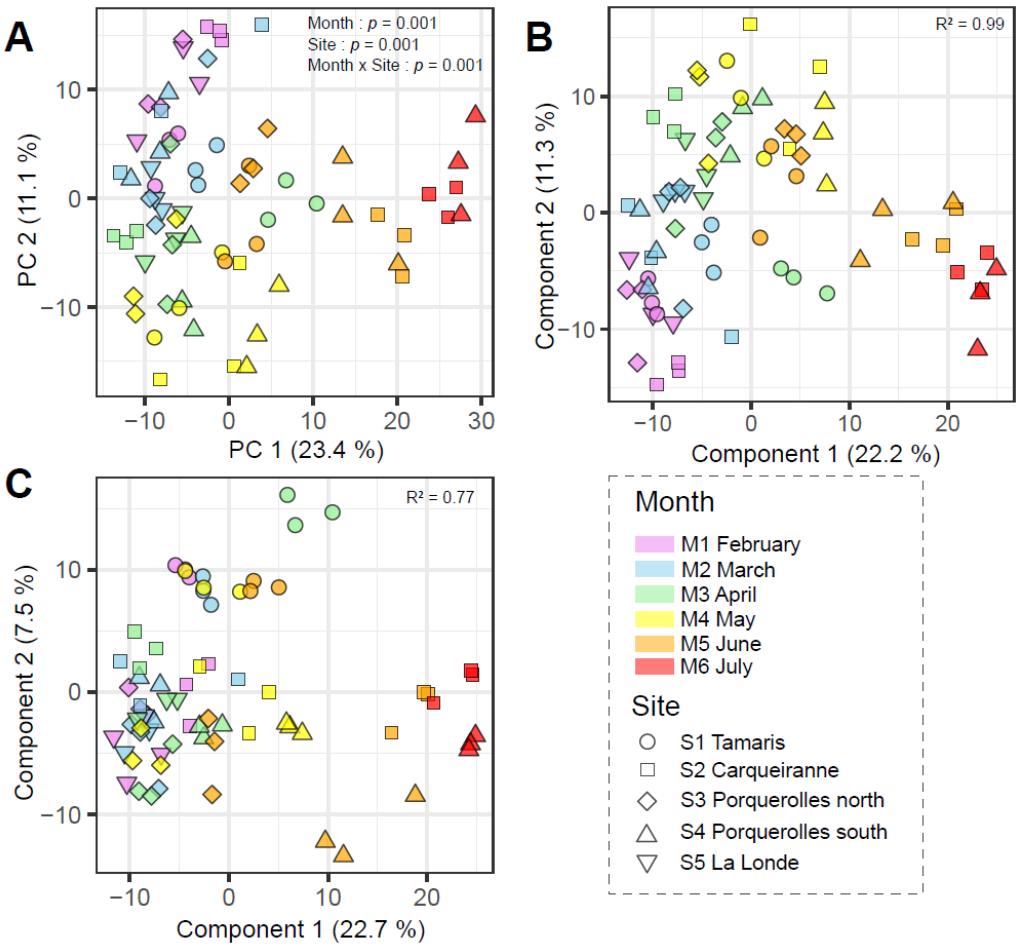

Figure VI.4. Diversity surface metabolome profiles assessed through LC-(+)-ESI-MS metabolomics. Score plots of (A) PCA, and PLS-DA constructed either with months (B) or sites (C) as supervised groups. *p* values corresponded to results of a two-way PERMANOVA using "Month" and "Site" as factors.

2.4.6. Surface compounds characterization and dynamics

Molecular networking gave an overview of the surface metabolome by gathering the main chemical families (Fig. SVI.15). Clusters A and F were composed by terpenes (mainly diterpenes and sesquiterpenes). Clusters B and D revealed di- and monoacylglycerylhydroxymethyl-*N*,*N*,*N*-trimethyl-*β*-alanines (DGTAs and *lyso*-DGTAs), respectively, while cluster C gathered monogalactosyldiacylglycerols (MGDGs) and diacylglycerols (DGs). Cluster E was characterized by di- and monoacylglyceryl-3-*O*-carboxy-(hydroxymethyl)-choline (DGCCs and *lyso*-DGCCs) and cluster G by pheophytin a and other chlorophyll derivatives.

Furthermore, a focus was made on the annotation of discriminant features (VIP score > 2), differentially expressed among months or sites (Table SVI.11 and SVI.12). Among the 15 most discriminant features according to the different months, 7 compounds were identified as DGTAs and showed the same pattern

with increasing concentrations during the seasonal monitoring (**Figure VI.5A**, Table SVI.11). Several other compounds showed similar seasonal variations, in particular *lyso*-DGCC (C16:0), *lyso*-phosphatidylcholine (*lyso*-PC, C20:5) and DMSP (**Figure VI.5A**, Table SVI.11). Despite lower VIP scores, sesquiterpenes (such as gleenol and cadina-4(14),5-diene) together with a geranylgeranylglycerol derivative showed a common pattern characterized by a significant decrease from May to July, while no clear change was observed before (**Figure VI.5A**).

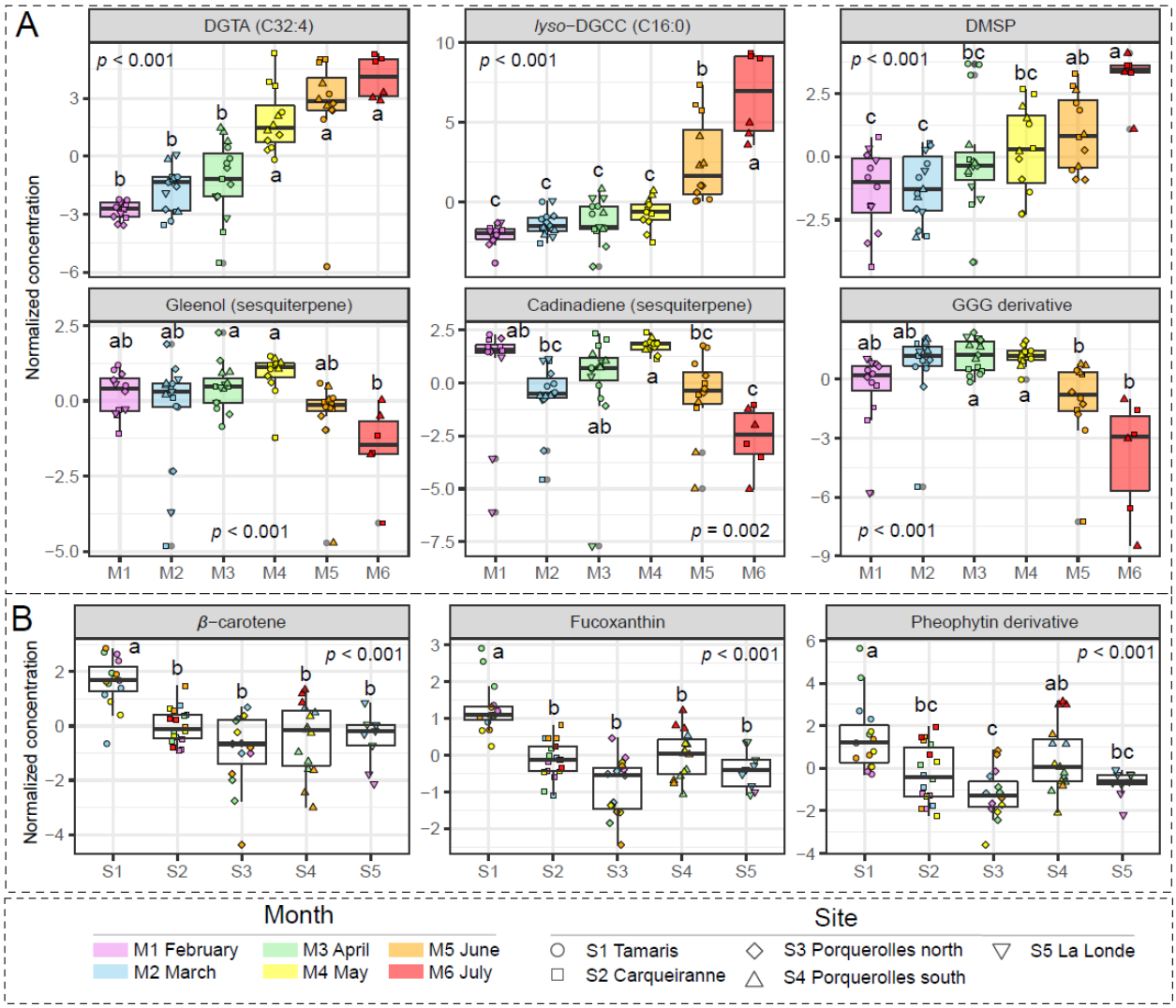

Figure VI.5. Normalized concentrations of significant and discriminant surface metabolites. (A) Discriminant metabolites according to temporal differences. *p* values corresponded to the results of a one-way ANOVA using "Month" as factor. (B) Discriminant metabolites according to spatial differences. *p* values corresponded to the results of a one-way ANOVA using "Site" as factor.

When focusing on features differentially expressed according to sampling sites (VIP score > 2), all selected metabolites, including DG (C20:5/C16:4), pigments such as fucoxanthin, *β*-carotene, and a

pheophytin derivative (**Figure VI.5B**, Table SVI.12), were identified as biomarkers of S1. These compounds were found in significantly higher concentrations at S1 compared to the other sites, excepted for the pheophytin derivative at S4 (**Figure VI.5B**, Table SVI.12).

2.4.7. Multi-omics network analysis

A multi-omics-based network (**Figure VI.6**) revealed correlations between the most discriminant features from each dataset (OTUs from 16S rRNA gene metabarcoding, predicted KEGG pathways from Tax4Fun, surface metabolites from metabolomics and environmental data). The whole network showed two clusters mainly characterized by positive correlations (82.2%). Temperature and copper concentrations were the two main environmental parameters showing correlations with features of other datasets, one in each cluster. The first cluster, associated to the seawater temperature, gathered variables involved in the temporal variations. This cluster was found to be composed by variables mostly observed during the summer period such as surface metabolites corresponding to several DGTAs, *lyso*-DGCC (C16:0) and DMSP. OTUs positively associated to this cluster were also found with increasing abundances during the seasonal monitoring and were mainly affiliated to the family *Rhodobacteraceae* (*e.g*. genera *Pseudoruegeria*, *Silicimonas* and *Octadecabacter*). Pathways associated to biofilm formation and bacterial chemotaxis showed negative correlations with features of this cluster (excepted with phosphates), while cysteine/methionine and arginine/proline metabolisms showed positive correlations.

The second cluster was composed by features specific to S1, copper concentrations being the central environmental parameter. Among surface metabolites, fucoxanthin, pheophytin derivatives and DG (C36:9) were positively correlated to copper. Two OTUs of this cluster affiliated to the family *Rubritaleaceae* (genera *Rubritalea* and *Roseibacillus*) were also positively correlated to copper and the metabolites previously mentioned.

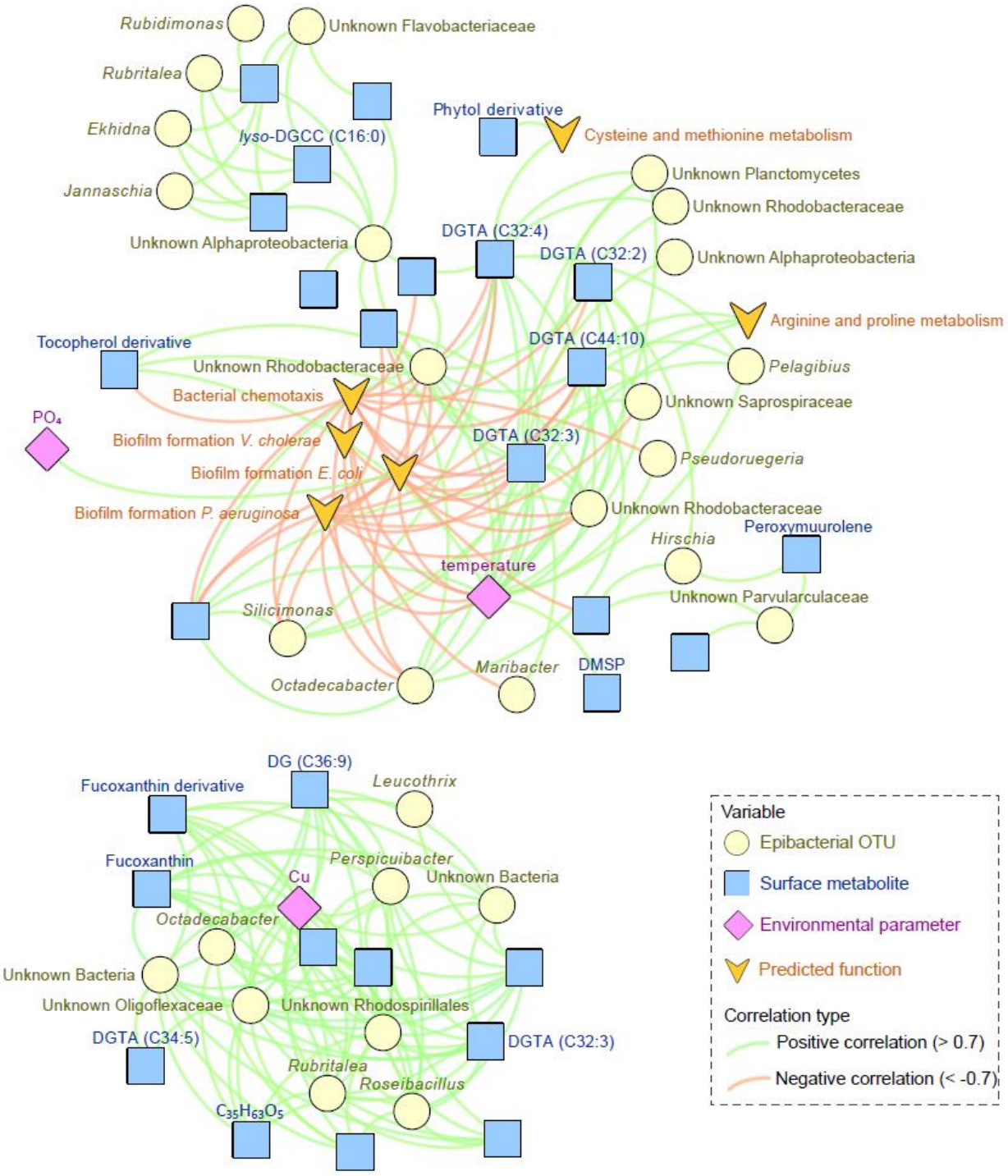

Figure VI.6. Spatiotemporal correlation network (multi-block sPLS-DA, DIABLO analysis) of the surface metabolome, epibacterial community, predicted functions and environmental variables. Using a sparse method, the network was constructed with an optimal number of variables according to the tuning procedure, which corresponded to a total of 29 metabolites, 28 OTUs, 6 predicted pathways and 3 environmental parameters with only positive correlations above 0.7 and negative correlations below -0.7.

2.5. Discussion

As the holobiont concept required to consider both hosts and their associated microbiota in integrative studies, an original multi-omics approach coupling metabolome and microbiota analyses at the surface of *T. atomaria* was conducted on five environmentally different sites to investigate how environmental parameters may control the host-microbiota relationships.

β-diversity and predicted functions from surface communities on *T. atomaria* appeared clearly dissimilar from those from neighboring rocky surface or seawater. This indicated for the first time for this Mediterranean seaweed that its epiphytic microbiota was highly host-specific. Moreover, the Shannon index was lower for algal samples compared to rocky biofilms irrespective of time or site, which also support the hypothesis of a control of the surface microbiota by the algal host. The β-diversity dissimilarity between algal epiphytic communities and epilithic ones have also been observed in few studies conducted within other environments with Canadian kelps and *Mastocarpus* spp. (Lemay et al., 2018b, 2018a) or *Fucus vesiculosus* from the Baltic sea (Stratil et al., 2014). Additional mechanisms of selection must be involved, including the role of algal physical properties (*e.g.* surface structuration and rigidity), but results from the integrated multi-omics analysis indicated that metabolites expressed at the surface, together with environmental constraints, should be viewed as the main factors shaping the structure and the physiology of the epiphytic microbiota, consequently influencing the whole dynamics of interactions in the holobiont.

2.5.1. A winter, low diversified and host-specific pioneer community

The pioneer microbiota observed in the early stage of *T. atomaria* was mainly characterized by the occurrence of *Hyphomonadaceae* and *Thiohalorhabdaceae* whatever the site, as previously reported at S1 and S2 (Paix et al., 2019, 2020). Hyphomonadaceae, mainly represented by the genus *Litorimonas*, appeared as a major contributor of the core and host enriched microbial consortia associated to the algal surface. This family was already described on eukaryotic surfaces (Abraham and Rohde, 2014), notably *Litorimonas cladophorae* isolated from the *Chlorophyta Cladophora stimpsoni* and *Algimonas porphyrae* from the *Rhodophyta Porphyra yezoensis* (Fukui et al., 2013; Nedashkovskaya et al., 2013). Moreover, a recent study showed that two OTUs affiliated to the genus *Litorimonas* were also reported as core OTUs of the *Rhodophyta Mastocarpus* spp. and showed a higher abundance on these algal surfaces compared to seawater and rocks (Lemay et al., 2018a). This observation strengthened the idea that *Hyphomonadaceae*, and especially the genus *Litorimonas*, are particularly well adapted to the macroalgal

niche. This high specificity was hypothesized to be linked to several functions including the use of algal exudates or oxygen produced by the host (Abraham and Rohde, 2014).

Moreover, *Hyphomonadaceae* are known to produce a polar holdfast which facilitates the surface anchoring (Dang and Lovell, 2016). In the case of *Hyphomonas* strain VP-6, this holdfast synthesizes specific EPS implied in the first step of the cell attachment (Langille and Weiner, 1998). These functions described in the literature could provide selective advantages for the attachment of pioneer taxa at the surface of uncolonized young algal tissues. Here, the major predicted functions associated to pioneer taxa (mainly in February) were linked to flagellar assembly, chemotaxis, secretion system, biofilm formation and lipopolysaccharide metabolism. These functions appear clearly essential for the establishment of pioneer taxa, which generally required the production of motility proteins, surface chemo- and mechanosensors, and EPS (Dang and Lovell, 2016). During the two following months, *Hyphomonadaceae*, and notably *Litorimonas*, showed a decrease in relative abundance. Conversely, cell densities and α-diversities increased from February to April, indicating the maturation of biofilms at the algal surface after the early colonization process of pioneer, low diversified, core and algal preferential taxa.

2.5.2. Temperature as a major temporal shaping factor

The occurrence of *Hyphomonadaceae* at the early algal stage could have been linked to low temperatures but they are probably more psychrotrophs than psychrophyles (i.e. more tolerant than adapted), since they seemed to reappear as a major family when a second generation of thalli started at S1 in May, when seawater temperature is high. Similarly, the beginning of a new generation in May at S1 could also explained lower α-diversity metrics and higher percentages of AEC and ACC associated to the pioneer community.

In contrast, the family Rhodobacteraceae constitutes a major taxon increasing during the monitoring. This family was mainly represented by genera of the Roseobacter group such as *Octadecabacter*, *Litoreibacter*, *Sulfitobacter*, *Loktanella*, *Pseudoruegeria*, *Silicimonas* and distinct from those dominating in the surrounding seawater such as *Planktotalea* and *Litorimicrobium*. Six OTUs among this family affiliated to *Octadecabacter*, *Silicimonas* and *Pseudoruegeria* were found positively correlated to the seawater temperature. The *Rhodobacteraceae* family was already described at the surface of many macroalgae and several taxa within this family were recurrently associated to high temperature conditions (Fernandes et al., 2011; Stratil et al., 2013; Mancuso et al., 2016; Dogs et al., 2017; Serebryakova et al., 2018; Yan et al., 2019). Especially, in the case of *D. pulchra*, the temperature was associated to the development of several pathogens from the *Roseobacter* group such as *Nautella italica* (Case et al., 2011; Fernandes et al., 2011).

Moreover, other taxa of the *Roseobacter* group have been described to be attracted by DMSP and they are able to use it as carbon and sulfur sources (Mou et al., 2005; Curson et al., 2011; Reisch et al., 2011; Bullock et al., 2017). DMSP constitutes an important osmolyte, synthetized by many microalgae but also seaweeds (Karsten et al., 1992; Sunda et al., 2002; Lyons et al., 2010), which is involved in various seaweed-bacterial interactions (Saha et al., 2011, 2012; Kessler et al., 2018; Wichard and Beemelmanns, 2018). As for (Paix et al., 2019), metabolomics showed here that DMSP also increased from February to July and appeared correlated with seawater temperature. The increasing production of DMSP at the algal surface could allow a better development of an adapted community specialized in the use of DMSP, notably for several taxa of the *Roseobacter* group showing DMSP catabolic pathways in their genomes (*e.g. Octadecabacter antarticus*) (Curson et al., 2011). The degradation pathway of methionine and cysteine predicted by Tax4Fun increased during the survey. As methionine constitutes a common precursor in the DMSP biosynthesis pathways (Bullock et al., 2017), a higher production of methionine could then also promotes specific bacterial functions involving DMSP.

In contrast with *T. atomaria*, the DMSP content of *Codium fragile* was found to decrease with seawater temperature but to increase with sunlight intensity (Lyons et al., 2010). Concurrently to temperature, irradiance increased from February to July along the French Mediterranean coast. Thus, irradiance could also explain the seasonal variations of DMSP at the surface of *T. atomaria* rather than temperature itself. This hypothesis was strengthened by other studies revealing positive correlations between the DMSP content of five *Chlorophyta* from Antartica and day-length and sunlight intensity (Karsten et al., 1990, 1992). Similar observations were also noticed in phytoplankton species (*e.g. Phaeocystis* sp.) and the related emission of dimethylsulfide in the atmosphere was even proposed to participate to climatic changes (see the CLAW hypothesis, (Stefels and Leeuwe, 1998; Sunda et al., 2002; Stefels et al., 2007; Reisch et al., 2011)). Considering that biofilms at the seaweed surface are more mature and that irradiance is higher during the summer period, a higher density of DMSP-producing microorganisms (*e.g.* diatoms, dinoflagellates and coccolithophores, but also some bacteria from the *Alphaproteobacteria*) may be expected (Keller and Korjeff-Bellows, 1996; Curson et al., 2017), substantially participating to the DMSP production at the algal surface.

Sesquiterpenes and a geranylgeranylglycerol derivative observed at the surface of *T. atomaria* showed a significant decrease after May. Among these terpenes, gleenol and geranylgeranylglycerol were previously described for their anti-adhesion activities against marine bacteria (Othmani et al., 2016a). Sesquiterpenes are also known as volatile chemical defenses against pathogens in the case of terrestrial

plants (Junker and Tholl, 2013; Boachon et al., 2019). In a similar way to *D. pulchra* with halogenated furanones (Longford et al., 2019), the late decrease of chemical defenses could be linked to the reduction of the host fitness caused by the stress of increasing temperature, irradiance, fouling pressure or also by the aging process. Consequently, the lower level of chemical defenses expressed notably in July, could promote the development of opportunistic epibacterial pathogens, but also specific macrofoulers. Indeed, for some *T. atomaria* individuals collected in July, the colonization of encrusting coralline algae was occasionally observed on the thalli together with bleached apical tips (data not shown).

2.5.3. Trace metal contamination plays locally a key role on the holobiont fitness

For both surface metabolomics and microbiota profiles, a clear discrimination of the samples in relation with trace metals contamination was reported. In the case of S1, a high enrichment factor for copper, and to a lesser extend for zinc and lead, was observed compared to the uncontaminated sites S2, S3 and S4, or the occasionally contaminated site S5, and reflected the high level of anthropogenic pressures of Toulon Bay (Coclet et al., 2018, 2019). Furthermore, contamination profile at S5 appeared specific to April with high concentrations of lead, zinc and cadmium (but not copper) in both dissolved and total fractions but without clear effects on the epibacterial community. The strong Mediterranean rain events occurring in March and April (notably the 25/03/2017, 02/04/2017 and 26/04/2017) could have generated a water spill from the river close to S5 (Le Maravenne) and then a subsequent resuspension of the metals in the coastal sea. In particular, lead is known to be easily remobilized from contaminated particles in coastal water column (Dang et al., 2020; Layglon et al., 2020). The specific metabolomics and microbiota profiles at S1 could probably be linked to high metal contaminations, especially in copper, as dissimilar biofilm communities were already reported between contaminated *vs* uncontaminated areas in the Toulon Bay (Coclet et al.). Considering the relative role of metals, lead was shown to have limited effect compared to copper on microbial communities during a mesocosms experiment mimicking the environmental conditions of the Toulon Bay (Coclet et al., 2020).

Several epibacterial taxa appeared specific to the copper-rich site S1, notably the *Rubritaleaeceae* family (*Verrucomicrobia* phylum), mainly represented by two OTUs of the genera *Rubritalea* and *Roseibacillus*. Interestingly, *Rubritalea* has been already observed as a specific epiphytic taxon of the *Chlorophyta Ulva* spp. in copper-rich environment (Hengst et al., 2010). Another study shows that *Rubritalea squalenifaciens* biosynthesizes antioxidative carotenoids to prevent lipid peroxidation (Shindo et al., 2007). Despite bioassays conducted with higher copper concentrations (from 0 to 8 mM), copper stress is actually known to quickly induce peroxidation of membrane lipids of bacteria (Hong et al., 2012)

and, similarly to algae, production of carotenoids could constitute a selective advantage against related oxidative stress conditions (Pinto et al., 2003).

However, hypotheses of direct or indirect effects of copper on surface community selection remain difficult to address with field analyses. For example, indirect effects through copper toxicity to phytoplankton and consecutive specific organic matter release have been suggested to select copiotroph taxa (Coclet et al., 2019). In the case of epibacterial communities, host surface metabolites could also play a major role. Among discriminant surface metabolites in these copper-rich conditions, the overexpression of photosynthetic pigments, including fucoxanthin, pheophytin derivatives and *β*-carotene, was observed. These results were in accordance with previous studies showing that several macroalgae, exposed to similar copper concentrations than those found at S1, increased their production of pigments (carotenoids and chlorophylls) as an adaptation strategy in response to photo-inhibition and reactive oxygen species (ROS) production induced by copper (Costa et al., 2016; Rodríguez et al., 2018; Ryabushko et al., 2017). For several macroalgae submitted to high copper stress, electron transport rate have been found to be inhibited (Connan and Stengel, 2011) and Cu^{2+} also competes with Mg^{2+} located in the chlorin ring of chlorophyll a, inactivating the associated light-harvesting function and leading to high toxicity (Küpper et al., 2002b). Similarly, *T. atomaria* could express, under copper-rich conditions, higher concentrations of pigments to prevent photo-inhibition and, more specifically, carotenoids known for their antioxidant properties to avoid ROS-induced damage. The oxidative stress promoted by such copper contamination has been also shown as a major factor of changes of the lipidome for several seaweeds (Jones and Harwood, 1993; Ritter et al., 2008, 2014). Here, in addition to photosynthetic pigments, high copper concentrations could be the cause of the changes observed in the algal surface lipidome, especially with a higher production of DG (C20:5/C16:4). In addition, as no clear relationship could be conversely established between copper concentrations and communities from rocky biofilms for the sampled sites, the indirect effect of copper through its impact on the host could be preferential in the selection of a specific community at Tamaris (S1).

Consequently, the shift of the surface algal metabolome potentially induced by copper stress, with notably a higher expression of fucoxanthin, could be a key parameter involved in the spatial dissimilarities of the epiphytic microbiota. In the case of *Dictyota* sp., but also for the more phylogenetically distant *F. vesiculosus,* this xanthophyll implied in the photosynthesis process has been identified as an inhibitor of the bacterial adhesion (Viano et al., 2009; Saha et al., 2011). Moreover, fucoxanthin was observed as an inhibitor of bacterial settlement in field studies for *F. vesiculosus*, and consequently considered as a part

of its chemical defenses (Lachnit et al., 2013). However, no clear effect was observed on the microbial community composition at the surface of *F. vesiculosus* (Lachnit et al., 2013) and the potential role of this compound in the selection of specific epiphytic communities needs to be more deeply investigated (Egan et al., 2013).

2.6. Conclusion

In conclusion, we found that (i) epibacterial communities were highly specific to *T. atomaria*, especially in the case of winter and low diversified pioneer bacterial colonizers, (ii) epibacterial densities and α-diversity measures increased over months and witnessed the attachment of new colonizers reducing the proportion of core and algal preferential taxa, (iii) strong spatio-temporal co-variations occurred between surface metabolites and epibacterial communities suggesting a whole holobiont dynamics, (iv) the temperature increase and trace metal contaminations constituted major direct and/or indirect environmental factors shaping seaweed-epibacterial interactions. This study constituted the first multi-omics approach coupling metabolomics and metabarcoding analyses to investigate the dynamics of seaweed-epibacteria interactions in connection with environmental parameters. Especially, in the case of trace metals contamination, whose impact has been rarely considered, this work brought new insights to decipher anthropogenic effects on marine coastal ecosystems.

2.7. Declarations

2.7.1. Ethics approval and consent to participate

Not applicable

2.7.2. Consent for publication

Not applicable

2.7.3. Availability of data and materials

Sequences data were deposited and are publicly available in the NCBI Sequences Read Archive (SRA) under the BioProject ID PRJNA639819, accession number. Raw data for LC-ESI-(+)-MS/MS experiments were deposited and are publicly available in the MassIVE platform under the IDs MSV000082277. Cytometry raw data are available on request from the authors.

2.7.4. Competing interests

The authors declare that they have no conflict of interest.

2.7.5. Funding

This work was funded by the French “Sud Provence-Alpes-Côte d’Azur (Sud PACA)” regional council (PhD grant of B.P.). LC-MS experiments were conducted on the regional platform MALLABAR funded by the Institute of Ecology and Environment (INEE) of the French National Centre for Scientific Research (CNRS) and the French Sud PACA regional council.

2.7.6. Authors' contributions

BP, JFB and GC have designed the study. BP, GC, and JFB performed field sampling. BP has performed the experiments and data acquisition of metabolomics, flow cytometry and metabarcoding analyses. NL, CLP, SDO and CG performed chemical analyses of seawater samples. BM has contributed to the treatment of the flow cytometry raw data. BP, JFB and GC have contributed to the data analysis. BP, JFB and GC have written the article.

2.7.7. Acknowledgements

The authors are grateful to Dr. M. Peirache, I. Masinski, G. Esposito and L. Maxime (National Park of Port-Cros, Hyères-les-Palmiers, France) for the sampling at Porquerolles Island, to Dr S. Greff (Aix-Marseille University, IMBE, France) for the acquisition of LC-MS profiles and to N. Carriot (Toulon University, MAPIEM, France) for the annotation of MS/MS data.

3. Bilan du chapitre

La variabilité spatio-temporelle de la structure des communautés épiphytes ainsi que celle de l'hôte, via son métabolome de surface, a été étudiée sur cinq sites de l'aire toulonnaise (incluant la Petite Rade de Toulon très anthropisée et deux sites sur l'ile de Porquerolles) afin d'identifier l'influence des paramètres environnementaux sur *T. atomaria*. Cette étude multi-omiques a permis de révéler trois résultats majeurs de la thèse en montrant

(i) que la communauté épibactérienne est spécifique à *Taonia* par comparaison à celle de substrats inertes et des communautés planctoniques présentes à proximité. Cette spécificité est observée durant tout le suivi et long de l'étude, ainsi qu'une augmentation des densités et une diversification au cours du temps.

(ii) un effet spatial (**Figure VI.7**) : les fortes concentrations en cuivre **(A)** observées dans la Petite Rade de Toulon (en comparaison avec des sites moins impactés tels que ceux de l'île de Porquerolles), semblent impacter le métabolome de surface de l'algue via l'induction d'un stress oxydatif induisant la surexpression de fucoxanthine **(B)**]. Le cuivre et cette modification du métabolome pourraient expliquer par ailleurs la sélection de taxa épibactériens spécifiques **(C).**

(iii) un effet temporel (**Figure VI.7**) : l'augmentation de la température **(D)** apparait comme un facteur majeur, corrélé par exemple à l'augmentation des Rhodobacteraceae **(E)** et du DMSP exsudé **(F)**. Un tel résultat suggère que la température constitue un facteur essentiel impactant les interactions algue-microbiote, avec l'utilisation du DMSP comme source de carbone par les Rhodobacteraceae.

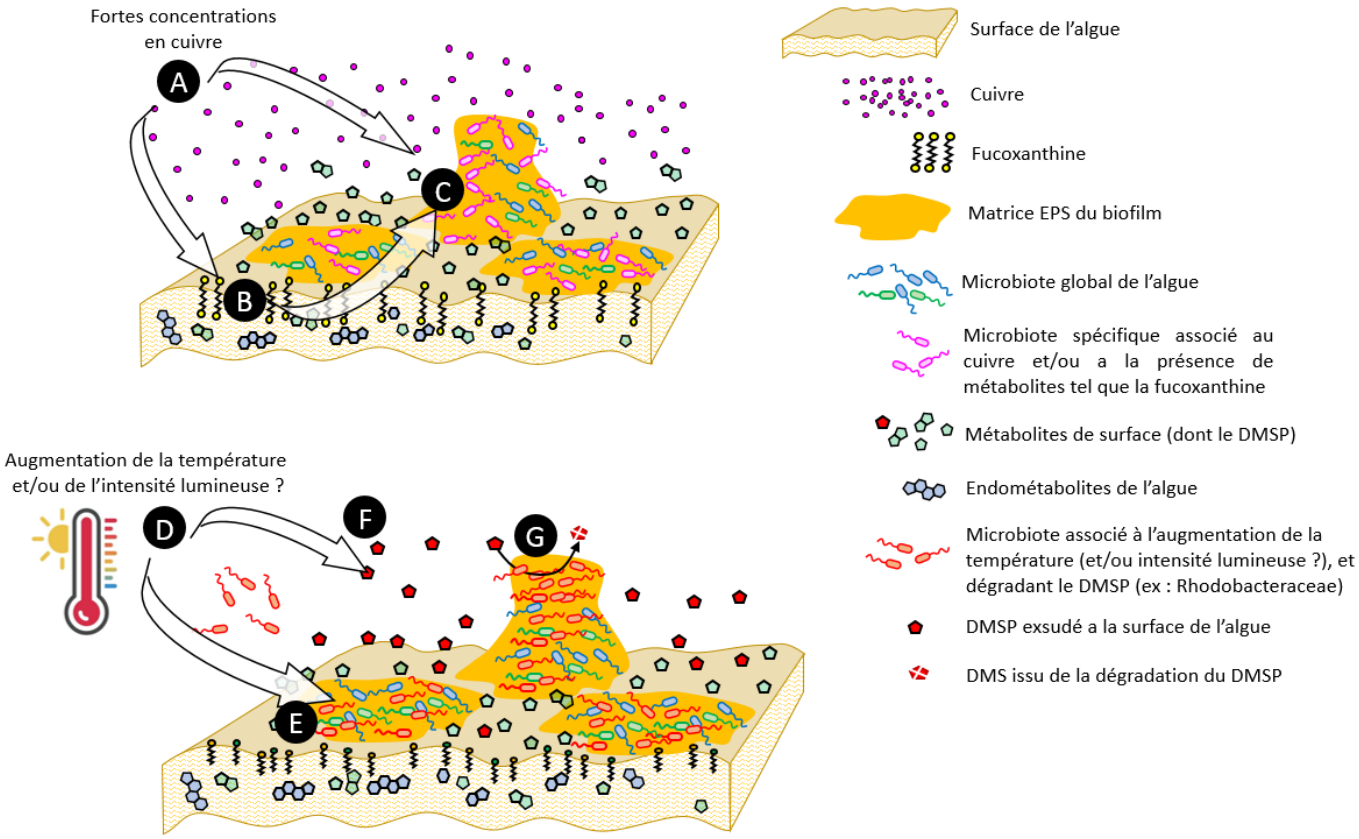

Figure VI.7. Schéma bilan expliquant les effets des deux principaux facteurs environnementaux observés dans le cadre de l'étude spatio-temporelle : la température et la concentration en cuivre

CHAPITRE VII : ETUDE EN MESOCOSMES

Vue de l'île de Batz depuis l'estacade de Roscoff

1. Avant-propos

Les résultats de l'étude préliminaire et du suivi spatio-temporel montrant une variation temporelle marquée au niveau du microbiote et du métabolome de surface de *T. atomaria*, la question de l'importance relative de la température et de l'intensité lumineuse, deux facteurs environnementaux qui co-varient en milieu naturel, a été abordée. Dans un contexte d'élévation globale des températures et d'intensification des épisodes météorologiques extrêmes tels que les vagues de chaleurs marines, il semble important de pouvoir dissocier l'impact respectif de ces deux facteurs.

Cette étude menée en mésocosmes en conditions contrôlées avec des spécimens de *T. atomaria* échantillonnées au nord de la Bretagne (Locquirec) vise à observer l'évolution de l'impact de changements de température et d'intensité lumineuse sur les variations du microbiote et du métabolome de surface de l'algue à court (24h) et moyens termes (jusqu'à 2 semaines). Cette étude est présentée sous la forme d'un article de recherche, en préparation en vue d'une soumission dans la revue *Environmental Microbiology*. Les références bibliographiques citées dans cet article sont indexées en fin de manuscrit. La partie *Supplementary Information* de cet article est presentée dans l'annexe VII du manuscrit (annexe électronique).

2. Article: Synergistic effects of temperature and light affect the relationship between *Taonia atomaria* and its epibacterial community: a mesocosm study

Benoit Paix[1], Philippe Potin[2], Christophe Le Poupon[3], Benjamin Misson[3], Catherine Leblanc[2], Gérald Culioli[1*] and Jean-François Briand[1*]

[1]*Université de Toulon, Laboratoire MAPIEM, EA 4323, Toulon, France*

[2]*Sorbonne Université, CNRS, Integrative Biology of Marine Models (LBI2M), UMR 8227, Station Biologique de Roscoff (SBR), Roscoff, France*

[3]*Université de Toulon, Aix Marseille Université, CNRS, IRD, Mediterranean Institute of Oceanography (MIO), UM110, France*

*corresponding authors : briand@univ-tln.fr, culioli@univ-tln.fr

2.1. Abstract

Marine macroalgae and their epiphytic microbiota displayed a large diversity of specific interactions which allow to consider them as holobiont systems. In a context of global warming and increasing marine heatwaves, this study aimed to assess the effect of combined conditions of temperature and irradiance on the macroalgal *Taonia atomaria* holobiont dynamics. We developed an experimental approach using mesocosm with three temperatures combined with three irradiances monitored at three sampling times (24h, 7 days and 14 days) with a multi-omics approach coupling algal surface metabolomics and metabarcoding. Both temperature and irradiance appeared to shape the microbiota and the surface metabolome of the holobiont, but with a distinct temporality. Epibacterial community structure firstly changed according to temperatures, and secondarily in relation to irradiance, while the opposite situation was found for the surface metabolome. The impact of an increased temperature revealed a decreasing richness of the epiphytic community together with an increase of several taxa such as *Sulfitobacter*, *Congregibacter* and *Parvularcula*. Irradiance changes appeared to impact surface metabolites production linked with the host photosynthesis (e.g. mannitol, fucoxanthin, DMSP) which was hypothesized to explain community structure modifications. Algal host may adapt directly its surface metabolome to changing temperature (e.g. lipids content) but also to changing microbiota (e.g. chemical defenses). Finally, this study brought new insights to consider seaweeds and their microbiota under changing environmental conditions, but also the reciprocal effect on each component of the holobiont system.

2.2. Introduction

As marine holobionts, macroalgae are known to establish intimate relationships with their epiphytic microbiota (Hollants et al., 2013). Notably, macroalgae are capable to control their epibacterial consortia through chemical defenses but also chemo-attracting compounds released at their surface (Harder et al., 2012; Wahl et al., 2012; Wichard et al., 2015). Such negative or positive chemical mediations play an important role for the host physiology and, for example, can be associated to immune or development processes (Wichard and Beemelmanns, 2018). As sessile organisms of intertidal zones, macroalgae are subject to many environmental changes often linked to anthropogenic stresses, such as global warming or marine coastal pollutions (Dittami et al., 2014; van der Loos et al., 2019). Concerns are notably raised to understand how climate changes will drive seaweed-bacteria interactions in the future (Campbell et al., 2011; Egan et al., 2014; Egan and Gardiner, 2016). As for other marine holobionts such as corals and sponges, temperature increase and seawater acidification are the most investigated factors for macroalgae in this context of global changes (van der Loos et al., 2019).

Among macroalgae, the bleaching disease of the Rhodophyta *Delisea pulchra* has been directly correlated to the temperature increase. This alga produces chemical defenses, identified as halogenated furanones, known to act as quorum sensing inhibitors and protecting the seaweed against bleaching disease (Maximilien et al., 1998; Harder et al., 2012). However, such defenses decrease in bleached algae in comparison to healthy ones in association to water temperature increases (Campbell et al., 2011; Case et al., 2011). In these specific conditions, several opportunistic bacteria (e.g. *Nautella italica* and *Phaeobacter* sp.) are observed at the algal surface and proposed to be involved in the bleaching phenomenon (Case et al., 2011; Fernandes et al., 2011; Campbell et al., 2014; Kumar et al., 2016). Even if temperature alone failed to explain the bleaching disease (Zozaya-Valdés et al., 2016), a global decrease of macroalgal health should be a plausible scenario to anticipate in the context of global warming (Egan et al., 2014).

In the last few years, the combined effect of the rise of temperature and seawater acidification on macroalgal physiology and surface microbiota has been increasingly studied through mesocosm experiments. While for the Chlorophyta *Caulerpa taxifolia* mitigating effects are observed (Roth-Schulze et al., 2018), future climate conditions influence the microbiota structure for the Ochrophyta *Eklonia radiata* (Qiu et al., 2019), *Macrocystis pyrifera* (Minich et al., 2018), *Fucus mytili* (Mensch et al., 2016) and the Rodophyta *Amphiroa gracilis* (Huggett et al., 2018). Moreover, the host physiology is also disturbed with blistered tissues and reduced photosynthetic efficency for *E. radiata*, bleaching disease for *A. gracilis*

and growth reduction for *C. taxifolia*, *M. pyrifera*, and *F. mytili*. In the case of the well-studied Ochrophyta *Fucus vesiculosus* (Saha et al., 2014), effect of both light and temperature has been investigated through the study of the surface concentrations of three metabolites [i.e. proline, dimethylsulfoniopropionate (DMSP) and fucoxanthin], known as bacterial settlement inhibitors, and the potential effect of their variations on the epibacterial community structure. To our knowledge, this is the only mesocosm study focusing simultaneously on surface microbiota and metabolites, knowing that chemical analyses have been limited specifically on these three compounds. The impact of both parameters appears relatively limited on these metabolites but variations of their surface concentrations could possibly shape the overall epibacterial community structure. For example, two major bacterial families (Rhodobacteraceae and Flavobacteriaceae) appear in higher percentages when DMSP concentration increases. However, as light and temperature have not been investigated together, this study has not allowed to decipher their combined effects.

Taonia atomaria (Woodward) J. Agardh is an annual photophilic marine Phaeophyta widely reported along the Mediterranean and the NE Atlantic coasts (Guiry and Guiry, 2020). This seaweed is known to produce at its surface several compounds displaying anti-adhesion activities (e.g. gleenol and geranylgeranylglycerol) (Othmani et al., 2016a) against a panel of marine bacteria. Such metabolites have been hypothesized to be part of the algal chemical defenses and involved in the selection of a specific epibacterial community. Furthermore, strong seasonal correlations occur, notably during spring and summer, between specific surface metabolites and some epibacterial taxa (Paix et al., 2019). The increase of temperature has been hypothesized as a key factor shaping the dynamics of such interactions. However, these *in situ* experiments have not allowed to unravel the respective significance of colinear factors such as temperature and light.

Here, a mesocosm approach was designed to decipher the respective and synergistic effects of temperature and irradiance on the interactions between *T. atomaria* and its epibacterial community. In this study, three different temperatures (13, 18 and 22°C) and three irradiance (20, 120 and 350 μmol.photons.m^{-2}.s^{-1}) were combined and the resulting data were subjected to an integrative multi-omics analysis. Untargeted LC-(+)-ESI-MS metabolomics, for the analysis of surface metabolites, was coupled to 16S rRNA gene metabarcoding and flow cytometry, for the analysis of epiphytic prokaryotes to investigate three different response times (one day, one and two weeks).

2.3. Materials and methods

2.3.1. Aquarium experimental device

The whole experimental device was set up at the "Roscoff Aquarium Services" structure (CRBM, Station Biologique de Roscoff, France) in a thermostated room at 16°C. The room had three shelves and each had three floors. Each floor gathered three replicate mesocosms (15L each), resulting in a total of 27 mesocosms (Fig. SVII.1 and SVII.2). They are supplied with pre-treated running seawater pumped from Roscoff coast [details in Supplementary information (SI)]. Each shelves system was supplied by the same independent semi-open water circuit. At first, the pre-treated seawater from Roscoff coast went through a 50L tank and was UV-treated with a Reeflex UV 800 system (Eheim, Deiziau, Germany). The water temperature within each tank was conditioned by TK500/TR10 chiller/heater systems (TECO refrigeration technologies, Ravenna, Italy). Seawater was then distributed to each mesocosm through a Compacton 2100 pump (Eheim, Deiziau, Germany). When arriving to mesocosms, the mean water flow was 36.5 $L.h^{-1}$ [Standard deviation (SD): ± 7.5]. Finally, the water from each mesocosm went back by overflowing to the first tank through a micron bag (100 μm; Red Sea, Düsseldorf, Germany). Two rows of 12V LED ribbons (Inovatlantic, Nantes, France) were set up on the top of each shelf, resulting in an irradiance of 120 $\mu mol.photons.m^{-2}.s^{-1}$ at the bottom of each mesocosm. This irradiance intensity corresponds approximatively to the mean *in situ* irradiance going up to 5m depth on NW French Atlantic coasts in summer (Martin et al., 2006). Each light system was set on a 16h:8h light:dark cycle during the whole experiment, which corresponds to the natural day:night cycle at that time.

2.3.2. Sampling and biological material

Approximatively 120 thalli of *Taonia atomaria* (Woodward) J. Agardh (Dictyotaceae, Phaeophyceae) were collected by scuba diving at Locquirec (The Channel, [48°41'39.9"N 3°41'50.7"W]) in July 2018 at low tide (2 to 4m depth). Thalli were stored in cool boxes filled with surrounding seawater and transported at lab within one hour after sampling.

Once at lab, only thalli with a length between 20 and 30 cm were kept to consider only individuals within the same development period. Furthermore, thalli showing evidence of macrofouling at their surface were not considered and ultimately a total of 87 thalli were kept. Among them, three thalli were considered as triplicates of field samples and directly used for cytometry, metabarcoding and metabolomics analyses.

2.3.3. Mesocosms experiment

The 84 remaining thalli were distributed in the 27 mesocosms as described in **Figure VII.1**. The whole study was conducted with triplicates of mesocosms for each condition. For each thallus, holdfasts were carefully attached to stainless steel screws in order to ballast the thallus at the bottom of the mesocosm. The seawater temperature and the irradiance intensity in all aquaria were set to field conditions at 18°C (SD: ± 0.2) and 120 μmol photons.m^{-2}.s^{-1} (SD: ± 10.5), respectively, and used for an acclimation period of one week. At the end of the acclimation period (t_0), three replicates were sampled (t_0 samples, **Figure VII.1**) and analyzed. After this sampling, all the mesocosms contained three thalli and the conditioning period was started with 9 distinct conditions: three temperature coupled with three irradiances. The three chiller/heater systems from each shelve were set to 13°C (SD: ± 0.6), kept to 18°C (SD: ± 0.2) or set to 22°C (SD: ± 0.5). These "low", "ambient" and "high" temperature conditions were named LT, AT and HT, respectively. The change of temperature was progressively done during 3h. For each floor, the irradiance of (i) bottom floors was set to 20 μmol.photons.m^{-2}.s^{-1} (SD: ± 0.75) by adding a solar film (F339-2000 , d-c Fix®), (ii) mid floors was kept to 120 μmol.photons.m^{-2}.s^{-1} (SD: ± 10.5), (iii) top floors was set to 350 μmol.photons.m^{-2}.s^{-1} (SD: ± 10.6) by turning on two supplementary LED ribbons. These "low", "ambient" and "high" irradiances conditions were named LI, AI and HI, respectively.

One day after, one thallus per mesocosm was chosen haphazardly and sampled, consisting in 27 t_1 samples (9 cross-conditions in triplicates, **Figure VII.1**). One and two weeks after t_0, two other samplings were performed in the same way with 27 t_2 and 27 t_3 samples, respectively (**Figure VII.1**).

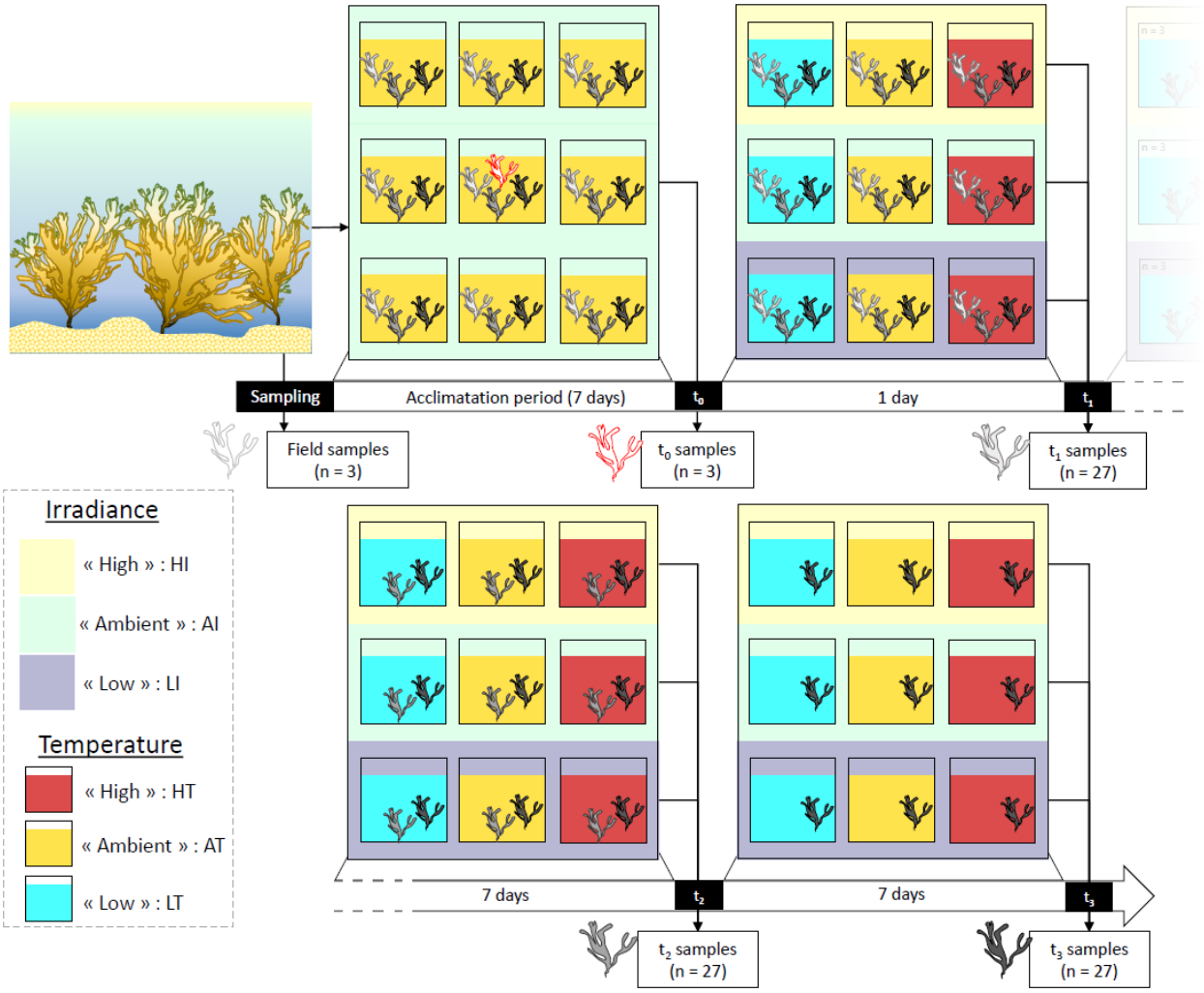

Figure VII.1. Experimental design of the study. Each square representing an aquarium in this workflow, actually correspond to a triplicate of aquaria.

2.3.4. *Physicochemical parameters measurements*

Temperature, irradiance, pH, salinity and O_2 were monitored daily in each mesocosm (details in SI). Concentrations of nitrates (NO_3^-), orthophosphates (PO_4^{3-}), silicates ($Si[OH]_4$) were determined at each sampling time (details in SI). Measurement methods were done as described in Briand et al., 2017.

2.3.5. *Physiological assessment*

Before extraction procedures, the maximum quantum yield (F_v/F_m) of photosynthetic energy conversion of the photosystem II (PSII) of each sample was measured using a pulse-amplitude modulated chlorophyll fluorometer (JUNIOR-PAM teaching Chlorophyll Flurorometer, Walz, Germany). A frond of each replicate was kept 2 min in the dark and three measures were done by placing directly the optic fiber

along three areas chosen haphazardly on the frond. Furthermore, a particular attention was paid during the whole experiment to identify any visual evidence of thallus deteriorations such as bleaching or other types of tissue degradation.

2.3.6. Flow cytometry analyses

Flow cytometry (FCM) analyses were used to assess the densities of heterotrophic prokaryotes at the surface of the algal samples. Epiphytic cells were collected by scraping the surface with a sterile scalpel fixed in 4 mL of 1% glutaraldehyde filtered seawater solution and conserved at -80°C. Aggregated cells were dissociated with an optimized sonication time of 2 min, stained using SYBR green I (Invitrogen, Carlsbad, CA, USA) and enumerated using a BD Accuri C6 flow cytometer (BD Biosciences, San Jose, CA, USA) as previously described (Paix et al., 2020). Results were expressed as densities of cells (cells.cm^{-2}) using the measured surface area of each sample.

2.3.7. 16S rRNA gene metabarcoding analyses

Epiphytic cells were collected by scraping the surface with a sterile scalpel. DNA extraction was performed using the DNeasy PowerBiofilm kit (MoBio, Qiagen, Germantown, MD, USA) and samples were conserved at -80°C (Paix et al., 2019, 2020).

The NOCHL primers were previously designed specifically to minimize the contamination from plastid 16S rRNA gene (Thomas et al., 2020). At first, they were tested in this study to estimate their efficiency to avoid amplification of chloroplastic 16S rRNA gene and compared to the 515F-Y/926R primers sets (Parada et al., 2016). Both primers were tested on triplicates of t_0 and t_1 (AT/AI) samples. The treatment of sequences for these analyses with both primers pairs was performed as described below.

Following these analyses, 16S rRNA genes of all samples were amplified using the NOCHL primers. Amplicons were sent to Eurofins Genomics (Ebersberg, Germany) for MiSeq Illumina sequencing (2×300 bp). 16S rRNA gene reads were processed using the FROGS workflow under the Galaxy environment (Escudié et al., 2018). Clustering step for generating operational taxonomic units (OTUs) was performed using SWARM with a clustering aggregation distance set to 3 (Mahé et al., 2014). Chimeric sequences were *de novo* removed using VSEARCH (Rognes et al., 2016). OTUs representing less than 0.005% of all the sequences were removed. OTUs were affiliated with the silva132 16S rRNA gene database. The final matrix was obtained by performing a rarefaction to the minimum library size (21 642 reads) using the “phyloseq” R package (McMurdie and Holmes, 2013).

α-diversity was estimated using Chao1 and Shannon indexes. β-diversity was analyzed with a non-metric multidimensional scaling (NMDS) using weighted UniFrac distances allowing to consider phylogenetic relationships between OTUs. These analyses were performed using the "phyloseq" R package and graphical outputs were generated using the "ggplot2" R package.

A Venn diagram was constructed to reveal percentages of OTUs and sequences shared between the samples collected at different sampling times. An OTU was considered as common to all the sampling times when it was found a least in one replicate of each sampling time. The Venn diagram was calculated with the Venn webtool (http://bioinformatics.psb.ugent.be/webtools/Venn/). LEfSe analyses were conducted to reveal discriminant taxa whether specific to a sampling time (from field to t_3 samples) or a particular mesocosm cross-condition ($n = 9$). LEfSe analyses were performed under the Galaxy environment with a LDA threshold set to 3.4. A focus on specific comparisons was made with SIMPER analyses to reveal the main contributing genera involved in the dissimilarity between field and t_0 samples. SIMPER analyses were conducted with the "vegan" R package with *p* values calculated through 999 permutations.

2.3.8. UHPLC metabolomics analyses

Extraction of surface metabolites and sample preparation were performed as described in Paix et al., 2019, and detailed in SI. Surface extracts were analyzed using a UHPLC-ESI-HRMS system (Dionex Ultimate 3000 rapid Separation; Thermo Fisher Scientific) equipped with an analytical core-shell reversed phase column (150 × 2.1 mm, 1.7 μm, Kinetex Phenyl-Hexyl; Phenomenex, Le Pecq, France) and coupled with an ESI-QToF Impact II mass spectrometer (Bruker Daltonics, Bremen, Germany) using a positive ionization mode (more details are given in SI).

Raw UPLC-MS data were converted into netCDF files using DataAnalysis software (v. 4.3; Bruker, Germany) and processed for peak finding, integration and alignment using MzMine 2 (version 2.53, Pluskal et al., 2010; details in SI). Data were filtered according to Favre et al., 2017, by taking into account signal/noise ratio, coefficient of variation and coefficient of correlation. The resulting data matrix (101 features) was $\log_{10}$-transformed, mean-centered, normalized using the sum of the chromatographic peak areas according to Paix et al., 2020. The data matrix was then analyzed using principal component analysis (PCA) and partial least-square discriminant analysis to determine the chemical biomarkers of a specific condition of temperature and irradiance.

The global annotation was performed as described in Paix et al., 2019, 2020. A particular attention was paid on compounds with a Variable Importance in Projection (VIP) score above 0.6. Thus, among the 101 features of the data matrix, the 30 first VIPs were annotated. In brief, annotation was assessed by comparison of MS/MS spectra with those of our in-house database (purified compounds and commercial standards listed in SI), and public databases such as MetLin, MoNA or Lipidmaps. To confirm the annotation, elucidation of the MS/MS fragmentation pathway was performed and when possible compared to the literature (details in SI).

2.3.9. Statistical tests

ANOVA tests were conducted to assess the significance of PAM measures, metabolites, densities, and taxa according to each experimental condition (time, irradiance and temperature). ANOVA test were followed by pairwise multiple comparison tests. Tukey's post-hoc tests were performed for PAM measures, discriminant metabolites, densities and α-diversity metrics. Duncan test with Benjamini-Hochberg method for *p*-value correction was performed as a multiple testing method to evaluate differences between groups for discriminant taxa. Following NMDS and PCA, overall differences between conditions were statistically tested with PERMANOVA and followed by a multivariate pairwise test. All these analyses were conducted on R with "ade4", "agricolae", "vegan" and "RVAideMemoire" packages. PLS-DA were subjected to cross validations using MetaboAnalyst 4.0 (https://www.metaboanalyst.ca).

2.4. Results

2.4.1. Physicochemical parameters

Several physicochemical parameters observed in mesocosm conditions showed low variability during the whole study, such as salinity, pH, O_2, and $[Si(OH)_4]$ with mean values of 35.8 ppt (SD: ± 0.2 ppt), 8.1 (SD: ± 0.05), 90% (SD: ± 1.4%), and 1.93 μM (SD: ± 0.28 μM), respectively (Table SVII.1). However, some parameters showed higher variability, such as $[NO_3^-]$ and $[PO_4^{3-}]$ with mean values of 1.27 μM (SD: ±0.58 μM) and 0.209 μM (SD: ±0.097 μM), respectively. $[NO_3^-]$ and $[PO_4^{3-}]$ appeared to increase significantly with time according to ANOVA ($p < 0.001$ and $p = 0.03$, respectively) and Tukey's tests, with higher values for $[NO_3^-]$ at t_3 compared to t_1 and t_2, and for $[PO_4^{3-}]$ at t_3 compared to t_1 (Table SVII.1). Moreover, only $[Si(OH)_4]$ exhibited differences between natural and mesocosm seawater, with means values from field to mesocosms decreasing by a 3-fold factor (Table SVII.1).

2.4.2. Physiological assessment

The maximum quantum yield of photosynthetic energy conversion (F_v/F_m) measured for all samples showed mean values of 0.71 (SD: ± 0.1, Fig. SVII.3). A three-way ANOVA test did not allow to observe any significant change whatever the condition (sampling time, temperature or irradiance) (*p*-values > 0.05 and F-values < 1.5). Moreover, no visible evidence of thallus deterioration (e.g. bleaching or fragmentation) was observed throughout the time of the experiment.

2.4.3. Flow cytometry analyses

Abundances of heteroprokaryotic cells at the surface of *T. atomaria* were estimated through flow cytometry and revealed densities ranging from 1.2×10^5 to 1.8×10^7 cells.cm^{-2} (Fig. SVII.4). When comparing samples over time, a significant increase was observed from field to t_2 and t_3 samples (Table SVII.2, Fig. SVII.4). However, no significant differences in cell densities have been observed between the different irradiance and temperature conditions (Table SVII.2).

2.4.4. Comparison of NOCHL and 515F-Y/926R primers

Chloroplast 16S rRNA gene sequences represented up to 46% of the sequences (mean : 31.4%, SD: ±12.6 %) when using the 515F-Y/926R primer set. Among the 7 842 700 16S rRNA gene reads obtained with the NOCHL primers, none have been affiliated to chloroplasts or Cyanobacteria whatever the replicate. After removing sequences affiliated to the chloroplast 16S rRNA gene from the OTU-table constructed with samples amplified with the 515F-Y/926R primer set, the community structures at the order level were compared for the six samples tested (Fig. SVII.5). Despite Verrucomicrobiae, Planctomycetacia and Cyanobacteria were less or not amplified with NOCHL primers, their percentage remained also low with 515F-926R primers (mean percentage for NOCHL *vs* 515F-926R primers: 0 *vs* 0.012 ; <0.001 *vs* 0.012 ; 0 *vs* 0.06) and a high correlation was observed between the two community structures at the order level [Mantel test (with 999 permutations) : $p = 0.001$, $r = 0.8$].

2.4.5. Epibacterial community diversity

A global increase of the Shannon index was observed with time (Fig. SVII.6). More precisely, field, t_0 and t_1 samples exhibited a significantly lower α-diversity in comparison with t_2 and t_3 samples. Moreover, at t_3 and for AI, Shannon index showed significant lower values for samples at HT (Fig. SVII.6, Table SVII.2).

Chao1 values for field samples were significantly lower than those of all the mesocosm samples (Fig. SVII.6, Table SVII.2). At t_3, whatever the irradiance condition, Chao1 showed significant lower values for HT samples compared to those at AT. At AI and HI, HT samples showed also lower values than those of LT

samples (Fig. SVII.6, Table SVII.2). A Venn diagram (Fig. SVII.7) revealed that the percentage of OTUs and sequences shared between all samples (field and mesocosm samples) reached 53.8 and 88.7%, respectively. The percentages of OTUs and sequences common to only mesocosm samples (t_0, t_1, t_2 and t_3) corresponded to 20 and 8.3%, respectively.

Considering the β-diversity, the first axis of the weighted-Unifrac based NMDS revealed a global shift from field to mesocosm samples (**Figure VII.2A**).

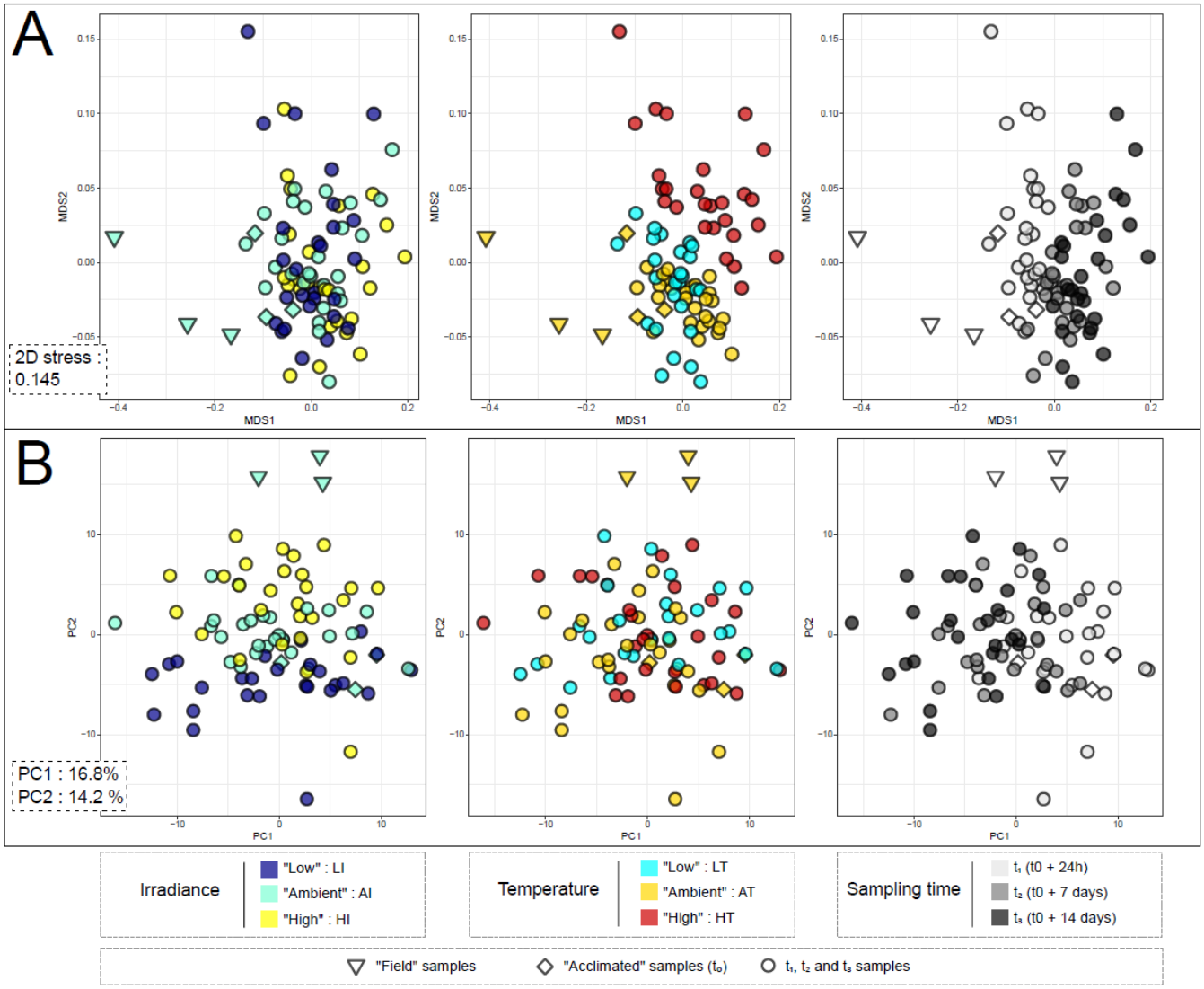

Figure VII.2. Multivariate analyses of surface microbiota and surface metabolomes including all samples of *T. atomaria*. (A) weighted UniFrac based NMDS plots showing β-diversity differences of epibacterial communities. (B) PCA score plots showing differences of surface metabolomes.

Moreover, a shift of the prokaryotic community was observed on the same axis from t_1 to t_3 samples. Three-factor PERMANOVA results validated and specified significant differences within each factor (time, temperature and irradiance) taken independently (Table SVII.3). A multivariate pairwise test showed that field, t_1, t_2 and t_3 samples appeared significantly different from each other except that t_0 samples were not differentiated from field and t_1 ones (Table SVII.4). In the case of temperature, the three conditions (LT, AT and HT) appeared significantly distinct from each other. For irradiance, HI samples were significantly differentiated from AI and LI ones, while no differences were observed between the two latter groups. When considering t_1, t_2, or t_3 samples independently **Figure VII.3**), the resulting NMDS plots showed separated clusters for each temperature (PERMANOVA and pairwise tests, Tables SVII.3 and SVII.4). However, no significant differences were observed within the three irradiance for t_1 or t_2 samples (Table SVII.4). Finally, t_3 samples were discriminated according to irradiance as HI and LI samples were significantly different (Table SVII.3 and SVII.4).

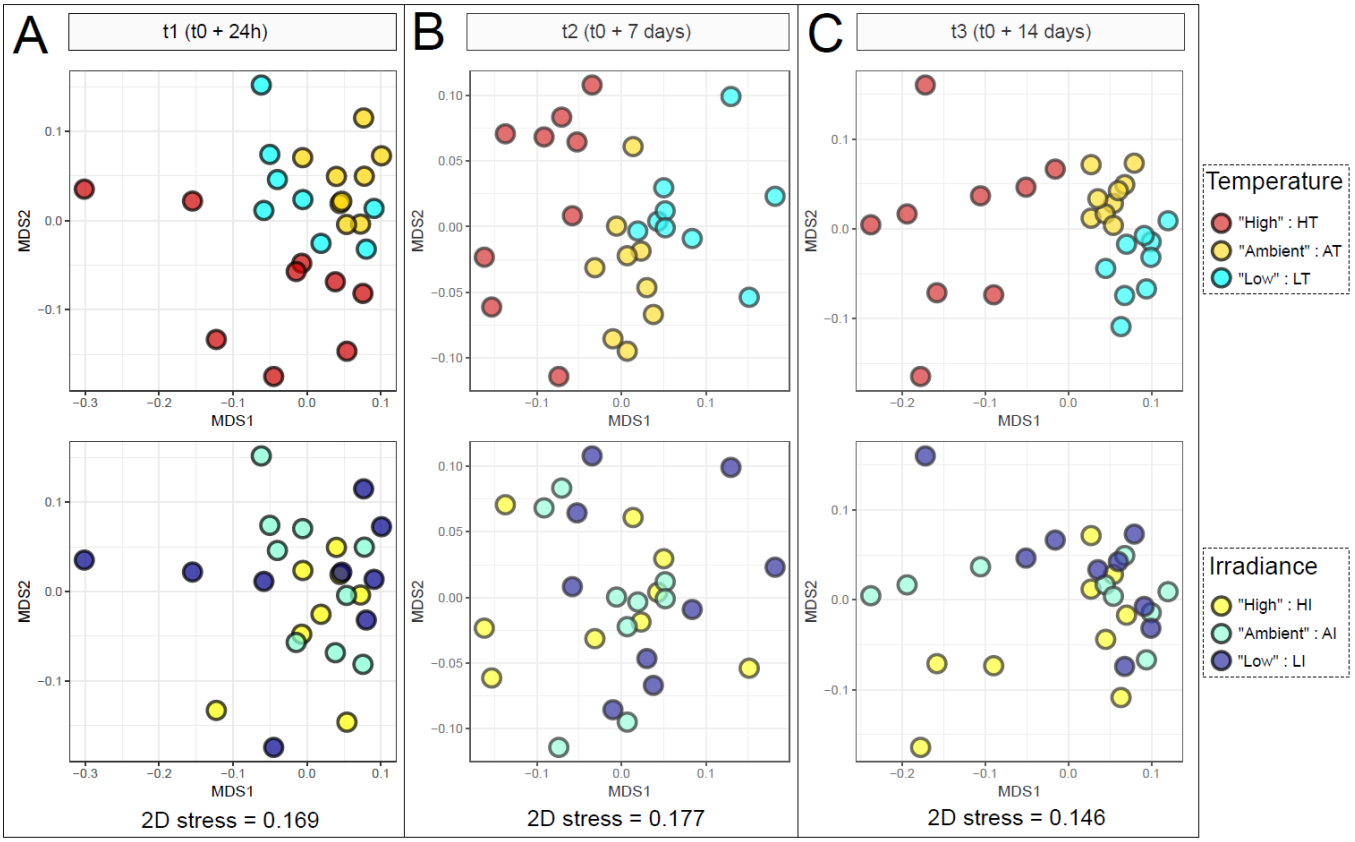

Figure VII.3. Weighted UniFrac based NMDS plots showing differences of β-diversity of epibacterial communities of *T. atomaria* samples collected at a specific sampling time: (A) t_1, (B) t_2, and (C) t_3.

Considering the taxa affiliation of the epibacterial community, differences between field and mesocosm samples were observed at the family level, (Fig. SVII.8). In field samples, the main families observed were

Hyphomonadaceae (Alphaproteobacteria), Alteromonadaceae, Thiohalorbdaceae (Gammaproteobacteria) and Saprospiraceae (Bacteroidetes) representing 21, 15, 15 and 14 % of the community, respectively. Hyphomonadaceae appeared as a biomarker taxon of field samples (LDA > 4, Table SVII.5). Thioharlobdaceae and Hyphomonadaceae were mainly represented by the genera *Granulosicoccus* and *Litorimonas* contributing up to 8 and 6% to the dissimilarity between field and t_0 samples, respectively (Table SVII.6).

In contrast, the community structure of mesocosm samples was mainly characterized by the occurrence of Alteromonadaceae and Rhodobacteraceae with relative percentages ranging from 9 to 61% and 9 to 44%, respectively (Fig. SVII.8). The Alteromonadaceae family appeared mainly represented by the genera *Alteromonas* and *Paraglaciecola* which were biomarkers of t_0 samples (Table SVII.5) and contributed to 13 and 3% of the overall dissimilarity between field and t_0 samples, respectively (Tables SVII.6).

From t_0 to t_3, and whatever the temperature/irradiance conditions, a clear decrease of Alteromonadaceae and an increase of Spongiibacteraceae, Rhizobiaceae (mainly represented by the genus *Lentilitoribacter*) and Cellvibrionaceae was noticed (Fig. SVII.8). These three latter families appeared as biomarker taxa of t_3 samples (LDA > 4, Table SVII.5).

A focus was made on t_3 samples since they gathered the highest number of biomarker taxa of a specific irradiance/temperature condition for a same LDA threshold (LDA > 3.4) (Table SVII.7 ; **Figure VII.4** ; Fig. SVII.9). Overall, biomarker taxa mostly differed according to the temperature. The genus *Oleiphilus* occurred mainly among LT samples whatever the irradiance, and appears as an example of taxa displaying a similar trend for t_1 and t_2 samples. Several other genera showed a similar tendency under particular conditions of irradiance, such as *Kordia* at AI and *Neptuniibacter* at LI. In contrast, some genera occurred mainly in samples at HT, such as *Sulfitobacter*, *Congregibacter* and *Parvularcula* at AI, *Hirschia* at LI, *Congregibacter* and *Parvularcula* at HI. Moreover, some genera also differed according to the irradiance conditions, such as *Kordia* at LT which occurred mainly at AI compared to LI and HI. At HT, *Lentilitoribacter* and *Parvularcula* were found in significant higher percentages at HI compared to LI. A similar tendency was observed for samples subjected to AT for the genus *Jannaschia*.

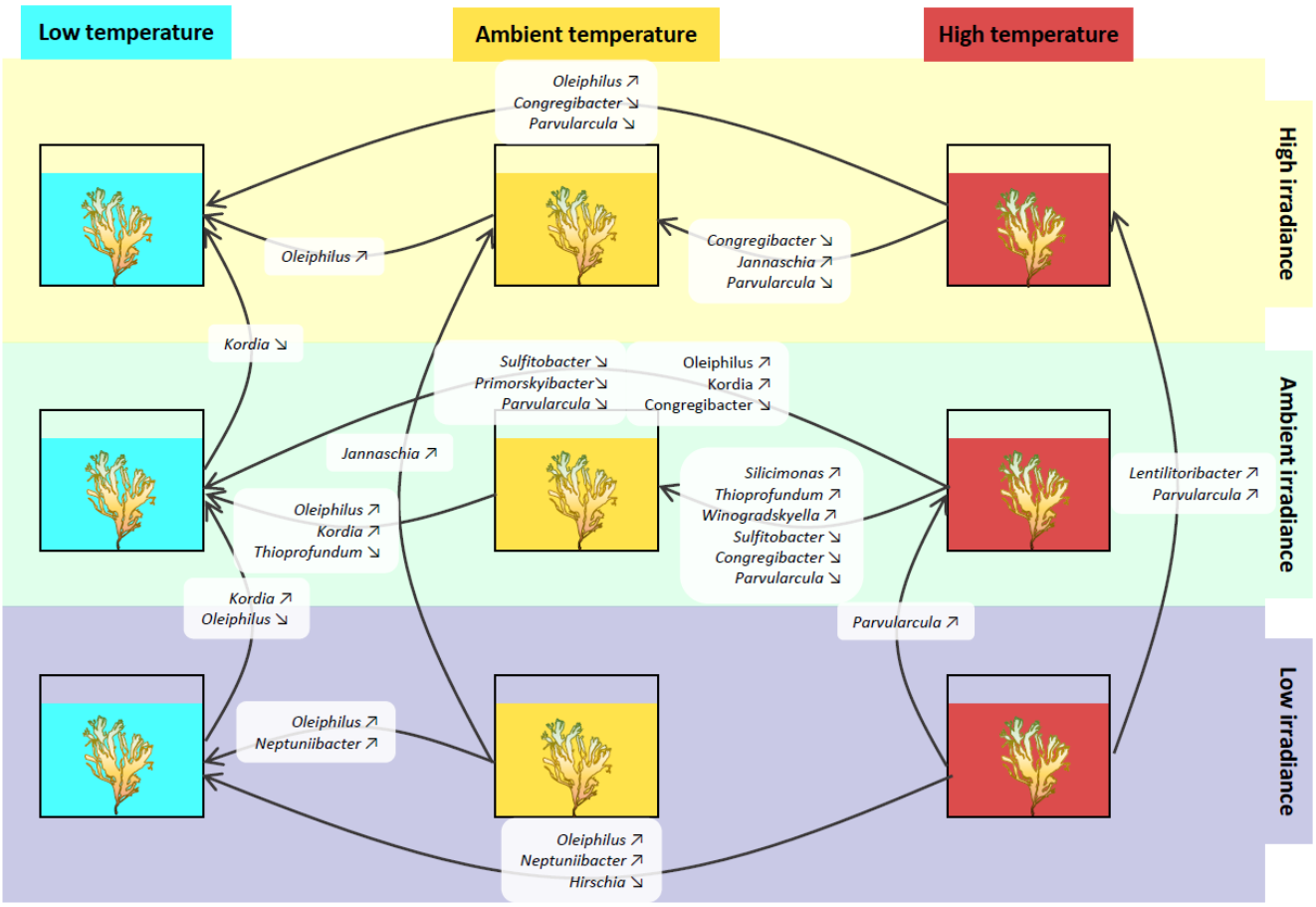

Figure VII.4. Summary of significant variations of discriminant bacterial genera at the surface of *T. atomaria* samples collected at t_3 according to cross-conditions of temperature and irradiance. An arrow between two aquaria indicates a significant difference of relative abundance of a biomarker genus (Duncan's test and Benjamini-Hochberg *p*-value adjustment) between two conditions. ↗ and ↘ symbols after a genus name indicate whether a significant increase or decrease is respectively observed from the condition where the arrow starts to the condition where the arrow ends.

2.4.6. Surface metabolome fingerprinting and VIP variations

Including all the samples, the main differences of surface metabolome profiles appeared on the second component of the PCA plot between field and mesocosm samples (**Figure VII.2B**). Moreover, a global shift of the surface metabolomes was observed on the first component from t_1 to t_3. Finally, a discrimination was also observed on the second component of the PCA between HI and LI samples. The PERMANOVA test conducted with the three experimental factors (time, temperature, and irradiance) validated and specified significant differences within each factor, but also a significant interactive effect of the three factors (Table SVII.8). The multivariate pairwise analysis revealed at first that all sampling times were significantly different from each other except t_3 samples with field, t_0 and t_2 samples on one hand, and t_1 samples with t_0 samples on the other hand (Table SVII.9). When comparing the three groups of samples obtained with

different irradiance, all of them were significantly different from each other, while for temperature conditions, HT samples were significantly discriminated from AT and LT samples on the basis of their surface metabolome.

The PCA plot obtained only with the t_1 samples did not reveal any clear differences between the temperature/irradiance conditions (**Figure VII.5A**). However, multivariate tests showed that LI and HI samples were statistically different (Table SVII.9). In the case of t_2 samples, the resulting PCA plot (**Figure VII.5B**) allowed to discriminate, on the first component, HT samples from the two other temperature conditions on the first component. On the second component, a discrimination was also observed between LI and HI samples. More precisely, these findings were confirmed by PERMANOVA tests and pairwise comparisons which showed significant differences between HT samples and those at the two other temperatures on one hand, and between LI samples and those obtained at the two other irradiances on the other hand (Table SVII.8 and SVII.9). Finally, the corresponding PCA plot (**Figure VII.5C**) for t_3 samples showed a discrimination between HI and LI samples on one hand, and between HT and LT samples on the other hand. In term of pairwise comparisons, samples were significantly different between each temperature (Tables SVII.9). LI samples appeared also significantly different from samples obtained at the two other irradiance (Table SVII.9).

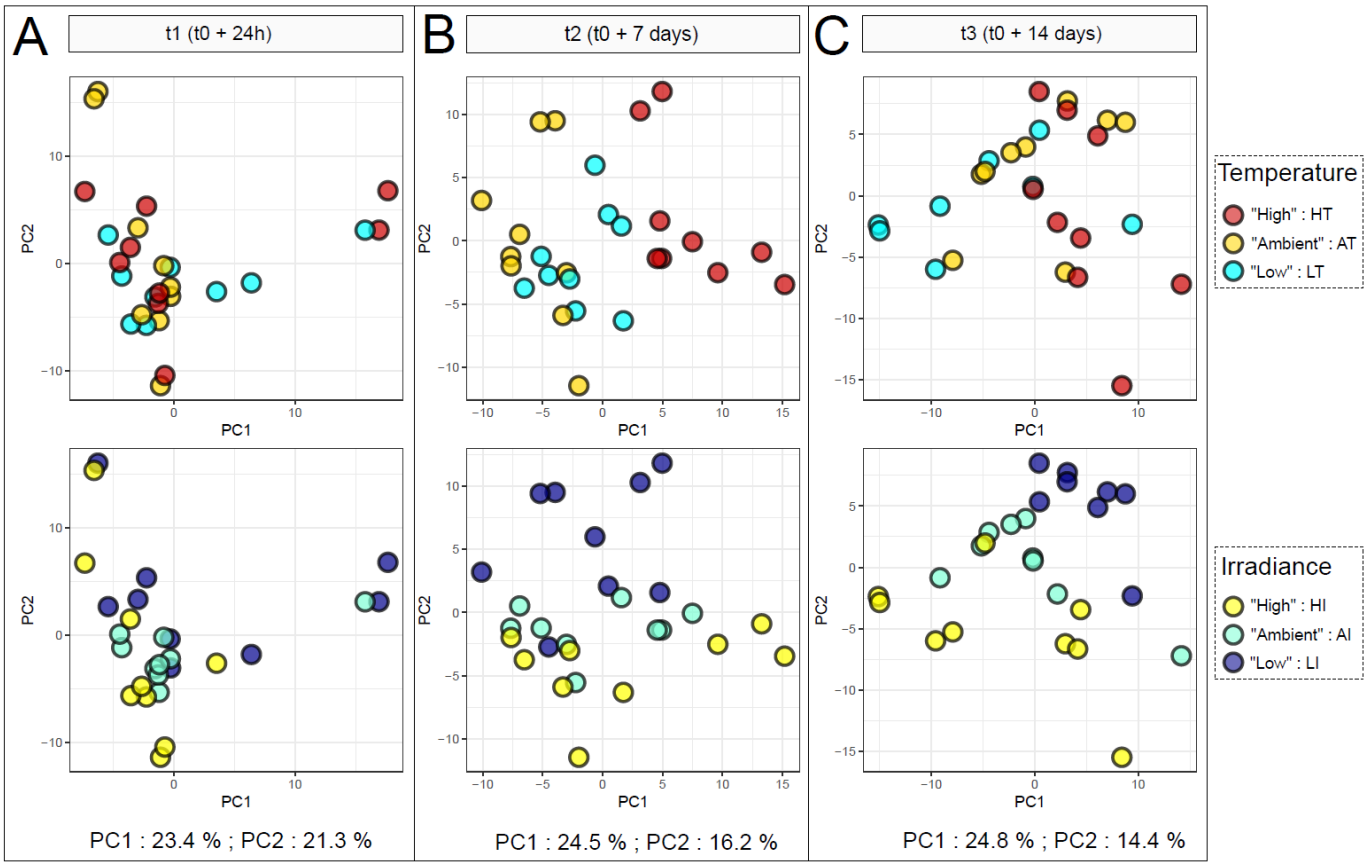

Figure VII.5. PCA score plots showing differences of surface metabolomes of *T. atomaria* depending on the sampling time: (A) t_1 samples, (B) t_2 samples, and (C) t_3 samples.

When comparing field and t_0 samples, the most discriminant compounds identified were fucoxanthin (VIP score: 1.87) and phenylalanine (VIP score: 1.85). These two compounds were more produced in t_0 samples compared to field samples (Fig. SVII.10) with a fold change of 7.0 and 6.2, respectively.

Subsequently, a focus was made on the variations of a panel of annotated surface compounds (**Figure VII.6**; Fig. SVII.10; Table SVII.10) discriminately expressed in t_3 samples according to each condition (VIP score > 0.6), since this sampling time offered the largest number of significant and discriminant variations. Such variations were not systematically observed in samples collected at previous sampling times (Fig. SVII.10).

At LT, DMSP, mannitol, several diacylglycerylhydroxymethyl-*N*,*N*,*N*-trimethyl-*β*-alanine (DGTAs) [such as DGTA (C42:11), DGTA (C40:8), DGTA (C36:4) and DGTA (C36:9)] and a diacylglycerol [DG (C36:9)] were found in higher concentrations in HI samples compared to those at LI. Moreover, mannitol and DGTA (C36:4) were also more produced in AI compared to LI, while DGTA (C42:11) and DG (C36:9) were found in higher concentrations at HI rather than AI. At AT, mannitol was found in higher amounts at AI and HI

rather than at LI and gleenol was also found in higher concentrations in AI rather than at LI. A quite opposite tendency was observed for fucoxanthin which appeared in higher amounts in samples at LI compared to those obtained at HI. At HT, fucoxanthin, tryptophan and an unknown sesquiterpene with the molecular formula $C_{15}H_{18}O_2$ were produced in lower concentrations in samples at LI rather than those at HI while the opposite tendency was observed for mannitol.

At LI, DGTA (C36:4), gleenol and phenylalanine were more produced in HT samples rather than those at LT. At AI, proline betaine and DG (C36:9) were found in higher concentrations in LT samples compared to HT ones. DG (C36:9) was also more produced in samples at LT compared to those obtained AT. Gleenol was found in higher concentrations in AT samples compared to those at HT. At HI, DGTA (C42:11) and DGTA (C36:0) were produced in higher concentrations in LT samples compared to AT and HT samples.

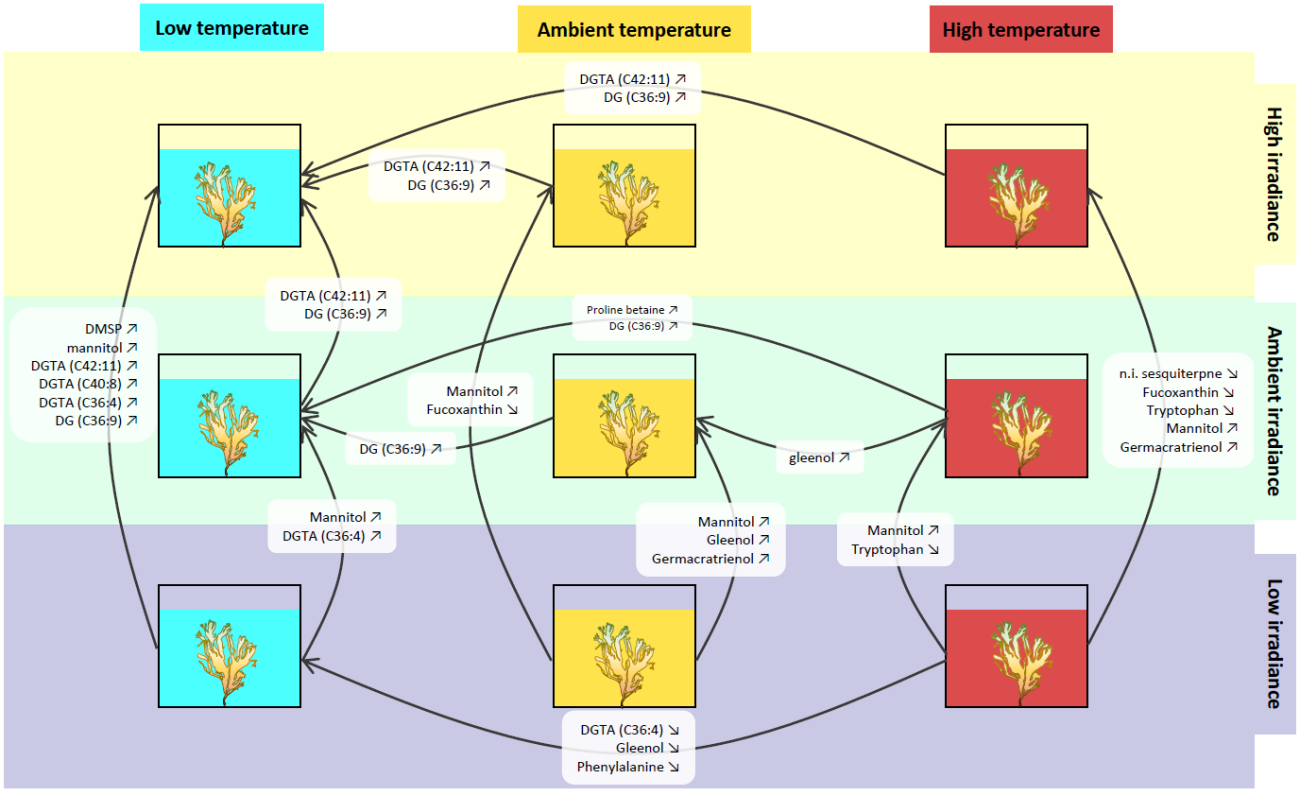

Figure VII.6. Summary of significant variations of discriminant surface metabolites of *T. atomaria* according to cross-conditions of temperature and irradiance at t_3. An arrow between two aquaria indicates a significant difference of the normalized concentrations of a chemical biomarker (ANOVA and Tukey's tests) between two conditions. ↗ and ↘ symbols after a compound name indicate whether a significant increase and decrease is respectively observed, from the condition where the arrow starts to the condition where the arrow ends.

2.5. Discussion

In a general context of global change, the impact of environmental factors on the surface microbiota of marine holobionts is still poorly studied through mesocosm-based approaches and the combination with the surface host's metabolome characterization remains rare. In the case of *T. atomaria*, the concurrent temporal increase of temperature and irradiance has been hypothesized to play a key role in controlling seaweed-microbiota interactions (Paix et al., 2019, Paix et al., *in prep.*). The aim of this study was to decorrelate these two factors to understand their specific and synergistic effects on the host-surface microbiota interactions.

Through this study, we also aimed to confirm the efficiency of NOCHL primers to avoid plastidal 16S rDNA gene amplification. Their amplification lead to a decrease of the sequencing depth for prokaryotic 16S rDNA sequences which can constitute an issue to investigate the diversity of prokaryotic communities associated to plants or algae. We compared this set of primers with 515F-Y/926R primers which previously lead up to 36% of chloroplast 16S rRNA gene sequences (Paix et al., 2020). We confirmed the results from Thomas et al., 2020, since the efficiency of NOCHL primers was clearly observed with no sequences affiliated to chloroplasts.

2.5.1. Effect of mesocosm conditioning on the holobiont system

Heteroprokaryotic densities and richness of the epiphytic community appeared higher for mesocosm samples compared to field ones, together with a distinct β-diversity. Besides, a relative high percentage of OTUs (20%) were specific to mesocosm samples. However, these OTUs represented a lower proportion in term of sequences (8.3%). Two plausible scenario could explain the presence of such epibionts at the surface of mesocosm samples despite they had not been observed within field samples. Firstly, these OTUs could be rare taxa in field samples, removed with the 0.005% filtering process of the FROGS pipeline or with the rarefaction of the OTU-table. These taxa may benefit from the algal conditioning and become more abundant at the algal surface in aquaria. Another source could be the pre-filtration process of the running seawater. Once pretreated, the running coastal seawater provided to the aquarium device was filtered (with ultimately 1 to 3 μm filters) and then sterilized using UV radiations. However, despite these filtrations steps, some exogenous colonizers might come from the planktonic community from the coastal sea, or also from biofilms on the surfaces of the experimental devices (e.g. tubes or filters). The effect of mesocosm conditioning on the surface microbiota was already investigated for the Rhodophyta *Delisea pulchra* and a similar scenario was also proposed by the authors (Zozaya-Valdés et al., 2016). 15 days after the transfer of *D. pulchra* from field to aquaria, a change of microbiota structure was observed with specific

enriched OTUs. The main ones were affiliated to Kordiimonadales (mainly the genus *Kordiimonas*), Alteromonadales (mainly the genus *Glaciecola*) and Cytophagales. In our study, the main taxa promoted after one week of acclimation also belonged to Alteromonadales with the genera *Alteromonas* and *Paraglaciecola*. Several strains belonging to these two genera have been previously described for their ability to degrade seaweed polysaccharides (Akagawa-Matsushita et al., 1992; Schultz-Johansen et al., 2016; Bech et al., 2017). Moreover, the genus *Alteromonas* was already identified as increasing during mesocosm experiments (Schäfer et al., 2000). *Alteromonas macleodii* in particular is well known as a r-strategist, taking quickly advantage of nutrient-enriched environments (Zemb et al., 2010; Romera-Castillo et al., 2011; Tada et al., 2011; Lawes et al., 2016). Despite we used a metabolomics approach which did not allowed to investigate algal polysaccharides, we hypothesized that a shift of the global chemical composition at the algal surface (e.g. an increase of polysaccharides biosynthesis) after the conditioning might constitute a selective advantage for *Alteromonas* and *Paraglaciecola* spp., which could metabolize such a carbon source and quickly grow at the surface of *T. atomaria*.

In contrast, two other genera of the Alteromonadales, *Litorimonas* and *Granulosicoccus* spp. significantly decreased when algal samples were transferred in mesocosms. These two genera have been already described at the surface of *T. atomaria* as specific, core and pioneer taxa and are known to quickly decrease over time on Mediterranean sites (Paix et al., 2019, 2020, Paix et al., *in prep.*). Even if environmental conditions from the sampling site of this study clearly differ from those of the Mediterranean ones, we suggested that these taxa could be sensitive to environmental changes. Among changes mediated by the conditioning from field to mesocosms, a decrease of hydrodynamics or predation pressure might also constitute important factors to consider.

For the surface metabolome, several metabolites were differentially produced after the transfer of *T. atomaria* from field to aquaria. For example, phenylalanine and fucoxanthin were observed with higher concentrations after the transfer in mesocosms while field samples were characterized by a higher expression of DGTAs. As hypothesized for polysaccharides, such chemical variations at the algal surface might also be considered as potential factors shaping differences of epibacterial composition.

2.5.2. Short-term responses of algal surface microbiota and metabolome

Through multivariate analyses conducted with t_1 samples, the short-term responses (24h) of the surface microbiota and metabolome were found to clearly differ. On one hand, short-term differences of prokaryotic β-diversity only appeared with the change of temperature. More particularly, the *Oleiphilus* genus was a major discriminant taxon which differs after t_1, with higher percentages at LT compared to AT

and HT. Conversely, the absence of a direct effect of irradiance on the global structure of the bacterial community at t_1 can be explained since the community composition was not characterized by major phototrophic taxa. The NOCHL primers did not allow to amplify sequences of 16S rRNA gene from Cyanobacteria (Thomas et al., 2020). However, Cyanobacteria sequences constituted less than 0.1% of the overall community for samples tested (t_0 and t_1) with the 515F-Y/926R primers. Moreover, the main aerobic anoxygenic phototrophs (AAP) identified in the data set were *Roseobacter*, *Erythrobacter* and *Jannaschia*, but these genera represented less than 0.01% of all sequences and did not vary significantly according to irradiance conditions in t_1 samples.

On the other hand, short term differences between surface metabolomes were observed only when the irradiance conditions varied. The highest irradiance rapidly induced an increase of the production of mannitol at the algal surface. This polyol is a photosynthetic product which constitutes the main form of energy storage for brown algae (Lehvo et al., 2001; Rousvoal et al., 2011; Weinberger et al., 2011) and a similar observation has previously been made for *F. vesiculosus* (Saha et al., 2014).

Interestingly, these results indicated that the short term response of the two components of the holobiont system are not susceptible to the same factor. Consequently, we hypothesized that adaptation of the algal host and its surface microbiota would be firstly inherent to their respective physiological specificities, and that reciprocal interactions at the holobiont scale could only occur later.

2.5.3. Effect of irradiance on surface microbiota: an indirect long-term effect mediated by the algal host?

After one week of conditioning, no effect of irradiance was observed on the microbiota structure. However, such differences appeared after two weeks between samples exposed to HI and LI, and this even more in the case of HT. The genera *Lentilitoribacter*, *Parvularcula* (at HT), and *Jannaschia* (at AT) constituted taxa which seemed to be especially adapted to higher irradiance. *Pelagimonas* and *Kordia* were genera especially adapted to AI conditions in the case of HT and LT, respectively. The case of *Jannaschia* is interesting since one species is known to produce the bacteriochlorophyll *a* pigment and is described as AAP (Yoon et al., 2010; Pujalte et al., 2014). Higher irradiances could have constituted a beneficial condition thanks to its phototrophic metabolism, and the delayed response is consistent with clear effects of light observed on natural AAP communities in the long terms (Koblížek, 2015). As no evidence of phototrophic metabolism was observed for *Parvularcula*, *Pelagimonas* and *Kordia*, irradiance could then constitute an indirect factor explaining the selection of these taxa. Moreover, it was clearly established that surface metabolome was directly impacted by the irradiance changes during the whole

experiment. Consequently, several surface algal metabolites differentially expressed according to light intensity could be considered as potential factors shaping microbiota light-dependent differences with time.

After two weeks, mannitol, fucoxanthin and DMSP were the main metabolites involved in the surface metabolome changes in connection with irradiance conditions. As already observed after one day, mannitol remained discriminant but with increasing concentrations in the case of HI, which may still result from a higher algal photosynthetic activity. Mannitol constitutes a preferential source of carbon for a large bacterial diversity but it is also a compatible solute known to play a role in osmoprotection (Kets et al., 1996; Sand et al., 2013; Zahid et al., 2015). Mannitol catabolism has been notably investigated through a genomic approach with *Zobellia galactanivorans*, a Flavobacteriia closely associated to several macroalgae (Barbeyron et al., 2001; Groisillier et al., 2015). The operon associated to mannitol assimilation for this bacterial strain has been identified and also found in other genomes among Flavobacteriaceae (Groisillier et al., 2015). Interestingly, this bacteria has the ability to degrade various algal polysaccharides such as alginate and fucans of Ochrophyta, or agars and carrageenans of Rhodophyta (Thomas et al., 2012, 2013; Barbeyron et al., 2016). In addition to mannitol, algal polysaccharides could also constitute an important source of carbon for epiphytic bacteria particularly adapted to macroalgal niches (Gobet et al., 2018). Consequently, such primary or secondary products of the algal photosynthesis could then be considered as key factors involved in the shaping of epibacterial communities, especially in the case of changing irradiance. An interesting perspective would be to investigate the polysaccharide production of *T. atomaria*, notably under distinct irradiance and to focus on microbial functions associated with the degradation of such biopolymers.

For fucoxanthin, a higher expression was observed in the case of a LI. Increasing amounts of this carotenoid have been observed with depth or shade increase in other macroalgae such as *F. vesiculosus*, *Ascophyllum nodosum*, *Udotea petiolate*, and *Dictyota dichotoma*. These data illustrating the adaptation of the photosynthetic performances of seaweeds with a lower quantity and quality of light (Ramus et al., 1977; Perez-Bermudez et al., 1981). Here, we suggested that a similar shade-light adaptation occurred in *T. atomaria* to compensate the irradiance decrease. Through culture dependent approaches, fucoxanthin was also found to display inhibiting activities against bacterial adhesion (Viano et al., 2009; Saha et al., 2011). However, the selective effect of fucoxanthin on the epibacterial community structure of macroalgae is always a matter of discussion (Lachnit et al., 2010; Saha et al., 2011; Egan et al., 2013). In Saha et al., 2014, correlations between fucoxanthin and several bacterial taxa were investigated and

several “fucoxanthin-positive” and “-negative” taxa have been determined. The Flavobacteriaceae family was notably found positively correlated to fucoxanthin suggesting that members of this family could be attracted by this compound. Here, no clear correlation was observed between Flavobacteriaceae and fucoxanthin (linear regression: $R^2 < 0.2$). Through *in vitro* and *in vivo* field experimental approaches, the anti-adhesion activity of fucoxanthin and of potential unidentified compounds of a non-polar fraction of the surface extracts of *F. vesiculosus*, has been previously supported. However, fucoxanthin has not been found to impact the community structure of *F. vesiculosus* and cautions have been raised to avoid any premature causality links (Lachnit et al., 2013). A low selective range of activity may be important to consider (Egan et al., 2013) and further investigations still need to be conducted to clearly understand the effect of fucoxanthin on macroalgal epibacterial communities under ecological relevant conditions.

In a previous work on Mediterranean samples of *T. atomaria*, DMSP was found to increase at the algal surface from February to July and such a variation was hypothesized to be correlated with the temporal increase of temperature and/or irradiance (Paix et al., 2019). In the present study, DMSP increased significantly with the irradiance intensity in the case of LT conditions. The DMSP concentrations of total extracts have been previously investigated under different light conditions in other seaweeds, such as *Ulothrix implexa, Ulothrix subflaccida, Enteromorpha bulbosa*, *Acrosiphonia arcta*, *Ulva rigida*, *Blidingia minima* (Karsten et al., 1990, 1992)*, Ulva lactuca* (Van Alstyne and Puglisi, 2007), *Codium fragile* (Lyons et al., 2010) and *F. vesiculosus* (Saha et al., 2014). In accordance with our results, Karsten et al., 1990, 1992 and Lyons et al., 2010, have found in their respective algal models that DMSP concentrations were higher with increasing irradiance. Taken together, these results may strengthen the hypothesis of a light-dependent DMSP biosynthesis, especially in the case of low temperature (Karsten et al., 1992). Moreover, DMSP is also produced by many microalgae, including dinoflagellates and diatoms (Bullock et al., 2017), and the potential origin of DMSP at the surface of *T. atomaria* could also be linked to such epiphytes that we identify on several Dictyotaceae including *T. atomaria* (Ternon et al., 2020). Besides, DMSP constitutes a source of carbon and sulfur for a large diversity of bacteria, especially those from the *Roseobacter* clade (Howard et al., 2008; Curson et al., 2011; Dogs et al., 2017). DMSP is also known as a chemo-attracting compound released at the surface of *Ulva mutabilis* which allows the gardening and mutualistic interactions with *Roseovarius* sp. (Wichard et al., 2015; Kessler et al., 2018). At the surface of *T. atomaria*, several discriminant taxa such as *Sulfitobacter* and *Jannaschia*, specific to a condition of temperature and irradiance at t_3, have been already described for their DMSP catabolic activity (Mou et al., 2005; Curson et al., 2008; Howard et al., 2008). More precisely, an interactive effect of temperature and irradiance was observed for the genus *Jannaschia*, with an optimum abundance under HI and AT conditions as mentioned

above. Then the higher DMSP production induced by a higher irradiance could also positively affect the growth and development of members of this genus at the surface of *T. atomaria*.

2.5.4. Effect of temperature on the holobiont dynamics in a context of global warming and marine heatwaves

The increase of seawater temperature was predicted to potentially affect macroalgae health at a global scale (Egan and Gardiner, 2016; Bindoff et al., 2019; van der Loos et al., 2019). Here, the HT condition with an increase of +4°C from ambient temperature corresponded to predictions made for 2081-2100 with the RCP 8.5 model (Collins et al., 2013). This increase constitutes also a representative scenario of a marine heatwaves in a near future, since temperature could also drastically increase during a limited time. Global climatic change is likely to increase the intensity, frequency and duration of marine heatwaves, which constitute major risks for marine biodiversity, notably for seaweeds (Meehl and Tebaldi, 2004; Perkins et al., 2012; Wernberg et al., 2016; Frölicher et al., 2018; Oliver et al., 2018; Collins et al., 2019; Smale et al., 2019).

At the holobiont scale, temperature appears to be implied in microbial shifts for a large number of seaweeds in mesocosm studies, such as *D. pulchra* from the Tasman sea (Zozaya-Valdés et al., 2016), *Neogoniolithon fosliei* from the Coral sea (Webster et al., 2011), *Macrocystis pyrifera* from NE Pacific coasts (Minich et al., 2018), *Amphiroa gracilis* from the SE Indian ocean (Huggett et al., 2018), *Fucus mytili* from the North sea (Mensch et al., 2016) and *F. vesiculosus* from the Baltic sea (Stratil et al., 2013). Concerns are notably raised since lower health conditions and chemical defenses caused by increasing temperature can result to a microbiota dysbiosis (Egan et al., 2014; Egan and Gardiner, 2016; Minich et al., 2018). More precisely, the development of opportunistic pathogens could be promoted through the activation of virulence factors (Case et al., 2011; Fernandes et al., 2011; Gardiner et al., 2017).

Among epiphytic bacteria which are known to be favored by an increase of seawater temperature, the Rhodobacteraceae family is particularly represented (Case et al., 2011; Fernandes et al., 2011; Stratil et al., 2013; Saha et al., 2014; Qiu et al., 2019). In the case of *D. pulchra*, pathogens from the Roseobacter group have been particularly observed, especially for bleached algae under high temperature conditions (Case et al., 2011; Zozaya-Valdés et al., 2015, 2016). However, pathogens of *D. pulchra* are not specifically restricted to this family (Kumar et al., 2016). In the present study, Rhodobacteraceae family appeared to be the main family increasing with the temperature, with notably the genus *Sulfitobacter*. Attention was also paid on the variation of several taxa from this family known as potential pathogens, such as *Nautella*, *Phaeobacter* and *Aquimarina* (Fernandes et al., 2011; Kumar et al., 2016). The contribution of these

potential pathogens to the overall microbiota shift in response to an increase of temperature was not significant. Moreover, no clear disease event (bleaching, blistered or disrupted tissues) was observed on thalli of *T. atomaria* during the whole study and the photosynthetic activity assessed with the maximum quantum yield of PSII (F_v/F_m) did not change significantly.

However, a lower α-diversity, especially in terms of richness, was observed when temperature increases under AI and HI conditions. In the case of human holobiont, a decrease of α-diversity constitutes a biomarker of a potential dysbiosis (Pitlik and Koren, 2017). For marine holobionts, including seaweeds, a high diversity is often considered to be essential for the stability and the resilience of the holobiont system under changing conditions (Loreau et al., 2001; Moore, 2005; Longford et al., 2019). Consequently, even if no clear pathogens were identified at the surface of *T. atomaria*, a decreasing richness under higher temperatures may indicate a lower fitness of the holobiont.

A global shift of the β-diversity of the surface microbiota of *T. atomaria* was observed after one day under high temperature while modifications of the surface metabolome were only observed after one week. The fact that temperature may directly modify the microbiota community structure and induce a later adaptive response of the algal metabolome to regulate its epibiosis could constitute an explanation of this observation. In Othmani et al., 2016, the anti-adhesion activity of several sesquiterpenes found at the surface of *T. atomaria* has been investigated against several bacterial strains isolated from marine biofilms. Gleenol, a spiroaxane sesquiterpene, showed strong anti-adhesion activities at relevant natural concentrations. This compound has been proposed to play an important role on the chemical selection of a specific microbial community at the surface of *T. atomaria* (Othmani et al., 2016a). In the present study, the amounts of gleenol at the algal surface appeared to reach their maximal level at HT/LI and AT/AI conditions for t_3 samples. The differential production of this metabolite could possibly constitute a host adaptation to limit quantitatively and/or qualitatively the dynamics of the microbiota composition induced by the change of temperature.

Changes of the surface metabolome of *T. atomaria* linked to temperature variations could also be attributed directly to physiological processes inherent to the algal host. Among other metabolites which differ significantly according to temperature conditions, several polyunsaturated membrane lipids were identified, including diacylglycerols (DGs) and DGTAs. These lipids were mainly expressed in the case of LT. Here, we hypothesized that thalli of *T. atomaria* exposed to HT express less polyunsaturated lipids in order to decrease the fluidity of its membrane. Such changes in membrane lipid composition for seaweeds has been already described as a means to maintain an optimal membrane fluidity under changing temperature

conditions (Eggert, 2012). Besides, this process is also well known in the case of microalgae (Sato and Murata, 1980, 1982; Schüler et al., 2017). This adaptation to temperature change could thus play a crucial role to maintain the integrity of several membrane process, including enzymatic mechanisms such as the induction of heat-shock genes during the membrane rigidification of *Synechocystis* (Inaba et al., 2003; Los and Murata, 2004; Eggert, 2012).

Thus, the impact of algal adaptation to heat-stress and microbiota changes has to be considered in a context of global warming, and even more in the case of increasing and intensifying marine heatwave events. To our knowledge, marine heatwaves have been experimentally studied only once on seaweeds together with their epibacterial community with the model *F. vesiculosus* (Saha et al., 2020a). Despite the study did not focus on the epibacterial diversity, a decrease of density was observed after the first heatwave while a recovery to the initial densities was observed after the third heatwave suggesting a potential mechanism of resilience to such repeated events.

In this study, we investigated the dynamics of the response of the holobiont system several times after changing the temperature/irradiance conditions. However, under a scenario of marine heatwave, an interesting perspective would be also to investigate the resilience of the seaweed holobiont system after the thermal stress with a progressive return to control conditions. While the resilience of corals is increasingly studied in the light of the holobiont concept, only few studies addressed such investigations for seaweed holobionts (Bourne et al., 2016; Cavalcanti et al., 2018; Longford et al., 2019; Saha et al., 2020a).

2.6. Conclusion

To our knowledge, this is the first multi-omics study on a seaweed holobiont investigating both surface metabolome and microbiota responses to experimentally controlled environmental conditions. Through a mesocosm-based approach, we showed that the seaweed-holobiont dynamics of the Ochrophyta *T. atomaria* is shaped by both temperature and irradiance. The response to temperature changes appeared to be faster for the microbiota than for the metabolome at the surface of the alga. On the contrary, irradiance changes may impact firstly the algal surface metabolome and, only then, its associated microbiota. We suggested that indirect effects could occur only after few days of conditioning. Algal metabolome variations resulting from a differential photosynthetic activity induced by a shift of irradiance could be a factor shaping thereafter the epiphytic microbiota. Several metabolites, such as mannitol, fucoxanthin and DMSP, known to play important roles on seaweed-microbiota interactions could be implied. Overall, bacterial richness appeared lower in the case of higher temperature with the selection of several specific taxa (notably from the Rhodobacteraceae family), which may indicate a decrease in the algal fitness.

2.7. Acknowledgments

This work was supported by the “Sud Provence-Alpes-Côte d’Azur” regional council (B.P. PhD grant). This work was also funded by the EMBRC-FRANCE project “EMPREINTES” supported by the Roscoff Marine Station, the CNRS and Sorbonne University. We are grateful to G. Schires for his help during the construction of the whole experimental device, to N. Carriot (MAPIEM, University of Toulon, France) for his help with annotation of the metabolomics data set, to S. Greff (IMBE, Aix-Marseille University, France), to N. Layglon for chemical analyses of seawater, to C. Leroux and E. Bourrigaux (Roscoff Marine Station, Sorbonne university, France) for their technical supports. We acknowledge F. Thomas and A. Gobet for sharing their useful work on the NOCHL primers.

3. Bilan du chapitre

Dans le cadre du changement global observé au niveau des océans, les effets respectifs et combinés de changements de la température et de l'intensité lumineuse ont été étudiés sur des thalles de *T. atomaria* prélevés sur la côte nord de la Bretagne par une approche en mésocosmes. L'étude a permis de révéler que ces deux facteurs impactent à la fois le métabolome et le microbiote de surface (**Figure VII.7**). Cependant les réponses de ces deux composantes ne sont pas simultanées puisqu'à court terme (24h) l'intensité lumineuse influence d'abord le métabolome (via l'activité photosynthétique) **(A)**, alors que le microbiote semble être d'abord impacté par la température **(B)**. Après deux semaines, la température apparait comme un facteur impactant le métabolome, soit directement **(C)** via un effet sur le lipidome, avec par exemple la modification de la proportion de lipides fortement insaturés (pouvant modifier la fluidité membranaire à la surface), soit indirectement **(D)** en réponse à la modification préalable de la composition du microbiote. Enfin, à plus long terme, l'intensité lumineuse semble être impliquée dans les différences de β-diversité. De manière réciproque, la modification du microbiote par l'intensité lumineuse peut s'expliquer directement **(E)** via un effet sur certaines bactéries photohétérotrophes (ex : *Jannaschia*), ou encore indirectement **(F)** via l'effet d'une modification préalable du métabolome, avec des différences d'expressions de composés connus pour être impliqués dans les interactions algue-microbiote tels que la fucoxanthine ou le DMSP.

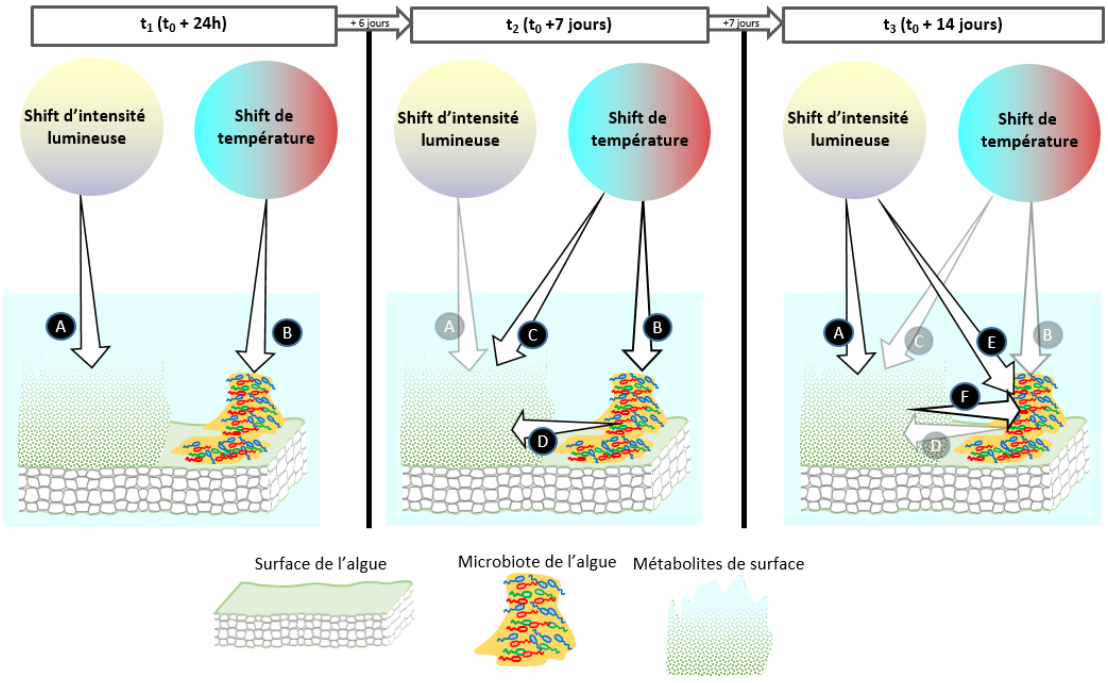

Figure VII.7. Schéma bilan expliquant les effets de changements d'intensité lumineuse et de température, et les cinétiques associées, sur le microbiote et métabolome de surface

CHAPITRE VIII : DISCUSSION GENERALE

Vue sur la ville de Roscoff, depuis son estacade

1. Rappels sur les objectifs de la thèse

Les interactions étroites entre les macroalgues et leurs bactéries épiphytes associées justifient de considérer ces systèmes biologiques en tant qu'holobiontes soulignant ainsi l'importance de rassembler ces deux ensembles au sein d'une analyse conjointe. Cette thèse s'inscrit dans le cadre d'une telle vision intégrative en proposant non seulement d'étudier les variations du microbiote et du métabolome à la surface des macroalgues-holobiontes du genre *Taonia* mais également l'impact de paramètres environnementaux sur de potentielles interactions réciproques. L'approche générale qui a été développée s'est principalement basée sur une analyse multi-omiques couplant notamment la métabolomique pour l'étude des molécules présentes à la surface de l'hôte algal et le metabarcoding pour l'étude des communautés épibactériennes.

La première étude (**chapitre II**) menée dans le cadre de cette thèse correspond à une analyse préliminaire dont l'objectif était de caractériser le microbiote et le métabolome de surface de *Taonia atomaria* sur un site de la Rade de Toulon (Carqueiranne) où elle était abondante. Nous souhaitions notamment mettre en évidence d'éventuelles variations temporelles et commencer à étudier les interactions potentielles entre le microbiote et l'algue via son métabolome. De cette étude a résulté un certain nombre de questionnements écologiques et méthodologiques :

a) Il s'avérait tout d'abord important d'évaluer l'existence de possibles différences phylogénétiques au sein d'échantillons de *Taonia* récoltés sur une large aire géographique, ainsi que l'effet de ces différences phylogénétiques sur la variabilité du métabolome et du microbiote de surface (**chapitre III**). Cette étude permettait enfin de déterminer l'influence de la zone géographique, et donc des paramètres climatiques généraux associés, sur cet holobionte algal. Cette étude financée par l'appel à projets EC2CO 2019 a été réalisée en partenariat avec le laboratoire de Biologie Intégrative des Modèles Marins de la Station Biologique de Roscoff (C. Leblanc, P. Potin) et le laboratoire de Phycologie de Gand en Belgique (O. De Clerck, C. Vieira).

b) Par ailleurs, d'un point de vue méthodologique, l'annotation des métabolites s'est révélée constituer une étape cruciale lors des analyses métabolomiques. Un second objectif a donc été d'initier et d'optimiser des méthodes analytiques destinées à l'élaboration d'une base de données permettant une annotation rapide des métabolites d'intérêt pour les études ultérieures (**chapitre IV**).

c) Un autre questionnement a consisté à prendre en compte, au niveau de l'hôte algal, l'échelle de l'individu afin de déterminer l'existence potentielle et les causes d'une différenciation le long du thalle (de la partie basale à la zone apicale) du métabolome et du microbiote de surface (**chapitre V**).

d) A la suite de ces premiers travaux, un objectif majeur de la thèse a permis, grâce à un suivi spatio-temporel durant un an de cinq sites de la Rade de Toulon et du Parc National de Port-Cros, de mieux appréhender l'effet des paramètres environnementaux majeurs impliquées dans les interactions à l'échelle de l'holobionte (**chapitre VI**). Un objectif complémentaire a été également de déterminer la spécificité du microbiote algal par rapport aux communautés présentes dans l'eau de mer environnante et au niveau de substrats abiotiques (roches) prélevés sur les mêmes sites.

e) Finalement, à partir de l'étude *in situ* précédente, des travaux portant sur l'influence potentielle de la température et de l'intensité lumineuse sur le métabolome et le microbiote de surface de *T. atomaria* ont été mis en œuvre dans le cadre d'un projet financé par EMBRC France en partenariat avec la station biologique de Roscoff (C. Leblanc, P. Potin). L'effet de ces deux paramètres a donc été étudié en conditions contrôlées par une approche expérimentale en mésocosmes (**chapitre VII**).

2. Bilan des approches utilisées

2.1. L'annotation du métabolome

L'étape d'annotation constitue très souvent un verrou méthodologique en métabolomique. Ce challenge est d'autant plus important dans le cadre de l'étude d'organismes non-modèles, et particulièrement d'organismes marins pour lesquels une grande part de la diversité chimique reste encore inexplorée (Blunt et al., 2007; Carroll et al., 2019). Afin de pouvoir interpréter au mieux les données obtenues par métabolomique dans l'ensemble des travaux menés sur *T. atomaria*, le **chapitre IV** s'est focalisée sur cette étape cruciale d'annotation. Afin d'initier une base de données permettant de référencer les principales informations expérimentales (masse moléculaire, formule brute, temps de rétention, données MS/MS) et d'annoter les différents composés observés dans les extraits, une première approche a consisté à purifier les métabolites majoritaires d'un extrait brut de *T. atomaria*. Cette étape de purification dite « approche phytochimique » a permis notamment de caractériser par spectroscopies (RMN 1D et 2D, SM…) la structure chimique de 12 composés, dont 8 avaient déjà été décrits lors de précédentes études menées au laboratoire (Viano et al., 2009; Othmani et al., 2016a, 2016b). Ces composés purs ont alors pu être utilisés en tant que standards chimiques ; leur analyse

chromatographique (LC-MS et GC-MS) permettant ainsi de déterminer leurs données expérimentales (temps de rétention, spectre de masse…) dans les conditions choisies pour l'étude ultérieure des extraits de *T. atomaria*. Parmi ces composés, le gleenol et le géranylgéranylglycérol (GGG) ont été retrouvés de manière récurrente dans le cadre des études métabolomiques réalisées par la suite sur *T. atomaria*. Cependant, une limite majeure associée à cette approche est de ne pouvoir identifier que des métabolites isolés en quantités suffisantes pour leur analyse structurale ultérieure par RMN. Ainsi, de manière globale, seuls les principaux composés majoritaires dans les extraits de *T. atomaria* ont pu être identifiés via cette approche phytochimique qui laisse ainsi un grand nombre de métabolites, détectés par la suite par des techniques sensibles de profilage telles que la LC-MS, encore non caractérisés de façon catégorique.

Depuis quelques années, une nouvelle approche d'annotation par réseaux moléculaires utilisant les données LC-MS/MS permet d'identifier rapidement, et sans purification, des métabolites qui montrent des spectres de masse similaires et présentent donc des structures chimiques potentiellement proches (Wang et al., 2016). Au cours de cette thèse, la construction de réseaux moléculaires via la plateforme GNPS s'est avéré être un outil précieux. Cette méthodologie a effectivement permis de faciliter l'annotation du métabolome de *T. atomaria,* notamment en utilisant comme points de référence des métabolites (appelés nœuds initiaux ou « *seeds* ») identifiés soit lors de l'approche phytochimique, soit via l'obtention de « *hit*s » dans des bases de données publiques. Ainsi, cette méthode a permis d'annoter un grand nombre de métabolites présentant une forte similarité spectrale avec ces nœuds initiaux mais elle a également conduit à identifier des molécules rassemblées dans des groupes communs (« *clusters* ») grâce à la mise en évidence de d'ions fragments ou de pertes de masse spécifiques. Cela a notamment été le cas de métabolites appartenant à des familles de lipides, telles que les DGTAs, les PCs ou les DGCCs, qui montrent des fragmentations caractéristiques en spectrométrie de masse (Maciel et al., 2016; da Costa et al., 2019).

Cependant, l'optimisation de certains paramètres s'est avérée nécessaire lors de la mise en œuvre des réseaux moléculaires afin, par exemple, d'identifier les seuils permettant de regrouper les membres des différentes familles de lipides au sein d'un même cluster qui leur serait spécifique. Les principaux paramètres impliqués dans les étapes de comparaison des spectres ont fait l'objet de différents tests présentés dans le **chapitre IV**. Parmi ces paramètres, trois sont cruciaux pour la structuration du réseau en fonction des seuils choisis :

- Le score de similarité (« *Cosine Score* » ou CS) entre deux spectres MS/MS (variant de 0, absence de similarité entre les spectres, à 1, spectres identiques).

- Le nombre minimum de fragments communs aux deux spectres MS/MS comparés.

Si les valeurs obtenues pour ces deux paramètres lors de la comparaison entre deux spectres MS/MS sont supérieures aux seuils fixés alors les conditions sont réunies pour créer un lien entre les deux nœuds correspondants dans le réseau moléculaire.

- Le nombre maximal de nœuds voisins pour un nœud donné.

À la suite des différents tests effectués, le choix du CS s'avère particulièrement important pour permettre le regroupement de chaque famille chimique au sein d'un même cluster, avec notamment une valeur seuil supérieure à 0,7.

En plus de la construction d'un réseau moléculaire dans le cadre du **chapitre IV** qui s'est focalisée sur l'annotation et la construction d'une base de données, des réseaux moléculaires ont par la suite été utilisés lors des **chapitres II**, **V**, **VI** et de l'étude présentée en **annexe I** avec des échantillons spécifiques. Au sein des réseaux moléculaires construits en utilisant les données MS/MS obtenues à partir des extraits de surface de *T. atomaria*, les métabolites qui composent les clusters les plus denses sont principalement les DGTAs et les *lyso*-DGTAs (**Tableau VIII.1**). Ces dérivés lipidiques témoignent d'une grande diversité en termes de longueur de chaine carbonée et de nombre d'insaturations au sein de ces extraits de surface.

	Chapitre II	**Chapitre V**	**Chapitre VI**	**Annexe I**
Lyso-DGTAs/DGTAs	35	32	28	6
Lyso-PCs/PCs	0	5	0	11
MGs/DGs/TGs	0	8	8	0
MGDGs/DGDGs	0	2	5	0
Lyso-DGCCs/DGCCs	0	0	6	7
GGG et dérivés	1	2	2	0
Sesquiterpènes	1	5	2	4
Diterpènes	4	3	2	10
Dipeptides	4	0	0	0

Tableau VIII.1. Tableau récapitulatif du nombre de métabolites identifiés par famille chimique en utilisant l'approche des réseaux moléculaires dans le cadre d'études sur les extraits de surface de *T. atomaria*

2.2.Le choix de la méthode analytique pour la métabolomique

En parallèle de l'optimisation de l'annotation par LC-MS en mode d'ionisation positif [LC-ESI-(+)-MS], une deuxième question méthodologique était de déterminer si d'autres approches analytiques complémentaires, telles la LC-MS en mode d'ionisation négatif [LC-ESI-(-)-MS] ou la GC-MS, pouvaient apporter des informations supplémentaires au niveau du métabolome de surface de *T. atomaria*. Cette étude s'est intégrée aux travaux menés sur les variations intra-thalles (**chapitre V**). Dans les conditions expérimentales que nous avons choisies, la comparaison de ces différents types d'analyse a permis de montrer qu'un plus grand nombre de métabolites étaient observés et identifiés par LC-ESI-(+)-MS (**Tableau VIII.2**).

	LC-ESI-(+)-MS	**LC-ESI-(-)-MS**	**GC-MS**
Nombre d'ions observés	433	135	261
Nombres de métabolites identifiés	54	34	25
Familles majeures de métabolites identifiés	DGTAs, PCs, GGG et dérivés	PEs, SQDGs et SQMGs	Sesquiterpènes

Tableau VIII.2. Comparaison du nombre de métabolites observés et annotés ainsi que des principales familles chimiques identifiées en fonction de trois méthodes d'analyses métabolomiques

Dans le cadre de cette étude, les trois approches s'avèrent complémentaires étant donnée la diversité des familles chimiques des métabolites annotés. Dans le cadre de l'approche LC-(+)-ESI-MS, les composés identifiés étaient des DGTAs, des PCs, ainsi que le GGG et ses dérivés acylés, alors que l'utilisation du mode d'ionisation négatif a permis de mettre en évidence d'autre composés tels que des PEs et des SQMGs/SQDGs. Enfin, l'avantage de la GC-MS réside principalement dans l'annotation de sesquiterpènes grâce aux bases de données Wiley 2008 et NIST 2011 ; annotation renforcée par le calcul des indices de rétention (van Den Dool and Kratz, 1963). Parmi ces dérivés sesquiterpéniques, seul le gleenol a été caractérisé lors de l'approche phytochimique par LC-ESI-(+)-MS, tandis que la majeure partie d'entre eux se retrouvent donc identifiés uniquement par GC-MS.

En définitive, bien que ces trois approches soient complémentaires et permettent d'analyser une large gamme de composés présents à la surface de *T. atomaria*, il faut cependant noter qu'elles ne conduisent pas à une couverture totale de la diversité chimique de la phycosphère, en ne permettant pas notamment l'étude des molécules ayant de plus hautes masses moléculaires (> 1 500 Da) telles que les polysaccharides et les protéines, par exemple. Cependant, il est par ailleurs important de noter qu'aucune méthode en métabolomique ne permet à ce jour de couvrir de manière exhaustive l'intégralité de la chimiodiversité

d'un organisme. Cette problématique de « matière noire », représentant la diversité chimique encore non observée ou non identifiée (da Silva et al., 2015), reste encore peu considérée et la possibilité d'intégrer de nouvelles méthodes complémentaires d'analyse constitue une perspective potentielle pour y remédier.

2.3.Quelle est l'origine des métabolites de surface étudiés ?

Dans le cadre d'une analyse métabolomique ciblant des extraits de surface, il était particulièrement important de pouvoir élucider l'origine biosynthétique des composés, notamment ceux observés comme étant discriminants au cours des différentes études. En effet, en plus d'échantillonner les métabolites de la macroalgue, l'étape d'extraction à la surface est aussi susceptible de collecter des métabolites provenant directement des organismes épiphytes ou de la matrice du biofilm. Dans l'optique de déterminer leur origine biosynthétique par comparaison avec la bibliographie, les différents composés annotés et discriminants observés au cours des diverses études sont présentées dans le **Tableau VIII.3** :

	Discriminations observées	**Reference**	**Origine potentielle**
DGTAs	Variations saisonnières	Chapitre II et VI	Macro et micro-algues (Dembitsky, 1996; López-Lara et al., 2003)
	Variations intra-thalles	Chapitre V Parrot et al., 2019	
	Variations d'intensité lumineuse	Chapitre VII	
DMSP	Variations saisonnières	Chapitre II et VI	Macro et micro-algues (Karsten et al., 1992; Yoch, 2002; Lyons et al., 2010; Kessler et al., 2017, 2018)
	Variations intra-thalles	Chapitre V	
	Différences taxonomiques	Annexe X	
	Variations d'intensité lumineuse	Chapitre VII Karsten et al., 1990 Lyons et al., 2010	
Fucoxanthine	Variations spatiales	Chapitre III et VI	Surface de macroalgues (Grosser et al., 2012)
	Variations d'intensité lumineuse	Chapitre VII Ramus et al., 1977 Perez-Bermudez et al., 1981	
Sesquiterpènes, GGG et dérivés	Variations saisonnières	Chapitre II et VII	*Taonia atomaria* (De Rosa et al., 1994; Tringali et al., 1995; Othmani et al., 2016b; Jerković et al., 2019)
	Variations de température et d'intensité lumineuse (gleenol)	Chapitre VII	
	Différences taxonomiques	Chapitre III et Annexe I	

Tableau VIII.3. Origine biosynthétique potentielle des principaux métabolites de surfaces déterminés comme étant des biomarqueurs

Ces métabolites semblent majoritairement provenir d'organismes eucaryotes et très certainement de *T. atomaria*, même si l'on ne peut pas exclure qu'une partie de la production métabolique de surface, dans le cas notamment du DMSP, soit aussi liée à des colonisateurs eucaryotes tels que les microalgues. En résumé, il semble donc très peu probable que les métabolites impliqués dans les principales discriminations observées, dans le cadre de ces études, au niveau du métabolome de surface de *T. atomaria* soient produits par des bactéries. Les différences observées sont certainement dues principalement au métabolome de l'hôte lui-même ou, dans une moindre mesure, à celui d'eucaryotes épiphytes.

2.4.Le choix des amorces pour l'approche par metabarcoding

Avec les avancées technologiques dans le domaine du séquençage haut-débit et la diminution des coûts d'analyses, l'approche par metabarcoding constitue à présent une méthode employée en routine par l'ensemble de la communauté scientifique dans le domaine de l'écologie microbienne. Cependant, le choix des amorces constitue une étape essentielle dans la réalisation d'une telle étude. Dans le cadre de cette thèse, l'objectif principal était de considérer l'ensemble de la communauté procaryote à la surface de l'algue. Nos recherches se sont donc orientées vers des amorces universelles qui ciblent le gène codant l'ARN 16S. Trois jeux d'amorces ont été utilisés au cours des différentes études (**Tableau VIII.4**).

Noms des amorces	Régions ciblées	Etudes	Références
775F/1103R	V5-V6	Chapitre II	Youssef et al., 2009
515F-Y/926R	V4-V5	Chapitre III ; V ; VI et VII	Parada et al., 2016
NOCHL	V3-V4	Chapitre VII	Thomas et al., 2020

Tableau VIII.4. Liste des amorces codant l'ARN 16S utilisées pour l'étude des communautés procaryotiques à la surface de *T. atomaria*

Le premier couple (775F/1103R) a été utilisé dans le cadre de l'étude préliminaire (**chapitre II**) dont les échantillons ont été traités en 2013 en suivant le protocole de Youssef et al., (2009). Ces auteurs avaient comparé la richesse en OTUs obtenue dans le cadre d'études environnementales pour les différentes régions variables du gène codant l'ARNr 16S. Suite aux travaux de Parada et al., (2016), notre choix s'est porté sur de nouvelles amorces (515F-Y/926R) destinées à optimiser la couverture globale de la communauté procaryote, spécifiquement en milieu marin, mais sur des communautés planctoniques. Cette optimisation s'est faite notamment par comparaison à une communauté de référence (« *mock community* ») avec laquelle une excellente corrélation a été obtenue (R^2 = 0,95) (Parada et al., 2016). Ces

travaux ont notamment permis de montrer que ces amorces amélioraient considérablement la couverture en comparaison avec un autre couple d'amorces (515F/806R) (Caporaso et al., 2011, 2012) qui était majoritairement utilisé au sein de la communauté scientifique, et pour lequel la comparaison avec la « *mock community* » révèle une corrélation bien plus faible ($R^2 \sim 0.5$). Par ailleurs, il est important de noter que ce couple d'amorce (515F/806R) a par la suite été modifié au niveau de l'amorce *reverse* (515F/806Rb), montrant alors une meilleure couverture notamment chez le clade SAR11 et les Thaumarcheota (Apprill et al., 2015; Walters et al., 2016). Ce dernier couple d'amorce (515F/806Rb), dont la couverture s'avère extrêmement comparable à celle du couple (515F-Y/926R) (test de Mantel : r = 0,975) (Walters et al., 2016), est actuellement celui qui est le plus utilisé dans la littérature récente portant sur les communauté épibactérienne de macrophytes (Bengtsson et al., 2017; Lemay et al., 2018b, 2018a; Lin et al., 2018; Marzinelli et al., 2018; Weigel and Pfister, 2019; Califano et al., 2020). Cependant, on peut noter que le couple (515F/806R) a aussi fait l'objet de nombreux travaux, parfois encore récents, malgré une plus faible couverture comparée à celle des couples (515F/806Rb) et (515F-Y/926R) (Marzinelli et al., 2015; Zozaya-Valdés et al., 2015, 2016; Chen and Parfrey, 2018). Un tel choix d'amorces (515F/806R et par la suite 806Rb) a notamment été justifié par certains auteurs avec l'objectif de correspondre aux normes standardisées du « *Earth Microbiome Project* » (EMP).

Par ailleurs, les travaux de Pollet et al., 2018 ont permis de mettre en évidence *in silico* la meilleure couverture d'un certain nombre de taxa avec le couple d'amorces (515F-Y/926R) en comparaison avec le couple (775F/1103R) (**Tableau VIII.5**). Ceci est notamment vrai pour les Flavobacteriia et les Rhodobacterales qui sont très souvent des taxa dominants au sein des biofilms marins (Dang and Lovell, 2016), que ce soit sur des surfaces abiotiques (Briand et al., 2017; Catão et al., 2019) ou biotiques, notamment les macroalgues (Dogs et al., 2017; de Mesquita et al., 2019).

Taxa bactériens	775F/1103R	515F-Y/926R
Bacteroidetes	15%	90%
Sphingobacteria	59%	91%
Flavobacteriia	1.70%	92%
Alpha-proteobacteria	63%	93%
Rhodobacterales	7%	95%
Gamma-proteobacteria	87%	93%
Alteromonadales	62%	92%
Cyanobacteria	0.87%	89%
Firmicutes	70%	88%
Planctomycetes	1.10%	86%
Verrucomicrobia	14%	88%

Tableau VIII.5. Couverture in silico des amorces 775F/1103R et 515F-Y/926R d'après Pollet et al., (2018)

En comparant à l'échelle de la famille, les communautés observées dans le cadre de l'étude préliminaire (**chapitre II**) et l'étude spatio-temporelle (**chapitre VI**), on peut d'abord noter la présence commune de certaines familles majeures telles que celles des Hyphomonadaceae, des Granulosicoccaceae [dont la dénomination a été modifiée en Thiohalorbdaceae suite à la mise à jour Silva 132] et des Saprospiraceae. Par contre, en accord avec les résultats de Pollet et al., (2018), on remarque que les Flavobacteriaceae et les Rhodobacteraceae sont très peu amplifiées dans le cadre de l'étude menée avec les amorces (775F/1103R), alors que les pourcentages relatifs de séquences amplifiées sont bien plus importants dans le cadre d'études conduites avec les amorces (515F-Y/926R). Ces deux familles seraient donc sous-représentées avec le premier couple d'amorces, confirmant ainsi que les amorces développées par Parada et al., (2016) sont plus adaptées dans le cadre de nos études.

Cependant, nous avons pu constater que ces amorces conduisaient aussi à l'amplification du gène de l'ARNr 16S d'origine chloroplastique. Une telle contamination dans les librairies est variable mais représente en moyenne 35% des séquences (±21%), diminuant ainsi la profondeur de séquençage pour l'analyse du gène codant pour l'ARNr 16S. Parmi les hypothèses développées pour expliquer l'importance relative de cette contamination, la première est qu'elle puisse provenir de cellules endommagées de l'hôte algal, en particulier lors de la récupération des cellules épiphytes par grattage au scalpel. La possibilité que la contamination chloroplastique provienne des taxa eucaryotes (notamment diatomées et dinoflagellés) au sein de la communauté épiphyte peut aussi être envisagée. De plus, suite à l'observation par microscopie de coupes transversales (**Figure VIII.1**), certains échantillons de *T. atomaria* présentaient une forte proportion de tétrasporanges qui se développaient à la surface de l'algue. Les tétrasporanges

constituent des structures contenant quatre spores haploïdes, se développant alors sous la forme d'un gamétophyte sexué. Chaque spore haploïde présente un certain nombre de plastes appelées « phaeoplastes » (Robinson, 1932). Un tel phénomène de développement des tétrasporanges à la surface a précédemment été décrit par les travaux de Robinson, 1932.

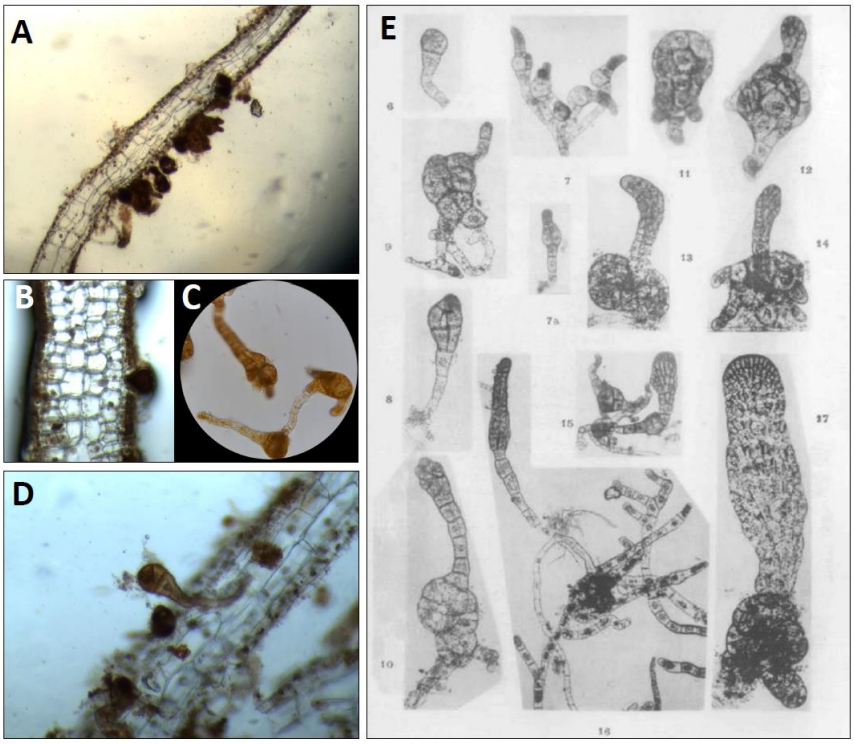

Figure VIII.1. Observations au microscope optique des tétrasporanges de *T. atomaria*. A et D : Coupes transversales de thalles présentant des tétraspores à leur surface. B : Coupe transversale d'un thalle présentant la germination du tétrasporange depuis la surface. C : Observation de tétrasporanges libres dans le milieu. Grossissements : A (× 100), B, C et D (× 400). E : Observation des différents stades de croissance des tétraspores de *T. atomaria* par Robinson, (1932).

Dans l'optique de développer des amorces universelles limitant la contamination chloroplastique, les travaux récents de Thomas et al., (2020), ont permis de décrire le couple d'amorce NOCHL. Ces amorces ont fait l'objet d'une étude méthodologique dans le cadre du **chapitre VII** en étant comparées au couple 515F-Y/926R. Les résultats ont montré que le couple d'amorce NOCHL n'amplifiait aucune séquence d'origine chloroplastique. De manière similaire aux résultats *in silico* présentés dans Thomas et al., (2020), une faible couverture est cependant observée pour certains taxa tels que les Cyanobactéries et les Verrucomicrobiae. L'absence de séquences de Cyanobactéries s'explique en particulier par le fait que le génome des chloroplastes soit issu de l'évolution du génome des Cyanobactéries ayant persistées lors de l'endosymbiose primaire. L'absence ou la faible couverture de ces groupes peut s'avérer problématique dans certains contextes d'études, en particulier si leur contribution relative est discriminante entre

différentes conditions. C'est notamment le cas lorsque l'on compare les échantillons d'eau et de biofilms, ou les Cyanobactéries et les Verrucomicrobiae sont généralement observés respectivement en tant que biomarqueurs des communautés planctoniques et épiphytes (**chapitre V et VI**). Néanmoins, dans le cadre du **chapitre VII** (n'abordant pas la communauté planctonique) nous avons remarqué que ces deux groupes étaient également très peu représentés lorsque les amorces 515F-Y/926R étaient utilisées. Ainsi, il est très probable que le faible recouvrement de ces deux groupes n'impacte que de manière très limitée les analyses de β-diversité dans ce contexte et le choix des amorces NOCHL a donc été effectué dans cette étude. En résumé, le choix des amorces 515F-Y/926R et NOCHL dépend de l'importance que l'on accorde soit à la réduction, parfois importante, du nombre de séquences liées à la contamination chloroplastique, soit à la perte de séquences de certains taxa, notamment les Cyanobactéries et les Verrucomicrobiae.

2.5.Les approches multi-omiques pour le couplage de jeux de données hétérogènes

Le développement de différentes méthodes d'analyses statistiques proposant un couplage de plusieurs jeux de données « -omiques » au sein d'une même étude est particulièrement récent (Lê Cao et al., 2009; Meng et al., 2014; Argelaguet et al., 2018).

Différentes méthodologies sont actuellement employées afin d'analyser conjointement plusieurs jeux de données –omiques au sein d'une même étude. Kim and Tagkopoulos, (2018) proposent ainsi de les classer en trois catégories, avec les approches « *data to data* », « *data to knowledge* » et « *knowledge to knowledge* ». Alors que l'approche « *data to data* » est une méthode généralement exploratoire qui a pour objectif d'analyser les différents jeux de données au sein d'une même analyse, l'approche « *knowledge to knowledge* » vise elle à interpréter d'abord les résultats de chaque analyse « -omique » en amont et indépendamment, pour ensuite rassembler les connaissances qui en résultent, au sein d'une méta-analyse permettant une vue d'ensemble des mécanismes moléculaires étudiés. Enfin l'approche « *data to knowledge* » constitue une approche intermédiaire ou les données d'une des approches « -omiques » sont analysées avec les connaissances d'une autre déjà interprétée. La génomique et la protéomique constituent les sciences « -omiques » les plus souvent intégrées au sein d'études multi-omiques de type « *data to data* », notamment grâce à l'essor de méthode permettant la reconstruction de réseaux d'interactions basée sur les voies fonctionnelles de référence associées aux gènes et protéines identifiés (Yeger-Lotem et al., 2004; Nguyen and Ho, 2012; Szklarczyk et al., 2015). Une telle méthode nécessite donc d'étudier des organismes modèles, ou les fonctions renseignées sont répertoriées au sein de bases de données telles que KEGG. A défaut de pouvoir corréler les différentes variables par rapport à leurs voies

fonctionnelles associées, une méthode « *data to data* » qui est néanmoins envisageable pour les organismes « non-modèles » constitue l'intégration, via des analyses multivariées basées sur la corrélation statistique, des différents jeux de données. Un exemple récent pour une analyse regroupant métabolomique et métabarcoding est la méthode « mmvec », permettant par une méthode de *machine learning*, la construction d'un réseau corrélant métabolites et microorganismes en calculant la probabilité de co-occurrence de chaque variable (Morton et al., 2019).

Dans cette même optique d'analyse statistique conjointe, le package MixOmics propose aussi diverses méthodes d'analyses d'intégration multivariées, notamment les analyses DIABLO et MINT. L'analyse DIABLO permet une intégration horizontale des données (divers jeux de données partageant les mêmes échantillons mais avec des variables différentes) tandis que l'analyse MINT propose une intégration verticale (divers jeux de données avec des échantillons différents mais les mêmes variables). Par exemple, l'analyse MINT se révèle intéressante dans le cas d'études métabolomiques mêlant différentes approches analytiques telles que RMN, GC-MS, ou encore LC-MS. Dans le cadre de cette dernière, différentes méthodes peuvent être mises en œuvre en fonction du type de phase stationnaire (C18, phénylhexyl, HILIC…) ou du type d'ionisation (ESI, APCI...) et du mode d'ionisation (positif ou négatif). Une telle méthode d'analyse statistique permet alors d'intégrer l'ensemble des approches analytiques afin d'autoriser une couverture plus large du métabolome. Dans cette optique, cette analyse aurait pu être appliquée dans le cadre de l'étude « *cross* »-métabolomique (**chapitre V**) ciblant la différenciation chimique le long des thalles de *T. atomaria* par GC-MS, LC-(+)-ESI-MS et LC-(-)-ESI-MS. Cependant, le problème majeur dans la mise en œuvre de telles analyses réside dans l'identification des variables. Du fait de l'annotation partielle des matrices de données obtenues, il était impossible de faire correspondre une variable d'une matrice à une autre lorsqu'elles n'étaient pas annotées. Ce type d'analyse multi-omiques n'a donc pas été employée lors de cette étude.

De la même manière que la PLSD-DA utilisée couramment en métabolomique, l'analyse DIABLO est basée sur la fonction *block.splsda()* et constitue une analyse statistique supervisée. Ce type d'analyse a été développé avec l'objectif d'étendre l'approche multivariée rCCA en utilisant une méthode supervisée qui permette d'intégrer un nombre de jeux de données -omiques supérieur à deux (Lê Cao et al., 2009). Le package MixOmics fournit avec l'approche DIABLO un certain nombre de fonctions permettant d'explorer en détails non seulement la discrimination entre échantillons, en prenant en compte l'ensemble des jeux de données intégrés, mais aussi les potentielles corrélations entre les variables. Parmi ces fonctions, *plot.arrow()* permet de visualiser les différences respectives entre échantillons tandis que *network()* aide

à la mise en forme d'un réseau de corrélation de variables en fixant un seuil de corrélation. Ce réseau permet alors d'initier une approche exploratoire et d'approfondir l'analyse des corrélations potentielles entre métabolites et taxa bactériens. Par exemple, une telle analyse a permis de fournir des hypothèses concernant le rôle du DMSP dans le cadre des **chapitre II** et **chapitre VI**.

3. Les communautés pionnières, cœurs et spécifiques à la surface de *Taonia*

3.1. Les taxa pionniers sont aussi des taxa cœurs et spécifiques à l'algue

Les **chapitres II, V et VI** ont permis de s'intéresser aux taxa pionniers pouvant coloniser les surfaces « jeunes » des algues du genre *Taonia* en mer Méditerranée, qu'il s'agisse de thalles complets prélevés en début de croissance des sporophytes (février) ou d'échantillons correspondant à des zones apicales où se situent les méristèmes. Pour ces trois études, la famille des Hyphomonadaceae est observée comme étant un taxon majeur de la communauté pionnière. Plus particulièrement, cette famille est représentée par le genre pionnier *Robiginitomaculum* au cours du premier suivi temporel (**chapitre II**) ainsi que par le genre *Litorimonas* pour les études portant sur les variations intra-thalles (**chapitre V**) et spatio-temporelles (**chapitre VI**). En outre, le genre *Nitratireductor* est aussi présenté, dans le cadre de l'étude des variations intra-thalles, comme étant un genre pionnier et l'étude spatio-temporelle permet de confirmer la présence de ce genre et de sa famille (Rhizobiaceae) majoritairement en février et mars (période de croissance initiale de l'algue). Enfin, le genre *Granulosicoccus* appartenant à la famille des Thiohalorhabdaceae est également observé comme étant un genre pionnier majeur lors du suivi temporel de 2013 (**chapitre II**) et du suivi spatio-temporel de 2017 (**chapitre VI**).

La notion de communauté de cœur (« *core community* ») caractérise ici la partie stable, en termes de composition, de l'ensemble de la communauté. Cependant, elle est dépendante de l'étude réalisée en fonction de choix méthodologiques : elle peut par exemple être aussi définie par les fonctions communes et non la taxonomie (Burke et al., 2011a, 2011b; Roth-Schulze et al., 2018). Dans le cadre de ces travaux de thèse, cette terminologie a été définie par la présence des OTUs en question dans au moins un des réplicats (n = 3) pour chaque condition. Un tel choix a notamment été considéré afin de prendre en compte la possibilité que certains taxa rares observés sur l'ensemble des conditions puissent ne pas être systématiquement retrouvés dans l'ensemble des réplicats, suite au seuil de filtration des séquences de 0.005% imposé en amont, par exemple. Cette définition permet d'exclure systématiquement de la communauté de cœur les OTUs absents des trois réplicats d'au moins une des conditions. La notion de

taxa cœurs est souvent très subjective en fonctions des études (Astudillo-García et al., 2017) et d'autres travaux portant sur les macroalgues holobiontes ont, par exemple, défini comme critère un seuil minimal d'abondance relative (Marzinelli et al., 2015).

La communauté cœur est alors définie par l'ensemble des OTUs stables (i) d'un point de vue temporel dans le cadre du **chapitre II**, (ii) d'un point de vue géographique dans le cadre du **chapitre III**, et (iii) d'un point de vue spatio-temporel dans le cadre du **chapitre VI**.

En comparant les différentes études (**Tableau VIII.6**), certains des taxa pionniers apparaissent aussi comme étant à la fois membres de la communauté de cœur et de la communauté spécifique à l'algue. Ces taxa sont notamment *Granulosicoccus* et *Litorimonas* ; ils contribuent de manière significative à ces deux sous-ensembles de la communauté globale. Deux genres appartenant aux Bacteroidetes, *Rubidimonas* et *Algitalea* (Saprospiraceae et Flavobacteriaceae), apparaissent aussi en tant que taxa spécifiques et membres de la communauté de cœur, mais eux ne sont pas identifiés comme étant pionniers.

	Chapitre II	**Chapitre III**	**Chapitre V**	**Chapitre VII**
Genres pionniers	*Robiginitomaculum* *Granulosicoccus*	n.d.	*Litorimonas* *Nitratireductor* *Rubritalea*	*Litorimonas* *Granulosicoccus*
Genres cœurs	*Robiginitomaculum* *Erythrobacter* *Granulosicoccus* *Thiothrix*	*Litorimonas* *Granulosicoccus* *Algitalea* *Rubidimonas*	n.d.	*Litorimonas* *Granulosicoccus*
Genres spécifiques	n.d.	n.d.	*Granulosicoccus* *Algitalea*	*Litorimonas* *Nitratireductor* *Granulosicoccus* *Algitalea* *Rubidimonas*

Tableau VIII.6. Liste des genres bactériens identifiés au cours des différentes études, comme étant les principaux contributeurs des communautés pionnières, cœurs ou spécifiques. n.d. : non déterminé

Par ailleurs, *Granulosicoccus* et *Litorimonas* constituent des genres particulièrement représentés au sein de la communauté des algues prélevées *in situ* en Bretagne avec des pourcentages d'abondance relative pouvant aller jusqu'à 31% et 18%, respectivement.

Ces deux genres sont très largement décrits dans la littérature comme étant abondants au sein des communautés épiphytes d'une vaste diversité d'autres macroalgues modèles issues d'environnements contrastés. C'est notamment le cas au sud-ouest de la Norvège où les algues *Laminaria hyperboreae* sont exposées à des modes battus variables (Bengtsson et al., 2012), ou le long des côtes Pacifique et Atlantique d'Amérique du Nord, avec par exemple les kelps *Nereocystis luetkeana* et *Macrocystis pyrifera* (Weigel

and Pfister, 2019) ou Pacifique (Chen and Parfrey, 2018; Lemay et al., 2018b; Lin et al., 2018), ou encore des *Mastocarpus* spp. provenant de la côte Pacifique nord-américaine (Lemay et al., 2018a). Plus précisément, dans le cadre d'une étude sur l'algue *L. hyperborea*, un OTU du genre *Granulosicoccus* a été identifié à la surface de jeunes spécimens d'algues et présenté comme étant pionnier. Ce taxon présente une adaptation potentielle permettant un attachement et une croissance rapides à la surface de la macroalgue et il se trouve ainsi impliqué dans les premiers stades de formation du biofilm (Bengtsson et al., 2012). Pour les algues du genre *Mastocarpus*, Lemay et al., (2018a) ont observé qu'un OTU du genre *Granulosicoccus* était l'un des représentants majeurs de la communauté de cœur, tout en étant associé aux deux modes de vies des algues (sporophyte et gamétophyte). Dans cette même étude, deux OTUs appartenant au genre *Litorimonas* ont aussi été identifiés comme faisant partie des principaux taxa de la communauté de cœur, car présents dans plus de 90% des échantillons.

De telles caractéristiques laissent donc supposer que ces deux genres sont particulièrement adaptés pour adhérer et se développer à la surface des macroalgues. Bien que les caractéristiques fonctionnelles associées au genre *Granulosicoccus* restent relativement peu décrites dans la littérature (Ivanova and Webb, 2014), de récents travaux ont permis via une approche de type CLASI-FISH de localiser précisément ce taxon au sein du biofilm à la surface de la macroalgue brune *Necrocystis luetkeana* (Ramirez-Puebla et al., 2020). Ces résultats obtenus par imagerie ont pu montrer que la localisation des *Granulosicoccus* spp. correspondait à des zones proches de la surface de l'algue par comparaison à d'autres taxa plus abondants à l'interface biofilm/eau de mer. Ces résultats permettent donc de renforcer l'idée que *Granulosicoccus* serait un taxa pionnier au sein du biofilm et serait caractérisé par une association étroite avec la macroalgue-hôte. Etant donné qu'un certain nombre de fonctions associées aux flagelles ont aussi été identifiées dans le génome de *Granulosicoccus* sp. (Kang et al., 2018), Ramirez-Puebla et al., (2020) soulignent l'importance de la motilité chez ce taxon, ce qui le rend particulièrement adapté à la colonisation précoce des frondes/thalles des algues.

En ce qui concerne *Litorimonas* et plus généralement les Hyphomonadaceae, certaines caractéristiques morphologiques leur permettraient de faciliter la colonisation de la surface des macroalgues (Dang and Lovell, 2016). En particulier, pour *Hyphomonas*, [un autre genre également décrit au sein des Hyphomonadaceae et communément retrouvé à la surface d'autres macroalgues (Hollants et al., 2013; Minich et al., 2018; Quigley et al., 2018)], la présence d'un crampon semble être potentiellement induite suite au contact direct avec la surface algale (Langille and Weiner, 1998; Weiner et al., 2000). Ce crampon est caractérisé par des adhésines extracellulaires constituées d'EPS [principalement des polysaccharides

(Merker and Smit, 1988)], qui permet chez la souche VP-6 d'induire les premières étapes de l'adhésion lors de la formation du biofilm (Langille and Weiner, 1998).

Cependant, les mécanismes associés au recrutement et au développement d'autrestaxa pionniers à la surface de l'algue restent encore à élucider dans le cadre de *T. atomaria*. Par exemple, l'implication de certains métabolites exprimés à la surface de l'algue dans le recrutement spécifique de ces taxa pionniers pourrait être envisagée. En effet, la surface des macroalgues constitue une niche microbienne spécifique pour les communautés épiphytes de biofilms et la production de certains constituants spécifiques, tels que par exemple des polysaccharides produits par l'hôte, pourrait constituer un facteur-clé dans l'adaptation et le développement de bactéries pionnières. Les travaux de Gobet et al., (2018) ont ainsi montré la présence de voies de dégradation des glucides codés par les gènes CAZymes chez la bactérie *Pseudoalteromonas carrageenovora*. Cette étude laisse supposer que l'acquisition de ces gènes résulterait d'une évolution associée à l'adaptation au mode de vie épiphyte à la surface des algues. Les voies de catabolisme associées à la dégradation des carraghénanes seraient notamment acquises via des transferts de gènes horizontaux. D'autres bactéries isolées à la surface d'algues, dont *Zobellia galactanivorans*, ont également été étudiées pour leurs voies fonctionnelles associées à la dégradation de polysaccharides d'algues (Thomas et al., 2012, 2013).

Par ailleurs, l'importance fonctionnelle des taxa pionniers pour l'hôte algal constitue une question encore très peu explorée dans la littérature (Morrissey et al., 2019). Les travaux menés en conditions de culture sur les Ulvales (*U. mutabilis* et *U. intestinalis*) soulignent cependant l'importance de la communauté bactérienne pour les stades précoces du développement de l'algue (Wichard et al., 2015; Ghaderiardakani et al., 2017; Kessler et al., 2018). Des combinaisons de souches de *Roseovarius* sp. et *Maribacter* sp. assurent la bonne morphogenèse de l'algue via la synthèse de facteurs de croissance telle que la thallusine et permettent la division cellulaire, la différenciation du rhizoïde et la formation de la paroi de l'algue (Ghaderiardakani et al., 2017; Alsufyani et al., 2020).

D'autre part, Longford et al., (2019) se sont aussi intéressés à l'importance fonctionnelle des premiers colonisateurs recrutés à la surface de *D. pulchra* après une expérience de manipulation du microbiote. Les auteurs ont incubé l'algue *D. pulchra* pendant 24h avec un mélange d'antibiotiques afin d'induire une perturbation du microbiote de surface, avec l'objectif de s'intéresser à la restructuration de la communauté une fois que l'algue est replacée dans son milieu naturel. Bien qu'il ne s'agisse pas de taxa pionniers *stricto sensu*, il s'avère que trois primo-colonisateurs cultivés (*Kytococcus sedentarius*, *Thalassobius aestuarii* et *Altererythrobacter ishigakiensis*) permettent de protéger *D. pulchra* d'autres

colonisateurs plus tardifs qui sont des pathogènes de l'algue induisant son blanchissement (*Phaeobacter gallaciensis,* cf **chapitre I**). Ainsi, la succession des colonisateurs joue un rôle particulièrement important pour la physiologie de l'algue, en particulier chez celles dépourvues de défenses chimiques (ex. : furanones halogénées). De manière similaire au concept de « *microbial gardening* » exploré notamment par (Saha and Weinberger, 2019), les taxa pionniers pourraient alors être recrutés spécifiquement par l'algue afin de constituer une communauté défendant l'algue contre l'arrivée successive et le développement de potentiels pathogènes.

Dans le cadre de l'algue *T. atomaria*, une telle hypothèse pourrait s'avérer particulièrement intéressante à tester expérimentalement sachant que les principaux taxa pionniers sont déjà identifiés, avec en particulier les genres *Litorimonas* et *Granusosicoccus*.

3.2.Une dynamique associée à la maturation du biofilm et la croissance de l'algue.

Le **Chapitre V** : Etude intra-thalle a permis de mettre en évidence des différenciations de microbiome et de métabolome le long des thalles de *T. atomaria* qui semblaient potentiellement associées à la croissance de cette algue. Des DGTAs ont notamment été observées comme étant des lipides sur-exprimés à la surface des parties apicales. Chez l'algue *Sargassum honeyri*, les teneurs en DGTAs semblent augmenter lors de la phase de croissance de l'algue, ce qui laisse supposer que ces métabolites pourraient constituer des marqueurs des zones de croissance. Les travaux de Robinson, (1932) ont montré que les zones de croissance méristématiques chez *T. atomaria* étaient situées dans les parties apicales, ce qui expliquerait donc la surexpression de DGTAs aux extrémités de cette algue.

Pour ce qui est des variations de la communauté épibactérienne de *T. atomaria*, en accord avec les résultats des **chapitre II** et **chapitre VI**, le pourcentage relatif du genre pionnier *Litorimonas* diminue au cours du temps et en relation avec la croissance de l'algue. Par ailleurs, il est intéressant de noter que lorsqu'une deuxième génération de thalles de *T. atomaria* apparait à Tamaris en mai (la température de l'eau a alors augmenté), l'abondance relative de ce taxon, mais aussi de *Granulosicoccus*, augmente de nouveau. Ceci laisse donc supposer que la forte abondance relative de ces taxa semble être associée aux stades précoces du développement des thalles plutôt qu'aux faibles températures hivernales.

Alors que les taxa pionniers diminuent, l'α-diversité et la densité bactérienne augmentent avec la croissance de l'algue. Par ailleurs, la seconde génération de thalles à Tamaris présente une faible α-diversité avec des valeurs similaires à celles observées pour la période d'apparition des thalles (février-

mars). Ces observations laissent supposer que les communautés pionnières sont peu diversifiées et qu'elles s'enrichissent par la suite, non pas directement en lien avec l'évolution des paramètres physico-chimiques comme la température, mais plutôt en lien avec la croissance de l'algue et en relation avec la maturation du biofilm présent à la surface de l'algue.

En identifiant les principaux taxa (via les analyses SIMPER et LEfSe) associés à la diversification de la communauté, d'une part liée à la croissance le long de l'algue (des zones apicales vers la base, **chapitre V**) et d'autre part à la temporalité (de février à juillet, **chapitre II** et **chapitre VI**), on peut cependant remarquer qu'aucun taxon ne se retrouve en commun (ni à l'échelle de la famille, ni du genre). Ainsi la diversification de la communauté épibactérienne après la colonisation des taxa pionniers serait en grande partie influencée par les conditions environnantes, que ce soit par un effet direct sur les communautés, ou par un effet indirect via un effet initial sur le métabolome de surface qui impacte ensuite les bactéries. L'augmentation de la température constituerait alors un facteur majeur associé à la temporalité, intimement lié à la diversification des colonisateurs de février à juillet. En revanche, ce facteur ne peut pas être explicatif de la diversification du sommet vers la base de l'algue. Ainsi cela expliquerait par exemple pourquoi les Rhodobacteraceae et Flavobacteriaceae, et leurs genres associés, constituent les principaux taxa augmentant de février à juillet sans toutefois présenter d'augmentation de la base vers le sommet des thalles de *T. atomaria*.

4. Impact de l'environnement sur la dynamique de l'holobionte

4.1. La dynamique des Rhodobacteraceae : quels sont les liens avec le DMSP, la température et la luminosité ?

La famille des Rhodobacteraceae constitue l'une des plus diversifiée en milieu marin avec plus de 100 genres décrits (Pujalte et al., 2014). Cette famille est particulièrement ubiquiste au sein des Alphaproteobacteria, que ce soit dans la colonne d'eau ou fixée à des surfaces biotiques ou inertes (Pujalte et al., 2014; Dang and Lovell, 2016). La famille des Rhodobacteraceae est subdivisée en différents clades dont le « marine Roseobacter clade » (MRC). Le MRC est très largement décrit à la surface des microalgues, telles que les diatomées ou les dinoflagellés (Seymour et al., 2017), mais aussi des macroalgues (Stratil et al., 2013; Zozaya-Valdés et al., 2015; Dogs et al., 2017). Ce clade rassemble plus de 70 genres dont *Octadecabacter*, *Sulfitobacter*, *Litoreibacter*, *Jannaschia*, *Loktanella, Aquimarina, Nautella et Ruegeria,* qui constituent les genres dominants retrouvés à la surface de macroalgues situées dans des environnements diverses tels que *Fucus spiralis* (Dogs et al., 2017) et *Fucus vesiculosus* en mer Baltique (Stratil et al., 2013), *Cystoseira compressa* en mer Méditerranée (Mancuso et al., 2016), *Sargassum muticum* au nord-est de l'Atlantique (Serebryakova et al., 2018), *Pyropia yzeoensis* en mer de Chine Orientale (Yan et al., 2019) et *Delisea pulchra* en mer de Tasman (Campbell et al., 2011; Fernandes et al., 2011). Dans le cadre des travaux réalisés au cours de cette thèse, les principaux genres identifiés au sein des Rhodobacteraceae appartiennent aussi à ceux cités précédemment (**Figure VIII.2**), avec une dominance toute particulière de *Octadecabacter*, *Loktanella* et *Litoreibacter* observée au cours du suivi spatio-temporel (**chapitre VI**) tandis que *Sulfitobacter* apparaissait comme taxon majeur au sein de cette famille lors de l'étude en mésocosmes menée avec des échantillons de *T. atomaria* prélevés sur les côtes du nord de la Bretagne (**chapitre VII**). Cette différence apparait donc aussi dans l'étude comparant les algues du genre *Taonia* provenant de Manche et de mer Méditerranée (**chapitre III**). Les différences phylogénétiques entre les algues ainsi que les différences de l'environnement et du métabolome associé sont alors considérées comme autant de facteurs pouvant influencer la structure de cette famille.

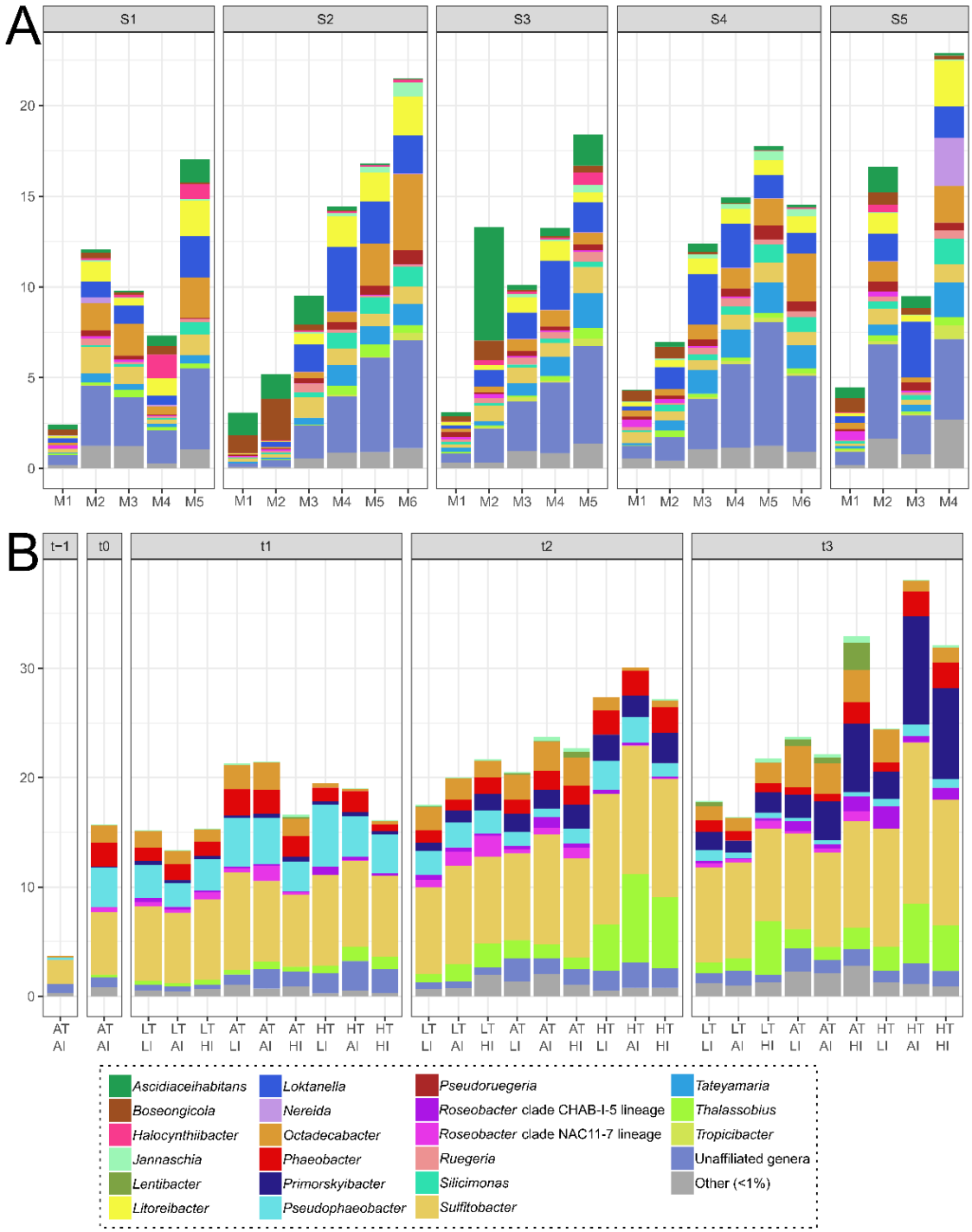

Figure VIII.2. Dynamique des pourcentages relatifs des différents genres affiliés au Rhodobacteraceae observés à la surface de *T. atomaria* lors (A) des études spatio-temporelles (**chapitre VI**) et (B) en mésocosmes (**chapitre VII**). Les indices M1 à M6 correspondent aux mois allant de février à juillet. Les sites S1, S2, S3, S4 et S5 correspondent à Tamaris, Carqueiranne, Porquerolles côtes nord, Porquerolles côtes sud et La-Londe-les-Maures, respectivement. Les indices LT, AT, HT correspondent aux conditions de température faible, ambiante et forte. Les indices LI, AI, HI correspondent aux conditions d'intensité lumineuse faible, ambiante et forte. Les indices t-1 ; t0 ; t1 ; t2 et t3 correspondent aux échantillons de terrains, aux échantillons acclimatés, aux échantillons après 24h, 7 jours et 14 jours de conditionnement, respectivement.

Plusieurs travaux montrent une augmentation des Rhodobacteraceae avec la température à la surface de *F. vesiculosus* (Stratil et al., 2013; Saha et al., 2014), *D. pulchra* (Case et al., 2011; Fernandes et al., 2011) et *Ecklonia radiata* (Qiu et al., 2019). Dans le cadre du suivi spatio-temporel présenté dans le **chapitre VI**, les Rhodobacteraceae constituait l'une des familles majeures de la communauté de surface et l'augmentation de sa proportion relative au sein de la communauté globale au cours du temps était l'une des plus marquée, et ce de manière continue de février à juillet. Par ailleurs, cette famille apparaissait aussi comme biomarqueur de ce dernier mois (juillet) avec l'analyse LEfSe. Le réseau de corrélation multi-omiques obtenu à partir de l'analyse DIABLO a permis également de révéler de forts liens de corrélation entre l'augmentation temporelle de certains OTUs appartenant à cette famille et l'augmentation de la température de l'eau de mer. Plus particulièrement, des OTUs appartenant aux genres *Silicomonas*, *Octadecabacter*, *Maribacter*, *Pseudoruegeria*, ainsi que d'autres genres non affiliés, étaient corrélés positivement à la température et regroupés au sein d'un même cluster. On peut aussi noter que le genre *Jannaschia* apparaissait au sein du même cluster sans être directement corrélé à la température, tout en présentant une augmentation durant la période du suivi temporel. L'augmentation des Rhodobacteraceae avec la température a été par la suite confirmée lors de l'étude réalisée en conditions contrôlées en mésocosmes (**chapitre VII**). En effet, après une et deux semaines de conditionnement, des pourcentages relatifs plus élevés atteignant plus de 30% ont été observés pour la température la plus élevée (22°C) et plus particulièrement pour certains genres dont *Sulfitobacter*, *Pelagimonas*, *Thalassobius* et *Primorskyibacter.*

La famille des Rhodobacteraceae représente un groupe très diversifié d'un point de vue fonctionnel avec notamment un certain nombre de fonctions reflétant une adaptation à des modes de vies épiphytes, et plus particulièrement dans le cadre d'association avec des algues (Wagner-Döbler et al., 2010; Thole et al., 2012; Luo and Moran, 2014). Les MRC (*Marine Roseobacter Clade*) sont particulièrement décrits pour certains mécanismes d'interactions symbiotiques avec le phytoplancton (Geng and Belas, 2010), en constituant pour leur hôte une source de vitamines (Croft et al., 2005; Wagner-Döbler et al., 2010; Buchan et al., 2014) ou de sidérophores (Thole et al., 2012). L'étude des génomes des MRC a également montré certains gènes codants des fonctions associés au système du c-*di*-GMP, au QS, à la motilité, ainsi qu'à divers mécanismes de reconnaissance chimique impliquant notamment des protéines réceptrices (Dang and Lovell, 2016). Ces fonctions seraient alors particulièrement importantes pour les bactéries pour localiser leur hôte algal mais aussi pour établir des interactions étroites avec celui-ci (Geng and Belas, 2010; Dang and Lovell, 2016).

Le catabolisme du DMSP est particulièrement présent au sein du groupe Roseobacter (Curson et al., 2011) avec notamment deux voies décrites : celle de la déméthylation et celle du clivage (Curson et al., 2011; Reisch et al., 2011). Le DMSP constitue alors une source de carbone mais aussi de soufre pour ces bactéries. Certaines séquences codantes pour des enzymes impliquées dans les voies de dégradation du DMSP ont notamment été observées au sein des génomes de souches appartenant aux genres *Octadecabacter* et *Jannaschia* (Curson et al., 2011). Pour ces souches (*Octadecabacter antarticus* str. 238 et 307, et *Jannaschia* sp. CCS1), les deux voies de dégradation du DMSP impliqueraient l'enzyme *DmdA* catalysant la première étape de déméthylation et l'enzyme *DddP* impliquée dans la première étape de clivage.

Dans le cadre de cette étude spatio-temporelle, l'hypothèse fournie pour expliquer l'augmentation de certains de ces taxa avec la température est basée sur ce lien étroit avec le DMSP. En effet, la teneur de cet osmolyte à la surface présente une variation temporelle très similaire, du fait de son augmentation continuelle de février à juillet, à celle de certains OTUs appartenant aux Rhodobacteraceae et à celle de la température. Par ailleurs, la même tendance est observée dans le cadre du premier suivi temporel réalisé sur le site Carqueiranne (**chapitre II**). Le DMSP, étant donné son augmentation durant le suivi, apparaissait alors comme l'un des principaux biomarqueurs associés à la temporalité.

Comme le DMSP est d'un part connu comme ayant des effets attracteurs vis-à-vis de certaines souches bactériennes (Kessler et al., 2018; Wichard and Beemelmanns, 2018) et, d'autre part en tant que source de carbone et de soufre pour de nombreux de taxa dont certains appartenant aux Rhodobacteraceae, il a donc été envisagé que l'augmentation temporel du DMSP à la surface de *T. atomaria* pouvait favoriser le recrutement et le développement préférentiel de certains taxa.

Pour ce qui est de la production de DMSP chez les algues, il a été montré chez un certain nombre de modèles, dont *Codium fragile*, que l'augmentation de la production de cet osmolyte était corrélée positivement à l'intensité lumineuse (Lyons et al., 2010). Par conséquent, ces observations ont permis de s'interroger sur la nature de l'effet de la température sur l'augmentation de la production de DMSP à la surface de *Taonia* lors du suivi spatio-temporel. En effet, la durée d'exposition et l'intensité de l'ensoleillement augmentent de manière similaire à la température de février à juillet. De la même façon, la question de l'impact direct de la température ou de l'intensité lumineuse sur certains taxa épibacteriens se pose également.

L'étude menée en conditions contrôlées en mésocosmes présentée au **chapitre VII** a alors permis de répondre en partie à cette problématique de covariation de ces deux paramètres environnementaux. Les

résultats ont permis de confirmer que les teneurs en DMSP à la surface de *T. atomaria* augmentaient avec l'intensité lumineuse et cela, plus particulièrement en conditions de faible température (13°C). Ces observations permettent de supporter l'hypothèse que la biosynthèse du DMSP serait liée à la luminosité avec une production maximale lorsque les températures sont faibles (Karsten et al., 1992; Lyons et al., 2010). En outre, aucun effet significatif d'une augmentation de température n'a été observé sur la production de DMSP à la surface de l'algue, ce qui suggère donc que les variations en DMSP observées dans le cadre de l'étude spatio-temporelle pourraient alors être principalement liées à l'augmentation de l'intensité lumineuse au cours du suivi. L'abondance relative d'un certain nombre de genres de Rhodobacteraceae s'avère quant à elle en augmentation avec la température et non pas avec l'intensité lumineuse. Il s'agit notamment des genres *Sulfitobacter*, *Pelagimonas* et *Primorskyibacter.* Par conséquent, bien que *Sulfitobacter* et *Primoskybacter* soient aussi décrits comme étant des taxa pouvant potentiellement dégrader le DMSP, leur dynamique ne semble donc pas être directement liée à cet osmolyte. Cependant, l'abondance relative du genre *Jannaschia* augmente avec l'intensité lumineuse, notamment en condition de température ambiante en mésocosmes (**chapitre VII**). Dans ce cas précis, l'effet combiné d'une température ambiante entrainant une augmentation de la production de DMSP avec de fortes intensités lumineuses pourrait alors expliquer les variations observées pour ce taxon.

Enfin, l'origine biosynthétique du DMSP reste encore à confirmer même si, dans le cadre de ces travaux, l'hypothèse a été faite que cet osmolyte est produit majoritairement à sa surface par l'algue elle-même. En effet, le DMSP est aussi produit par un grand nombre de microorganismes photosynthétiques et leur participation à la production de DMSP à la surface de l'hôte algal doit être envisagée. Ainsi, la dynamique bactérienne associée au DMSP pourrait être intimement liée à celle de la communauté photosynthétique présente à la surface de *T. atomaria*.

4.2.Importance de la fucoxanthine en tant que photopigment antioxydant et antimicrobien

La fucoxanthine est un composé (xanthophylle) de la famille des caroténoïdes retrouvé de manière récurrente dans les différents extraits de surface de *Taonia* étudiés au cours de cette thèse (généralement sous la forme des ions suivants : $[M + H]^+$, $[M - H_2O + H]^+$ et $[M + Na]^+$). Ce photopigment majeur chez les macroalgues brunes a aussi été identifié comme étant présent à la surface de *Fucus vesiculosus* (Saha et al., 2011; Lachnit et al., 2013) et des expériences menées par spectroscopie Raman ont pu déterminer sa localisation précise à la surface de cette algue (Grosser et al., 2012). Ces expériences d'imagerie ont notamment montré que ce composé était libéré à la surface des cellules de l'algue avec des concentrations

décroissantes allant de la membrane des cellules vers le milieu environnant au niveau de la zone limite de surface. Ces travaux ont par ailleurs démontré que la présence de cette molécule n'était pas liée à celle de microalgues épiphytes ou à des cellules endommagées (Grosser et al., 2012). Alors que la fucoxanthine est connue en tant que photopigment faisant partie des photosystèmes localisés de manière intracellulaire à la surface des thylakoïdes, le mécanisme d'exsudation de ce composé à la surface des algues reste encore à élucider.

L'étude portant sur les variations spatio-temporelles en lien avec les paramètres environnementaux (**chapitre VI**) a montré que ce photopigment est surexprimé dans un site particulièrement contaminé en cuivre situé dans la Petite Rade de Toulon (Tamaris). Par ailleurs, le β-carotène ainsi que d'autres pigments photosynthétiques tels que la phéophytine a (chlorophylle dépourvue de l'ion Mg^{2+}) et certains de ses dérivés oxydés, présentent des variations similaires à celles de la fucoxanthine. Ces résultats sont en accord avec d'autres études menées précédemment sur *Sargassum cymosum*, *Cystoseira crinita* et *Cystoseira barbata* qui montrent une surexpression de pigments photosynthétiques (et notamment de fucoxanthine) en présence de fortes concentrations en cuivre (Costa et al., 2016; Ryabushko et al., 2017). Deux hypothèses sont alors proposées pour expliquer l'augmentation de ces composés à la surface de l'algue en présence de cuivre. D'une part, cet élément trace métallique est connu pour son effet toxique chez les algues via un mécanisme de photo-inhibition produit lorsqu'il remplace le magnésium dans le complexe porphyrine-Mg^{2+} de la chlorophylle (Küpper et al., 1996, 1998). Cette compétition au sein du noyau induit alors l'inactivation du transfert d'électrons au sein de la chlorophylle et, par conséquent, une diminution globale de l'activité photosynthétique de l'algue. Une augmentation globale de l'expression en pigment photosynthétique, avec notamment la fucoxanthine et la chlorophylle *a* comme principaux composants de l'appareil photosynthétique, permettrait alors d'assurer au minimum une certaine activité photosynthétique malgré l'antagonisme issu de la complexation de la chlorophylle avec l'ion Cu^{2+}. D'autre part, de fortes concentrations en cuivre constituent aussi une source de stress oxydatif chez les algues (Pinto et al., 2003; Costa et al., 2016). Dans ces conditions, il a été décrit que la capacité de production d'électrons au sein de l'appareil photosynthétique pouvait excéder la capacité de leur prise en charge par les mécanismes de la photosynthèse, ce qui génère alors un excès d'électrons induisant l'apparition d'espèces réactives de l'oxygènes (ROS). La surexpression de composés antioxydants tels que la fucoxanthine et le β-carotène à la surface de *T. atomaria* pourrait donc constituer une stratégie adaptative développée par cette algue pour réduire l'impact des ROS à sa surface.

Par ailleurs, de fortes intensités lumineuses induisent aussi un stress oxydatif et, de manière similaire à la réponse potentielle au cuivre, une surexpression de caroténoïdes pourrait aussi réduire l'effet des ROS produits (Mikami and Hosokawa, 2013). Ainsi, ce mécanisme pourrait expliquer les plus fortes teneurs en fucoxanthine observées au niveau des échantillons de *T. atomaria* prélevés en Méditerranée par rapport à ceux provenant de Bretagne (**chapitre III**).

Cependant, une autre dynamique a été observée en réponse à des intensités lumineuses croissantes lors de l'étude en conditions contrôlées (**chapitre VII**). En effet, une augmentation de la production en fucoxanthine a été observée lorsque l'intensité lumineuse diminuait, notamment dans les conditions de température ambiante et élevée. De manière opposée, la concentration en mannitol, un polyol servant aux algues de stockage du carbone issu de la photosynthèse, apparaissait la plus faible dans les conditions de faible intensité lumineuse. Cette diminution est en accord avec une diminution de l'activité photosynthétique de l'algue en condition de faible intensité lumineuse. Par conséquent, une hypothèse proposée est que l'augmentation de la fucoxanthine corresponde à une photo-adaptation de l'algue afin d'assurer une activité photosynthétique suffisante malgré les conditions de faible luminosité. Ce résultat est en accord avec d'autres études précédentes portant sur *F. vesiculosus*, *Ascophyllum nodosum* (Ramus et al., 1977), *Udotea petiolata* et *Dictyota dichotoma* (Perez-Bermudez et al., 1981), pour lesquelles l'expression de la fucoxanthine augmentait avec la profondeur, et donc lorsque l'intensité lumineuse diminuait.

En définitive, il est possible d'envisager que ces deux hypothèses liées à l'expression de la fucoxanthine à la surface de *T. atomaria*, en fonction de l'intensité lumineuse, ne soient pas exclusives avec à la fois un optimum lié à la photo-adaptation et un second lié au stress oxydatif.

Alors que la fucoxanthine a été décrite comme étant un composé présent à la surface de *F. vesiculosus*, son activité antimicrobienne a fait l'objet d'autres études chez cette même macroalgue (Lachnit et al., 2010; Grosser et al., 2012; Saha et al., 2014). Notamment, il a été montré qu'une fraction d'un extrait de *F. vesiculosus* contenant de la fucoxanthine, en plus d'autre composés ayant la même polarité, pouvait inhiber de manière significative l'adhésion bactérienne *in situ* lorsqu'elle était incorporée dans du phytagel au sein d'un dispositif expérimental de diffusion en continu (Lachnit et al., 2010). Cependant, l'expérience n'as pas permis de conclure qu'il y avait un effet significatif sur la structure des communautés bactériennes observées à la surface de ce dispositif. Il a donc été suggéré que l'effet sélectif de la fucoxanthine pouvait être limité, bien que son activité vis-à-vis de l'adhésion bactérienne puisse s'observer de manière globale sur l'ensemble de la communauté (Egan et al., 2013). Néanmoins, la fucoxanthine est un composé dont la

stabilité est souvent variable en fonction des conditions, avec notamment la possibilité d'une photo-dégradation qui peut réduire son contenu total dans une fraction (Piovan et al., 2013). Ainsi l'activité de la fucoxanthine au sein de la fraction pourrait être sensiblement différente de son activité réelle à la surface. Par ailleurs, l'hypothèse d'une régulation active de l'expression de la fucoxanthine par l'algue à sa surface, en tant que mécanisme de défense chimique, n'a pour le moment pas été démontrée.

Au cours de ces travaux de thèse, la fucoxanthine apparait comme étant un métabolite principalement exprimé pour permettre à l'algue de s'adapter à des contraintes environnementales, que ce soit un stress oxydatif, ou une faible intensité lumineuse. Cependant, on peut aussi noter que la variation temporelle de la fucoxanthine apparait limitée, que ce soit dans le cadre du suivi temporel réalisé à Carqueiranne en 2013 (**chapitre II**) ou du suivi spatio-temporel réalisé sur cinq sites en 2017 (**chapitre VI**). L'éventuelle implication de la fucoxanthine dans le contrôle de la quantité de bactéries à la surface de l'algue n'a pu être clairement mise en évidence par cytométrie en flux. Pour ce qui est de la structure de la communauté, l'effet direct réel de la fucoxanthine reste difficile à déterminer puisque les paramètres environnementaux potentiellement impliqués dans les variations de fucoxanthine à la surface de *T. atomaria*, tels que le cuivre et l'intensité lumineuse, peuvent aussi impacter directement la structure de la communauté épibactérienne.

4.3. Observation d'un phénomène de blanchissement chez *T. atomaria* : vers l'identification d'une éventuelle dysbiose médiée par l'augmentation de la température, l'abaissement des défenses chimiques de l'algue et la colonisation par des algues coralligènes ?

Les prélèvements des thalles de *T. atomaria* en juillet ont permis d'observer des zones blanchies accompagnées d'un certain nombre de macrophytes colonisant l'algue, notamment au niveau des zones apicales, à Carqueiranne et sur la côte sud de Porquerolles. Ces zones ont fait l'objet d'observations par microscopies numérique (microscope HIROX - KH-7700) et confocale (Zeiss Confocal LSM 510 Meta).

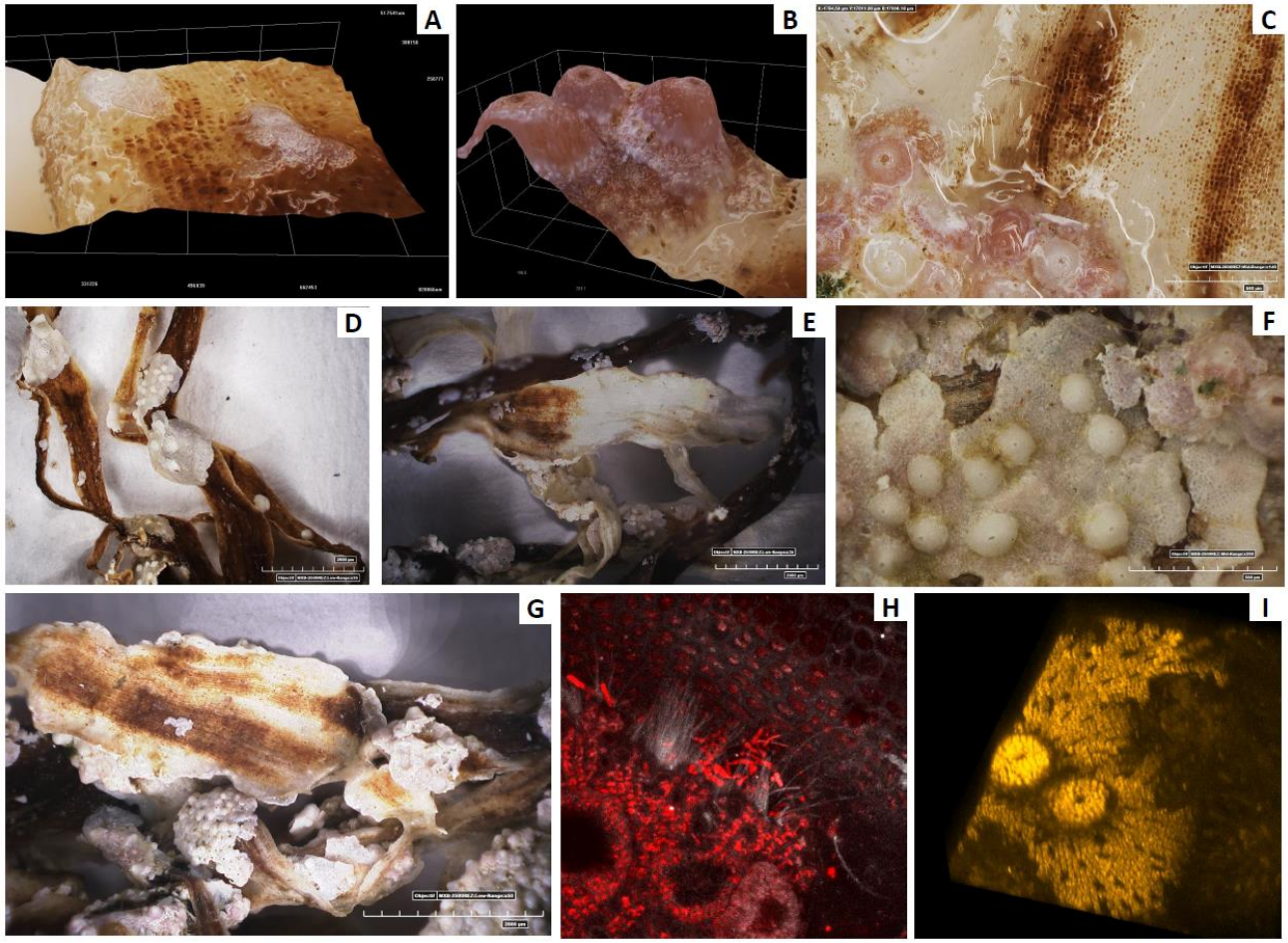

Figure VIII.3. Images 2D (**A**, **C**-**H**) et 3D (**B** et **I**) de thalles humides (**A**-**C**, **H** et **I**) et de thalles séchés (**D**-**G**) de *T. atomaria* obtenues par microscopie numérique (**A**-**F**) et par microscopie confocale (**H** et **I**) montrant des zones blanchies et/ou la présence d'algues coralligènes encroûtantes. Grossissements : **A** (×350), **B** et **C** (×140), **D** et **E** (x35), **F**, **H** et **I** (×200), et **G** (×50)

Sur les photos obtenues par microscopie numérique (**Figure VIII.3A**-**G**), on peut observer des zones « blanchies » avec des cellules de l'algue vidées de leur contenu cellulaire. Ces zones blanchies sont généralement observées à proximité de la présence de macrophytes épiphytes dont la morphologie permet de supposer qu'il s'agit d'algues calcaires encroûtantes (**Figure VIII.3D**, **F** et **G**). La structure morphologique de ces épiphytes a été observée en trois dimensions grâce aux microscopes numérique et confocal à balayage laser et a permis de révéler des formes coniques (**Figure VIII.3B** et **I**). Par comparaison avec d'autres études (Borges et al., 2014; Peña et al., 2014), ces structures ressemblent aux conceptacles d'algues coralligènes. Ces épiphytes ont été grattés spécifiquement afin d'extraire leur ADN. Le résultat du séquençage partiel du gène codant l'ARNr 18S (Illumina MiSeq, amorces 960F et NSR1438R ciblant la région V7) a permis d'observer que 84% des séquences étaient regroupées au sein d'un unique OTU affilié à l'ordre des Corallinales confirmant ainsi qu'il s'agit bien d'une algue rouge encroûtante (FROGS propose

une multi-affiliation au niveau des familles, c'est-à-dire que la séquence de cet OTU « blast » avec la même qualité pour plusieurs séquences affiliées à des familles différentes dans SILVA 132 : entre autre, les familles multi-affiliées correspondent à Mastophoraceae (avec le genre *Metamastophora*), et Corallinaceae (*Marginisporum*, *Corallina*, *Chiharaea*, *Bossiella* et *Arthrocardia*). La diversité et l'étude taxonomique allant de l'échelle de la famille à celle de l'espèce reste donc encore à élucider à l'aide d'autres marqueurs taxonomiques plus précis tel que le COI-5P dont l'efficacité a été montrée pour l'étude d'algues appartenant à cet ordre (Peña et al., 2014). Les genres *Hydrolithon* (Hydrolithaceae) ou *Melobesia* (Hapalidiaceae) pourraient par exemple correspondre à ce type d'épiphytes du fait des caractéristiques morphologiques de leur conceptacle mais aussi de leur écologie. En effet, ces algues sont retrouvées de manière ubiquiste sur diverses surfaces en mer Méditerranée, que ce soit sur des substrats rocheux, des algues ou des plantes aquatiques telles que les posidonies (Rindi et al., 2019).

Au cours de l'étude spatio-temporelle, la proportion de surface colonisée par ces épiphytes encroûtants a été estimée et montre en particulier une augmentation temporelle pour les sites S2 et S4 (respectivement Carqueiranne et la côte sud de Porquerolles) avec des pourcentages parmi les plus importants en juin et juillet (**Figure VIII.4**).

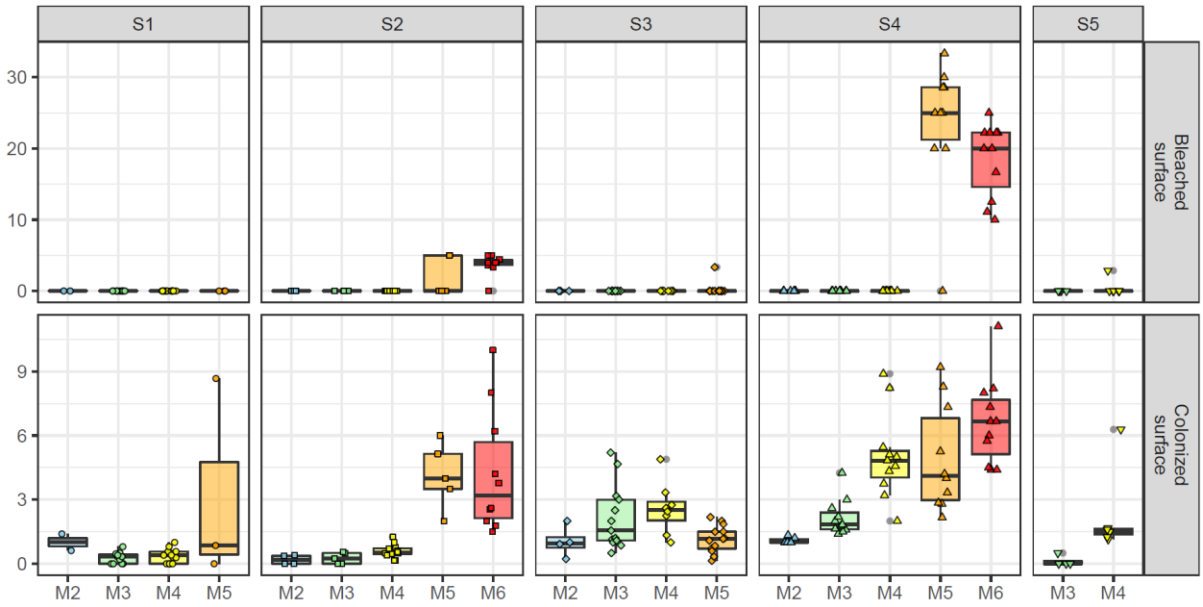

Figure VIII.4. Estimation de la proportion du thalle blanchie et colonisée par des macroalgues encroûtantes.

De manière similaire, les thalles présentant un phénomène de blanchissement ont été observés au niveau des site S2 mais surtout S4 avec des pourcentages de surfaces blanchies dépassant 20% en juin et

juillet. Il est aussi intéressant de noter que les parties les plus colonisées et les plus blanchies à ces deux périodes sont situées au niveau des zones apicales (**Figure VIII.5**).

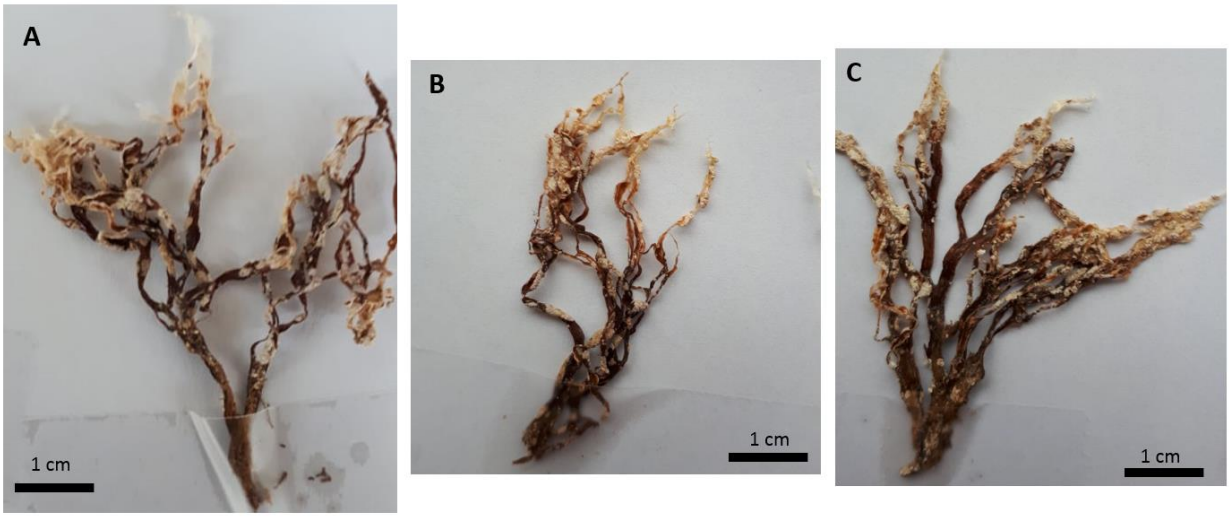

Figure VIII.5. Photographies des thalles séchés provenant du site S2 (Carqueiranne) (**A** et **B**) et du site S4 (côte sud de Porquerolles) (**C**) récoltées en Juillet.

L'apparition de macrophytes encroûtants à la surface des algues du genre *Taonia* pourrait potentiellement diminuer l'efficacité photosynthétique et provoquer ainsi un stress chez l'hôte, se traduisant par le blanchissement des tissus. De par l'augmentation de la colonisation en juin et juillet, il est possible que l'apparition de ces macrophytes encroûtant soit liée à l'augmentation de la température, mais aussi au shift concomitant du métabolome et/ou du microbiome de surface de l'algue. Bien que de telles corrélations soient observées, il est cependant important de noter que les liens de causalités suggérés restent encore à vérifier expérimentalement.

Les sesquiterpènes ainsi que le GGG correspondent aux principaux métabolites secondaires purifiés chez l'algue *T. atomaria* (De Rosa et al., 1994; Tringali et al., 1995; Othmani et al., 2016b; Jerković et al., 2019) via des approches dites « phytochimiques ». Les travaux d'Othmani et al., (2016a) ont permis de mettre en évidence des activités anti-adhésions pour le GGG et deux sesquiterpènes, le gleenol et le *trans*-calaménène, vis-à-vis de certaines souches bactériennes marines de référence. Par ailleurs, lors de cette étude le GGG est présenté comme l'un des métabolites majoritairement exprimés à la surface de *T. atomaria*. Au cours des différentes études menées dans le cadre de cette thèse, l'approche métabolomique a permis de mettre en évidence différents types de variations (temporelle, spatiale, intra-thalle) associées à certains de ces métabolites de surface. L'étude des variations intra-thalles du métabolome de surface de *T. atomaria* a ainsi révélé que des sesquiterpènes étaient majoritairement

exprimés au niveau des zones apicales de l'algue et a permis d'envisager l'importance de ces molécules potentiellement impliquée dans la défense chimique vis-à-vis de la protection spécifique de ces zones de croissance. Bien que la première étude préliminaire menée en 2013 sur le site de Carqueiranne **(chapitre II**) n'ait pas révélé de différences significatives dans les variations temporelles des sesquiterpènes et du GGG, l'étude spatio-temporelle de 2017, décrite dans le cadre du **chapitre VI**, a montré une diminution globale des sesquiterpènes (mis à part du péroxymuurolène) et des dérivés du GGG et ce, principalement au cours des deux derniers mois de prélèvement. Aucune corrélation claire n'est observée au sein des réseaux de corrélations entre ces métabolites et des paramètres environnementaux, cependant il est possible d'envisager que cette diminution tardive des sesquiterpènes et du GGG soit liée à l'augmentation de la température. En effet, dans le cas d'un sesquiterpène en particulier, le gleenol, l'étude en mésocosmes sur des spécimens de *T. atomaria* prélevés en Bretagne a permis d'observer que son expression était optimale à la surface de l'algue après deux semaines de conditionnement et dans les conditions de température et d'intensité lumineuse ambiantes. Pour ce même composé, en conservant les mêmes conditions d'intensité lumineuse mais en augmentant la température (+4°C), une diminution significative était observée après deux semaines. Ainsi, certains composés potentiellement impliqués dans la défense chimique de l'algue seraient impactés par une élévation de la température de l'eau. Ce sont donc les parties apicales pour lesquelles les défenses chimiques joueraient un rôle privilégié qui seraient les plus impactées par l'effet de l'augmentation de la température. De manière similaire à *D. pulchra* (Harder et al., 2012), la diminution locale de ces défenses pourrait engendrer l'apparition de certains microorganismes pathogènes ou de macroorganismes épiphytes, telles que des algues rouges encroûtantes, provoquant ainsi le phénomène de blanchissement de l'algue évoqué ci-dessus.

En outre, il a été également montré que certains mécanismes de communication (QS) utilisés par les bactéries pouvaient avoir un impact sur le recrutement des spores des macroalgues *Ulva* spp. (Tait et al., 2005; Wheeler et al., 2006). En effet, les auteurs ont observé que les spores étaient attirées par la présence de HSLs et que l'inactivation de ces molécules empêchait l'attraction des spores à la surface d'un biofilm bactérien (Tait et al., 2005). Par ailleurs, d'autre bactéries, dont *Pseudoalteromonas tunicata*, sont aussi connues pour présenter des activités liées à l'inhibition de la germination des spores de l'algue *Ulva lactuca* (Egan et al., 2001). Ces études laissent ainsi supposer que la structure de la communauté épibactérienne joue un rôle essentiel dans le recrutement ou non de certaines spores d'algues macrophytes à la surface de l'hôte algal. Une diminution des défenses de l'algue ciblant les taxa bactériens impliqués dans le recrutement de spores de macrophytes coralligènes pourrait donc, dans ce contexte, constituer un scenario envisageable.

5. Quid de la communauté microbienne eucaryote ?

A ce jour, très peu de travaux ont étudié le microbiote eucaryote associé à la surface des macroalgues (Lemay et al., 2018a; Liang et al., 2019; Wang et al., 2020). Cependant, du fait des interactions potentielles entre procaryotes et eucaryotes à la surface de l'hôte, ces travaux soulignent l'importance de combiner l'étude de ces deux communautés. Bien que l'objectif général de cette thèse concernait *T. atomaria* et ses procaryotes épiphytes, la communauté eucaryote associée a aussi été abordée (**annexe I**) (Ternon et al., 2020). Ces travaux ont permis d'observer la spécificité des communautés eucaryotes, notamment le dinoflagellé *Ostreopsis* cf. *ovata*, sur quatre macroalgues de la famille des Dictyotaceae : *T. atomaria*, *Dictyota dichotoma*, *Dictyota spiralis* et *Padina pavonica*. Plus précisément, l'objectif de cette étude était de comprendre le rôle potentiel de certains métabolites présents à la surface de ces macroalgues dans la colonisation par *O.* cf. *ovata*. Les données de dénombrement des microalgues au microscope optique et de metabarcoding ciblant le gène codant l'ARNr 18S (région V7, Illumina MiSeq) ont notamment pu montrer que la colonisation par *O.* cf. *ovata* était plus importante à la surface de *D. dichotoma* que sur celle des trois autres macroalgues. De manière plus globale, les différences de composition des communautés eucaryotes montrent une forte spécificité pour chaque hôte, laissant ainsi supposer que les différences relatives du métabolome de surface pourraient être impliquées dans ces différences de colonisation. Parmi les métabolites-clés impliqués dans les différences entre chaque algue, on observe notamment : (i) des diterpènes exprimés préférentiellement à la surface des deux *Dictyota* et (ii) le géranylgéranylglycérol quasi-exclusivement produit à la surface de *T. atomaria*. Cependant, des différences associées à la présence de prédateurs de microalgues tels que les copépodes, en lien ou non avec les métabolites produits à la surface des macroalgues, peuvent aussi constituer des facteurs cruciaux de la structuration des communautés de surface.

En accord avec les précédentes observations concernant la présence d'algues coralligènes sur *T. atomaria* (**Figure VIII.3** et **Figure VIII.5**), 10 OTUs appartenant à la famille des Corallinophycideae ont été identifiés préférentiellement dans les échantillons prélevés à la surface de *T. atomaria*, suggérant une colonisation spécifique de cette macroalgue. En lien avec les hypothèses citées précédemment, il pourrait être envisagé que les différences de colonisation par ces algues coralligènes, et donc de recrutement de ses spores, soient dues à un abaissement des métabolites de défenses à la surface ou encore à des communautés épibactériennes spécifiques.

6. Conceptualisation de la dynamique hôte-microbiote-environnement chez l'holobionte *T. atomaria*

Dans le cadre de l'holobionte algal étudié dans cette thèse, une tentative de conceptualisation globale de la dynamique de la relation tripartite entre l'hôte, son microbiote procaryote et l'environnement basée sur trois hypothèses non exclusives et probablement concomitantes est proposée.

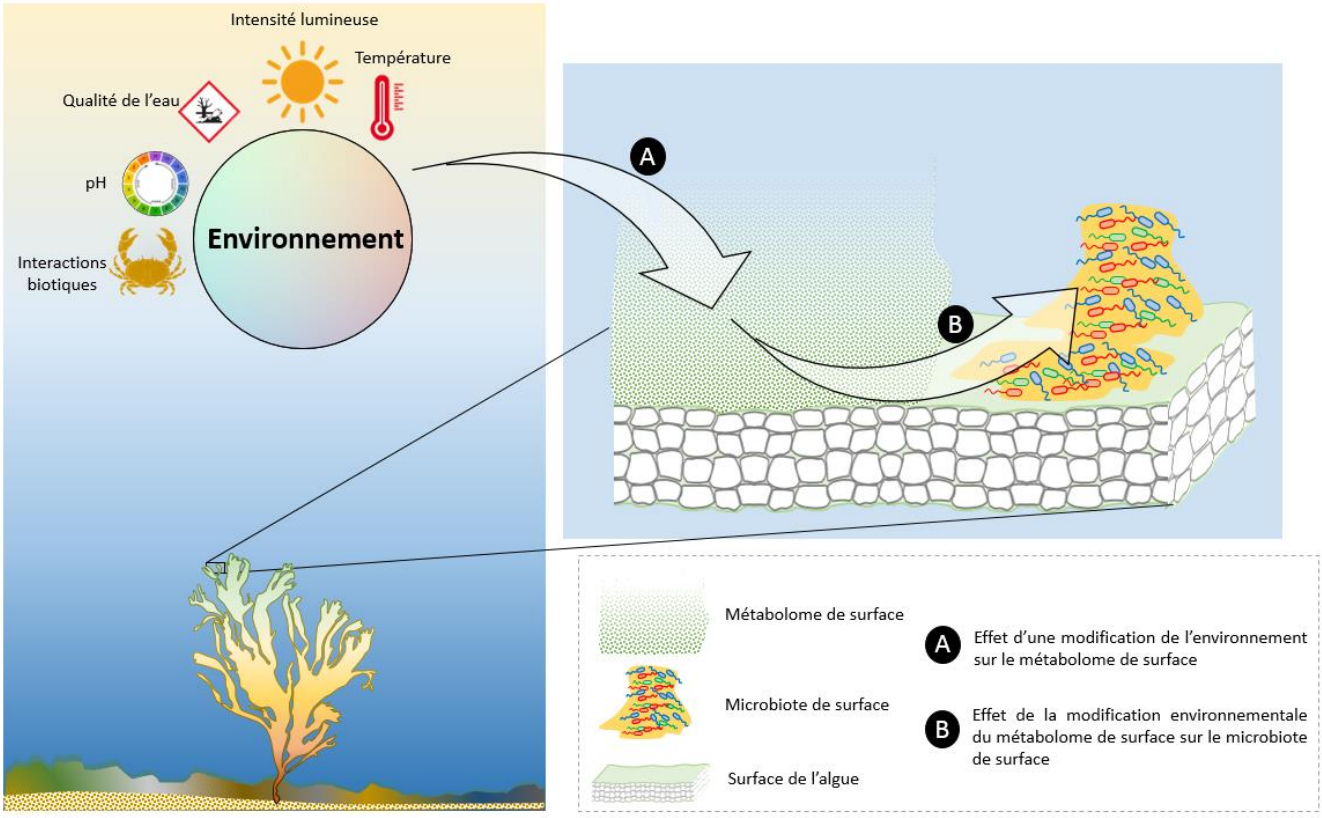

Figure VIII.6. Premier cas de figure : l'environnement impacte la physiologie de l'algue et donc d'abord son métabolome

Le premier processus implique que certains changements environnementaux induisent une modification physiologique chez l'algue, modifiant ainsi la composition de son métabolome de surface et impactant indirectement le microbiote de surface (**Figure VIII.6**). Par exemple, l'hypothèse que l'augmentation de l'intensité lumineuse induisait chez l'algue une augmentation de son activité photosynthétique et donc une surexpression de mannitol (étude en mésocosmes, **chapitre VII**) illustre ce mécanisme. En considérant que le mannitol constitue une source de carbone pour certaines bactéries, la surexpression de ce substrat par l'algue, notamment à sa surface, induirait potentiellement une modification de la diversité microbienne avec un enrichissement potentiel de taxa utilisant

préférentiellement cette source de carbone. De manière générale, il est bien établi que la production et la composition chimique des algues en oligosaccharides est dépendante de l'activité photosynthétique (Stiger-Pouvreau et al., 2016). Ainsi, une différence de composition en carbohydrates au niveau des parois cellulaires, en lien avec la qualité et l'intensité lumineuse, peut sensiblement modifier la structure de la communauté épibactérienne de par ses préférences en termes de source de carbone.

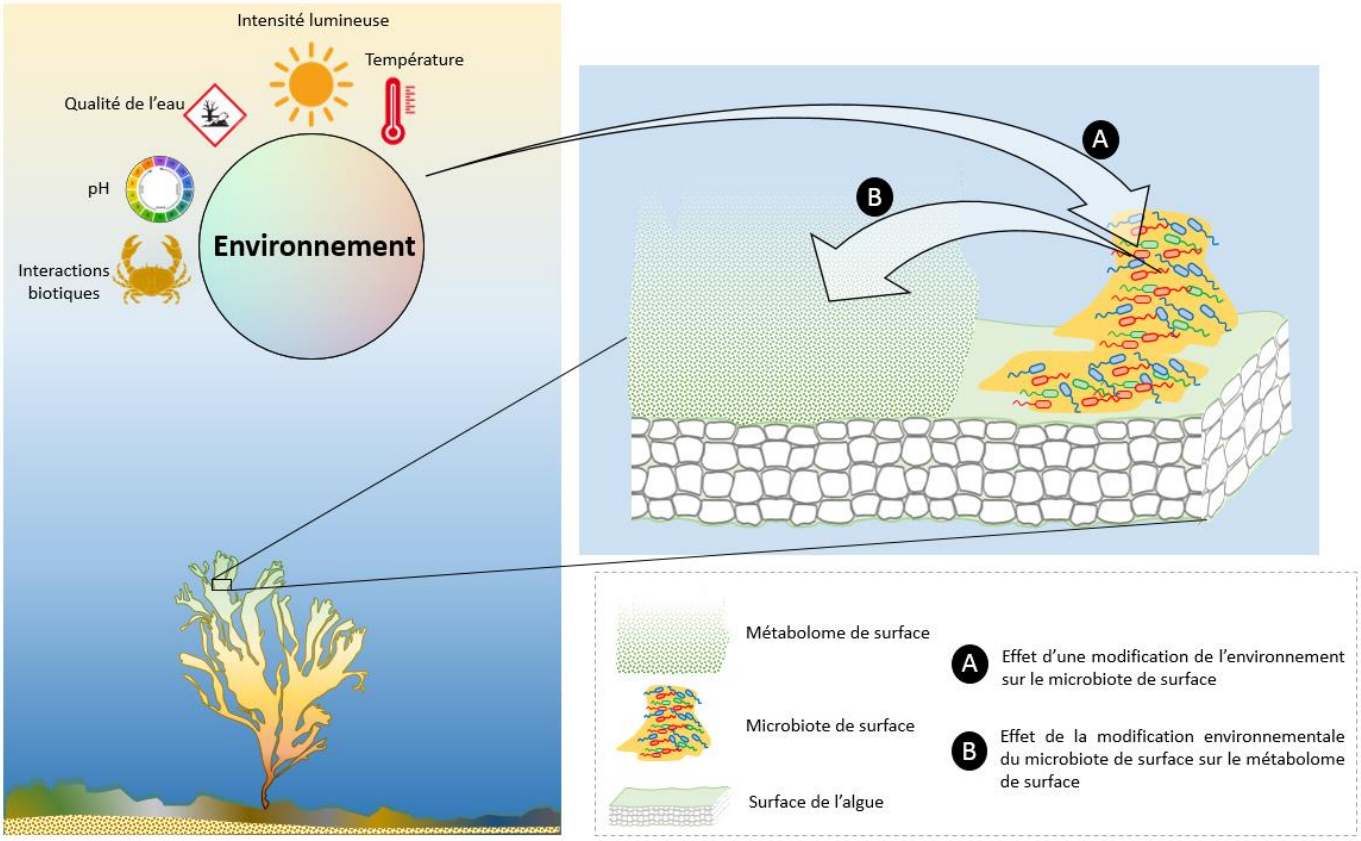

Figure VIII.7. Deuxième cas de figure : l'environnement impacte d'abord le microbiote

Pour le deuxième processus (**Figure VIII.7**), l'environnement affecterait directement le microbiote et la modification de la structure des communautés épiphytes induirait alors un changement physiologique chez l'algue. Ce changement physiologique peut correspondre à deux scenarii différents : (i) l'algue est impactée négativement par la modification environnementale du microbiote, pouvant aboutir par exemple à une dysbiose, (ii) l'algue s'adapte à son nouveau microbiote et modifie ses interactions à sa surface, que ce soit pour se défendre contre le développement de pathogènes, ou développer des interactions positives suite à la colonisation de sa surface par des bactéries mutualistes.

Le premier scénario peut être illustré en prenant pour exemple les travaux de Rohde et al., (2008). Ces derniers ont pu montrer que l'eutrophisation de la colonne d'eau constitue un facteur favorisant la

colonisation des épibiontes à la surface de *F. vesiculosus*. La présence d'algues filamenteuses (*Enteromorpha* sp., *Ceramium* sp.), de polychaetes (*Polydora* sp.) ou de balanes (*Balanus improvisus*) réduit alors l'intensité lumineuse accessible pour l'algue. Ce phénomène est notamment observé en profondeur ou l'intensité lumineuse est plus basse, ce qui limite la croissance de l'hôte. La limite de profondeur à laquelle *F. vesiculosus* peut se développer se situe ainsi entre 4 et 6m sur le site étudié (Kiel, mer Baltique).

Le second scénario suppose la présence de mécanismes moléculaires chez l'algue qui seraient adaptés à la présence ou l'action de bactéries spécifiques, elles-mêmes étant favorisées dans certaines conditions environnementales. Plusieurs études illustrent l'induction de mécanismes de défense associée à la dégradation de la paroi de l'algue (Potin et al., 1999; Weinberger et al., 1999; Weinberger, 2007). En effet, il a été montré chez l'agarophyte *Gracilaria conferta* qu'un « *burst* » oxydatif est déclenché lorsque l'algue détecte la présence d'oligosaccharides (Weinberger et al., 1999; Weinberger and Friedlander, 2000). La présence de tels composés est induite par l'action de bactéries dégradant les polysaccharides pariétaux de l'algue ; la réponse oxydative de l'algue a alors pour vocation d'induire leur élimination. Ce mécanisme d'immunité est aussi retrouvé de manière similaire chez d'autres modèles, notamment *Laminaria digitata*, *Saccharina latissima*, *Macrocystis pyrifera*, *Lessonia nigrescens* et *Saccorhiza polyschides* (Küpper et al., 2001, 2002a).

Enfin, le troisième processus (**Figure VIII.8**) correspond à un scenario pour lequel les paramètres environnementaux agissent directement à la fois sur l'hôte et sur son microbiote. En outre, à la suite de ces changements, une seconde réponse d'un des deux compartiments (microbiome ou métabolome), donc indirecte, peut également survenir. Ce cas est notamment illustré dans la littérature avec le modèle *D. pulchra* pour lequel l'augmentation de la température induirait une diminution des défenses chimiques de l'algue via la diminution de la production en furanones halogénées, mais aussi l'activation de facteur de virulence chez d'autres bactéries (Campbell et al., 2011, 2014; Case et al., 2011; Zozaya-Valdés et al., 2016, 2017). Par conséquent, ces deux phénomènes constituent deux facteurs propices au développement ultérieur de bactéries pathogènes opportunistes causant la dégradation de la paroi et de la membrane algales et induisant par la suite le blanchissement des tissus.

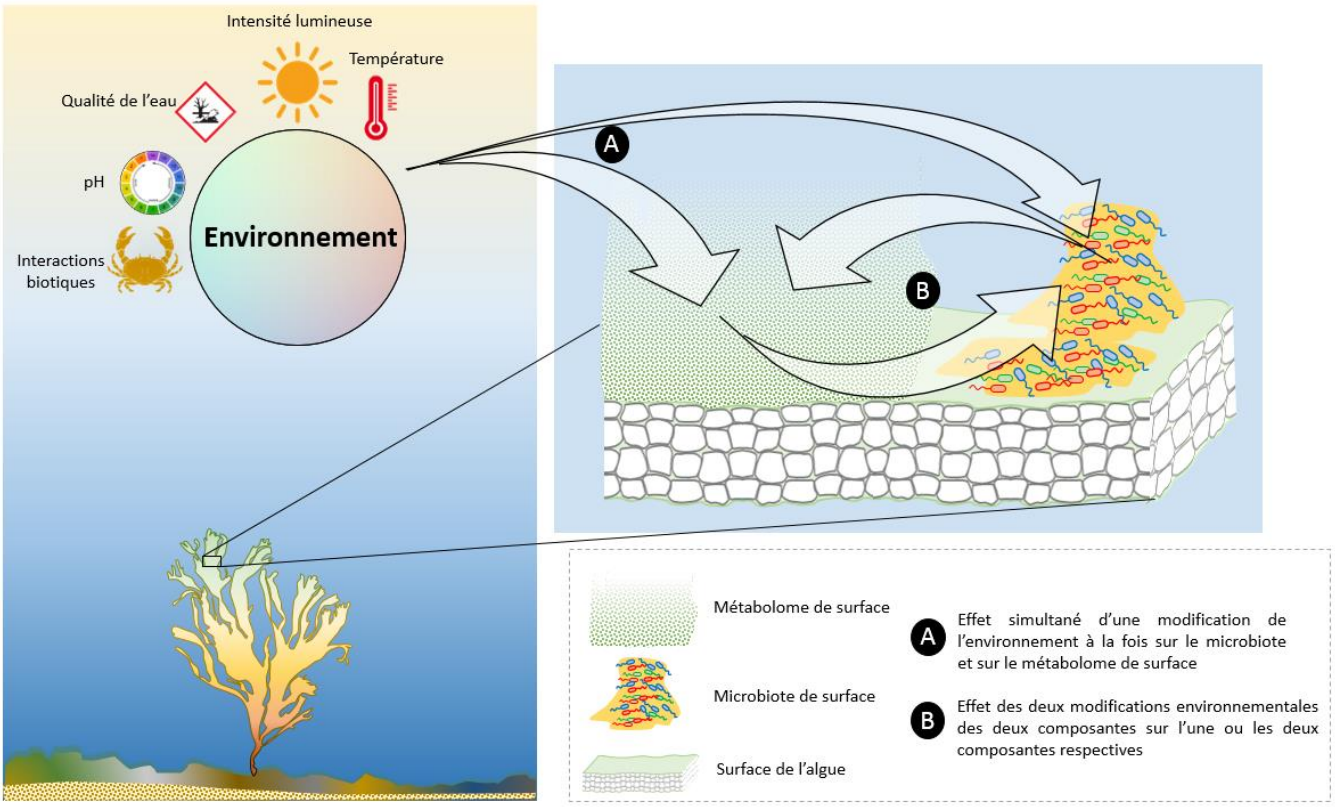

Figure VIII.8. Troisième cas de figure : l'environnement impacte simultanément l'algue et le microbiote

Ce scénario pourrait aussi expliquer l'effet du cuivre sur la communauté épibactérienne de *T. atomaria* (**chapitre VI**). En effet, il est possible d'envisager que l'adaptation métabolique de l'algue avec la sur-expression en caroténoïdes, en réponse à un stress oxydatif dû à la présence importante de cuivre dans l'environnement, puisse aussi constituer un facteur de sélection supplémentaire pour les bactéries. Ainsi, les taxa sélectionnés dans ces conditions seraient à la fois adaptés directement à la présence de cuivre et à la présence de la fucoxanthine sur-exprimée à la surface de l'algue.

CONCLUSION GENERALE ET PERSPECTIVES

Vue depuis l'un des laboratoires d'accueil de la Station Biologique de Roscoff

1. Conclusions

L'objectif général de cette thèse a été de comprendre comment variait la structure et la spécificité de la communauté bactérienne du microbiote de surface de *T. atomaria* en lien avec les variations de la production métabolique de surface de l'hôte et quelle était l'influence de l'environnement sur ces variations qui affectent et façonnent l'holobionte.

Un tel objectif a nécessité le développement initial d'une approche originale, employée pour l'ensemble de ces travaux, capable de coupler l'étude de la communauté des procaryotes épiphytes de *T. atomaria* (par metabarcoding) à celle des métabolites présents à sa surface (par métabolomique non-ciblée). Cette approche combinant écologie microbienne et chimique avec des analyses multi-omiques a constitué une gageure car, outre le fait que son emploi n'avait été que très rarement reporté dans la littérature en général, ce type de couplage n'avait jamais été appliqué auparavant à l'étude de macroalgues holobiontes. Plus particulièrement, l'intégration des différents jeux de données expérimentaux via des analyses statistiques multi-omiques a constitué une partie exploratoire et particulièrement innovante des travaux décrits dans ce manuscrit. Les résultats ainsi obtenus ont conduit à mettre en lumière de potentielles relations entre les variations du microbiote et celles du métabolome de surface de *T. atomaria* et ce, en lien avec des paramètres environnementaux tels que la température de l'eau, l'intensité lumineuse ou la pollution métallique.

La première étape de cette thèse a consisté à analyser les résultats d'une étude préliminaire portant sur les variations temporelles du microbiote et du métabolome de surface d'échantillons de *T. atomaria* prélevés en un site (Carqueiranne, Var) durant toute la période de présence de l'algue (février à juillet). En couplant les deux jeux de données, nous avons révélé d'importantes covariations entre le métabolome et le microbiote à la surface de l'algue, principalement lors de la période printanière et estivale. L'analyse par réseaux a alors suggéré qu'une dynamique globale s'effectuait à l'échelle de l'holobionte en relation avec l'environnement. Cette étude a ainsi permis de poser un certain nombre de questions et d'objectifs concernant non seulement la méthodologie employée mais également la compréhension des interactions à l'échelle de l'holobionte algal

Étant donné que l'identification des métabolites constitue une étape cruciale -et souvent limitante dans le cas d'organisme non-modèle tels que *T. atomaria*- en métabolomique, il a été tout d'abord essentiel d'optimiser une méthodologie permettant d'annoter de manière exhaustive le métabolome de l'algue. Dans ce contexte, l'élaboration d'une banque de données permettant d'identifier rapidement les métabolites d'intérêt pour la suite de la thèse a été entreprise. Le couplage des approches phytochimique

(par purification des composés) et par réseaux moléculaire s'est avéré extrêmement performant et a permis d'annoter une grande diversité de lipides, dont certaines familles encore jamais décrites dans la littérature.

Un autre objectif méthodologique destiné à l'analyse métabolomique a été de pouvoir déterminer dans quelle mesure une meilleure couverture du métabolome était possible via une approche analytique multi-plateformes. Des profilages chimiques par LC-ESI-(+)-MS, LC-(-)-ESI-MS et GC-MS ont montré un bonne complémentarité du fait de la vaste chimiodiversité présente dans les échantillons étudiés. Néanmoins, les analyses réalisées par LC-ESI-(+)-MS se sont révélées être les plus adaptées car elles ont permis de considérer une large gamme de métabolites en englobant à la fois une grande variété de glycérolipides ainsi que des terpènes, et notamment des sesquiterpènes.

Par ailleurs, étant donné que l'ensemble des analyses réalisées jusqu'alors ont porté sur la totalité du thalle, un autre objectif a été de déterminer à l'échelle d'un individu de *T. atomaria* : quelles étaient les variations du métabolome et des communautés épibactériennes et quels étaient les liens unissant ces deux jeux de données. L'étude de la variabilité intra-thalle a alors permis d'observer une différentiation progressive entre la base et l'apex aussi bien pour le métabolome que pour le microbiote de surface et que la croissance de l'algue pouvait expliquer en partie une telle variabilité. En effet, des composés de défense (sesquiterpènes) ont été déterminés comme étant majoritairement exprimés au niveau des zones de croissance (zones apicales) tandis qu'une communauté de procaryotes épiphytes plus dense, mais également plus diversifiée et moins spécifique, a été caractérisée au niveau des zones basales, c'est-à-dire les plus matures, des thalles de *T. atomaria*.

Une étude biogéographique à grande échelle intégrant vingt sites le long des côtes méditerranéennes françaises et un site situé au nord de la Bretagne a permis d'évaluer l'importance respective de la phylogénie de l'hôte et de l'environnement sur d'éventuelles différences de microbiote et de métabolome à la surface de *T. atomaria*. De fortes différences en termes de microbiote, de métabolome et de phylogénie ont ainsi été observées entre les échantillons méditerranéens et bretons, suggérant que l'environnement et la phylogénie étaient deux paramètres potentiellement impliqués dans une telle dissimilarité intraspécifique.

Un suivi spatio-temporel a ensuite été conduit sur cinq sites contrastés de l'aire toulonnaise (incluant le Parc national de Port-Cros) afin de mieux appréhender l'effet des paramètres environnementaux impliquées dans les interactions entre l'hôte algal et son microbiote et de déterminer la spécificité du microbiote algal. Les communautés épiphytes de l'algue sont apparues ainsi très largement distinctes de

celles de substrats rocheux et de l'eau de mer environnante, soulignant la spécificité du microbiote à la surface de *T. atomaria*. Par exemple, certains taxa ont été observés préférentiellement à la surface de l'algue, tels que *Granulosicoccus* et *Litorimonas*, et représentent par ailleurs des colonisateurs pionniers. Confirmant l'importante covariation temporelle déjà observée, cette étude a montré en outre que la température et la contamination en cuivre constituent les principaux paramètres explicatifs associés aux variations spatiales et temporelles du microbiote et du métabolome de surface de *T. atomaria*. En particulier, une augmentation de la production de fucoxanthine à la surface de l'algue en conditions de fortes concentrations en cuivre dans le milieu constituerait une adaptation de *T. atomaria* contre le stress oxydatif induit par le cuivre qui impacterait ainsi directement et indirectement sa communauté épiphytique.

Enfin, une dernière question induite par l'étude précédente s'est focalisée sur l'effet spécifique des variations de la température et de l'intensité lumineuse vis-à-vis du microbiote et du métabolome de surface de *T. atomaria*. Ces deux facteurs environnementaux co-varient généralement *in situ* ce qui rend difficile la détermination de leur rôle respectif. Cette étude menée en mésocosmes en conditions contrôlées a révélé que ces deux paramètres pouvaient impacter à la fois le microbiote et le métabolome mais avec des cinétiques de réponses différentes. En effet, la température a initialement impacté le microbiote tandis que les variations du métabolome de surface étaient d'abord dues aux variations d'intensité lumineuse. Des effets indirects ont par ailleurs été proposés, avec par exemple une augmentation de l'intensité lumineuse pouvant induire une production plus importante de DMSP à la surface de l'algue. La présence de cet osmolyte pourrait alors favoriser certains taxa bactériens adaptés et connus pour leurs fonctions associées à son catabolisme (e.g. *Jannaschia*).

De manière générale, l'ensemble de ce travail de thèse a permis d'observer dans différentes conditions de fortes similarités au niveau des variations du métabolome de surface de l'algue et de son microbiote. De telles covariations ont permis alors de suggérer un certain nombre d'interaction hôte-microbiote en lien étroit avec l'environnement (avec notamment la température, l'intensité lumineuse et la contamination en cuivre), mais aussi la phylogénie et la croissance de l'algue. Dans un contexte de fortes pressions anthropiques sur l'environnement, ces éléments constituent donc des paramètres essentiels pour la compréhension de l'évolution et l'adaptation des interactions à l'échelle de l'holobionte, et s'inscrivent alors dans un contexte plus global visant à mieux comprendre la dynamique des écosystèmes marins face à de tels changements.

2. Perspectives

Afin de poursuivre l'étude de *T. atomaria* en tant que modèle d'algue holobionte, diverses perspectives peuvent être envisagées avec notamment deux axes prometteurs.

Une première étape pourrait consister à étudier de façon plus approfondie le blanchissement de *T. atomaria* observé sur certains sites en mer Méditerranée lors de la période estivale, et notamment à estimer le rôle du microbiote dans l'induction d'un tel phénomène. Diverses hypothèses pourraient être testées : (i) le développement de bactéries pathogènes opportunistes provoquerait le blanchissement, ce qui a été observé chez d'autres algues et (ii) le développement de certaines bactéries permettrait le recrutement de spores de macroalgues coralligènes encroûtantes qui induisent par la suite le blanchissement de *T. atomaria*. Ainsi, une perspective intéressante serait d'étudier certaines souches bactériennes isolées à partir des zones blanchies de l'algue et d'identifier par génomique, transcriptomique ou par RT-qPCR l'expression de facteurs de virulence. Le développement méthodologique d'une approche culturale permettant d'isoler des souches représentatives de la communauté épiphyte des zones blanchies constituerait alors une première étape de cette analyse. Par ailleurs, il est très probable que le blanchissement de l'algue soit lié à certains facteurs environnementaux, notamment l'augmentation de la température. Dans un contexte où les vagues de chaleurs marines constituent des évènements de plus en plus fréquents et intenses, il serait intéressant d'étudier expérimentalement l'effet d'une augmentation de la température sur le blanchissement de l'algue en mer Méditerranée, mais aussi la résilience de l'holobionte dans le cadre d'un retour aux conditions normales.

Une deuxième perspective porterait sur le rôle fonctionnel des polysaccharides de l'algue. D'autres méthodes analytiques seraient alors nécessaires pour caractériser cette chimiodiversité, puisque seuls les composés de faibles masses moléculaires sont généralement analysés en métabolomique. Une première étape consisterait alors à caractériser la composition en polysaccharides de la paroi algale ou plus largement à la surface de l'algue, à l'aide de protocoles d'extraction spécifiques et de méthodes analytiques adaptées (IR-TF, Pyr-GC-MS, MALDI… ou autres). L'étude de la modification de la composition en polysaccharides en fonction des différentes conditions environnementales et de la variation du microbiote pourrait ainsi fournir des hypothèses quant aux rôles écologiques de ces biopolymères à l'échelle de l'holobionte. De manière complémentaire, la recherche de voies de dégradation spécifiques des polysaccharides chez *T. atomaria* pourrait s'avérer très intéressante, via une étude de génomique/transcriptomique de certaines souches isolées (notamment parmi les bactéries pionnières qui

s'avèrent particulièrement spécifiques à la niche algale) ou encore de métagénomique/métatranscriptomique sur l'ensemble de la communauté.

ANNEXE I : FOCUS SUR *OSTREOPSIS* CF. *OVATA*

1. Avant-propos

Cette étude a été conduite sur quatre Dictyotacées prélevées à Villefrance-sur-Mer (*Taonia atomaria, Padina pavonica*, *Dictyota dichotoma* et *Dictyota spiralis*) où des proliférations du dinoflagellé toxique *Ostreopsis* cf. *ovata* sont observées régulièrement. L'étude avait alors pour objectif de déterminer si la colonisation par O. *cf*. ovata à la surface de ces macroalgues pouvait être influencée par la production métabolique de surface de ces Dictyotacées.

Cette étude est présentée sous la forme d'un article de recherche accepté et en cours de parution dans la revue *Frontiers in Marine Science* [Ternon et al., (2020). *Front. Mar. Sci*. *In press*]. Les références bibliographiques citées dans cet article sont indexées en fin de manuscrit. La partie *Supplementary Information* de cet article est presentée dans l'annexe VIII du manuscrit (annexe électronique).

2. Article: Exploring the role of macroalgal surface metabolites on the settlement of the benthic dinoflagellate *Ostreopsis* cf. *ovata*.

Eva Ternon[a,b,c *ǂ], Benoît Paix[d ǂ], Olivier P. Thomas[e], Jean-François Briand[d], Gérald Culioli [d*]

[ǂ] These authors contributed equally contributed to this work

a. Université Côte d'Azur, CNRS, OCA, IRD, Géoazur, 250 rue Albert Einstein, 06560 Valbonne, France, eva.ternon@imev-mer.fr (* corresponding author)

b. Sorbonne Universités, CNRS UMR7093, Laboratoire d'Océanographie de Villefranche, 06234 Villefranche-sur-Mer, France

c. Center for Marine Biotechnology and Biomedicine, Scripps Institution of Oceanography, University of California San Diego, La Jolla, CA, 92093, United States

d. Université de Toulon, Laboratoire MAPIEM, EA 4323, Toulon, France., paix@univ-tln.fr, briand@univ-tln.fr, culioli@univ-tln.fr (* corresponding author)

e. Marine Biodiscovery, School of Chemistry and Ryan Institute, National University of Ireland Galway (NUI Galway), University Road, H91 TK33 Galway, Ireland, olivier.thomas@nuigalway.ie

Keywords: *Ostreopsis* cf. *ovata*, Dictyotaceae, surface colonization, metabolomics, metabarcoding, eukaryotes, biofilms.

2.1. Abstract

Macroalgae constitute one of the preferred substrates of the benthic dinoflagellate *Ostreopsis* cf. *ovata*. Across the Mediterranean Sea, this toxic microalga has been shown to thrive on the surface of various species of macroalgae, including Chlorophyta, Rhodophyta and Phaeophyceae. Interestingly, some Dictyotaceae are characterized by a low abundance of cells of *O.* cf. *ovata* on their surface. Based on the antifouling properties of some specialized metabolites produced by seaweeds, macroalgal metabolites have been proposed to contribute to the settlement and development of *O*. cf. *ovata*. To address this question, the composition of the surface of four Dictyotaceae, *Dictyota dichotoma*, *Dictyota spiralis*, *Taonia atomaria* and *Padina pavonica* was investigated through an integrative approach combining the analysis of their eukaryotic diversity (18S rRNA gene metabarcoding), their surface metabolome (untargeted LC-MS-based metabolomics) as well as the bioactivity of their surface extracts on *O.* cf. *ovata*. Altogether, the data suggest an influence of the macroalgal surface chemistry on the growth of the dinoflagellate, with *D. dichotoma* being the most bioactive. Some metabolites are proposed to be involved in the observed bioactivity. Other biotic factors are also likely to be entailed in the control of the *O*. cf. *ovata* population and they may even prevail on the influence of the macroalgal surface chemistry.

2.2. Introduction

Recurrent outbreaks of the toxic dinoflagellate *Ostreopsis* cf. *ovata* have been reported over the past 15 years in Mediterranean coastal waters (Ciminiello et al., 2006; Mangialajo et al., 2011). Despite recent research efforts (reviewed in Pistocchi et al., 2011; Carnicer et al., 2015), the abiotic factors fostering the proliferation of this species remain unclear (Cohu et al., 2011; Meroni et al., 2018) although high temperature, low hydrodynamic conditions seem to constitute a pre-requisite (Totti et al., 2010; Pezzolesi et al., 2012; Meroni et al., 2018). *O.* cf. *ovata* is a benthic species that colonizes a variety of substrates, including macrophytes (Totti et al., 2010; Mangialajo et al., 2011). The surface of these seaweeds can constitute an ideal microenvironment for the growth of highly diverse prokaryotic and eukaryotic communities, including benthic microalgae. While the interactions between bacteria and macroalgae have been investigated to some extent during the past decades (Egan et al., 2013; Hollants et al., 2013), less information has been provided about the drivers guiding the settlement of microalgae on the surface of macroalgae.

O. cf. *ovata* has been shown to thrive on the surface of various species of macroalgae across the Mediterranean Sea, including Chlorophyta (Battocchi et al., 2010; Accoroni et al., 2015; Hosny and Labib, 2019), Rhodophyta (Vila et al., 2001; Battocchi et al., 2010; Cohu et al., 2013; Blanfuné et al., 2015; Gémin et al., 2019; Hosny and Labib, 2019) and Phaeophyceae (Vila et al., 2001; Battocchi et al., 2010; Cohu et al., 2013; Blanfuné et al., 2015; Gémin et al., 2019; Hosny and Labib, 2019), without any clear species preference. Remarkably, some Phaeophyceae of the family Dictyotaceae are usually characterized by a low abundance of *O*. cf. *ovata* as for instance *Taonia atomaria*, *Dictyota fasciola* or *Padina pavonica* (Blanfuné et al., 2015; Gémin et al., 2019; Hosny and Labib, 2019). The antifouling properties of some specialized metabolites produced by Dictyotaceae have been proposed to drive the settlement and development of *O*. cf. *ovata* (Cohu et al., 2013; Blanfuné et al., 2015; Gémin et al., 2019). Approaches in chemical ecology have revealed that metabolites produced by macroalgae can be detrimental or beneficial to the settlement of bacteria and microalgae (Hellio et al., 2002; Goecke et al., 2010; Wichard and Beemelmanns, 2018). In particular, several metabolites produced by species of the family Dictyotaceae have been shown to inhibit the growth of bacteria (*e.g.* dictyol C and fucoxanthin; Salvador Soler et al., 2007; Viano et al., 2009), microalgae (*e.g.* dictyolactone and sanadaol; Kim et al., 2006), bryozoan (*e.g.* dictyol E, pachydictyol A, dictyodial; Schmitt et al., 1998) and various other benthic species (*e.g.* diterpenoids, gleenol and geranylgeranylglycerol; Bianco et al., 2009; Othmani et al., 2016b).

To the best of our knowledge, only one study has investigated the effect of the metabolites from brown, red and green macroalgae (*Dictyota dichotoma*, *Rhodymenia pseudopalmata* and *Ulva rigida*, respectively) on the growth of the dinoflagellate *O*. cf. *ovata* (Accoroni et al., 2015). The exposure to dried algal cells, fresh thalli and dissolved metabolites of *D. dichotoma* caused an intense stress to *O.* cf. *ovata* cells yielding to growth inhibition as well as formation of double-walled cysts. Conversely, this inhibiting activity of *D. dichotoma* metabolites on the toxic dinoflagellate does not mirror the frequent development of *O*. cf. *ovata* on *D. dichotoma* observed in previous studies performed in the NW Mediterranean Sea (Cohu et al., 2013; Blanfuné et al., 2015; Gémin et al., 2019). Following common practices in the chemical ecology of macroalgae (Puglisi et al., 2014), the authors used whole-cell macroalgal extracts which are not representative of real ecological situations occurring at the surface of macroalgae. Therefore, the influence of the surface metabolome of brown algae on the growth and settlement of *O*. cf. *ovata* remains largely to be assessed. Results of such studies will provide valuable information on the pattern of colonization of this toxic dinoflagellate along the NW Mediterranean shoreline that leads to ecological (Gorbi et al., 2013; Giussani et al., 2016; Pavaux et al., 2019) and health (Ciminiello et al., 2006; Casabianca et al., 2013) concerns.

The epiphytic community colonizing the surface of macroalgae is not only expected to contribute to the surface metabolome but also to directly interact with *O.* cf. *ovata*, adding another level of complexity to its settlement preferences. Among co-occurring species on surfaces colonized by *O*. cf. *ovata*, *Roseobacter* bacteria (Vanucci et al., 2016; Guidi et al., 2018), diatoms of the genera *Licmophora*, *Navicula* and *Amphora*, and the dinoflagellates *Prorocentrum lima*, *Amphidinium caetera* and *Coolia monotis* (Accoroni et al., 2015; Marro et al., 2019; Pavaux et al., 2019) have been reported to be the most abundant. Recent evidences of chemically-mediated interactions between microalgae and their predators (Ianora et al., 2004; Selander et al., 2015), competitors (Tillmann and Hansen, 2009; Poulson-Ellestad et al., 2014; Ternon et al., 2018) and the bacterial community (Wichard and Beemelmanns, 2018 and references therein) suggest that biotic interactions within members of the epiphytic community may also influence the settlement of *O.* cf. *ovata* on macroalgal surfaces.

This study aims to investigate the influence of the surface metabolome of four brown algae of the Dictyotaceae family (*Taonia atomaria*, *Padina pavonica*, *Dictyota dichotoma* and *Dictyota spiralis*) on the settlement of the toxic dinoflagellate *O.* cf. *ovata* in the NW Mediterranean. An integrative approach was used to investigate both the chemical and eukaryotic compositions at the surface of each algal species combining untargeted LC-MS-based metabolomics and high throughput sequencing (18S rRNA Illumina

MiSeq sequencing), respectively. Applications of dedicated experimental protocols allowed the selective extraction of the surface metabolites of each algal species (Othmani et al., 2016a) and the activity of these extracts were further tested on monocultures of the toxic dinoflagellate.

2.3. Materials and methods

Field sampling was performed at 9 a.m. on the 7th of July 2017 during an *O.* cf. *ovata* bloom at the Rochambeau site in the bay of Villefranche-sur-Mer (France, Ligurian Sea; 43°41'34.83" N, 7°18'31.66" E) known for the recurrence of such events (Cohu et al., 2013; Jauzein et al., 2018; Gémin et al., 2019). The seawater temperature and salinity were 23.9 °C and 39, respectively, at the time of the collection. Thirteen specimens of each macroalgal species (*D. dichotoma*, *D. spiralis*, *P. pavonica* and *T. atomaria*) were collected at 0.5m depth by snorkeling. The collection of the macroalgae followed the protocol recommended by Totti et al., (2010) and consisted in holding specimens of each species with zip bags avoiding any agitation of the surrounding seawater and resuspension of benthic cells, followed by a careful removing of their holdfast from the rocky substrate using tweezers. All zip bags containing macroalgae specimens and surrounding seawater were immediately closed underwater and processed in the lab the same morning using: (i) four specimens of each species to measure the abundance of *O.* cf. *ovata* and diatoms at the algal surface, (ii) six specimens of each species to extract the surface and the whole macroalgal metabolomes, and (iii) three specimens of each species for the analysis of epiphytic eukaryotic communities through 18S rRNA gene high-throughput sequencing. After sampling for macroalgae, a volume of 1L of seawater was also collected from the water column at the sampling site for 18S rRNA gene high-throughput sequencing.

2.3.1. Microalgal cell abundance at the surface of the macroalgae

Four specimens of each macroalga were transferred from their zip bag to 15 mL Falcon tubes filled with 4 mL of filtered seawater (0.2 μm) and 150 μL of acidic Lugol's iodine solution. The tubes were vigorously shaken and then vortexed during 5s to remove epiphytes. Supernatants were kept in the Falcon tubes while the macroalgal thalli were removed with tweezers and air-dried on a filter paper. No pre-filtration of the supernatant was needed (Totti et al., 2010) as sediments were not abundant. Pictures of the macroalgae were taken to further estimate their surface area using the Mesurim® software and to allow the expression of the cell abundance in cell cm^{-2}. Epiphytic cell abundances in the rinsed water were determined in a 1 mL volume Sedgwick Rafter counting chamber under an inverted phase contrast microscope (Zeiss Axiovert 40C) at a magnification of ×40. Identification of dinoflagellates and diatoms was performed using data from the literature (Bertalot et al., 2000; Horiguchi, 2014, respectively).

2.3.2. Chemical extraction and analysis of macroalgal samples

The surface metabolome of the four seaweed species was investigated on six replicates by a dipping method previously developed for *T. atomaria* (Othmani et al., 2016a) that caused no disruption of its membranes. *P. pavonica* is expected to have similar membrane strength as its surface is calcified (Benita et al., 2018). The integrity of the cell walls of the two softer *Dictyota* species was confirmed after soaking using an optical microscope. Briefly, Surface Extracts (SEs) were obtained by soaking each algal thallus during 5s in an 8 mL glass vial filled with 5 mL of methanol (MeOH). The Total Extracts (TEs) were obtained by soaking each thallus in 7 mL of MeOH during 18h. Both resulting extracts (SEs and TEs) were concentrated under reduced pressure and stored at −20°C until analyses and bioassays. The approximate extracted surface area of each thallus was measured therefore leading to an estimation of the amount of extracts per cm² of macroalga (**Table AI.1**).

Species	Natural concentration		Tested concentration		Macroalgal surface	
	Mean	stdv	Concentration	Enrichment factor	Mean	stdv
	mg cm^{-2}		mg cm^{-2}		cm²	
Taonia atomaria	0.5	0.1	2.5	5	7.4	1.8
Padina pavonica	0.9	0.3	3.5	4	7.3	2.3
Dictyota dichotoma	0.8	0.2	1.0	1	2.5	1.8
Dictyota spiralis	0.7	0.1	2.0	3	6.0	2.3

Table AI.1. Mean concentration (mg.cm^{-2}) of the SEs obtained from each macroalgal species given with the mean surface area measured for each species (n = 4). The concentration of the SEs tested in the bioassays is also given together with an estimation of the enrichment factors compared to natural concentrations. The enrichment factor was calculated as follow: $Enrichment\ factor = Concentration(\frac{tested}{natural})$.

2.3.3. DNA extraction and amplification of the epiphytic communities

The epiphytic microbiota was sampled using a sterile scalpel, introduced into plastic Eppendorf tubes (2 mL) and flash frozen in liquid nitrogen. DNA extraction was carried out using the PowerBiofilm DNA isolation Kit (Qiagen) and samples were preserved at -80°C. After DNA extraction, the V7 region of 18S rRNA gene was amplified using 960F and NSR1438R primers following Debroas et al., (2017). Amplicons were sent to GeT Platform (Toulouse, France) for MiSeq Illumina sequencing (2 × 250 bp).

2.3.4. 18S rRNA gene metabarcoding data processing and analysis

18S rRNA gene reads were processed using the FROGS workflow under Galaxy environment (Escudié et al., 2018). Sequences were quality filtered by removing those for which primers sequences were not present. The primer search accepts 10% of differences. Primers sequences were then removed in the remaining sequence using “cutadapt”. Clustering step was performed using SWARM with a clustering aggregation distance set to 3 (Mahé et al., 2014). Chimeric sequences were removed *de novo* using

VSEARCH (Rognes et al., 2016). Rare OTUs representing less than 0.005% of all sequences were removed. OTUs were affiliated with the Silva 132 18S rRNA. The final matrix was obtained by performing a rarefaction to the minimum library size (8975 reads) using the "phyloseq" R package (McMurdie and Holmes, 2013). Eukaryotic *β*-diversity was analyzed with a non-metric multidimensional scaling (NMDS) using Jaccard distances with the "phyloseq" package (McMurdie and Holmes, 2013). PERMANOVA test was performed using the distance matrix constructed with the Jaccard index, using the "vegan" R package (Oksanen et al., 2019).

2.3.5. Bioassays

A bioassay was designed to test the activity of the SEs in 48-well plates for which the well surface is ~1 cm^2. The low amounts of SEs available (0.2 to 5 mg) allowed only one bioassay. The activity of compounds of the SEs being unknown, the highest concentrations prepared from the SEs were tested to ensure a biological response: 2.5, 3.5, 1 and 2 mg cm^{-2} for *T. atomaria*, *P. pavonica*, *D. dichotoma* and *D. spiralis*, respectively. These concentrations are higher than those naturally encountered at the surface of the macroalgae by a factor 5, 4, 1 and 3, respectively (**Table AI.1**). All SEs were re-suspended in dimethyl sulfoxide (DMSO) to reach concentrations of 50, 70, 20 and 40 mg mL^{-1}, respectively for each alga. A volume of 50 μL of each SE was added to the wells containing a thin layer of fresh unsolidified agar and further dried at room temperature (0.3% of DMSO final volume). A same volume of DMSO was similarly added to six more wells as a control.

A monoclonal strain of *O.* cf. *ovata* obtained from the MCCV (Mediterranean Culture Collection of Villefranche, MCCV054) was grown in L1 medium (Guillard and Ryther, 1962) prepared with autoclaved aged and filtered seawater (from the Bay of Villefranche), adjusted to a salinity of 38 and maintained at 24°C under a 14:10 light/dark cycle with a light intensity of 250 μmol m^{-2} s^{-1}. After four days of growth (early exponential phase), 2 mL of the microalgal culture were sampled and fixed with acidic Lugol's iodine solution (4% v/v) and the cell abundance was determined using a Sedgwick rafter counting chamber and an inverted phase contrast microscope (Zeiss Axiovert 40C) at a magnification of ×40. Appropriate volumes of culture and L1 medium were added to each well previously filled with SEs or DMSO (blank) to obtain a concentration of 100 cell mL^{-1} of *O.* cf. *ovata* cells with a final volume of 1.4 mL. All well plates were incubated 24h in the same conditions as for the cultures.

To monitor the bioactivity of the SEs on *O.* cf. *ovata*, both the physiological state and the abundance of the cells were measured after 24h of incubation. All well plates were placed in the dark for 15 min and the well content are successively transferred to a 2 mL glass cuvette immediately moved to a MC-PAM (Multi-

Color Pulse-Amplitude-Modulated, Heinz Walz Gmbh, Effeltrich, Germany) equipped with a blue LED (440 nm) as a source for the actinic light and a white LED used for the saturating pulses. The maximum quantum yield (F_v/F_m) of the photosystem II (PSII) was used as a proxy of the microalga physiological state. It was calculated as $(F_m - F_0)/F_m$, where F_0 is the fluorescence of a dark-adapted sample and F_m is measured after application of a saturation pulse of light (intensity 431 μE m^{-2} s^{-1}, 300 ms duration). Curve-fitting software provided with the instrument (PAMwin V3.20W) was used to obtain F_v/F_m. All curve fits and fluorescence transients were manually inspected in real time. Each sample was placed back in its well after the PAM measurement and immediately fixed with acidic Lugol's iodine solution (4% v/v) for cell counting under microscope as described earlier. The growth rate of *O*. cf. *ovata* was calculated for each well as follows:

$$\mu = \frac{\ln(N2/N1)}{t2 - t1}$$

where N1 and N2 are the cell abundances at times t1 (beginning of the experiment) and t2 (sampling after 24h).

2.3.6. UHPLC-HRMS analysis of macroalgal extracts

Before injection, samples were solubilized in 1 mL of LC-MS grade MeOH. Eleven quality control samples (QCs) and four analytical blanks were also prepared as described in (Paix et al., 2020), and all samples were randomly injected to avoid systematic errors. Acquisition was performed by UHPLC-HRMS using a Dionex Ultimate 3000 rapid Separation chromatographic system (Thermo Fisher Scientific, Waltham, MA, USA) coupled to a QToF Impact II mass spectrometer (Bruker Daltonics, Bremen, Germany) equipped with an electrospray source. A volume of 5 μL of each sample was injected and analysed on a reversed phase column (150 × 2.1 mm, 1.7 μm, Kinetex Phenyl-Hexyl equipped with a SecurityGuard cartridge; Phenomenex, Le Pecq, France) with a column temperature of 40°C and a flow rate of 0.5 mL min^{-1}. Mobile phases were (A) water and (B) acetonitrile (Chromasolv; Sigma-Aldrich-Merck, Darmstadt, Germany) containing each 0.1% (v/v) of formic acid (Ultra grade; Fluka, Fischer Scientific, Illkirch, France). The elution gradient started at 5% B and kept for 2 min, then to 100% B (linear ramp) in 8 min and kept for 4 min; then back to 5% B (linear ramp) over 0.01 min and maintained 1.99 min, for a total run time of 16 min. Mass spectrometry (MS) analyses were performed in the full scan positive mode (ESI +). The capillary voltage of the MS spectrometer was set at 4500V and the nebulizing parameters were set as follows: nebulizing gas (N_2) pressure at 0.4 bar, drying gas (N_2) flow at 4 L min^{-1}, and drying temperature at 180 °C. Mass spectra were recorded from *m/z* 50 to 1200. Tandem mass spectrometry analyses were

performed with a collision induced dissociation (CID) and collision energy of 25 eV. A solution of formate/acetate forming clusters was automatically injected before each sample for internal mass calibration, and the mass spectrometer was calibrated with the same solution before each sequence of samples. Raw UHPLC-HRMS data were analysed using DataAnalysis (version 4.3; Bruker Daltonics), converted into netCDF files and processed for peak finding, integration and alignment using the open source XCMS package (version 1.46.0; Smith et al., 2006) in the R 3.2.3 environment. The resulting variables list was filtered using three successive steps (signal/noise ratio, coefficient of variation and coefficient of autocorrelation) with an in-house script running on R. These variables were $\log_{10}$-transformed, mean-centred and normalized using the sum of the chromatographic peak areas as described in Paix et al., (2020), and analysed by Principal Component Analysis (PCA) and partial least-square discriminant analysis (PLS-DA) using the MetaboAnalyst 3.5 online resource (http://www.metaboanalyst.ca). The global annotation was assessed by comparison of MS/MS spectra with those of an in-house database (purified compounds and commercial standards), and public databases (MarinLit, MetLin, MoNA or Lipidmaps). Subsequently, the annotation procedure of analogs of known compounds was facilitated by molecular networking using the GNPS platform (https://gnps.ucsd.edu/ProteoSAFe/static/gnps-splash.jsp).

2.4. Results

2.4.1. Assessment of the natural abundance of benthic microalgae using microscopy

All the four macroalgal species had their surface colonized by diatoms, including species of the genera *Licmophora*, *Amphora*., *Navicula*, *Cylindrotheca*, *Striatella* and *Gyrosigma*, as well as the dinoflagellate *O.* cf. *ovata* (**Figure AI.1**). *O.* cf. *ovata* showed a lower abundance than diatoms, representing 14 to 23% of the total number of counted cells, with densities ranging from 1.5 to 7.9×10^3 cell cm^{-2}. Significant different concentrations of *O.* cf. *ovata* cells were observed between macroalgal hosts (ANOVA: $p = 0.0175$). Post-hoc analysis revealed a significantly higher concentration of cells on *D. dichotoma* compared to *D. spiralis* and *P. pavonica*, while no significant differences were detected between *T. atomaria*, *P. pavonica* and *D. spiralis*, and neither between *T. atomaria* and *D. dichotoma* – due to one outlier sample.

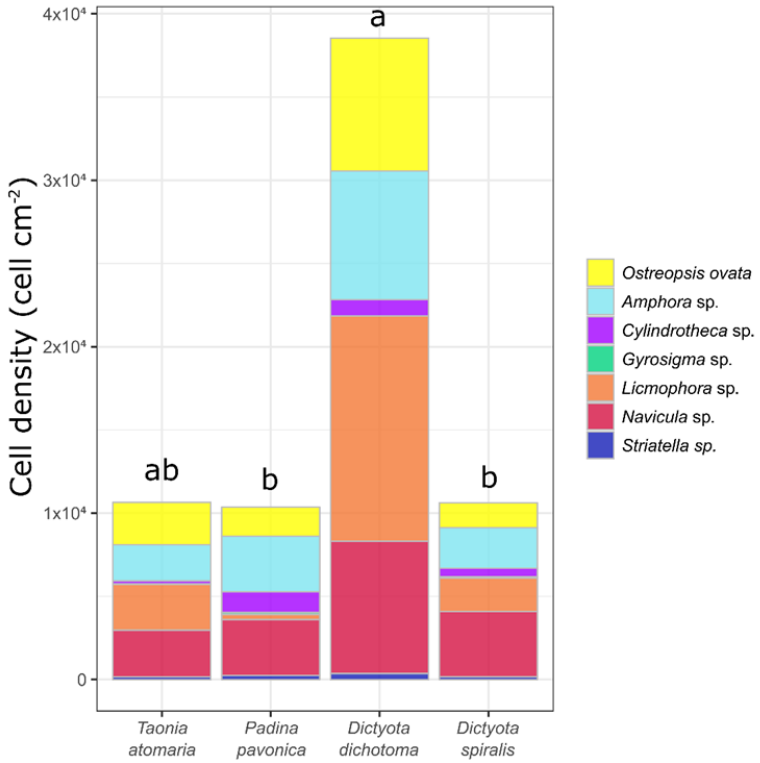

Figure AI.1. Cell density (cell cm^{-2}) of major diatoms and *O.* cf. *ovata* at the surface of the four macroalgae. Statistical significance was evaluated only for *O.* cf. *ovata* abundances using an ANOVA test (*$p = 0.0175$) followed by a post-hoc Tukey's test.

2.4.2. Diversity of epiphytic eukaryotes through 18S rRNA gene HTS

When compared to the number of OTUs, the Chao1 index reflects the richness that could be reached if a higher number of sequences has been obtained. Here, Chao1 indicated that the highest richness of eukaryotic communities was observed in seawater as well as on the surface of *T. atomaria* and *P. pavonica* (SI Figure SVIII.1). Considering the β-diversity, seawater communities were clearly dissimilar from those found on the macroalgal surfaces (**Figure AI.2** and SI Figure SVIII.2). The dinobiontes seemed to constitute the major taxa in seawater, with *Amphidinium* being the most represented genus (54%) followed by *Alexandrium* (9%), while *Ostreopsis* only represented 3%. Among epiphytes, a clear clustering at the algal species level could be noticed, with the two *Dictyota* species communities on the one hand, and *T. atomaria* and *P. pavonica* communities on the other hand (**Figure AI.2**). Using the Jaccard index with a NMDS analysis, the β-diversity of the eukaryotic communities revealed clear differences between the epiphytic and the planktonic communities, but also between macroalgal hosts (**Figure AI.2** and SI Figure SVIII.2, PERMANOVA: $p = 0.001$).

Even though they serve as support of common taxa, like Dinoflagellata, Arthropoda, Ochrophyta, Annelida, Florideophycideae, and Mollusca, the four macroalgae species exhibited a contrasted composition of their epiphytic eukaryotic communities. Among the major detected taxa, two belonged to microalgae (Ochrophyta and Dinoflagellata), one to copepods (Arthropoda), two to red algae (Florideophycideae) and two to upper benthic organisms (Annelida and Mollusca). The major species of diatoms present on the macroalgae belonged to the genera *Berkeleya*, *Navicula*, *Haslea*, *Nitzschia*, *Actoncyclus*, *Amphora*, *Cylindrotheca*, *Cocconeis*, *Psammoneis*, *Hyalosira* and *Frustulia* and their relative abundance was the highest on *P. pavonica* (19%) and the lowest on *D. spiralis* (2%). The abundance of Dinoflagellata in the epiphytic community determined by cell counting was highly consistent with the results obtained by 18S rDNA gene sequencing. The major OTU identified belonged to the genus *Ostreopsis*, while other dinoflagellate taxa, without specific affiliation at the genus level, were also detected with very few sequences. Dinoflagellates represented only 1% of the total eukaryotic diversity on *T. atomaria*, *P. pavonica* and *D. spiralis* while it reached 6% on *D. dichotoma*. The Harpacticoids Amphiascoides and Paramphiascella were the main Arthropoda families and the species *Amonardia coreana*, *Parastenhelia* sp., *Amphiascoides atopus* and *Paramphiascella fulvofasciata* were annotated. Several Annelida species of the Phyllodocida family were detected, including *Platynereis dumerilii* and *Syllis pigmentate*; they were mainly distributed on *D. dichotoma* and *P. pavonica*. The major plathyhelminthe species was *Convoluta convoluta* which was reported on the two *Dictyota* spp. The Arthropoda were particularly represented on *D. spiralis* (67%) and *T. atomaria* (32.5%) while *P. pavonica* showed the highest

Annelida community (39.5%). The Florideophycideae also largely contributed to the eukaryotic diversity on *T. atomaria* (22.4%). These same taxa were shown to colonize *D. dichotoma*, none of them being predominant: Dinoflagellata (6%), Arthropoda (18%), Ochrophyta (10%), Annelida (23%), Florideophycideae (12%), Mollusca (8%) and Xenacoelomorpha (16%).

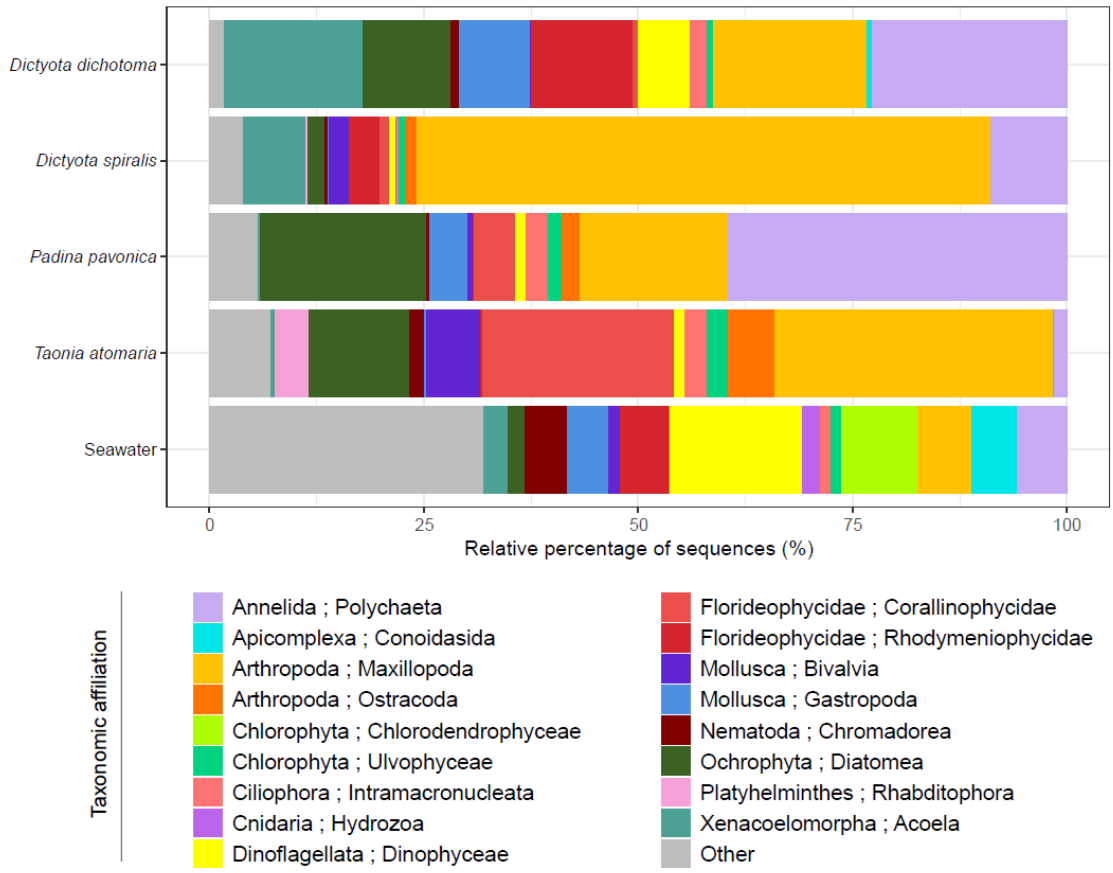

Figure AI.2. Eukaryotic communities colonizing the surface of the four macroalgae and present in the surrounding seawater. Replicate samples of a same species were averaged (n = 3) and relative colonization to all sequences is given (%). Taxonomic affiliation corresponds to the Phylum and Class level. "Other" combines Classes that represent less than 2% of the total diversity.

2.4.3. Chemical analysis of macroalgal extracts

The chemical diversity of the four macroalgal extracts was assessed by untargeted LC-MS-based metabolomics and led to 375 features after filtering. The PCA score plot of the surface and total (SEs and TEs) macroalgal extracts (**Figure AI.3**) showed a clear separation between the two *Dictyota* spp. and the two other species (*T. atomaria* and *P. pavonica*), mainly on the first component (48% of the total variance)

highlighting a distinct chemical composition between these species. Furthermore, the second component (18.5% of the total variance) highlighted differences between SEs and TEs within each of these two algal groups. A list of the features responsible for the differences between SEs and TEs for each species is provided in SI (SI Table SVIII.1). The vast majority of these metabolites being minor ions on the chromatograms, very few could be annotated. Most metabolites specific to the SEs were small/polar compounds as suggested by their retention time (RT < 1 min) whereas TEs were more enriched in less polar metabolites (RT > 8 min). Dimethylsulfoniopropionate (DMSP), *Lyso*-diacylglyceryl-3-*O*-carboxyhydroxymethylcholine (C16:0) and a compound, putatively annotated as acetyl-*L*-cysteine, were found to be enriched in the SEs of *T. atomaria, P. pavonica* and *D. dichotoma*, respectively.

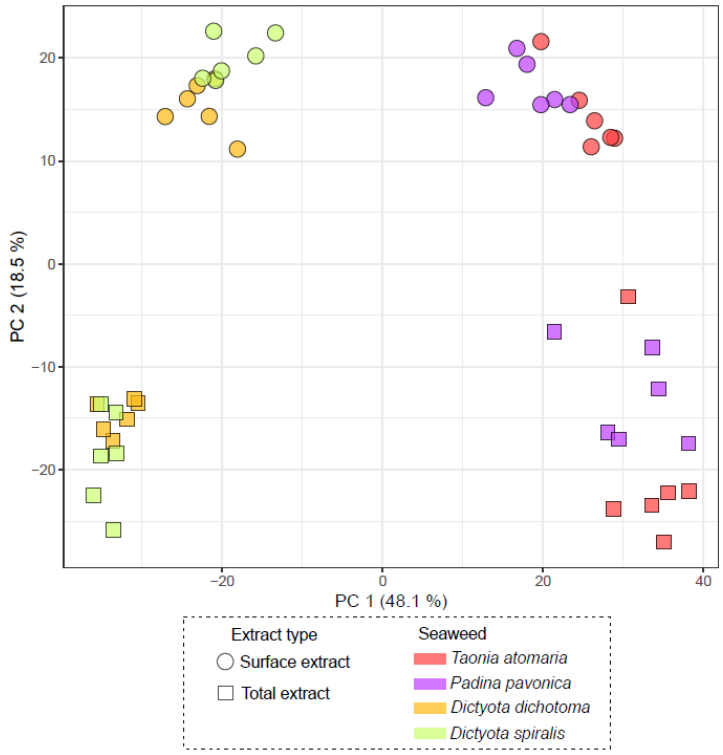

Figure AI.3. PCA score plot obtained from LC-(+)-ESI-MS metabolomics analyses of both the total extracts (TEs) and surface extracts (SEs) of the four macroalgae.

The score plot of the PLS-DA only built with SEs (**Figure AI.4**) offered a more focused view of the distribution of these extracts. None of the SEs overlapped with 95% confidence, suggesting significant differences in their chemical content, even for the two *Dictyota* spp. The distribution of the samples on both the PCA and the PLS-DA score plots was highly driven by the large number of metabolites produced by *D. dichotoma* and *D. spiralis*. The first 50 Variable Importance of Projection (VIPs) responsible for the separation of the samples on the PLS-DA score plot (VIP score > 1.1) are listed in **Table AI.2**.

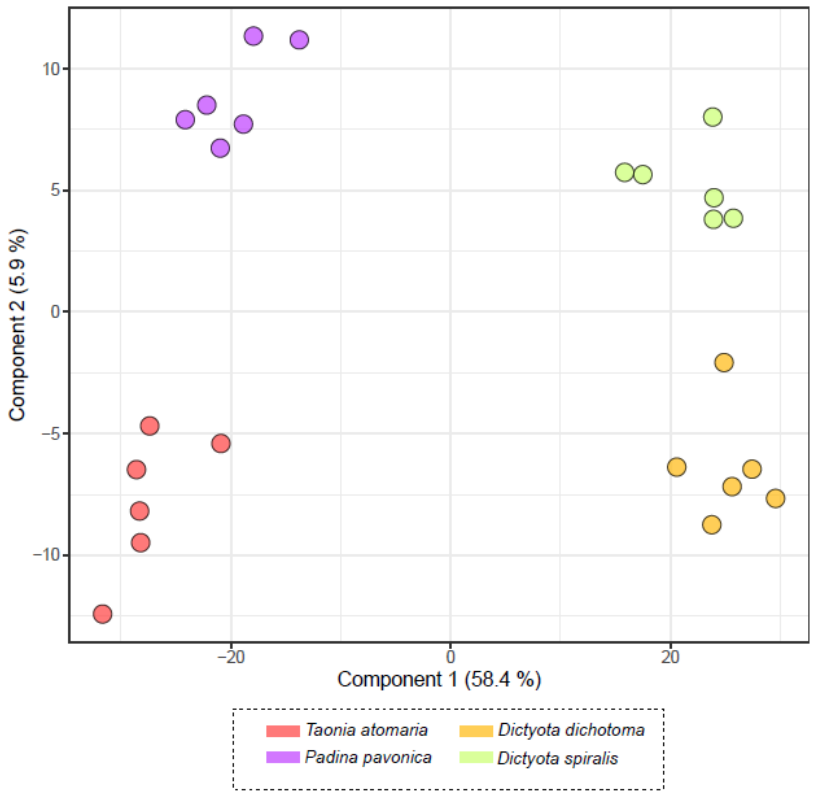

Figure AI.4. PLS-DA score plot obtained from LC-(+)-ESI-MS metabolomics analyses of the surface extracts (SEs) of the four macroalgae.

Search of matches of MS data from compounds of our in-house database, the MarinLit database and molecular network built from MS/MS spectra analysis (**Figure AI.5**) allowed the annotation of several of the VIPs characteristic of each macroalga (**Table AI.2**).

Several chemical markers enriched in *D. dichotoma* and *D. spiralis* SEs were detected in cluster B and I of the molecular network, allowing their putative annotation as diterpene derivatives. More precisely, the diterpenes dictyotalide A (or an isomer) (VIP n°4), *ent*-erogorgiaene (VIP n°10), dictyotetraene (VIP n°14), dictyol A (VIP n°15), isopachydictyol A (VIP n°19), 17,18-18,19-bisepoxyxenic-19-methoxy-6,9,13-triene (VIP n°25) and tricyclodictyofuran C (VIP n°6 and 41) were putatively identified in cluster B, and dictyotadimer A (VIP n°13) in cluster I. Finally, even if not appearing in the molecular network, dictyol B (VIP n°29) was also putatively annotated. Several other VIPs were not identified but were characterized as diterpenes or diterpene derivatives using their MS and MS/MS data.

Both the lipid geranylgeranylglycerol and the sulphur compound DMSP (VIPs n°20 and 27, respectively) were identified by the mean of chemical standards as the major markers found in *T. atomaria* SEs. Five other compounds (VIPS n°31, 36, 37, 40 and 42), putatively identified as diacylglyceryl-3-*O*-

carboxyhydroxymethylcholines [DGCCs (C22:6), (C44:12), (C36:6); *Lyso*-DGCCs (C16:0) and (C38:6), respectively), were also detected in *T. atomaria* and gathered in cluster D. Finally, the VIP n°46 was putatively annotated as the sesquiterpene *trans*-calamenene using an in-house standard.

P. pavonica was the algal species that showed the least chemical richness on its surface with only two unidentified markers (VIPs n°34 and 49) being found in its corresponding SEs.

More compounds not listed as VIPs were identified from other clusters of the molecular network: diacylglycerylhydroxymethyl-*N*,*N*,*N*-trimethyl-β-alanines (DGTAs) and phosphatidylcholines (PCs) present in cluster A, other PCs in cluster E, carotenoids in cluster F, sesquiterpenoids in cluster G, and pheophytin a derivatives in cluster N.

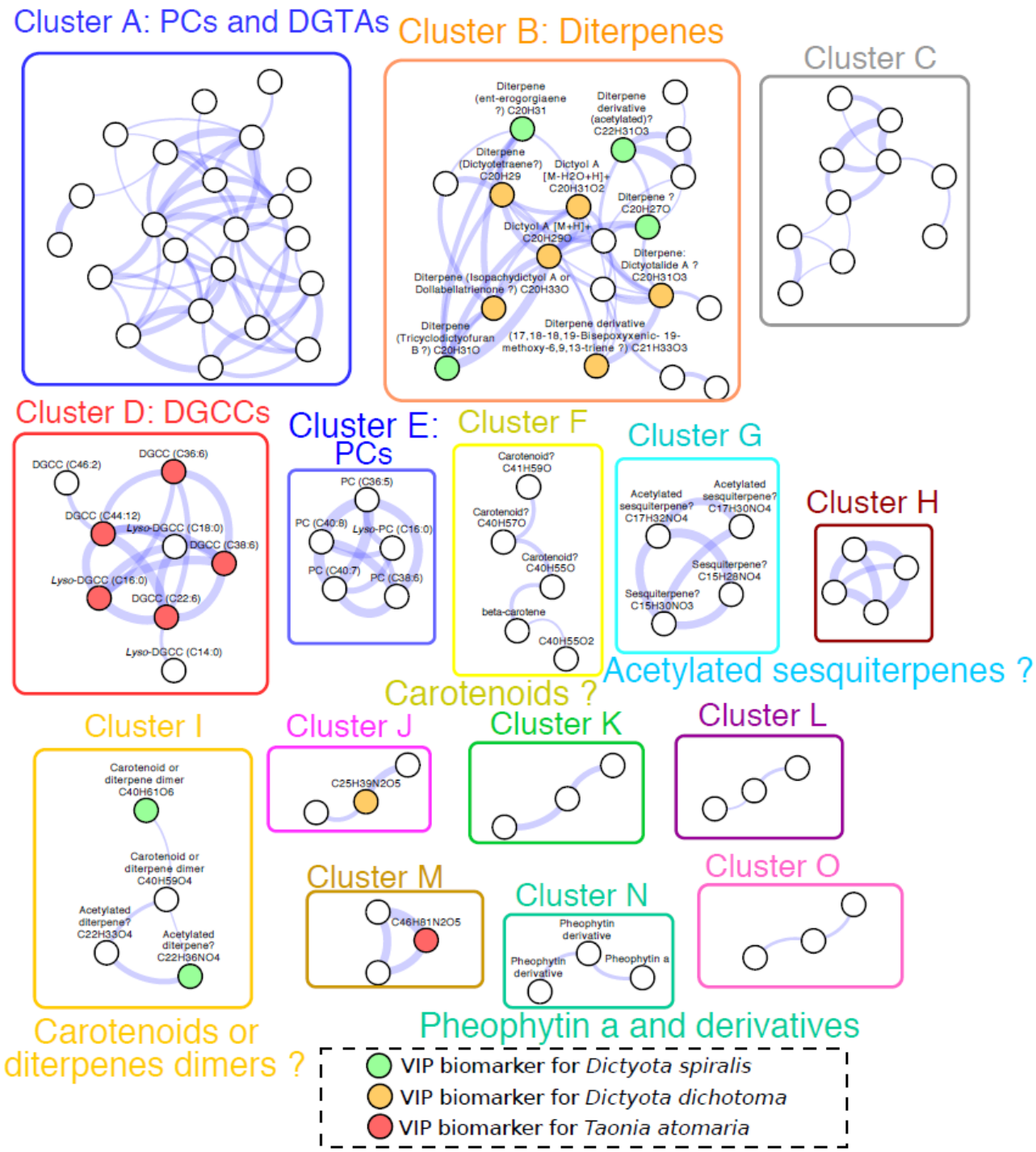

Figure AI.5. Molecular network obtained from LC-(+)-ESI-MS/MS data of the SEs of the four macroalgal species. Only clusters with 3 or more nodes are represented. Nodes represent MS/MS spectra which are connected based on their spectral similarity. Colored nodes indicate biomarkers according to the four macroalgae (orange: *D.* dichotoma, green: *D. spiralis*, red: *T. atomaria*, no VIPs for *P. pavonica* were observed). The edge width is proportional to the cosine score.

VIP	Cluster	*m/z*	Annotation	Formula	err	msigma	*D. dichotoma*	*D. spiralis*	*P. pavonica*	*T. atomaria*
1	-	472.236753	Unknown	$C_{26}H_{34}NO_7$	-9.6	9.5				
2	-	390.263585	Diterpene derivative (methoxylated & acetylated)?	$C_{23}H_{36}NO_4$	-2.8	1.1				
3	SL	461.300916	Unknown	$C_{26}H_{41}N_2O_5$	1.0	13.0				
4	B	319.226939	Dictyotalide A or isomer	$C_{20}H_{31}O_3$	-1.0	12.9				
5	J	447.285584	Unknown	$C_{25}H_{39}N_2O_5$	-0.6	6.7				
6	-	317.247489	Tricyclodictyofurane C or isomer	$C_{21}H_{33}O_2$	-1.2	12.4				
7	-	422.254062	Diterpene derivative (methoxylated & acetylated)?	$C_{23}H_{36}NO_6$	-1.6	4.6				
8	I	378.264217	Diterpene derivative (acetylated)	$C_{22}H_{36}NO_4$	-3.8	9.3				
9	-	364.284964	Diterpene derivative (acetylated)	$C_{22}H_{38}NO_3$	-2.7	17.0				
10	B	271.242119	*ent*-erogorgiaene	$C_{20}H_{31}$	-1.0	4.4				
11	-	342.242938	4-methylaminoacarone	$C_{22}H_{32}NO_2$	-2.7	11.9				
12	-	573.466831	Carotenoid (pirardixanthin derivative?)	$C_{40}H_{61}O_2$	-0.3	28.1				
13	I	637.448128	Dictyotadimer A	$C_{40}H_{61}O_6$	-2.7	14.0				
14	B	269.226492	Dictyotetraene	$C_{20}H_{29}$	-0.3	66.9				
15	B	285.221393	Dictyol A *	$C_{20}H_{29}O$	-1.8	12.4				
16	-	413.280297	*Apo*-carotenoid	$C_{30}H_{37}O$	8.5	4.4				
17	B	283.20567	Unknown	$C_{20}H_{27}O$	-1.0	7.9				
18	-	743.450601	Unknown	$C_{46}H_{63}O_8$	-1.0	38.4				
19	B	289.252582	Isopachydictyol A or dollabellatrienone	$C_{20}H_{33}O$	0.5	6.7				
20	-	382.331504	Geranylgeranylglycerol *	$C_{23}H_{44}NO_3$	-1.7	6.1				
21	-	373.235224	Unknown	$C_{21}H_{34}NaO_4$	-0.3	2.6				
22	-	410.290343	Diterpene derivative (methoxylated & acetylated)?	$C_{23}H_{40}NO_5$	-3.4	4.7				
23	(B)	333.242627	17,18:18,19-bisepoxyxenic-methoxy-triene	$C_{21}H_{33}O_3$	-1.8	7.7				
24	SL	446.290738	Phormacin B	$C_{26}H_{40}NO_5$	-1.0	7.2				
25	B	333.242496	17,18:18,19-bisepoxyxenic-methoxy-triene	$C_{21}H_{33}O_3$	-0.8	4.4				
26	-	406.258778	Diterpene derivative (methoxylated & acetylated)?	$C_{23}H_{36}NO_5$	-2.9	5.0				
27	-	135.047248	DMSP *	$C_5H_{11}O_2S$	0.2	1.0				
28	-	489.343493	Unknown	$C_{26}H_{49}O_8$	-3.5	13.7				
29	-	327.229615	Dictyol B	$C_{20}H_{32}NaO_2$	-0.5	14.2				
30	-	654.47347	carotenoid	$C_{40}H_{64}NO_6$	-5.5	18.9				
31	D	562.374243	DGCC (C22:6)	$C_{32}H_{52}NO_7$	-2.3	1.4				
32	-	356.25884	Unknown	$C_{23}H_{34}NO_2$	-2.7	16.0				
33	-	426.231272	Unknown	$C_{22}H_{36}NO_5S$	-2.6	15.7				
34	SL	653.297738	Unknown	$C_{29}H_{49}O_{16}$	2.3	10.3				
35	E	741.614801	Unknown	$C_{46}H_{81}N_2O_5$	-2.5	9.7				
36	D	872.605027	DGCC (C44:12)	$C_{54}H_{82}NO_8$	-3.1	2.1				
37	D	772.573549	DGCC (C36:6)	$C_{46}H_{78}NO_8$	-2.7	2.1				
38	-	317.247669	Tricyclodictyofuran C or isomer	$C_{21}H_{33}O_2$	-3.0	3.5				
39	SL	318.242795	Unknown	$C_{20}H_{32}NO_2$	-1.6	18.5				
40	D	490.374196	*Lyso*-DGCC (C16:0)	$C_{26}H_{52}NO_7$	-0.7	14.3				
41	B	287.237035	Tricyclodictyofuran B	$C_{20}H_{31}O$	-0.8	27.2				
42	D	800.604167	DGCC (C38:6)	$C_{48}H_{82}NO_8$	-2.1	6.6				
43	B	343.226662	Diterpene derivative (acetylated)	$C_{22}H_{31}O_3$	-2.2	9.6				
44	SL	260.112865	Unknown	$C_{11}H_{18}NO_6$	-0.6	3.2				
45	-	453.27291	*Apo*-carotenoid	$C_{30}H_{38}NaO_2$	4.0	10.3				
46	-	201.16362	*Trans*-calamenene *	$C_{15}H_{21}$	-2.8	25.8				
47	SL	376.787236	FA (C24:5)	$C_{24}H_{42}NO_2$	3.3	9.9				
48	SL	445.292694	Amphidinolide	$C_{25}H_{42}NaO_5$	-0.1	5.3				
49	-	704.546719	Unknown	$C_{42}H_{74}NO_7$	-2.5	7.7				
50	-	319.226828	Dictyotalide A or isomer	$C_{20}H_{31}O_3$	-0.3	27.0				

Colour code: -4, -2, 0, 2, 4

Table AI.2. Putative annotation of the first 50 chemical markers (VIP score > 1.1) driving the distribution of the samples on the PLS-DA score plot obtained from LC-(+)-ESI-MS metabolomics analyses of the SEs of the four macroalgae. Identification of the compounds marked by * was confirmed with a chemical standard. Clusters "SL" corresponds to a self-loop (a metabolite only connected to itself). The colour code represents the mean concentration values obtained for each macroalga.

2.4.4. Bioactivity of surface extracts (SEs) on O. cf. ovata

To ensure a measurable effect on *O.* cf. *ovata* cells, the maximal concentration that could be obtained from the SEs was tested for their bioactivity. Therefore, tested concentrations varied from 1 to 3.5 mg cm^{-2} according to the species and comparison between bioactivities should be treated cautiously. Three macroalgal SEs out of four induced a significant growth reduction of *O*. cf. *ovata* ($p < 0.001$; **Figure AI.6A**), with *D. spiralis* SE found to be not statistically active. Despite tested at the lowest concentration (1 mg cm^{-2}), the inhibition of *O.* cf. *ovata* growth induced by *D. dichotoma* SEs was similar to those of *P. pavonica* while being significantly lower than the one of *T. atomaria*. Although similar concentrations were used for *T. atomaria* and *D. spiralis* SEs (2.5 and 2 mg cm^{-2}, respectively), the inhibition on *O.* cf. *ovata* growth induced by *T. atomaria* SEs was significantly higher.

All but *P. pavonica* macroalgal SEs induced a significant stress on *O*. cf. *ovata* physiology as conveyed by the significant alteration of the efficiency of the photosystem II (PSII) shown by the Fv/Fm ratio ($p < 0.001$, **Figure AI.6B**). Despite being tested at the lowest concentration, the SEs of *D. dichotoma* caused among the most intense inhibition of the PSII efficiency. Such an inhibition was comparable to those observed for *D. spiralis* and *T. atomaria* SEs. Whether the growth rate of *O.* cf. *ovata* was not affected by *D. spiralis*, the PSII efficiency was significantly altered to a similar extent than with *D. dichotoma*. Mirroring the effects on *O.* cf. *ovata* growth rate, *T. atomaria* SEs tested at 2.5 mg cm^{-2} also caused an intense stress on the photosystem II of the dinoflagellate. The related reduction in the Fv/Fm ratio measured was significantly higher than for *D. spiralis* and *P. pavonica*, although tested at a similar and lower concentration, respectively.

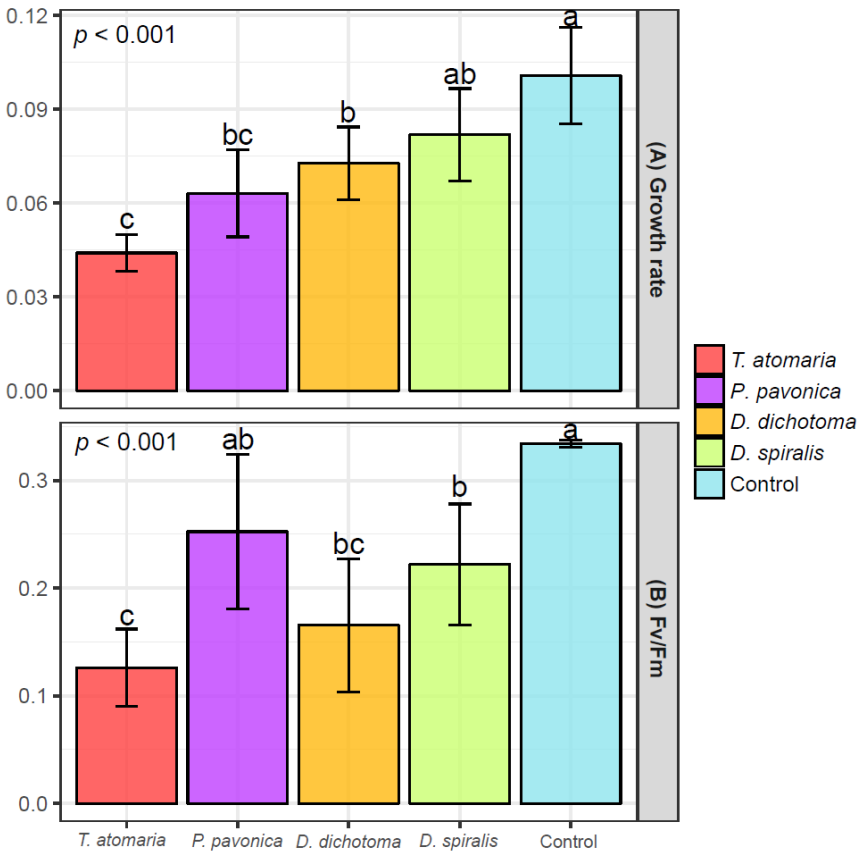

Figure AI.6. (A) Growth rate (μ) of *O.* cf. *ovata* and (B) Maximum quantum yield of PSII (F_v/F_m) of dark-adapted samples of *O.* cf. *ovata* after exposure of 24h to macroalgal surface extracts (SEs) and blanks (n = 6 per condition). p values and a, b, c, d indexes correspond to results of the one-way ANOVA and Tukey's tests, respectively.

2.5. Discussion

The simultaneous monitoring of both the abundance and toxin content of benthic *O.* cf. *ovata* cells undertaken by Gémin et al., (2019) at the same sampling site in the bay of Villefranche showed that the development of this bloom followed a classic trend. In terms of intensity, the bloom peaked at $9.2 \pm 7.5\ 10^5$ cells g^{-1} FW (Gémin et al., 2019) corresponding to a moderate bloom for this site (Guidi-Guilvard et al., 2012; Cohu et al., 2013) or other Mediterranean sampling sites (Totti et al., 2010). Consistently with our results but also with other observations from the NW Mediterranean Sea (Cohu et al., 2013; Blanfuné et al., 2015), Gémin et al., (2019) found the highest cell concentration of *O.* cf. *ovata* on *Dictyota* spp. and the lowest on *P. pavonica*.

2.5.1. Potential control of the abundance of O. cf. ovata by the epiphytic community

A preferred colonization by *O.* cf. *ovata* on branched, three-dimensional thalli with a high surface/volume ratio has been previously suggested by several authors (Vila et al., 2001; Totti et al., 2010; Gémin et al., 2019) but such an hypothesis is not fully supported by the low abundance of *O.* cf. *ovata*

measured on the highly branched *T. atomaria* or by settlement differences observed between morphologically similar *Dictyota* species (this study and Blanfuné et al., 2015). The 18S rRNA gene sequencing revealed a high diversity of eukaryotes colonizing the macroalgae, suggesting that various biotic interactions may take place within the epiphytic community having the potential to regulate the colonization of *O.* cf. *ovata*.

Inter-specific competition for nutrients, light and space may occur between the dinoflagellate *O.* cf. *ovata* and the various species of diatoms that co-occurred within the epiphytes of the macroalgae. Species of the genera *Licmophora*, *Navicula*, and *Amphora* were the most abundant diatoms co-occurring with *O*. cf. *ovata*, in line with previous findings (Accoroni et al., 2016), while *Coscinodiscus* spp. usually detected in the Catalan Sea (Vila et al., 2001; Carnicer et al., 2015) was missing. Other dinoflagellate species were barely detectable conversely to previous studies that reported the co-occurrence of *Prorocentrum lima* and *Coolia monotis* in various sampling sites across the Mediterranean Sea, including the bay of Villefranche (Vila et al., 2001; Aligizaki and Nikolaidis, 2006; Cohu et al., 2011; Blanfuné et al., 2015; Accoroni et al., 2016). In recent co-culture experiments, weak deleterious allelopathic effects induced by *Licmophora paradoxa*, *Coolia monotis*, *Prorocentrum lima* and *Navicula arenaria* towards *O.* cf. *ovata* were highlighted (Ternon et al., *in review*, Ternon et al., 2018). A chemical control of the colonization of *O.* cf. *ovata* by co-occurring benthic microalgae is therefore possible although it may be counterbalanced by the existence of an additional weak inhibiting allelopathic effects applied by *O*. cf. *ovata* on the diatoms *L. paradoxa* and *N. arenaria* and the dinoflagellate *P. lima* (Ternon et al., *in review*).

Predation by benthic copepods is another factor that may modulate the colonization pattern of benthic microalgae. Benthic harpaticoids, such as *Sphaeroma serratum*, *Tigriopus fulvus*, *Acartia clausi*, and *Sarsamphiascus cf. propinquus*, have been recently shown to feed on *O.* cf. *ovata* (Prato et al., 2011; Faimali et al., 2012; Furlan et al., 2013; Pavaux et al., 2019) with similar ingestion rates as for diatoms (Boisnoir et al., 2020). The resistance of benthic copepods to *O*. cf. *ovata*'s toxicity was found to be highly variable among species, with LC_{50} ranging from 10 to 20,000 cells mL^{-1} (Prato et al., 2011; Faimali et al., 2012; Pavaux et al., 2019). Ingestion of *O*. cf. *ovata* leads to reduced fecal pellets production and fecundity rates indicating a reprotoxic effect (Pavaux et al., 2019) that may cause a reduction in nauplii abundance (Guidi-Guilvard et al., 2012) but not on adults' abundance. Our study was conducted at the peak of the bloom, when the highest concentrations of O. cf. *ovata* and toxin content per cell were reported (Gémin et al., 2019). *In situ* cell concentrations reported in cells per g of macroalga fresh weight ($9.2 \pm 7.5\ 10^5$ cells g^{-1} FW; Gémin et al., 2020) likely exceeded the toxic level of 20,000 cells per mL (Pavaux et al., 2019).

Nevertheless, the amount of toxins per cell reported *in situ* was lower compared to the MCCV054 strain of *O.* cf. *ovata* used in Pavaux et al. study (5-10 against 13 pg cell^{-1}; Gémin et al., 2019; Pavaux et al., 2020, respectively). Additionally, Gémin et al., (2019) showed that the toxin content in *O.* cf. *ovata* varied according to the macroalgal species they colonized. The toxicity of *O.* cf. *ovata* towards grazers may therefore vary according to the substrate. Therefore, it is difficult to conclude whether the maxillopods are suffering from the natural concentrations of *O.* cf. *ovata* encountered on the four macroalgae. Moreover, the resistance of the copepod species (*Paramphiascella fulvofasciata*, *Amphiascoides atopus*, *Amonardia coreana*, *Harpaticus* spp., and *Nemesis* spp.) detected on the four macroalgae to *O.* cf. *ovata* has not been experimentally tested and may differ from already tested species. It is worth noting that the relative abundance of benthic copepods and *O.* cf. *ovata* did not show any obvious correlation. In contrast, if maxillopods have the capacity to feed on *O.* cf. *ovata*, they unlikely are the major factor that regulates its colonization on the macroalgae. Indeed, the toxic dinoflagellate was found to be similarly abundant on *D. spiralis*, *T. atomaria* and *P. pavonica* (1,505; 2,251 and 1,759 cells cm^{-2}, respectively), not mirroring their different ratio *Ostreopsis*:maxillopods (1:67, 1:33 and 1:17, respectively) in term of comparison of 18S rRNA gene sequences.

Other predators, like polychaetes, were also shown to graze *O.* cf. *ovata* despite an important sensitivity to the ovatoxins (Simonini et al., 2011). Concentrations of *O*. cf. *ovata* as low as 200 cells mL^{-1} caused the death of 100% of a population of *Dinophylus gyrociliatus* in less than 48h (Simonini et al., 2011). However, similarly to copepods, the capacity to feed on *O.* cf. *ovata* as well as the resistance to the ovatoxins may differ among species and according to the toxicity of *O.* cf. *ovata* cells linked with the substrate they colonize (Gémin et al., 2019). The species *Syllis pigmentata*, *Platynereis dumerilii* and *Neodexiospira brasiliensis,* for which no LC_{50} is available yet, were the most abundant while *D. gyrociliatus* was not detected on the macroalgae.

The eukaryotic richness of the epiphytic macroalgal communities was high, particularly on *T. atomaria* and *P. pavonica*, and interactions that may result from it have not been fully investigated yet. For instance, the bacterial community which was not described in this study may play an important role in the regulation of epiphytic communities (Tait et al., 2005; Wheeler et al., 2006; Saha and Weinberger, 2019), including *O.* cf. *ovata*. The present data set did not highlight a specific biotic interaction within the epiphytic community that may favor or inhibit the settlement of *O*. cf. *ovata* on the different macroalgal species.

2.5.2. Algal surface chemistry influences the growth of O. cf. ovata

Several studies have shown deleterious effects of macroalgal metabolites on microalgae using whole cells dried and grounded (Tang and Gobler, 2011; Accoroni et al., 2015) or organic whole-cell extracts (Hellio et al., 2002; Nagayama et al., 2003). To our knowledge, this study is the first attempt in evaluating the bioactivity of SEs on settlement and growth of a microalgal species. Previous study on *T. atomaria* demonstrated a satisfying extraction of surface metabolites without disturbance of the macroalgal membranes by the soaking protocol used in the present study (Othmani et al., 2016a). The differences observed in the chemistry of the SEs and TEs for all four macroalgae species further validated the soaking protocol as an efficient method to extract surface metabolites of the three other species *P. pavonica*, *D. spiralis* and D. *dichotoma*. Most chemical markers characteristics of the SEs were found to be polar metabolites (RT < 1 min), including DMSP, whereas TEs were characterized by less polar compounds (RT > 8 min).

The chemical fingerprint of the four macroalgae species draws two distinct groups: the two *Dictyota* spp. clustering together and *P. pavonica* and *T. atomaria* gathering in the second group. In terms of eukaryotic β-diversity, the same two groups emerged, suggesting that the metabolites at the surface of the macroalgae are influencing the settlement of eukaryotes. Since both *T. atomaria* and *P. pavonica* showed a higher richness of their overall epiphytic eukaryotic community, their surface metabolites could be considered less bioactive towards these communities, although higher antibacterial activities have been previously observed for *Taonia* and *Dictyota* spp. among Phaeophyceae species (Salvador Soler et al., 2007). When looking specifically at *O.* cf. *ovata*, the surface chemistry of the four macroalgae has the potential to influence the settlement of the toxic dinoflagellate by altering both its physiology and its growth. Nevertheless, the use of different concentrations (1 to 3.5 mg cm^{-2}) in the bioassay does not allow to order the bioactivity of the four macroalgae, however *D. dichotoma* clearly induced a strong inhibition of both the growth and the PSII efficiency of *O.* cf. *ovata* at ecological concentrations (1 mg cm^{-2}) and can therefore be considered as the most bioactive species. Many diterpenes isolated from *Dictyota* spp. have been found to exhibit antifouling properties as for instance the algicidal dictyolactone towards the red-tide microalgae *Heterosigma akashiwo* (Kim et al., 2006), dictyol C that reduces the adhesion of *Pseudoalteromonas* spp. (Viano et al., 2009), as well as dictyol E, dictyol B acetate, pachydictyol A and dictyodial that all cause significant larval mortalities of invertebrates (Schmitt et al., 1998). Although none of the cited compounds were major chemical markers in any of the two *Dictyota* spp., the high diterpenes content of their SEs suggests that this family of metabolites could be responsible for the observed bioactivity of both species. Nevertheless, considering the higher stress induced by *D. dichotoma* compared

to *D. spiralis* on *O.* cf. *ovata*, chemical markers more specific to *D. dichotoma* were sought. Two metabolites listed as VIPs n°5 and 12 were significantly more enriched in *D. dichotoma* SEs (SI, Figure SVIII.3) with the molecular formulae $C_{25}H_{39}N_2O_5$ and $C_{40}H_{61}O_2$ corresponding to an unidentified compound (cluster J) and a carotenoid-like compound likely to belong to the pirardixanthin family (Tsushima et al., 2001), respectively. While the activity of these families of compounds has not been determined so far, some carotenoids like fucoxanthin are known to possess inhibiting properties against bacteria (Viano et al., 2009; Saha et al., 2011) which could also target benthic microalgae.

T. atomaria showed a higher bioactivity than *D. spiralis* and *P. pavonica*, tested at a similar and higher concentration, respectively. This bioactivity is, however, likely overestimated compared to an ecological situation (enrichment factor of 5). Both geranylgeranylglycerol and DMSP were the major biomarkers in *T. atomaria* SEs, in agreement with previous findings (Othmani et al., 2016a; Paix et al., 2019), and were therefore enriched in this species compared to the three others (SI Figure SVIII.3). These two metabolites have shown activity against bacterial settlement (Saha et al., 2012; Othmani et al., 2016a, 2016b) and may have the potential for inhibiting the growth of *O*. cf. *ovata*. However, DMSP is a metabolite largely biosynthesized by *O*. cf. *ovata* itself (pers. data; Chen et al., 2020), leaving geranylgeranlyglycerol as the most likely candidate. The present dataset did not allow to propose any metabolite for *P. pavonica* that could explain the unspecific bioactivity of its SEs. If all four macroalgae species have the ability to affect *O.* cf. *ovata*'s growth or physiology, bidirectional effects may also be considered since some macroalgae have been shown to rely on microbial metabolites for cell division and differentiation (Wichard and Beemelmanns, 2018). The bioactive metabolites produced by the benthic dinoflagellate (Ternon et al., *in review*; Pavaux et al., 2020) may be detrimental or beneficial to the macroalgal host.

The bioactivity of the SEs combined to the natural settlement of *O*. cf. *ovata* suggests that the colonization preferences of *O.* cf. *ovata* are not driven by the sole bioactivity of the surface chemistry of macroalgae. Indeed, the highest abundance of *O.* cf. *ovata*'s cells were found on *D. dichotoma* that simultaneously presented the highest bioactivity at ecological concentrations (1 mg cm^{-2}). The toxicity of *D. dichotoma* surface chemistry is likely faded by other unknown factors that may include reduced grazing and interspecific competition as shown by the lower ratio dinoflagellates:maxillopods and dinoflagellates:diatoms observed at the surface of *D. dichotoma* compared to other macroalgae. Diterpenes of *Dictyota* spp. have been shown to have deterrent effects on a wide range of herbivores (Hay and Steinberg, 1992; Pereira et al., 2000) and could also target grazers like copepods since they have been shown to be sensitive to various allelochemicals (Ianora et al., 2004). The lower bioactivity of *D. spiralis*

SEs compared to those of *D. dichotoma* (tested at 2 mg cm^{-2}) could not explain the low abundance of *O.* cf. *ovata* on its surface, suggesting the existence of other inhibiting factors controlling the colonization of the dinoflagellate on this macroalga as for instance the large relative abundance of copepods compared to that found at the surface of *D. dichotoma*.

The outcome of this experiment considered neither a spatial nor temporal variability, and rather describes an interaction between macroalgae and *O*. cf. *ovata* at high temperature (~24°C) and salinity (~39) conditions commonly found in the NW Mediterranean coastal waters in summer (Vila et al., 2001). If *O.* cf. *ovata* mostly blooms in summer across the Mediterranean Sea (Ciminiello et al., 2006; Cohu et al., 2013), late blooms are also reported in several areas (Aligizaki and Nikolaidis, 2006; Accoroni et al., 2012). The macroalgae colonized by *O.* cf. *ovata* were shown to differ throughout the year (Aligizaki and Nikolaidis, 2006; Battocchi et al., 2010; Hosny and Labib, 2019) likely in link to the macroalgal seasonality that modifies both their distribution and chemotypes (Paix et al., 2019) as well as their related bioactivity (Salvador Soler et al., 2007). In addition, the growth of *O.* cf. *ovata* was shown to be salinity sensitive (Pistocchi et al., 2011) and is optimal at salinity 36. Salinity also determines the distribution of seaweeds species (Martins et al., 1999) by altering various physiological aspects, including the production of metabolites (Polo et al., 2015). Therefore, at lower salinities areas (e.g Northern Adriatic) a modified macroalgal bioactivity may lead to a different colonization pattern by *O.* cf. *ovata* (Accoroni et al., 2016).

2.6. Conclusion

The present dataset confirms that some Phaeophyceae of the family Dictyotaceae like *T. atomaria*, *Dictyota spp.* or *P. pavonica* may be characterized by a lower abundance of *O*. cf. *ovata* cells. Whether the surface chemistry of the macroalgae have the potential to handicap the growth of *O.* cf. *ovata*, it is not enough to explain the settlement preference on *D. dichotoma* that was found to be the most bioactive species. Complex interlacing factors involving several members of the epiphytic community are likely to modulate the growth of the toxic benthic dinoflagellate *O*. cf. *ovata* on macroalgae.

2.7. Acknowledgments

This work benefited from the support of the project OCEAN-15 (ANR-15-CE35-0002-01) of the French National Research Agency (ANR) and from the project CMAPO (2017) of the French GdR Mediatec. This work was also funded by the French “Sud Provence-Alpes-Côte d’Azur (Sud PACA)” regional council (PhD grant of Benoît Paix). The open access publication was supported by the MSCA project CHEMICROS (H2020-MSCA-IF-841051). The authors are grateful to Anaïs Lebrun for her help with bioassays and to Dr Stéphane Greff (Aix-Marseille University, IMBE) for his help during the acquisition of LC-MS profiles. LC-

MS experiments were conducted on the regional platform MALLABAR funded by the Institute of Ecology and Environment (INEE) of the French National Centre for Scientific Research (CNRS) and the French Sud PACA regional council. The authors declare no conflict of interest.

ANNEXES ELECTRONIQUES

Les **annexes II** à **VIII** pour les parties « *Supplementary information* » des articles des **chapitres II** à **VII** et de l'**Annexe I** : Focus sur *Ostreopsis* cf. *ovata* sont disponibles au format électronique.

Ces annexes électroniques sont les suivantes :

Annexe II : Annexe de l'article presenté dans le **Chapitre II** : Etude préliminaire - *Supplementary information for « Temporal covariation of epibacterial community and surface metabolome in the Mediterranean seaweed holobiont* Taonia atomaria *»*

Annexe III : Annexe de l'article presenté dans le **Chapitre III** : Etude biogéographique - *Supplementary information for « Host phylogeny and biogeography shape the surface microbiota and metabolome of the brown alga* Taonia *(Dictyotales) »*

Annexe IV : Annexe de l'article presenté dans le **Chapitre IV** : Annotation du métabolome - *Supplementary information for « Integration of LC/MS-based molecular networking and classical phytochemical approach allows in-depth annotation of the metabolome of non-model organisms - The case study of the brown seaweed* Taonia atomaria *»*

Annexe V : Annexe de l'article presenté dans le **Chapitre V** : Etude intra-thalle - *Supplementary information for « A multi-omics analysis suggests links between the differentiated surface metabolome and epiphytic microbiota along the thallus of a Mediterranean seaweed holobiont »*

Annexe VI : Annexe de l'article presenté dans le **Chapitre VI** : Suivi spatio-temporel - *Supplementary information for « A multi-omics approach deciphers how temperature and copper stress shape seaweed-microbiota interactions at the surface of* Taonia atomaria *on the NW Mediterranean coast »*

Annexe VIII : Annexe de l'article presenté dans le **Chapitre VII** : Etude en mésocosmes - *Supplementary information for « Synergistic effects of temperature and light affect the relationship between* Taonia atomaria *and its epibacterial community: a mesocosm study »*

Annexe VIII : Annexe de l'article presenté dans l'**Annexe I** : Focus sur *Ostreopsis* cf. *ovata* - *Supplementary information for « Exploring the role of macroalgal surface metabolites on the settlement of the benthic dinoflagellate* Ostreopsis *cf.* ovata *»*

LISTE DES COMMUNICATIONS SCIENTIFIQUES

Publications acceptées (chapitres II, V et annexe I)

Paix, B., Othmani, A., Debroas, D., Culioli, G., and Briand, J.-F. (2019). Temporal covariation of epibacterial community and surface metabolome in the Mediterranean seaweed holobiont *Taonia atomaria*. *Environ. Microbiol.* 21, 3346–3363. doi:10.1111/1462-2920.14617.

Paix, B., Carriot, N., Barry-Martinet, R., Greff, S., Misson, B., Briand, and Culioli, G. (2020). A multi-omics analysis suggests links between the differentiated surface metabolome and epiphytic microbiota along the thallus of a Mediterranean seaweed holobiont. *Front. Microbiol.* 11, 494. doi:10.3389/fmicb.2020.00494.

Ternon, E., **Paix, B.**, Thomas, O. P., Briand, J.-F., and Culioli, G. (2020). Exploring the role of macroalgal surface metabolites on the settlement of the benthic dinoflagellate *Ostreopsis* cf. *ovata*. *Front. Mar. Sci. in press*.

Publication soumise (chapitre VI)

Paix, B., Layglon, N., Le Poupon, C., D'Onofrio, S., Misson, B., Garnier, C., Culioli, G., and Briand, J.-F. (*in prep.*). A multi-omics approach deciphers how temperature and copper stress shape seaweed-microbiota interactions at the surface of *Taonia atomaria* on the NW Mediterranean coast. *Submitted to Microbiome (in review)*

Publications en préparations (chapitres III, IV et VII)

Paix, B., Vieira, C., Potin, P., Leblanc, C., De Clerck, O., Briand, J.-F., and Culioli, G. (*in prep.*). Host phylogeny and biogeography shape the surface microbiota and metabolome of the brown alga *Taonia* (Dictyotales).

Carriot, N., **Paix, B.**, Greff, S., Viguier, B., Briand, J.-F., and Culioli, G. (*in prep.*). Integration of LC/MS-based molecular networking and classical phytochemical approach allows in-depth annotation of the metabolome of non-model organisms - The case study of the brown seaweed *Taonia atomaria*.

Paix, B., Potin, P., Layglon, N., Misson, B., Leblanc, C., Culioli, G., and Briand, J.-F. (*in prep.*). Synergistic effects of temperature and light affect the relationship between *Taonia atomaria* and its epibacterial community: a mesocosm study.

Communications orales

Carriot N., **Paix B.**, Greff S., Briand J.-F., and Culioli G. Variabilité zonale du métabolome de la macroalgue brune *Taonia atomaria*: annotation par l'approche des réseaux moléculaires et liens avec le microbiote associé. MétaSUD 2019 - Journées de métabolomique en Région Sud - Provence Alpes Côte d'Azur, Toulon (France), June 2019.

Paix B., Othmani A., Carriot N., Debroas D., Greff S., Briand J.-F., and Culioli G. Couplage des analyses du métabolome et du microbiome pour comprendre les interactions chimiques saisonnières entre l'algue brune *Taonia atomaria* et ses communautés bactériennes épiphytes. MétaSUD 2019 - Journées de métabolomique en Région SUD - Provence Alpes Côte d'Azur, Toulon (France), June 2019.

Paix, B., Layglon, N., Le Poupon, C., D'Onofrio, S., Misson, B., Peirache, M., Culioli, G., and Briand, J.-F. Effets du métabolome de surface, de la température et de la contamination en métaux traces, sur le microbiote de surface de l'holobionte algal *Taonia atomaria*. IXe Colloque de l'Association Francophone d'Ecologie Microbienne (AFEM), Bussang (France), November 2019.

Communications par affiches

Paix, B., Othmani, A., Catao, E., Debroas, D., Culioli, G., and Briand, J.-F. Seasonal covariation of epibacterial community and surface metabolome in the Mediterranean seaweed holobiont of *Taonia atomaria*. 17th International Symposium on Microbial Ecology, Leipzig (Germany), August 2018.

Paix, B., Layglon, N., Le Poupon, C., D'Onofrio, S., Misson, B., Peirache, M., Culioli, G., and Briand, J.-F. Surface metabolome together with sea water temperature and trace metals contamination shape the surface microbiote of the Mediterranean brown seaweed holobiont *Taonia atomaria*. The Second International Conference on Holobionts, Montréal (QC, Canada), May 2019.

Paix, B., Othmani, A., Carriot, N., Debroas, D., Greff, S., Briand, J.-F., and Culioli, G. Couplage des analyses du métabolome et du microbiome pour comprendre les interactions chimiques saisonnières entre l'algue brune Taonia atomaria et ses communautés bactériennes épiphytes. MétaSUD 2019 - Journées de métabolomique en Région SUD - Provence Alpes Côte d'Azur, Toulon (France), June 2019.

Carriot, N., **Paix, B.**, Greff, S., Briand, J.-F., and Culioli, G. Utilisation de l'approche des réseaux moléculaires pour l'annotation de nouvelles classes de glycérolipides au sein du métabolome de la macroalgue brune Taonia atomaria. MétaSUD 2019 - Journées de métabolomique en Région SUD - Provence Alpes Côte d'Azur, Toulon (France), June 2019.

Autres présentations et actions de vulgarisations

Paix, B., Culioli, G., and Briand, J.-F. Comment la chimie peut-elle aider l'ecologie dans la lutte antifouling ? Conférence – Point Rencontre, Maison du Parc, Porquerolles. July 2017.

Paix, B., and Culioli, G. A la découverte d'un monde microscopique à la surface des algues. Atelier – Fête de la Nature, Maison du Parc, Porquerolles. July 2017.

Paix, B. Atelier microscopie – Fête des la science. Université de Toulon, MAPIEM. Mai 2017

REFERENCES BIBLIOGRAPHIQUES

Abatis, D., Vagias, C., Galanakis, D., Norris, J. N., Moreau, D., Roussakis, C., et al. (2005). Atomarianones A and B: two cytotoxic meroditerpenes from the brown alga *Taonia atomaria*. *Tetrahedron Lett.* 46, 8525–8529. doi:10.1016/j.tetlet.2005.10.007.

Abdul Malik, S. A., Bedoux, G., Garcia Maldonado, J. Q., Freile-Pelegrín, Y., Robledo, D., and Bourgougnon, N. (2019). "Defence on surface: macroalgae and their surface-associated microbiome," in *Advances in Botanical Research* (Academic Press), 327–368. doi:10.1016/bs.abr.2019.11.009.

Abraham, W.-R., and Rohde, M. (2014). "The Family Hyphomonadaceae," in *The Prokaryotes: Alphaproteobacteria and Betaproteobacteria*, eds. E. Rosenberg, E. F. DeLong, S. Lory, E. Stackebrandt, and F. Thompson (Berlin, Heidelberg: Springer Berlin Heidelberg), 283–299. doi:10.1007/978-3-642-30197-1_260.

Accoroni, S., Percopo, I., Cerino, F., Romagnoli, T., Pichierri, S., Perrone, C., et al. (2015). Allelopathic interactions between the HAB dinoflagellate *Ostreopsis* cf. *ovata* and macroalgae. *Harmful Algae* 49, 147–155. doi:10.1016/j.hal.2015.08.007.

Accoroni, S., Romagnoli, T., Pichierri, S., Colombo, F., and Totti, C. (2012). Morphometric analysis of *Ostreopsis* cf. *ovata* cells in relation to environmental conditions and bloom phases. *Harmful Algae* 19, 15–22. doi:10.1016/j.hal.2012.05.003.

Accoroni, S., Romagnoli, T., Pichierri, S., and Totti, C. (2016). Effects of the bloom of harmful benthic dinoflagellate *Ostreopsis* cf. *ovata* on the microphytobenthos community in the northern Adriatic Sea. *Harmful Algae* 55, 179–190. doi:10.1016/j.hal.2016.03.003.

Aires, T., Moalic, Y., Serrao, E. A., and Arnaud-Haond, S. (2015). Hologenome theory supported by cooccurrence networks of species-specific bacterial communities in siphonous algae (*Caulerpa*). *FEMS Microbiol. Ecol.* 91, fiv067. doi:10.1093/femsec/fiv067.

Aires, T., Serebryakova, A., Viard, F., Serrão, E. A., and Engelen, A. H. (2018). Acidification increases abundances of Vibrionales and Planctomycetia associated to a seaweed-grazer system: potential consequences for disease and prey digestion efficiency. *PeerJ* 6, e4377. doi:10.7717/peerj.4377.

Aires, T., Serrão, E. A., and Engelen, A. H. (2016). Host and environmental specificity in bacterial communities associated to two highly invasive marine species (genus *Asparagopsis*). *Front. Microbiol.* 7, 559. doi:10.3389/fmicb.2016.00559.

Aires, T., Serrão, E. A., Kendrick, G., Duarte, C. M., and Arnaud-Haond, S. (2013). Invasion is a community affair: Clandestine followers in the bacterial community associated to green

algae, *Caulerpa racemosa*, track the invasion source. *PLoS One* 8, e68429. doi:10.1371/journal.pone.0068429.

Akagawa-Matsushita, M., Matsuo, M., Koga, Y., and Yamasato, K. (1992). *Alteromonas atlantica* sp. nov. and *Alteromonas carrageenovora* sp. nov., bacteria that decompose algal polysaccharides. *Int. J. Syst. Evol. Microbiol.* 42, 621–627. doi:10.1099/00207713-42-4-621.

Aligizaki, K., and Nikolaidis, G. (2006). The presence of the potentially toxic genera *Ostreopsis* and *Coolia* (Dinophyceae) in the North Aegean Sea, Greece. *Harmful Algae* 5, 717–730. doi:10.1016/j.hal.2006.02.005.

Alsufyani, T., Califano, G., Deicke, M., Grueneberg, J., Weiss, A., Engelen, A. H., et al. (2020). Macroalgal-bacterial interactions: identification and role of thallusin in morphogenesis of the seaweed *Ulva* (Chlorophyta). *J. Exp. Bot.* 71, 3340–3349. doi:10.1093/jxb/eraa066.

Amico, V., Oriente, G., Piattelli, M., Tringali, C., Fattorusso, E., Magno, S., et al. (1977). (-)-(R)-1-O-Geranylgeranylglycerol from the brown alga *Dilophus fasciola*. *Experientia* 33, 989–990. doi:10.1007/BF01945922.

Amico, V., Oriente, G., Piattelli, M., Tringali, C., Fattorusso, E., Magno, S., et al. (1978). Sesquiterpenes based on the cadalane skeleton from the brown alga *Dilophus fasciola*. *Experientia* 35, 450–451. doi:10.1007/BF01922698.

Apprill, A., McNally, S., Parsons, R., and Weber, L. (2015). Minor revision to V4 region SSU rRNA 806R gene primer greatly increases detection of SAR11 bacterioplankton. *Aquat. Microb. Ecol.* 75, 129–137. doi:10.3354/ame01753.

Areche, C., San-Martín, A., Rovirosa, J., Soto-Delgado, J., and Contreras, R. (2009). An unusual halogenated meroditerpenoid from *Stypopodium flabelliforme*: studies by NMR spectroscopic and computational methods. *Phytochemistry* 70, 1315–1320. doi:10.1016/j.phytochem.2009.07.017.

Argelaguet, R., Velten, B., Arnol, D., Dietrich, S., Zenz, T., Marioni, J. C., et al. (2018). Multi-Omics Factor Analysis-a framework for unsupervised integration of multi-omics data sets. *Mol. Syst. Biol.* 14, e8124. doi:10.15252/msb.20178124.

Aßhauer, K. P., Wemheuer, B., Daniel, R., and Meinicke, P. (2015). Tax4Fun: predicting functional profiles from metagenomic 16S rRNA data. *Bioinformatics* 31, 2882–2884. doi:10.1093/bioinformatics/btv287.

Astudillo-García, C., Bell, J. J., Webster, N. S., Glasl, B., Jompa, J., Montoya, J. M., et al. (2017). Evaluating the core microbiota in complex communities: A systematic investigation. *Environ. Microbiol.* 19, 1450–1462. doi:10.1111/1462-2920.13647.

Baedke, J., Fábregas-Tejeda, A., and Delgado, A. N. (2020). The holobiont concept before Margulis. *J. Exp. Zool.* 334, 149–155. doi:10.1002/jez.b.22931.

Baek, K., Choi, A., Kang, I., Im, M., and Cho, J.-C. (2014). *Granulosicoccus marinus* sp. nov., isolated from Antarctic seawater, and emended description of the genus *Granulosicoccus*. *Int. J. Syst. Evol. Microbiol.* 64, 4103–4108. doi:10.1099/ijs.0.070045-0.

Barbeyron, T., L'Haridon, S., Corre, E., Kloareg, B., and Potin, P. (2001). *Zobellia galactanovorans* gen. nov., sp. nov., a marine species of Flavobacteriaceae isolated from a red alga, and classification of [*Cytophaga*] *uliginosa* (ZoBell and Upham 1944) Reichenbach 1989 as *Zobellia uliginosa* gen. nov., comb. nov. *Int. J. Syst. Evol. Microbiol.* 51, 985–997. doi:10.1099/00207713-51-3-985.

Barbeyron, T., Thomas, F., Barbe, V., Teeling, H., Schenowitz, C., Dossat, C., et al. (2016). Habitat and taxon as driving forces of carbohydrate catabolism in marine heterotrophic bacteria: example of the model algae-associated bacterium *Zobellia galactanivorans* DsijT. *Environ. Microbiol.* 18, 4610–4627. doi:10.1111/1462-2920.13584.

Barboza, F. R., Kotta, J., Weinberger, F., Jormalainen, V., Kraufvelin, P., Molis, M., et al. (2019). Geographic variation in fitness-related traits of the bladderwrack *Fucus vesiculosus* along the Baltic Sea-North Sea salinity gradient. *Ecol. Evol.* 9, 9225–9238. doi:10.1002/ece3.5470.

Barott, K. L., Rodriguez-Brito, B., Janouškovec, J., Marhaver, K. L., Smith, J. E., Keeling, P., et al. (2011). Microbial diversity associated with four functional groups of benthic reef algae and the reef-building coral *Montastraea annularis*. *Environ. Microbiol.* 13, 1192–1204. doi:10.1111/j.1462-2920.2010.02419.x.

Bartsev, A. V., Deakin, W. J., Boukli, N. M., McAlvin, C. B., Stacey, G., Malnoë, P., et al. (2004). NopL, an effector protein of *Rhizobium* sp. NGR234, thwarts activation of plant defense reactions. *Plant Physiol.* 134, 871–879. doi:10.1104/pp.103.031740.

Battocchi, C., Totti, C., Vila, M., Masó, M., Capellacci, S., Accoroni, S., et al. (2010). Monitoring toxic microalgae *Ostreopsis* (dinoflagellate) species in coastal waters of the Mediterranean Sea using molecular PCR-based assay combined with light microscopy. *Mar. Pollut. Bull.* 60, 1074–1084. doi:10.1016/j.marpolbul.2010.01.017.

Baumann, P. (2005). Biology bacteriocyte-associated endosymbionts of plant sap-sucking insects. *Annu. Rev. Microbiol.* 59, 155–189. doi:10.1146/annurev.micro.59.030804.121041.

Bech, P. K., Schultz-Johansen, M., Glaring, M. A., Barbeyron, T., Czjzek, M., and Stougaard, P. (2017). *Paraglaciecola hydrolytica* sp. nov., a bacterium with hydrolytic activity against multiple seaweed-derived polysaccharides. *Int. J. Syst. Evol. Microbiol.* 67, 2242–2247. doi:10.1099/ijsem.0.001933.

Bednarz, V. N., Grover, R., and Ferrier-Pagès, C. (2020). Elevated ammonium delays the impairment of the coral-dinoflagellate symbiosis during labile carbon pollution. *Aquat. Toxicol.* 218, 105360. doi:10.1016/j.aquatox.2019.105360.

Bengtsson, M. M., Bühler, A., Brauer, A., Dahlke, S., Schubert, H., and Blindow, I. (2017). Eelgrass leaf surface microbiomes are locally variable and highly correlated with epibiotic eukaryotes. *Front. Microbiol.* 8, 1312. doi:10.3389/fmicb.2017.01312.

Bengtsson, M. M., and Øvreås, L. (2010). Planctomycetes dominate biofilms on surfaces of the kelp *Laminaria hyperborea*. *BMC Microbiol.* 10, 261. doi:10.1186/1471-2180-10-261.

Bengtsson, M. M., Sjøtun, K., Lanzén, A., and Ovreås, L. (2012). Bacterial diversity in relation to secondary production and succession on surfaces of the kelp *Laminaria hyperborea*. *ISME J.* 6, 2188–2198. doi:10.1038/ismej.2012.67.

Bengtsson, M. M., Sjtun, K., and Øvreås, L. (2010). Seasonal dynamics of bacterial biofilms on the kelp *Laminaria hyperborea*. *Aquat. Microb. Ecol.* 60, 71–83. doi:10.3354/ame01409.

Benita, M., Dubinsky, Z., and Iluz, D. (2018). *Padina pavonica*: morphology and calcification functions and mechanism. *Am. J. Plant. Sci.* 09, 1156. doi:10.4236/ajps.2018.96087.

Bertalot, H. L., Witowski, A., and Metzeltin, D. (2000). "Iconographia Diatomologica: Annotated Diatom Micrographs, vol. 7: Diversity - Taxonomy - Identification, Iconographia Diatomologica," in *Diatom flora of Marine Coasts, Vol. 1* (Koeltz).

Bertness, M. D., Leonard, G. H., Levine, J. M., Schmidt, P. R., and Ingraham, A. O. (1999). Testing the relative contribution of positive and negative interactions in rocky intertidal communities. *Ecology* 80, 2711–2726. doi:10.1890/0012-9658(1999)080[2711:TTRCOP]2.0.CO;2.

Béthoux, J. P., Morin, P., Chaumery, C., Connan, O., Gentili, B., and Ruiz-Pino, D. (1998). Nutrients in the Mediterranean Sea, mass balance and statistical analysis of concentrations with respect to environmental change. *Mar. Chem.* 63, 155–169. doi:10.1016/S0304-4203(98)00059-0.

Bianco, É. M., Rogers, R., Teixeira, V. L., and Pereira, R. C. (2009). Antifoulant diterpenes produced by the brown seaweed *Canistrocarpus cervicornis*. *J. Appl. Phycol.* 21, 341–346. doi:10.1007/s10811-008-9374-9.

Bindoff, N. L., Cheung, W. W. L., Kairo, J. G., Arístegui, J., Guinder, V. A., Hallberg, R., et al. (2019). "Chapter 5: Changing ocean, marine ecosystems, and dependent communities," in *IPCC Special Report on the Ocean and Cryosphere in a Changing Climate*.

Bittner, L., Payri, C. E., Couloux, A., Cruaud, C., de Reviers, B., and Rousseau, F. (2008). Molecular phylogeny of the Dictyotales and their position within the Phaeophyceae, based on

nuclear, plastid and mitochondrial DNA sequence data. *Mol. Phylogenet. Evol.* 49, 211–226. doi:10.1016/j.ympev.2008.06.018.

Bland, J. A., and Brock, T. D. (1973). The marine bacterium *Leucothrix mucor* as an algal epiphyte. *Mar. Biol.* 23, 283–292. doi:10.1007/BF00389335.

Blanfuné, A., Boudouresque, C. F., Grossel, H., and Thibaut, T. (2015). Distribution and abundance of *Ostreopsis* spp. and associated species (Dinophyceae) in the northwestern Mediterranean: the region and the macroalgal substrate matter. *Environ. Sci. Pollut. Res.* 22, 12332–12346. doi:10.1007/s11356-015-4525-4.

Blanfuné, A., Boudouresque, C. F., Verlaque, M., Beqiraj, S., Kashta, L., Nasto, I., et al. (2016). Response of rocky shore communities to anthropogenic pressures in Albania (Mediterranean Sea): Ecological status assessment through the CARLIT method. *Mar. Pollut. Bull.* 109, 409–418. doi:10.1016/j.marpolbul.2016.05.041.

Blunt, J. W., Munro, M. H. G., and Munro, M. H. G. (2007). *Dictionary of Marine Natural Products with CD-ROM*. Chapman and Hall/CRC doi:10.1201/9780849382178.

Boachon, B., Lynch, J. H., Ray, S., Yuan, J., Caldo, K. M. P., Junker, R. R., et al. (2019). Natural fumigation as a mechanism for volatile transport between flower organs. *Nat. Chem. Biol.* 15, 583. doi:10.1038/s41589-019-0287-5.

Boisnoir, A., Pavaux, A.-S., Schizas, N. V., Marro, S., Blasco, T., Lemée, R., et al. (2020). The use of stable isotopes to measure the ingestion rate of potentially toxic benthic dinoflagellates by harpacticoid copepods. *J. Exp. Mar. Biol. Ecol.* 524, 151285. doi:10.1016/j.jembe.2019.151285.

Bondoso, J., Godoy-Vitorino, F., Balagué, V., Gasol, J. M., Harder, J., and Lage, O. M. (2017). Epiphytic Planctomycetes communities associated with three main groups of macroalgae. *FEMS Microbiol. Ecol.* 93. doi:10.1093/femsec/fiw255.

Bondoso, J., Harder, J., and Lage, O. M. (2013). rpoB gene as a novel molecular marker to infer phylogeny in Planctomycetales. *Antonie Van Leeuwenhoek* 104, 477–488. doi:10.1007/s10482-013-9980-7.

Bordenstein, S. R., and Theis, K. R. (2015). Host biology in light of the microbiome: ten principles of holobionts and hologenomes. *PLoS Biol.* 13, e1002226. doi:10.1371/journal.pbio.1002226.

Borges, V. P., Bastos, E., Batista, M. B., Bouzon, Z., Lhullier, C., Schmidt, E. C., et al. (2014). The genus *Melobesia* (Corallinales, Rhodophyta) from the subtropical South Atlantic, with the addition of *M. rosanoffii* (Foslie) Lemoine. *Phytotaxa* 190, 268–276. doi:10.11646/phytotaxa.190.1.16.

Boudouresque, C. F., Blanfuné, A., Ruitton, S., and Thibaut, T. (2020). “Chapter 17 - Macroalgae as a tool for coastal management in the Mediterranean Sea,” in *Handbook of Algal Science, Technology and Medicine*, ed. O. Konur (Academic Press), 277–290. doi:10.1016/B978-0-12-818305-2.00017-6.

Boudouresque, C.-F., Bertrand, J.-C., Caumette, P., and Normand, P. (2011). “Systématique et évolution des micro-organismes : concepts généraux.,” in *Ecologie microbienne. Microbiologie des milieux naturels et anthropisés.*, eds. B. J.C, C. P, L. P, M. R, and N. P (Presses Universitaires de Pau et des Pays de l’Adour), 119–157. Available at: https://hal.archives-ouvertes.fr/hal-00808568 [Accessed June 10, 2020].

Bourne, D. G., Morrow, K. M., and Webster, N. S. (2016). Insights into the coral microbiome: underpinning the health and resilience of reef ecosystems. *Annu. Rev. Microbiol.* 70, 317–340. doi:10.1146/annurev-micro-102215-095440.

Bourne, D. G., and Munn, C. B. (2005). Diversity of bacteria associated with the coral *Pocillopora damicornis* from the Great Barrier Reef. *Environ. Microbiol.* 7, 1162–1174. doi:10.1111/j.1462-2920.2005.00793.x.

Bourne, D., Iida, Y., Uthicke, S., and Smith-Keune, C. (2008). Changes in coral-associated microbial communities during a bleaching event. *ISME J.* 2, 350–363. doi:10.1038/ismej.2007.112.

Briand, J.-F., Barani, A., Garnier, C., Réhel, K., Urvois, F., LePoupon, C., et al. (2017). Spatio-temporal variations of marine biofilm communities colonizing artificial substrata including antifouling coatings in contrasted french coastal environments. *Microb. Ecol.* 74, 585–598. doi:10.1007/s00248-017-0966-2.

Brock, E., Nylund, G. M., and Pavia, H. (2007). Chemical inhibition of barnacle larval settlement by the brown alga *Fucus vesiculosus*. *Mar. Ecol. Prog. Ser.* 337, 165–174. doi:10.3354/meps337165.

Brown, B. E. (1997). Coral bleaching: causes and consequences. *Coral Reefs* 16, S129–S138. doi:10.1007/s003380050249.

Bruno, J. F., Stachowicz, J. J., and Bertness, M. D. (2003). Inclusion of facilitation into ecological theory. *Trends Ecol. Evol.* 18, 119–125. doi:10.1016/S0169-5347(02)00045-9.

Buchan, A., LeCleir, G. R., Gulvik, C. A., and González, J. M. (2014). Master recyclers: features and functions of bacteria associated with phytoplankton blooms. *Nat. Rev. Microbiol.* 12, 686–698. doi:10.1038/nrmicro3326.

Bullock, H. A., Luo, H., and Whitman, W. B. (2017). Evolution of dimethylsulfoniopropionate metabolism in marine phytoplankton and bacteria. *Front. Microbiol.* 8, 637. doi:10.3389/fmicb.2017.00637.

Burgunter-Delamare, B., KleinJan, H., Frioux, C., Fremy, E., Wagner, M., Corre, E., et al. (2020). Metabolic complementarity between a brown alga and associated cultivable bacteria provide indications of beneficial interactions. *Front. Mar. Sci.* 7. doi:10.3389/fmars.2020.00085.

Burke, C., Steinberg, P., Rusch, D., Kjelleberg, S., and Thomas, T. (2011a). Bacterial community assembly based on functional genes rather than species. *Proc. Natl. Acad. Sci. U.S.A.* 108, 14288–14293. doi:10.1073/pnas.1101591108.

Burke, C., Thomas, T., Lewis, M., Steinberg, P., and Kjelleberg, S. (2011b). Composition, uniqueness and variability of the epiphytic bacterial community of the green alga *Ulva australis*. *ISME J.* 5, 590–600. doi:10.1038/ismej.2010.164.

Buschmann, A. H., Riquelme, V. A., Hernández-González, M. C., Varela, D., Jiménez, J. E., Henríquez, L. A., et al. (2006). A review of the impacts of salmonid farming on marine coastal ecosystems in the southeast Pacific. *ICES J. Mar. Sci.* 63, 1338–1345. doi:10.1016/j.icesjms.2006.04.021.

Califano, G., Kwantes, M., Abreu, M. H., Costa, R., and Wichard, T. (2020). Cultivating the macroalgal holobiont: effects of integrated multi-trophic aquaculture on the microbiome of *Ulva rigida* (Chlorophyta). *Front. Mar. Sci.* 7. doi:10.3389/fmars.2020.00052.

Campbell, A. H., Harder, T., Nielsen, S., Kjelleberg, S., and Steinberg, P. D. (2011). Climate change and disease: bleaching of a chemically defended seaweed. *Glob. Change Biol.* 17, 2958–2970. doi:10.1111/j.1365-2486.2011.02456.x.

Campbell, A. H., Vergés, A., and Steinberg, P. D. (2014). Demographic consequences of disease in a habitat-forming seaweed and impacts on interactions between natural enemies. *Ecology* 95, 142–152.

Camps, M., Barani, A., Gregori, G., Bouchez, A., Berre, B. L., Bressy, C., et al. (2014). Antifouling coatings influence both abundance and community structure of colonizing biofilms: a case study in the Northwestern Mediterranean sea. *Appl. Environ. Microbiol.* 80, 4821–4831. doi:10.1128/AEM.00948-14.

Caporaso, J. G., Lauber, C. L., Walters, W. A., Berg-Lyons, D., Huntley, J., Fierer, N., et al. (2012). Ultra-high-throughput microbial community analysis on the Illumina HiSeq and MiSeq platforms. *ISME J.* 6, 1621–1624. doi:10.1038/ismej.2012.8.

Caporaso, J. G., Lauber, C. L., Walters, W. A., Berg-Lyons, D., Lozupone, C. A., Turnbaugh, P. J., et al. (2011). Global patterns of 16S rRNA diversity at a depth of millions of sequences per sample. *Proc. Natl. Acad. Sci. U.S.A.* 108 Suppl 1, 4516–4522. doi:10.1073/pnas.1000080107.

Carnicer, O., Guallar, C., Andree, K. B., Diogène, J., and Fernández-Tejedor, M. (2015). *Ostreopsis* cf. *ovata* dynamics in the NW Mediterranean Sea in relation to biotic and abiotic factors. *Environ. Res.* 143, 89–99. doi:10.1016/j.envres.2015.08.023.

Carroll, A. R., Copp, B. R., Davis, R. A., Keyzers, R. A., and Prinsep, M. R. (2019). Marine natural products. *Nat. Prod. Rep.* 36, 122–173. doi:10.1039/C8NP00092A.

Casabianca, S., Casabianca, A., Riobó, P., Franco, J. M., Vila, M., and Penna, A. (2013). Quantification of the toxic dinoflagellate *Ostreopsis* spp. by qPCR assay in marine aerosol. *Environ. Sci. Technol.* 47, 3788–3795. doi:10.1021/es305018s.

Case, R. J., Longford, S. R., Campbell, A. H., Low, A., Tujula, N., Steinberg, P. D., et al. (2011). Temperature induced bacterial virulence and bleaching disease in a chemically defended marine macroalga. *Environ. Microbiol.* 13, 529–537. doi:10.1111/j.1462-2920.2010.02356.x.

Catania, F., Krohs, U., Chittò, M., Ferro, D., Ferro, K., Lepennetier, G., et al. (2017). The hologenome concept: we need to incorporate function. *Theory Biosci.* 136, 89–98. doi:10.1007/s12064-016-0240-z.

Catão, E. C. P., Pollet, T., Misson, B., Garnier, C., Ghiglione, J.-F., Barry-Martinet, R., et al. (2019). Shear stress as a major driver of marine biofilm communities in the NW Mediterranean sea. *Front. Microbiol.* 10. doi:10.3389/fmicb.2019.01768.

Cavalcanti, G. S., Shukla, P., Morris, M., Ribeiro, B., Foley, M., Doane, M. P., et al. (2018). Rhodoliths holobionts in a changing ocean: host-microbes interactions mediate coralline algae resilience under ocean acidification. *BMC Genomics* 19, 701. doi:10.1186/s12864-018-5064-4.

Chaleckis, R., Meister, I., Zhang, P., and Wheelock, C. E. (2019). Challenges, progress and promises of metabolite annotation for LC-MS-based metabolomics. *Curr. Opin. Biotechnol.* 55, 44–50. doi:10.1016/j.copbio.2018.07.010.

Chang, Y.-C., and Lee, T.-M. (1999). High temperature-induced free proline accumulation in *Gracilaria tenuistipitata* (Rhodophyta). *Bot. Bull. Acad. Sinica* 40, 289–294.

Chen, L., Kieber, D. J., Amato, F., Vila, M., Viure, L., Alastuey, A., et al. (2020). Dimethylsulfoniopropionate concentrations in Mediterranean coastal water and ambient aerosols during *Ostreopsis* cf. *ovata* blooms. in (AGU). Available at: https://agu.confex.com/agu/osm20/meetingapp.cgi/Paper/649841 [Accessed June 24, 2020].

Chen, M. Y., and Parfrey, L. W. (2018). Incubation with macroalgae induces large shifts in water column microbiota, but minor changes to the epibiota of co-occurring macroalgae. *Mol. Ecol.* 27, 1966–1979. doi:10.1111/mec.14548.

Chong, J., Soufan, O., Li, C., Caraus, I., Li, S., Bourque, G., et al. (2018). MetaboAnalyst 4.0: towards more transparent and integrative metabolomics analysis. *Nucleic Acids Res.* 46, W486–W494. doi:10.1093/nar/gky310.

Chong, J., Wishart, D. S., and Xia, J. (2019). Using Metaboanalyst 4.0 for comprehensive and integrative metabolomics data analysis. *Curr. Protoc. Bioinformatics* 68, e86. doi:10.1002/cpbi.86.

Ciminiello, P., Dell'Aversano, C., Fattorusso, E., Forino, M., Magno, G. S., Tartaglione, L., et al. (2006). The Genoa 2005 outbreak. Determination of putative palytoxin in Mediterranean *Ostreopsis ovata* by a new liquid chromatography tandem mass spectrometry method. *Anal. Chem.* 78, 6153–6159. doi:10.1021/ac060250j.

Cirri, E., Grosser, K., and Pohnert, G. (2016). A solid phase extraction based non-disruptive sampling technique to investigate the surface chemistry of macroalgae. *Biofouling* 32, 145–153. doi:10.1080/08927014.2015.1130823.

Clerck, O. D., Leliaert, F., Verbruggen, H., Lane, C. E., Paula, J. C. D., Payo, D. A., et al. (2006). A revised classification of the Dictyoteae (Dictyotales, Phaeophyceae) based on rbcL and 26S ribosomal DNA sequence analyses. *J. Phycol.* 42, 1271–1288. doi:10.1111/j.1529-8817.2006.00279.x.

Coclet, C., Garnier, C., Delpy, F., Jamet, D., Durrieu, G., Le Poupon, C., et al. (2018). Trace metal contamination as a toxic and structuring factor impacting ultraphytoplankton communities in a multicontaminated Mediterranean coastal area. *Prog. Oceanogr.* 163, 196–213. doi:10.1016/j.pocean.2017.06.006.

Coclet, C., Garnier, C., Durrieu, G., D'onofrio, S., Layglon, N., Briand, J.-F., et al. (2020). Impacts of copper and lead exposure on prokaryotic communities from contaminated contrasted coastal seawaters: the influence of previous metal exposure. *FEMS Microbiol. Ecol.* 96. doi:10.1093/femsec/fiaa048.

Coclet, C., Garnier, C., Durrieu, G., Omanović, D., D'Onofrio, S., Le Poupon, C., et al. (2019). Changes in bacterioplankton communities resulting from direct and indirect interactions with trace metal gradients in an urbanized marine coastal area. *Front. Microbiol.* 10, 257. doi:10.3389/fmicb.2019.00257.

Coclet, C., Garnier, C., Durrieu, G., Omanović, D., D'onofrio, S., Le Poupon, C., et al. Metal contamination and relationships with bacterioplankton community appear as marginal drivers for biofilm communities in an anthropized coastal area. *Submitted to Sci. Total Environ.*

Coelho-Souza, S. A., Jenkins, S. R., Casarin, A., Baeta-Neves, M. H., Salgado, L. T., Guimaraes, J. R. D., et al. (2017). The effect of light on bacterial activity in a seaweed holobiont. *Microb. Ecol.* 74, 868–876. doi:10.1007/s00248-017-0995-x.

Cohu, S., Mangialajo, L., Thibaut, T., Blanfuné, A., Marro, S., and Lemée, R. (2013). Proliferation of the toxic dinoflagellate *Ostreopsis* cf. *ovata* in relation to depth, biotic substrate and environmental factors in the North West Mediterranean Sea. *Harmful Algae* 24, 32–44. doi:10.1016/j.hal.2013.01.002.

Cohu, S., Thibaut, T., Mangialajo, L., Labat, J.-P., Passafiume, O., Blanfuné, A., et al. (2011). Occurrence of the toxic dinoflagellate *Ostreopsis* cf. *ovata* in relation with environmental factors in Monaco (NW Mediterranean). *Mar. Pollut. Bull.* 62, 2681–2691. doi:10.1016/j.marpolbul.2011.09.022.

Coll, M., Piroddi, C., Steenbeek, J., Kaschner, K., Lasram, F. B. R., Aguzzi, J., et al. (2010). The biodiversity of the Mediterranean sea: Estimates, patterns, and threats. *PLoS One* 5, e11842. doi:10.1371/journal.pone.0011842.

Collins, M., Knutti, R., Arblaster, J., Dufresne, J.-L., Fichefet, T., Friedlingstein, P., et al. (2013). "Chapter 12: Long-term climate change: Projections, commitments and irreversibility," in *IPCC, 2013: Climate Change 2013: The Physical Science Basis. Contribution of Working Group I to the Fifth Assessment Report of the Intergovernmental Panel on Climate Change*.

Collins, M., Sutherland, M., Bouwer, L., Cheong, S.-M., Frölicher, T., Jacot Des Combes, H., et al. (2019). "Chapitre 6: Extremes, abrupt changes and managing risk," in *IPCC Special Report on the Ocean and Cryosphere in a Changing Climate*.

Compère, C., Bellon-Fontaine, M.-N., Bertrand, P., Costa, D., Marcus, P., Poleunis, C., et al. (2001). Kinetics of conditioning layer formation on stainless steel immersed in seawater. *Biofouling* 17, 129–145. doi:10.1080/08927010109378472.

Connan, S., and Stengel, D. B. (2011). Impacts of ambient salinity and copper on brown algae: 1. Interactive effects on photosynthesis, growth, and copper accumulation. *Aquat. Toxicol.* 104, 94–107. doi:10.1016/j.aquatox.2011.03.015.

Cosse, A., Potin, P., and Leblanc, C. (2009). Patterns of gene expression induced by oligoguluronates reveal conserved and environment-specific molecular defense responses in the brown alga *Laminaria digitata*. *New Phytol.* 182, 239–250. doi:10.1111/j.1469-8137.2008.02745.x.

Costa, G. B., de Felix, M. R. L., Simioni, C., Ramlov, F., Oliveira, E. R., Pereira, D. T., et al. (2016). Effects of copper and lead exposure on the ecophysiology of the brown seaweed *Sargassum cymosum*. *Protoplasma* 253, 111–125. doi:10.1007/s00709-015-0795-4.

Costerton, J. W., Cheng, K. J., Geesey, G. G., Ladd, T. I., Nickel, J. C., Dasgupta, M., et al. (1987). Bacterial biofilms in nature and disease. *Annu. Rev. Microbiol.* 41, 435–464. doi:10.1146/annurev.mi.41.100187.002251.

Croft, M. T., Lawrence, A. D., Raux-Deery, E., Warren, M. J., and Smith, A. G. (2005). Algae acquire vitamin B12 through a symbiotic relationship with bacteria. *Nature* 438, 90–93. doi:10.1038/nature04056.

Curson, A. R. J., Liu, J., Bermejo Martínez, A., Green, R. T., Chan, Y., Carrión, O., et al. (2017). Dimethylsulfoniopropionate biosynthesis in marine bacteria and identification of the key gene in this process. *Nat. Microbiol.* 2, 17009. doi:10.1038/nmicrobiol.2017.9.

Curson, A. R. J., Rogers, R., Todd, J. D., Brearley, C. A., and Johnston, A. W. B. (2008). Molecular genetic analysis of a dimethylsulfoniopropionate lyase that liberates the climate-changing gas dimethylsulfide in several marine alpha-proteobacteria and *Rhodobacter sphaeroides*. *Environ. Microbiol.* 10, 757–767. doi:10.1111/j.1462-2920.2007.01499.x.

Curson, A. R. J., Todd, J. D., Sullivan, M. J., and Johnston, A. W. B. (2011). Catabolism of dimethylsulphoniopropionate: microorganisms, enzymes and genes. *Nat. Rev. Microbiol.* 9, 849–859. doi:10.1038/nrmicro2653.

da Costa, E., Azevedo, V., Melo, T., Rego, A. M., V Evtuguin, D., Domingues, P., et al. (2018). High-Resolution lipidomics of the early life stages of the red seaweed *Porphyra dioica*. *Molecules* 23, 187. doi:10.3390/molecules23010187.

da Costa, E., Domingues, P., Melo, T., Coelho, E., Pereira, R., Calado, R., et al. (2019). Lipidomic signatures reveal seasonal shifts on the relative abundance of high-valued lipids from the brown algae *Fucus vesiculosus*. *Mar. Drugs* 17, 335. doi:10.3390/md17060335.

da Gama, B. A. P., Plouguerné, E., and Pereira, R. C. (2014). "Chapter fourteen - The antifouling defence mechanisms of marine macroalgae," in *Advances in Botanical Research* Sea Plants., ed. N. Bourgougnon (Academic Press), 413–440. Available at: http://www.sciencedirect.com/science/article/pii/B9780124080621000147 [Accessed November 7, 2016].

da Silva, R. R., Dorrestein, P. C., and Quinn, R. A. (2015). Illuminating the dark matter in metabolomics. *Proc. Natl. Acad. Sci. U.S.A.* 112, 12549–12550. doi:10.1073/pnas.1516878112.

Dang, D. H., Layglon, N., Ferretto, N., Omanović, D., Mullot, J.-U., Lenoble, V., et al. (2020). Kinetic processes of copper and lead remobilization during sediment resuspension of marine polluted sediments. *Sci. Total Environ.* 698, 134120. doi:10.1016/j.scitotenv.2019.134120.

Dang, H., and Lovell, C. R. (2016). Microbial surface colonization and biofilm development in marine environments. *Microbiol. Mol. Biol. Rev.* 80, 91–138. doi:10.1128/MMBR.00037-15.

Davy, S. K., Allemand, D., and Weis, V. M. (2012). Cell biology of cnidarian-dinoflagellate symbiosis. *Microbiol. Mol. Biol. Rev.* 76, 229–261. doi:10.1128/MMBR.05014-11.

de Mesquita, M. M. F., Crapez, M. A. C., Teixeira, V. L., and Cavalcanti, D. N. (2019). Potential interactions bacteria-brown algae. *J. Appl. Phycol.* 31, 867–883. doi:10.1007/s10811-018-1573-4.

de Nys, R., Dworjanyn, S. A., and Steinberg, P. D. (1998). A new method for determining surface concentrations of marine natural products on seaweeds. *Mar. Ecol. Prog. Ser.* 162, 79–87. doi:10.3354/meps162079.

de Nys, R., Steinberg, P. D., Willemsen, P., Dworjanyn, S. A., Gabelish, C. L., and King, R. J. (1995). Broad spectrum effects of secondary metabolites from the red alga *Delisea pulchra* in antifouling assays. *Biofouling* 8, 259–271. doi:10.1080/08927019509378279.

de Nys, R., Wright, A. D., König, G. M., and Sticher, O. (1993). New halogenated furanones from the marine alga *Delisea pulchra* (cf. *fimbriata*). *Tetrahedron* 49, 11213–11220. doi:10.1016/S0040-4020(01)81808-1.

De Rosa, S., De Giulio, A., Iodice, C., and Zavodink, N. (1994). Sesquiterpenes from the brown alga *Taonia atomaria*. *Phytochemistry* 37, 1327–1330. doi:10.1016/S0031-9422(00)90407-2.

Debroas, D., Mone, A., and Ter Halle, A. (2017). Plastics in the North Atlantic garbage patch: A boat-microbe for hitchhikers and plastic degraders. *Sci. Total Environ.* 599–600, 1222–1232. doi:10.1016/j.scitotenv.2017.05.059.

Della Sala, G., Hochmuth, T., Teta, R., Costantino, V., and Mangoni, A. (2014). Polyketide synthases in the microbiome of the marine sponge *Plakortis halichondrioides*: a metagenomic update. *Mar. Drugs* 12, 5425–5440. doi:10.3390/md12115425.

Dembitsky, V. M. (1996). Betaine ether-linked glycerolipids: chemistry and biology. *Prog. Lipid Res.* 35, 1–51. doi:10.1016/0163-7827(95)00009-7.

Dettmer, K., Aronov, P. A., and Hammock, B. D. (2007). Mass spectrometry-based metabolomics. *Mass. Spectrom. Rev.* 26, 51–78. doi:10.1002/mas.20108.

Dittami, S. M., Arboleda, E., Auguet, J.-C., Bigalke, A., Briand, E., Cardenas, P., et al. (2020). A community perspective on the concept of marine holobionts: current status, challenges, and future directions. PeerJ Inc. doi:10.7287/peerj.preprints.27519v3.

Dittami, S. M., Duboscq-Bidot, L., Perennou, M., Gobet, A., Corre, E., Boyen, C., et al. (2016). Host–microbe interactions as a driver of acclimation to salinity gradients in brown algal cultures. *ISME J.* 10, 51–63. doi:10.1038/ismej.2015.104.

Dittami, S. M., Eveillard, D., and Tonon, T. (2014). A metabolic approach to study algal–bacterial interactions in changing environments. *Mol. Ecol.* 23, 1656–1660. doi:10.1111/mec.12670.

Dittami, S. M., Gravot, A., Renault, D., Goulitquer, S., Eggert, A., Bouchereau, A., et al. (2011). Integrative analysis of metabolite and transcript abundance during the short-term response to saline and oxidative stress in the brown alga *Ectocarpus siliculosus*. *Plant Cell Environ.* 34, 629–642. doi:10.1111/j.1365-3040.2010.02268.x.

Dobretsov, S., Dahms, H., Harder, T., and Qian, P. (2006). Allelochemical defense against epibiosis in the macroalga *Caulerpa racemosa* var. *turbinata*. *Mar. Ecol. Prog. Ser.* 318, 165–175. doi:10.3354/meps318165.

Dobretsov, S., Dahms, H.-U., Tsoi, M. Y., and Qian, P.-Y. (2005). Chemical control of epibiosis by Hong Kong sponges: the effect of sponge extracts on micro- and macrofouling communities. *Mar. Ecol. Prog. Ser.* 297, 119–129. doi:10.3354/meps297119.

Dobretsov, S., and Qian, P.-Y. (2004). The role of epibotic bacteria from the surface of the soft coral *Dendronephthya* sp. in the inhibition of larval settlement. *J. Exp. Mar. Biol. Ecol.* 299, 35–50. doi:10.1016/j.jembe.2003.08.011.

Dogs, M., Wemheuer, B., Wolter, L., Bergen, N., Daniel, R., Simon, M., et al. (2017). Rhodobacteraceae on the marine brown alga *Fucus spiralis* are predominant and show physiological adaptation to an epiphytic lifestyle. *Syst. Appl. Microbiol.* 40, 370–382. doi:10.1016/j.syapm.2017.05.006.

Domingo-Almenara, X., Brezmes, J., Vinaixa, M., Samino, S., Ramirez, N., Ramon-Krauel, M., et al. (2016). eRah: A computational tool integrating spectral deconvolution and alignment with quantification and identification of metabolites in GC/MS-based metabolomics. *Anal. Chem.* 88, 9821–9829. doi:10.1021/acs.analchem.6b02927.

Donlan, R. M. (2002). Biofilms: microbial life on surfaces. *Emerg. Infect. Dis.* 8, 881–890. doi:10.3201/eid0809.020063.

Dray, S., and Dufour, A.-B. (2007). The ade4 package: implementing the duality diagram for ecologists. *J. Stat. Softw.* 22, 1–20. doi:10.18637/jss.v022.i04.

Duncan, K. R., Crüsemann, M., Lechner, A., Sarkar, A., Li, J., Ziemert, N., et al. (2015). Molecular networking and pattern-based genome mining improves discovery of biosynthetic gene clusters and their products from *Salinispora* species. *Chem. Biol.* 22, 460–471. doi:10.1016/j.chembiol.2015.03.010.

Dunne, W. M. (2002). Bacterial adhesion: seen any good biofilms lately? *Clin. Microbiol. Rev.* 15, 155–166. doi:10.1128/CMR.15.2.155-166.2002.

Dworjanyn, S. A., De Nys, R., and Steinberg, P. D. (1999). Localisation and surface quantification of secondary metabolites in the red alga *Delisea pulchra*. *Mar. Biol.* 133, 727–736. doi:10.1007/s002270050514.

Dworjanyn, S. A., Nys, R. de, and Steinberg, P. D. (2006). Chemically mediated antifouling in the red alga *Delisea pulchra*. *Mar. Ecol. Prog. Ser.* 318, 153–163. doi:10.3354/meps318153.

Edgar, R. C. (2004). MUSCLE: multiple sequence alignment with high accuracy and high throughput. *Nucleic Acids Res.* 32, 1792–1797. doi:10.1093/nar/gkh340.

Egan, S., Fernandes, N. D., Kumar, V., Gardiner, M., and Thomas, T. (2014). Bacterial pathogens, virulence mechanism and host defence in marine macroalgae. *Environ. Microbiol.* 16, 925–938. doi:10.1111/1462-2920.12288.

Egan, S., and Gardiner, M. (2016). Microbial dysbiosis: rethinking disease in marine ecosystems. *Front. Microbiol.* 7, 991. doi:10.3389/fmicb.2016.00991.

Egan, S., Harder, T., Burke, C., Steinberg, P., Kjelleberg, S., and Thomas, T. (2013). The seaweed holobiont: understanding seaweed–bacteria interactions. *FEMS Microbiol. Rev.* 37, 462–476. doi:10.1111/1574-6976.12011.

Egan, S., James, S., Holmström, C., and Kjelleberg, S. (2001). Inhibition of algal spore germination by the marine bacterium *Pseudoalteromonas tunicata*. *FEMS Microbiol. Ecol.* 35, 67–73.

Eggert, A. (2012). "Seaweed responses to temperature," in *Seaweed Biology: Novel Insights into Ecophysiology, Ecology and Utilization* Ecological Studies., eds. C. Wiencke and K. Bischof (Berlin, Heidelberg: Springer), 47–66. doi:10.1007/978-3-642-28451-9_3.

Escudié, F., Auer, L., Bernard, M., Mariadassou, M., Cauquil, L., Vidal, K., et al. (2018). FROGS: Find, Rapidly, OTUs with Galaxy Solution. *Bioinformatics* 34, 1287–1294. doi:10.1093/bioinformatics/btx791.

Evans, R. D., Wilson, S. K., Field, S. N., and Moore, J. A. Y. (2014). Importance of macroalgal fields as coral reef fish nursery habitat in north-west Australia. *Mar. Biol.* 161, 599–607. doi:10.1007/s00227-013-2362-x.

Faimali, M., Giussani, V., Piazza, V., Garaventa, F., Corrà, C., Asnaghi, V., et al. (2012). Toxic effects of harmful benthic dinoflagellate *Ostreopsis ovata* on invertebrate and vertebrate marine organisms. *Mar. Environ. Res.* 76, 97–107. doi:10.1016/j.marenvres.2011.09.010.

Fattorusso, E., Magno, S., Mayol, L., Santacroce, C., Sica, D., Amico, V., et al. (1976). Dictyol A and B, two novel diterpene alcohols from the brown alga *Dictyota dichotoma*. *J. Chem. Soc. Chem. Comm.* 0, 575–576. doi:10.1039/C39760000575.

Faust, K., and Raes, J. (2016). CoNet app: inference of biological association networks using Cytoscape. *F1000Res* 5, 1519. doi:10.12688/f1000research.9050.2.

Favre, L., Ortalo-Magné, A., Greff, S., Pérez, T., Thomas, O. P., Martin, J.-C., et al. (2017). Discrimination of four marine biofilm-forming bacteria by LC-MS metabolomics and

influence of culture parameters. *J. Proteome Res.* 16, 1962–1975. doi:10.1021/acs.jproteome.6b01027.

Fernandes, N., Case, R. J., Longford, S. R., Seyedsayamdost, M. R., Steinberg, P. D., Kjelleberg, S., et al. (2011). Genomes and virulence factors of novel bacterial pathogens causing bleaching disease in the marine red alga *Delisea pulchra*. *PLoS One* 6, e27387. doi:10.1371/journal.pone.0027387.

Fernandes, N., Steinberg, P., Rusch, D., Kjelleberg, S., and Thomas, T. (2012). Community structure and functional gene profile of bacteria on healthy and diseased thalli of the red seaweed *Delisea pulchra*. *PLoS One* 7, e50854. doi:10.1371/journal.pone.0050854.

Flemming, H.-C., Wingender, J., Szewzyk, U., Steinberg, P., Rice, S. A., and Kjelleberg, S. (2016). Biofilms: an emergent form of bacterial life. *Nat. Rev. Microbiol.* 14, 563–575. doi:10.1038/nrmicro.2016.94.

Flemming, H.-C., and Wuertz, S. (2019). Bacteria and archaea on Earth and their abundance in biofilms. *Nat. Rev. Microbiol.* 17, 247–260. doi:10.1038/s41579-019-0158-9.

Florez, J. Z., Camus, C., Hengst, M. B., and Buschmann, A. H. (2017). A functional perspective analysis of macroalgae and epiphytic bacterial community interaction. *Front. Microbiol.* 8, 2561. doi:10.3389/fmicb.2017.02561.

Florez, J. Z., Camus, C., Hengst, M. B., Marchant, F., and Buschmann, A. H. (2019). Structure of the epiphytic bacterial communities of *Macrocystis pyrifera* in localities with contrasting nitrogen concentrations and temperature. *Algal Res.* 44, 101706. doi:10.1016/j.algal.2019.101706.

Flórez, L. V., Biedermann, P. H. W., Engl, T., and Kaltenpoth, M. (2015). Defensive symbioses of animals with prokaryotic and eukaryotic microorganisms. *Nat. Prod. Rep.* 32, 904–936. doi:10.1039/C5NP00010F.

Flot, J.-F., Bauermeister, J., Brad, T., Hillebrand-Voiculescu, A., Sarbu, S. M., and Dattagupta, S. (2014). *Niphargus–Thiothrix* associations may be widespread in sulphidic groundwater ecosystems: evidence from southeastern Romania. *Mol. Ecol.* 23, 1405–1417. doi:10.1111/mec.12461.

Frölicher, T. L., Fischer, E. M., and Gruber, N. (2018). Marine heatwaves under global warming. *Nature* 560, 360–364. doi:10.1038/s41586-018-0383-9.

Fukui, Y., Abe, M., Kobayashi, M., Saito, H., Oikawa, H., Yano, Y., et al. (2013). *Algimonas porphyrae* gen. nov., sp. nov., a member of the family Hyphomonadaceae, isolated from the red alga *Porphyra yezoensis*. *Int. J. Syst. Evol. Microbiol.* 63, 314–320. doi:10.1099/ijs.0.040485-0.

Furlan, M., Antonioli, M., Zingone, A., Sardo, A., Blason, C., Pallavicini, A., et al. (2013). Molecular identification of *Ostreopsis* cf. *ovata* in filter feeders and putative predators. *Harmful Algae* 21–22, 20–29. doi:10.1016/j.hal.2012.11.004.

Gaillard, J. (1972). Quelques remarques sur le cycle reproducteur des Dictyotales et sur ses variations. *Bull. Soc. Bot. France* 119, 145–150. doi:10.1080/00378941.1972.10839084.

Galand, P. E., Pereira, O., Hochart, C., Auguet, J. C., and Debroas, D. (2018). A strong link between marine microbial community composition and function challenges the idea of functional redundancy. *ISME J.* 12, 2470–2478. doi:10.1038/s41396-018-0158-1.

Gardiner, M., Bournazos, A. M., Maturana-Martinez, C., Zhong, L., and Egan, S. (2017). Exoproteome analysis of the seaweed pathogen *Nautella italica* R11 reveals temperature-dependent regulation of RTX-like proteins. *Front. Microbiol.* 8. doi:10.3389/fmicb.2017.01203.

Gardiner, M., Fernandes, N. D., Nowakowski, D., Raftery, M., Kjelleberg, S., Zhong, L., et al. (2015). VarR controls colonization and virulence in the marine macroalgal pathogen *Nautella italica* R11. *Front. Microbiol.* 6. doi:10.3389/fmicb.2015.01130.

Gaubert, J., Payri, C. E., Vieira, C., Solanki, H., and Thomas, O. P. (2019). High metabolic variation for seaweeds in response to environmental changes: a case study of the brown algae *Lobophora* in coral reefs. *Sci. Rep.* 9, 993. doi:10.1038/s41598-018-38177-z.

Gémin, M.-P., Réveillon, D., Hervé, F., Pavaux, A.-S., Tharaud, M., Séchet, V., et al. (2019). Toxin content of *Ostreopsis* cf. *ovata* depends on bloom phases, depth and macroalgal substrate in the NW Mediterranean Sea. *Harmful Algae* 92, 101727. doi:10.1016/j.hal.2019.101727.

Geng, H., and Belas, R. (2010). Molecular mechanisms underlying *Roseobacter*–phytoplankton symbioses. *Curr. Opin. Biotechnol.* 21, 332–338. doi:10.1016/j.copbio.2010.03.013.

Gerlich, M., and Neumann, S. (2013). MetFusion: integration of compound identification strategies. *J. Mass Spectrom.* 48, 291–298. doi:10.1002/jms.3123.

Gerwick, W. H., and Fenical, W. (1981). Ichthyotoxic and cytotoxic metabolites of the tropical brown alga *Stypopodium zonale* (Lamouroux) Papenfuss. *J. Org. Chem.* 46, 22–27. doi:10.1021/jo00314a005.

Ghaderiardakani, F., Califano, G., Mohr, J. F., Abreu, M. H., Coates, J. C., and Wichard, T. (2019). Analysis of algal growth- and morphogenesis-promoting factors in an integrated multi-trophic aquaculture system for farming *Ulva* spp. *Aquac. Environ. Interact.* 11, 375–391. doi:10.3354/aei00319.

Ghaderiardakani, F., Coates, J. C., and Wichard, T. (2017). Bacteria-induced morphogenesis of *Ulva intestinalis* and *Ulva mutabilis* (Chlorophyta): a contribution to the lottery theory. *FEMS Microbiol. Ecol.* 93. doi:10.1093/femsec/fix094.

Giacomoni, F., Le Corguillé, G., Monsoor, M., Landi, M., Pericard, P., Pétéra, M., et al. (2015). Workflow4Metabolomics: a collaborative research infrastructure for computational metabolomics. *Bioinformatics* 31, 1493–1495. doi:10.1093/bioinformatics/btu813.

Gil, B., Ferrándiz, M. L., Sanz, M. J., Terencio, M. C., Ubeda, A., Rovirosa, J., et al. (1995). Inhibition of inflammatory responses by epitaondiol and other marine natural products. *Life Sci.* 57, PL25–PL30. doi:10.1016/0024-3205(95)00260-D.

Gil, R., Sabater-Muñoz, B., Latorre, A., Silva, F. J., and Moya, A. (2002). Extreme genome reduction in *Buchnera* spp.: toward the minimal genome needed for symbiotic life. *Proc. Natl. Acad. Sci. U.S.A.* 99, 4454–4458. doi:10.1073/pnas.062067299.

Gillan, D. C., and Dubilier, N. (2004). Novel epibiotic thiothrix bacterium on a marine amphipod. *Appl. Environ. Microbiol.* 70, 3772–3775. doi:10.1128/AEM.70.6.3772-3775.2004.

Giussani, V., Costa, E., Pecorino, D., Berdalet, E., De Giampaulis, G., Gentile, M., et al. (2016). Effects of the harmful dinoflagellate *Ostreopsis* cf. *ovata* on different life cycle stages of the common moon jellyfish *Aurelia* sp. *Harmful Algae* 57, 49–58. doi:10.1016/j.hal.2016.05.005.

Gobet, A., Barbeyron, T., Matard-Mann, M., Magdelenat, G., Vallenet, D., Duchaud, E., et al. (2018). Evolutionary evidence of algal polysaccharide degradation acquisition by *Pseudoalteromonas carrageenovora* 9T to adapt to macroalgal niches. *Front. Microbiol.* 9, 2740. doi:10.3389/fmicb.2018.02740.

Goecke, F., Labes, A., Wiese, J., and Imhoff, J. F. (2010). Chemical interactions between marine macroalgae and bacteria. *Mar. Ecol. Prog. Ser.* 409, 267–299. doi:10.3354/meps08607.

González, A. G., Darias, J., and Martín, J. D. (1971). Taondiol, a new component from *Taonia atomaria*. *Tetrahedron Lett.* 12, 2729–2732. doi:10.1016/S0040-4039(01)96964-3.

González, A. G., Darias, J., Martín, J. D., and Norte, M. (1974). Atomaric acid, a new component from *Taonia atomaria*. *Tetrahedron Lett.* 15, 3951–3954. doi:10.1016/S0040-4039(01)92054-4.

Gorbi, S., Avio, G. C., Benedetti, M., Totti, C., Accoroni, S., Pichierri, S., et al. (2013). Effects of harmful dinoflagellate *Ostreopsis* cf. *ovata* exposure on immunological, histological and oxidative responses of mussels *Mytilus galloprovincialis*. *Fish Shellfish Immunol.* 35, 941–950. doi:10.1016/j.fsi.2013.07.003.

Graham, L. E., and Wilcox, L. W. (2000). *Algae*. Upper Saddle River, N.J.: Prentice Hall.

Grim, C. M., Luu, G. T., and Sanchez, L. M. (2019). Staring into the void: demystifying microbial metabolomics. *FEMS Microbiol. Lett.* 366. doi:10.1093/femsle/fnz135.

Groisillier, A., Labourel, A., Michel, G., and Tonon, T. (2015). The mannitol utilization system of the marine bacterium *Zobellia galactanivorans*. *Appl. Environ. Microbiol.* 81, 1799–1812. doi:10.1128/AEM.02808-14.

Grosser, K., Zedler, L., Schmitt, M., Dietzek, B., Popp, J., and Pohnert, G. (2012). Disruption-free imaging by Raman spectroscopy reveals a chemical sphere with antifouling metabolites around macroalgae. *Biofouling* 28, 687–696. doi:10.1080/08927014.2012.700306.

Grueneberg, J., Engelen, A. H., Costa, R., and Wichard, T. (2016). Macroalgal morphogenesis induced by waterborne compounds and bacteria in coastal seawater. *PLoS One* 11, e0146307. doi:10.1371/journal.pone.0146307.

Guidi, F., Pezzolesi, L., and Vanucci, S. (2018). Microbial dynamics during harmful dinoflagellate *Ostreopsis* cf. *ovata* growth: Bacterial succession and viral abundance pattern. *Microbiologyopen* 7, e00584. doi:10.1002/mbo3.584.

Guidi-Guilvard, L. D., Gasparini, S., and Lemée, R. (2012). The negative impact of *Ostreopsis* cf. *ovata* on phytal meiofauna from the coastal NW Mediterranean. *Cryptogam. Algol.* 33, 121–128. doi:10.7872/crya.v33.iss2.2011.121.

Guillard, R. R. L., and Ryther, J. H. (1962). Studies of marine planktonic diatoms: i. *Cyclotella nana* Hustedt, and *Detonula confervacea* (Cleve) gran. *Can. J. Microbiol.* 8, 229–239. doi:10.1139/m62-029.

Guiry, M. D., and Guiry, M. D. (2020). *AlgaeBase*. World-wide electronic publication, National University of Ireland, Galway. https://www.algaebase.org; searched on 05 June 2020.

Hall, E. R., Muller, E. M., Goulet, T., Bellworthy, J., Ritchie, K. B., and Fine, M. (2018). Eutrophication may compromise the resilience of the Red Sea coral *Stylophora pistillata* to global change. *Mar. Pollut. Bull.* 131, 701–711. doi:10.1016/j.marpolbul.2018.04.067.

Handelsman, J. (2004). Metagenomics: application of genomics to uncultured microorganisms. *Microbiol. Mol. Biol. Rev.* 68, 669–685. doi:10.1128/MMBR.68.4.669-685.2004.

Harder, T. (2009). “Marine epibiosis: concepts, ecological consequences and host defence,” in *Marine and Industrial Biofouling*, eds. P. D. H.-C. Flemming, D. P. S. Murthy, D. R. Venkatesan, and P. D. K. Cooksey (Springer Berlin Heidelberg), 219–231. Available at: http://link.springer.com/chapter/10.1007/978-3-540-69796-1_12 [Accessed November 21, 2016].

Harder, T., Campbell, A. H., Egan, S., and Steinberg, P. D. (2012). Chemical mediation of ternary interactions between marine holobionts and their environment as exemplified by the red alga *Delisea pulchra*. *J. Chem. Ecol.* 38, 442–450. doi:10.1007/s10886-012-0119-5.

Harder, T., Dobretsov, S., and Qian, P.-Y. (2004). Waterborne polar macromolecules act as algal antifoulants in the seaweed *Ulva reticulata*. *Mar. Ecol. Prog. Ser.* 274, 133–141. doi:10.3354/meps274133.

Harder, T., Lau, S. C. K., Dobretsov, S., Fang, T. K., and Qian, P.-Y. (2003). A distinctive epibiotic bacterial community on the soft coral *Dendronephthya* sp. and antibacterial activity of coral tissue extracts suggest a chemical mechanism against bacterial epibiosis. *FEMS Microbiol. Ecol.* 43, 337–347. doi:10.1111/j.1574-6941.2003.tb01074.x.

Harrison, J. J., Rabiei, M., Turner, R. J., Badry, E. A., Sproule, K. M., and Ceri, H. (2006). Metal resistance in *Candida* biofilms. *FEMS Microbiol. Ecol.* 55, 479–491. doi:10.1111/j.1574-6941.2005.00045.x.

Harrison, J. J., Turner, R. J., and Ceri, H. (2005). Persister cells, the biofilm matrix and tolerance to metal cations in biofilm and planktonic *Pseudomonas aeruginosa*. *Environ. Microbiol.* 7, 981–994. doi:10.1111/j.1462-2920.2005.00777.x.

Harvey, W. H. (1849). *A manual of the British marine Algae...* London,: J. Van Voorst, doi:10.5962/bhl.title.3973.

Hay, M. E. (2009). Marine chemical ecology: chemical signals and cues structure marine populations, communities, and ecosystems. *Annu. Rev. Mar. Sci.* 1, 193–212. doi:10.1146/annurev.marine.010908.163708.

Hay, M. E., and Steinberg, P. D. (1992). “Chapter 10 - The chemical ecology of plant–herbivore interactions in marine versus terrestrial communities,” in *Herbivores: Their Interactions with Secondary Plant Metabolites (Second Edition)*, eds. G. A. Rosenthal and M. R. Berenbaum (San Diego: Academic Press), 371–413. doi:10.1016/B978-0-08-092545-5.50015-8.

Hellio, C., Berge, J. P., Beaupoil, C., GAL, Y. L., and Bourgougnon, N. (2002). Screening of marine algal extracts for anti-settlement activities against microalgae and macroalgae. *Biofouling* 18, 205–215. doi:10.1080/08927010290010137.

Hengst, M. B., Andrade, S., González, B., and Correa, J. A. (2010). Changes in epiphytic bacterial communities of intertidal seaweeds modulated by host, temporality, and copper enrichment. *Microb. Ecol.* 60, 282–290. doi:10.1007/s00248-010-9647-0.

Hernandez-Agreda, A., Leggat, W., Bongaerts, P., Herrera, C., and Ainsworth, T. D. (2018). Rethinking the coral microbiome: simplicity exists within a diverse microbial biosphere. *Mbio* 9, e00812-18. doi:10.1128/mBio.00812-18.

Hervé, M. (2020). *RVAideMemoire: testing and plotting procedures for biostatistics*. Available at: https://CRAN.R-project.org/package=RVAideMemoire [Accessed January 15, 2020].

Heydorn, A., Ersbøll, B., Kato, J., Hentzer, M., Parsek, M. R., Tolker-Nielsen, T., et al. (2002). Statistical analysis of *Pseudomonas aeruginosa* biofilm development: impact of mutations in genes involved in twitching motility, cell-to-cell signaling, and stationary-phase sigma factor expression. *Appl. Environ. Microbiol.* 68, 2008–2017. doi:10.1128/AEM.68.4.2008-2017.2002.

Hollants, J., Decleyre, H., Leliaert, F., De Clerck, O., and Willems, A. (2011a). Life without a cell membrane: Challenging the specificity of bacterial endophytes within *Bryopsis* (Bryopsidales, Chlorophyta). *BMC Microbiol.* 11, 255. doi:10.1186/1471-2180-11-255.

Hollants, J., Leliaert, F., De Clerck, O., and Willems, A. (2013). What we can learn from sushi: a review on seaweed-bacterial associations. *FEMS Microbiol. Ecol.* 83, 1–16. doi:10.1111/j.1574-6941.2012.01446.x.

Hollants, J., Leroux, O., Leliaert, F., Decleyre, H., De Clerck, O., and Willems, A. (2011b). Who is in there? Exploration of endophytic bacteria within the siphonous green seaweed *Bryopsis*(Bryopsidales, Chlorophyta). *PLoS One* 6, e26458. doi:10.1371/journal.pone.0026458.

Hong, R., Kang, T. Y., Michels, C. A., and Gadura, N. (2012). Membrane lipid peroxidation in copper alloy-mediated contact killing of *Escherichia coli*. *Appl. Environ. Microbiol.* 78, 1776–1784. doi:10.1128/AEM.07068-11.

Horiguchi, E. : M. H. S. A. M. N. C. T. ed. (2014). *Marine benthic dinoflagellates - unveiling their worldwide biodiversity*. Stuttgart, Germany: Schweizerbart Science Publishers Available at: http://www.schweizerbart.de//publications/detail/isbn/9783510614028/Kleine_Sencke nberg_Reihe_Nr_54_Marine_b.

Hosny, S., and Labib, W. (2019). Ecology of the epiphytic potentially harmful dinoflagellate *Ostreopsis* cf. *ovata* (fukuyo) from coastal waters off Alexandria Egypt. *J. Oceanogr. Mar. Sci.* 7, 1–9. doi:10.35248/2572-3103.19.7.189.

Howard, E. C., Sun, S., Biers, E. J., and Moran, M. A. (2008). Abundant and diverse bacteria involved in DMSP degradation in marine surface waters. *Environ. Microbiol.* 10, 2397–2410. doi:10.1111/j.1462-2920.2008.01665.x.

Huang, R., Zhou, X., Xu, T., Yang, X., and Liu, Y. (2010). Diketopiperazines from marine organisms. *Chem. Biodivers.* 7, 2809–2829. doi:10.1002/cbdv.200900211.

Huggett, M. J., McMahon, K., and Bernasconi, R. (2018). Future warming and acidification result in multiple ecological impacts to a temperate coralline alga. *Environ. Microbiol.* 20, 2769–2782. doi:10.1111/1462-2920.14113.

Ianora, A., Miralto, A., Poulet, S. A., Carotenuto, Y., Buttino, I., Romano, G., et al. (2004). Aldehyde suppression of copepod recruitment in blooms of a ubiquitous planktonic diatom. *Nature* 429, 403–407. doi:10.1038/nature02526.

Inaba, M., Suzuki, I., Szalontai, B., Kanesaki, Y., Los, D. A., Hayashi, H., et al. (2003). Gene-engineered rigidification of membrane lipids enhances the cold inducibility of gene expression in *Synechocystis*. *J. Biol. Chem.* 278, 12191–12198. doi:10.1074/jbc.M212204200.

Isaac, G., Jeannotte, R., Esch, S. W., and Welti, R. (2007). New mass-spectrometry-based strategies for lipids. *Genet. Eng. (N.Y.)* 28, 129–157. doi:10.1007/978-0-387-34504-8_8.

Ivanova, E. P., and Webb, H. K. (2014). "The family Granulosicoccaceae," in *The Prokaryotes: Gammaproteobacteria*, eds. E. Rosenberg, E. F. DeLong, S. Lory, E. Stackebrandt, and F. Thompson (Berlin, Heidelberg: Springer), 315–317. doi:10.1007/978-3-642-38922-1_247.

Jauzein, C., Açaf, L., Accoroni, S., Asnaghi, V., Fricke, A., Hachani, M. A., et al. (2018). Optimization of sampling, cell collection and counting for the monitoring of benthic harmful algal blooms: Application to *Ostreopsis* spp. blooms in the Mediterranean Sea. *Ecol. Indic.* 91, 116–127. doi:10.1016/j.ecolind.2018.03.089.

Jerković, I., Kranjac, M., Marijanović, Z., Roje, M., and Jokić, S. (2019). Chemical diversity of headspace and volatile oil composition of two brown algae (*Taonia atomaria* and *Padina pavonica*) from the Adriatic Sea. *Molecules* 24, 495. doi:10.3390/molecules24030495.

Johnson, C. H., Ivanisevic, J., and Siuzdak, G. (2016). Metabolomics: beyond biomarkers and towards mechanisms. *Nat. Rev. Mol. Cell Biol.* 17, 451–459. doi:10.1038/nrm.2016.25.

Johnson, M. D., Price, N. N., and Smith, J. E. (2014). Contrasting effects of ocean acidification on tropical fleshy and calcareous algae. *PeerJ* 2, e411. doi:10.7717/peerj.411.

Jones, A. L., and Harwood, J. L. (1993). Lipid metabolism in the brown marine algae *Fucus vesiculosus* and *Ascophyllum nodosum*. *J. Exp. Bot.* 44, 1203–1210. doi:10.1093/jxb/44.7.1203.

Jones, C. G., Lawton, J. H., and Shachak, M. (1994). Organisms as ecosystem engineers. *Oikos* 69, 373–386. doi:10.2307/3545850.

Junker, R. R., and Tholl, D. (2013). Volatile organic compound mediated interactions at the plant-microbe interface. *J. Chem. Ecol.* 39, 810–825. doi:10.1007/s10886-013-0325-9.

Kang, I., Lim, Y., and Cho, J.-C. (2018). Complete genome sequence of *Granulosicoccus antarcticus* type strain IMCC3135T, a marine gammaproteobacterium with a putative dimethylsulfoniopropionate demethylase gene. *Mar. Genomics* 37, 176–181. doi:10.1016/j.margen.2017.11.005.

Karsten, U., Kirst, G. O., and Wiencke, C. (1992). Dimethylsulphoniopropionate (DMSP) accumulation in green macioalgae from polar to temperate regions: interactive effects of light versus salinity and light versus temperature. *Polar Biol.* 12, 603–607. doi:10.1007/BF00236983.

Karsten, U., Wiencke, C., and Kirst, G. O. (1990). The effect of light intensity and daylength on the *β*-dimethylsulphoniopropionate (DMSP) content of marine green macroalgae from Antarctica. *Plant Cell Environ.* 13, 989–993. doi:10.1111/j.1365-3040.1990.tb01991.x.

Kelecom, A., and Laneuville Teixeira, V. (1986). Diterpenes of marine brown algae of the family Dictyotaceae: Their possible role as defense compounds and their use in chemotaxonomy. *Sci. Total Environ.* 58, 109–115. doi:10.1016/0048-9697(86)90081-1.

Keller, M. D., and Korjeff-Bellows, W. (1996). “Physiological aspects of the production of dimeyhtlsulfoniopropionate (DMSP) by marine phytoplankton,” in *Biological and Environmental Chemistry of DMSP and Related Sulfonium Compounds*, eds. R. P. Kiene, P. T. Visscher, M. D. Keller, and G. O. Kirst (Boston, MA: Springer US), 131–142. doi:10.1007/978-1-4613-0377-0_12.

Kermarrec, L., Franc, A., Rimet, F., Chaumeil, P., Humbert, J. F., and Bouchez, A. (2013). Next-generation sequencing to inventory taxonomic diversity in eukaryotic communities: a test for freshwater diatoms. *Mol. Ecol. Resour.* 13, 607–619. doi:10.1111/1755-0998.12105.

Kessler, R. W., Crecelius, A. C., Schubert, U. S., and Wichard, T. (2017). In situ monitoring of molecular changes during cell differentiation processes in marine macroalgae through mass spectrometric imaging. *Anal. Bioanal. Chem.* 409, 4893–4903. doi:10.1007/s00216-017-0430-7.

Kessler, R. W., Weiss, A., Kuegler, S., Hermes, C., and Wichard, T. (2018). Macroalgal-bacterial interactions: Role of dimethylsulfoniopropionate in microbial gardening by *Ulva* (Chlorophyta). *Mol. Ecol.* 27, 1808–1819. doi:10.1111/mec.14472.

Kets, E. P., Galinski, E. A., de Wit, M., de Bont, J. A., and Heipieper, H. J. (1996). Mannitol, a novel bacterial compatible solute in *Pseudomonas putida* S12. *J. Bacteriol.* 178, 6665–6670. doi:10.1128/jb.178.23.6665-6670.1996.

Ki, J.-S., Zhang, R., Zhang, W., Huang, Y.-L., and Qian, P.-Y. (2009). Analysis of RNA polymerase beta subunit (rpoB) gene sequences for the discriminative power of marine *Vibrio* species. *Microb. Ecol.* 58, 679. doi:10.1007/s00248-009-9519-7.

Kim, J. Y., Alamsjah, M. A., Hamada, A., Fujita, Y., and Ishibashi, F. (2006). Algicidal diterpenes from the brown alga *Dictyota dichotoma*. *Biosci. Biotechnol. Biochem.* 70, 2571–2574. doi:10.1271/bbb.60281.

Kim, M., and Tagkopoulos, I. (2018). Data integration and predictive modeling methods for multi-omics datasets. *Mol. Omics* 14, 8–25. doi:10.1039/C7MO00051K.

Kind, T., Meissen, J. K., Yang, D., Nocito, F., Vaniya, A., Cheng, Y.-S., et al. (2012). Qualitative analysis of algal secretions with multiple mass spectrometric platforms. *J. Chromatogr. A* 1244, 139–147. doi:10.1016/j.chroma.2012.04.074.

Kinlan, B. P., and Gaines, S. D. (2003). Propagule dispersal in marine and terrestrial environments: A community perspective. *Ecology* 84, 2007–2020.

Koblížek, M. (2015). Ecology of aerobic anoxygenic phototrophs in aquatic environments. *FEMS Microbiol. Rev.* 39, 854–870. doi:10.1093/femsre/fuv032.

Konkol, N. R., Bruckner, J. C., Aguilar, C., Lovalvo, D., and Maki, J. S. (2010). Dominance of epiphytic filamentous *Thiothrix* spp. on an aquatic macrophyte in a hydrothermal vent flume in Sedge Bay, Yellowstone Lake, Wyoming. *Microb. Ecol.* 60, 528–538. doi:10.1007/s00248-010-9656-z.

Kon-ya, K., Shimidzu, N., Otaki, N., Yokoyama, A., Adachi, K., and Miki, W. (1995). Inhibitory effect of bacterial ubiquinones on the settling of barnacle, *Balanus amphitrite*. *Experientia* 51, 153–155. doi:10.1007/BF01929360.

Kramer, P., and Bressan, P. (2015). Humans as superorganisms: How microbes, viruses, imprinted genes, and other selfish entities shape our behavior. *Perspect. Psychol. Sci.* 10, 464–481. doi:10.1177/1745691615583131.

Krebs, H. A. (1975). The August Krogh principle: “For many problems there is an animal on which it can be most conveniently studied.” *J. Exp. Zool.* 194, 221–226. doi:10.1002/jez.1401940115.

Kroeker, K. J., Kordas, R. L., Crim, R., Hendriks, I. E., Ramajo, L., Singh, G. S., et al. (2013). Impacts of ocean acidification on marine organisms: quantifying sensitivities and interaction with warming. *Glob. Chang. Biol.* 19, 1884–1896. doi:10.1111/gcb.12179.

Kuhl, C., Tautenhahn, R., Böttcher, C., Larson, T. R., and Neumann, S. (2012). CAMERA: An integrated strategy for compound spectra extraction and annotation of LC/MS data sets. *Anal. Chem.* 84, 283–289. doi:10.1021/ac202450g.

Kuhlisch, C., and Pohnert, G. (2015). Metabolomics in chemical ecology. *Nat. Prod. Rep.* 32, 937–955. doi:10.1039/C5NP00003C.

Kumar, V., Zozaya-Valdes, E., Kjelleberg, S., Thomas, T., and Egan, S. (2016). Multiple opportunistic pathogens can cause a bleaching disease in the red seaweed *Delisea pulchra*. *Environ. Microbiol.* 18, 3962–3975. doi:10.1111/1462-2920.13403.

Küpper, F. C., Kloareg, B., Guern, J., and Potin, P. (2001). Oligoguluronates elicit an oxidative burst in the brown algal kelp *Laminaria digitata*. *Plant Physiol.* 125, 278–291. doi:10.1104/pp.125.1.278.

Küpper, F. C., Müller, D. G., Peters, A. F., Kloareg, B., and Potin, P. (2002a). Oligoalginate recognition and oxidative burst play a key role in natural and induced resistance of sporophytes of Laminariales. *J. Chem. Ecol.* 28, 2057–2081. doi:10.1023/A:1020706129624.

Küpper, H., Küpper, F., and Spiller, M. (1996). Environmental relevance of heavy metal-substituted chlorophylls using the example of water plants. *J. Exp. Bot.* 47, 259–266. doi:10.1093/jxb/47.2.259.

Küpper, H., Küpper, F., and Spiller, M. (1998). In situ detection of heavy metal substituted chlorophylls in water plants. *Photosynth. Res.* 58, 123–133. doi:10.1023/A:1006132608181.

Küpper, H., Šetlík, I., Spiller, M., Küpper, F. C., and Prášil, O. (2002b). Heavy metal-induced inhibition of photosynthesis: Targets of *in vivo* heavy metal chlorophyll formation. *J. Phycol.* 38, 429–441. doi:10.1046/j.1529-8817.2002.01148.x.

Kusumi, T., Ishitsuka, M., Iwashita, T., Naoki, H., Konno, T., and Kakisawa, H. (1981). A novel type of glycerides bearing a methacrylic acid moiety from the brown alga, *Sargassum fulvellum*. *Chem. Lett.* 10, 1393–1396. doi:10.1246/cl.1981.1393.

Kyrpides, N. C. (2009). Fifteen years of microbial genomics: meeting the challenges and fulfilling the dream. *Nat. Biotechnol.* 27, 627–632. doi:10.1038/nbt.1552.

La Barre, S., Potin, P., Leblanc, C., and Delage, L. (2010). The halogenated metabolism of brown algae (Phaeophyta), its biological importance and its environmental significance. *Mar. Drugs* 8, 988–1010. doi:10.3390/md8040988.

Lachnit, T., Blümel, M., Imhoff, J. F., and Wahl, M. (2009). Specific epibacterial communities on macroalgae: phylogeny matters more than habitat. *Aquat. Biol.* 5, 181–186. doi:10.3354/ab00149.

Lachnit, T., Bosch, T. C. G., and Deines, P. (2019). Exposure of the host-associated microbiome to nutrient-rich conditions may lead to dysbiosis and disease development—an evolutionary perspective. *Mbio* 10. doi:10.1128/mBio.00355-19.

Lachnit, T., Fischer, M., Künzel, S., Baines, J. F., and Harder, T. (2013). Compounds associated with algal surfaces mediate epiphytic colonization of the marine macroalga *Fucus vesiculosus*. *FEMS Microbiol. Ecol.* 84, 411–420. doi:10.1111/1574-6941.12071.

Lachnit, T., Meske, D., Wahl, M., Harder, T., and Schmitz, R. (2011). Epibacterial community patterns on marine macroalgae are host-specific but temporally variable. *Environ. Microbiol.* 13, 655–665. doi:10.1111/j.1462-2920.2010.02371.x.

Lachnit, T., Wahl, M., and Harder, T. (2010). Isolated thallus-associated compounds from the macroalga *Fucus vesiculosus* mediate bacterial surface colonization in the field similar to that on the natural alga. *Biofouling* 26, 247–255. doi:10.1080/08927010903474189.

Lackner, G., Peters, E. E., Helfrich, E. J. N., and Piel, J. (2017). Insights into the lifestyle of uncultured bacterial natural product factories associated with marine sponges. *Proc. Natl. Acad. Sci. U.S.A.* 114, E347–E356. doi:10.1073/pnas.1616234114.

Lami, R. (2019). "Chapter 3 - Quorum Qensing in marine biofilms and environments," in *Quorum Sensing*, ed. G. Tommonaro (Academic Press), 55–96. doi:10.1016/B978-0-12-814905-8.00003-4.

Lanctôt, C. M., Bednarz, V. N., Melvin, S., Jacob, H., Oberhaensli, F., Swarzenski, P. W., et al. (2020). Physiological stress response of the scleractinian coral *Stylophora pistillata* exposed to polyethylene microplastics. *Environ. Pollut.* 263, 114559. doi:10.1016/j.envpol.2020.114559.

Langille, M. G. I., Zaneveld, J., Caporaso, J. G., McDonald, D., Knights, D., Reyes, J. A., et al. (2013). Predictive functional profiling of microbial communities using 16S rRNA marker gene sequences. *Nat. Biotechnol.* 31, 814–821. doi:10.1038/nbt.2676.

Langille, S. E., and Weiner, R. M. (1998). Spatial and temporal deposition of *Hyphomonas* strain VP-6 capsules involved in biofilm formation. *Appl. Environ. Microbiol.* 64, 2906–2913. doi:10.1128/AEM.64.8.2906-2913.1998.

Lawes, J. C., Neilan, B. A., Brown, M. V., Clark, G. F., and Johnston, E. L. (2016). Elevated nutrients change bacterial community composition and connectivity: high throughput sequencing of young marine biofilms. *Biofouling* 32, 57–69. doi:10.1080/08927014.2015.1126581.

Layglon, N., Misson, B., Durieu, G., Coclet, C., D'Onofrio, S., Dang, D. H., et al. (2020). Long-term monitoring emphasizes impacts of the dredging on dissolved Cu and Pb contamination along with ultraplankton distribution and structure in Toulon Bay (NW Mediterranean Sea, France). *Mar. Pollut. Bull.* 156, 111196. doi:10.1016/j.marpolbul.2020.111196.

Lê Cao, K.-A., González, I., and Déjean, S. (2009). integrOmics: an R package to unravel relationships between two omics datasets. *Bioinformatics* 25, 2855–2856. doi:10.1093/bioinformatics/btp515.

Leblanc, C., Schaal, G., Cosse, A., Destombe, C., Valero, M., Riera, P., et al. (2011). Trophic and biotic interactions in *Laminaria digitata* beds: which factors could influence the persistence of marine kelp forests in northern Brittany? *Cah. Biol. Mar.* 52, 415–427.

Leggat, W., Ainsworth, T., Bythell, J., Dove, S., Gates, R., Hoegh-Guldberg, O., et al. (2007). The hologenome theory disregards the coral holobiont. *Nat. Rev. Microbiol.* 5, 826–826. doi:10.1038/nrmicro1635-c1.

Lehvo, A., Bäck, S., and Kiirikki, M. (2001). Growth of *Fucus vesiculosus* L. (Phaeophyta) in the Northern Baltic proper: Energy and nitrogen storage in seasonal environment. *Botanica Marina* 44, 345–350. doi:10.1515/BOT.2001.044.

Lejeusne, C., Chevaldonné, P., Pergent-Martini, C., Boudouresque, C. F., and Pérez, T. (2010). Climate change effects on a miniature ocean: the highly diverse, highly impacted Mediterranean Sea. *Trends Ecol. Evol.* 25, 250–260. doi:10.1016/j.tree.2009.10.009.

Lemay, M. A., Martone, P. T., Hind, K. R., Lindstrom, S. C., and Parfrey, L. W. (2018a). Alternate life history phases of a common seaweed have distinct microbial surface communities. *Mol. Ecol.* 27, 3555–3568. doi:10.1111/mec.14815.

Lemay, M. A., Martone, P. T., Keeling, P. J., Burt, J. M., Krumhansl, K. A., Sanders, R. D., et al. (2018b). Sympatric kelp species share a large portion of their surface bacterial communities. *Environ. Microbiol.* 20, 658–670. doi:10.1111/1462-2920.13993.

Li, H., Yu, Y., Luo, W., Zeng, Y., and Chen, B. (2009). Bacterial diversity in surface sediments from the Pacific Arctic Ocean. *Extremophiles* 13, 233–246. doi:10.1007/s00792-009-0225-7.

Liang, Z., Liu, F., Wang, W., Zhang, P., Sun, X., Wang, F., et al. (2019). High-throughput sequencing revealed differences of microbial community structure and diversity between healthy and diseased *Caulerpa lentillifera*. *BMC Microbiol.* 19. doi:10.1186/s12866-019-1605-5.

Lin, J. D., Lemay, M. A., and Parfrey, L. W. (2018). Diverse bacteria utilize alginate within the microbiome of the giant kelp *Macrocystis pyrifera*. *Front. Microbiol.* 9, 1914. doi:10.3389/fmicb.2018.01914.

Liu, B., and Benning, C. (2013). Lipid metabolism in microalgae distinguishes itself. *Curr. Opin. Biotechnol.* 24, 300–309. doi:10.1016/j.copbio.2012.08.008.

Lloyd, E. A., and Wade, M. J. (2019). Criteria for holobionts from community genetics. *Biol. Theory* 14, 151–170. doi:10.1007/s13752-019-00322-w.

Loeb, G. I., and Neihof, R. A. (1975). “Marine conditioning films,” in *Applied Chemistry at Protein Interfaces* Advances in Chemistry. (American Chemical Society), 319–335. doi:10.1021/ba-1975-0145.ch016.

Longford, S. R., Campbell, A. H., Nielsen, S., Case, R. J., Kjelleberg, S., and Steinberg, P. D. (2019). Interactions within the microbiome alter microbial interactions with host chemical defences and affect disease in a marine holobiont. *Sci. Rep.* 9, 1363. doi:10.1038/s41598-018-37062-z.

López-Lara, I. M., Sohlenkamp, C., and Geiger, O. (2003). Membrane lipids in plant-associated bacteria: their biosyntheses and possible functions. *Mol. Plant Microbe Interact.* 16, 567–579. doi:10.1094/MPMI.2003.16.7.567.

Loreau, M., Naeem, S., Inchausti, P., Bengtsson, J., Grime, J. P., Hector, A., et al. (2001). Biodiversity and ecosystem functioning: current knowledge and future challenges. *Science* 294, 804–808. doi:10.1126/science.1064088.

Los, D. A., and Murata, N. (2004). Membrane fluidity and its roles in the perception of environmental signals. *Biochim. Biophys. Acta* 1666, 142–157. doi:10.1016/j.bbamem.2004.08.002.

Louca, S., Parfrey, L. W., and Doebeli, M. (2016). Decoupling function and taxonomy in the global ocean microbiome. *Science* 353, 1272–1277. doi:10.1126/science.aaf4507.

Luo, H., and Moran, M. A. (2014). Evolutionary ecology of the Marine Roseobacter Clade. *Microbiol. Mol. Biol. Rev.* 78, 573–587. doi:10.1128/MMBR.00020-14.

Luter, H. M., Gibb, K., and Webster, N. S. (2014). Eutrophication has no short-term effect on the *Cymbastela stipitata* holobiont. *Front. Microbiol.* 5, 216. doi:10.3389/fmicb.2014.00216.

Lyons, D. A., Scheibling, R. E., and Alstyne, K. L. V. (2010). Spatial and temporal variation in DMSP content in the invasive seaweed *Codium fragile* ssp. *fragile*: effects of temperature, light and grazing. *Mar. Ecol. Prog. Ser.* 417, 51–61. doi:10.3354/meps08818.

Maciel, E., Leal, M. C., Lillebø, A. I., Domingues, P., Domingues, M. R., and Calado, R. (2016). Bioprospecting of marine macrophytes using MS-based lipidomics as a new approach. *Mar. Drugs* 14, 49. doi:10.3390/md14030049.

Mahé, F., Rognes, T., Quince, C., Vargas, C. de, and Dunthorn, M. (2014). Swarm: robust and fast clustering method for amplicon-based studies. *PeerJ* 2, e593. doi:10.7717/peerj.593.

Mancuso, F. P., D'Hondt, S., Willems, A., Airoldi, L., and De Clerck, O. (2016). Diversity and temporal dynamics of the epiphytic bacterial communities associated with the canopy-forming seaweed *Cystoseira compressa* (Esper) Gerloff and Nizamuddin. *Front. Microbiol.* 7, 476. doi:10.3389/fmicb.2016.00476.

Manefield, M., de Nys, R., Naresh, K., Roger, R., Givskov, M., Peter, S., et al. (1999). Evidence that halogenated furanones from *Delisea pulchra* inhibit acylated homoserine lactone (AHL)-mediated gene expression by displacing the AHL signal from its receptor protein. *Microbiology* 145, 283–291. doi:10.1099/13500872-145-2-283.

Manefield, M., Rasmussen, T. B., Henzter, M., Andersen, J. B., Steinberg, P., Kjelleberg, S., et al. (2002). Halogenated furanones inhibit quorum sensing through accelerated LuxR turnover. *Microbiology* 148, 1119–1127. doi:10.1099/00221287-148-4-1119.

Mangialajo, L., Ganzin, N., Accoroni, S., Asnaghi, V., Blanfuné, A., Cabrini, M., et al. (2011). Trends in *Ostreopsis* proliferation along the Northern Mediterranean coasts. *Toxicon* 57, 408–420. doi:10.1016/j.toxicon.2010.11.019.

Mann, K. H. (2000). *Ecology of coastal waters: With implications for management*. John Wiley & Sons.

Marbà, N., and Duarte, C. M. (2010). Mediterranean warming triggers seagrass (*Posidonia oceanica*) shoot mortality. *Glob. Change Biol.* 16, 2366–2375. doi:10.1111/j.1365-2486.2009.02130.x.

Margulis, L. (1990). Words as battle cries—symbiogenesis and the new field of endocytobiology. *Bioscience* 40, 673–677. doi:10.2307/1311435.

Margulis, L., 1938-2011 (viaf)108159261, and Fester, R. (1991). *Symbiosis as a source of evolutionary innovation : speciation and morphogenesis*. Cambridge (Mass.) : MIT press Available at: http://lib.ugent.be/catalog/rug01:000265232.

Marie, C., Deakin, W. J., Viprey, V., Kopciñska, J., Golinowski, W., Krishnan, H. B., et al. (2003). Characterization of Nops, nodulation outer proteins, secreted via the type III secretion system of NGR234. *Mol. Plant Microbe Interact.* 16, 743–751. doi:10.1094/MPMI.2003.16.9.743.

Marro, S., Pavaux, A.-S., Drouet, K., and Lemée, R. (2019). Diversity of benthic microphytoplankton associated to *Ostreopsis* cf. *ovata* bloom in the NW Mediterranean Sea. in.

Martin, S., Castets, M.-D., and Clavier, J. (2006). Primary production, respiration and calcification of the temperate free-living coralline alga *Lithothamnion corallioides*. *Aquat. Bot.* 85, 121–128. doi:10.1016/j.aquabot.2006.02.005.

Martin-Platero, A. M., Cleary, B., Kauffman, K., Preheim, S. P., McGillicuddy, D. J., Alm, E. J., et al. (2018). High resolution time series reveals cohesive but short-lived communities in coastal plankton. *Nat. Commun.* 9, 1–11. doi:10.1038/s41467-017-02571-4.

Martins, I., Oliveira, J. M., Flindt, M. R., and Marques, J. C. (1999). The effect of salinity on the growth rate of the macroalgae *Enteromorpha intestinalis* (Chlorophyta) in the Mondego estuary (west Portugal). *Acta Oecol.* 20, 259–265. doi:10.1016/S1146-609X(99)00140-X.

Marzinelli, E. M., Campbell, A. H., Zozaya Valdes, E., Vergés, A., Nielsen, S., Wernberg, T., et al. (2015). Continental-scale variation in seaweed host-associated bacterial communities is a function of host condition, not geography. *Environ. Microbiol.* 17, 4078–4088. doi:10.1111/1462-2920.12972.

Marzinelli, E. M., Qiu, Z., Dafforn, K. A., Johnston, E. L., Steinberg, P. D., and Mayer-Pinto, M. (2018). Coastal urbanisation affects microbial communities on a dominant marine holobiont. *NPJ Biofilms Microbiomes* 4, 1. doi:10.1038/s41522-017-0044-z.

Matsuo, Y., Imagawa, H., Nishizawa, M., and Shizuri, Y. (2005). Isolation of an algal morphogenesis inducer from a marine bacterium. *Science* 307, 1598. doi:10.1126/science.1105486.

Maximilien, R., Nys, R. de, Holmstrm, C., Gram, L., Givskov, M., Crass, K., et al. (1998). Chemical mediation of bacterial surface colonisation by secondary metabolites from the red alga *Delisea pulchra*. *Aquat. Microb. Ecol.* 15, 233–246. doi:10.3354/ame015233.

McKey, D. (1979). "The distribution of secondary compounds within plants," in *Herbivores-their interaction with secondary plant metabolites*, 55–134. Available at: https://ci.nii.ac.jp/naid/10012096248/ [Accessed July 19, 2019].

McMurdie, P. J., and Holmes, S. (2013). phyloseq: an R package for reproducible interactive analysis and graphics of microbiome census data. *PLoS One* 8, e61217. doi:10.1371/journal.pone.0061217.

McNeil, null, Nuccio, null, and Hanson, null (1999). Betaines and related osmoprotectants. Targets for metabolic engineering of stress resistance. *Plant Physiol.* 120, 945–950. doi:10.1104/pp.120.4.945.

Meehl, G. A., and Tebaldi, C. (2004). More intense, more frequent, and longer lasting heat waves in the 21st century. *Science* 305, 994–997. doi:10.1126/science.1098704.

Mendiburu, F. de (2019). *Agricolae: Statistical procedures for agricultural research*. Available at: https://CRAN.R-project.org/package=agricolae [Accessed July 9, 2019].

Meng, C., Kuster, B., Culhane, A. C., and Gholami, A. M. (2014). A multivariate approach to the integration of multi-omics datasets. *BMC Bioinformatics* 15, 162. doi:10.1186/1471-2105-15-162.

Mensch, B., Neulinger, S. C., Graiff, A., Pansch, A., Künzel, S., Fischer, M. A., et al. (2016). Restructuring of epibacterial communities on *Fucus vesiculosus* forma *mytili* in response to elevated pCO_2 and increased temperature levels. *Front. Microbiol.* 7, 434. doi:10.3389/fmicb.2016.00434.

Merker, R. I., and Smit, J. (1988). Characterization of the adhesive holdfast of marine and freshwater Caulobacters. *Appl. Environ. Microbiol.* 54, 2078–2085.

Meroni, L., Chiantore, M., Petrillo, M., and Asnaghi, V. (2018). Habitat effects on *Ostreopsis* cf. *ovata* bloom dynamics. *Harmful Algae* 80, 64–71. doi:10.1016/j.hal.2018.09.006.

Meyer-Abich, A. (1943). I. Das typologische grundgesetz und seine folgerungen für phylogenie und entwicklungsphysiologie. *Acta Biotheor.* 7, 1–80. doi:10.1007/BF01603792.

Michaelson, L. V., Napier, J. A., Molino, D., and Faure, J.-D. (2016). Plant sphingolipids: Their importance in cellular organization and adaption. *Biochim. Biophys. Acta* 1861, 1329–1335. doi:10.1016/j.bbalip.2016.04.003.

Michelou, V. K., Caporaso, J. G., Knight, R., and Palumbi, S. R. (2013). The ecology of microbial communities associated with *Macrocystis pyrifera*. *PLoS One* 8, e67480. doi:10.1371/journal.pone.0067480.

Mikami, K., and Hosokawa, M. (2013). Biosynthetic pathway and health benefits of fucoxanthin, an algae-specific xanthophyll in brown seaweeds. *Int. J. Mol. Sci.* 14, 13763–13781. doi:10.3390/ijms140713763.

Minich, J. J., Morris, M. M., Brown, M., Doane, M., Edwards, M. S., Michael, T. P., et al. (2018). Elevated temperature drives kelp microbiome dysbiosis, while elevated carbon dioxide induces water microbiome disruption. *PLoS One* 13, e0192772. doi:10.1371/journal.pone.0192772.

Moenne, A., González, A., and Sáez, C. A. (2016). Mechanisms of metal tolerance in marine macroalgae, with emphasis on copper tolerance in Chlorophyta and Rhodophyta. *Aquat. Toxicol.* 176, 30–37. doi:10.1016/j.aquatox.2016.04.015.

Monroe, D. (2007). Looking for chinks in the armor of bacterial biofilms. *PLoS Biol.* 5, e307. doi:10.1371/journal.pbio.0050307.

Monte, A. A., Brocker, C., Nebert, D. W., Gonzalez, F. J., Thompson, D. C., and Vasiliou, V. (2014). Improved drug therapy: triangulating phenomics with genomics and metabolomics. *Human Genomics* 8, 16. doi:10.1186/s40246-014-0016-9.

Moore, P. D. (2005). Roots of stability. *Nature* 437, 959–961. doi:10.1038/437959a.

Moran, N. A., McCutcheon, J. P., and Nakabachi, A. (2008). Genomics and evolution of heritable bacterial symbionts. *Annu. Rev. Genet.* 42, 165–190. doi:10.1146/annurev.genet.41.110306.130119.

Moran, N. A., and Sloan, D. B. (2015). The Hologenome concept: helpful or hollow? *PLoS Biol.* 13, e1002311. doi:10.1371/journal.pbio.1002311.

Morrissey, K. L., Çavaş, L., Willems, A., and De Clerck, O. (2019). Disentangling the influence of environment, host specificity and thallus differentiation on bacterial communities in siphonous green seaweeds. *Front. Microbiol.* 10, 717. doi:10.3389/fmicb.2019.00717.

Morton, J. T., Aksenov, A. A., Nothias, L. F., Foulds, J. R., Quinn, R. A., Badri, M. H., et al. (2019). Learning representations of microbe-metabolite interactions. *Nat. Methods* 16, 1306–1314. doi:10.1038/s41592-019-0616-3.

Mou, X., Moran, M. A., Stepanauskas, R., González, J. M., and Hodson, R. E. (2005). Flow-cytometric cell sorting and subsequent molecular analyses for culture-independent identification of bacterioplankton involved in dimethylsulfoniopropionate transformations. *Appl. Environ. Microbiol.* 71, 1405–1416. doi:10.1128/AEM.71.3.1405-1416.2005.

Muscatine, L., and Porter, J. W. (1977). Reef corals: mutualistic symbioses adapted to nutrient-poor environments. *Bioscience* 27, 454–460. doi:10.2307/1297526.

Nagayama, K., Shibata, T., Fujimoto, K., Honjo, T., and Nakamura, T. (2003). Algicidal effect of phlorotannins from the brown alga *Ecklonia kurome* on red tide microalgae. *Aquaculture* 218, 601–611. doi:10.1016/S0044-8486(02)00255-7.

Nahas, R., Abatis, D., Anagnostopoulou, M. A., Kefalas, P., Vagias, C., and Roussis, V. (2007). Radical-scavenging activity of Aegean Sea marine algae. *Food Chem.* 102, 577–581. doi:10.1016/j.foodchem.2006.05.036.

Nasrolahi, A., Stratil, S. B., Jacob, K. J., and Wahl, M. (2012). A protective coat of microorganisms on macroalgae: inhibitory effects of bacterial biofilms and epibiotic microbial assemblages on barnacle attachment. *FEMS Microbiol. Ecol.* 81, 583–595. doi:10.1111/j.1574-6941.2012.01384.x.

Nedashkovskaya, O. I., Kukhlevskiy, A. D., Zhukova, N. V., Kim, S.-J., and Rhee, S.-K. (2013). *Litorimonas cladophorae* sp. nov., a new alphaproteobacterium isolated from the Pacific green alga *Cladophora stimpsoni*, and emended descriptions of the genus *Litorimonas* and *Litorimonas taeaensis*. *Antonie Van Leeuwenhoek* 103, 1263–1269. doi:10.1007/s10482-013-9906-4.

Nelson, C. E., Carlson, C. A., Ewart, C. S., and Halewood, E. R. (2014). Community differentiation and population enrichment of Sargasso Sea bacterioplankton in the euphotic zone of a mesoscale mode-water eddy. *Environ. Microbiol.* 16, 871–887. doi:10.1111/1462-2920.12241.

Nguyen, T.-P., and Ho, T.-B. (2012). Detecting disease genes based on semi-supervised learning and protein-protein interaction networks. *Artif. Intell. Med.* 54, 63–71. doi:10.1016/j.artmed.2011.09.003.

Nizzamudin, M., and Godeh, M. (1993). Observations on *Taonia atomaria* f. *ciliata* (Lamour.) Nizamuddin. *Pak. J. Bot.* 25, 199–207.

Nothias, L.-F., Nothias-Esposito, M., da Silva, R., Wang, M., Protsyuk, I., Zhang, Z., et al. (2018). Bioactivity-based molecular networking for the discovery of drug leads in natural product bioassay-guided fractionation. *J. Nat. Prod.* 81, 758–767. doi:10.1021/acs.jnatprod.7b00737.

Nylund, G. M., Persson, F., Lindegarth, M., Cervin, G., Hermansson, M., and Pavia, H. (2010). The red alga *Bonnemaisonia asparagoides* regulates epiphytic bacterial abundance and community composition by chemical defence. *FEMS Microbiol. Ecol.* 71, 84–93. doi:10.1111/j.1574-6941.2009.00791.x.

OBIS (2020). Ocean Biogeographic Information System. Intergovernmental Oceanographic Commission of UNESCO. www.iobis.org.

Ogier, J.-C., Pagès, S., Galan, M., Barret, M., and Gaudriault, S. (2019). rpoB, a promising marker for analyzing the diversity of bacterial communities by amplicon sequencing. *BMC Microbiol.* 19, 171. doi:10.1186/s12866-019-1546-z.

Oksanen, J., Blanchet, F. G., Friendly, M., Kindt, R., Legendre, P., McGlinn, D., et al. (2019). *vegan: Community ecology package*. Available at: https://CRAN.R-project.org/package=vegan [Accessed January 15, 2020].

Olguin-Uribe, G., Abou-Mansour, E., Boulander, A., Débard, H., Francisco, C., and Combaut, G. (1997). 6-Bromoindole-3-carbaldehyde, from an *Acinetobacter* sp. bacterium associated with the ascidian *Stomozoa murrayi*. *J. Chem. Ecol.* 23, 2507–2521. doi:10.1023/B:JOEC.0000006663.28348.03.

Oliver, E. C. J., Donat, M. G., Burrows, M. T., Moore, P. J., Smale, D. A., Alexander, L. V., et al. (2018). Longer and more frequent marine heatwaves over the past century. *Nat. Commun.* 9, 1–12. doi:10.1038/s41467-018-03732-9.

Oliver, S. G., Winson, M. K., Kell, D. B., and Baganz, F. (1998). Systematic functional analysis of the yeast genome. *Trends Biotechnol.* 16, 373–378. doi:10.1016/S0167-7799(98)01214-1.

Olsen, G. J., Lane, D. J., Giovannoni, S. J., Pace, N. R., and Stahl, D. A. (1986). Microbial ecology and evolution: a ribosomal RNA approach. *Annu. Rev. Microbiol.* 40, 337–365. doi:10.1146/annurev.mi.40.100186.002005.

Orr, J. C., Fabry, V. J., Aumont, O., Bopp, L., Doney, S. C., Feely, R. A., et al. (2005). Anthropogenic ocean acidification over the twenty-first century and its impact on calcifying organisms. *Nature* 437, 681–686. doi:10.1038/nature04095.

Ortiz-Castro, R., Díaz-Pérez, C., Martínez-Trujillo, M., del Río, R. E., Campos-García, J., and López-Bucio, J. (2011). Transkingdom signaling based on bacterial cyclodipeptides with auxin activity in plants. *Proc. Natl. Acad. Sci. U.S.A.* 108, 7253–7258. doi:10.1073/pnas.1006740108.

Othmani, A., Briand, J.-F., Ayé, M., Molmeret, M., and Culioli, G. (2016a). Surface metabolites of the brown alga *Taonia atomaria* have the ability to regulate epibiosis. *Biofouling* 32, 801–813. doi:10.1080/08927014.2016.1198954.

Othmani, A., Bunet, R., Bonnefont, J.-L., Briand, J.-F., and Culioli, G. (2016b). Settlement inhibition of marine biofilm bacteria and barnacle larvae by compounds isolated from the Mediterranean brown alga *Taonia atomaria*. *J. Appl. Phycol.* 28, 1975–1986. doi:10.1007/s10811-015-0668-4.

O'Toole, G. A., and Kolter, R. (1998). Flagellar and twitching motility are necessary for *Pseudomonas aeruginosa* biofilm development. *Mol. Microbiol.* 30, 295–304. doi:10.1046/j.1365-2958.1998.01062.x.

O'Toole, G., Kaplan, H. B., and Kolter, R. (2000). Biofilm formation as microbial development. *Annu. Rev. Microbiol.* 54, 49–79. doi:10.1146/annurev.micro.54.1.49.

Paix, B., Carriot, N., Barry-Martinet, R., Greff, S., Misson, B., Briand, J.-F., et al. (2020). A multi-omics analysis suggests links between the differentiated surface metabolome and epiphytic microbiota along the thallus of a Mediterranean seaweed holobiont. *Front. Microbiol.* 11, 494. doi:10.3389/fmicb.2020.00494.

Paix, B., Layglon, N., Le Poupon, C., D'Onofrio, S., Misson, B., Garnier, C., et al. (*in prep.*). A multi-omics approach deciphers how temperature and copper stress shape seaweed-microbiota interactions at the surface of *Taonia atomaria* on the NW Mediterranean coast.

Paix, B., Othmani, A., Debroas, D., Culioli, G., and Briand, J.-F. (2019). Temporal covariation of epibacterial community and surface metabolome in the Mediterranean seaweed holobiont *Taonia atomaria*. *Environ. Microbiol.* 21, 3346–3363. doi:10.1111/1462-2920.14617.

Paix, B., Potin, P., Layglon, N., Misson, B., Leblanc, C., Culioli, G., et al. (*in prep.*). Synergistic effects of temperature and light affect the relationship between *Taonia atomaria* and its epibacterial community: a mesocosm study.

Palmer, J., Flint, S., and Brooks, J. (2007). Bacterial cell attachment, the beginning of a biofilm. *J. Ind. Microbiol. Biotechnol.* 34, 577–588. doi:10.1007/s10295-007-0234-4.

Parada, A. E., Needham, D. M., and Fuhrman, J. A. (2016). Every base matters: assessing small subunit rRNA primers for marine microbiomes with mock communities, time series and global field samples. *Environ. Microbiol.* 18, 1403–1414. doi:10.1111/1462-2920.13023.

Park, S., Jung, Y.-T., Won, S.-M., Park, J.-M., and Yoon, J.-H. (2014). *Granulosicoccus undariae* sp. nov., a member of the family Granulosicoccaceae isolated from a brown algae reservoir and emended description of the genus *Granulosicoccus*. *Antonie Van Leeuwenhoek* 106, 845–852. doi:10.1007/s10482-014-0254-9.

Parrot, D., Blümel, M., Utermann, C., Chianese, G., Krause, S., Kovalev, A., et al. (2019). Mapping the surface microbiome and metabolome of brown seaweed *Fucus vesiculosus* by amplicon sequencing, integrated metabolomics and imaging techniques. *Sci. Rep.* 9, 1061. doi:10.1038/s41598-018-37914-8.

Paula, J. C. D., Vallim, M. A., and Teixeira, V. L. (2011). What are and where are the bioactive terpenoids metabolites from Dictyotaceae (Phaeophyceae). *Rev. Bras. Farmacogn.* 21, 216–228. doi:10.1590/S0102-695X2011005000079.

Pavaux, A.-S., Rostan, J., Guidi-Guilvard, L., Marro, S., Ternon, E., Olivier, T., et al. (2019). Effects of the toxic dinoflagellate *Ostreopsis* cf. *ovata* on survival, feeding and reproduction of a phytal harpacticoid copepod. *J. Exp. Mar. Biol. Ecol.* 516, 103–113. doi:10.1016/j.jembe.2019.05.004.

Pavaux, A.-S., Ternon, E., Dufour, L., Marro, S., Gémin, M.-P., Thomas, O. P., et al. (2020). Efficient, fast and inexpensive bioassay to monitor benthic microalgae toxicity: Application to *Ostreopsis* species. *Aquat. Toxicol.* 223, 105485. doi:10.1016/j.aquatox.2020.105485.

Peixoto, R. S., Rosado, P. M., Leite, D. C. de A., Rosado, A. S., and Bourne, D. G. (2017). Beneficial microorganisms for corals (BMC): Proposed mechanisms for coral health and resilience. *Front. Microbiol.* 8. doi:10.3389/fmicb.2017.00341.

Pellegrini, M., Valls, R., and Pellegrini, L. (1997). Chimiotaxonomie et marqueurs chimiques dans les algues brunes. *Lagascalia* 19, 145–164.

Peña, V., Hernández-Kantún, J. J., Grall, J., Pardo, C., López, L., Bárbara, I., et al. (2014). Detection of gametophytes in the maerl-forming species *Phymatolithon calcareum* (Melobesioideae, Corallinales) assessed by DNA barcoding. *Cryptogam. Algol.* 35, 15–25. doi:10.7872/crya.v35.iss1.2014.15.

Pereira, R. C., Cavalcanti, D. N., and Teixeira, V. L. (2000). Effects of secondary metabolites from the tropical Brazilian brown alga *Dictyota menstrualis* on the amphipod *Parhyale hawaiensis*. *Mar. Ecol. Prog. Ser.* 205, 95–100. doi:10.3354/meps205095.

Perez-Bermudez, P., Garcia-Carrascosa, M., Cornejo, M. J., and Segura, J. (1981). Water-depth effects in photosynthetic pigment content of the benthic algae *Dictyota dichotoma* and *Udotea petiolata*. *Aquat. Bot.* 11, 373–377. doi:10.1016/0304-3770(81)90070-X.

Perkins, S. E., Alexander, L. V., and Nairn, J. R. (2012). Increasing frequency, intensity and duration of observed global heatwaves and warm spells. *Geophys. Res. Lett.* 39, L20714. doi:10.1029/2012GL053361.

Pettus, J. A., Wing, R. M., and Sims, J. J. (1977). Marine natural products XII isolation of a family of multihalogenated gamma-methylene lactones from the red seaweed *Delisea fimbriata*. *Tetrahedron Lett.* 18, 41–44. doi:10.1016/S0040-4039(01)92545-6.

Pezzolesi, L., Guerrini, F., Ciminiello, P., Dell'Aversano, C., Iacovo, E. D., Fattorusso, E., et al. (2012). Influence of temperature and salinity on *Ostreopsis* cf. *ovata* growth and evaluation of toxin content through HR LC-MS and biological assays. *Water Res.* 46, 82–92. doi:10.1016/j.watres.2011.10.029.

Picioreanu, C., van Loosdrecht, M. C., and Heijnen, J. J. (2001). Two-dimensional model of biofilm detachment caused by internal stress from liquid flow. *Biotechnol. Bioeng.* 72, 205–218.

Pineda, M.-C., Strehlow, B., Sternel, M., Duckworth, A., Jones, R., and Webster, N. S. (2017). Effects of suspended sediments on the sponge holobiont with implications for dredging management. *Sci. Rep.* 7, 4925. doi:10.1038/s41598-017-05241-z.

Pinto, E., Sigaud-kutner, T. C. S., Leitão, M. A. S., Okamoto, O. K., Morse, D., and Colepicolo, P. (2003). Heavy metal–induced oxidative stress in algae. *J. Phycol.* 39, 1008–1018. doi:10.1111/j.0022-3646.2003.02-193.x.

Piovan, A., Seraglia, R., Bresin, B., Caniato, R., and Filippini, R. (2013). Fucoxanthin from *Undaria pinnatifida*: photostability and coextractive effects. *Molecules* 18, 6298–6310. doi:10.3390/molecules18066298.

Pistocchi, R., Pezzolesi, L., Guerrini, F., Vanucci, S., Dell'Aversano, C., and Fattorusso, E. (2011). A review on the effects of environmental conditions on growth and toxin production of *Ostreopsis ovata*. *Toxicon* 57, 421–428. doi:10.1016/j.toxicon.2010.09.013.

Pita, L., Rix, L., Slaby, B. M., Franke, A., and Hentschel, U. (2018). The sponge holobiont in a changing ocean: from microbes to ecosystems. *Microbiome* 6, 46. doi:10.1186/s40168-018-0428-1.

Pitlik, S. D., and Koren, O. (2017). How holobionts get sick-toward a unifying scheme of disease. *Microbiome* 5, 64. doi:10.1186/s40168-017-0281-7.

Pollet, T., Berdjeb, L., Garnier, C., Durrieu, G., Le Poupon, C., Misson, B., et al. (2018). Prokaryotic community successions and interactions in marine biofilms: the key role of Flavobacteriia. *FEMS Microbiol. Ecol.* 94. doi:10.1093/femsec/fiy083.

Polo, L. K., Felix, M. R. L., Kreusch, M., Pereira, D. T., Costa, G. B., Simioni, C., et al. (2015). Metabolic profile of the brown macroalga *Sargassum cymosum* (Phaeophyceae, Fucales) under laboratory UV radiation and salinity conditions. *J. Appl. Phycol.* 27, 887–899. doi:10.1007/s10811-014-0381-8.

Popendorf, K. J., Fredricks, H. F., and Van Mooy, B. A. S. (2013). Molecular ion-independent quantification of polar glycerolipid classes in marine plankton using triple quadrupole MS. *Lipids* 48, 185–195. doi:10.1007/s11745-012-3748-0.

Potin, P., Bouarab, K., Küpper, F., and Kloareg, B. (1999). Oligosaccharide recognition signals and defence reactions in marine plant-microbe interactions. *Curr. Opin. Microbiol.* 2, 276–283. doi:10.1016/S1369-5274(99)80048-4.

Poulson-Ellestad, K. L., Jones, C. M., Roy, J., Viant, M. R., Fernández, F. M., Kubanek, J., et al. (2014). Metabolomics and proteomics reveal impacts of chemically mediated competition on marine plankton. *Proc. Natl. Acad. Sci. U.S.A.* 111, 9009–9014. doi:10.1073/pnas.1402130111.

Prato, E., Biandolino, F., Bisci, A. P., and Caroppo, C. (2011). Preliminary assessment of *Ostreopsis* cfr. *ovata* acute toxicity by using a battery bioassay. *Chem. Ecol.* 27, 117–125. doi:10.1080/02757540.2011.625930.

Price, M. N., Dehal, P. S., and Arkin, A. P. (2010). FastTree 2 – Approximately Maximum-Likelihood trees for large alignments. *PLoS One* 5, e9490. doi:10.1371/journal.pone.0009490.

Pruesse, E., Quast, C., Knittel, K., Fuchs, B. M., Ludwig, W., Peplies, J., et al. (2007). SILVA: a comprehensive online resource for quality checked and aligned ribosomal RNA sequence data compatible with ARB. *Nucleic Acids Res.* 35, 7188–7196. doi:10.1093/nar/gkm864.

Puglisi, M. P., Sneed, J. M., Sharp, K. H., Ritson-Williams, R., and Paul, V. J. (2014). Marine chemical ecology in benthic environments. *Nat. Prod. Rep.* 31, 1510–1553. doi:10.1039/C4NP00017J.

Pujalte, M. J., Lucena, T., Ruvira, M. A., Arahal, D. R., and Macián, M. C. (2014). "The family Rhodobacteraceae," in *The Prokaryotes: Alphaproteobacteria and Betaproteobacteria*, eds. E. Rosenberg, E. F. DeLong, S. Lory, E. Stackebrandt, and F. Thompson (Berlin, Heidelberg: Springer), 439–512. doi:10.1007/978-3-642-30197-1_377.

Qiu, Z., Coleman, M. A., Provost, E., Campbell, A. H., Kelaher, B. P., Dalton, S. J., et al. (2019). Future climate change is predicted to affect the microbiome and condition of habitat-forming kelp. *Proc. Biol. Sci.* 286, 20181887. doi:10.1098/rspb.2018.1887.

Quigley, C. T. C., Morrison, H. G., Mendonça, I. R., and Brawley, S. H. (2018). A common garden experiment with *Porphyra umbilicalis* (Rhodophyta) evaluates methods to study spatial differences in the macroalgal microbiome. *J. Phycol.* 54, 653–664. doi:10.1111/jpy.12763.

Ragonese, C., Tedone, L., Beccaria, M., Torre, G., Cichello, F., Cacciola, F., et al. (2014). Characterisation of lipid fraction of marine macroalgae by means of chromatography techniques coupled to mass spectrometry. *Food Chem.* 145, 932–940. doi:10.1016/j.foodchem.2013.08.130.

Ramirez-Puebla, S. T., Weigel, B. L., Jack, L., Schlundt, C., Pfister, C. A., and Welch, J. L. M. (2020). Spatial organization of the kelp microbiome at micron scales (preprint). *bioRxiv*, 2020.03.01.972083. doi:10.1101/2020.03.01.972083.

Ramus, J., Lemons, F., and Zimmerman, C. (1977). Adaptation of light-harvesting pigments to downwelling light and the consequent photosynthetic performance of the eulittoral rockweeds *Ascophyllum nodosum* and *Fucus vesiculosus*. *Mar. Biol.* 42, 293–303. doi:10.1007/BF00402191.

Reisch, C. R., Moran, M. A., and Whitman, W. B. (2011). Bacterial catabolism of dimethylsulfoniopropionate (DMSP). *Front. Microbiol.* 2, 172. doi:10.3389/fmicb.2011.00172.

Reshef, L., Koren, O., Loya, Y., Zilber-Rosenberg, I., and Rosenberg, E. (2006). The coral probiotic hypothesis. *Environ. Microbiol.* 8, 2068–2073. doi:10.1111/j.1462-2920.2006.01148.x.

Rickert, E., Karsten, U., Pohnert, G., and Wahl, M. (2015). Seasonal fluctuations in chemical defenses against macrofouling in *Fucus vesiculosus* and *Fucus serratus* from the Baltic Sea. *Biofouling* 31, 363–377. doi:10.1080/08927014.2015.1041020.

Rickert, E., Lenz, M., Barboza, F. R., Gorb, S. N., and Wahl, M. (2016a). Seasonally fluctuating chemical microfouling control in *Fucus vesiculosus* and *Fucus serratus* from the Baltic Sea. *Mar. Biol.* 163, 203. doi:10.1007/s00227-016-2970-3.

Rickert, E., Wahl, M., Link, H., Richter, H., and Pohnert, G. (2016b). Seasonal variations in surface metabolite composition of *Fucus vesiculosus* and *Fucus serratus* from the Baltic Sea. *PLoS One* 11, e0168196. doi:10.1371/journal.pone.0168196.

Rimet, F., Gusev, E., Kahlert, M., Kelly, M. G., Kulikovskiy, M., Maltsev, Y., et al. (2019). Diat.barcode, an open-access curated barcode library for diatoms. *Sci. Rep.* 9, 1–12. doi:10.1038/s41598-019-51500-6.

Rindi, F., Braga, J. C., Martin, S., Peña, V., Le Gall, L., Caragnano, A., et al. (2019). Coralline algae in a changing Mediterranean Sea: how can we predict their future, if we do not know their present? *Front. Mar. Sci.* 6, 723. doi:10.3389/fmars.2019.00723.

Ritter, A., Dittami, S. M., Goulitquer, S., Correa, J. A., Boyen, C., Potin, P., et al. (2014). Transcriptomic and metabolomic analysis of copper stress acclimation in *Ectocarpus siliculosus* highlights signaling and tolerance mechanisms in brown algae. *BMC Plant Biol.* 14, 116. doi:10.1186/1471-2229-14-116.

Ritter, A., Goulitquer, S., Salaün, J.-P., Tonon, T., Correa, J. A., and Potin, P. (2008). Copper stress induces biosynthesis of octadecanoid and eicosanoid oxygenated derivatives in the brown algal kelp *Laminaria digitata*. *New Phytol.* 180, 809–821. doi:10.1111/j.1469-8137.2008.02626.x.

Rizzo, L., Fraschetti, S., Alifano, P., Pizzolante, G., and Stabili, L. (2016). The alien species *Caulerpa cylindracea* and its associated bacteria in the Mediterranean Sea. *Mar. Biol.* 163, 4. doi:10.1007/s00227-015-2775-9.

Robinson, W. (1932). Observations on the Development of *Taonia atomaria*, Ag. *Ann. Bot.* os-46, 113–120. doi:10.1093/oxfordjournals.aob.a090311.

Roche, S. A., and Leblond, J. D. (2010). Betaine lipids in Chlorarachniophytes. *Phycological Res.* 58, 298–305. doi:10.1111/j.1440-1835.2010.00590.x.

Rodríguez, F. E., Laporte, D., González, A., Mendez, K. N., Castro-Nallar, E., Meneses, C., et al. (2018). Copper-induced increased expression of genes involved in photosynthesis, carotenoid synthesis and C assimilation in the marine alga *Ulva compressa*. *BMC Genomics* 19, 829. doi:10.1186/s12864-018-5226-4.

Rognes, T., Flouri, T., Nichols, B., Quince, C., and Mahé, F. (2016). VSEARCH: a versatile open source tool for metagenomics. *PeerJ* 4, e2584. doi:10.7717/peerj.2584.

Rohde, S., Hiebenthal, C., Wahl, M., Karez, R., and Bischof, K. (2008). Decreased depth distribution of *Fucus vesiculosus* (Phaeophyceae) in the Western Baltic: effects of light deficiency and epibionts on growth and photosynthesis. *Eur. J. Phycol.* 43, 143–150. doi:10.1080/09670260801901018.

Rohwer, F., Seguritan, V., Azam, F., and Knowlton, N. (2002). Diversity and distribution of coral-associated bacteria. *Mar. Ecol. Prog. Ser.* 243, 1–10. doi:10.3354/meps243001.

Romera-Castillo, C., Sarmento, H., Alvarez-Salgado, X. A., Gasol, J. M., and Marrasé, C. (2011). Net production and consumption of fluorescent colored dissolved organic matter by natural bacterial assemblages growing on marine phytoplankton exudates. *Appl. Environ. Microbiol.* 77, 7490–7498. doi:10.1128/AEM.00200-11.

Rosenberg, E., Koren, O., Reshef, L., Efrony, R., and Zilber-Rosenberg, I. (2007). The role of microorganisms in coral health, disease and evolution. *Nat. Rev. Microbiol.* 5, 355–362. doi:10.1038/nrmicro1635.

Rosenberg, E., Sharon, G., and Zilber-Rosenberg, I. (2009). The hologenome theory of evolution contains Lamarckian aspects within a Darwinian framework. *Environ. Microbiol.* 11, 2959–2962. doi:10.1111/j.1462-2920.2009.01995.x.

Rosenberg, E., and Zilber-Rosenberg, I. (2018). The hologenome concept of evolution after 10 years. *Microbiome* 6, 78. doi:10.1186/s40168-018-0457-9.

Roth-Schulze, A. J., Pintado, J., Zozaya-Valdés, E., Cremades, J., Ruiz, P., Kjelleberg, S., et al. (2018). Functional biogeography and host specificity of bacterial communities associated with the Marine Green Alga *Ulva* spp. *Mol. Ecol.* 27, 1952–1965. doi:10.1111/mec.14529.

Roth-Schulze, A. J., Thomas, T., Steinberg, P., Deveney, M. R., Tanner, J. E., Wiltshire, K. H., et al. (2018). The effects of warming and ocean acidification on growth, photosynthesis, and bacterial communities for the marine invasive macroalga *Caulerpa taxifolia*. *Limnol. Oceanogr.* 63, 459–471. doi:10.1002/lno.10739.

Rousvoal, S., Groisillier, A., Dittami, S. M., Michel, G., Boyen, C., and Tonon, T. (2011). Mannitol-1-phosphate dehydrogenase activity in *Ectocarpus siliculosus*, a key role for mannitol synthesis in brown algae. *Planta* 233, 261–273. doi:10.1007/s00425-010-1295-6.

Rovirosa, J., Sepulveda, M., Quezada, E., and San-Martin, A. (1992). Isoepitaondiol, a diterpenoid of *Stypopodium flabelliforme* and the insecticidal activity of stypotriol, epitaondiol and derivatives. *Phytochemistry* 31, 2679–2681. doi:10.1016/0031-9422(92)83610-B.

Rowan, R. (1998). Review-Diversity and ecology of zooxanthellae on coral reefs. *J. Phycol.* 34, 407–417. doi:10.1046/j.1529-8817.1998.340407.x.

Ryabushko, V. I., Prazukin, A. V., Gureeva, E. V., Bobko, N. I., Kovrigina, N. P., and Nekhoroshev, M. V. (2017). Fucoxanthin and heavy metals in brown algae of genus *Cystoseira* C. Agardh from water areas with different anthropogenic influences (Black Sea). *Mar. Biol. J.* 2, 70–79. doi:10.21072/mbj.2017.02.2.07.

Sabry, O. M. M., Andrews, S., McPhail, K. L., Goeger, D. E., Yokochi, A., LePage, K. T., et al. (2005). Neurotoxic meroditerpenoids from the tropical marine brown alga *Stypopodium flabelliforme*. *J. Nat. Prod.* 68, 1022–1030. doi:10.1021/np050051f.

Saha, M., Barboza, F. R., Somerfield, P. J., Al-Janabi, B., Beck, M., Brakel, J., et al. (2020a). Response of foundation macrophytes to near-natural simulated marine heatwaves. *Glob. Change Biol.* 26, 417–430. doi:10.1111/gcb.14801.

Saha, M., Ferguson, R. M. W., Dove, S., Künzel, S., Meichssner, R., Neulinger, S. C., et al. (2020b). Salinity and time can alter epibacterial communities of an invasive seaweed. *Front. Microbiol.* 10. doi:10.3389/fmicb.2019.02870.

Saha, M., Rempt, M., Gebser, B., Grueneberg, J., Pohnert, G., and Weinberger, F. (2012). Dimethylsulphopropionate (DMSP) and proline from the surface of the brown alga *Fucus vesiculosus* inhibit bacterial attachment. *Biofouling* 28, 593–604. doi:10.1080/08927014.2012.698615.

Saha, M., Rempt, M., Grosser, K., Pohnert, G., and Weinberger, F. (2011). Surface-associated fucoxanthin mediates settlement of bacterial epiphytes on the rockweed *Fucus vesiculosus*. *Biofouling* 27, 423–433. doi:10.1080/08927014.2011.580841.

Saha, M., Rempt, M., Stratil, S. B., Wahl, M., Pohnert, G., and Weinberger, F. (2014). Defence chemistry modulation by light and temperature shifts and the resulting effects on associated epibacteria of *Fucus vesiculosus*. *PLoS One* 9, e105333. doi:10.1371/journal.pone.0105333.

Saha, M., and Weinberger, F. (2019). Microbial “gardening” by a seaweed holobiont: Surface metabolites attract protective and deter pathogenic epibacterial settlement. *J. Ecol.* 107, 2255–2265. doi:10.1111/1365-2745.13193.

Saha, M., Wiese, J., Weinberger, F., and Wahl, M. (2016). Rapid adaptation to controlling new microbial epibionts in the invaded range promotes invasiveness of an exotic seaweed. *J. Ecol.* 104, 969–978. doi:10.1111/1365-2745.12590.

Sala, E., and Boudouresque, C. F. (1997). The role of fishes in the organization of a Mediterranean sublittoral community.: I: Algal communities. *J. Exp. Mar. Biol. Ecol.* 212, 25–44. doi:10.1016/S0022-0981(96)02745-1.

Salvador Soler, N., Gómez Garreta, M. A., Lavelli, L., and Ribera Siguán, M. A. (2007). Antimicrobial activity of Iberian macroalgae. *Sci. Mar.* 71, 101–113. doi:10.3989/scimar.2007.71n1101.

Samburova, V., Lemos, M. S., Hiibel, S., Kent Hoekman, S., Cushman, J. C., and Zielinska, B. (2013). Analysis of triacylglycerols and free fatty acids in algae using Ultra-Performance Liquid Chromatography Mass Spectrometry. *J. Am. Oil Chem. Soc.* 90, 53–64. doi:10.1007/s11746-012-2138-3.

Sand, M., Mingote, A. I., Santos, H., Müller, V., and Averhoff, B. (2013). Mannitol, a compatible solute synthesized by *Acinetobacter baylyi* in a two-step pathway including a salt-induced and salt-dependent mannitol-1-phosphate dehydrogenase. *Environ. Microbiol.* 15, 2187–2197. doi:10.1111/1462-2920.12090.

Sato, N., and Murata, N. (1980). Temperature shift-induced responses in lipids in the blue-green alga, *Anabaena variabilis*: the central role of diacylmonogalactosylglycerol in thermo-adaptation. *Biochim. Biophys. Acta* 619, 353–366. doi:10.1016/0005-2760(80)90083-1.

Sato, N., and Murata, N. (1982). Lipid biosynthesis in the blue-green alga, *Anabaena variabilis*: II. Fatty acids and lipid molecular species. *Biochim. Biophys. Acta* 710, 279–289. doi:10.1016/0005-2760(82)90110-2.

Schäfer, H., Servais, P., and Muyzer, G. (2000). Successional changes in the genetic diversity of a marine bacterial assemblage during confinement. *Arch. Microbiol.* 173, 138–145. doi:10.1007/s002039900121.

Scheubert, K., Hufsky, F., Petras, D., Wang, M., Nothias, L.-F., Dührkop, K., et al. (2017). Significance estimation for large scale metabolomics annotations by spectral matching. *Nat. Commun.* 8, 1–10. doi:10.1038/s41467-017-01318-5.

Schiel, D. R. (2006). Rivets or bolts? When single species count in the function of temperate rocky reef communities. *J. Exp. Mar. Biol. Ecol.* 338, 233–252. doi:10.1016/j.jembe.2006.06.023.

Schiel, D. R., and Foster, M. S. (2006). The population biology of large brown seaweeds: Ecological consequences of multiphase life histories in dynamic coastal environments. *Annu. Rev. Ecol. Evol. Syst.* 37, 343–372. doi:10.1146/annurev.ecolsys.37.091305.110251.

Schmitt, T. M., Hay, M. E., and Lindquist, N. (1995). Constraints on chemically mediated coevolution: Multiple functions for seaweed secondary metabolites. *Ecology* 76, 107–123. doi:10.2307/1940635.

Schmitt, T. M., Lindquist, N., and Hay, M. E. (1998). Seaweed secondary metabolites as antifoulants: effects of *Dictyota* spp. diterpenes on survivorship, settlement, and development of marine invertebrate larvae. *Chemoecology* 8, 125–131. doi:10.1007/s000490050017.

Schoch, C. L., Seifert, K. A., Huhndorf, S., Robert, V., Spouge, J. L., Levesque, C. A., et al. (2012). Nuclear ribosomal internal transcribed spacer (ITS) region as a universal DNA barcode marker for Fungi. *Proc. Natl. Acad. Sci. U.S.A.* 109, 6241–6246. doi:10.1073/pnas.1117018109.

Schüler, L. M., Schulze, P. S. C., Pereira, H., Barreira, L., León, R., and Varela, J. (2017). Trends and strategies to enhance triacylglycerols and high-value compounds in microalgae. *Algal Res.* 25, 263–273. doi:10.1016/j.algal.2017.05.025.

Schultz-Johansen, M., Glaring, M. A., Bech, P. K., and Stougaard, P. (2016). Draft genome sequence of a novel marine bacterium, *Paraglaciecola* sp. strain s66, with hydrolytic activity against seaweed polysaccharides. *Genome Announc.* 4. doi:10.1128/genomeA.00304-16.

Selander, E., Kubanek, J., Hamberg, M., Andersson, M. X., Cervin, G., and Pavia, H. (2015). Predator lipids induce paralytic shellfish toxins in bloom-forming algae. *Proc. Natl. Acad. Sci. U.S.A.* 112, 6395–6400. doi:10.1073/pnas.1420154112.

Serebryakova, A., Aires, T., Viard, F., Serrão, E. A., and Engelen, A. H. (2018). Summer shifts of bacterial communities associated with the invasive brown seaweed *Sargassum muticum* are location and tissue dependent. *PLoS One* 13, e0206734. doi:10.1371/journal.pone.0206734.

Seymour, J. R., Amin, S. A., Raina, J.-B., and Stocker, R. (2017). Zooming in on the phycosphere: the ecological interface for phytoplankton–bacteria relationships. *Nat. Microbiol.* 2, 1–12. doi:10.1038/nmicrobiol.2017.65.

Shankar, V., Agans, R., and Paliy, O. (2017). Advantages of phylogenetic distance based constrained ordination analyses for the examination of microbial communities. *Sci. Rep.* 7, 6481. doi:10.1038/s41598-017-06693-z.

Shindo, K., Mikami, K., Tamesada, E., Takaichi, S., Adachi, K., Misawa, N., et al. (2007). Diapolycopenedioic acid xylosyl ester, a novel glyco-C30-carotenoic acid produced by a new marine bacterium *Rubritalea squalenifaciens*. *Tetrahedron Lett.* 48, 2725–2727. doi:10.1016/j.tetlet.2007.02.065.

Shoji, J., Kamimura, Y., and Fujiki, C. (2009). “Macro-algae habitat as fish nursery: Evaluation of function a predation refuge,” in *Integrated Coastal Zone Management* (John Wiley & Sons, Ltd), 50–56. doi:10.1002/9781444316285.ch4.

Simister, R., Taylor, M. W., Tsai, P., and Webster, N. (2012). Sponge-microbe associations survive high nutrients and temperatures. *PLoS One* 7, e52220. doi:10.1371/journal.pone.0052220.

Simonini, R., Orlandi, M., and Abbate, M. (2011). Is the toxic dinoflagellate *Ostreopsis* cf. *ovata* harmful to Mediterranean benthic invertebrates? Evidences from ecotoxicological tests with the polychaete *Dinophilus gyrociliatus*. *Mar. Environ. Res.* 72, 230–233. doi:10.1016/j.marenvres.2011.08.009.

Smale, D. A., Wernberg, T., Oliver, E. C. J., Thomsen, M., Harvey, B. P., Straub, S. C., et al. (2019). Marine heatwaves threaten global biodiversity and the provision of ecosystem services. *Nat. Clim. Change* 9, 306–312. doi:10.1038/s41558-019-0412-1.

Smith, C. A., Want, E. J., O'Maille, G., Abagyan, R., and Siuzdak, G. (2006). XCMS: processing mass spectrometry data for metabolite profiling using nonlinear peak alignment, matching, and identification. *Anal. Chem.* 78, 779–787. doi:10.1021/ac051437y.

Sneed, J. M., Ritson-Williams, R., and Paul, V. J. (2015). Crustose coralline algal species host distinct bacterial assemblages on their surfaces. *ISME J.* 9, 2527–2536. doi:10.1038/ismej.2015.67.

Soares, A. R., Teixeira, V. L., Pereira, R. C., and Villaça, R. (2003). Variation on diterpene production by the Brazilian alga *Stypopodium zonale* (Dictyotales, Phaeophyta). *Biochem. Syst. Ecol.* 31, 1347–1350. doi:10.1016/S0305-1978(03)00116-9.

Sohlenkamp, C., and Geiger, O. (2016). Bacterial membrane lipids: diversity in structures and pathways. *FEMS Microbiol. Rev.* 40, 133–159. doi:10.1093/femsre/fuv008.

Spoerner, M., Wichard, T., Bachhuber, T., Stratmann, J., and Oertel, W. (2012). Growth and thallus morphogenesis of *Ulva mutabilis* (Chlorophyta) depends on a combination of two bacterial species excreting regulatory factors. *J. Phycol.* 48, 1433–1447. doi:10.1111/j.1529-8817.2012.01231.x.

Spring, S., Scheuner, C., Göker, M., and Klenk, H.-P. (2015). A taxonomic framework for emerging groups of ecologically important marine gammaproteobacteria based on the reconstruction of evolutionary relationships using genome-scale data. *Front. Microbiol.* 6, 281. doi:10.3389/fmicb.2015.00281.

Steen, F., Vieira, C., D'Hondt, S., Tyberghein, L., Fernandez-García, C., Wysor, B., et al. (*in review*). Global diversification and biogeography of a group of brown seaweeds driven by different evolutionary processes across clades. *Submitted to J. Biogeogr.*

Steen, F., Vieira, C., Leliaert, F., Payri, E. C., and Clerck, O. D. (2015). Biogeographic affinities of Dictyotales from madagascar: a phylogenetic approach. *Cryptogam. Algol.* 36, 129–141. doi:10.7872/crya.v36.iss2.2015.129.

Stefels, J., and Leeuwe, M. A. van (1998). Effects of iron and light stress on the biochemical composition of antarctic *Phaeocystis* sp. (Prymnesiophyceae). i. Intracellular DMSP concentrations. *J. Phycol.* 34, 486–495. doi:10.1046/j.1529-8817.1998.340486.x.

Stefels, J., Steinke, M., Turner, S., Malin, G., and Belviso, S. (2007). Environmental constraints on the production and removal of the climatically active gas dimethylsulphide (DMS) and implications for ecosystem modelling. *Biogeochemistry* 83, 245–275. doi:10.1007/s10533-007-9091-5.

Stencel, A., and Wloch-Salamon, D. M. (2018). Some theoretical insights into the hologenome theory of evolution and the role of microbes in speciation. *Theory Biosci.* 137, 197–206. doi:10.1007/s12064-018-0268-3.

Stiger-Pouvreau, V., Bourgougnon, N., and Deslandes, E. (2016). "Chapter 8 - Carbohydrates from seaweeds," in *Seaweed in Health and Disease Prevention*, eds. J. Fleurence and I. Levine (San Diego: Academic Press), 223–274. doi:10.1016/B978-0-12-802772-1.00008-7.

Stoodley, P., Sauer, K., Davies, D. G., and Costerton, J. W. (2002). Biofilms as complex differentiated communities. *Annu. Rev. Microbiol.* 56, 187–209. doi:10.1146/annurev.micro.56.012302.160705.

Stratil, S. B., Neulinger, S. C., Knecht, H., Friedrichs, A. K., and Wahl, M. (2013). Temperature-driven shifts in the epibiotic bacterial community composition of the brown macroalga *Fucus vesiculosus*. *Microbiologyopen* 2, 338–349. doi:10.1002/mbo3.79.

Stratil, S. B., Neulinger, S. C., Knecht, H., Friedrichs, A. K., and Wahl, M. (2014). Salinity affects compositional traits of epibacterial communities on the brown macroalga *Fucus vesiculosus*. *FEMS Microbiol. Ecol.* 88, 272–279. doi:10.1111/1574-6941.12292.

Suárez-García, S., Arola, L., Pascual-Serrano, A., Arola-Arnal, A., Aragonès, G., Bladé, C., et al. (2017). Development and validation of a UHPLC-ESI-MS/MS method for the simultaneous quantification of mammal lysophosphatidylcholines and lysophosphatidylethanolamines in serum. *J. Chromatogr. B* 1055, 86–97. doi:10.1016/j.jchromb.2017.04.028.

Sunda, W., Kieber, D. J., Kiene, R. P., and Huntsman, S. (2002). An antioxidant function for DMSP and DMS in marine algae. *Nature* 418, 317–320. doi:10.1038/nature00851.

Szklarczyk, D., Franceschini, A., Wyder, S., Forslund, K., Heller, D., Huerta-Cepas, J., et al. (2015). STRING v10: protein-protein interaction networks, integrated over the tree of life. *Nucleic Acids Res.* 43, D447-452. doi:10.1093/nar/gku1003.

Tada, Y., Taniguchi, A., Nagao, I., Miki, T., Uematsu, M., Tsuda, A., et al. (2011). Differing growth responses of major phylogenetic groups of marine bacteria to natural phytoplankton blooms in the western North Pacific Ocean. *Appl. Environ. Microbiol.* 77, 4055–4065. doi:10.1128/AEM.02952-10.

Taib, N., Mangot, J.-F., Domaizon, I., Bronner, G., and Debroas, D. (2013). Phylogenetic affiliation of SSU rRNA genes generated by massively parallel sequencing: new insights into the freshwater protist diversity. *PLoS One* 8, e58950. doi:10.1371/journal.pone.0058950.

Tait, K., Joint, I., Daykin, M., Milton, D. L., Williams, P., and Cámara, M. (2005). Disruption of quorum sensing in seawater abolishes attraction of zoospores of the green alga *Ulva* to bacterial biofilms. *Environ. Microbiol.* 7, 229–240. doi:10.1111/j.1462-2920.2004.00706.x.

Tait, L. W., and Schiel, D. R. (2011). Legacy effects of canopy disturbance on ecosystem functioning in macroalgal assemblages. *PLoS One* 6, e26986. doi:10.1371/journal.pone.0026986.

Tang, Y. Z., and Gobler, C. J. (2011). The green macroalga, *Ulva lactuca*, inhibits the growth of seven common harmful algal bloom species via allelopathy. *Harmful Algae* 10, 480–488. doi:10.1016/j.hal.2011.03.003.

Tappin, A. D., and Millward, G. E. (2015). The English Channel: Contamination status of its transitional and coastal waters. *Mar. Pollut. Bull.* 95, 529–550. doi:10.1016/j.marpolbul.2014.12.012.

Tautenhahn, R., Cho, K., Uritboonthai, W., Zhu, Z., Patti, G. J., and Siuzdak, G. (2012). An accelerated workflow for untargeted metabolomics using the METLIN database. *Nat. Biotechnol.* 30, 826–828. doi:10.1038/nbt.2348.

Teitzel, G. M., and Parsek, M. R. (2003). Heavy metal resistance of biofilm and planktonic *Pseudomonas aeruginosa*. *Appl. Environ. Microbiol.* 69, 2313–2320. doi:10.1128/AEM.69.4.2313-2320.2003.

Ternon, E., Paix, B., Thomas, O. P., Briand, J.-F., and Culioli, G. (2020). Exploring the role of macroalgal surface metabolites on the settlement of the benthic dinoflagellate *Ostreopsis* cf. *ovata*. *Front. Mar. Sci. in press*.

Ternon, E., Pavaux, A.-S., Marro, S., Thomas, O. P., and Lemée, R. (2018). Allelopathic interactions between the benthic toxic dinoflagellate *Ostreopsis* cf. *ovata* and a co-occurring diatom. *Harmful Algae* 75, 35–44. doi:10.1016/j.hal.2018.04.003.

Ternon, E., Pavaux, A.-S., Peltekis, A., Gémin, M., Jauzein, C., Bailleul, B., et al. (*in review*). Allelochemistry in the dynamics of microalgal species: case study of the toxic benthic dinoflagellate *Ostreopsis* cf. *ovata*. *Submitted to Aquat. Microb. Ecol.*

Theis, K. R., Dheilly, N. M., Klassen, J. L., Brucker, R. M., Baines, J. F., Bosch, T. C. G., et al. (2016). Getting the hologenome concept right: An eco-evolutionary framework for hosts and their microbiomes. *mSystems* 1. doi:10.1128/mSystems.00028-16.

Theodoridis, G. A., Gika, H. G., Want, E. J., and Wilson, I. D. (2012). Liquid chromatography-mass spectrometry based global metabolite profiling: a review. *Anal. Chim. Acta* 711, 7–16. doi:10.1016/j.aca.2011.09.042.

Theophilus, T., Vieira, C., Culioli, G., Thomas, O. P., N'Yeurt, A. D. R., Andréfouët, S., et al. (2020). "Chapter Six - Dictyotaceae (Dictyotales, Phaeophyceae) species from French Polynesia: current knowledge and future research," in *Advances in Botanical Research* Seaweeds Around the World: State of Art and Perspectives., ed. N. Bourgougnon (Academic Press), 163–211. doi:10.1016/bs.abr.2019.12.001.

Thingstad, T. F., Krom, M. D., Mantoura, R. F. C., Flaten, G. a. F., Groom, S., Herut, B., et al. (2005). Nature of phosphorus limitation in the ultraoligotrophic Eastern Mediterranean. *Science* 309, 1068–1071. doi:10.1126/science.1112632.

Thole, S., Kalhoefer, D., Voget, S., Berger, M., Engelhardt, T., Liesegang, H., et al. (2012). *Phaeobacter gallaeciensis* genomes from globally opposite locations reveal high similarity of adaptation to surface life. *ISME J.* 6, 2229–2244. doi:10.1038/ismej.2012.62.

Thomas, F., Barbeyron, T., Tonon, T., Génicot, S., Czjzek, M., and Michel, G. (2012). Characterization of the first alginolytic operons in a marine bacterium: from their emergence in marine Flavobacteriia to their independent transfers to marine Proteobacteria and human gut Bacteroides. *Environ. Microbiol.* 14, 2379–2394. doi:10.1111/j.1462-2920.2012.02751.x.

Thomas, F., Cosse, A., Panse, S. L., Kloareg, B., Potin, P., and Leblanc, C. (2014). Kelps feature systemic defense responses: insights into the evolution of innate immunity in multicellular eukaryotes. *New Phytol.* 204, 567–576. doi:10.1111/nph.12925.

Thomas, F., Dittami, S. M., Brunet, M., Duff, N. L., Tanguy, G., Leblanc, C., et al. (2020). Evaluation of a new primer combination to minimize plastid contamination in 16S rDNA metabarcoding analyses of alga-associated bacterial communities. *Environ. Microbiol. Rep.* 12, 30–37. doi:10.1111/1758-2229.12806.

Thomas, F., Lundqvist, L. C. E., Jam, M., Jeudy, A., Barbeyron, T., Sandström, C., et al. (2013). Comparative characterization of two marine alginate lyases from *Zobellia galactanivorans* reveals distinct modes of action and exquisite adaptation to their natural substrate. *J. Biol. Chem.* 288, 23021–23037. doi:10.1074/jbc.M113.467217.

Thompson, J. R., Rivera, H. E., Closek, C. J., and Medina, M. (2015). Microbes in the coral holobiont: partners through evolution, development, and ecological interactions. *Front. Cell. Infect. Microbiol.* 4. doi:10.3389/fcimb.2014.00176.

Thompson, L. R., Sanders, J. G., McDonald, D., Amir, A., Ladau, J., Locey, K. J., et al. (2017). A communal catalogue reveals Earth's multiscale microbial diversity. *Nature* 551, 457–463. doi:10.1038/nature24621.

Thomsen, M. S., Mondardini, L., Alestra, T., Gerrity, S., Tait, L., South, P. M., et al. (2019). Local extinction of bull kelp (*Durvillaea* spp.) due to a marine heatwave. *Front. Mar. Sci.* 6. doi:10.3389/fmars.2019.00084.

Tillmann, U., and Hansen, P. J. (2009). Allelopathic effects of *Alexandrium tamarense* on other algae: evidence from mixed growth experiments. *Aquat. Microb. Ecol.* 57, 101–112. doi:10.3354/ame01329.

Totti, C., Accoroni, S., Cerino, F., Cucchiari, E., and Romagnoli, T. (2010). *Ostreopsis ovata* bloom along the Conero Riviera (Northern Adriatic Sea): Relationships with environmental conditions and substrata. *Harmful Algae* 9, 233–239. doi:10.1016/j.hal.2009.10.006.

Tourneroche, A., Lami, R., Hubas, C., Blanchet, E., Vallet, M., Escoubeyrou, K., et al. (2019). Bacterial-fungal interactions in the kelp endomicrobiota drive autoinducer-2 Quorum Sensing. *Front. Microbiol.* 10, 1693. doi:10.3389/fmicb.2019.01693.

Tringali, C., Piattelli, M., and Spatafora, C. (1995). Sesquiterpenes and geranylgeranylglycerol from the brown algae *Taonia lacheana* and *Taonia atomaria* f. *ciliata*: their chemotaxonomic significance. *Phytochemistry* 40, 827–831. doi:10.1016/0031-9422(95)00357-D.

Tronholm, A., Sansón, M., Afonso-Carrillo, J., Verbruggen, H., and Clerck, O. D. (2010a). Niche partitioning and the coexistence of two cryptic *Dictyota* (Dictyotales, Phaeophyceae) species from the Canary islands. *J. Phycol.* 46, 1075–1087. doi:10.1111/j.1529-8817.2010.00912.x.

Tronholm, A., Steen, F., Tyberghein, L., Leliaert, F., Verbruggen, H., Siguan, M. A. R., et al. (2010b). Species delimitation, taxonomy, and biogeography of *Dictyota* in Europe (Dictyotales, Phaeophyceae). *J. Phycol.* 46, 1301–1321. doi:10.1111/j.1529-8817.2010.00908.x.

Tsushima, M., Maoka, T., and Matsuno, T. (2001). Structures of carotenoids with 5,6-dihydro-β-end groups from the spindle shell *Fusinus perplexus*. *J. Nat. Prod.* 64, 1139–1142. doi:10.1021/np010060y.

Tujula, N. A. (2006). Analysis of the epiphytic bacterial community associated with the green alga *Ulva australis*.

Tziveleka, L.-A., Abatis, D., Paulus, K., Bauer, R., Vagias, C., and Roussis, V. (2005). Marine polyprenylated hydroquinones, quinones, and chromenols with inhibitory effects on leukotriene formation. *Chem. Biodivers.* 2, 901–909. doi:10.1002/cbdv.200590066.

Vairappan, C. S., Suzuki, M., Ishii, T., Okino, T., Abe, T., and Masuda, M. (2008). Antibacterial activity of halogenated sesquiterpenes from Malaysian *Laurencia* spp. *Phytochemistry* 69, 2490–2494. doi:10.1016/j.phytochem.2008.06.015.

Vallim, M. A., De Paula, J. C., Pereira, R. C., and Teixeira, V. L. (2005). The diterpenes from Dictyotacean marine brown algae in the Tropical Atlantic American region. *Biochem. Syst. Ecol.* 33, 1–16. doi:10.1016/j.bse.2004.06.002.

Van Alstyne, K. L., and Puglisi, M. P. (2007). DMSP in marine macroalgae and macroinvertebrates: Distribution, function, and ecological impacts. *Aquat. Sci.* 69, 394–402. doi:10.1007/s00027-007-0888-z.

van de Water, J. A. J. M., Allemand, D., and Ferrier-Pagès, C. (2018). Host-microbe interactions in octocoral holobionts - recent advances and perspectives. *Microbiome* 6, 64. doi:10.1186/s40168-018-0431-6.

van Den Dool, H., and Kratz, P. (1963). A generalization of the retention index system including linear temperature programmed gas—liquid partition chromatography. *J. Chromatogr. A* 11, 463–471. doi:10.1016/S0021-9673(01)80947-X.

van der Loos, L. M., Eriksson, B. K., and Falcão Salles, J. (2019). The macroalgal holobiont in a changing sea. *Trends Microbiol.* 27, 635–650. doi:10.1016/j.tim.2019.03.002.

Vandenkoornhuyse, P., Quaiser, A., Duhamel, M., Le Van, A., and Dufresne, A. (2015). The importance of the microbiome of the plant holobiont. *New Phytol.* 206, 1196–1206. doi:10.1111/nph.13312.

Vaniya, A., and Fiehn, O. (2015). Using fragmentation trees and mass spectral trees for identifying unknown compounds in metabolomics. *Trends Anal. Chem.* 69, 52–61. doi:10.1016/j.trac.2015.04.002.

Vanucci, S., Guidi, F., Pistocchi, R., and Long, R. A. (2016). Phylogenetic structure of bacterial assemblages co-occurring with *Ostreopsis* cf. *ovata* bloom. *Harmful Algae* 55, 259–271. doi:10.1016/j.hal.2016.04.003.

Vargas, C. de, Audic, S., Henry, N., Decelle, J., Mahé, F., Logares, R., et al. (2015). Eukaryotic plankton diversity in the sunlit ocean. *Science* 348, 1261605. doi:10.1126/science.1261605.

Vasselon, V., Domaizon, I., Rimet, F., Kahlert, M., and Bouchez, A. (2017). Application of high-throughput sequencing (HTS) metabarcoding to diatom biomonitoring: Do DNA extraction methods matter? *Freshw. Sci.* 36, 162–177. doi:10.1086/690649.

Verhoeven, J. T. P., Kavanagh, A. N., and Dufour, S. C. (2017). Microbiome analysis shows enrichment for specific bacteria in separate anatomical regions of the deep-sea carnivorous sponge *Chondrocladia grandis*. *FEMS Microbiol. Ecol.* 93. doi:10.1093/femsec/fiw214.

Verpoorte, R., Choi, Y. H., Mustafa, N. R., and Kim, H. K. (2008). Metabolomics: back to basics. *Phytochem. Rev.* 7, 525–537. doi:10.1007/s11101-008-9091-7.

Viano, Y., Bonhomme, D., Camps, M., Briand, J.-F., Ortalo-Magné, A., Blache, Y., et al. (2009). Diterpenoids from the Mediterranean brown alga *Dictyota* sp. evaluated as antifouling substances against a marine bacterial biofilm. *J. Nat. Prod.* 72, 1299–1304. doi:10.1021/np900102f.

Vieira, C. (2020). *Lobophora*–coral interactions and phase shifts: summary of current knowledge and future directions. *Aquat. Ecol.* 54, 1–20. doi:10.1007/s10452-019-09723-2.

Vieira, C., D'hondt, S., De Clerck, O., and Payri, C. E. (2014). Toward an inordinate fondness for stars, beetles and *Lobophora*? Species diversity of the genus *Lobophora* (Dictyotales, Phaeophyceae) in New Caledonia. *J. Phycol.* 50, 1101–1119. doi:10.1111/jpy.12243.

Vieira, C., Engelen, A. H., Guentas, L., Aires, T., Houlbreque, F., Gaubert, J., et al. (2016). Species specificity of bacteria associated to the brown seaweeds *Lobophora* (Dictyotales, Phaeophyceae) and their potential for induction of rapid coral bleaching in *Acropora muricata*. *Front. Microbiol.* 7. doi:10.3389/fmicb.2016.00316.

Vila, M., Garcés, E., and Masó, M. (2001). Potentially toxic epiphytic dinoflagellate assemblages on macroalgae in the NW Mediterranean. *Aquat. Microb. Ecol.* 26, 51–60. doi:10.3354/ame026051.

Vos, M., Quince, C., Pijl, A. S., de Hollander, M., and Kowalchuk, G. A. (2012). A Comparison of rpoB and 16S rRNA as markers in pyrosequencing studies of bacterial diversity. *PLoS One* 7, e30600. doi:10.1371/journal.pone.0030600.

Wagner-Döbler, I., Ballhausen, B., Berger, M., Brinkhoff, T., Buchholz, I., Bunk, B., et al. (2010). The complete genome sequence of the algal symbiont *Dinoroseobacter shibae*: a hitchhiker's guide to life in the sea. *ISME J.* 4, 61–77. doi:10.1038/ismej.2009.94.

Wahl, M. (1989). Marine epibiosis. I. Fouling and antifouling: some basic aspects. *Mar. Ecol. Prog. Ser.* 58, 175–189. doi:10.3354/meps058175.

Wahl, M. (2008). Ecological lever and interface ecology: epibiosis modulates the interactions between host and environment. *Biofouling* 24, 427–438. doi:10.1080/08927010802339772.

Wahl, M. (2009). "Epibiosis," in *Biofouling*, eds. S. Dürr and J. C. Thomason (Wiley-Blackwell), 100–108. doi:10.1002/9781444315462.ch7.

Wahl, M., Goecke, F., Labes, A., Dobretsov, S., and Weinberger, F. (2012). The second skin: ecological role of epibiotic biofilms on marine organisms. *Front. Microbiol.* 3, 292. doi:10.3389/fmicb.2012.00292.

Wahl, M., Shahnaz, L., Dobretsov, S., Saha, M., Symanowski, F., David, K., et al. (2010). Ecology of antifouling resistance in the bladder wrack *Fucus vesiculosus*: patterns of microfouling and antimicrobial protection. *Mar. Ecol. Prog. Ser.* 411, 33–48. doi:10.3354/meps08644.

Walters, W., Hyde, E. R., Berg-Lyons, D., Ackermann, G., Humphrey, G., Parada, A., et al. (2016). Improved bacterial 16S rRNA gene (V4 and V4-5) and fungal internal transcribed spacer marker gene primers for microbial community surveys. *mSystems* 1, e00009-15. doi:10.1128/mSystems.00009-15.

Wang, L., Liu, X., Yu, S., Shi, X., Wang, X., and Zhang, X.-H. (2017). Bacterial community structure in intertidal sediments of Fildes Peninsula, maritime Antarctica. *Polar Biol.* 40, 339–349. doi:10.1007/s00300-016-1958-2.

Wang, M., Carver, J. J., Phelan, V. V., Sanchez, L. M., Garg, N., Peng, Y., et al. (2016). Sharing and community curation of mass spectrometry data with Global Natural Products Social Molecular Networking. *Nat. Biotechnol.* 34, 828–837. doi:10.1038/nbt.3597.

Wang, W., Wu, L., Xu, K., Xu, Y., Ji, D., Chen, C., et al. (2020). The cultivation of *Pyropia haitanensis* has important impacts on the seawater microbial community. *J. Appl. Phycol.*, 1–13. doi:10.1007/s10811-020-02068-6.

Ward, J. R., and Lafferty, K. D. (2004). The elusive baseline of marine disease: are diseases in ocean ecosystems increasing? *PLoS Biol.* 2, e120. doi:10.1371/journal.pbio.0020120.

Waters, C. M., and Bassler, B. L. (2005). Quorum sensing: cell-to-cell communication in bacteria. *Annu. Rev. Cell. Dev. Biol.* 21, 319–346. doi:10.1146/annurev.cellbio.21.012704.131001.

Weber, M. X., and Medina, M. (2012). "Chapter four - The role of microalgal symbionts (symbiodinium) in holobiont physiology," in *Advances in Botanical Research* Genomic Insights into the Biology of Algae., ed. G. Piganeau (Academic Press), 119–140. doi:10.1016/B978-0-12-391499-6.00004-9.

Webster, N. S., Soo, R., Cobb, R., and Negri, A. P. (2011). Elevated seawater temperature causes a microbial shift on crustose coralline algae with implications for the recruitment of coral larvae. *ISME J.* 5, 759–770. doi:10.1038/ismej.2010.152.

Weigel, B. L., and Pfister, C. A. (2019). Successional dynamics and seascape-level patterns of microbial communities on the canopy-forming kelps *Nereocystis luetkeana* and *Macrocystis pyrifera*. *Front. Microbiol.* 10, 346. doi:10.3389/fmicb.2019.00346.

Weinberger, F. (2007). Pathogen-induced defense and innate immunity in macroalgae. *Biol. Bull.* 213, 290–302. doi:10.2307/25066646.

Weinberger, F., and Friedlander, M. (2000). Response of *Gracilaria conferta* (Rhodophyta) to oligoagars results in defense against agar-degrading epiphytes. *J. Phycol.* 36, 1079–1086. doi:10.1046/j.1529-8817.2000.00003.x.

Weinberger, F., Friedlander, M., and Hoppe, H.-G. (1999). Oligoagars elicit a physiological response in *Gracilaria conferta* (Rhodophyta). *J. Phycol.* 35, 747–755. doi:10.1046/j.1529-8817.1999.3540747.x.

Weinberger, F., Rohde, S., Oschmann, Y., Shahnaz, L., Dobretsov, S., and Wahl, M. (2011). Effects of limitation stress and of disruptive stress on induced antigrazing defense in the bladder wrack *Fucus vesiculosus*. *Mar. Ecol. Prog. Ser.* 427, 83–94. doi:10.3354/meps09044.

Weiner, R. M., Melick, M., O'Neill, K., and Quintero, E. (2000). *Hyphomonas adhaerens* sp. nov., *Hyphomonas johnsonii* sp. nov. and *Hyphomonas rosenbergii* sp. nov., marine budding and prosthecate bacteria. *Int. J. Syst. Evol. Microbiol.* 50, 459–469. doi:10.1099/00207713-50-2-459.

Wernberg, T., Bennett, S., Babcock, R. C., Bettignies, T. de, Cure, K., Depczynski, M., et al. (2016). Climate-driven regime shift of a temperate marine ecosystem. *Science* 353, 169–172. doi:10.1126/science.aad8745.

Wessels, M., König, G. M., and Wright, A. D. (1999). A new tyrosine kinase inhibitor from the marine brown alga *Stypopodium zonale*. *J. Nat. Prod.* 62, 927–930. doi:10.1021/np990010h.

Wheeler, G. L., Tait, K., Taylor, A., Brownlee, C., and Joint, I. (2006). Acyl-homoserine lactones modulate the settlement rate of zoospores of the marine alga *Ulva intestinalis* via a novel chemokinetic mechanism. *Plant Cell Environ.* 29, 608–618.

Wichard, T., and Beemelmanns, C. (2018). Role of chemical mediators in aquatic interactions across the Prokaryote-Eukaryote boundary. *J. Chem. Ecol.* 44, 1008–1021. doi:10.1007/s10886-018-1004-7.

Wichard, T., Charrier, B., Mineur, F., Bothwell, J. H., Clerck, O. D., and Coates, J. C. (2015). The green seaweed *Ulva*: a model system to study morphogenesis. *Front. Plant Sci.* 6, 72. doi:10.3389/fpls.2015.00072.

Williams, G. A., and Seed, R. (1992). "Interactions between macrofaunal epiphytes and their host algae," in *Plant-animal interactions in the marine benthos*.

Wilson, K., Able, K., and Heck, K., Jr. (1989). Predation rates on juvenile blue crabs in estuarine nursery habitats: evidence for the importance of macroalgae (*Ulva lactuca*). *Mar. Ecol. Prog. Ser.* 58, 243–251. doi:10.3354/meps058243.

Wilson, S. K., Depczynski, M., Fisher, R., Holmes, T. H., O'Leary, R. A., and Tinkler, P. (2010). Habitat associations of juvenile fish at ningaloo reef, Western Australia: The importance of coral and algae. *PLoS One* 5, e15185. doi:10.1371/journal.pone.0015185.

Womersley, H. B. S., Study, A. B. R., Adelaide, B. G. of, Herbarium, S., Study, A. B. R., and Womersley, H. (1996). The marine benthic flora of Southern Australia. Rhodophyta. Part IIIB, Gracilariales, Rhodymeniales, Corallinales and Bonnemaisoniales. Available at: https://trove.nla.gov.au/version/45813849 [Accessed June 21, 2020].

Wright, J. T., Nys, R. de, and Steinberg, P. D. (2000). Geographic variation in halogenated furanones from the red alga *Delisea pulchra* and associated herbivores and epiphytes. *Mar. Ecol. Prog. Ser.* 207, 227–241. doi:10.3354/meps207227.

Yan, Y.-W., Yang, H.-C., Tang, L., Li, J., Mao, Y.-X., and Mo, Z.-L. (2019). Compositional shifts of bacterial communities associated with *Pyropia yezoensis* and surrounding seawater co-occurring with red rot disease. *Front. Microbiol.* 10, 1666. doi:10.3389/fmicb.2019.01666.

Yang, C.-Y., Yang, C.-Y., and Sung, C.-K. (2013a). Enhancing air retention by biomimicking *Salvinia molesta* structures. *Jpn. J. Appl. Phys.* 52, 06GF08. doi:10.7567/JJAP.52.06GF08.

Yang, J. Y., Sanchez, L. M., Rath, C. M., Liu, X., Boudreau, P. D., Bruns, N., et al. (2013b). Molecular networking as a dereplication strategy. *J. Nat. Prod.* 76, 1686–1699. doi:10.1021/np400413s.

Yeger-Lotem, E., Sattath, S., Kashtan, N., Itzkovitz, S., Milo, R., Pinter, R. Y., et al. (2004). Network motifs in integrated cellular networks of transcription–regulation and protein–protein interaction. *Proc. Natl. Acad. Sci. U.S.A.* 101, 5934–5939. doi:10.1073/pnas.0306752101.

Yoch, D. C. (2002). Dimethylsulfoniopropionate: its sources, role in the marine food web, and biological degradation to dimethylsulfide. *Appl. Environ. Microbiol.* 68, 5804–5815. doi:10.1128/AEM.68.12.5804-5815.2002.

Yoon, J., Adachi, K., and Kasai, H. (2015). Isolation and characterization of a novel marine Bacteroidetes as *Algitalea ulvae* gen. nov., sp. nov., isolated from the green alga *Ulva pertusa*. *Antonie Van Leeuwenhoek* 108, 505–513. doi:10.1007/s10482-015-0504-5.

Yoon, J.-H., Kang, S.-J., Park, S., Oh, K.-H., and Oh, T.-K. (2010). *Jannaschia seohaensis* sp. nov., isolated from a tidal flat sediment. *Int. J. Syst. Evol. Microbiol.* 60, 191–195. doi:10.1099/ijs.0.011270-0.

Youssef, N., Sheik, C. S., Krumholz, L. R., Najar, F. Z., Roe, B. A., and Elshahed, M. S. (2009). Comparison of species richness estimates obtained using nearly complete fragments and simulated pyrosequencing-generated fragments in 16S rRNA gene-based environmental surveys. *Appl. Environ. Microbiol.* 75, 5227–5236. doi:10.1128/AEM.00592-09.

Zahid, N., Schweiger, P., Galinski, E., and Deppenmeier, U. (2015). Identification of mannitol as compatible solute in *Gluconobacter oxydans*. *Appl. Microbiol. Biotechnol.* 99, 5511–5521. doi:10.1007/s00253-015-6626-x.

Zallen, D. T. (1993). The “light” organism for the job: green algae and photosynthesis research. *J. Hist. Biol.* 26, 269–279. doi:10.1007/BF01061970.

Zemb, O., West, N., Bourrain, M., Godon, J. J., and Lebaron, P. (2010). Effect of a transient perturbation on marine bacterial communities with contrasting history. *J. Appl. Microbiol.* 109, 751–762. doi:10.1111/j.1365-2672.2010.04706.x.

Zhang, P., Wang, X., Wang, T., Zhu, P., and Yang, L. (2018). The major changes in lipid composition of *Sargassum horneri* during different growth phases. *J. Appl. Phycol.* 30, 517–523. doi:10.1007/s10811-017-1219-y.

Zilber-Rosenberg, I., and Rosenberg, E. (2008). Role of microorganisms in the evolution of animals and plants: the hologenome theory of evolution. *FEMS Microbiol. Rev.* 32, 723–735. doi:10.1111/j.1574-6976.2008.00123.x.

Zozaya-Valdés, E., Egan, S., and Thomas, T. (2015). A comprehensive analysis of the microbial communities of healthy and diseased marine macroalgae and the detection of known and potential bacterial pathogens. *Front. Microbiol.* 6, 146. doi:10.3389/fmicb.2015.00146.

Zozaya-Valdés, E., Roth-Schulze, A. J., Egan, S., and Thomas, T. (2017). Microbial community function in the bleaching disease of the marine macroalgae *Delisea pulchra*. *Environ. Microbiol.* 19, 3012–3024. doi:10.1111/1462-2920.13758.

Zozaya-Valdés, E., Roth-Schulze, A. J., and Thomas, T. (2016). Effects of temperature stress and aquarium conditions on the red macroalga *Delisea pulchra* and its associated microbial community. *Front. Microbiol.* 7, 161. doi:10.3389/fmicb.2016.00161.

Zulkifly, S., Hanshew, A., Young, E. B., Lee, P., Graham, M. E., Graham, M. E., et al. (2012). The epiphytic microbiota of the globally widespread macroalga *Cladophora glomerata* (Chlorophyta, Cladophorales). *Am. J. Bot.* 99, 1541–1552. doi:10.3732/ajb.1200161.

Etude des dynamiques spatio-temporelles des interactions entre le microbiote et le métabolome de surface de la macroalgue *Taonia atomaria* par une approche multi-omiques

En tant qu'espèces ingénieures de leurs écosystèmes et que producteurs primaires, les macroalgues marines jouent un rôle crucial au sein de leur écosystème. Les interactions chimiques avec leurs microorganismes épiphytes semblent particulièrement essentielles pour leur physiologie. Cependant les relations macroalgues-microbiote et le rôle des paramètres environnementaux dans ces interactions restent encore peu explorées. L'objectif général de la thèse est de comprendre comment varie la structure de la communauté procaryotique épiphyte de l'algue brune *Taonia atomaria* en lien avec les variations de la production métabolique de surface de l'hôte et quelle est l'influence de l'environnement sur ces variations qui affectent et façonnent ce modèle d'holobionte. Une approche multi-omiques, couplant l'étude des communautés procaryotes épiphytes par metabarcoding et l'étude des métabolites de surface par des analyses optimisées en métabolomique, a ainsi été employée conjointement avec d'autres analyses telle que la cytométrie en flux. Les résultats obtenus ont révélé que la communauté microbienne épiphyte de *T. atomaria*, lui était spécifique en comparaison avec les communautés de biofilms de substrats rocheux et celles planctoniques, suggérant un rôle possible du métabolome de surface. Entre outre, d'importantes co-variations entre le métabolome et le microbiote à la surface de l'algue ont été observées à différents niveaux, que ce soit à l'échelle du thalle, de la dynamique temporelle ou encore d'un point de vue biogéographique. Certains paramètres environnementaux semblent être particulièrement impliqués dans les interactions au sein de l'holobionte, tels que la température, la contamination en cuivre, mais aussi l'intensité lumineuse. Dans un contexte de Changement Global, ces travaux apportent de nouvelles perspectives permettant de mieux appréhender la dynamique des macroalgues-holobiontes.

Mots clés : Macroalgues, Holobionte, Microbiote, Métabolome

Study of the spatio-temporal dynamics of interactions between the surface microbiota and metabolome of the macroalga *Taonia atomaria* through a multi-omics approach

As ecosystems engineers and primary producers, marine seaweeds play important roles for other organisms. Chemical interactions with epiphytic microorganisms seem particularly important for their physiology. However, macroalgae-microbiota relationships and the role of environmental parameters remains poorly investigated. The main objective of this PhD thesis was to understand how vary the epiphytic prokaryotic community of the brown alga *Taonia atomaria*, in relationship with variations of the surface metabolome of the host and what is the influence of the environment on these variations which shape this holobiont model. A multi-omics approach coupling prokaryotic communities studies by metabarcoding and surface metabolites studies by an optimized metabolomics analysis, has been jointly conducted, together with further analyses such as flow cytometry. Studies have thus revealed that the epiphytic microbial community of *T. atomaria* was specific in comparison with the biofilm communities of rocky substrates, and planktonic ones, suggesting a possible role of the surface metabolome in the structuring of the microbiota. Otherwise, important co-variations between the metabolome and the microbiota at the algal surface were observed at different levels, whether at the thallus or biogeographical scale, or during temporal dynamics. Some environmental parameters seem to be particularly involved in these interactions, such as temperature, copper contamination, but also irradiance. In a context of Global Change, this work provides new perspectives allowing to better understand dynamics of macroalgal-holobionts.

Keywords: Seaweeds, Holobiont, Microbiota, Metabolome

ÉCOLE DOCTORALE 548 – MER & SCIENCES

LABORATOIRE MATERIAUX POLYMERES INTERFACES ENVIRONNEMENT MARIN (MAPIEM)

THÈSE présentée par :

Benoît PAIX

Soutenue le 17 Septembre 2020

Pour obtenir le grade de Docteur en Sciences de la Vie et de la Santé

Spécialité : Ecologie microbienne

ANNEXES ELECTRONIQUES

Etude des dynamiques spatio-temporelles des interactions entre le microbiote et le métabolome de surface de la macroalgue *Taonia atomaria* par une approche multi-omiques

Thèse dirigée par Gérald Culioli et Jean-François Briand

JURY :

M^{me} Soizic Prado	Professeure des universités, Muséum national d'histoire naturelle	**Rapporteure**
M. Jean-François Ghiglione	Directeur de recherche CNRS, Sorbonne Université	**Rapporteur**
M^{me} Catherine Leblanc	Directrice de recherche CNRS, Sorbonne Université	**Examinatrice**
M^{me} Christine Ferrier-Pagès	Directrice de recherche, Centre Scientifique de Monaco	**Examinatrice**
M^{me} Marion Peirache	Référente Milieu Marin, Parc National de Port-Cros	**Invitée**
M. Gérald Culioli	Maître de conférences, HDR Université de Toulon	**Directeur de thèse**
M. Jean-François Briand	Maître de conférences, Université de Toulon	**Co-encadrant de thèse**

Table des matières

Annexe II ____ **8**

Temporal covariation of epibacterial community and surface metabolome in the Mediterranean seaweed holobiont Taonia atomaria ____ *9*

Detailed experimental procedures for metabolomics ____ 10

Figure SII.1. Chemical structures of some surface metabolites isolated from *Taonia atomaria** ____ 13

Figure SII.2. (+)-ESI-LC-MS profiles of surface extracts of *T. atomaria* (collected monthly from February to July) ____ 14

Figure SII.3. PCA score plot obtained from (+)-ESI-LC−MS profiles of surface extracts of *T. atomaria* collected monthly from February to July (*n* = 18), QCs sample (*n* = 8) and blanks (solvent blanks, *n* = 2; analytical blanks, *n* = 4) ____ 15

Figure SII.4. PLS-DA analysis from (+)-ESI-LC−MS profiles of surface extracts of *T. atomaria* collected monthly from February to July (one class per month; ____ 16

Figure SII.5. HRMS/MS data and hypothetical MS fragmentation* of VIP n°1 putatively identified as Proline betaine ** ____ 17

Figure SII.6. HRMS/MS data and hypothetical MS fragmentation of VIP n°2 identified as DMSP* ____ 18

Figure SII.7. HRMS/MS data and hypothetical MS fragmentation of VIP n°3 putatively identified as Ceramide (dC18:1/C16:0) ____ 19

Figure S8. HRMS/MS data and hypothetical MS fragmentation of VIP n°4 putatively identified as DGTA C44:10 ____ 20

Figure SII.9. HRMS/MS data and MS fragmentation of VIP n°5 identified as Proline* ____ 22

Figure SII/10. HRMS/MS data and hypothetical MS fragmentation of VIP n°6 putatively identified as DGTA C44:12 (DGTA C22:6/C22:6) ____ 23

Figure SII.11. HRMS/MS data of VIP n°7 identified as Sesquiterpene IV [(-)-*Trans*-Calamenene] ____ 24

Figure SII.12. HRMS/MS data of VIP n°8 ____ 24

Figure SII.13. HRMS/MS data and hypothetical MS fragmentation of VIP n°9 putatively identified as *Lyso*-DGTA (C20:5) ____ 25

Figure SII.14. HRMS/MS data and hypothetical MS fragmentation of VIP n°10 putatively identified as Glutaminevaline (Gln-Val)* ____ 26

Figure SII.15. HRMS/MS data of VIP n°11 ____ 27

Figure SII.16. HRMS/MS data and hypothetical MS fragmentation of VIP n°12 putatively identified as Ceramide (dC18:1/C14:0) ____ 28

Figure SII.17. HRMS/MS data and hypothetical MS fragmentation of VIP n°13 putatively identified as Glutamineleucine (Gln-Leu)* ____ 29

Figure SII.18. HRMS/MS data and hypothetical MS fragmentation of VIP n°14 putatively identified as DGTA C32:2 ____ 30

Figure SII.19. HRMS/MS data and hypothetical MS fragmentation of VIP n°15 ____ 32

Figure SII.20. HRMS/MS data and hypothetical MS fragmentation of VIP n°16 identified as Glutaminephenylalanine (Gln-Phe)* ____ 33

Figure SII.21. HRMS/MS data of VIP n°17 ____ 34

Figure SII.22. HRMS/MS data and hypothetical MS fragmentation of VIP n°18 identified as difucol-2-*O*-sulfate ____ 35

Figure SII.23. Seasonal variations (from February to July) of the epibacterial communities on *T. atomaria* at the class level ____ 36

Figure SII.24. Seasonal variations of the relative abundance of the core microbiome of *T. atomaria* ____ 37

Figure SII.25. Heatmap representation of the seasonal correlation (multi-block PLS-DA) between significant OTUs and metabolites found at the surface of *T. atomaria* ____ 38

Annexe III ____ **39**

Host phylogeny and biogeography shape the microbiota and metabolome of the surface of the brown alga Taonia (Dictyotales) ____ *40*

Table SIII.1. Environmental parameters, sampling dates, and GPS coordinates of the collection sites of *Taonia* ____ 41

Table SIII.2. SIMPER results of the most contributing genera to the dissimilarities of the epibacterial community between Mediterranean and Brittany samples of *Taonia*. 42
Figure SIII.1. Photographs of the herbarium of *Taonia* specimens (part1). 43
Figure SIII.1. Photographs of the herbarium of *Taonia* specimens (part2). 44
Figure SIII.2. Variations of cell densities and *α*-diversity indexes (Chao1 and Shannon) of the epiphytic community of samples of *Taonia* according to each sampling site. 45
Figure SIII.3. Normalized concentration of the two most discriminant metabolites (*δ*-cadinene and fucoxanthin) involved in the discrimination between surface metabolomes of Mediterranean and Brittany samples of *Taonia* 46

Annexe IV 47

Integration of LC/MS-based molecular networking and classical phytochemical approach allows in-depth annotation of the metabolome of non-model organisms - The case study of the brown seaweed Taonia atomaria *48*

Supplementary tables *49*
Table SIV.1. Summary of the 39 fractions obtained after Flash-chromatography 49
Table SIV.2. Summary of tested parameters for the MN-1, 2 and 3 50

Supplementary figures *51*
Figure SIV.1. Annotation of cluster 1A and proposed MS/MS fragmentation pattern for the compounds MGDG (18:4/18:1), SQDG(16:0/18:3) and TG (14:0/16:0/16:1) 51
Figure SIV.2. MN1 representing nodes with a color gradient according to the retention time 52
Figure SIV.3. Annotation of cluster 1B and proposed MS/MS fragmentation pattern for the compound DGDG (18:4/20:5) 53
Figure SIV.4. Annotation of the cluster 1C and proposed MS/MS fragmentation pattern for the compound MGTA (14:0) 54
Figure SIV.5. Annotation of cluster 1D and proposed MS/MS fragmentation pattern for the compound SQMG (18:1) 55
Figure SIV.6. Annotation of cluster 1E and proposed MS/MS fragmentation pattern for the compound *lyso*-PC (20:5) 56
Figure SIV.7. Annotation of cluster 1H and proposed MS/MS fragmentation pattern for the compound MFG (18:1) 57
Figure SIV.8. Annotation of cluster 1I and proposed MS/MS fragmentation pattern for the compound MFuA (20:4) 58
Figure SIV.9. Less restrained MN (MN-2) built with MS/MS data of fractions obtained from the crude extract of the brown alga *Taonia atomaria.* 59

Annexe V 60

A multi-omics analysis suggests links between the differentiated surface metabolome and epiphytic microbiota along the thallus of a Mediterranean seaweed holobiont *61*

Supplementary Materials & Methods *62*
Supplementary information for LC-ESI-MS analyses 62
Supplementary information for GC-MS analyses 63
Supplementary information for annotation procedure 63

Supplementary Tables *65*
Table SV.1. Parameters used for metabolomics data processing (part 1) 65
Table SV.1. Parameters used for metabolomics data processing (part 2) 66
Table SV.2. Surfaces of the thallus parts used for metabolomics and sum of the chromatographic peak areas (surface extracts, LC-(+)-ESI-MS) 67
Table SV.3. Summary of PERMANOVA results examining the effect of “site” and “sample types” factors for of the 16S rRNA gene dataset. 68
Table SV.4. Multivariate pairwise results (p values) examining differences between both sites and between each sample types, for of the 16S rRNA gene dataset. 68
Table SV.5. SIMPER results of the most contributing genera to the dissimilarities between water samples and algal samples collected at Carqueiranne. 69

Table SV.6. SIMPER results of the most contributing genera to the dissimilarities between water samples and algal samples collected at Tamaris. 70
Table SV.7. SIMPER results of the most contributing genera to the dissimilarities between rocky biofilms and algal samples collected at Carqueiranne. 71
Table SV.8. SIMPER results of the most contributing genera to the dissimilarities between rocky biofilms and algal samples collected at Tamaris. 71
Table SV.9. SIMPER results of the most contributing genera to the dissimilarities between basal and apical parts of algal samples collected at Carqueiranne. 73
Table SV.10. SIMPER results of the most contributing genera to the dissimilarities between basal and apical parts of algal samples collected at Tamaris. 74
Table SV.11. Summary of PERMANOVA results examining the effect of "site" and "thallus parts" factors for each normalized metabolomics dataset. 75
Table SV.12. Multivariate pairwise results (*p* values) examining differences between both sites and between each thallus parts for each metabolomics dataset. 76
Table SV.13. Summary of R^2 values obtained for the two first components after cross validation test for PLS-DA obtained with each metabolomics dataset. 76
Table SV.14. List of compounds identified through GC-MS analyses 77
Table SV.15. Putative annotation of VIPs from the LC-(+)-ESI-MS dataset of samples of *T. atomaria* collected at Tamaris 78
Table SV.16. Putative annotation of VIPs from the LC-(+)-ESI-MS dataset of samples of *T. atomaria* collected at Carqueiranne 79

Supplementary Figures *80*
Figure SV.1. Global workflow 80
Figure SV.2A. Methodologies used for the preparation of fronds and for extraction for metabolomics analysis 81
Figure SV.2B. Description of the separation in three parts (basal, median and apical) of the thalli of *T. atomaria*. 82
Figure SV.3. Discrimination of heterotrophic prokaryotes by flow cytometry. 83
Figure SV.4. Confocal microscopy images of basal and apical parts of *T. atomaria* collected at Tamaris. 84
Figure SV.5. Rarefaction curves obtained after data processing of 16S rRNA gene sequences. 85
Figure SV.6. Unifrac distances between rocky biofilms (R) and the three thallus parts [basal (B), median (M) and apical parts (A)], or between seawater samples (W) and the three thallus parts. 86
Figure SV.7. Cladogram obtained from the LEfSe analysis built with the 16S rRNA gene dataset of bacterial communities at the surface of *T. atomaria*, in rocky biofilms and in seawater at Tamaris. 87
Figure SV.8. Cladogram obtained from the LEfSe analysis built with the 16S rRNA gene dataset of bacterial communities at the surface of *T. atomaria*, in rocky biofilms and in seawater at Carqueiranne. 88
Figure SV.9. Co-occurrence network of OTUs from the 16S rRNA gene dataset of bacterial communities at the surface of *T. atomaria*, in rocky biofilms and in seawater at Tamaris 89
Figure SV.10. Venn diagrams showing shared percentages of sequences between: (i) the different thallus parts and rocky biofilms and (ii) the different thallus parts and sea water. 90
Figure SV.11. Chemodiversity indexes (Shannon) of surface extracts of *T. atomaria* (two sites: Carqueiranne and Tamaris; three algal parts: basal, median and apical) analyzed by LC-(+)-ESI-MS, LC-(-)-ESI-MS and GC-MS 91
Figure SV.12. PLS-DA plots of GC-MS, LC-(-)-ESI-MS and LC-(+)-ESI-MS metabolomics analyses of surface and total extracts of *T. atomaria* (two sites: Carqueiranne and Tamaris; three algal parts: basal, median and apical). 92
Figure SV.13. Molecular network for LC-(+)-ESI-MS dataset annotation. 93
Figure SV.14. Molecular network for LC-(-)-ESI-MS dataset annotation. 94
Figure SV.15. Heatmap of sesquiterpenes variations across samples identified in the GC-MS dataset. 95
Figure SV.16. Heatmap of annotated compounds variations identified in the LC-(+)-ESI-MS dataset (1/2). 96
Figure SV.16. Heatmap of annotated compounds variations identified in the LC-(+)-ESI-MS dataset (2/2). 97
Figure SV.17. Heatmap of annotated compounds variations identified in the LC-(-)-ESI-MS dataset. 98

Annexe VI **99**

A multi-omics approach deciphers how temperature and copper stress shape seaweed-microbiota interactions at the surface of Taonia atomaria on the NW Mediterranean coast ____ *100*

Supplementary information for Material and Methods ____ *101*
Supplementary information for sampling ____ 101
Supplementary information for dissolved organic carbon and total nitrogen analyses ____ 101
Supplementary information for dissolved and total concentrations trace metals analyses ____ 101
Supplementary information for flow cytometry analysis ____ 101
Supplementary information for 16S rRNA gene metabarcoding analyses (FROGSS pipeline) ____ 101
Supplementary information for Tax4Fun analysis ____ 102
Supplementary information for metabolomics analyses ____ 102
Supplementary information for the annotation procedure ____ 103
Supplementary information for multi-omics analysis ____ 104

Supplementary Tables ____ *106*
Table SVI.1. Environmental parameters and sampling dates (Part 1: from February to April 2017). ____ 106
Table SVI.1. Environmental parameters and sampling dates (Part 2 from May to July 2017). ____ 107
Table SVI.2. Multivariate pairwise results (*p* values) examining differences between "sample types" for the 16S rRNA gene dataset with all samples (999 permutations). ____ 108
Table SVI.3. Multivariate pairwise results (*p* values) examining differences between "months" and between "sites" for the 16S rRNA gene dataset with *Taonia atomaria* samples (999 permutations). ____ 108
Table SVI.4. Multivariate pairwise results (*p* values) examining differences between "months" and between "sites" for the 16S rRNA gene dataset with rocky biofilm samples (999 permutations). ____ 109
Table SVI.5. Multivariate pairwise results (*p* values) examining differences between "months" and between "sites" for the 16S rRNA gene dataset with seawater samples (999 permutations). ____ 109
Table SVI.6. SIMPER results of the most contributing genera to the dissimilarities between seawater and algal samples. ____ 110
Table SVI.7. SIMPER results of the most contributing genera to the dissimilarities between rocky biofilm samples and algal samples. ____ 111
Table SVI.8. Multivariate pairwise results (*p* values) examining differences between "sample types" for the dataset of KO predicted by Tax4Fun analysis (999 permutations). ____ 112
Table SVI.9. Multivariate pairwise results (*p* values) examining differences between "months" and between "sites" for the dataset of KO predicted by Tax4Fun analysis (999 permutations). ____ 112
Table SVI.10. Multivariate pairwise results (*p* values) examining differences between "months" and between "sites" for the LC-(+)-ESI-MS metabolomics dataset (999 permutations). ____ 113
Table SVI.11. List of biomarkers (VIP score > 2) identified by LC-HRMS and involved in the discrimination between months within surface extracts of *T. atomaria* (Part 1). ____ 114
Table SVI.11. List of biomarkers (VIP score > 2) identified by LC-HRMS and involved in the discrimination between months within surface extracts of *T. atomaria* (Part 2). ____ 115
Table SVI.12. List of biomarkers (VIP score > 2) identified by LC-HRMS and involved in the discrimination between sites within surface extracts of *T. atomaria*. ____ 116

Supplementary Figures ____ *117*
Figure SVI.1. Map with the location of the sampling sites. ____ 117
Figure SVI.2. Discrimination of heterotrophic prokaryotes by flow cytometry. ____ 118
Figure SVI.3. Variations of thalli length (cm) conducted with all algal samples collected during the study and pictures of thalli collected at S1 (one replicate per month). ____ 119
Figure SVI.4. Variations of cells densities at the surface of *T. atomaria* for each site (A) and heteroprokaryotic cell abundances in seawater samples (B). ____ 120
Figure SVI.5. Spatiotemporal dynamics of prokaryotic cell density (A), α-diversity (B), percentage of algal-core (C) and algal-enriched (D) taxa at the surface of *T. atomaria*. ____ 121
Figure SVI.6. NMDS (Bray-Curtis index) showing prokaryotic β-diversity of algal samples. ____ 122
Figure SVI.7. NMDS (Bray-Curtis index) showing prokaryotic β-diversity of rocky biofilm (A) and seawater (B) samples. ____ 123
Figure SVI.8. Cladogram obtained from the LEfSe analysis built with the 16S rRNA gene dataset of all samples and revealing discriminant prokaryotic taxa specific to *T. atomaria*, to rocky biofilms and to seawater samples (LDA threshold set to 4). ____ 124

Figure SVI.9. Cladogram obtained from the LEfSe analysis built with the 16S rRNA gene dataset of *T. atomaria* samples and revealing discriminant epibacterial taxa specific to each sampling month (LDA threshold set to 4.5). 125
Figure SVI.10. Cladogram obtained from the LEfSe analysis built with the 16S rRNA gene dataset of *T. atomaria* samples and revealing discriminant epibacterial taxa specific to each sampling site (LDA threshold set to 3.5). 126
Figure SVI.11. Percentage of core community sequences (A) and algal-enriched community sequences (B). 127
Figure SVI.12. PCA constructed with KEGG KO from Tax4Fun analysis with algal, rocky biofilm and seawater samples. *p* value corresponded to the results of the one-way PERMANOVA using "sample type" as the factor. 128
Figure SVI.13. PCA constructed with KEGG KO from Tax4Fun analysis with algal samples. *p* values corresponded to the results of the two-way PERMANOVA using "Month" and "Site" as factors. 129
Figure SVI.14. Complementary KEGG pathways predicted by Tax4Fun analysis. 130
Figure SVI.15. GNPS molecular network built with LC-ESI-(+)-MS/MS data. Levels of annotations were attributed according to Schymanski et al., 2014. 131

Annexe VII 132

Synergistic effects of temperature and light affect the relationship between Taonia atomaria and its epibacterial community: a mesocosm study 133

Supplementary materials 134
Supplementary information concerning the pre-treatment of running seawater 134
Supplementary information concerning the determination of the physico-chemical parameters of seawater 134
Supplementary information concerning the metabolomics analyses 134

Supplementary tables 137
Table SVII.1. Physico-chemical parameters (mean ± SD) measured *in situ* or in the aquaria. 137
Table SVII.2. Summary of three-way ANOVA tests examining the effect of sampling time, temperature and irradiance conditions for the cell densities at the algal surface, and the *α*-diversity indexes (Shannon and Chao1) of the epibacterial communities of *T. atomaria*. 138
Table SVII.3. Summary of three-way and two-way PERMANOVA results examining the effect of sampling time, temperature and irradiance conditions (for all samples, and for t_1, t_2, and t_3 samples, independently) for the 16S rRNA gene dataset obtained with the epibacterial communities of *T. atomaria*. 139
Table SVII.4. Multivariate pairwise results (*p*-values) examining differences between sampling times, temperature and irradiance conditions (for all samples, or for t_1, t_2, and t_3 samples, independently) for the 16S rRNA gene dataset (999 permutations) obtained with the epibacterial communities of *T. atomaria*. 140
Table SVII.5. Summary of taxa determined with LEfSe analysis (LDA > 4) corresponding to discriminating biomarkers of the epibacterial communities of *T. atomaria* for a specific sampling time (Part 1) 141
Table SVII.5. Summary of taxa determined with LEfSe analysis (LDA > 4) corresponding to discriminating biomarkers of the epibacterial communities of *T. atomaria* for a specific sampling time (Part 2) 142
Table SVII.6. SIMPER results of the most contributing genera to the dissimilarities between field and t_0 samples of the epibacterial communities of *T. atomaria*. 143
Table SVII.7. Summary of affiliated genera determined through LEfSe analysis corresponding to discriminating biomarker taxa of the epibacterial communities of *T. atomaria* for a specific condition of temperature and irradiance at t_3 (LDA > 3.4). 144
Table SVII.8. Summary of three-way and two-way PERMANOVA results examining the effect of sampling time, temperature and irradiance conditions (for all samples and for t_1, t_2, and t_3 samples, independently) for the LC-(+)-ESI-HRMS metabolomics dataset obtained with the surface extracts of *T. atomaria*. 145
Table SVII.9. Multivariate pairwise results (*p*-values) examining differences between sampling times, temperature and irradiance conditions (for all samples and for t_1, t_2, and t_3 samples, independently) for the LC-(+)-ESI-HRMS metabolomics dataset (999 permutations) obtained with the surface extracts of *T. atomaria.* 146

Table SVII.10. List of metabolites (VIP score > 0.6) identified by LC-(+)-ESI-HRMS and involved in the discrimination between each irradiance/temperature condition at t_3 within surface extracts of *T. atomaria* (Part 1). 147
Table SVII.10. List of metabolites (VIP score > 0.6) identified by LC-(+)-ESI-HRMS and involved in the discrimination between each irradiance/temperature condition at t_3 within surface extracts of *T. atomaria* (Part 2). 148
Table SVII.10. List of metabolites (VIP score > 0.6) identified by LC-(+)-ESI-HRMS and involved in the discrimination between each irradiance/temperature condition at t_3 within surface extracts of *T. atomaria* (Part 3). 149

Supplementary figures 150
Figure SVII.1. Representation of the experimental mesocosm systems used for the study. 150
Figure SVII.2. Photographs of the experimental setup used to cultivate samples of *T. atomaria*. 151
Figure SVII.3. Mean values (± SD) of maximum photosynthetic yield (F_v/F_m measures) of thalli of *T. atomaria* before extraction procedures. 152
Figure SVII.4. Variations of cells densities at the surface of *T. atomaria*. 152
Figure SVII.5. Comparison of the epibacterial community structure of *T. atomaria* at the order level analyzed with 515F-Y / 926R and NOCHL primers for triplicates samples collected at t_0 and t_1 sampling times with ambient temperature (AT) and irradiance (AI) conditions. 153
Figure SVII.6. Variations of *α*-diversity metrics (Shannon and Chao1 indexes) of the epibacterial communities of *T. atomaria*. 154
Figure SVII.7. Venn diagrams showing shared percentages of OTUs (A) and sequences (B) between samples of *T. atomaria* obtained at each sampling time. 154
Figure SVII.8. Structure of epibacterial communities of *T. atomaria* at the family level. 155
Figure SVII.9. Variation of biomarker genera identified through the LEfSe analysis conducted on t_3 samples (see Table SVII.7) (Part 1). 156
Figure SVII.9. Variation of biomarker genera identified through the LEfSe analysis conducted on t_3 samples (see Table SVII.7) (Part 2). 157
Figure SVII.9. Variation of biomarker genera identified through the LEfSe analysis conducted on t_3 samples (see Table SVII.7) (Part 3). 158
Figure SVII.10. Variation of annotated biomarker metabolites (VIPs, see Table SVII.10) involved in the discrimination between each condition at t_3 (Part 1) 159
Figure SVII.10. Variation of annotated biomarker metabolites (VIPs, see Table SVII.10) involved in the discrimination between each condition at t_3 (Part 2) 160
Figure SVII.10. Variation of annotated biomarker metabolites (VIPs, see Table SVII.10) involved in the discrimination between each condition at t_3 (Part 3) 161

Annexe VIII 162

Exploring the role of macroalgal surface metabolites on the settlement of the benthic dinoflagellate Ostreopsis cf. ovata. 163
Figure SVIII.1. Eukaryotic communities' alpha-diversity obtained by 18S rRNA gene metabarcoding for the four macroalgae species and the surrounding seawater. 164
Figure SVIII.2. Eukaryotic communities' beta-diversity obtained by 18S rRNA gene metabarcoding for the four macroalgae species and the surrounding seawater: NMDS plot determined using the Jaccard index. 164
Figure SVIII.3. Relative abundance in the surface extracts (SE) of the four macroalgal species of (A) geranylgeranylglycerol, (B) DMSP, and the two unidentified biomarkers of *D. dichotoma*, (C) unknown compound and (D) carotenoid-like compound, based on their ion intensity in LC-MS analysis. 165
Table SVIII.1. Putative annotation of the first few biomarkers (VIP > 1.42) driving the distribution of the surface extracts (SEs) and the total extracts (TEs) obtained by PLS-DA analyses performed for each macroalgal species. 166

Annexe II

Supporting information
for

Temporal covariation of epibacterial community and surface metabolome in the Mediterranean seaweed holobiont *Taonia atomaria*

Benoit Paix[1#], Ahlem Othmani[1#], Didier Debroas[2], Gérald Culioli[1*] and Jean-François Briand[1*]

[1]Université de Toulon, MAPIEM, EA 4323, Toulon, France.

[2]Université Clermont Auvergne, CNRS, Laboratoire Microorganismes: Génome et Environnement, UMR 6023, Clermont–Ferrand, France

#These authors contributed equally to this work

[*]Corresponding authors: J.-F. Briand (briand@univ-tln.fr) and G. Culioli (culioli@univ-tln.fr)

Detailed experimental procedures for metabolomics

Surface metabolome extraction

Prior to extraction, algal samples were gently spin-dried in a salad spinner for 30s at approximately 500 rpm. Algal pieces of 10–12 cm^2 were then selected and each sample was immersed 5s in 2 mL of methanol (Analytical grade, VWR, Fontenay-sous-Bois, France) in an 8-mL glass vial. This experimental protocol was previously defined to preserve the perfect integrity of the outer cell membrane (Othmani et al., 2016a). Particular care was taken to prevent contact between the cut portions of fronds and methanol to avoid the extraction of intracellular compounds. This experiment was performed in triplicate with algal pieces coming from three different individuals (n = 3).

Sample preparation for metabolomics

The resulting surface extracts were concentrated to dryness under reduced pressure at a temperature lower than 35°C. Dried surface extracts were then transferred in 2-mL HPLC vials and stored under inert atmosphere (N_2), in the dark at -20°C until analysis. Before injection, samples were solubilized in LC-MS grade methanol (Chromasolv, Sigma-Aldrich, St Louis, MO, USA) at a concentration of 10 $mg.mL^{-1}$. For all experiments, extraction and sample preparation were carried out by the same operator.

Quality control & Injection sequence

Analytical blanks were prepared with exactly the same protocol as those used for surface extracts but without algal pieces. These blanks allowed the subsequent subtraction of contaminants or components coming from solvents and vials. In order to ensure quality control, a pool sample was prepared by combining 100 μL of each surface extract. The pool sample was divided into seven 2-ml HPLC vials (around 250 μL of solution in each vial) that were used as quality-control samples (QCs). To ensure analytical repeatability, a first QC was injected ten times at the beginning of the sequence in order to stabilize the chromatographic system. Then, the injection sequence consisted of the iterative injection of one QC and five samples (surface extracts and analytical blanks) randomly selected to avoid any possible time-dependent changes in LC–MS chromatographic fingerprints. Moreover, to assess sample carry-over of the analytical process, two solvent blanks (LC-MS grade methanol) were injected before the first QC and at the end of the injection sequence.

UPLC-HRMS analysis

The UPLC-HRMS instrumentation consisted of a Dionex Ultimate 3000 Rapid Separation (Thermo Fisher Scientific, Waltham, MA, USA) chromatographic system equipped with a RS pump, a temperature-controlled autosampler, a thermostated column compartment and UV diode array detector. This system was coupled to a QToF Impact II mass spectrometer (Bruker Daltonics, Bremen, Germany). The analyses were performed using an analytical core-shell reversed-phase column (150 × 2.1 mm, 1.7 μm, Kinetex Phenyl-Hexyl equipped with a SecurityGuard cartridge, Phenomenex, Le Pecq, France) with a column temperature of 40°C and a flow rate of 0.5 $mL.min^{-1}$. The autosampler temperature was set at 4°C and the injection volume was 5 μL. Mobile phases were: (A) water and (B) acetonitrile (Chromasolv, Sigma-Aldrich) containing each 0.1% (*v*/*v*) of formic acid (Ultra grade, Fluka). The elution gradient started at 5% B and kept for 2 min, then to 100% B (linear ramp) in 8 min and kept for 4 min; then back to 5% B (linear ramp) over 0.01 min and maintained 1.99 min, for a total run time of 16 min.

The capillary voltage of the MS spectrometer was set at 4500V (positive mode), and the nebulizing parameters were set as follows: nebulizing gas (N_2) pressure at 0.4 bar, drying gas (N_2) flow at 4 $L.min^{-1}$, and drying temperature at 180 °C. Mass spectra were recorded from m/z 50 to 1200 at a mass resolving power of 25 000 full width at half-maximum (FWHM, m/z = 200) and a frequency of 2 Hz. Tandem mass spectrometry analyses were performed thanks to a collision induced dissociation (CID) with a collision energy of 25 eV. A solution of formate/acetate forming clusters was automatically injected before each sample for internal mass calibration, and the mass spectrometer was calibrated with the same solution before each sequence of samples. Data handling was done using DataAnalysis (version 4.3, Bruker Daltonics).

Data Preprocessing & Filtering

LC–MS raw data were automatically recalibrated using the calibration clusters found at the beginning of each chromatogram and converted into netCDF files (centroid mode) with a script developed within the DataAnalysis software. Converted files were preprocessed with the XCMS package (version 1.46.0) (Smith et al., 2006) in the R 3.2.3 environment: i) Peak picking was performed with the "centwave" method (peakwidth = c(2,20), ppm = 2) without threshold prefilter (Patti et al., 2012), ii) retention time correction was done with the "obiwarp" method (profstep = 0.1), iii) peaks were grouped using the following parameters bw = 10, minfrac = 0.5 and minsamp = 1, and iv) missing peaks were filled with default parameters.

The resulting variables list was further processed by the CAMERA package (version 1.26.0) (Kuhl et al., 2012) and to ensure data quality and remove redundant signals, three successive filtering steps were applied to preprocessed data using an in-house script on R. The first was based on the signal/noise (S/N) ratio to remove signals of QCs observed in analytical blanks (ratio set at 10 for features matching between QCs and analytical blanks). The second allowed suppression of signals based on the value of the coefficient of variation (CV) of the intensity of the variables in the QCs (cutoff set at 20%). A third filtering step was applied using the coefficient of the autocorrelation (with a cutoff set at 80%) between variables with a same retention time in the surface extract samples.

Statistical analyses

The resulting data were normalized, log10-transformed, mean-centered and analyzed by principal component analysis (PCA) and partial least-square discriminant analysis (PLS-DA) using the MetaboAnalyst 3.5 online resource (http://www.metaboanalyst.ca). Analyzed data from MetaboAnalyst were then exported and figures were generated in the R 3.2.3 environment using "ggplot2" package. The seasonal clustering observed with PCA and PLS-DA scores plots were statistically tested respectively with PERMANOVA test (999 permutations) using the "Vegan" R package, and a permutation test using MetaboaAnalyst webtool (Separation distance: B/W, 1000 permutations). Variation of each selected metabolites during each month was then statistically tested by one-way anova ANOVA followed by post-hoc test (HSD) using the "Agricolae" R package.

MS/MS molecular networking and annotation of metabolites

The MS/MS molecular network was generated on the GNPS online platform (https://gnps.ucsd.edu). Raw LC-MS/MS data were converted into .mzXML files with DataAnalysis. MS/MS data were clustered using default parameters for "medium data preset" with a precursor ion mass tolerance of 2 Da and a fragment ion mass tolerance of 0.5 Da. Data were analyzed with Cytoscape (version 3.4.0), using nodes to represent *m/z* detected features and edges to represent the MS/MS spectral similarity (with a cosine score (CS) > 0.7) between *m/z* features. Normalized concentrations for metabolites found commonly within the molecular network were imported into Cytoscape. By implementing these data, a pie chart was generated into each node revealing the relative seasonal distribution of each metabolite. Transparency of edges connecting each node was proportional to the spectral similarity using the cosine score.

Annotation of selected *m/z* features were done by: (i) comparison of MS, MS/MS and RT data with those of commercial or purified chemical standards [Level 1 of annotation from (Schymanski et al., 2014)], (ii) library match of MS and MS/MS data (Level 2a of annotation), or (iii) the use of a molecular networking approach together with the careful analysis of MS, MS/MS and retention time data (Level 3 of annotation).

References

Kuhl, C., Tautenhahn, R., Böttcher, C., Larson, T. R., and Neumann, S. (2012). CAMERA: An integrated strategy for compound spectra extraction and annotation of LC/MS data sets. *Anal Chem* 84, 283–289. doi:10.1021/ac202450g.

Othmani, A., Briand, J.-F., Ayé, M., Molmeret, M., and Culioli, G. (2016). Surface metabolites of the brown alga *Taonia atomaria* have the ability to regulate epibiosis. *Biofouling* 32, 801–813. doi:10.1080/08927014.2016.1198954.

Patti, G. J., Tautenhahn, R., and Siuzdak, G. (2012). Meta-analysis of untargeted metabolomic data from multiple profiling experiments. *Nat Protoc* 7, 508–516. doi:10.1038/nprot.2011.454.

Schymanski, E. L., Jeon, J., Gulde, R., Fenner, K., Ruff, M., Singer, H. P., et al. (2014). Identifying small molecules via high resolution mass spectrometry: Communicating confidence. *Environ. Sci. Technol.* 48, 2097–2098. doi:10.1021/es5002105.

Smith, C. A., Want, E. J., O'Maille, G., Abagyan, R., and Siuzdak, G. (2006). XCMS: processing mass spectrometry data for metabolite profiling using nonlinear peak alignment, matching, and identification. *Anal. Chem.* 78, 779–787. doi:10.1021/ac051437y.

Figure SII.1. Chemical structures of some surface metabolites isolated from *Taonia atomaria**

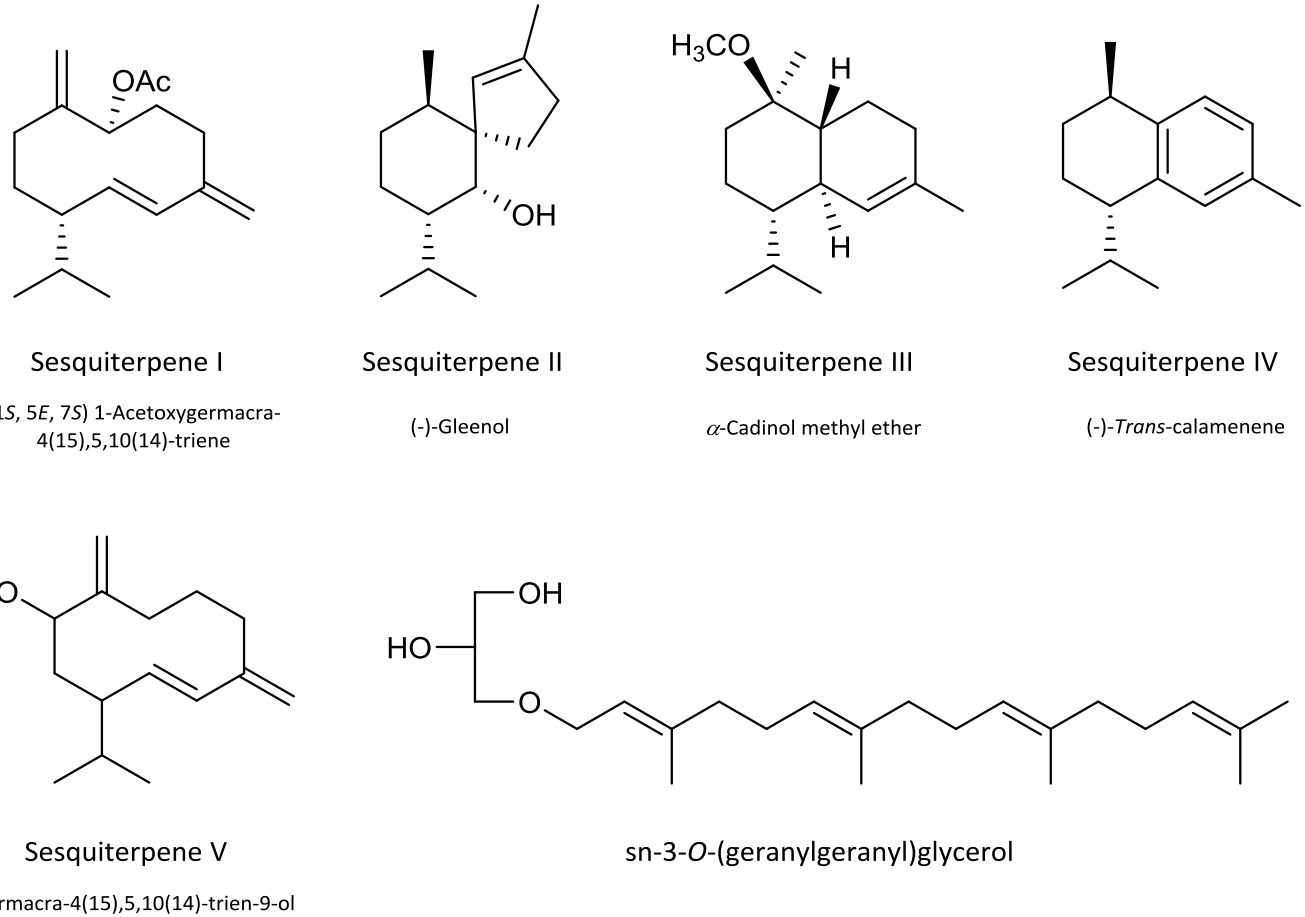

Sesquiterpene I

(1*S*, 5*E*, 7*S*) 1-Acetoxygermacra-4(15),5,10(14)-triene

Sesquiterpene II

(-)-Gleenol

Sesquiterpene III

α-Cadinol methyl ether

Sesquiterpene IV

(-)-*Trans*-calamenene

Sesquiterpene V

Germacra-4(15),5,10(14)-trien-9-ol

sn-3-*O*-(geranylgeranyl)glycerol

*See Othmani A, Bunet R, Bonnefont J-L, Briand J-F, Culioli G. 2016. Settlement inhibition of marine biofilm bacteria and barnacle larvae by compounds isolated from the Mediterranean brown alga *Taonia atomaria*. J Appl Phycol. 28:1975-1986.

Figure SII.2. (+)-ESI-LC-MS profiles of surface extracts of *T. atomaria* (collected monthly from February to July)

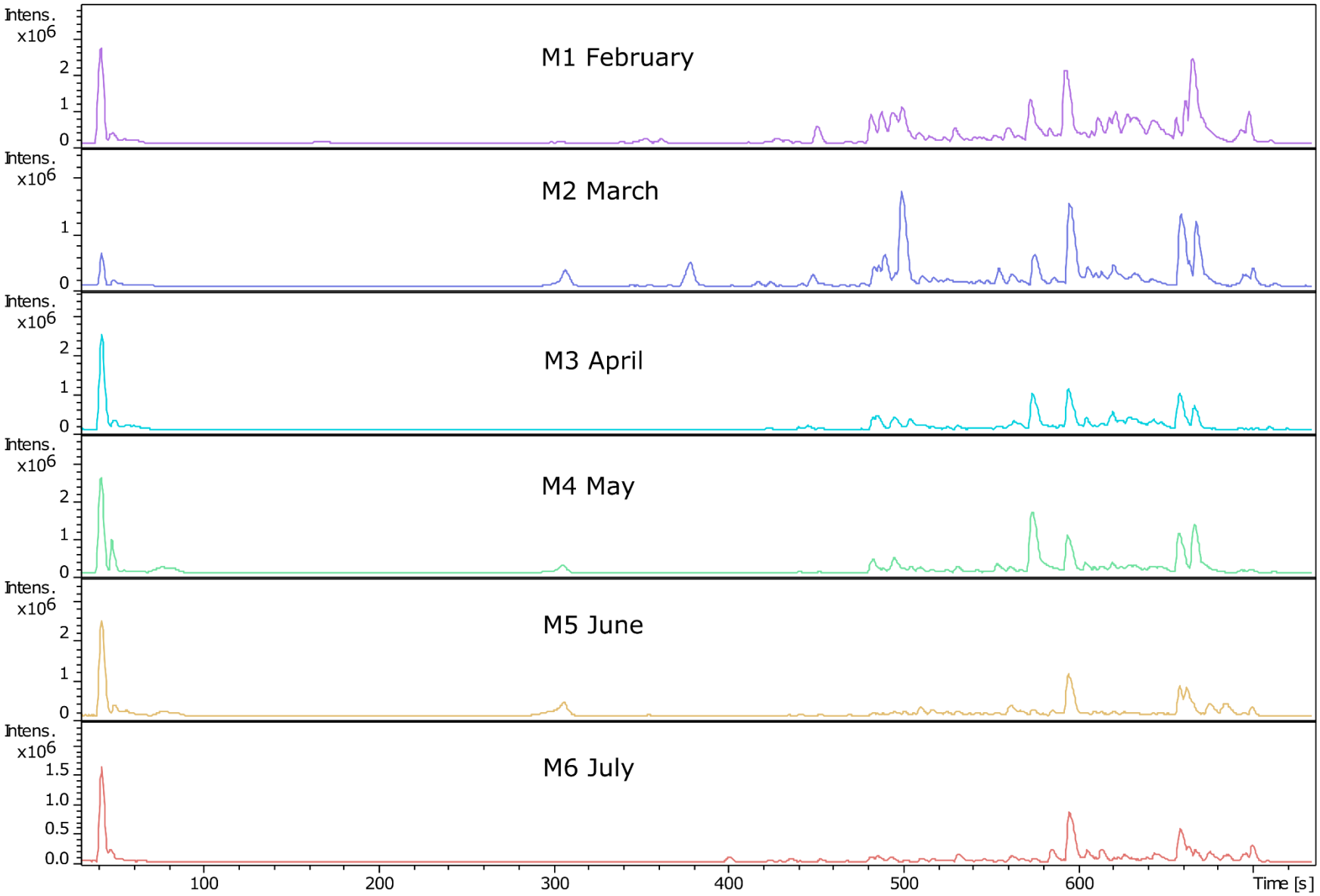

Figure SII.3. PCA score plot obtained from (+)-ESI-LC–MS profiles of surface extracts of *T. atomaria* collected monthly from February to July (n = 18), QCs sample (n = 8) and blanks (solvent blanks, n = 2; analytical blanks, n = 4)

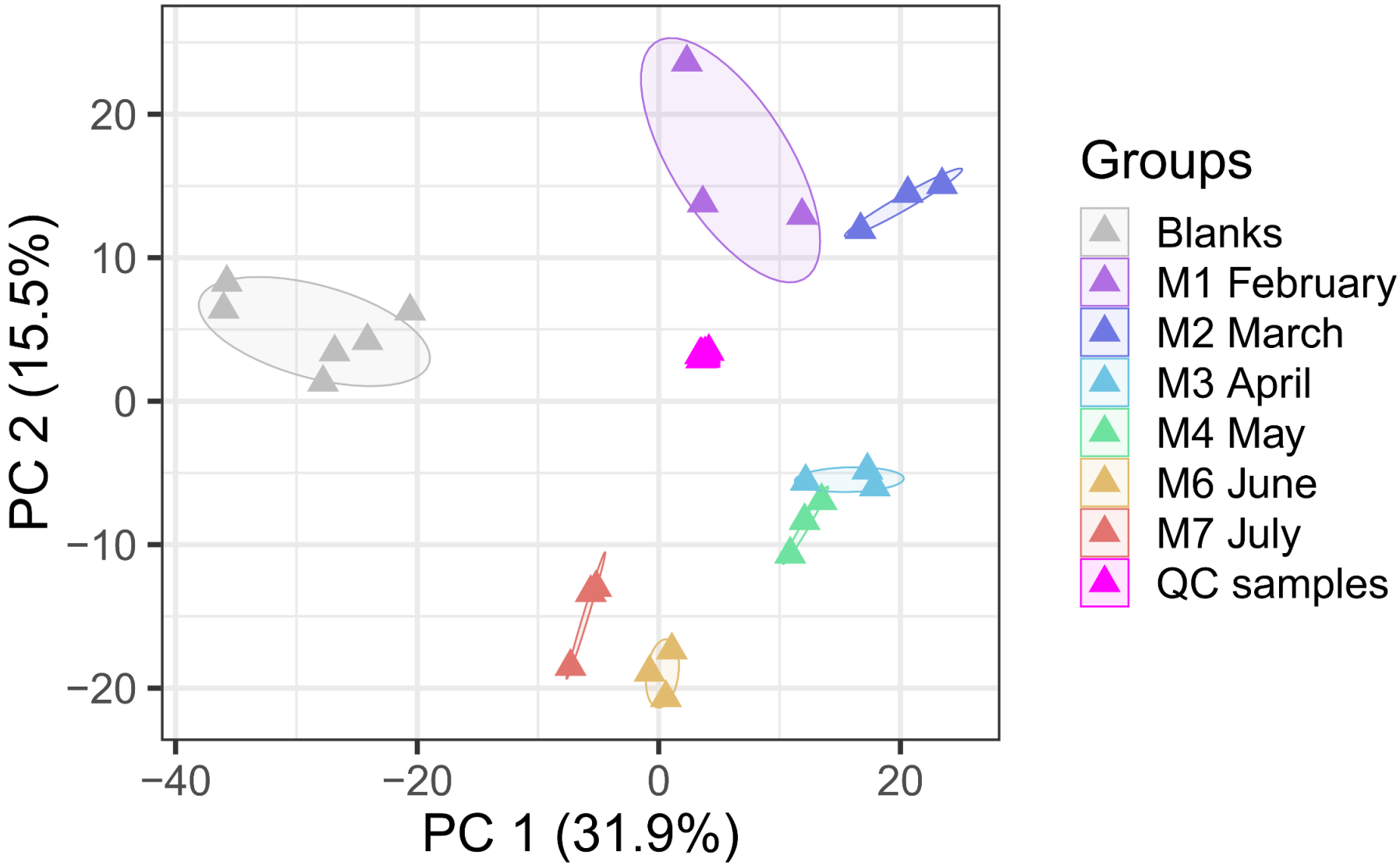

Figure SII.4. PLS-DA analysis from (+)-ESI-LC–MS profiles of surface extracts of *T. atomaria* collected monthly from February to July (one class per month;
"Class order matters" option was selected in MetaboAnalyst): (A) PLS-DA score plot, (B) VIP scores of the 100 first VIPs according to their rank (The rectangle in red showed the 18 first VIPs above the regression line in green which were selected for the analysis, (C) Permutation test results (Separation distance: B/W, 1000 permutations).

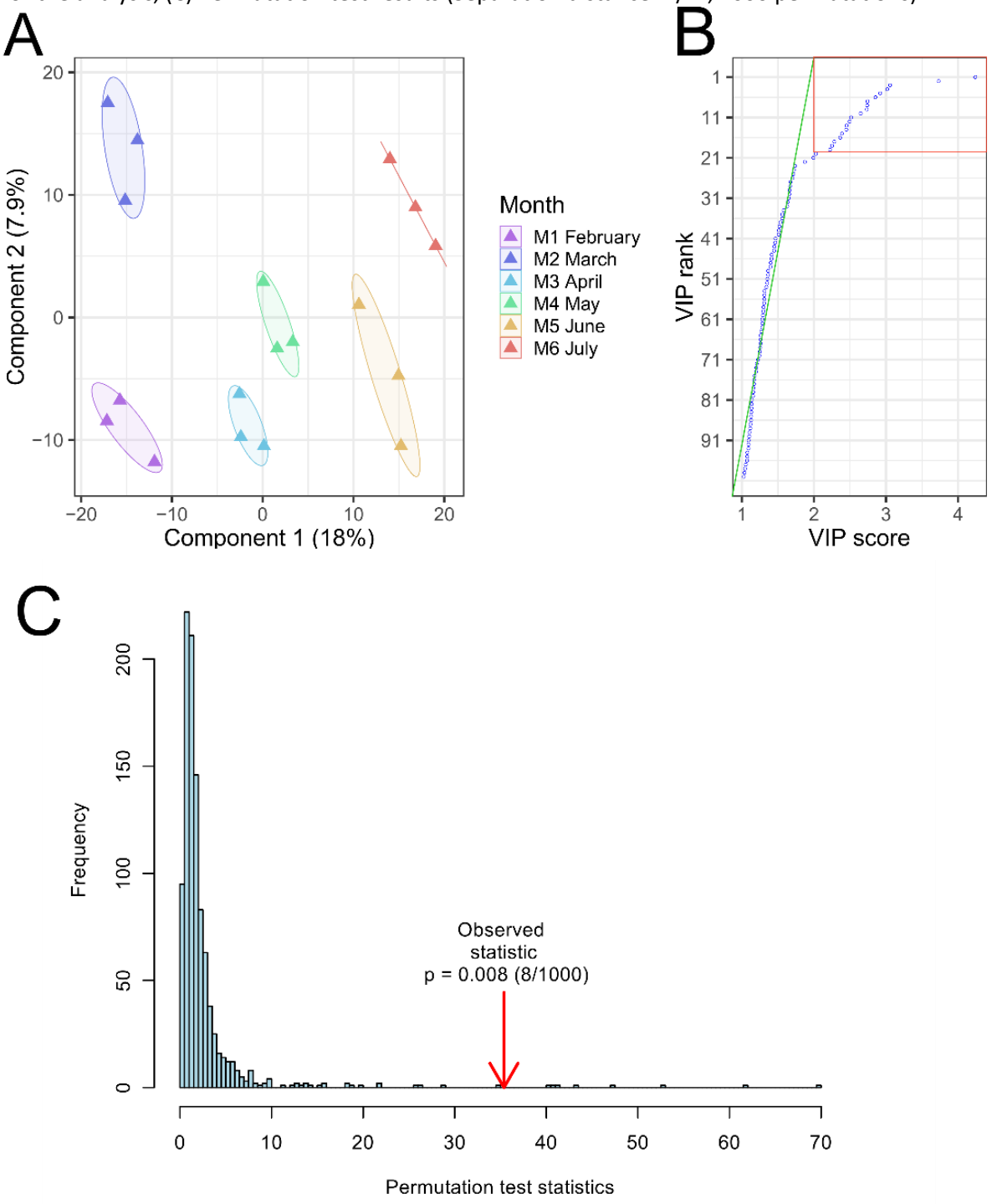

Figure SII.5. HRMS/MS data and hypothetical MS fragmentation* of VIP n°1 putatively identified as Proline betaine **

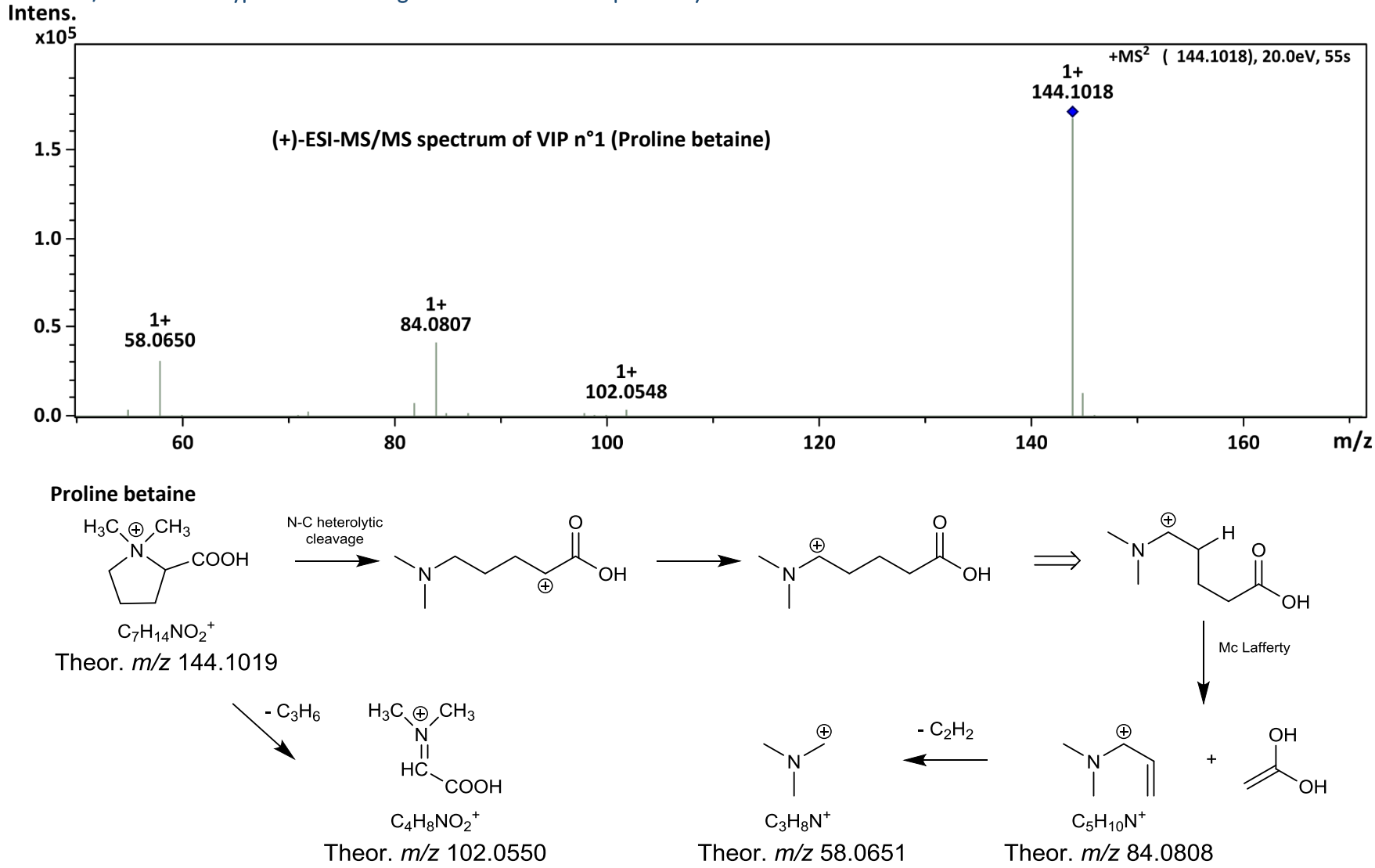

*Modified from Naresh Chary V, Dinesh Kumar C, Vairamani M, Prabhakar S. 2012. Characterization of amino acid-derived betaines by electrospray ionization tandem mass spectrometry. Journal of Mass Spectrometry. 47:79-88.

** The HRMS, HRMS/MS data and the retention time of VIP n°1 were identical to those of a commercial standard of Proline betaine (stachydrine).

Figure SII.6. HRMS/MS data and hypothetical MS fragmentation of VIP n°2 identified as DMSP*

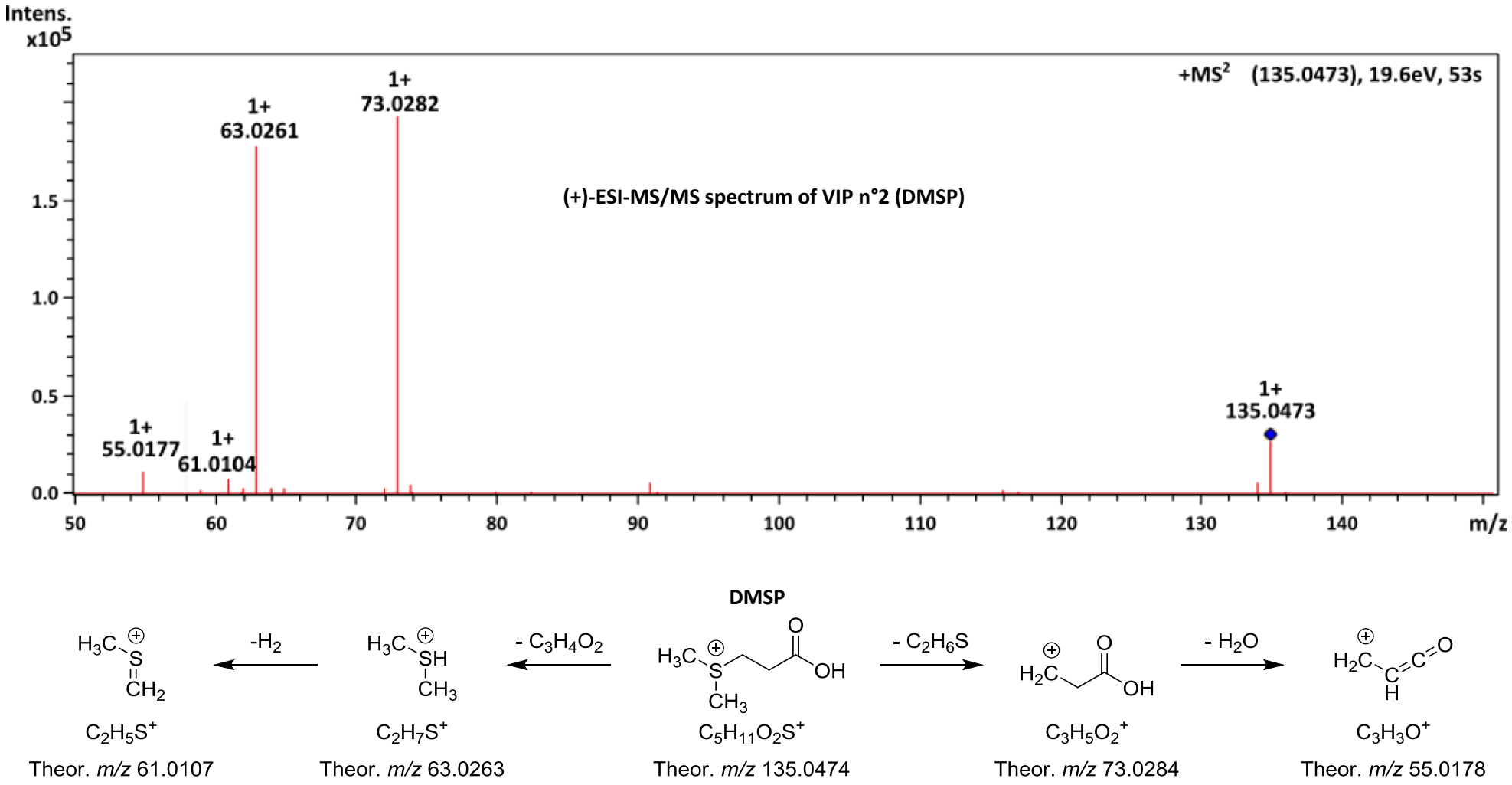

*The HRMS, HRMS/MS data and the retention time of VIP n°2 were identical to those of a commercial standard of DMSP.

Figure SII.7. HRMS/MS data and hypothetical MS fragmentation of VIP n°3 putatively identified as Ceramide (dC18:1/C16:0)

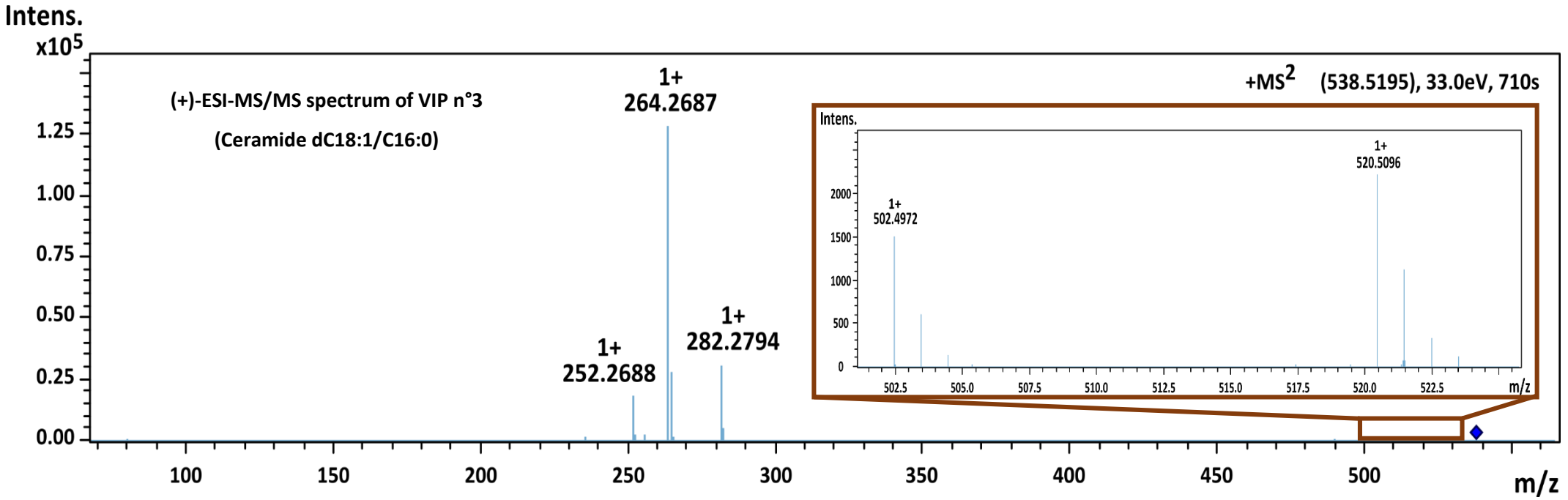

Ceramide (dC18:1/C16:0)

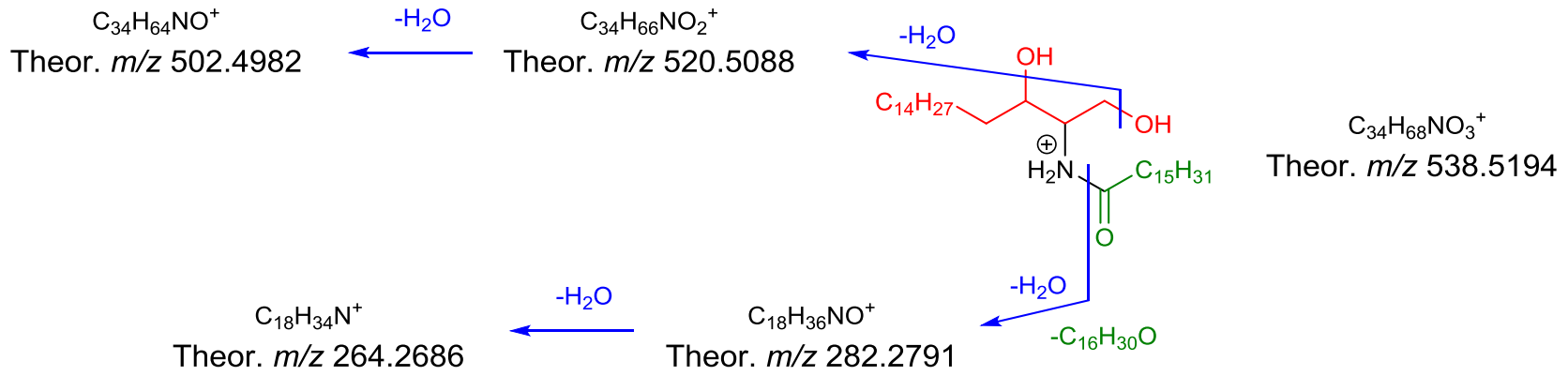

Figure S8. HRMS/MS data and hypothetical MS fragmentation of VIP n°4 putatively identified as DGTA C44:10

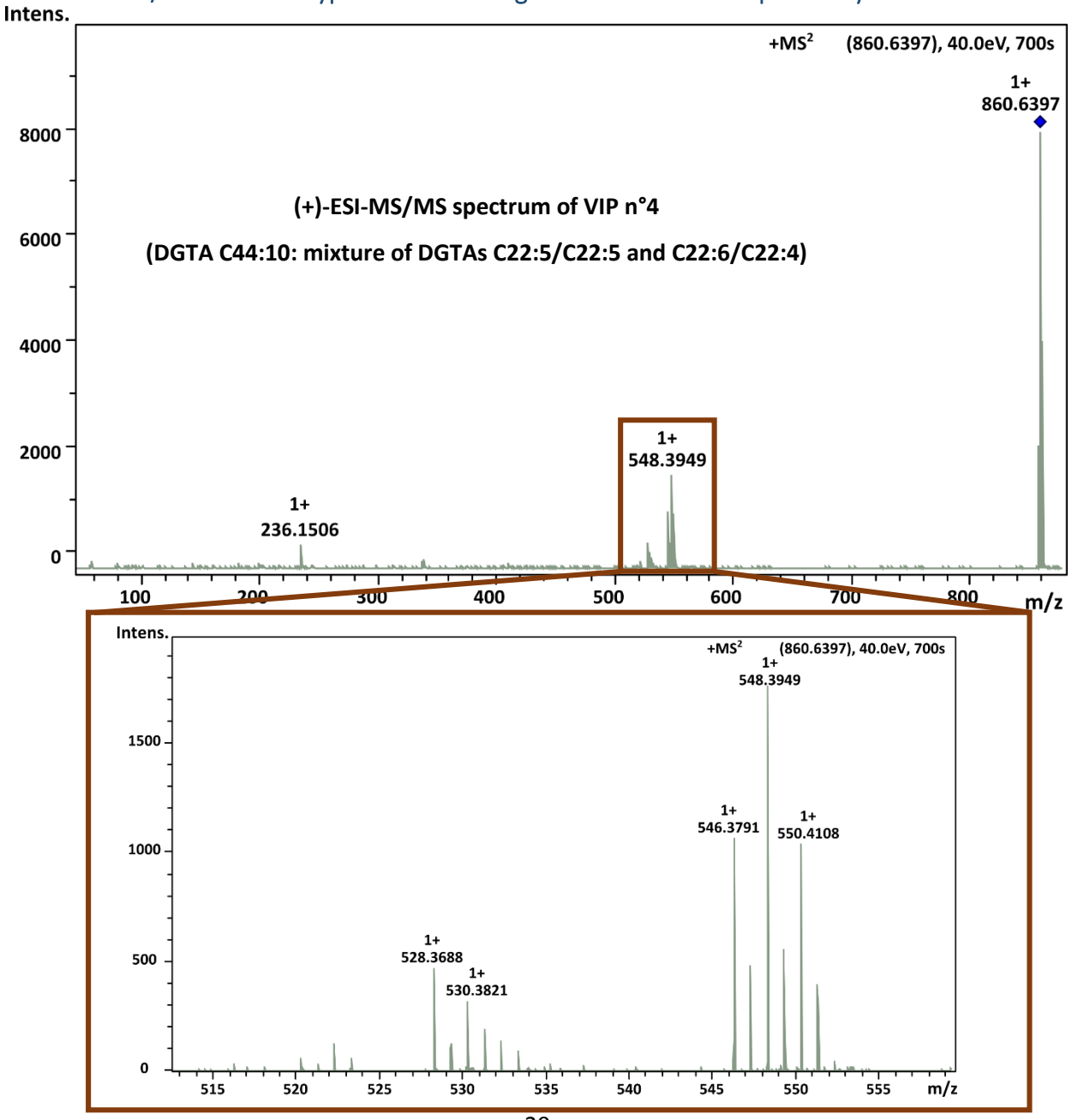

DGTA (C22:5/C22:5)

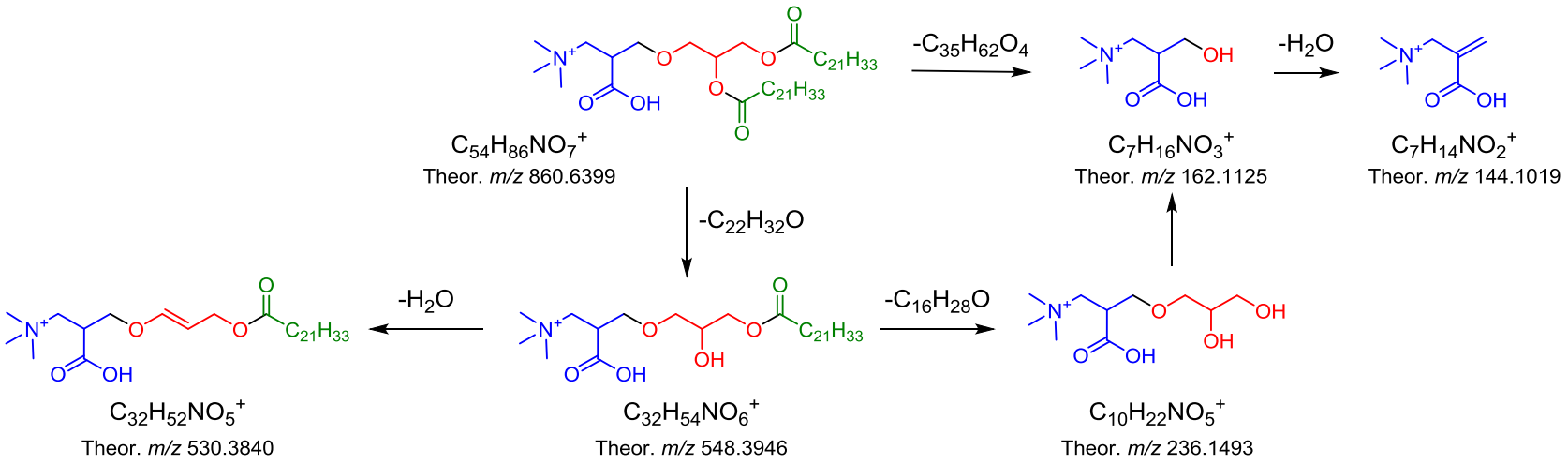

DGTA (C22:6/C22:4)*

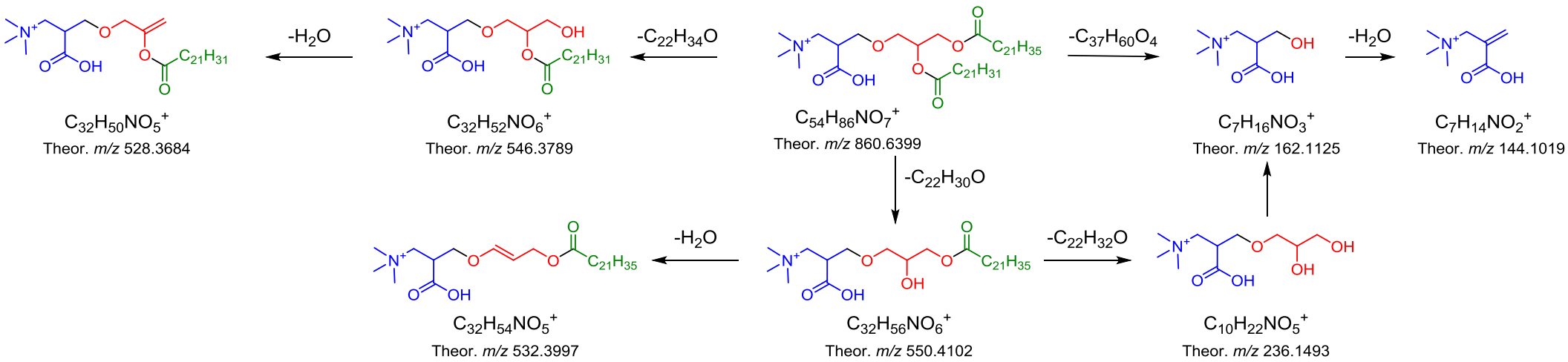

*Positions of the acyl moieties on the glycerol could be inverted.

Figure SII.9. HRMS/MS data and MS fragmentation of VIP n°5 identified as Proline*

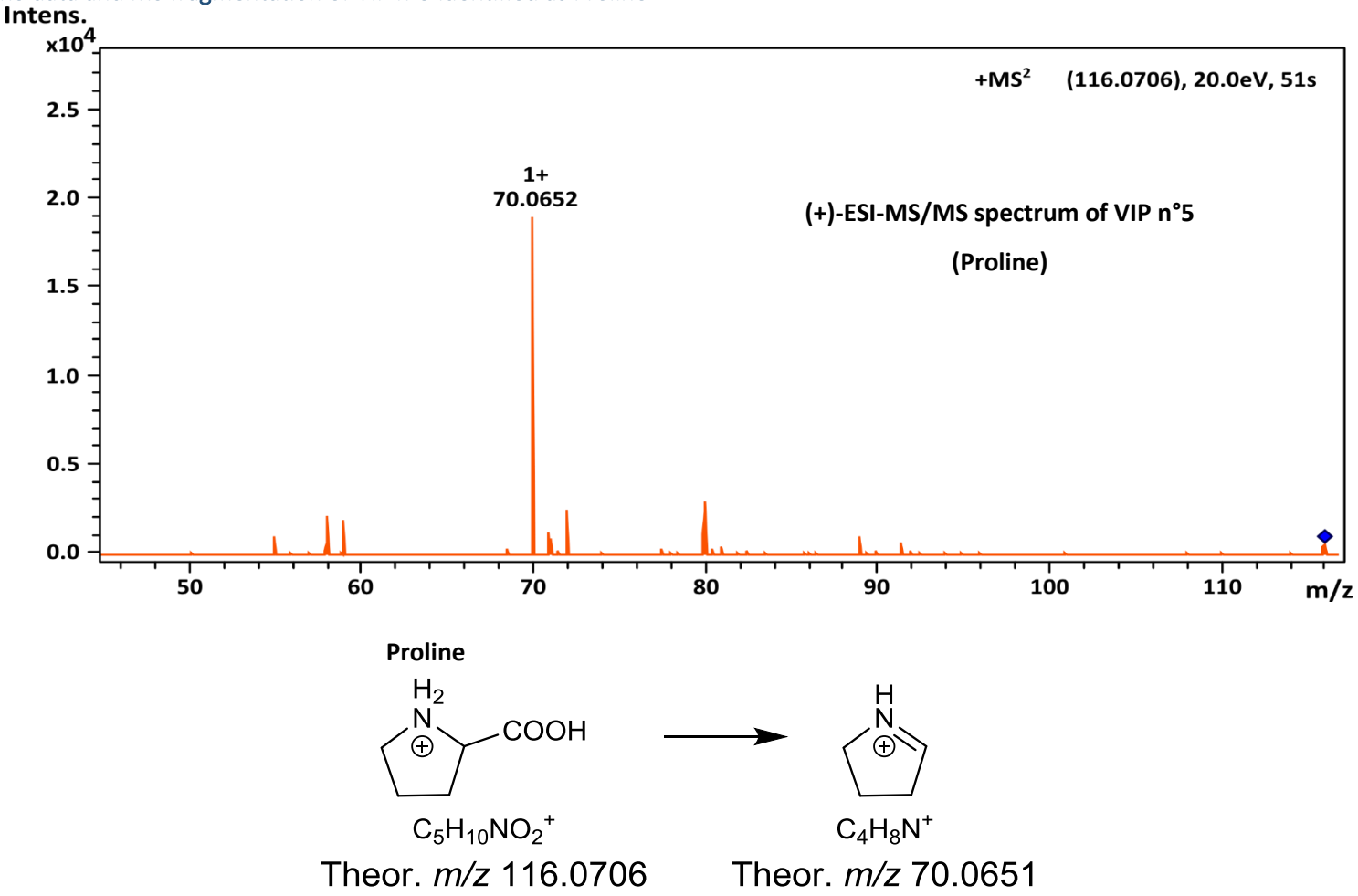

*The HRMS, HRMS/MS data and the retention time of VIP n°5 were identical to those of a commercial standard of Proline.

Figure SII/10. HRMS/MS data and hypothetical MS fragmentation of VIP n°6 putatively identified as DGTA C44:12 (DGTA C22:6/C22:6)

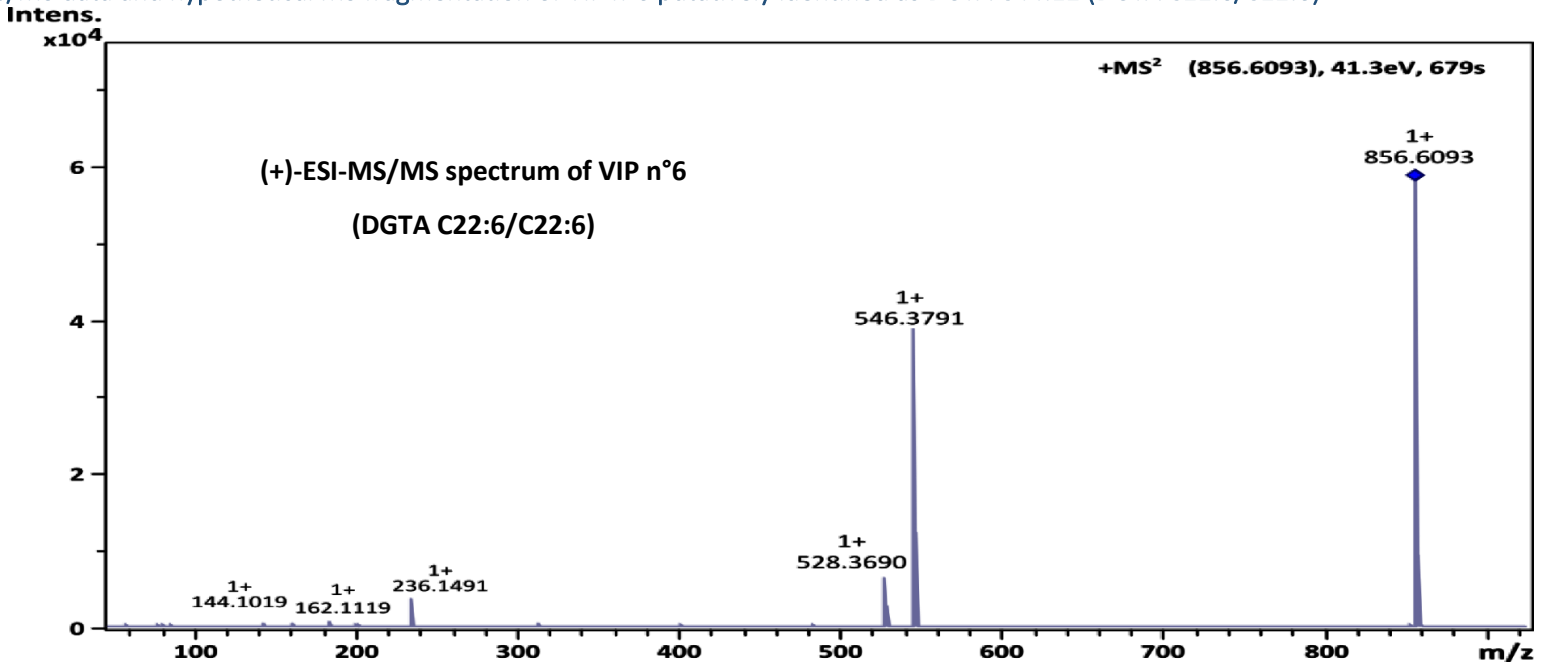

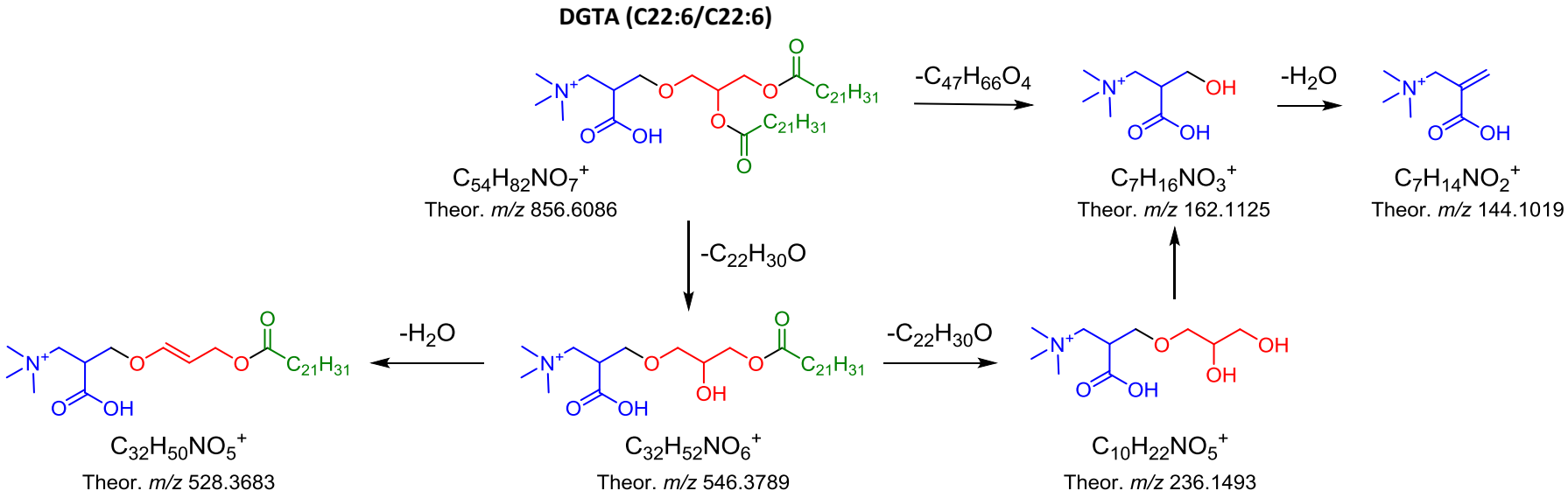

Figure SII.11. HRMS/MS data of VIP n°7 identified as Sesquiterpene IV [(-)-*Trans*-Calamenene]

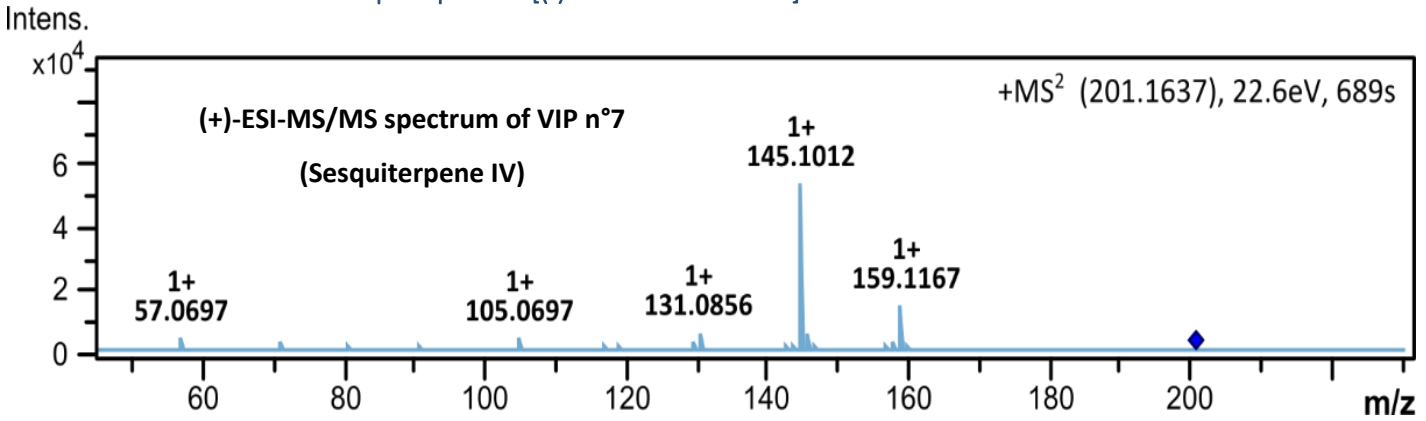

Figure SII.12. HRMS/MS data of VIP n°8

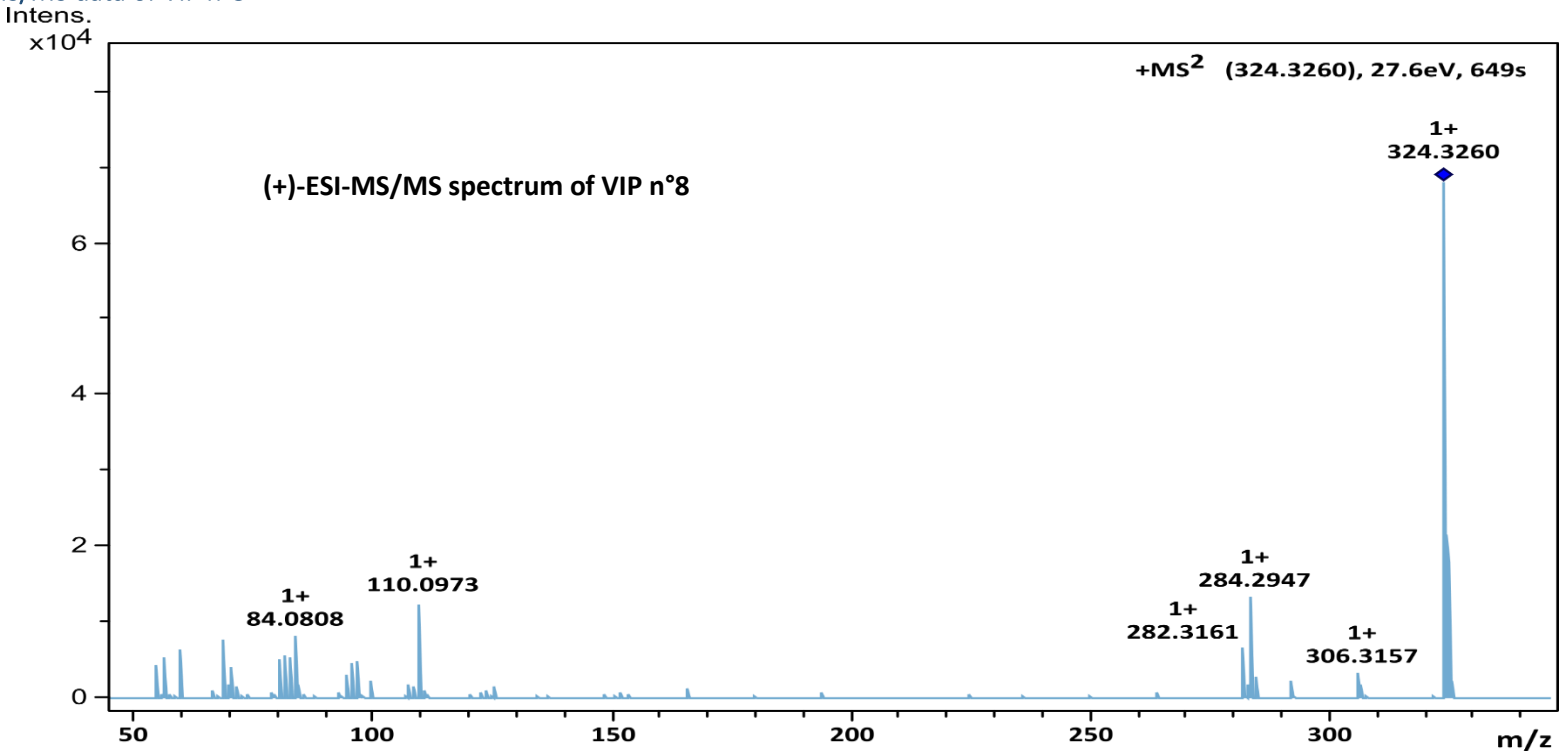

Figure SII.13. HRMS/MS data and hypothetical MS fragmentation of VIP n°9 putatively identified as *Lyso*-DGTA (C20:5)

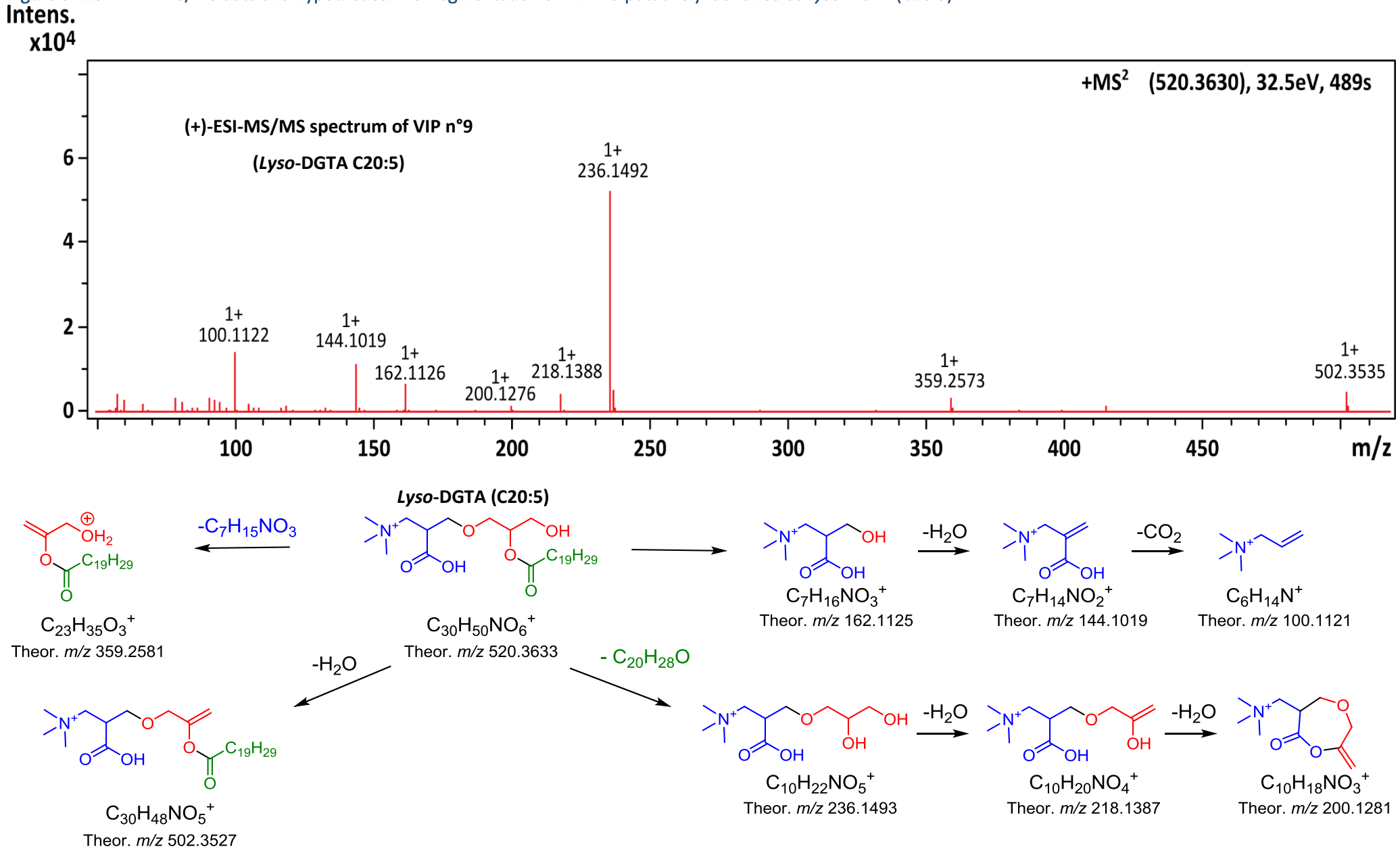

Figure SII.14. HRMS/MS data and hypothetical MS fragmentation of VIP n°10 putatively identified as Glutaminevaline (Gln-Val)*

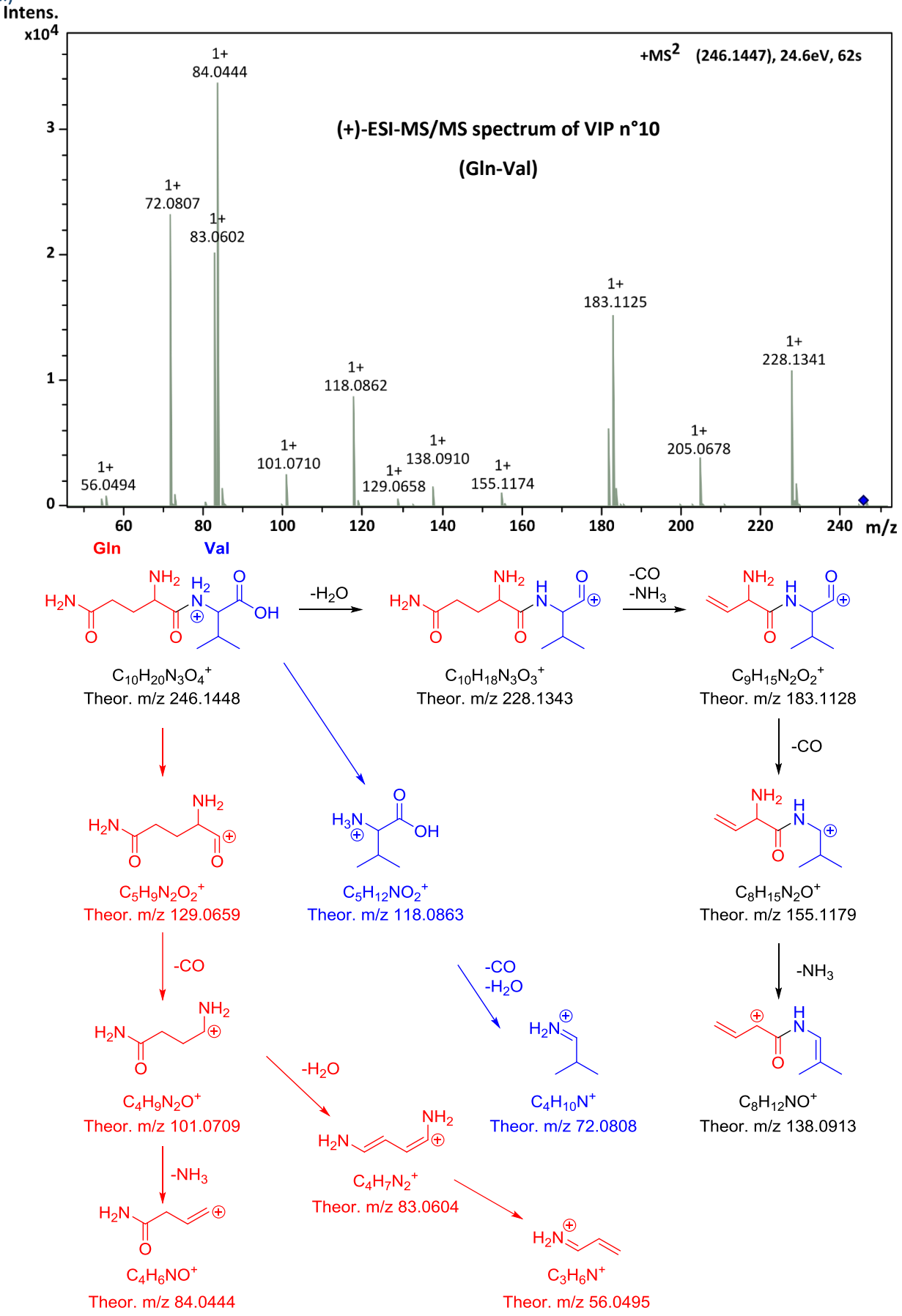

*The experimental HRMS/MS data of VIP n°10 matched perfectly with those of Gln-Val found in METLIN database (METLIN ID: 23765)

Figure SII.15. HRMS/MS data of VIP n°11

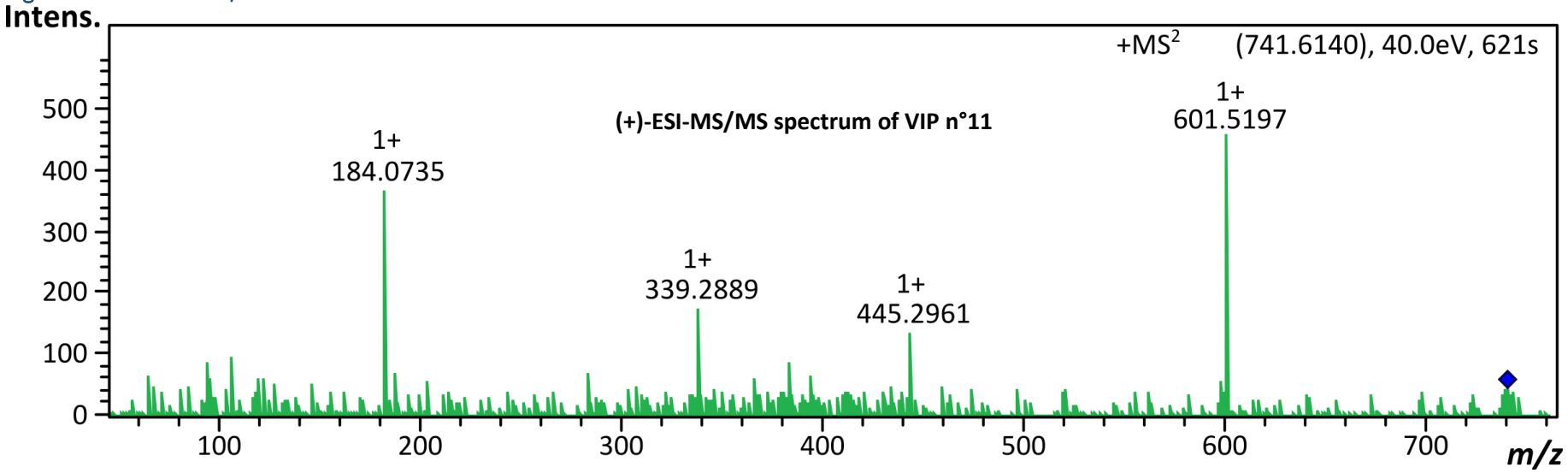

Figure SII.16. HRMS/MS data and hypothetical MS fragmentation of VIP n°12 putatively identified as Ceramide (dC18:1/C14:0)

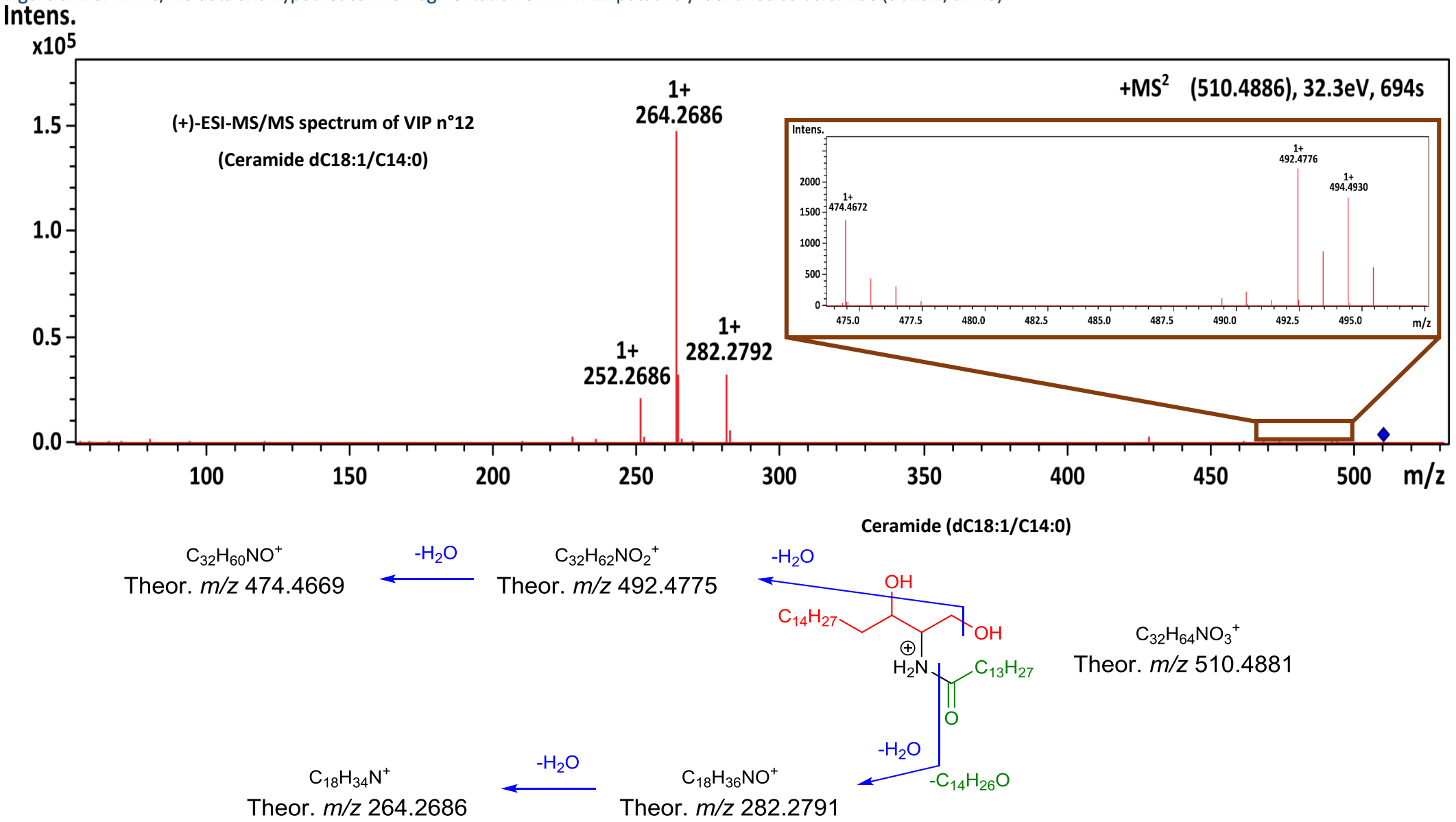

Figure SII.17. HRMS/MS data and hypothetical MS fragmentation of VIP n°13 putatively identified as Glutamineleucine (Gln-Leu)*

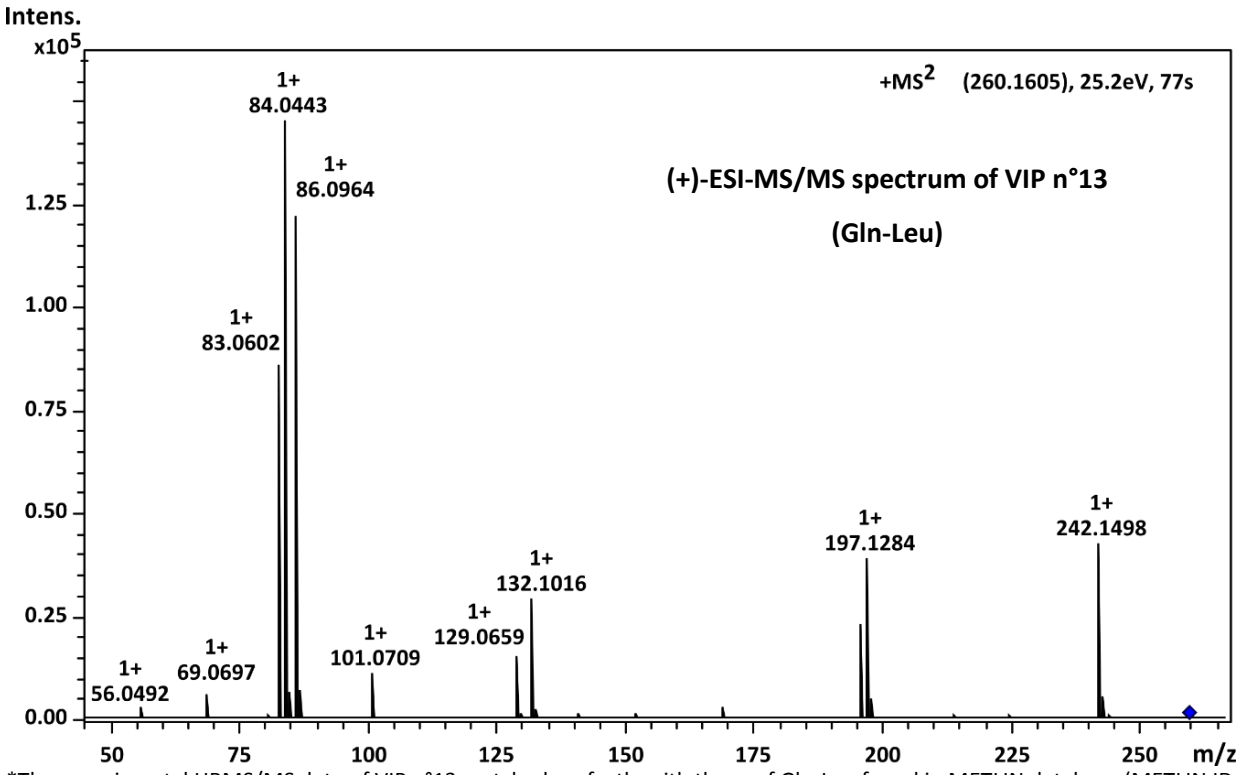

*The experimental HRMS/MS data of VIP n°13 matched perfectly with those of Gln-Leu found in METLIN database (METLIN ID: 23938)

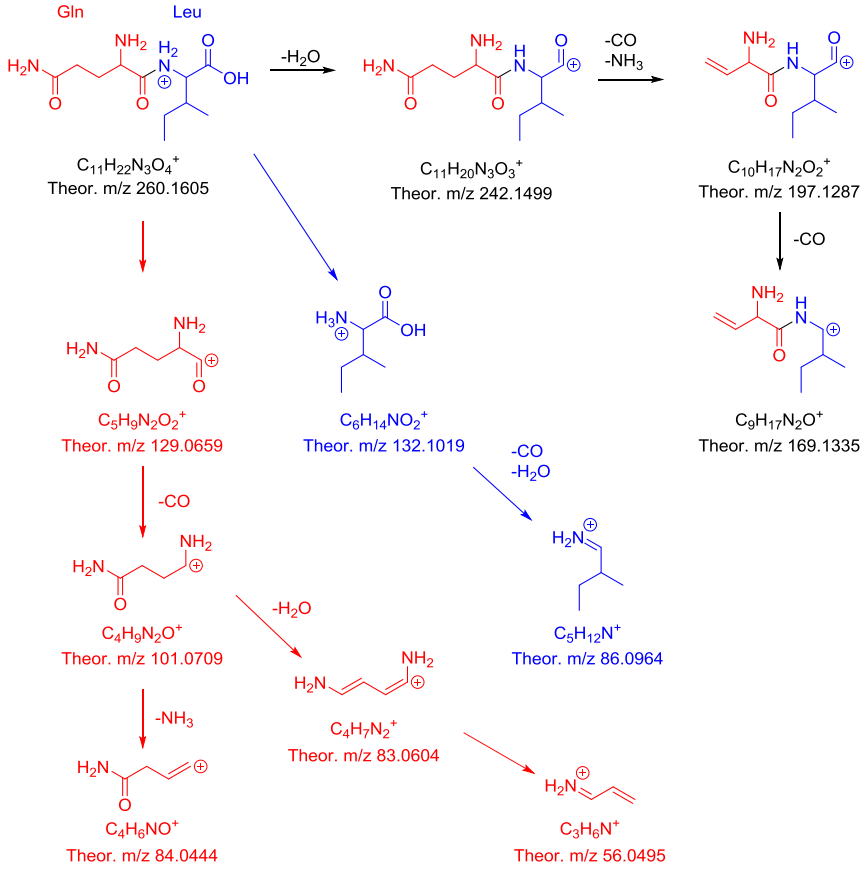

Figure SII.18. HRMS/MS data and hypothetical MS fragmentation of VIP n°14 putatively identified as DGTA C32:2

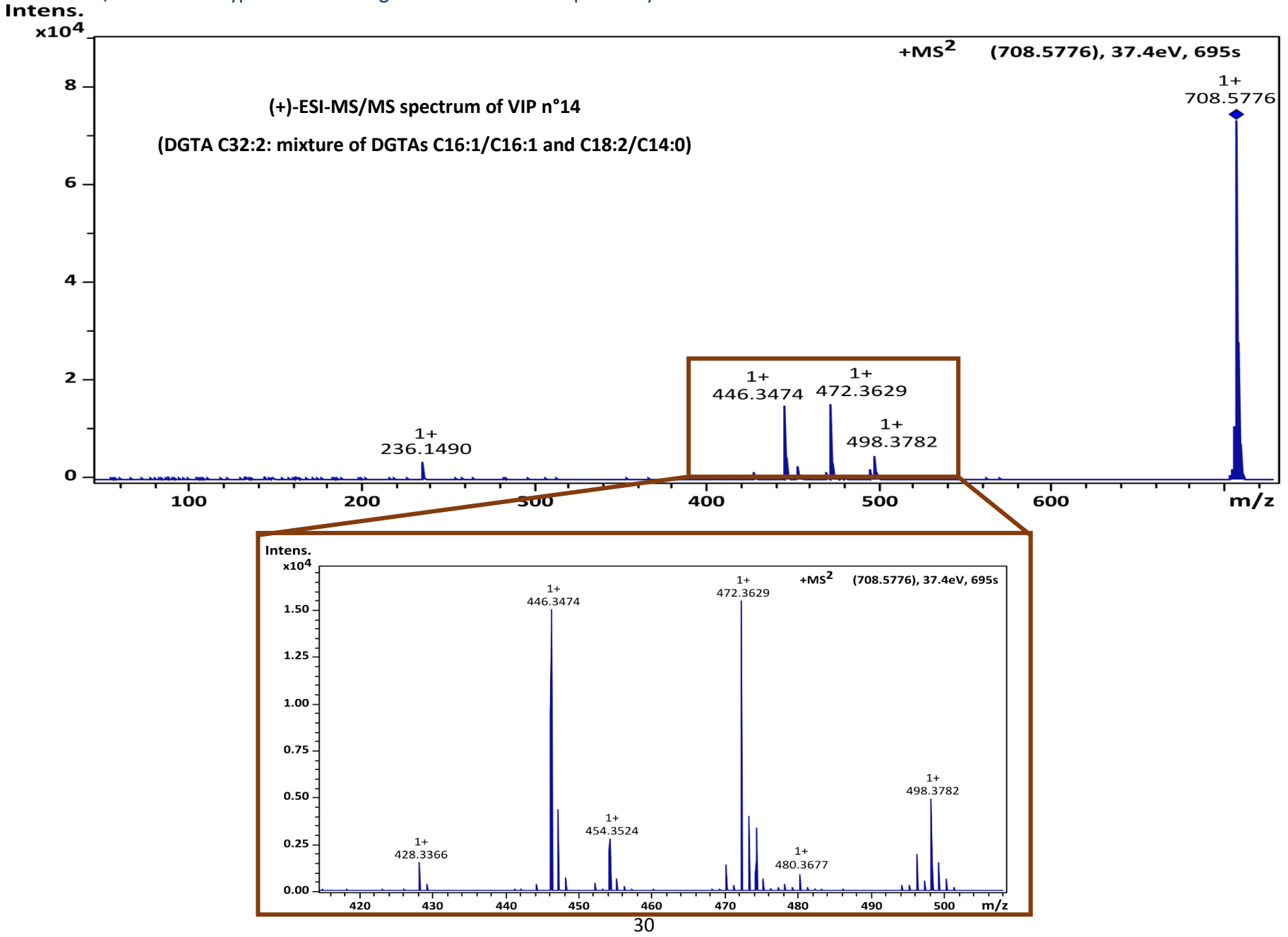

DGTA (C16:1/C16:1)

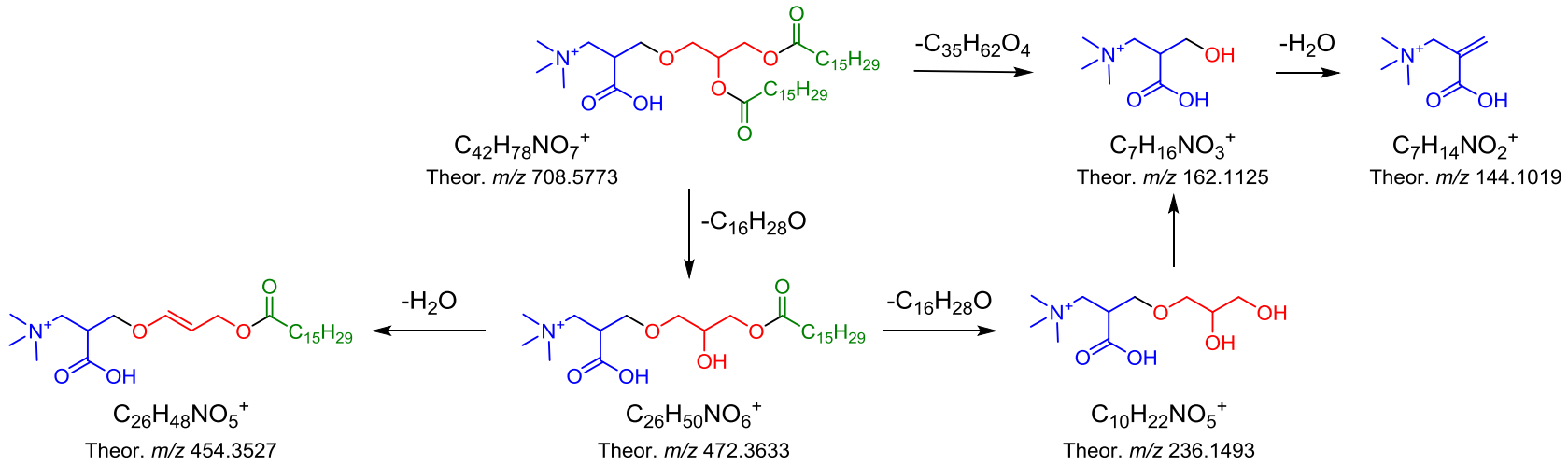

DGTA (C18:2/C14:0)*

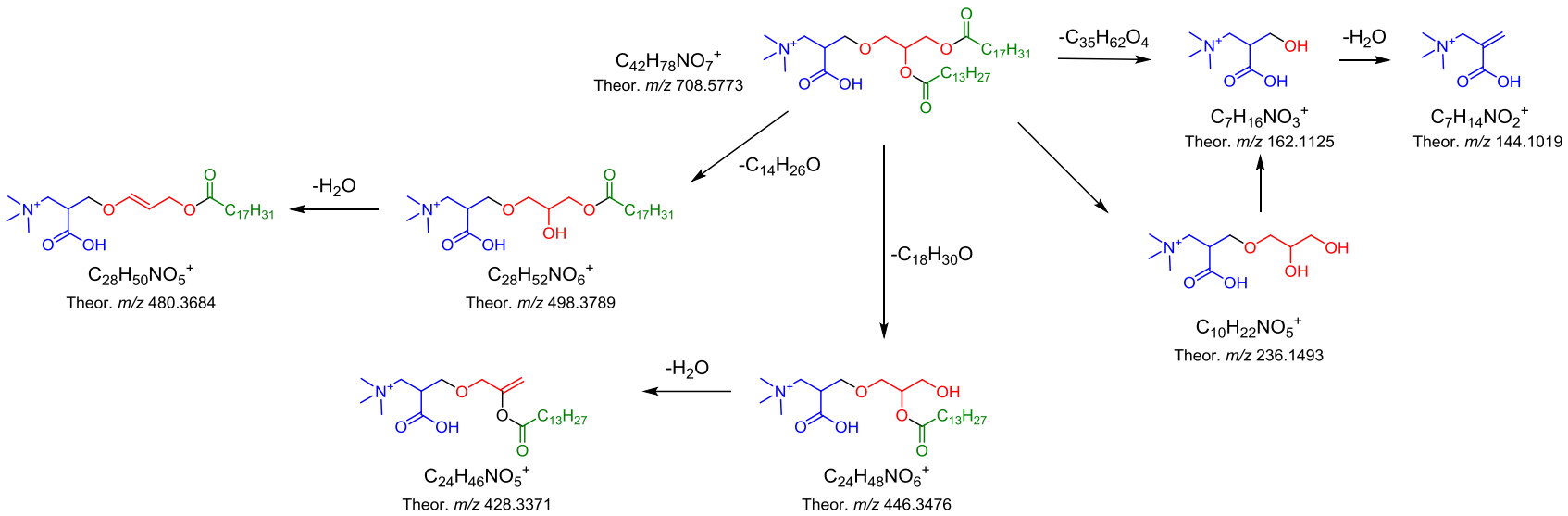

*Positions of the acyl moieties on the glycerol could be inverted.

Figure SII.19. HRMS/MS data and hypothetical MS fragmentation of VIP n°15

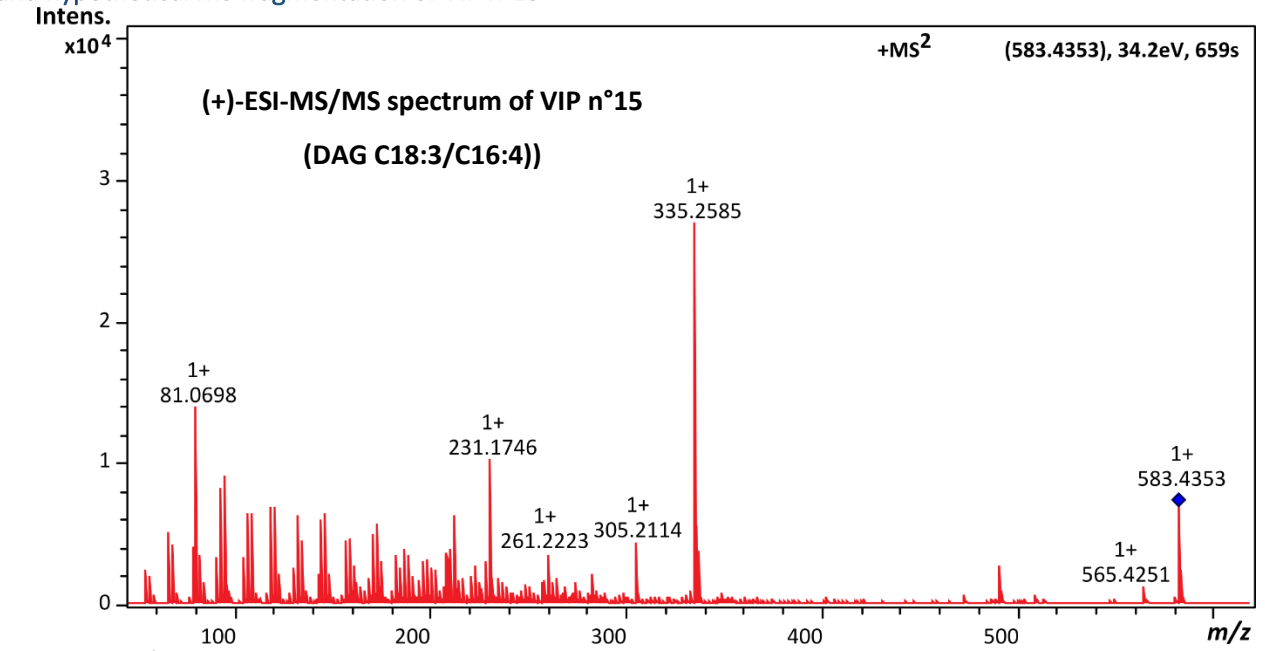

DAG (C18:3/C16:4)*

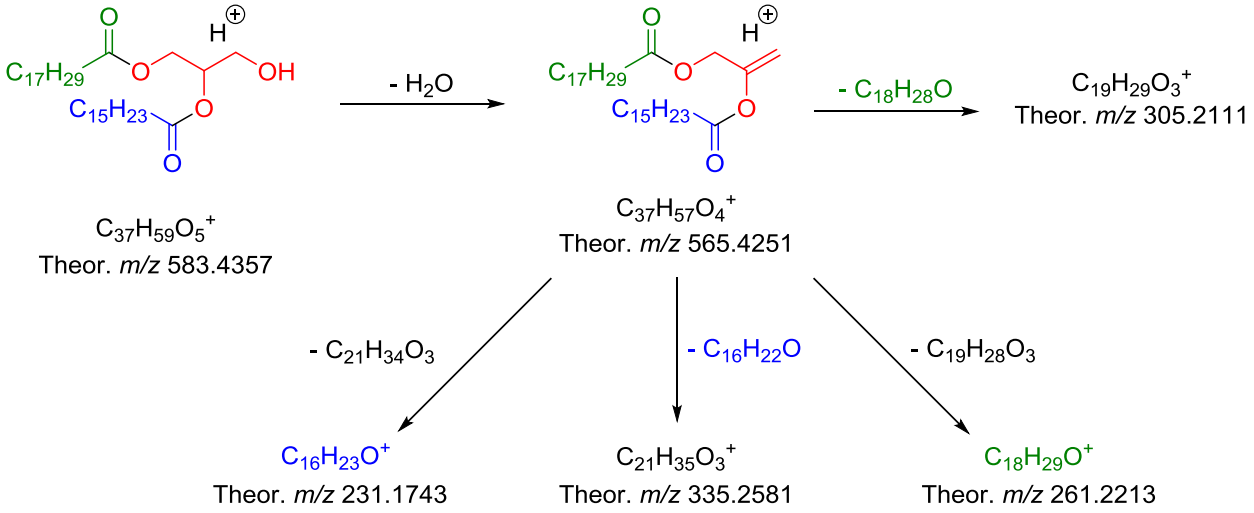

*Positions of the acyl moieties on the glycerol could be inverted.

Figure SII.20. HRMS/MS data and hypothetical MS fragmentation of VIP n°16 identified as Glutaminephenylalanine (Gln-Phe)*

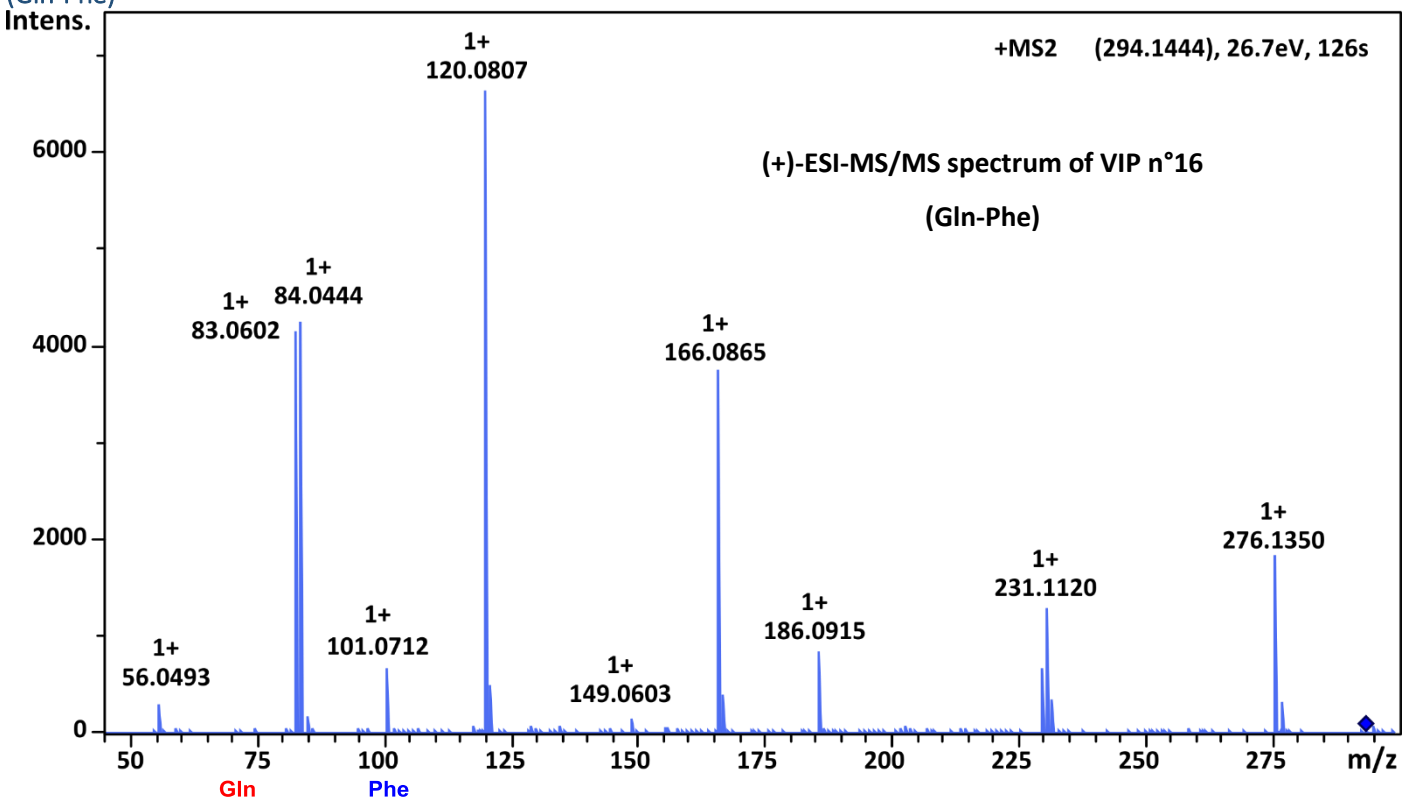

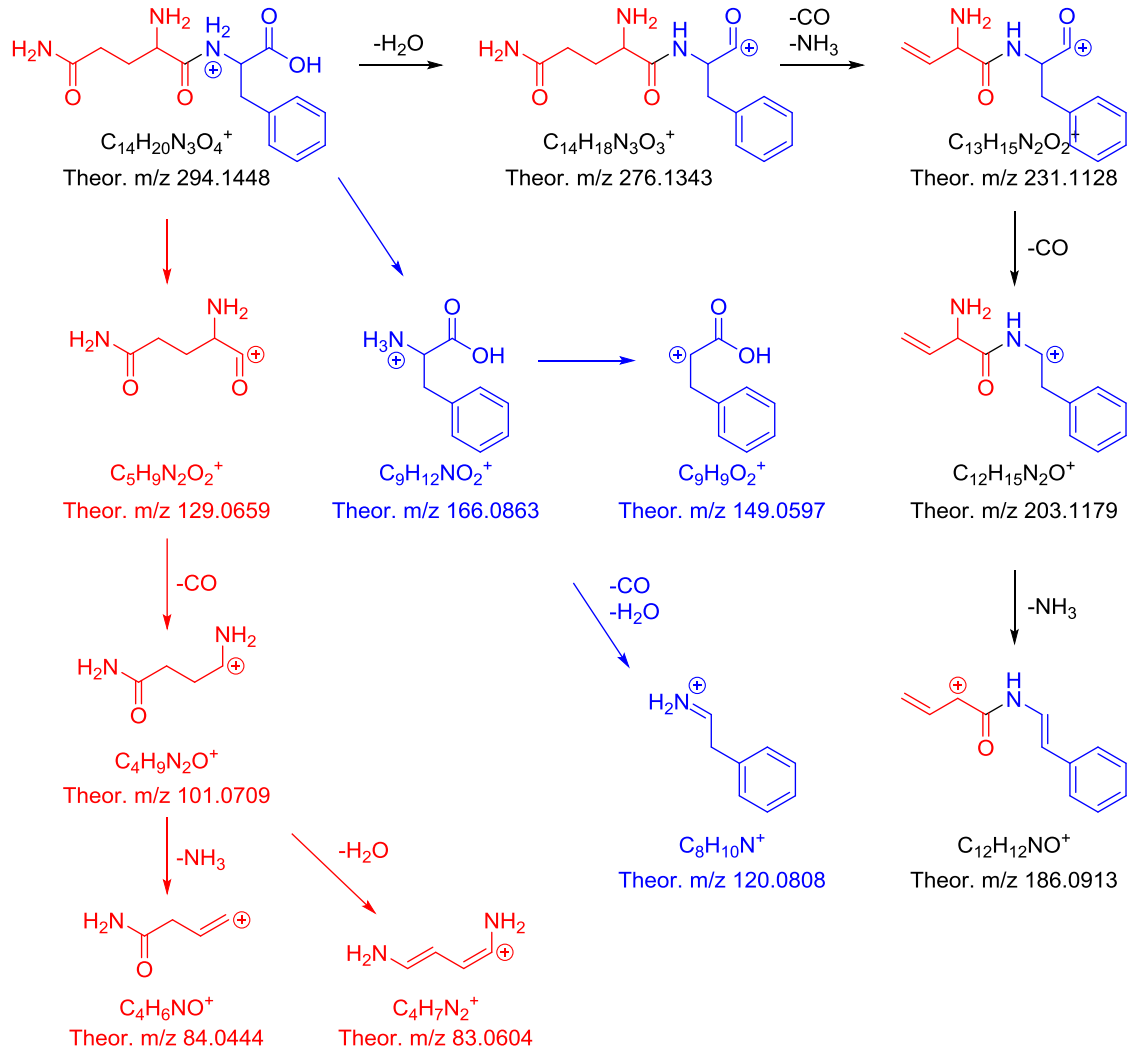

*The experimental HRMS/MS data of VIP n°17 matched perfectly with those of Gln-Phe found in METLIN database (METLIN ID: 23865)

Figure SII.21. HRMS/MS data of VIP n°17

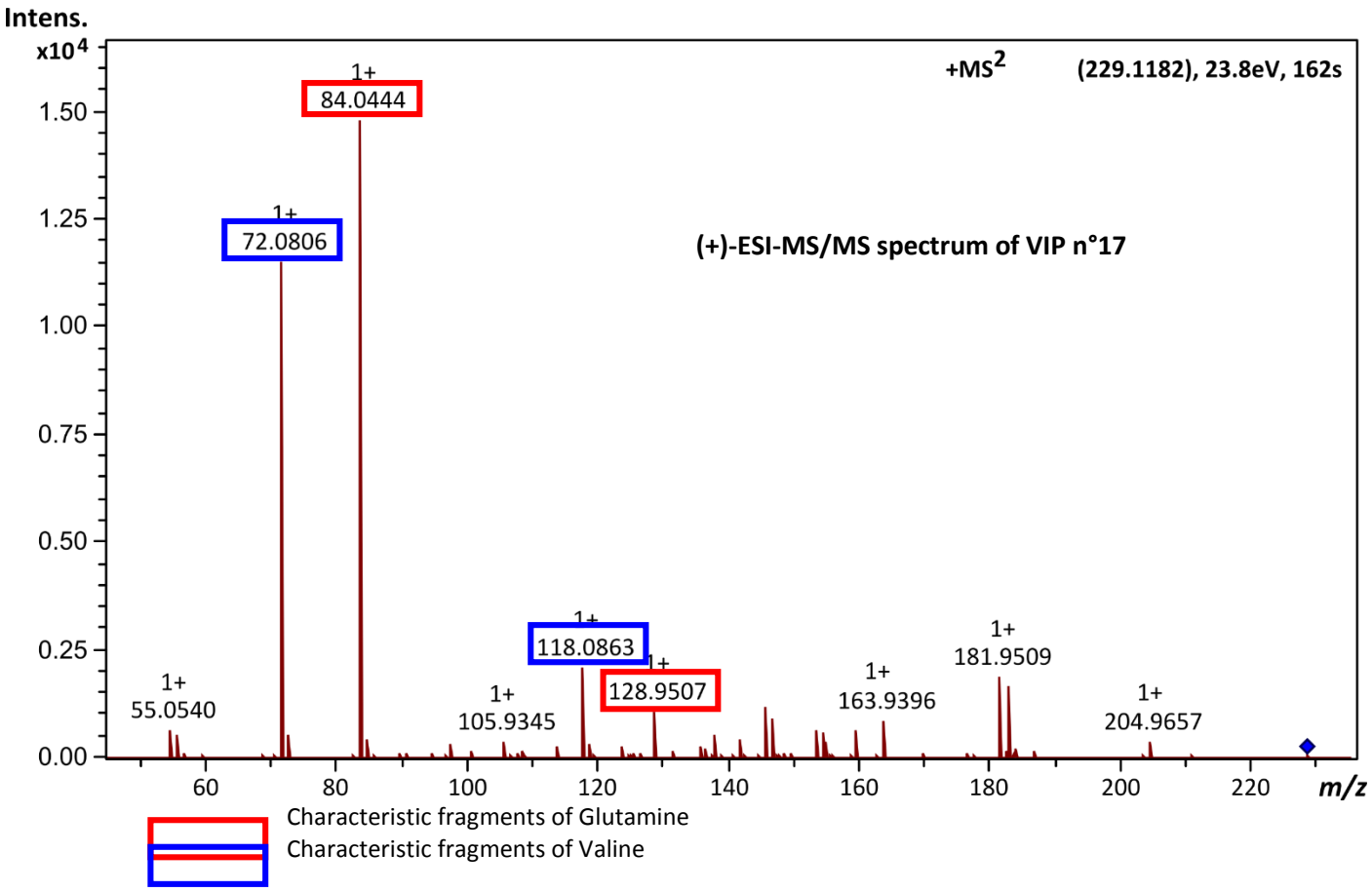

Figure SII.22. HRMS/MS data and hypothetical MS fragmentation of VIP n°18 identified as difucol-2-*O*-sulfate

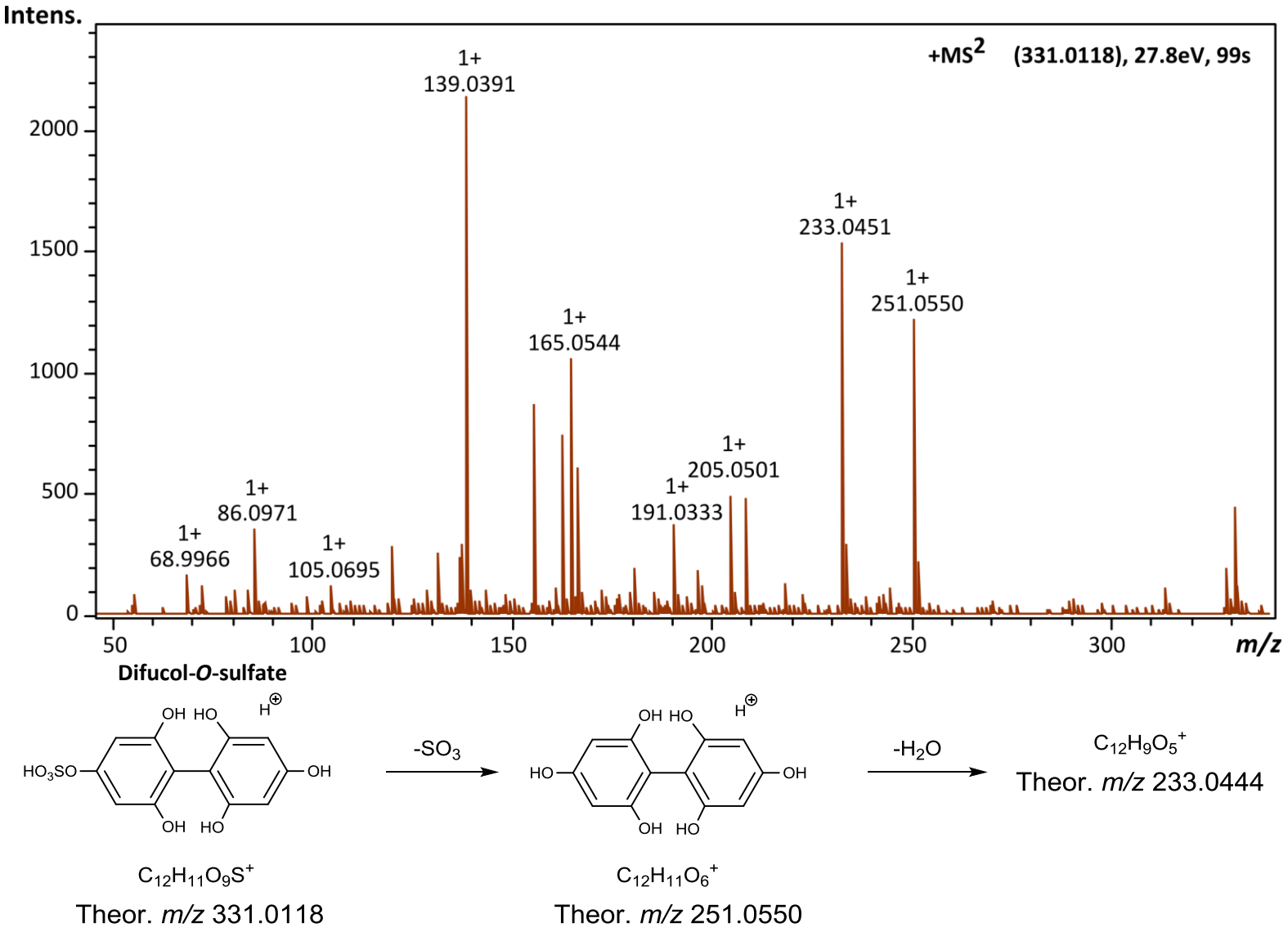

Figure SII.23. Seasonal variations (from February to July) of the epibacterial communities on *T. atomaria* at the class level

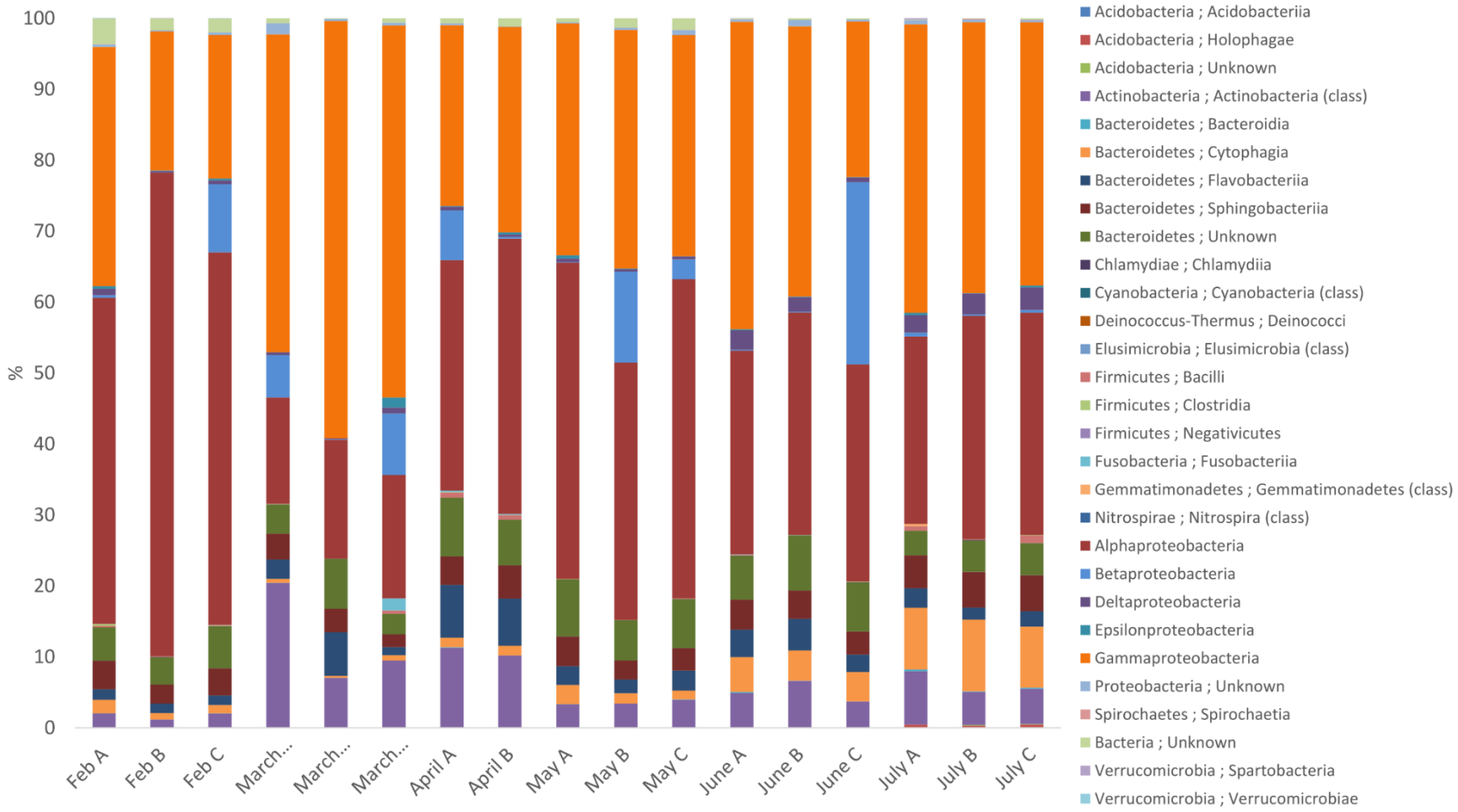

Figure SII.24. Seasonal variations of the relative abundance of the core microbiome of *T. atomaria*

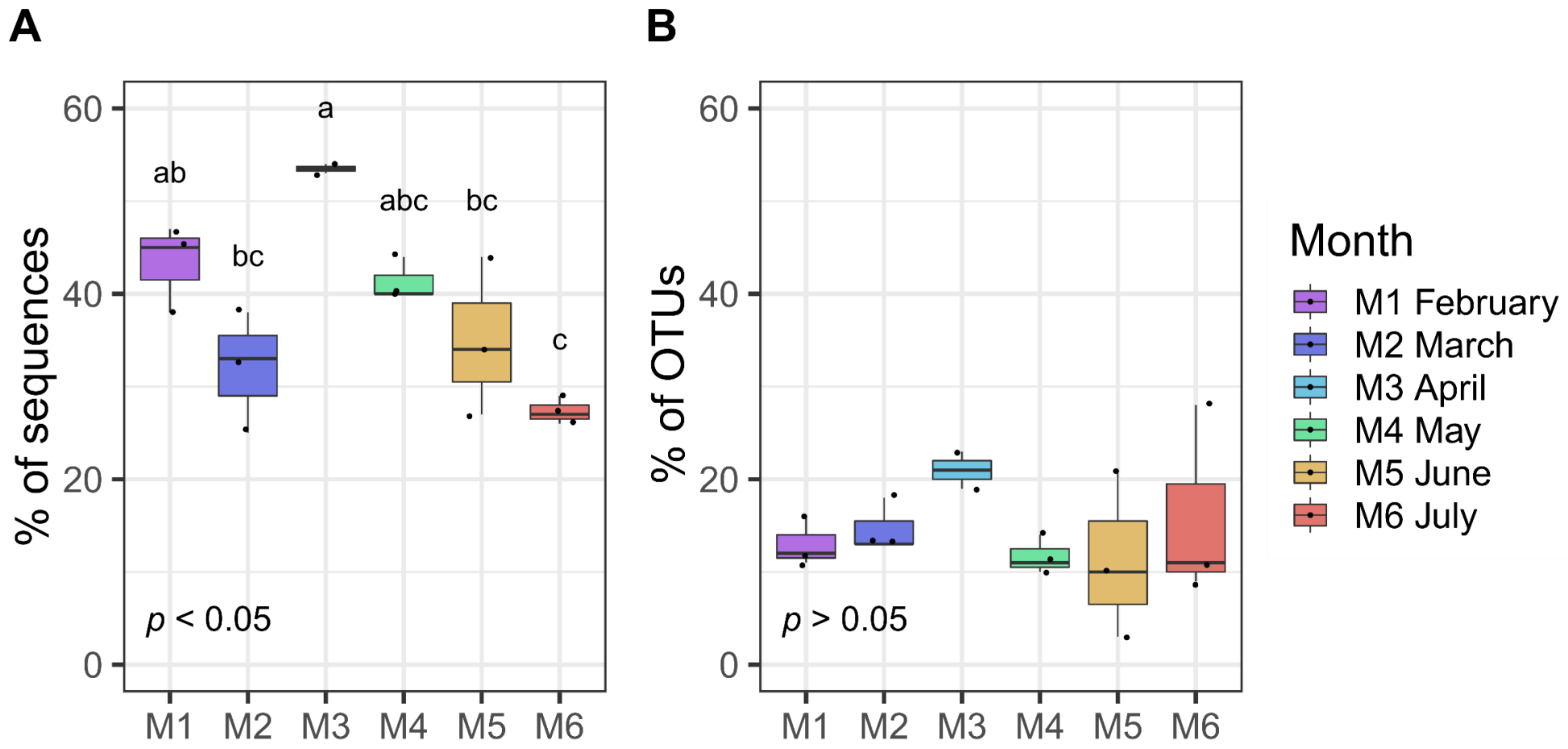

Figure SII.25. Heatmap representation of the seasonal correlation (multi-block PLS-DA) between significant OTUs and metabolites found at the surface of *T. atomaria*

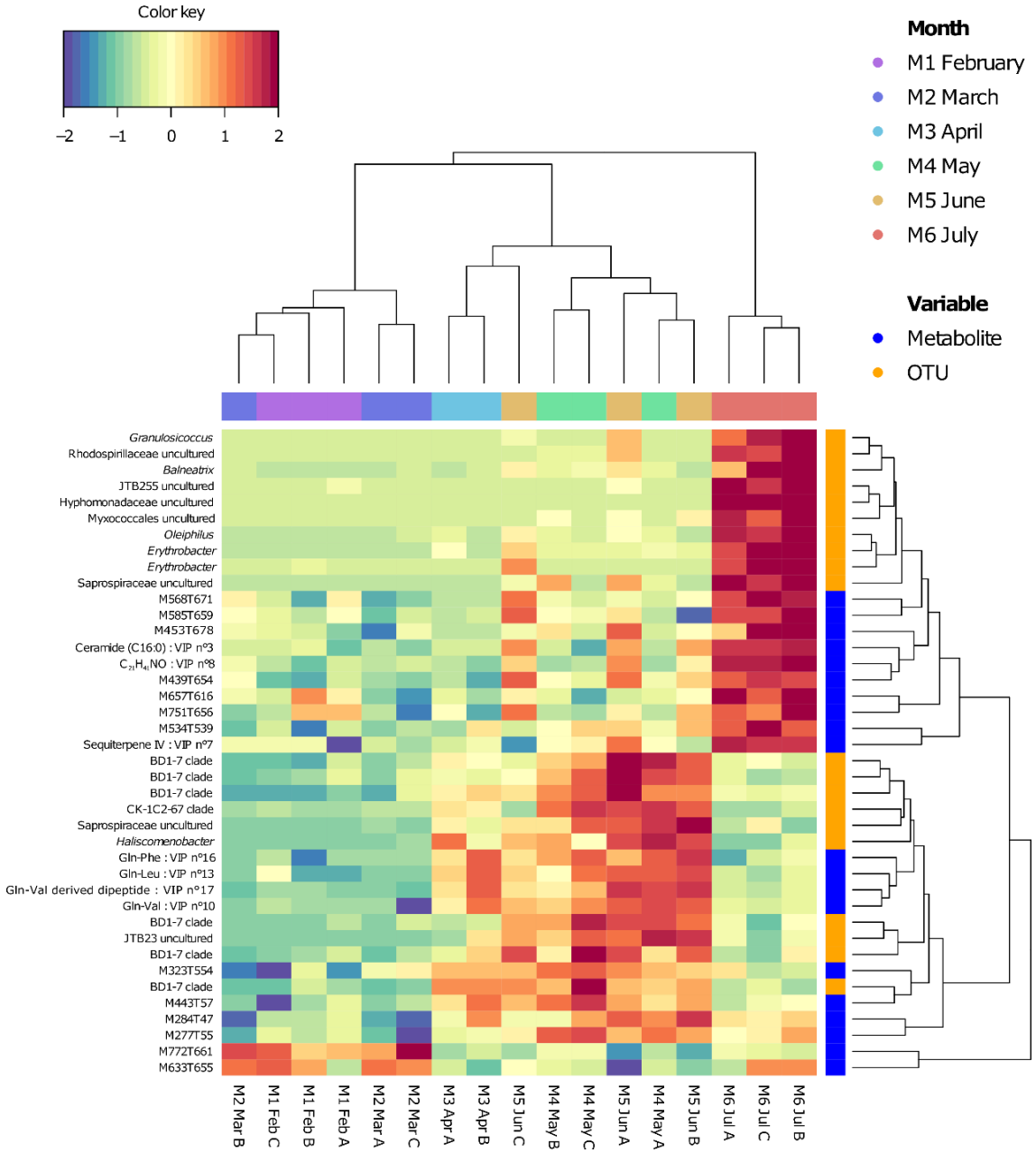

Annexe III

Supporting information

for

Host phylogeny and biogeography shape the microbiota and metabolome of the surface of the brown alga *Taonia* (Dictyotales)

Benoît Paix[1], Christophe Vieira[2], Philippe Potin[3], Catherine Leblanc[3], Olivier De Clerck[4], Jean-François Briand[1*], Gérald Culioli[1*]

[1] *Université de Toulon, Laboratoire MAPIEM, EA 4323, Toulon, France*

[2] *Kobe University Research Center for Inland Seas, Rokkodai, Kobe 657-8501, Japan*

[3] *Sorbonne Université, CNRS, Integrative Biology of Marine Models (LBI2M), Station Biologique de Roscoff (SBR), Roscoff, France*

[4] *Ghent University, Department of Biology, Phycology Research Group, Ghent, Belgium*

*corresponding authors : briand@univ-tln.fr, culioli@univ-tln.fr

Table SIII.1. Environmental parameters, sampling dates, and GPS coordinates of the collection sites of *Taonia*

Geographical area	Site abbreviation	Site name	GPS coordinates	Sampling date (dd/mm/yyyy)	Temperature (°C)	O_2 (%)	Turbidity (NTU)	Salinity (ppt)	pH -
Mediterranean coast	VILF	Villefranche-sur-Mer	43°41'34.8'' N ; 7°18'31.6'' E	30/05/2018	21.3	n.d.[a]	n.d.	37.8	8.2
	ANTB	Cap d'Antibes	43°34'23.2" N ; 7°07'37.6" E	30/05/2018	21.2	99.5	0.37	39.3	8.3
	THEO	Théoule-sur-Mer	43°31'24.2" N ; 6°56'37.2" E	30/05/2018	23.7	95.3	0.34	38.1	8.3
	DRAM	Le Dramont	43°25'11.2" N ; 6°51'30.7" E	30/05/2018	22.0	112.8	0.38	38.5	8.4
	STMA	Sainte Maxime	43°19'31.8" N ; 6°39'56.5" E	30/05/2018	23.3	122.8	0.40	38.7	8.6
	STCL	Saint-Clair (Le Lavandou)	43°08'16.0" N ; 6°22'41.8" E	30/05/2018	22.6	105.5	0.35	38.8	8.2
	TAMR	Tamaris	43°05'35.0" N ; 5°54'31.0" E	31/05/2018	21.0	85.3	0.31	38.5	8.3
	BRUS	Le Brusc	43°04'05.6" N ; 5°47'38.7" E	31/05/2018	22.0	81.5	0.31	39.0	8.2
	BAND	Bandol	43°07'47.8" N ; 5°45'07.2" E	31/05/2018	21.4	109.6	0.31	39.0	8.2
	CASS	Cassis	43°12'45.4" N ; 5°31'51.4" E	31/05/2018	21.3	11.7	0.31	38.6	8.3
	MRSL	Calanque Blanche (Marseille)	43°13'25.2" N ; 5°20'46.2" E	30/05/2018	21.9	99.5	0.35	37.6	8.3
	CERB	Cerbère	42°26'26.2" N ; 3°10'08.9" E	01/06/2018	21.7	117.6	0.32	36.6	8.5
	BANY	Banyuls	42°29'23.2" N ; 3°07'47.8" E	01/06/2018	22.5	121.7	0.31	37.2	8.5
	ADG	Agde	43°16'30.3" N ; 3°30'56.5" E	01/06/2018	23.0	103.2	0.31	38.6	8.4
	PRQN	Plage d'argent (Porquerolles island)	43°00'16.1" N ; 6°11'21.9" E	05/06/2018	21.1	93.0	0.31	38.3	8.2
	PRQS	Calanque du Brégançonnet (Porquerolles island)	42°59'41.7" N ; 6°10'53.3" E	05/06/2018	20.8	75.9	0.31	38.1	8.1
	LLND	La Londe	43°07'13.7" N ; 6°16'00.3" E	05/06/2018	22.1	118.1	0.31	38.0	8.3
	CARQ	Carqueiranne	43°05'12.2" N ; 6°05'02.1" E	05/06/2018	21.9	113.1	0.31	38.0	8.3
Brittany coast	LOCQ	Locquirec	48°41'39.9" N ; 3°41'50.7" W	16/06/2018	18.0	98.1	n.d.	35.2	8.3

[a] not determined (measures not performed).

Table SIII.2. SIMPER results of the most contributing genera to the dissimilarities of the epibacterial community between Mediterranean and Brittany samples of *Taonia*.

Only the first 50% of the cumulative contribution are shown. *p*-values were calculated with a permutation test (999 permutations).

Order	Family	Genus	Average contribution	SD[a]	Ratio	Average Mediterranean	Average Brittany	Cum. sum	*p*-value
Caulobacterales	Hyphomonadaceae	*Litorimonas*	6.5%	0.06	1.2	424	2424	9%	0.002
Alteromonadales	Alteromonadaceae	*Alteromonas*	6.0%	0.01	4.7	1	1859	18%	0.001
Thiohalorhabdales	Thiohalorhabdaceae	*Granulosicoccus*	4.9%	0.02	2.5	845	2331	25%	0.001
Rhodovibrionales	Kiloniellaceae	*Kiloniella*	4.5%	0.05	0.8	0	1383	31%	0.001
Caulobacterales	Hyphomonadaceae	*Hellea*	2.3%	0.02	1.0	131	809	35%	0.004
Flavobacteriales	Flavobacteriaceae	*Tenacibaculum*	1.8%	0.02	0.9	165	649	37%	0.044
Chitinophagales	Saprospiraceae	unknown genus	1.7%	0.01	1.3	1615	1419	40%	0.426
Flavobacteriales	Flavobacteriaceae	*Croceitalea*	1.7%	0.01	2.1	514	0	42%	0.005
Sphingomonadales	Sphingomonadaceae	*Sphingorhabdus*	1.6%	0.01	1.1	496	0	45%	0.173
Rhodobacterales	Rhodobacteraceae	unknown genus	1.2%	0.01	1.6	486	124	46%	0.050
Chitinophagales	Saprospiraceae	*Lewinella*	1.1%	0.01	1.2	513	193	48%	0.351

[a] Standard deviation.

Figure SIII.1. Photographs of the herbarium of *Taonia* specimens (part1).
Red and green labels correspond to sites from Mediterranean and Brittany coasts, respectively (see labels codes in Figure 1. Legend)

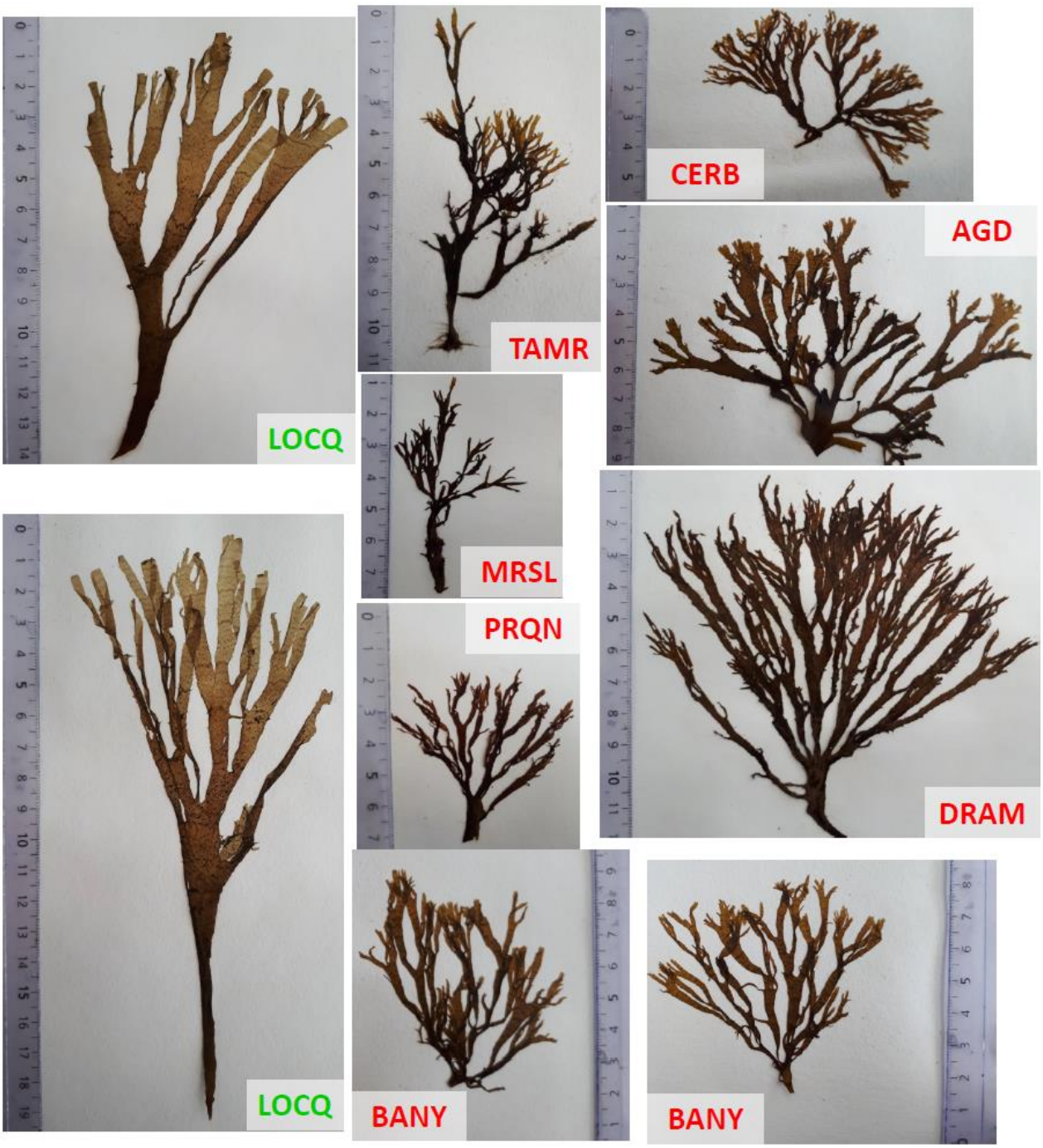

Figure SIII.1. Photographs of the herbarium of *Taonia* specimens (part2).
Red and green labels correspond to sites from Mediterranean and Brittany coasts, respectively (see labels codes in Figure 1. Legend)

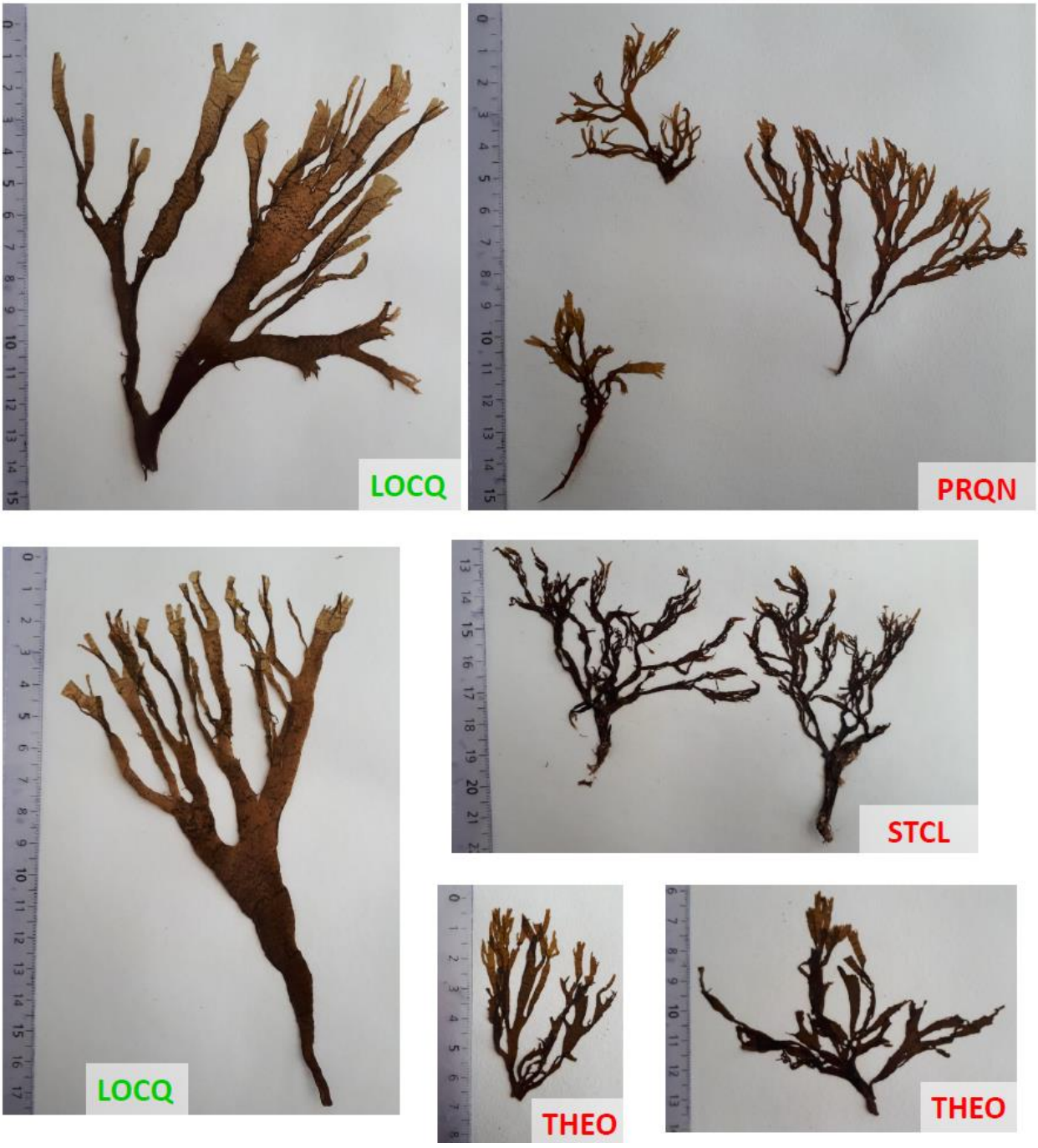

Figure SIII.2. Variations of cell densities and α-diversity indexes (Chao1 and Shannon) of the epiphytic community of samples of *Taonia* according to each sampling site.

p-values and lowercase letters (from **a** to **g**) correspond to the results of the comparison between sites with one-way ANOVA and post-hoc Tukey's tests, respectively.

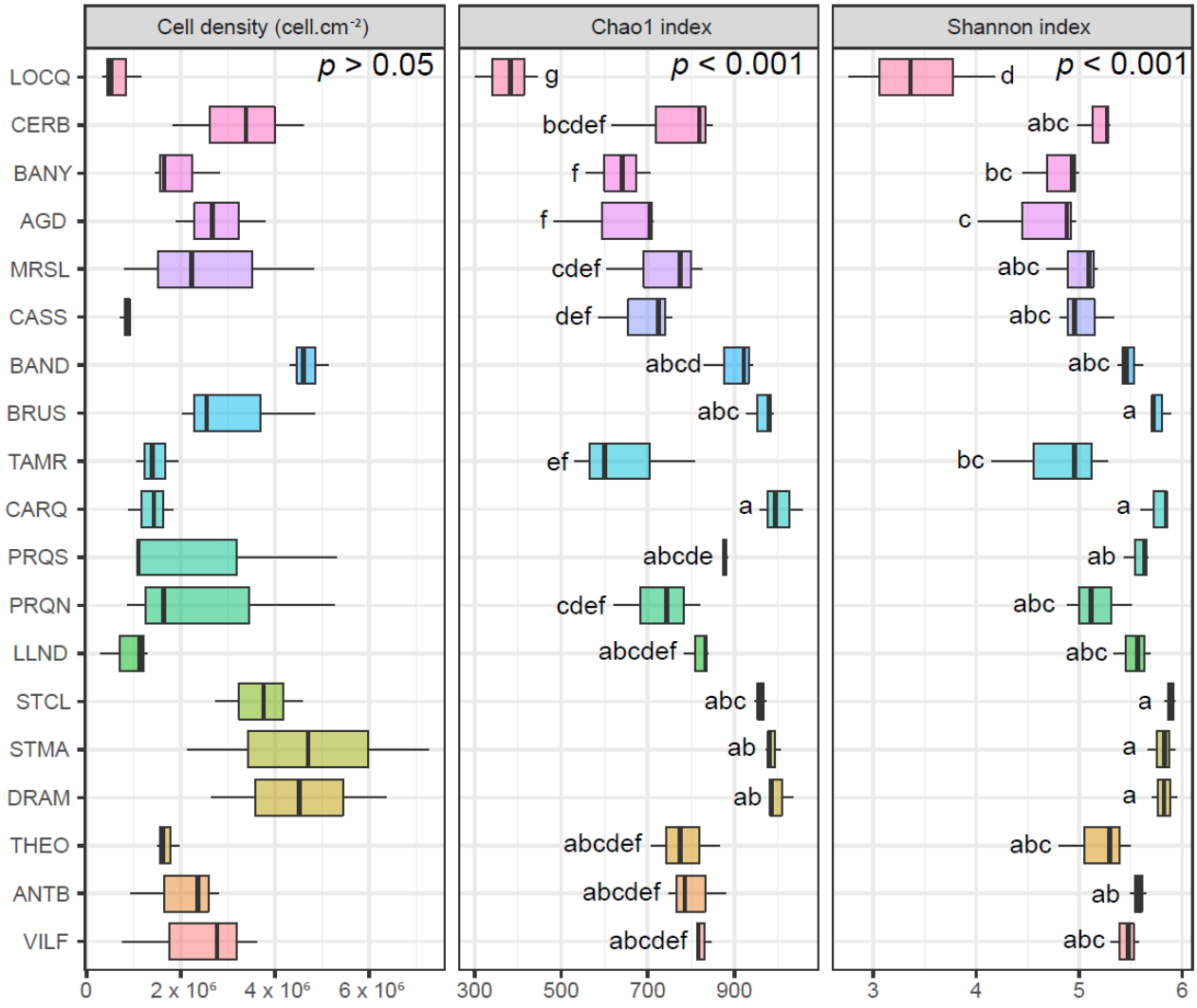

Figure SIII.3. Normalized concentration of the two most discriminant metabolites (*δ*-cadinene and fucoxanthin) involved in the discrimination between surface metabolomes of Mediterranean and Brittany samples of *Taonia*

p-values and lowercase letters (from **a** to **g**) correspond to the results of the comparison between sites with one-way ANOVA and Tukey's tests, respectively.

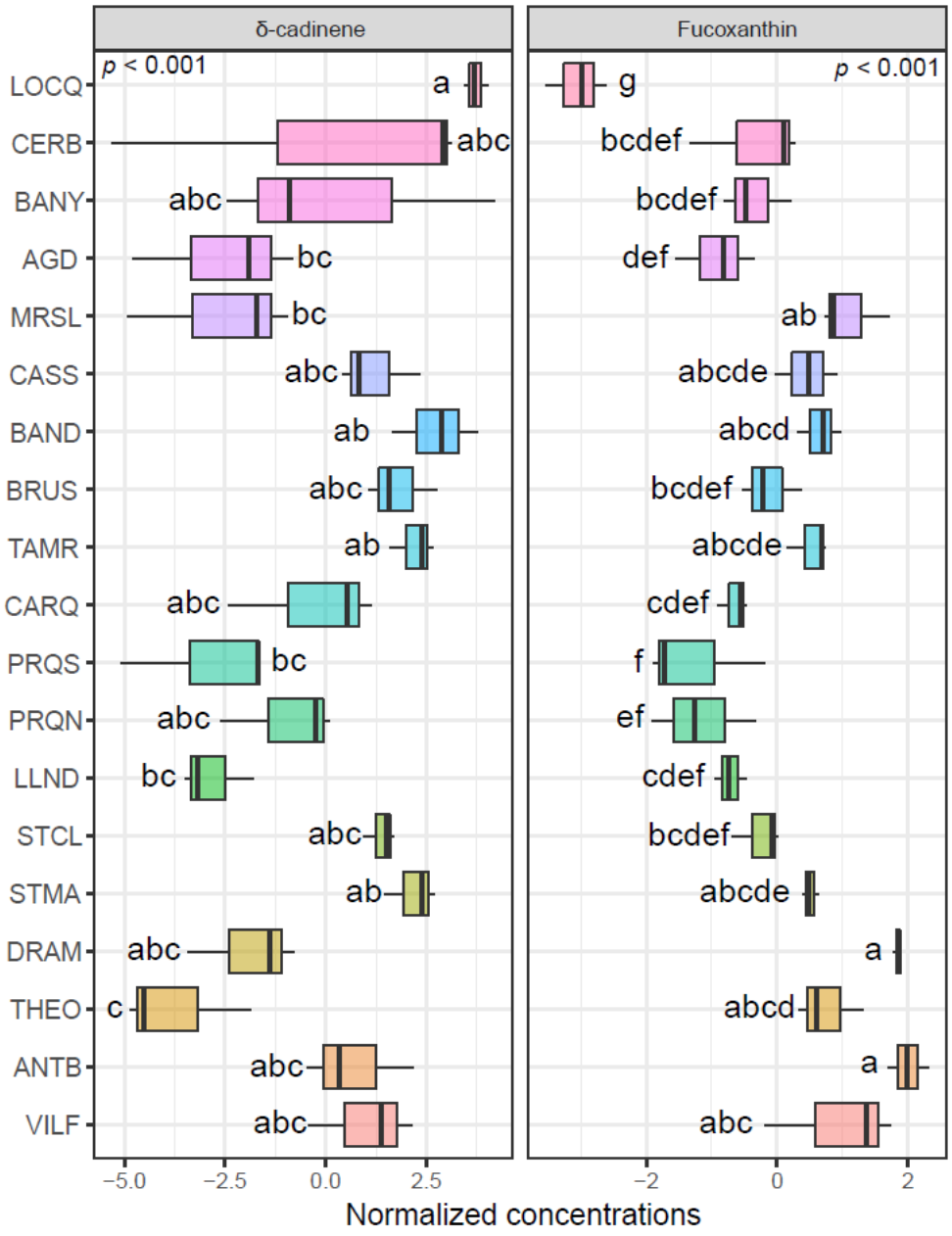

Annexe IV

Supporting information

for

Integration of LC/MS-based molecular networking and classical phytochemical approach allows in-depth annotation of the metabolome of non-model organisms - The case study of the brown seaweed Taonia atomaria

Nathan Carriot[a,1], Benoît Paix[a,1], Stéphane Greff[b], Bruno Viguier[a], Jean-François Briand[a], Gérald Culioli[a,*]

[a] Université de Toulon, MAPIEM, EA 4323, Toulon, France

[b] Aix Marseille Université, CNRS, IRD, Avignon Université, Institut Méditerranéen de Biodiversité et d'Ecologie marine et continentale (IMBE), Station marine d'Endoume, Marseille, France.

[1]These authors contributed equally to this work.

[*]Corresponding author.

E-mail address: culioli@univ-tln.fr (G. Culioli)

Supplementary tables

Table SIV.1. Summary of the 39 fractions obtained after Flash-chromatography

A: cadina-4(14),5-diene, **B**: cubebol, **C** : 4-*epi*-cubebol, **D** : (+)-gleenol, **E** : (1*S*, 5*E*, 7*S*) 1-acetoxygermacra-4(15),5,10(14)-triene, **F** : germacra-4(15),5,10(14)-trien-9-ol, **G** : geranylgeranylglycerol, **H** : dictyol A

Fraction number	Percentage of solvent used for Flash chromatography			Color of the fraction	Mass of the fraction (mg)	Fractions used for purification	Compounds purified	Fractions used for molecular networking approach
	CH_2Cl_2 (A)	MeOH (B)	Water (C)					
1	0	10	90	Transparent	>0.5			
2	0	10	90	Transparent	>0.5			
3	0	18	82	Light pink	>0.5			
4	0	27	73	Light purple	>0.5			
5	0	36	64	Light yellow	>0.5			
6	0	45	55	Light yellow	>0.5			
7	0	54	46	Light yellow	>0.5			
8	0	63	37	Light yellow	>0.5			
9	0	72	28	Light yellow	>0.5			
10	0	81	19	Light yellow	>0.5			X
11	0	90	10	Yellow - Orange	>0.5			
12	0	99	1	Yellow - Orange	22.1			
13	0	100	0	Orange	4.2			
14	0	100	0	Orange	11.5			X
15	0	100	0	Orange	98.9			X
16	0	100	0	Orange	241.3	X		X
17	0	100	0	Dark orange	326	X	D, E, G	X
18	0	100	0	Dark green	257.3	X	D, E, H	X
19	9	91	0	Green	215.5	X	A, B, C, D, E, F, G	X
20	19	81	0	Green	213.1	X	A, F	X
21	29	71	0	Light green	152.2	X	F	X
22	39	61	0	Light green	97.3			X
23	49	51	0	Green	64.1			X
24	59	41	0	Dark green	43.4			X
25	69	31	0	Dark green	53.2			X
26	79	21	0	Green - Dark orange	78.1			X
27	89	11	0	Green - Dark orange	131.7			X
28	99	1	0	Green - Dark orange	116.3			X
29	100	0	0	Green - Dark orange	32.4			
30	100	0	0	Green - Dark orange	28.4			
31	100	0	0	Yellow	20.1			
32	100	0	0	Yellow	10			
33	100	0	0	Light yellow	15.8			
34	100	0	0	Light yellow	7.5			
35	100	0	0	Light yellow	6.9			
36	100	0	0	Light yellow	11.4			
37	100	0	0	Light yellow	0.7			
38	100	0	0	Transparent	>0.5			
39	100	0	0	Transparent	>0.5			

Table SIV.2. Summary of tested parameters for the MN-1, 2 and 3

	MN-1	MN-2	MN-3
Minimum cosine score [a]	0.85	0.80	0.70
Minimum matched fragment ions [b]	10	8	6
Network TopK [c]	7	7	10

Descriptions of the following parameters according to the GNPs platform:

[a] **Minimum cosine score**: Minimum score that must occur between a pair of consensus MS/MS spectra in order for an edge to be formed in the molecular network. Default value is 0.7. Lower value will increase the size of the clusters by inducing the clustering of less related MS/MS spectra, higher value will limit do the opposite.

[b] **Minimum matched fragment ions**: Parameters used for molecular networking. Is the minimum number of common fragment ions that are shared by two separate consensus MS/MS spectra in order to be connected by an edge in the molecular network. A low value will permit linkages between spectra of molecules with few similar fragment ions, but it will result in many more less-related spectra being connected to the network. A higher value will do the opposite. Default value is 6, but note that these parameters should be adjusted depending on the experimental conditions for mass spectra acquisition (such as mode of ionization, fragmentation conditions, and the mobile phase, ...), and the collision-induced fragmentation behavior of the molecules of interest within the samples. High molecular weight (MW) compounds, and compounds with more hetero-atoms will generally tend to produce more fragment ions. However, this rule cannot be systematized. For example, some lipids with high MW generate only few fragment ions.

[c] **Network TopK**: Maximum number of neighbor nodes for one single node. The edge between two nodes are kept only if both nodes are within each other's TopK most similar nodes. For example, if this value is set at 20, then a single node may be connected to up to 20 other nodes. Keeping this value low makes very large networks (many nodes) much easier to visualize.

Supplementary figures

Figure SIV.1. Annotation of cluster 1A and proposed MS/MS fragmentation pattern for the compounds MGDG (18:4/18:1), SQDG(16:0/18:3) and TG (14:0/16:0/16:1)

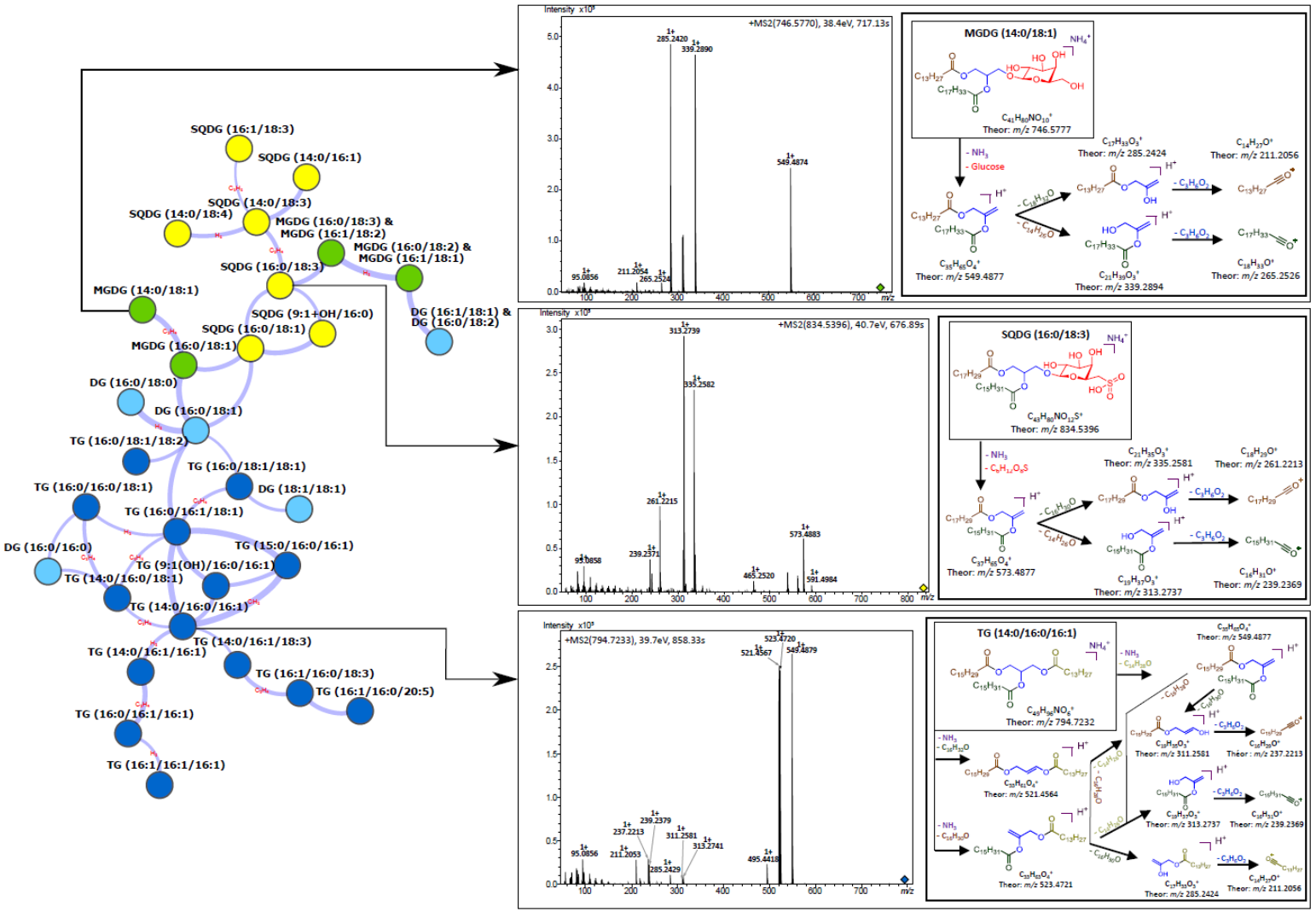

Figure SIV.2. MN1 representing nodes with a color gradient according to the retention time

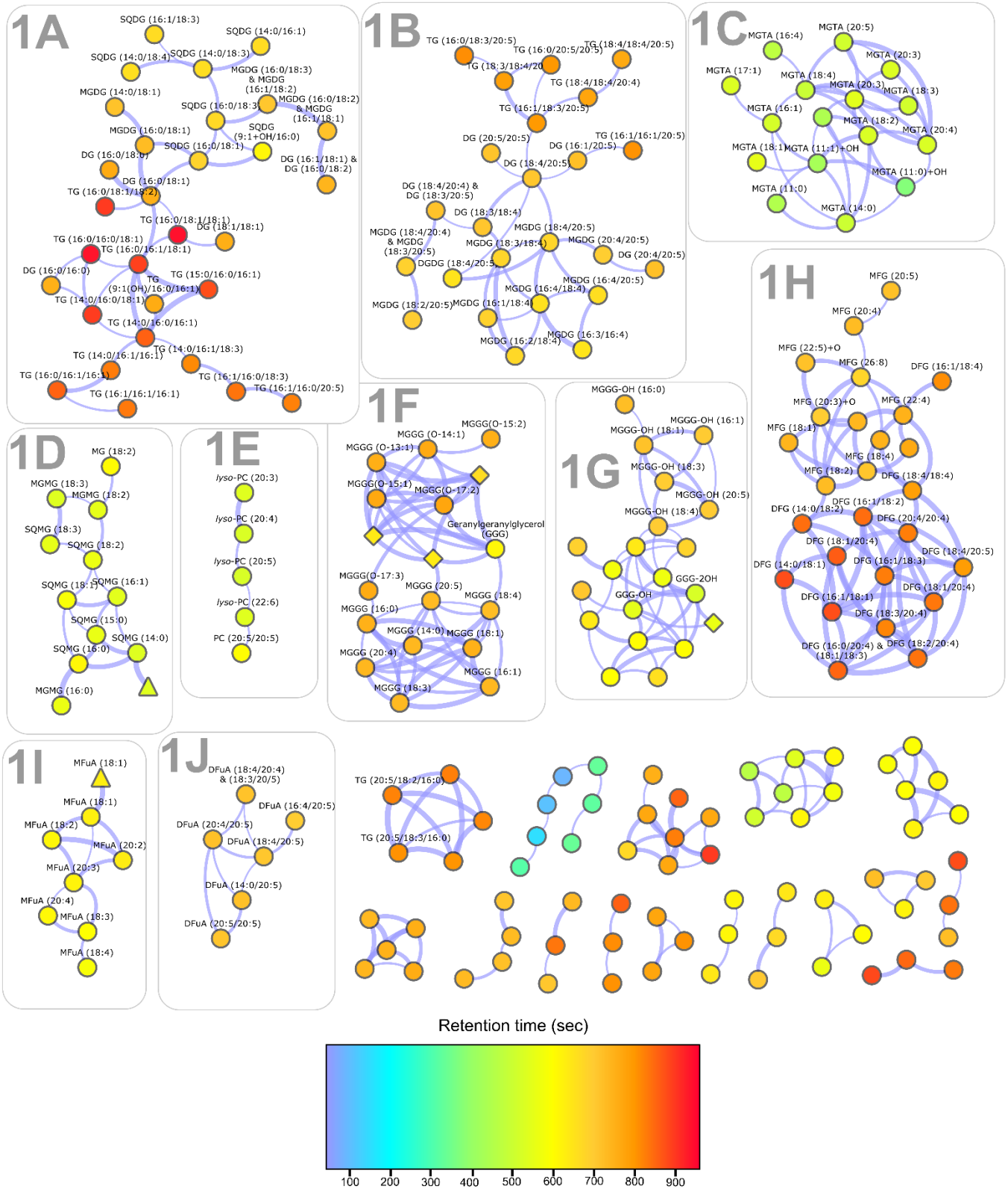

Figure SIV.3. Annotation of cluster 1B and proposed MS/MS fragmentation pattern for the compound DGDG (18:4/20:5)

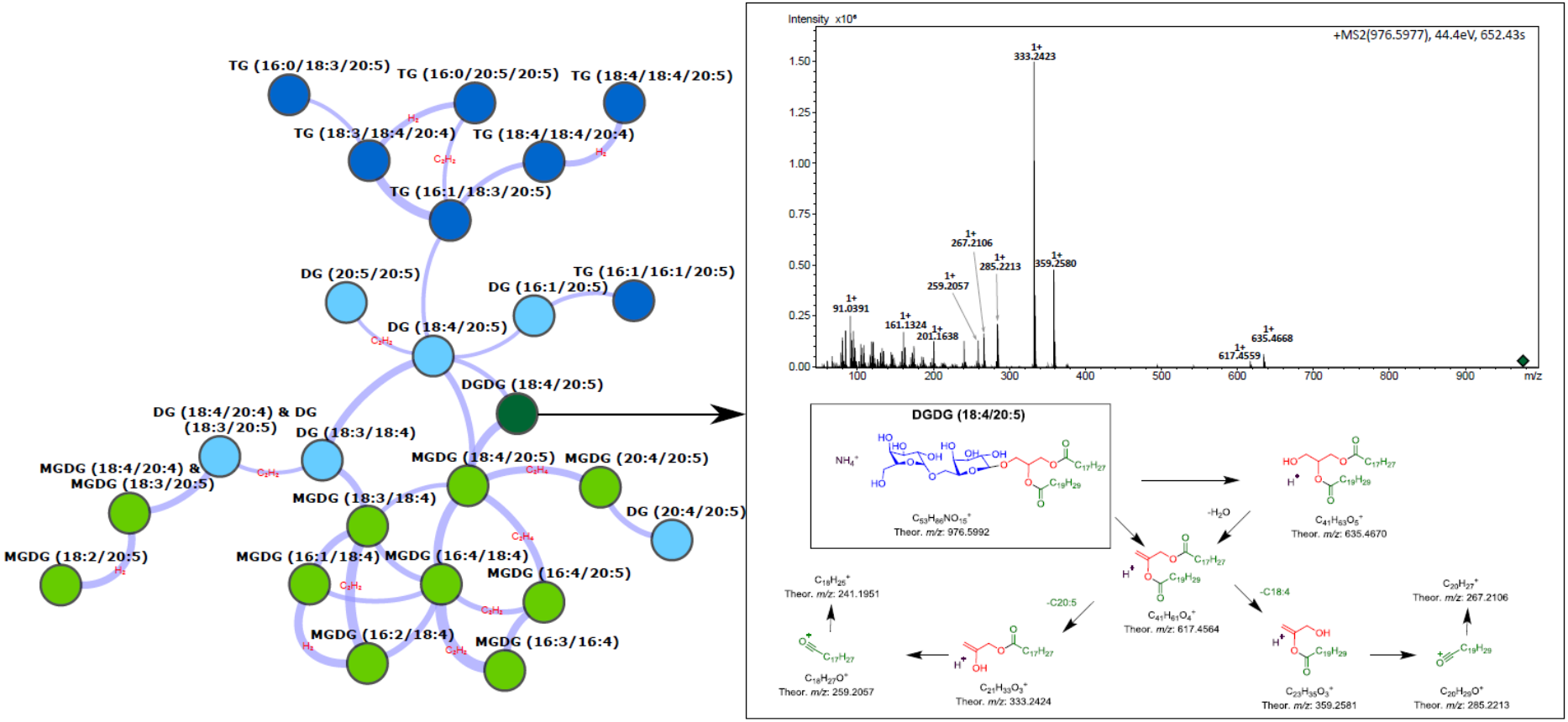

Figure SIV.4. Annotation of the cluster 1C and proposed MS/MS fragmentation pattern for the compound MGTA (14:0)

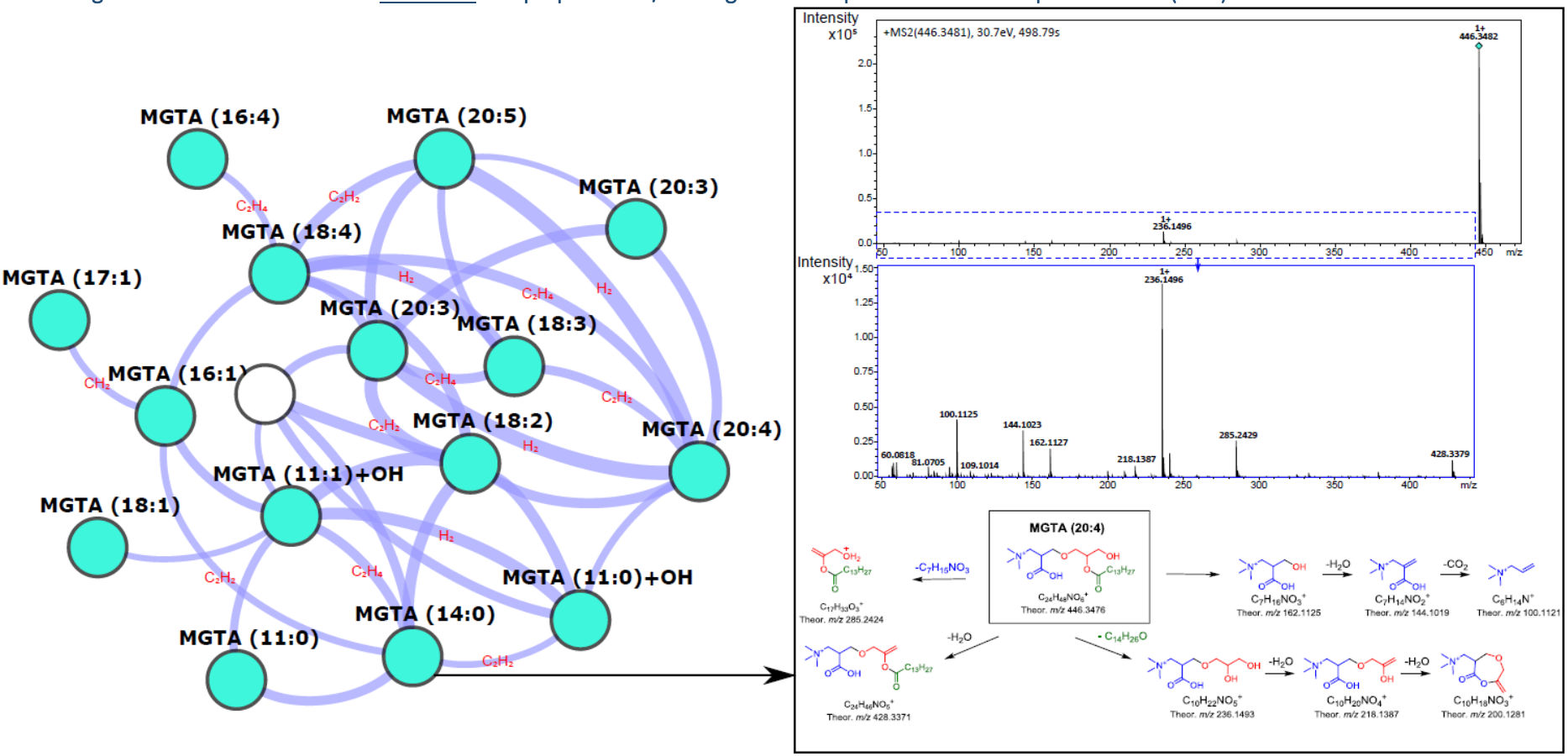

Figure SIV.5. Annotation of cluster 1D and proposed MS/MS fragmentation pattern for the compound SQMG (18:1)

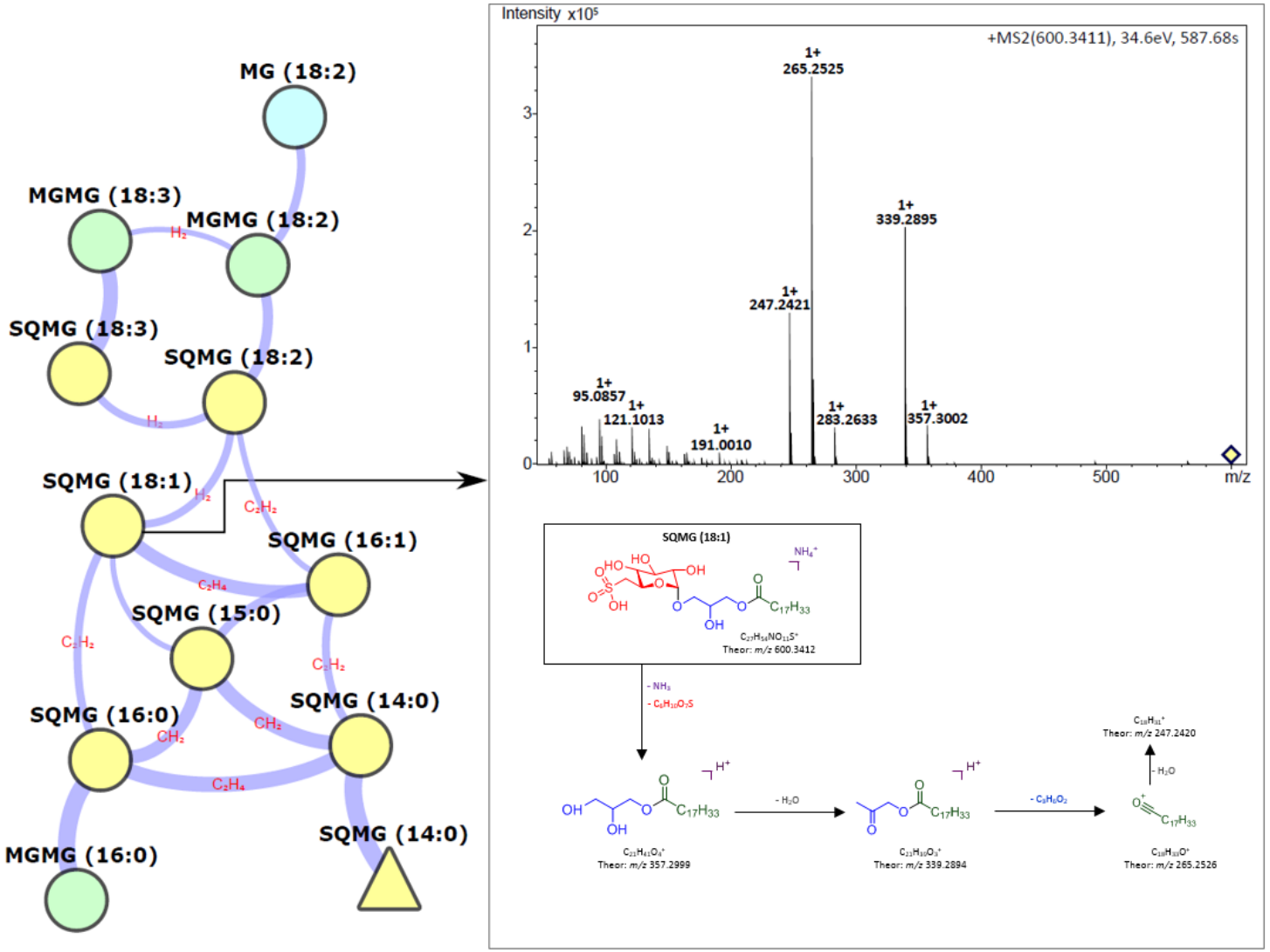

Figure SIV.6. Annotation of cluster 1E and proposed MS/MS fragmentation pattern for the compound *lyso*-PC (20:5)

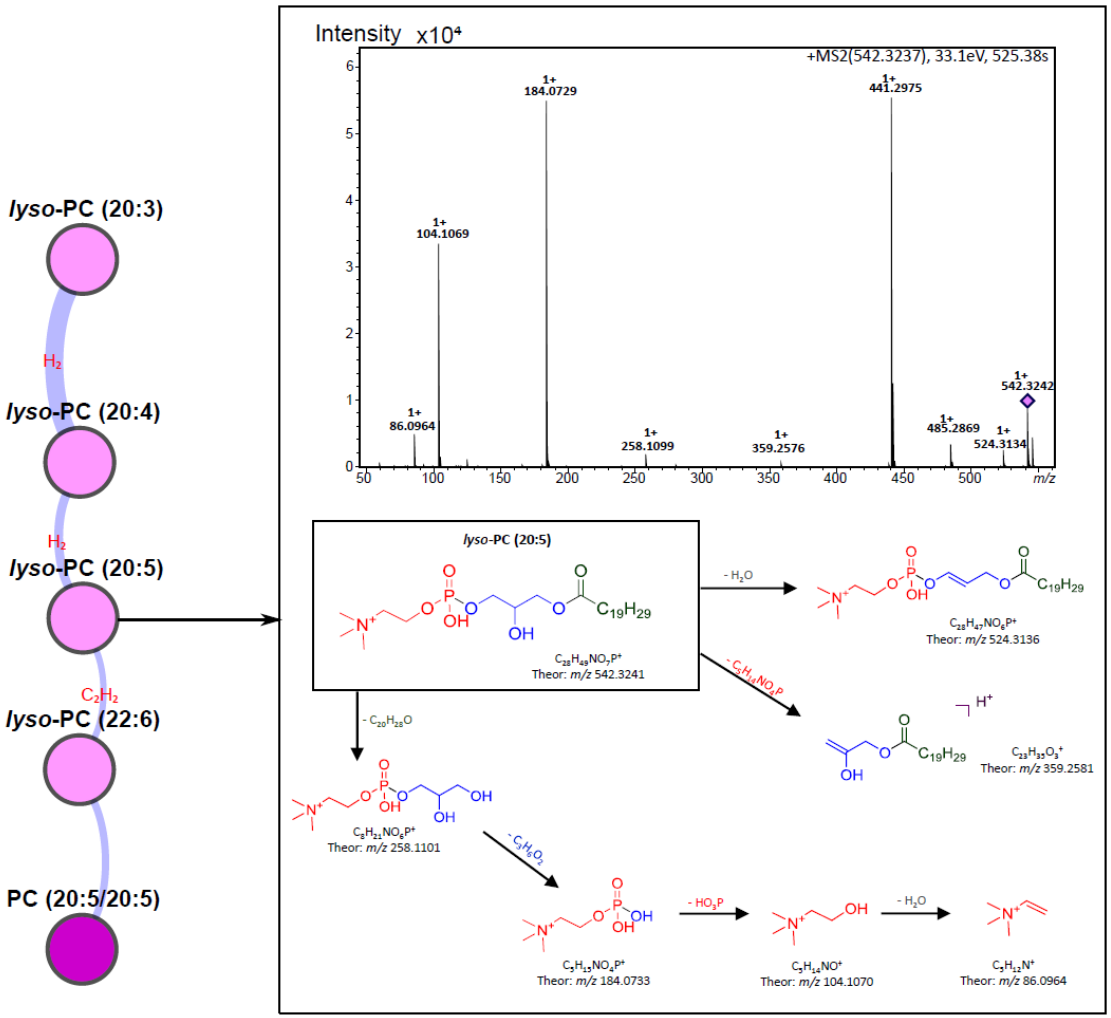

Figure SIV.7. Annotation of cluster 1H and proposed MS/MS fragmentation pattern for the compound MFG (18:1)

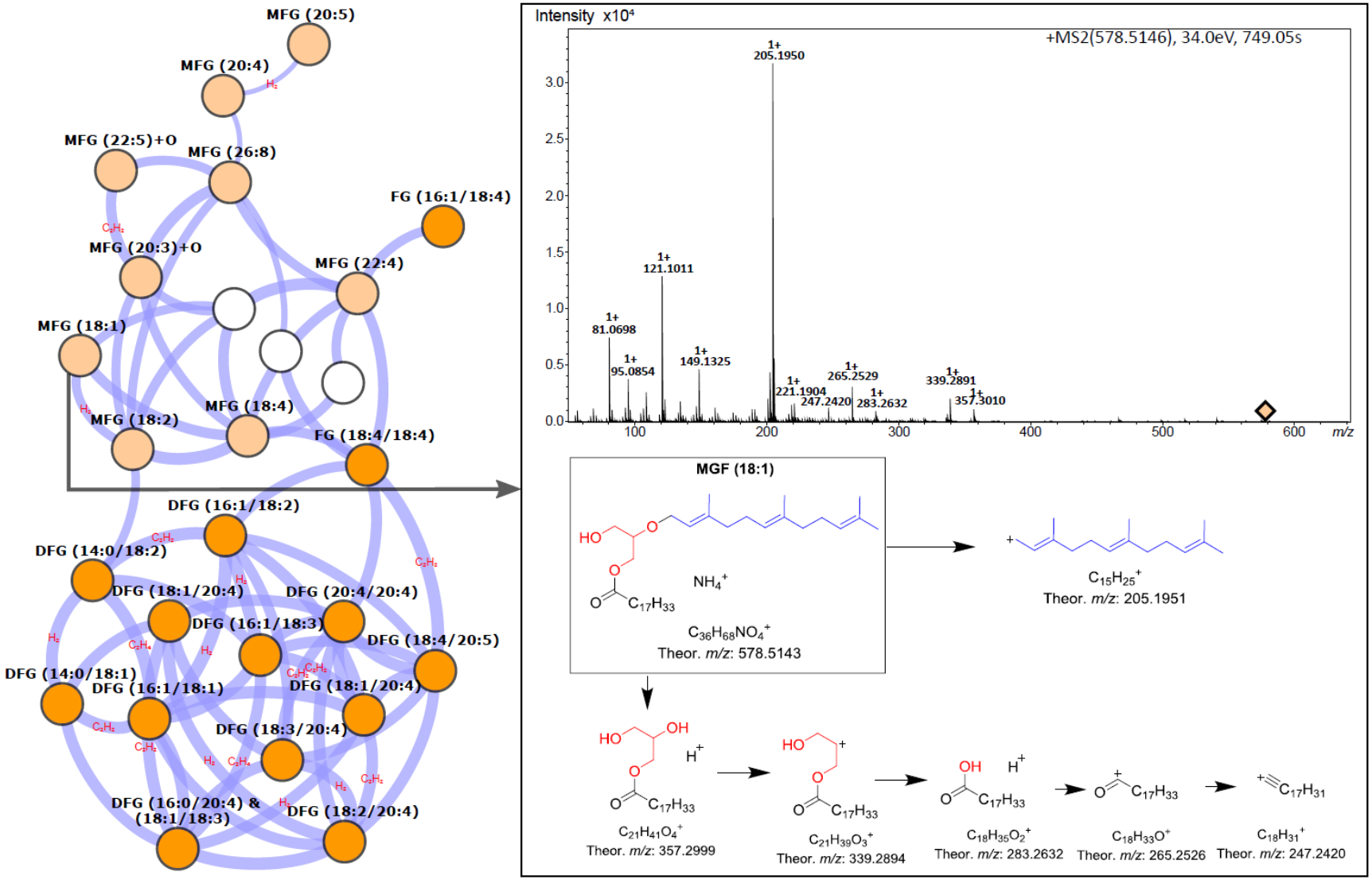

Figure SIV.8. Annotation of cluster 1l and proposed MS/MS fragmentation pattern for the compound MFuA (20:4)

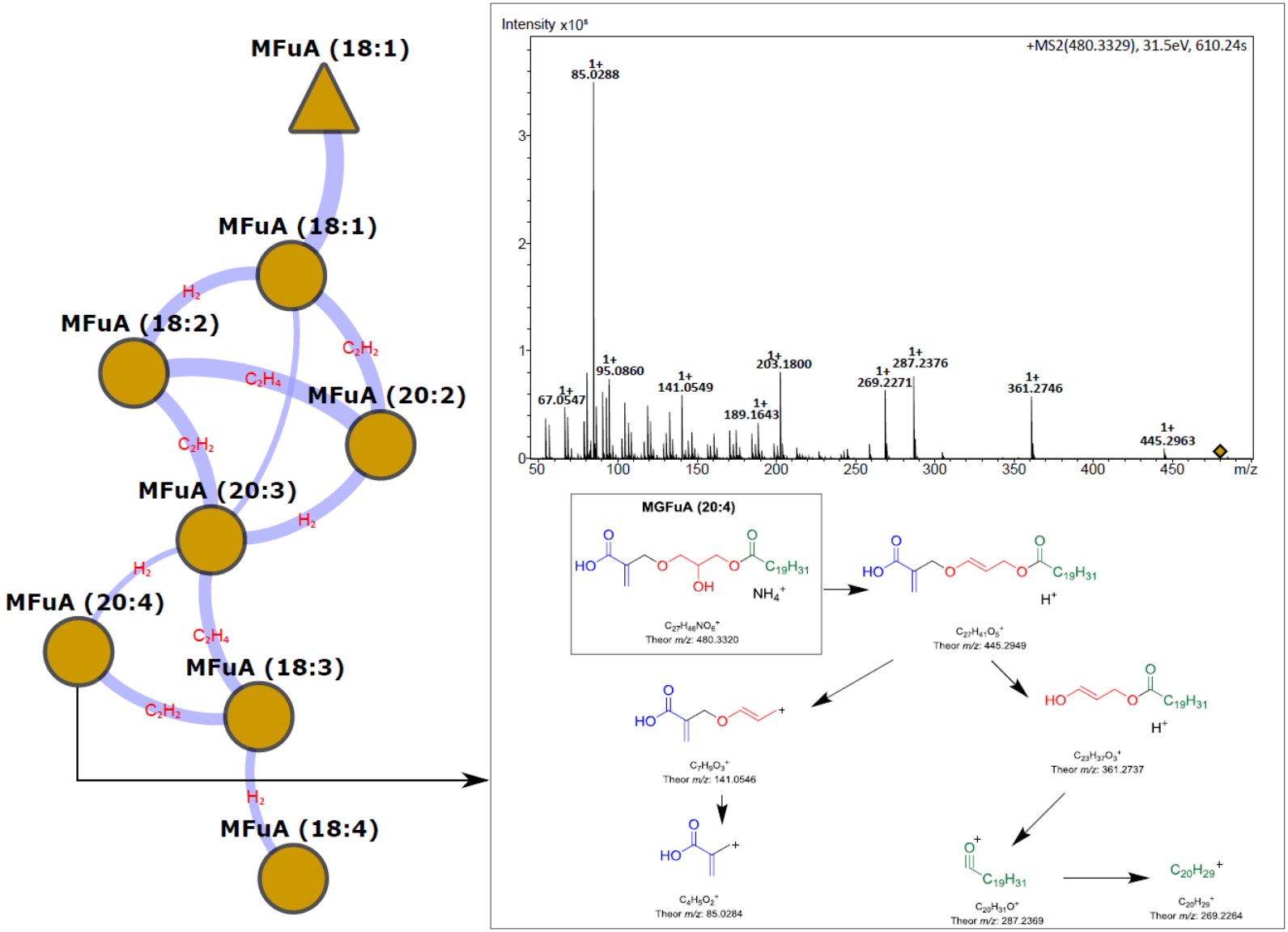

Figure SIV.9. Less restrained MN (MN-2) built with MS/MS data of fractions obtained from the crude extract of the brown alga *Taonia atomaria.*

Node colors were chosen according to their chemical classes (see color code in Table IV.1). Nodes with a diamond shape correspond to fragments ions, while those with a triangle shape are representing compounds with a distinct adduct from the rest of its cluster. Nodes with a thick border correspond to newly annotated compounds via the MN enlargement. Thickness of an edge between two nodes was proportional to the cosine score (CS, from 0.8 to 0.995). Only clusters with at least three nodes were represented. The whole network also includes 31 clusters of two nodes, together with 410 unbound nodes.

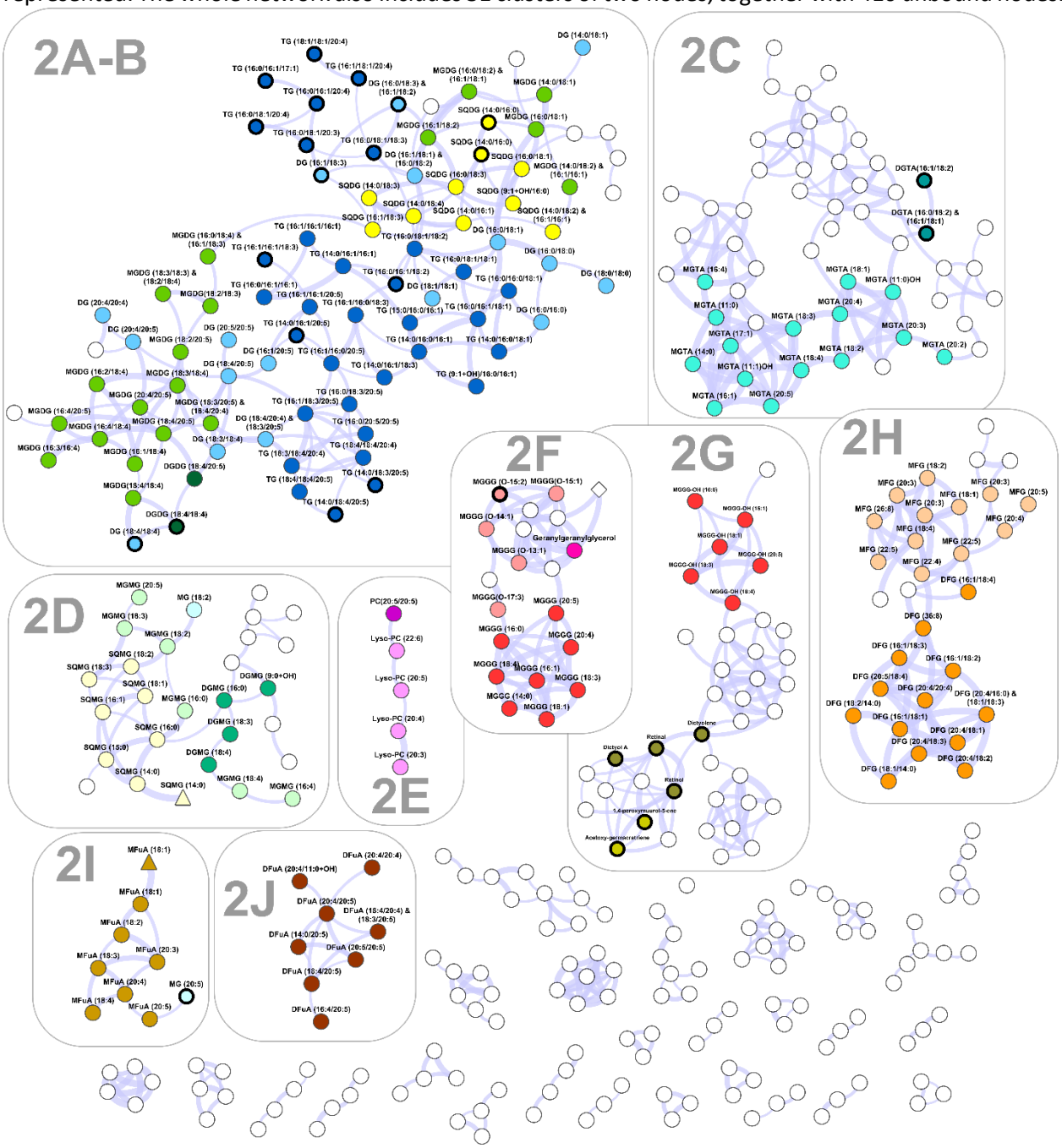

Annexe V

Supporting information

for

A multi-omics analysis suggests links between the differentiated surface metabolome and epiphytic microbiota along the thallus of a Mediterranean seaweed holobiont

Benoit Paix[1], Nathan Carriot[1], Raphaëlle Barry-Martinet[1], Stéphane Greff[2], Benjamin Misson[3], Jean-François Briand[1,*] and Gérald Culioli[1,*]

[1] Université de Toulon, MAPIEM, EA 4323, Toulon, France.

[2] CNRS, Aix Marseille Université, IRD, Avignon Université, Institut Méditerranéen de Biodiversité et d'Ecologie marine et continentale. Station marine d'Endoume, Marseille, France.

[3] Université de Toulon, Aix Marseille Université, CNRS, IRD, Mediterranean Institute of Oceanography (MIO), UM110, France.

[*]Corresponding authors: J.-F. Briand (briand@univ-tln.fr) and G. Culioli (culioli@univ-tln.fr)

Supplementary Materials & Methods

Supplementary information for LC-ESI-MS analyses

The UPLC-HRMS instrumentation consisted of a Dionex Ultimate 3000 Rapid Separation (Thermo Fisher Scientific, Waltham, MA, USA) chromatographic system equipped with a RS pump, a temperature-controlled autosampler, a thermostated column compartment and an UV-vis diode array detector. This system was coupled to a QToF Impact II mass spectrometer (Bruker Daltonics, Bremen, Germany). The analyses were performed using an analytical core-shell reversed-phase column (150 × 2.1 mm, 1.7 μm, Kinetex Phenyl-Hexyl equipped with a SecurityGuard cartridge, Phenomenex, Le Pecq, France) with a column temperature of 40°C and a flow rate of 0.5 mL.min^{-1}. The autosampler temperature was set at 4°C and the injection volume was 5 μL. Mobile phases were: (A) water and (B) acetonitrile (Chromasolv; Sigma-Aldrich-Merck, Darmstadt, Germany) containing each 0.1% (*v*/*v*) of formic acid (Ultra grade; Fluka, Fischer Scientific, Illkirch, France). The elution gradient started at 5% B and maintained for 2 min, then increased to 100% B (linear ramp) in 8 min and maintained for 4 min; then back to 5% B (linear ramp) over 0.01 min and maintained 1.99 min, for a total run time of 16 min.

The capillary voltage of the MS spectrometer was set at 4500V (positive mode), and the nebulizing parameters were set as follows: nebulizing gas (N_2) pressure at 0.4 bar, drying gas (N_2) flow at 4 L.min^{-1}, and drying temperature at 180°C. Mass spectra were recorded from *m/z* 50 to 1200 at a mass resolving power of 25 000 full width at half-maximum (FWHM, *m/z* = 200) and a frequency of 2 Hz. Tandem mass spectrometry analyses were performed thanks to a collision induced dissociation (CID) with a collision energy of 25 eV. A solution of formate/acetate forming clusters was automatically injected before each sample for internal mass calibration, and the mass spectrometer was calibrated with the same solution before each sequence of samples. Data handling was done using DataAnalysis software (version 4.3, Bruker Daltonics).

Supplementary information for GC-MS analyses

Separation of metabolites was performed on a HP-5MS 5% Phenyl-Methyl Silox column (30 m × 0.25 mm, 0.25 μm; Agilent Technologies, Santa Clara, CA, USA) with helium as mobile phase. The run started at 40°C for 5 min and increased by 10°C.min^{-1} up to 350°C for a total runtime of 31 min. A constant flow rate was set to 1 mL min^{-1}. A volume of 1 μL of each sample was injected in splitless mode and the injector temperature was set at 250°C. A solution with a mix of C_8-C_{20} alkanes (Fluka) was also injected for the determination of retention indices.

Supplementary information for annotation procedure

In this study, three levels of annotation were applied for the identification of metabolites, following the same methodology described in Paix et al., 2019.

The first approach, which corresponds to the level 1 of annotation according to Schymanski et al., 2014) was based on the use of several commercial standards described in Paix et al., 2019, as well as compounds previously purified from *T. atomaria* or *Dictyota* spp. by our team (Viano et al., 2009; Othmani et al., 2016b). These standards were solubilized in MeOH at a concentration of 0.1 mg.mL^{-1} and analyzed with the same experimental conditions used for the three metabolomics workflows.

The second strategy was to annotate putatively some *m/z* features by the comparison of their MS (and MS/MS for LC-MS analyses) data with reference databases. A match found with a MS (and MS/MS) library is considered with the level 2 of annotation. To facilitate the dereplication procedure with the two LC-MS datasets, the molecular networking approach was used, allowing the clustering of metabolites with a similar chemical structure in a same sub-network (cluster). Briefly, molecular networks were generated using GNPS platform with surface and total extracts (https://gnps.ucsd.edu/ProteoSAFe/static/gnps-splash.jsp, Wang et al., 2016). MS/MS raw data (.mzxml files) were clustered using MS cluster with a tolerance of 0.02 Da for precursor ions and 0.02 Da for MS/MS fragment ions. Minimum cosine score (CS) value used for the clustering was set to 0.7. Data were exported and analyzed using Cytoscape (v. 3.4.0). Positive and negative LC-ESI-MS/MS molecular networks were then analyzed and annotated based on MS/MS fragmentation pathways and comparison with in-house and public databases such as Metlin (https://metlin.scripps.edu/) or Lipidmaps (https://www.lipidmaps.org/).

When no characteristic fragmentation pathway was determined by comparison to the literature, the most probable chemical formula was proposed using the *Smart Formula* tool from DataAnalysis. This last step finally corresponded to the level 4 of annotation.

References

Othmani, A., Bunet, R., Bonnefont, J.-L., Briand, J.-F., and Culioli, G. (2016). Settlement inhibition of marine biofilm bacteria and barnacle larvae by compounds isolated from the Mediterranean brown alga *Taonia atomaria*. *J Appl Phycol* 28, 1975–1986. doi:10.1007/s10811-015-0668-4.

Paix, B., Othmani, A., Debroas, D., Culioli, G., and Briand, J.-F. (2019). Temporal covariation of epibacterial community and surface metabolome in the Mediterranean seaweed holobiont *Taonia atomaria*. *Environ. Microbiol.* 21, 3346–3363. doi:10.1111/1462-2920.14617.

Schymanski, E. L., Jeon, J., Gulde, R., Fenner, K., Ruff, M., Singer, H. P., et al. (2014). Identifying small molecules via high resolution mass spectrometry: Communicating confidence. *Environ. Sci. Technol.* 48, 2097–2098. doi:10.1021/es5002105.

Viano, Y., Bonhomme, D., Camps, M., Briand, J.-F., Ortalo-Magné, A., Blache, Y., et al. (2009). Diterpenoids from the Mediterranean brown alga *Dictyota* sp. evaluated as antifouling substances against a marine bacterial biofilm. *J. Nat. Prod.* 72, 1299–1304. doi:10.1021/np900102f.

Wang, M., Carver, J. J., Phelan, V. V., Sanchez, L. M., Garg, N., Peng, Y., et al. (2016). Sharing and community curation of mass spectrometry data with Global Natural Products Social Molecular Networking. *Nat. Biotechnol.* 34, 828–837. doi:10.1038/nbt.3597.

Supplementary Tables

Table SV.1. Parameters used for metabolomics data processing (part 1)

XCMS 3.0 parameters used for LC-ESI-MS data processing	**Selected parameters**
Extraction method for peaks detection	CentWave
Max tolerated ppm *m/z* deviation in consecutive scans in ppm	2
Min,Max peak width in seconds	2,20
Signal to Noise ratio cutoff	10
Prefilter step for for the first analysis step (ROI detection)	0,0
Method to use for first grouping	PeakDensity
Bandwidth	10* / 30**
Minimum fraction of samples	0.5
Minimum number of samples	1
Width of overlapping *m/z* slices	0.25
Maximum number of groups to identify in a single *m/z* slice	50
Method to use for retention time correction	Obiwarp
Bin size (in *m/z* dimension) to be used for the profile matrix generation	1
Method to use for second grouping	PeakDensity
Bandwidth	10
Minimum fraction of samples	0.5
Minimum number of samples	1
Width of overlapping *m/z* slices	0.25
PeakDensityAdv	
Maximum number of groups to identify in a single *m/z* slice	50
Fill peaking	
Value by which the *m/z* width of peaks should be expanded	0
Value by which the RT width of peaks should be expanded	0
Specifying a ppm by which the *m/z* width of the peak region should be expanded	0

* Value used for LC-(+)-ESI-MS dataset ; ** Value used for LC-(-)-ESI-MS dataset

Table SV.1. Parameters used for metabolomics data processing (part 2)

Erah parameters used for GC-MS data processing	**Selected parameters**
Peaks detection and deconvolution	
Minimum peak width	2.5
Minimum peak height	2500
Noise threshold	500
m/z to exclude	c(73:75,147:149,207:208)
Alignment	
Minimum correlation between spectra	0.90
Maximal time of misalignment	20
m/z range	40:500
Missing compound recovery	
Minimum number of samples	3

Table SV.2. Surfaces of the thallus parts used for metabolomics and sum of the chromatographic peak areas (surface extracts, LC-(+)-ESI-MS)

Site	Thallus part	Replicate	Surface of the thallus part (cm^2)	Sum of the chromatographic peak areas
Carqueiranne	Basal	R1	0.86	68 637 650
		R2	1.00	78 057 335
		R3	1.01	82 430 445
	Median	R1	1.66	81 888 073
		R2	1.55	89 157 091
		R3	2.42	98 612 317
	Apical	R1	1.90	82 826 045
		R2	3.10	103 448 844
		R3	3.40	117 397 130
Tamaris	Basal	R1	6.37	186 913 438
		R2	2.41	113 964 760
		R3	3.89	128 462 240
		R4	2.55	122 817 686
		R5	2.79	115 003 896
	Median	R1	5.92	183 219 063
		R2	9.62	201 502 962
		R3	6.12	194 114 469
		R4	5.22	147 675 204
		R5	2.72	111 884 657
	Apical	R1	6.02	157 565 425
		R2	10.27	230 346 718
		R3	4.28	153 539 839
		R4	3.64	118 921 859
		R5	8.14	182 534 138

Table SV.3. Summary of PERMANOVA results examining the effect of "site" and "sample types" factors for of the 16S rRNA gene dataset.
D. f; MS; F; R^2 and P correspond to degrees of freedom; mean square; F ratio; coefficient of determination and *p* value, respectively

	D. f	MS	F	R^2	*p value*
Site	1	0.44573	6.5772	0.10667	0.001
Sample type	4	0.4745	7.0017	0.4542	0.001
Site:Sample type	4	0.11992	1.7695	0.11479	0.012
Residuals	20	0.06777	0.32435		
Total	29			1	

Table SV.4. Multivariate pairwise results (*p* values) examining differences between both sites and between each sample types, for of the 16S rRNA gene dataset.

Comparison type	Samples compared	*p* values
Site comparison	Carqueiranne vs Tamaris	0.002853067
Sample type comparison	Basal vs median parts	0.12997305
	Basal vs apical parts	0.01248217
	Basal part vs seawater	0.00815162
	Basal part vs rocky surfaces	0.00815162
	Median vs apical parts	0.31954351
	Median parts vs seawater	0.00815162
	Median parts vs rocky surfaces	0.00815162
	Apical parts vs seawater	0.00815162
	Apical parts vs rocky surfaces	0.00815162
	Rocky surfaces vs seawater	0.00815162

Table SV.5. SIMPER results of the most contributing genera to the dissimilarities between water samples and algal samples collected at Carqueiranne. Only the first 50% of the cumulative contribution is showed. *p* values were calculated with a permutation test constructed with 999 permutations.

Order	Family	Genus	Average contribution	SD	Ratio	Av. water samples	Av. thallus samples	Cum. sum	*p* value
Synechococcales	Cyanobiaceae	*Synechococcus CC9902*	10.9%	0.10	1.09	1293	1	13.9%	0.008
Flavobacteriales	Flavobacteriaceae	*Algitalea*	5.1%	0.03	1.86	1	609	20.4%	0.009
Flavobacteriales	Flavobacteriaceae	*Polaribacter*	4.4%	0.06	0.75	543	38	26.0%	0.034
Chitinophagales	Saprospiraceae	unknown genus	3.3%	0.01	4.15	46	435	30.1%	0.020
Rhodobacterales	Rhodobacteraceae	*Litorimicrobium*	2.9%	0.02	1.65	357	8	33.9%	0.002
Pirellulales	Pirellulaceae	unknown genus	2.7%	0.02	1.52	324	0	37.3%	0.018
Chitinophagales	Saprospiraceae	*Lewinella*	2.2%	0.01	3.22	5	262	40.1%	0.001
Caulobacterales	Hyphomonadaceae	unknown genus	2.0%	0.01	3.38	12	253	42.7%	0.001
Chitinophagales	unknown family	unknown genus	1.7%	0.01	2.03	2	205	44.9%	0.011
Rhodobacterales	Rhodobacteraceae	unknown genus	1.7%	0.01	2.12	100	302	47.0%	0.622
Rhodobacterales	Rhodobacteraceae	*Planktotalea*	1.6%	0.01	2.72	244	50	49.1%	0.003

Table SV.6. SIMPER results of the most contributing genera to the dissimilarities between water samples and algal samples collected at Tamaris.

Only the first 50% of the cumulative contribution was showed. *p* values were calculated with a permutation test constructed with 999 permutations.

Order	**Family**	**Genus**	**Average contribution**	**SD**	**Ratio**	**Av. water samples**	**Av. thallus samples**	**Cum. sum**	***p* value**
Synechococcales	Cyanobiaceae	*Synechococcus*	9.0%	0.07	1.24	1067	1	10.3%	0.063
SAR11 clade	Clade I	Clade Ia	3.9%	0.05	0.81	462	0	14.7%	0.003
Thiohalorhabdales	Thiohalorhabdaceae	*Granulosicoccus*	3.3%	0.02	1.72	13	407	18.5%	0.019
Chitinophagales	Saprospiraceae	unknown genus	3.3%	0.02	2.18	16	406	22.3%	0.025
Flavobacteriales	Flavobacteriaceae	NS5 marine group	3.2%	0.02	1.75	385	1	26.0%	0.002
Rhodobacterales	Rhodobacteraceae	unknown genus	3.2%	0.02	1.40	80	447	29.6%	0.027
Caulobacterales	Hyphomonadaceae	*Litorimonas*	2.8%	0.03	0.94	2	331	32.8%	0.125
Pirellulales	Pirellulaceae	unknown genus	2.8%	0.03	1.02	329	0	36.0%	0.017
Synechococcales	Synechococcales Incertae Sedis	*Schizothrix*	2.7%	0.03	0.78	3	318	39.0%	0.141
Flavobacteriales	Flavobacteriaceae	NS4 marine group	2.2%	0.01	1.53	266	1	41.5%	0.002
Rhizobiales	Rhizobiaceae	*Nitratireductor*	1.9%	0.04	0.52	22	232	43.7%	0.144
Rhodobacterales	Rhodobacteraceae	*Planktomarina*	1.7%	0.01	2.32	202	1	45.7%	0.001
Rhodobacterales	Rhodobacteraceae	HIMB11	1.6%	0.02	0.72	191	0	47.5%	0.006
Betaproteobacteriales	Burkholderiaceae	*Limnobacter*	1.6%	0.02	0.69	191	0	49.3%	0.096
Cellvibrionales	Halieaceae	OM60(NOR5) clade	1.4%	0.01	1.60	171	2	51.0%	0.002

Table SV.7. SIMPER results of the most contributing genera to the dissimilarities between rocky biofilms and algal samples collected at Carqueiranne. Only the first 50% of the cumulative contribution was showed. *p* values were calculated with a permutation test constructed with 999 permutations.

Order	Family	Genus	Average contribution	SD	Ratio	Av. rocky biofilms	Av. thallus samples	Cum. sum	*p* value
Flavobacteriales	Flavobacteriaceae	*Algitalea*	5.1%	0.03	1.86	2	609	8.8%	0.005
Rhodobacterales	Rhodobacteraceae	*Loktanella*	2.3%	0.02	1.48	334	264	12.7%	0.074
Chitinophagales	Saprospiraceae	unknown genus	2.2%	0.01	1.60	479	435	16.4%	0.441
unknown order	unknown family	unknown genus	1.7%	0.02	0.88	216	46	19.4%	0.023
Thalassobaculales	unknown family	unknown genus	1.6%	0.01	1.35	195	0	22.2%	0.014
Flavobacteriales	Flavobacteriaceae	*Aquimarina*	1.6%	0.02	0.83	196	57	24.9%	0.129
Chitinophagales	unknown family	unknown genus	1.5%	0.01	1.79	25	205	27.5%	0.036
Caulobacterales	Hyphomonadaceae	unknown genus	1.4%	0.01	2.14	81	253	30.0%	0.053
Flavobacteriales	Flavobacteriaceae	*Croceitalea*	1.4%	0.01	1.78	30	197	32.4%	0.05
Verrucomicrobiales	Rubritaleaceae	*Rubritalea*	1.3%	0.01	1.16	4	155	34.6%	0.33
Flavobacteriales	Flavobacteriaceae	*Maritimimonas*	1.1%	0.01	1.46	140	5	36.5%	0.002
Chitinophagales	Saprospiraceae	*Lewinella*	1.0%	0.01	1.54	225	262	38.2%	0.758
Rhodobacterales	Rhodobacteraceae	unknown genus	0.9%	0.01	1.25	248	302	39.8%	0.996
Nostocales	Xenococcaceae	unknown genus	0.8%	0.01	0.70	97	0	41.2%	0.034
Nostocales	Xenococcaceae	*Chroococcidiopsis*	0.8%	0.01	0.72	97	2	42.6%	0.078
Nitrosopumilales	Nitrosopumilaceae	*Candidatus Nitrosopumilus*	0.8%	0.01	0.70	90	0	43.9%	0.07
Steroidobacterales	Woeseiaceae	JTB255 marine benthic group	0.7%	0.01	0.70	88	0	45.2%	0.034
Sphingomonadales	Sphingomonadaceae	*Erythrobacter*	0.7%	0.00	1.67	109	63	46.4%	0.024
Flavobacteriales	Flavobacteriaceae	*Tenacibaculum*	0.7%	0.00	2.49	1	83	47.6%	0.297
Steroidobacterales	Woeseiaceae	*Woeseia*	0.6%	0.01	1.00	80	8	48.7%	0.007
Pirellulales	Pirellulaceae	*Rhodopirellula*	0.6%	0.00	2.15	89	14	49.8%	0.017

Table SV.8. SIMPER results of the most contributing genera to the dissimilarities between rocky biofilms and algal samples collected at Tamaris. Only the first 50% of the cumulative contribution is showed. *p* values were calculated with a permutation test constructed with 999 permutations.

Order	**Family**	**Genus**	**Average contribution**	**sd**	**ratio**	**Av. rocky biofilms**	**Av. thallus samples**	**Cum. sum**	***p* value**
Thiohalorhabdales	Thiohalorhabdaceae	*Granulosicoccus*	2.8%	0.02	1.40	79	407	4.2%	0.045
Synechococcales	Synechococcales Incertae Sedis	*Schizothrix*	2.5%	0.03	0.74	16	318	8.0%	0.143
Caulobacterales	Hyphomonadaceae	*Litorimonas*	2.4%	0.03	0.84	85	331	11.6%	0.155
Chitinophagales	Saprospiraceae	unknown genus	2.1%	0.01	1.52	172	406	14.8%	0.448
Rhodobacterales	Rhodobacteraceae	unknown genus	2.1%	0.02	1.38	338	447	18.0%	0.296
Flavobacteriales	Flavobacteriaceae	*Aquimarina*	2.1%	0.01	1.41	279	36	21.2%	0.022
Rhizobiales	Rhizobiaceae	*Nitratireductor*	1.9%	0.04	0.51	7	232	24.1%	0.148
Rhodobacterales	Rhodobacteraceae	*Loktanella*	1.8%	0.01	1.34	278	103	26.8%	0.264
Nostocales	Xenococcaceae	*Pleurocapsa*	1.8%	0.02	0.95	226	67	29.5%	0.018
unknown order *	unknown family	unknown genus	1.5%	0.01	1.08	208	77	31.7%	0.024
Thalassobaculales	unknown family	unknown genus	1.4%	0.02	0.73	167	0	33.8%	0.074
Rhodobacterales	Rhodobacteraceae	*Sulfitobacter*	1.4%	0.01	1.69	188	23	35.9%	0.008
Flavobacteriales	Flavobacteriaceae	*Algitalea*	1.3%	0.01	1.26	184	144	37.9%	0.975
Verrucomicrobiales	Rubritaleaceae	*Rubritalea*	1.3%	0.02	0.86	12	166	39.9%	0.33
Flavobacteriales	Flavobacteriaceae	*Winogradskyella*	1.1%	0.01	0.90	116	99	41.6%	0.162
Verrucomicrobiales	Rubritaleaceae	*Roseibacillus*	1.1%	0.01	1.02	69	134	43.2%	0.125
Cytophagales	Amoebophilaceae	*Candidatus Amoebophilus*	1.0%	0.01	0.90	115	0	44.7%	0.002
Pirellulales	Pirellulaceae	*Blastopirellula*	1.0%	0.01	1.38	103	156	46.1%	0.329
Flavobacteriales	Flavobacteriaceae	*Tenacibaculum*	0.9%	0.01	1.75	76	105	47.5%	0.028
Sphingomonadales	Sphingomonadaceae	*Sphingorhabdus*	0.9%	0.00	1.82	28	131	48.8%	0.024
Phormidesmiales	Phormidesmiaceae	*Acrophormium*	0.9%	0.01	1.15	7	110	50.2%	0.13

*unknown Bacteria

Table SV.9. SIMPER results of the most contributing genera to the dissimilarities between basal and apical parts of algal samples collected at Carqueiranne.

Only the first 50% of the cumulative contribution is showed. *p* values were calculated with a permutation test constructed with 999 permutations.

Order	**Family**	**Genus**	**Average contribution**	**SD**	**Ratio**	**Av. basal parts**	**Av. apical parts**	**Cum. sum**	***p* value**
Flavobacteriales	Flavobacteriaceae	*Algitalea*	4.1%	0.01	3.17	417	609	9.6%	0.118
Rhodobacterales	Rhodobacteraceae	*Loktanella*	2.3%	0.01	2.67	142	410	14.9%	0.166
Verrucomicrobiales	Rubritaleaceae	*Rubritalea*	1.9%	0.01	1.39	44	265	19.2%	0.185
Flavobacteriales	Flavobacteriaceae	*Croceitalea*	1.6%	0.00	4.49	106	301	23.1%	0.033
Chitinophagales	unknown family	unknown genus	1.6%	0.01	2.20	296	108	26.8%	0.062
Rhodobacterales	Rhodobacteraceae	unknown genus	1.4%	0.01	2.43	391	227	30.0%	0.742
Caulobacterales	Hyphomonadaceae	unknown genus	1.1%	0.00	3.23	344	214	32.6%	0.501
Chitinophagales	Saprospiraceae	unknown genus	1.1%	0.01	1.54	467	346	35.1%	0.965
Flavobacteriales	Flavobacteriaceae	unknown genus	1.0%	0.01	2.01	61	181	37.5%	0.023
Rhodovibrionales	Kiloniellaceae	unknown genus	0.8%	0.00	2.84	9	105	39.4%	0.002
Flavobacteriales	Flavobacteriaceae	*Aquimarina*	0.8%	0.01	0.97	20	109	41.2%	0.51
unknown order	unknown family	unknown genus	0.7%	0.00	2.40	94	11	42.8%	0.179
Rhodobacterales	Rhodobacteraceae	*Octadecabacter*	0.6%	0.00	7.13	33	110	44.3%	0.018
Flavobacteriales	Flavobacteriaceae	*Winogradskyella*	0.6%	0.01	0.89	77	142	45.8%	0.385
Phormidesmiales	Phormidesmiaceae	*Acrophormium*	0.6%	0.00	1.79	88	16	47.2%	0.398
Thiohalorhabdales	Thiohalorhabdaceae	*Granulosicoccus*	0.5%	0.00	3.91	96	32	48.5%	0.829
Verrucomicrobiales	DEV007	unknown genus	0.5%	0.00	1.98	82	19	49.7%	0.032

Table SV.10. SIMPER results of the most contributing genera to the dissimilarities between basal and apical parts of algal samples collected at Tamaris. Only the first 50% of the cumulative contribution is showed. *p* values were calculated with a permutation test constructed with 999 permutations.

Order	**Family**	**Genus**	**Average contribution**	**sd**	**ratio**	**Av. basal part**	**Av. apical part**	**Cum. sum**	***p* value**
Rhizobiales	Rhizobiaceae	*Nitratireductor*	5.3%	0.05	1.05	5	638	8.8%	0.002
Caulobacterales	Hyphomonadaceae	*Litorimonas*	5.3%	0.03	1.78	92	721	17.6%	0.002
Synechococcales	Synechococcales Incertae Sedis	*Schizothrix*	3.8%	0.05	0.77	69	512	23.9%	0.129
Rhodobacterales	Rhodobacteraceae	unknown genus	2.5%	0.02	1.60	482	213	28.1%	0.22
Thiohalorhabdales	Thiohalorhabdaceae	*Granulosicoccus*	2.4%	0.02	1.44	403	467	32.1%	0.257
Flavobacteriales	Flavobacteriaceae	*Winogradskyella*	1.9%	0.02	0.84	56	217	35.2%	0.131
Chitinophagales	Saprospiraceae	unknown genus	1.8%	0.01	1.61	426	402	38.2%	0.704
Verrucomicrobiales	Rubritaleaceae	*Roseibacillus*	1.8%	0.01	1.22	30	242	41.1%	0.017
Flavobacteriales	Flavobacteriaceae	*Algitalea*	1.5%	0.01	1.38	222	41	43.6%	0.815
Chitinophagales	Saprospiraceae	*Portibacter*	1.5%	0.01	2.04	236	59	46.1%	0.017
Nostocales	Xenococcaceae	*Pleurocapsa*	1.2%	0.01	1.41	157	18	48.0%	0.232
Chitinophagales	Saprospiraceae	*Lewinella*	1.1%	0.00	4.24	174	39	49.9%	0.522

Table SV.11. Summary of PERMANOVA results examining the effect of "site" and "thallus parts" factors for each normalized metabolomics dataset.
D. f ; MS ; F ; R^2 and P correspond to degrees of freedom ; mean square ; F ratio ; coefficient of determination and *p* value, respectively

		Surface extracts					Total extracts				
		D. f	**MS**	**F**	**R^2**	**P**	**D. f**	**MS**	**F**	**R^2**	**P**
LC-(+)-ESI-MS	**Site**	1	4690	2.383	0.08725	0.002	1	14505	8.209	0.236	0.001
	Thallus parts	2	3997	2.031	0.14869	0.001	2	4747	2.687	0.154	0.002
	Site:Thallus parts	2	2825	1.436	0.10511	0.017	2	2828	1.601	0.092	0.036
	Residuals	18	1968		0.65895		18	1767		0.517	
	Total	23			1		23			1	
LC-(-)-ESI-MS	**Site**	1	367	5.371	0.1426	0.001	1	1890	28.2	0.471	0.001
	Thallus parts	2	350.1	5.124	0.27204	0.001	2	300.1	4.48	0.15	0.003
	Site:Thallus parts	2	138.3	2.025	0.1075	0.026	2	156.5	2.335	0.078	0.049
	Residuals	18	68.33	0.478			18	67	0.301		
	Total	23			1		23			1	
GC-MS	**Site**	1	16926	1.171	0.04856	0.248	1	2669	5.757	0.18	0.002
	Thallus parts	2	28282	1.957	0.1623	0.009	2	1550	3.344	0.209	0.002
	Site:Thallus parts	2	14675	1.015	0.08421	0.4	2	582.3	1.256	0.079	0.243
	Residuals	17	14452		0.70493		17	463.6		0.532	
	Total	22			1		22			1	

Table SV.12. Multivariate pairwise results (*p* values) examining differences between both sites and between each thallus parts for each metabolomics dataset.

		Surface extracts			**Total extracts**		
Comparison type	**Samples compared**	LC-(+)-ESI-MS	LC-(-)-ESI-MS	GC-MS	LC-(+)-ESI-MS	LC-(-)-ESI-MS	GC-MS
Site comparison	**Carqueiranne vs Tamaris**	0.001	0.005	0.258	0.001	0.001	0.002
Sample type comparison	**Basal vs median parts**	0.006	0.013	0.294	0.0345	0.161	0.0135
	Basal vs Apical parts	0.003	0.003	0.003	0.033	0.161	0.0135
	Median vs apical parts	0.058	0.013	0.0375	0.145	0.161	0.278

Table SV.13. Summary of R^2 values obtained for the two first components after cross validation test for PLS-DA obtained with each metabolomics dataset.
The method "leave-one-out cross-validation" (LOOCV) was chosen for the cross-validation.

	Surface extracts	**Total extracts**
LC-(+)-ESI-MS	0.972	0.970
LC-(-)-ESI-MS	0.866	0.907
GC-MS	0.717	0.858

Table SV.14. List of compounds identified through GC-MS analyses

Name	Molecular formula	Retention time (s)	Experimental RI	RI from reference	Reference	Match with NIST11 database (%)
α-cubebene	$C_{15}H_{24}$	23.639	1351	1352	Lucero, Fredrickson, et al., 2006	99
β-bourbonene	$C_{15}H_{24}$	24.584	1386	1387	Adams, 2008	97
β-cubebene	$C_{15}H_{24}$	24.717	1391	1387	Adams, 2008	89
β-ylangene	$C_{15}H_{24}$	25.495	1421	1421	Flamini, Luigi Cioni, et al., 2005	99
β-copaene	$C_{15}H_{24}$	25.723	1429	1430	Adams, 2008	97
trans-muurola-3,5-diene	$C_{15}H_{24}$	26.252	1452	1451	Adams, 2008	90
cis-muurola-4(14),5-diene	$C_{15}H_{24}$	26.673	1469	1465	Adams, 2008	72
trans-cadina-1(6),4-diene	$C_{15}H_{24}$	26.84	1476	1475	Adams, 2008	93
γ-muurolene	$C_{15}H_{24}$	26.929	1479	1477	Flamini, Cioni, et al., 2007	99
α-amorphene & germacrene D	$C_{15}H_{24}$	26.994	1482	1483-1484	Adams, 2008	93
α-muurolene	$C_{15}H_{24}$	27.489	1502	1501	Flamini, Tebano, et al., 2006	99
cis-calamenene	$C_{15}H_{22}$	28.026	1525	1522	Palmeira, Moura, et al., 2004	96
trans-cadina-1,4-diene	$C_{15}H_{24}$	28.295	1536	1536	Andrade, Sampaio, et al., 2007	93
α-calacorene	$C_{15}H_{20}$	28.45	1543	1543	Lucero, Estell, et al., 2003	53
unidentified sesquiterpene	$C_{15}H_{22}$	28.547	1547	-	-	-
unidentified sesquiterpene	$C_{15}H_{24}O$	28.895	1561	-	-	-
β-calacorene	$C_{15}H_{20}$	29.004	1566	1564	Javidnia, Miri, et al., 2006	96
unidentified sesquiterpene	$C_{15}H_{24}O_2$	29.103	1570	-	-	-
gleenol isomer (?)	$C_{15}H_{26}O$	29.261	1577	-	-	-
gleenol	$C_{15}H_{26}O$	29.619	1587	1587	Custer, 2009	94
unidentified sesquiterpene	$C_{15}H_{24}O_2$	33.139	1749	-	-	-
unidentified sesquiterpene	$C_{15}H_{24}O_2$	33.258	1755	-	-	-
unidentified sesquiterpene	$C_{15}H_{24}O_2$	33.354	1760	-	-	-
unidentified sesquiterpene	$C_{15}H_{24}O_2$	34.322	1808	-	-	-

Table SV.15. Putative annotation of VIPs from the LC-(+)-ESI-MS dataset of samples of *T. atomaria* collected at Tamaris

VIP N°	*m/z*	RT (s)	VIP score	Molecular formula	Mass error (ppm)	m[a]	MS/MS fragment ions (relative abundance in %)	Putative identification[b]
1	450.3355	684	3.8	$C_{30}H_{44}NO_2$	1.1	5.5	450.3355 $[M+NH_4]^+$ (2), 201.1641 $[C_{15}H_{21}]^+$ (69), 159.1166 $[C_{12}H_{15}]^+$ (55), 145.1011 $[C_{11}H_{13}]^+$ (100), 119.0854 $[C_9H_{11}]^+$ (27), 95.0856 $[C_7H_{11}]^+$ (30)	$C_{30}H_{40}O_2$ (*apo*-carotenoid?)
2	318.2790	587	3.7	$C_{21}H_{36}NO$	0.2	3.0	318.2790 $[M+H]^+$ (3), 286.2514 $[C_{20}H_{32}N]^+$ (2), 175.1458 $[C_{13}H_{19}]^+$ (4), 149.1321 $[C_{11}H_{17}]^+$ (5), 126.0909 $[C_7H_{12}NO]^+$ (36), 108.0802 $[C_7H_{10}N]^+$ (18), 95.0860 $[C_7H_{11}]^+$ (23), 93.0695 $[C_7H_9]^+$ (19), 81.0699 $[C_6H_9]^+$ (100), 69.0697 $[C_5H_9]^+$ (52)	3,4-epoxy-lobophorene B?
3	682.5617	683	3.0	$C_{40}H_{76}NO_7$	-0.4	5.5	n.o.	DGTA (C30:1)
4	482.3475	584	2.9	$C_{27}H_{48}NO_6$	0.2	2.5	482.3475 $[M+NH_4]^+$ (1), 271.2415 $[C_{20}H_{31}]^+$ (90), 215.1791 $[C_{16}H_{23}]^+$ (87), 201.1635 $[C_{15}H_{21}]^+$ (69), 189.1638 $[C_{14}H_{21}]^+$ (45), 175.1481 $[C_{13}H_{19}]^+$ (73), 161.1322 $[C_{12}H_{17}]^+$ (93), 135.1166 $[C_{10}H_{15}]^+$ (77), 109.1011 $[C_8H_{13}]^+$ (100), 95.0857 $[C_7H_{11}]^+$ (69), 81.0698 $[C_6H_9]^+$ (81), 69.0695 $[C_5H_9]^+$ (57)	GGG derivative
5	474.3793	546	2.7	$C_{26}H_{52}NO_6$	0.1	11.0	474.3793 $[M+H]^+$ (100), 456.3688 $[M-H_2O+H]^+$ (22), 412.3775 $[C_{25}H_{50}NO_3]^+$ (1), 369.3021 $[C_{22}H_{41}O_4]^+$ (1), 313.2733 $[C_{19}H_{37}O_3]^+$ (1), 236.1491 $[C_{10}H_{22}NO_5]^+$ (57)	*lyso*-DGTA (C16:0)
6	421.3167	573	2.6	$C_{22}H_{45}O_7$	-1.0	11.0	421.3167 $[M+H]^+$ (1), 385.2950 $[M-2H_2O+H]^+$ (2), 239.2372 $[C_{16}H_{31}O]^+$ (4), 165.0759 $[C_6H_{13}O_5]^+$ (14), 147.0653 $[C_6H_{11}O_4]^+$ (18), 129.0547 $[C_6H_9O_3]^+$ (35), 111.0445 $[C_6H_7O_2]^+$ (20), 99.0445 $[C_5H_7O_2]^+$ (21), 95.0858 $[C_7H_{11}]^+$ (20), 83.0494 $[C_5H_7O]^+$ (34), 69.0338 $[C_4H_5O]^+$ (100), 57.0704 $[C_4H_9]^+$ (26)	Mannitol + FA chain (C16 :0)?
7	623.2865	653	2.5	$C_{35}H_{43}O_{10}$	-1.0	8.5	623.2865 $[M+H]^+$ (100), 605.2755 $[M-H_2O+H]^+$ (67), 591.2604 $[C_{34}H_{39}O_9]^+$ (4), 573.2496 $[C_{34}H_{37}O_8]^+$ (12), 545.2546 $[C_{33}H_{37}O_7]^+$ (48), 217.1948 $[C_{16}H_{25}]^+$ (9)	$C_{35}H_{42}O_{10}$
8	524.3941	503	2.2	$C_{30}H_{54}NO_6$	-0.3	2.2	524.3941 $[M+H]^+$ (100), 363.2886 $[C_{23}H_{39}O_3]^+$ (0,5), 236.1496 $[C_{10}H_{22}NO_5]^+$ (5)	*lyso*-DGTA (C20:3)
9	423.3106	562	2.2	$C_{25}H_{43}O_5$	0.4	26.8	n.o.	$C_{25}H_{42}O_5$
10	375.2167	458	2.1	$C_{22}H_{31}O_5$	-0.1	16.8	375.2167 $[M+H]^+$ (1), 315.1928 $[C_{20}H_{27}O_3]^+$ (1), 205.0858 $[C_{12}H_{13}O_3]^+$ (7), 177.0909 $[C_{11}H_{13}O_2]^+$ (12), 159.0804 $[C_{11}H_{11}O]^+$ (23), 131.0853 $[C_{10}H_{11}]^+$ (14), 109.1012 $[C_8H_{13}]^+$ (100), 95.0493 $[C_6H_7O]^+$ (8), 67.0545 $[C_5H_7]^+$ (7)	$C_{22}H_{30}O_5$ (Acetylated diterpene)
11	135.0471	50	2.01	$C_5H_{11}O_2S$	2.0	6.9	135.0471 $[M+H]^+$ (19), 73.0283 $[C_3H_5O_2]^+$ (100), 63.0261 $[C_2H_7S]^+$ (100), 61.0108 $[C_2H_5S]^+$ (5), 55.0177 $[C_3H_3O]^+$ (7)	DMSP[d]
12	307.1517	378	1.9	$C_{17}H_{23}O_5$	7.2	18.4	307.1517 $[M+H]^+$ (100), 215.1039 $[C_{14}H_{15}O_2]^+$ (3), 121.1021 $[C_9H_{13}]^+$ (6), 115.0363 $[C_5H_7O_3]^+$ (8),	$C_{17}H_{22}O_5$
13	808.6099	628	1.9	$C_{47}H_{87}NO_7P$	14.4	7.9	808.6099 $[M+H]^+$ (100), 522.3794 $[C_{27}H_{57}NO_6P]^+$ (2), 504.3681 $[C_{27}H_{55}NO_5P]^+$ (2), 184.07 $[C_5H_{15}NO_4P]^+$ (13)	PC (C39:5)?
14	741.6138	618	1.9	$C_{44}H_{86}O_6P$	2.7	11.1	741.6138 $[M+H]+$ (100), 697.6233 $[C_{43}H_{86}O_4P]+$ (1), 571.4716 $[C_{34}H_{68}O_4P]+$ (1), 439.3891 $[C_{24}H_{56}O_4P]^+$ (9),	$C_{44}H_{85}O_6P$
15	577.5193	732	1.9	$C_{37}H_{69}O_4$	-0.4	21.1	577.5193 $[M+H]^+$ (100), 265.2523 $[C_{18}H_{33}O]^+$ (23), 247.2414 $[C_{18}H_{31}]^+$ (16), 239.2358 $[C_{16}H_{31}O]^+$ (25), 221.2275 $[C_{16}H_{29}]^+$ (3), 149.1329 [C11H17]$^+$ (9) , 135.1162 $[C_{10}H_{15}]^+$ (10) , 123.1158 $[C_9H_{15}]^+$ (17) , 109.1011 $[C_8H_{13}]^+$ (32), 95.0858 $[C_7H_{11}]^+$ (48), 83.0857 $[C_6H_{11}]^+$ (32) , 69.0699 $[C_5H_9]^+$ (28), 57.0698 $[C_4H_9]^+$ (14)	DG (C34:1) (C18:1, C16:0)
16	704.5474	661	1.9	$C_{42}H_{74}NO_7$	0.8	8.2	704.5474 $[M+H]^+$ (100), 494.3778 $[C_{28}H_{48}NO_6]^+$ (16), 446.3480 $[C_{24}H_{48}NO_6]^+$ (42), 236.1496 $[C_{10}H_{22}NO_5]^+$ (5)	DGTA (C32:0) (C18:4, C14:0)

[a] Constructor statistical match factor (comparison of theoretical and experimental isotopic patterns); [b] Abbreviations: PC: phosphatidylcholine, DGTA: diacylglycerylhydroxymethyl-*N*,*N*,*N*-trimethyl-*ß*-alanine, DG: diacylglycerol, GGG: geranylgeranylglycerol, FA: Fatty Acid; [c] not observed; [d] This identification was confirmed with a commercial standard.

Table SV.16. Putative annotation of VIPs from the LC-(+)-ESI-MS dataset of samples of *T. atomaria* collected at Carqueiranne

VIP N°	*m/z*	RT (s)	VIP score	Formula	Mass error (ppm)	m?[a]	MS/MS fragment ions (relative abundance in %)	Putative identification[b]
1	704.5468	607	3.1	$C_{39}H_{79}NO_7P$	17.1	17	604.5468 $[M+H]^+$ (100), 494.3487 $[C_{25}H_{53}NO_6P]^+$ (1), 476.3371 $[C_{25}H_{51}NO_5P]^+$ (1), 184.0722 $[C_5H_{15}NO_4P]^+$ (1)	PC (C31:1)?
2	706.5629	673	3.1	$C_{42}H_{76}NO_7$	-1.4	10.2	706.5629 $[M+H]^+$ (100), 496.3637 $[C_{28}H_{50}NO_6]^+$ (15), 494.3480 $[C_{28}H_{48}NO_6]^+$ (1), 478.3536 $[C_{28}H_{48}NO_5]^+$ (4), 446.3482 $[C_{24}H_{48}NO_6]^+$ (40), 428.3371 $[C_{24}H_{46}NO_5]^+$ (4), 236.1494 $[C_{10}H_{22}NO_5]^+$ (4)	DGTA (C32:3) (C14:0, C18:3)
3	758.5936	630	3.0	$C_{43}H_{85}NO_7P$	16.3	10.2	758.5936 $[M+H]^+$ (100), 520.3619 $[C_{27}H_{55}NO_6P]^+$ (1), 502.3523 $[C_{27}H_{53}NO_5P]^+$ (1), 184.0733 $[C_5H_{15}NO_4P]^+$ (8),	PC (C35:2)?
4	405.3519	694	2.9	$C_{30}H_{45}$	-3.7	21.5	405.3519 $[M+H]^+$ (100), 321.2574 $[C_{24}H_{33}]^+$ (5), 201.1641 $[C_{15}H_{21}]^+$ (100), 145.1009 $[C_{11}H_{13}]^+$ (6), 135.1168 $[C_{10}H_{15}]^+$ (17), 95.0857 $[C_7H_{11}]^+$ (7), 93.0702 $[C_7H_9]^+$ (8)	$C_{30}H_{44}$ (*apo*-carotenoid?)
5	810.6252	636	2.9	$C_{47}H_{89}NO_7P$	15.3	5.1	810.6252 $[M+H]^+$ (100), 522.3797 $[C_{27}H_{57}NO_6P]^+$ (2), 504.3683 $[C_{27}H_{55}NO_5P]^+$ (2), 184.0737 $[C_5H_{15}NO_4P]^+$ (40)	PC (C39:4)?
6	778.5619	602	2.8	$C_{45}H_{81}NO_7P$	14.6	8.7	778.5619 $[M+H]^+$ (100), 520.3585 $[C_{27}H_{55}NO_6P]^+$ (1), 502.3549 $[C_{27}H_{53}NO_5P]^+$ (1), 184.0732 $[C_5H_{15}NO_4P]^+$ (17)	PC (C37:6)?
7	542.3247	505	2.6	$C_{28}H_{49}NO_7P$	-1	8.8	542.3247 $[M+H]^+$ (100), 524.3157 $[M-H_2O+H]^+$ (1), 184.0732 $[C_5H_{15}NO_4P]^+$ (100)	*lyso*-PC (C20:5)
8	732.5781	623	2.5	$C_{41}H_{83}NO_7P$	16.2	6.3	732.5781 $[M+H]^+$ (100), 522.3788 $[C_{27}H_{57}NO_6P]^+$ (1), 504.3694 $[C_{27}H_{55}NO_5P]^+$ (1), 446.3471 $[C_{21}H_{53}NO_6P]^+$ (1), 428.3370 $[C_{21}H_{51}NO_5P]^+$ (1), 184.0735 $[C_5H_{15}NO_4P]^+$ (1)	PC (C33:1)?
9	496,3637	486	2.4	$C_{28}H_{50}NO_6$	-0.2	8.6	496.3637 $[M+H]^+$ (100), 478.3534 $[C_{28}H_{48}NO_5]^+$ (1), 391.2830 $[C_{24}H_{39}O_4]^+$ (1), 335.2590 $[C_{21}H_{35}O_3]^+$ (1), 236.1494 $[C_{10}H_{22}NO_5]^+$ (4), 218.1386 $[C_{10}H_{20}NO_4]^+$ (1), 144.1020 $[C_7H_{14}NO_2]^+$ (1), 100.1126 $[C_6H_{14}N]^+$ (2)	*lyso*-DGTA (C18:3)
10	203.1793	531	2.4	$C_{15}H_{23}$	0.7	17.4	203.1793 $[M+H]^+$ (31), 161.1321 $[C_{12}H_{17}]^+$ (26), 147.1167 $[C_{11}H_{15}]^+$ (71), 133.1010 $[C_{10}H_{13}]^+$ (32), 119.0855 $[C_9H_{11}]^+$ (50), 109.1011 $[C_8H_{13}]^+$ (27), 105.0698 $[C_8H_9]^+$ (83), 91.0544 $[C_7H_7]^+$ (46), 81.0697 $[C_6H_9]^+$ (81), 69.0697 $[C_5H_9]^+$ (56), 55.0541 $[C_4H_7]^+$ (14)	Germacra-4(15),5,10(14)-trien-9-ol $[M-H_2O+H]^+$ [d]
11	376.2598	486	2.2	$C_{26}H_{34}NO$	9.5	7.7	n.o.[c]	$C_{26}H_{33}NO$?
12	406.3598	750	2.2	$C_{29}H_{44}N$	-33.4	7.4	406.3598 $[M+NH_4]^+$ (4), 363.3048 $[C_{27}H_{39}]^+$ (100), 279.2114 $[C_{21}H_{27}]^+$ (6)	$C_{29}H_{40}$?
13	410.3274	638	2.1	$C_{24}H_{44}NO_4$	-2.2	14.7	410.3274 $[M+NH_4]^+$ (1), 273.2583 $[C_{20}H_{33}]^+$ (3), 217.1952 $[C_{16}H_{25}]^+$ (5), 203.1796 $[C_{15}H_{23}]^+$ (4), 177.1640 $[C_{13}H_{21}]^+$ (4), 163.1483 $[C_{12}H_{19}]^+$ (8), 149.1326 $[C_{11}H_{17}]^+$ (20), 135.1170 $[C_{10}H_{15}]^+$ (12), 121.1014 $[C_9H_{13}]^+$ (32), 109.1015 $[C_8H_{13}]^+$ (35), 95.0858 $[C_7H_{11}]^+$ (66), 81.0701 $[C_6H_9]^+$ (100), 69.0702 $[C_5H_9]^+$ (31)	GGG derivative
14	482.3489	587	2.0	$C_{27}H_{48}NO_6$	-1.7	2.4	482.3489 $[M+NH_4]^+$ (1), 271.2422 $[C_{20}H_{31}]^+$ (100), 215.1796 $[C_{16}H_{23}]^+$ (78), 201.1639 $[C_{15}H_{21}]^+$ (58), 189.1640 $[C_{14}H_{21}]^+$ (48), 175.1480 $[C_{13}H_{19}]^+$ (61), 161.1323 $[C_{12}H_{17}]^+$ (75), 135.1168 $[C_{10}H_{15}]^+$ (71), 121.1014 $[C_9H_{13}]^+$ (46), 109.1010 $[C_8H_{13}]^+$ (86), 95.0856 $[C_7H_{11}]^+$ (79), 81.0698 $[C_6H_9]^+$ (87), 69.0689 $[C_5H_9]^+$ (87)	GGG derivative
15	307.1520	378	2.0	$C_{17}H_{23}O_5$	7.2	18.4	307.1517 $[M+H]^+$ (100), 215.1039 $[C_{14}H_{15}O_2]^+$ (3), 121.1021 $[C_9H_{13}]^+$ (6), 115.0363 $[C_5H_7O_3]^+$ (8)	$C_{17}H_{22}O_5$

[a] Constructor statistical match factor (comparison of theoretical and experimental isotopic patterns); [b] Abbreviations: PC: phosphatidylcholine, DGTA: diacylglycerylhydroxymethyl-*N*,*N*,*N*-trimethyl-?-alanine, GGG: geranylgeranylglycerol; [c] not observed; [d] This identification was confirmed with a purified standard.

Supplementary Figures

Figure SV.1. Global workflow

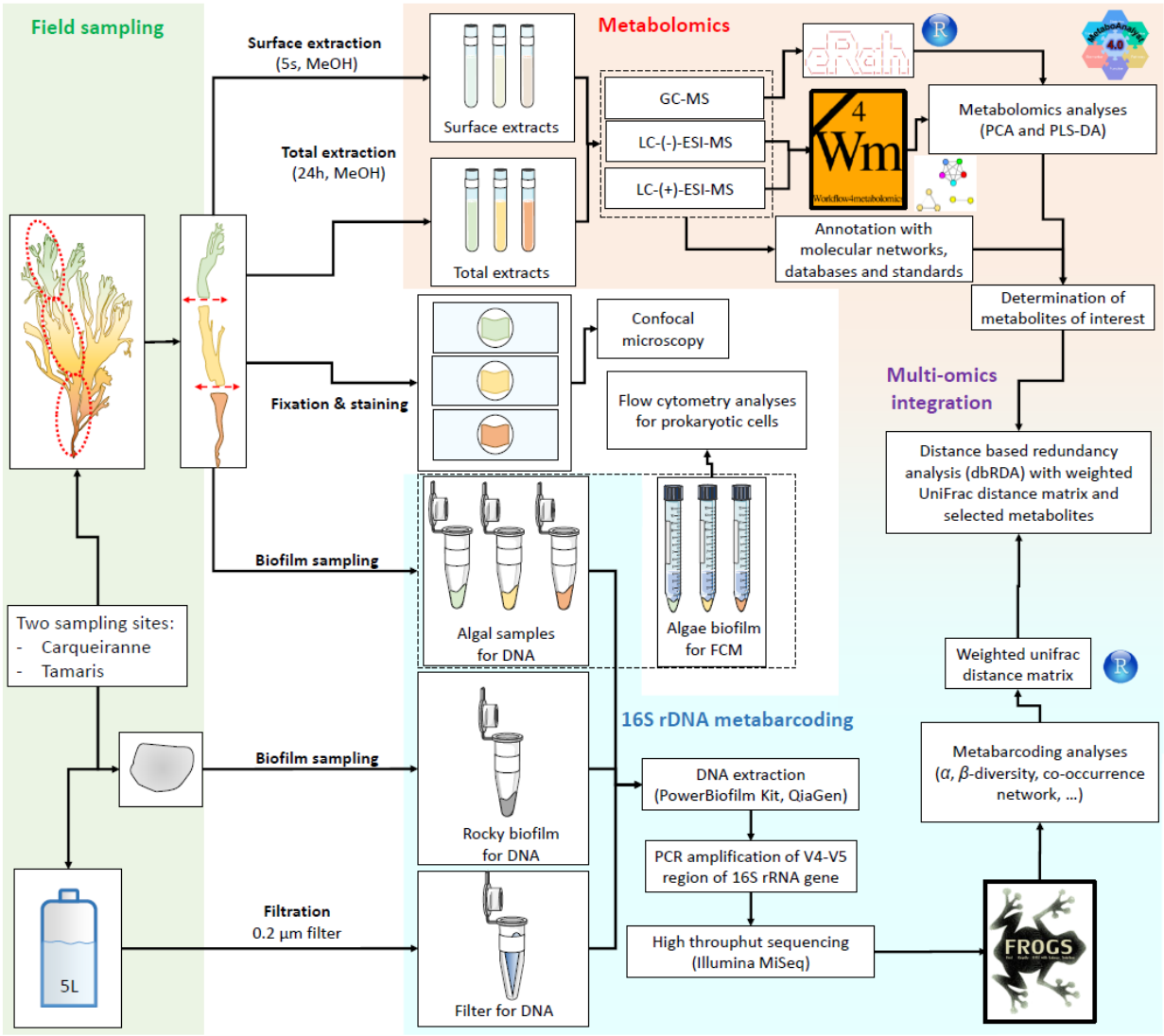

Figure SV.2A. Methodologies used for the preparation of fronds and for extraction for metabolomics analysis

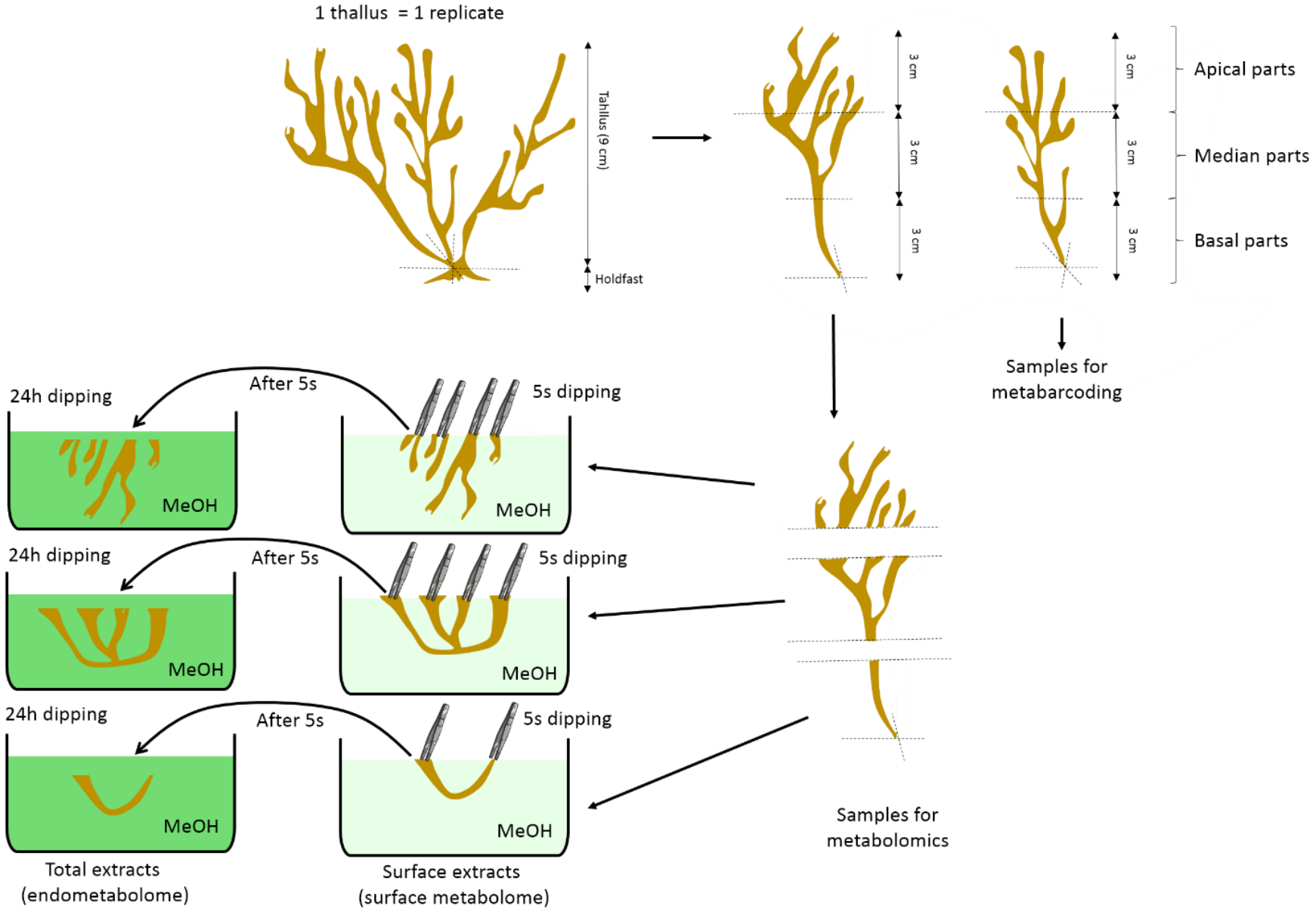

Figure SV.2B. Description of the separation in three parts (basal, median and apical) of the thalli of *T. atomaria*.
Dashed lines represent cut sections separating each part.

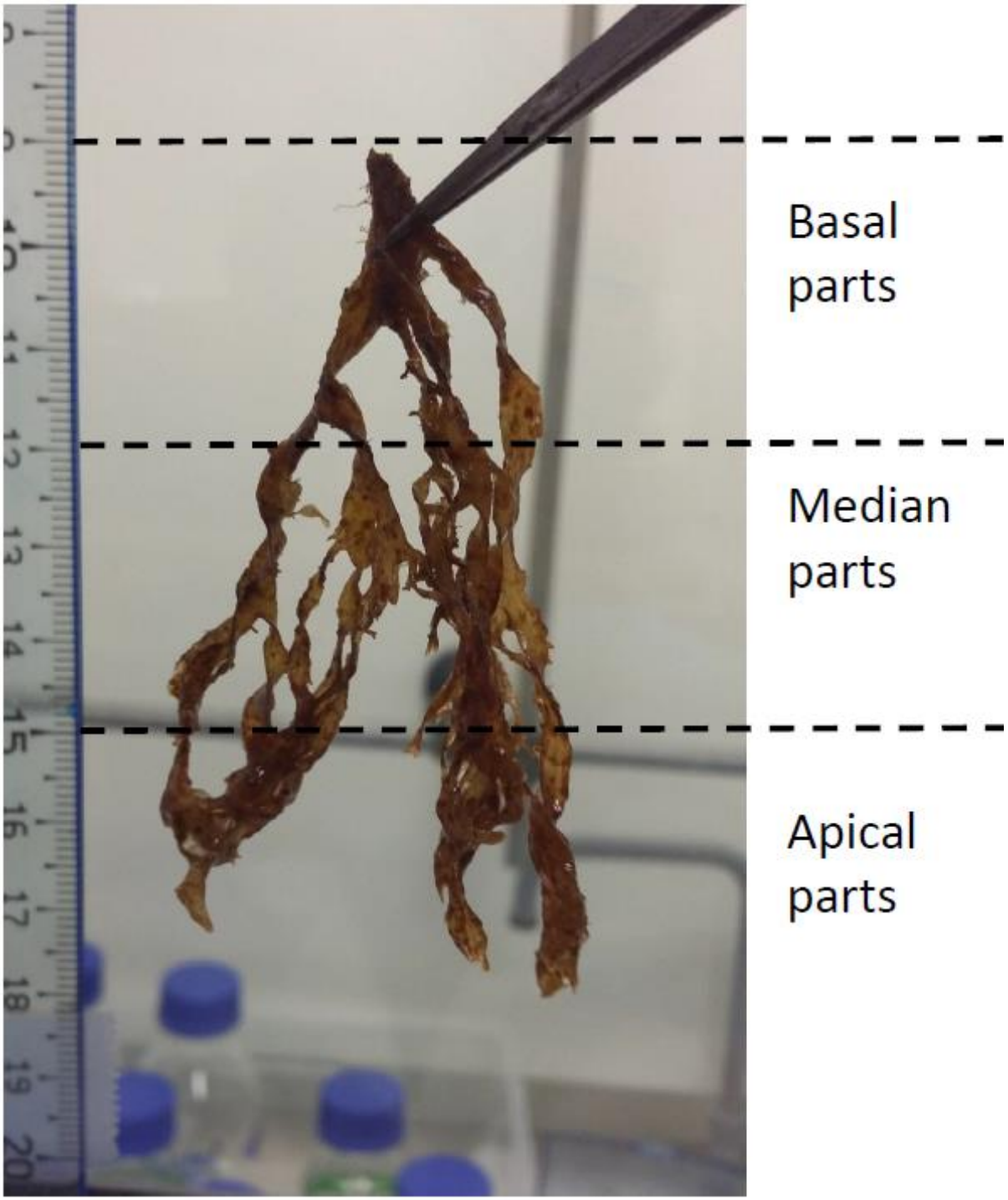

Figure SV.3. Discrimination of heterotrophic prokaryotes by flow cytometry.

A successive 3-steps workflow was used. A: Samples were first screened for the presence of potential doublets or aggregates. Sample dilution was eventually adjusted in order to keep doublets below 5% of the total signal. B: Particles showing a red fluorescence (FL3) were excluded in order to keep only strict heterotrophs (*i.e.* presenting only the SYBR green-induced fluorescence). C: High side scatter signal harboring particles were excluded in order to enumerate only prokaryotes.

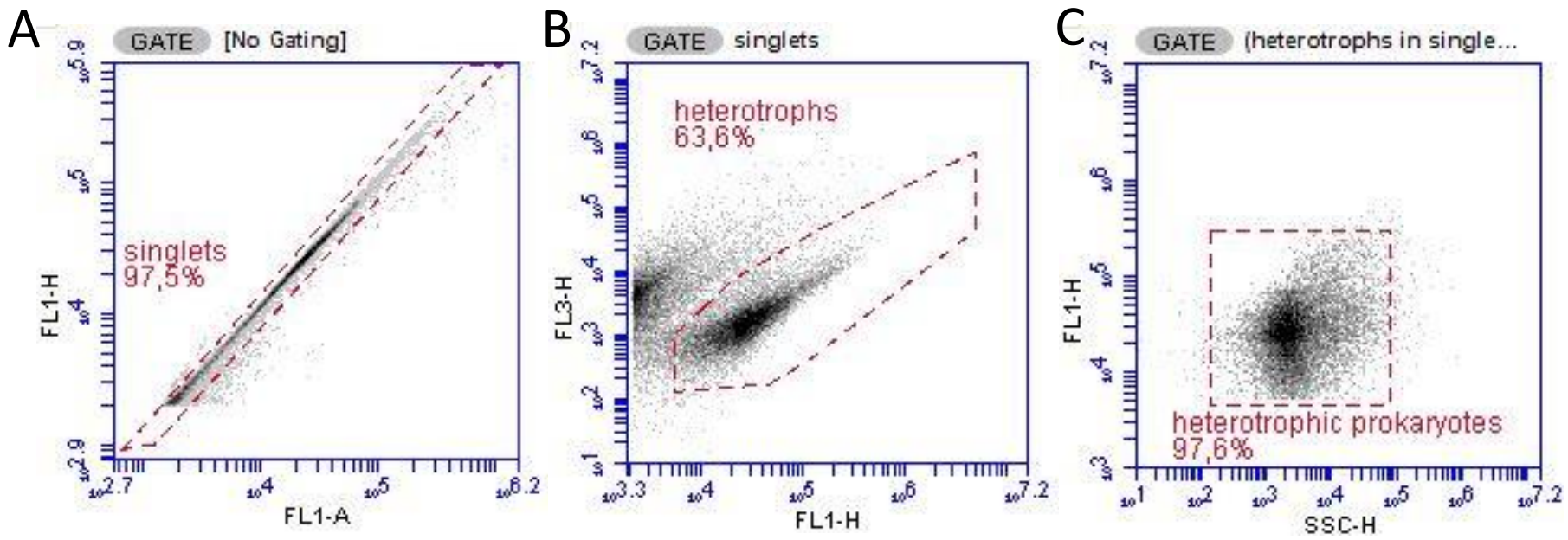

Figure SV.4. Confocal microscopy images of basal and apical parts of *T. atomaria* collected at Tamaris.
Images were acquired with a 20X/0.75NA objective. A, B and C corresponded to a first basal part; D, E and F corresponded to images acquired from replicates of basal parts, while G, H and I corresponded to images acquired from an apical part. A, D and G corresponded to images acquired with chlorophyll signal, B, E and H with Dapi signal, and C, F and I with both signals merged. Yellow arrows indicated diatom-like structures observed, blue arrows indicated filamentous bacteria-like structures.

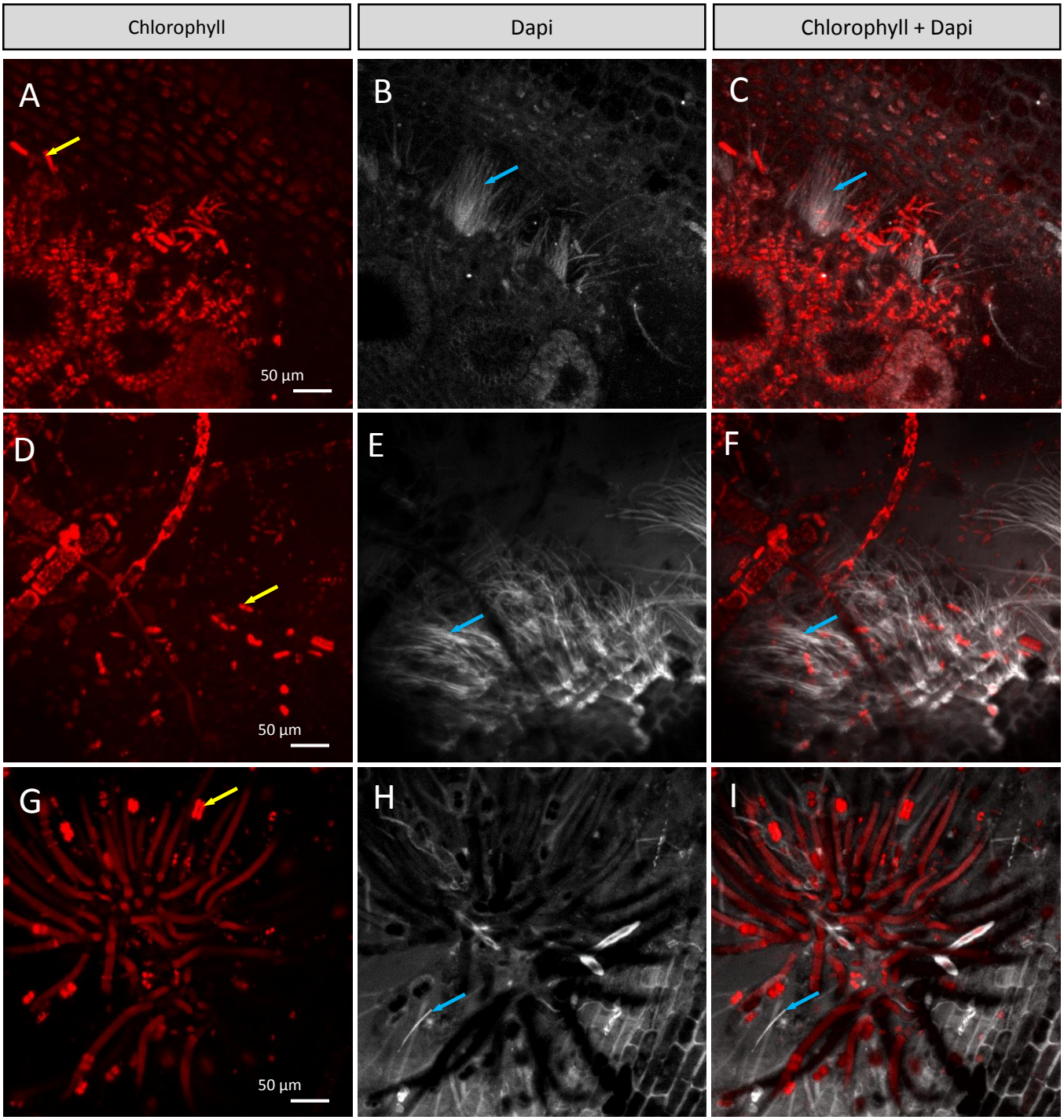

Figure SV.5. Rarefaction curves obtained after data processing of 16S rRNA gene sequences.

Red, yellow, green, grey and blue lines represented respectively samples from basal (.B) , median (.M) and apical (.A) algal parts, rocky biofilms and water samples. Dashed lines represented Carqueiranne samples (C.) and full lines represented Tamaris samples (T.).

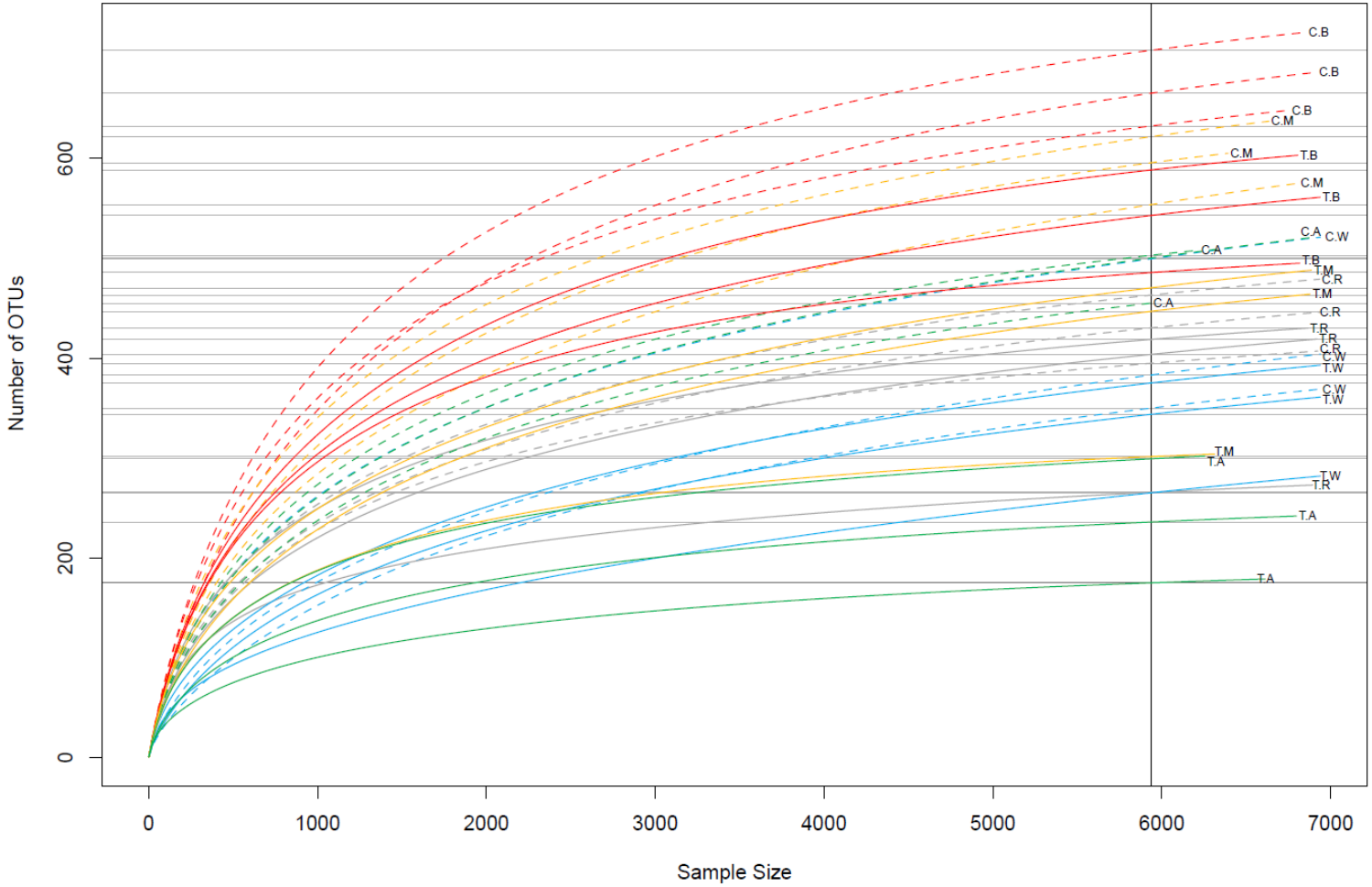

Figure SV.6. Unifrac distances between rocky biofilms (R) and the three thallus parts [basal (B), median (M) and apical parts (A)], or between seawater samples (W) and the three thallus parts.

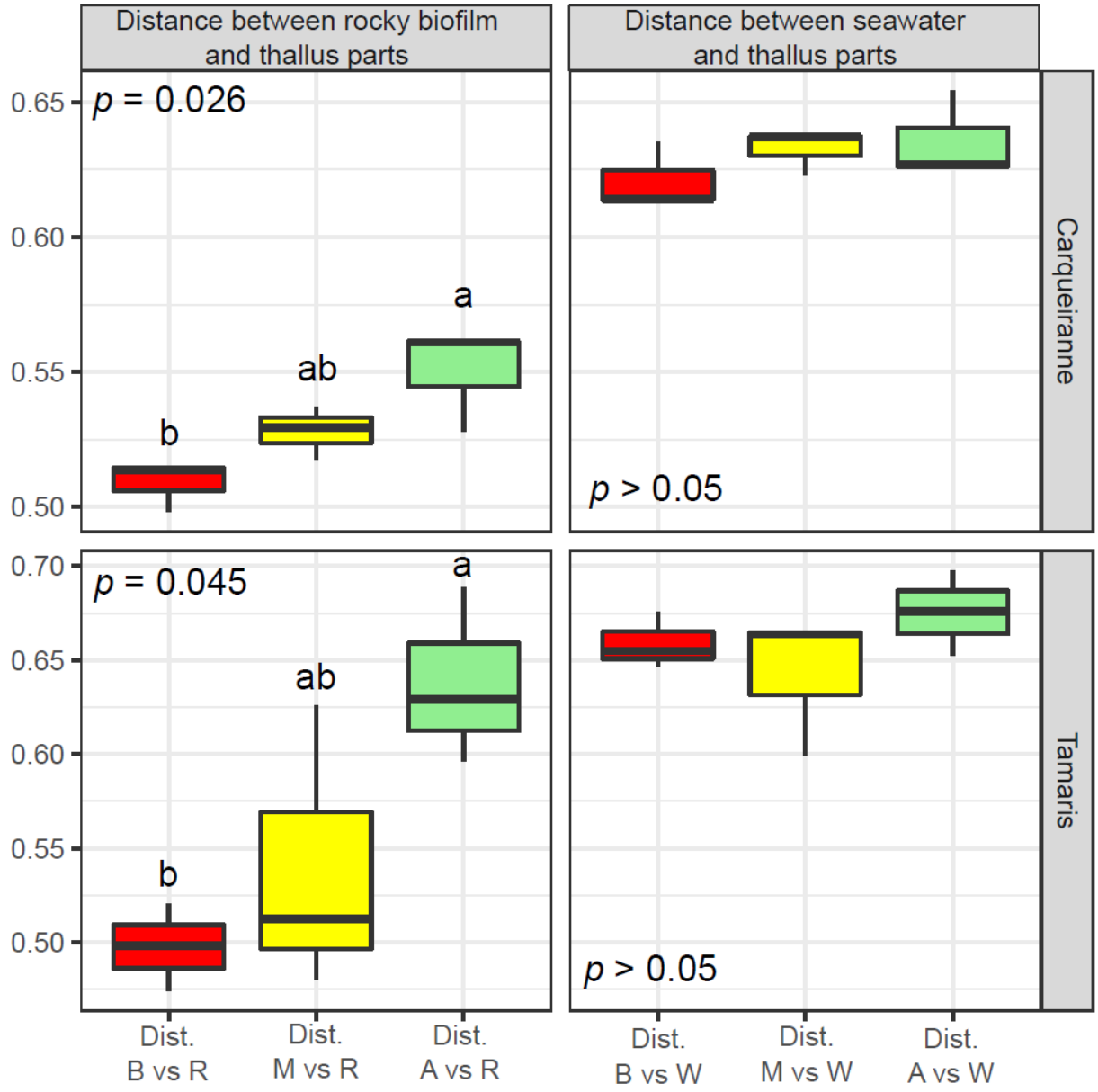

Figure SV.7. Cladogram obtained from the LEfSe analysis built with the 16S rRNA gene dataset of bacterial communities at the surface of *T. atomaria*, in rocky biofilms and in seawater at Tamaris.

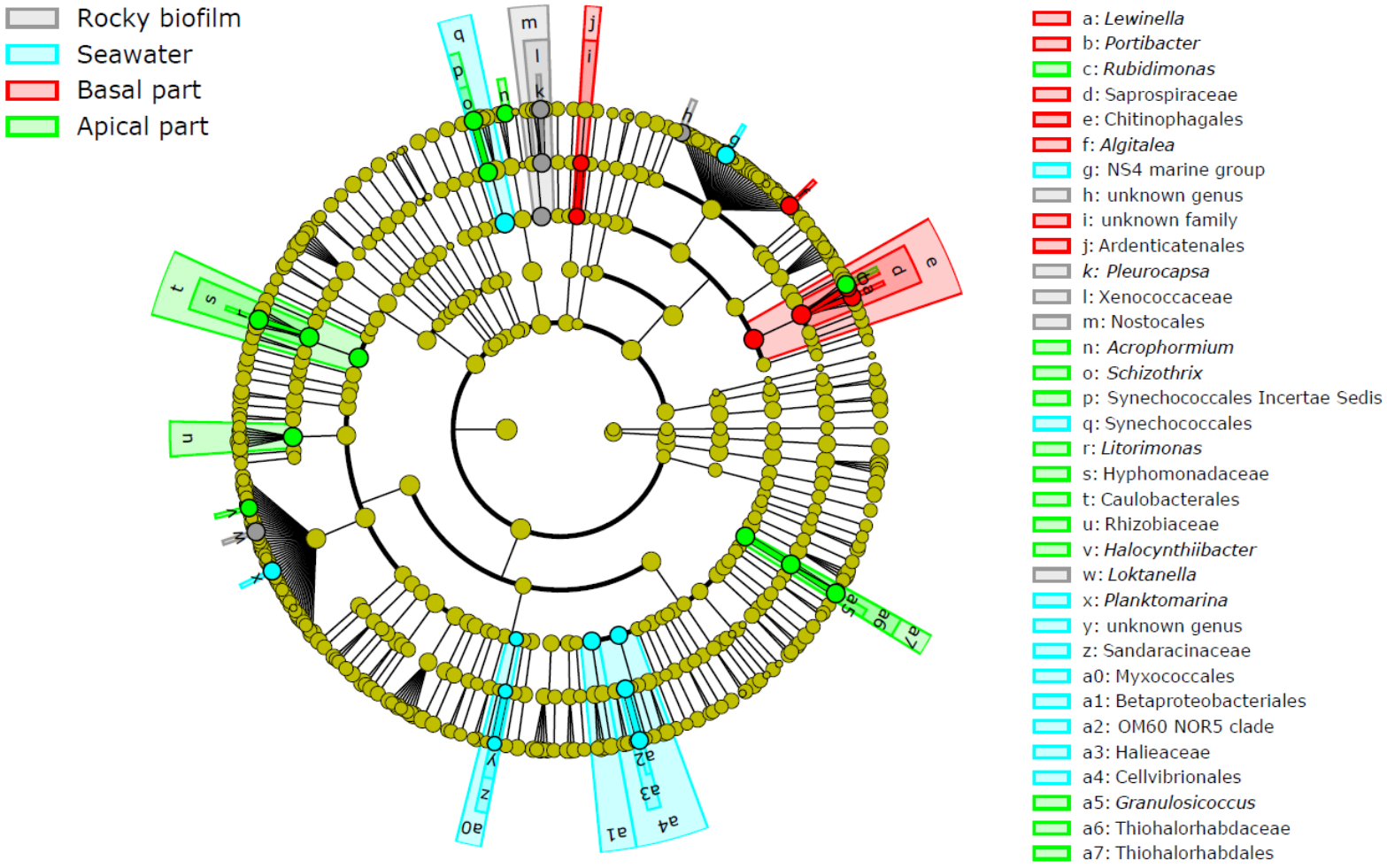

Figure SV.8. Cladogram obtained from the LEfSe analysis built with the 16S rRNA gene dataset of bacterial communities at the surface of *T. atomaria*, in rocky biofilms and in seawater at Carqueiranne.

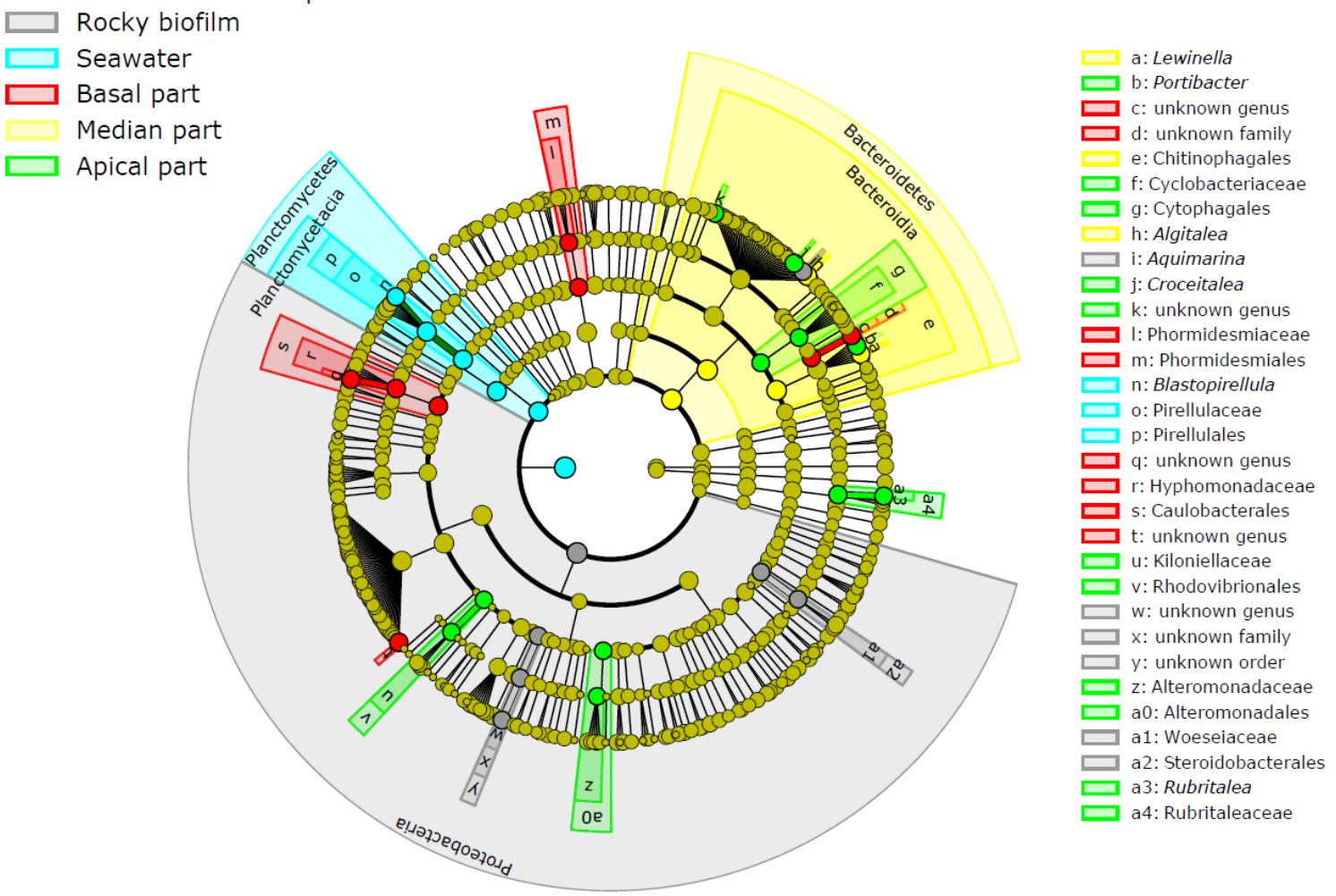

Figure SV.9. Co-occurrence network of OTUs from the 16S rRNA gene dataset of bacterial communities at the surface of *T. atomaria*, in rocky biofilms and in seawater at Tamaris

Pie-chart inside each node revealed the distribution of each OTU across the different sample groups (Red: basal part, yellow: median part, green: apical part, grey: rocky biofilm, blue: seawater). Thickness of edges between each node was proportional to correlation or dissimilarity distances. The size of each node was proportional to the relative percentage of sequences of each OTU in all samples.

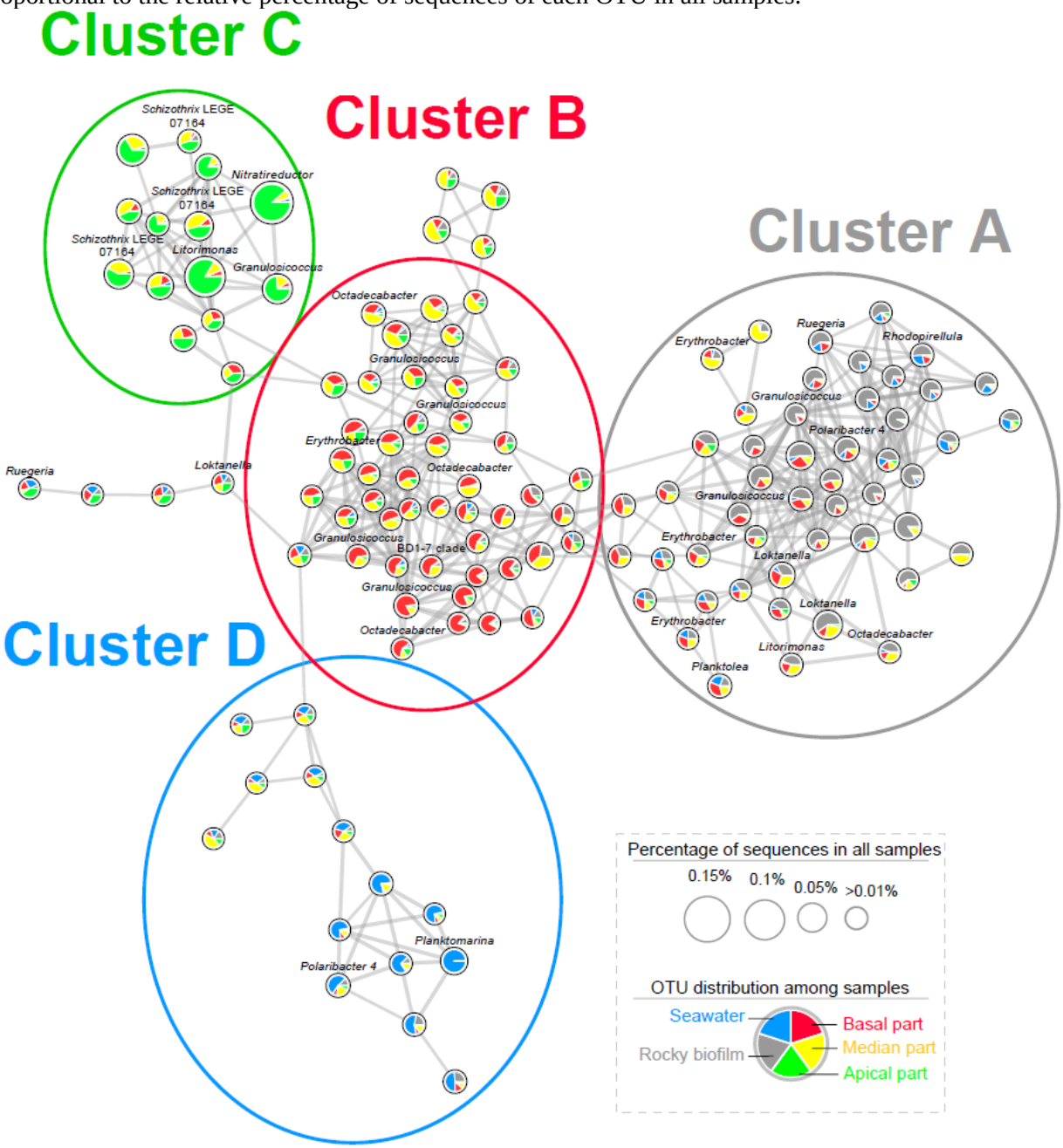

Figure SV.10. Venn diagrams showing shared percentages of sequences between: (i) the different thallus parts and rocky biofilms and (ii) the different thallus parts and sea water.

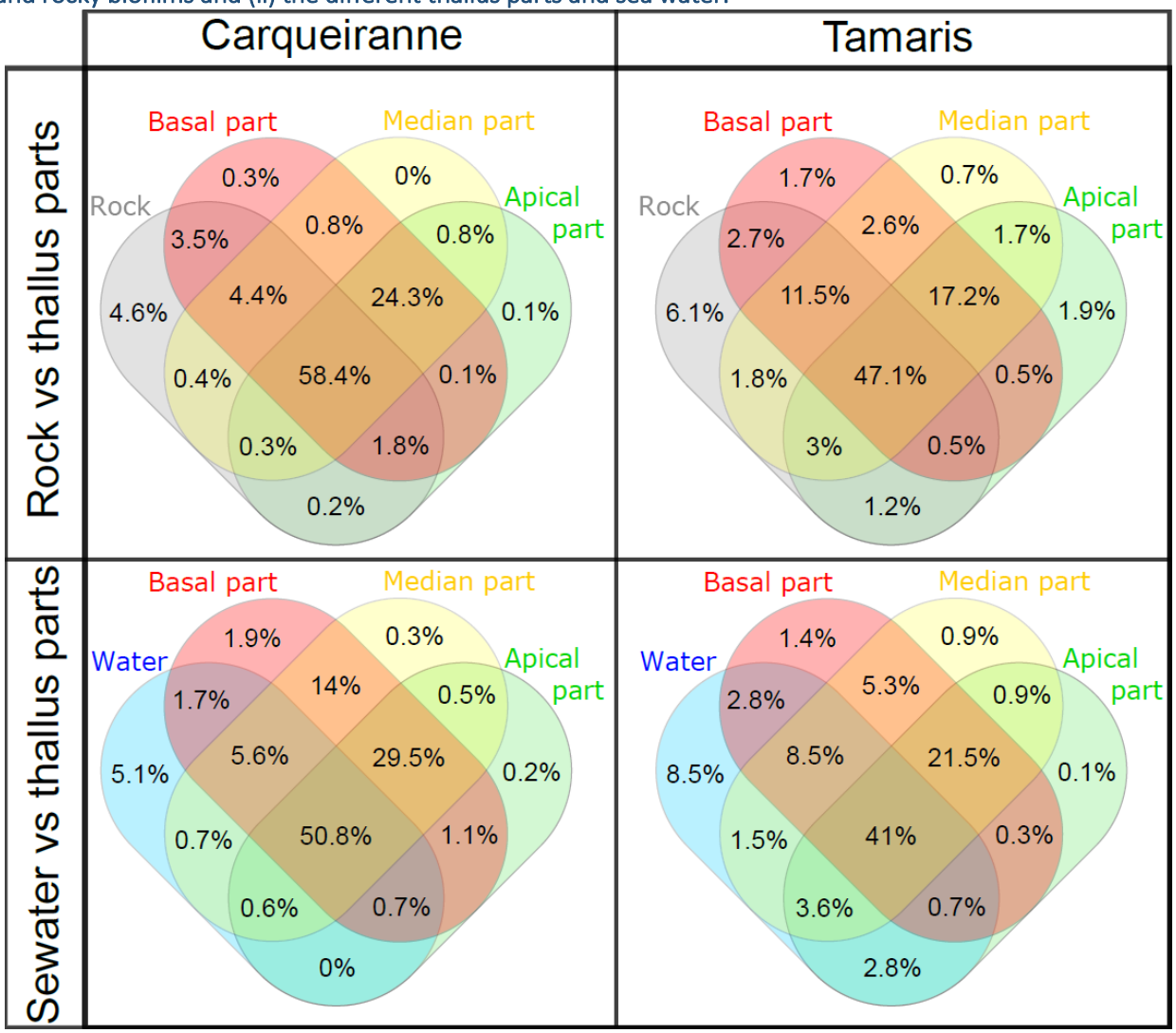

Figure SV.11. Chemodiversity indexes (Shannon) of surface extracts of *T. atomaria* (two sites: Carqueiranne and Tamaris; three algal parts: basal, median and apical) analyzed by LC-(+)-ESI-MS, LC-(-)-ESI-MS and GC-MS
Boxplots in red, yellow and green, respectively labeled ("B", "M" and "A") represented basal, median and apical algal parts.

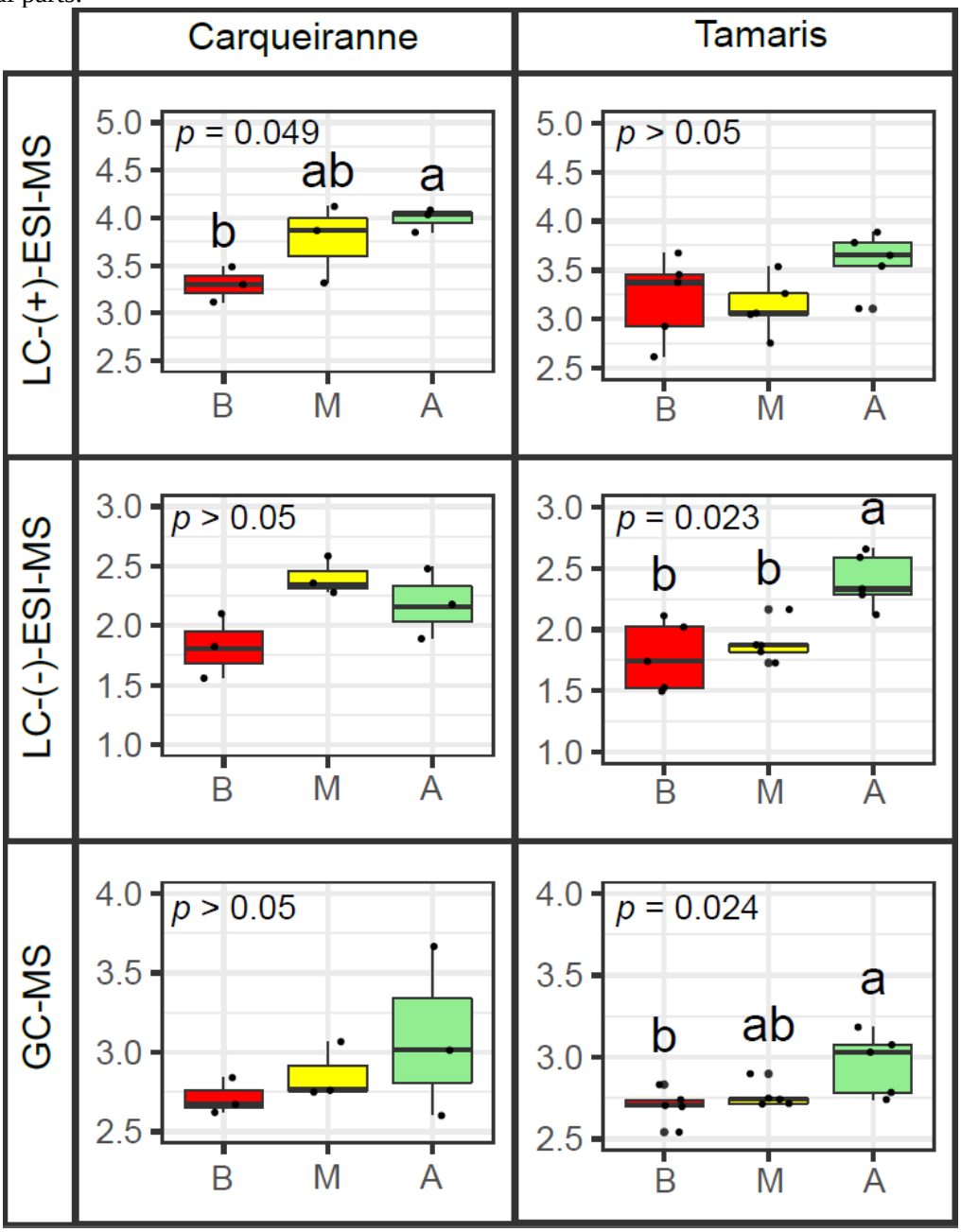

Figure SV.12. PLS-DA plots of GC-MS, LC-(-)-ESI-MS and LC-(+)-ESI-MS metabolomics analyses of surface and total extracts of *T. atomaria* (two sites: Carqueiranne and Tamaris; three algal parts: basal, median and apical).

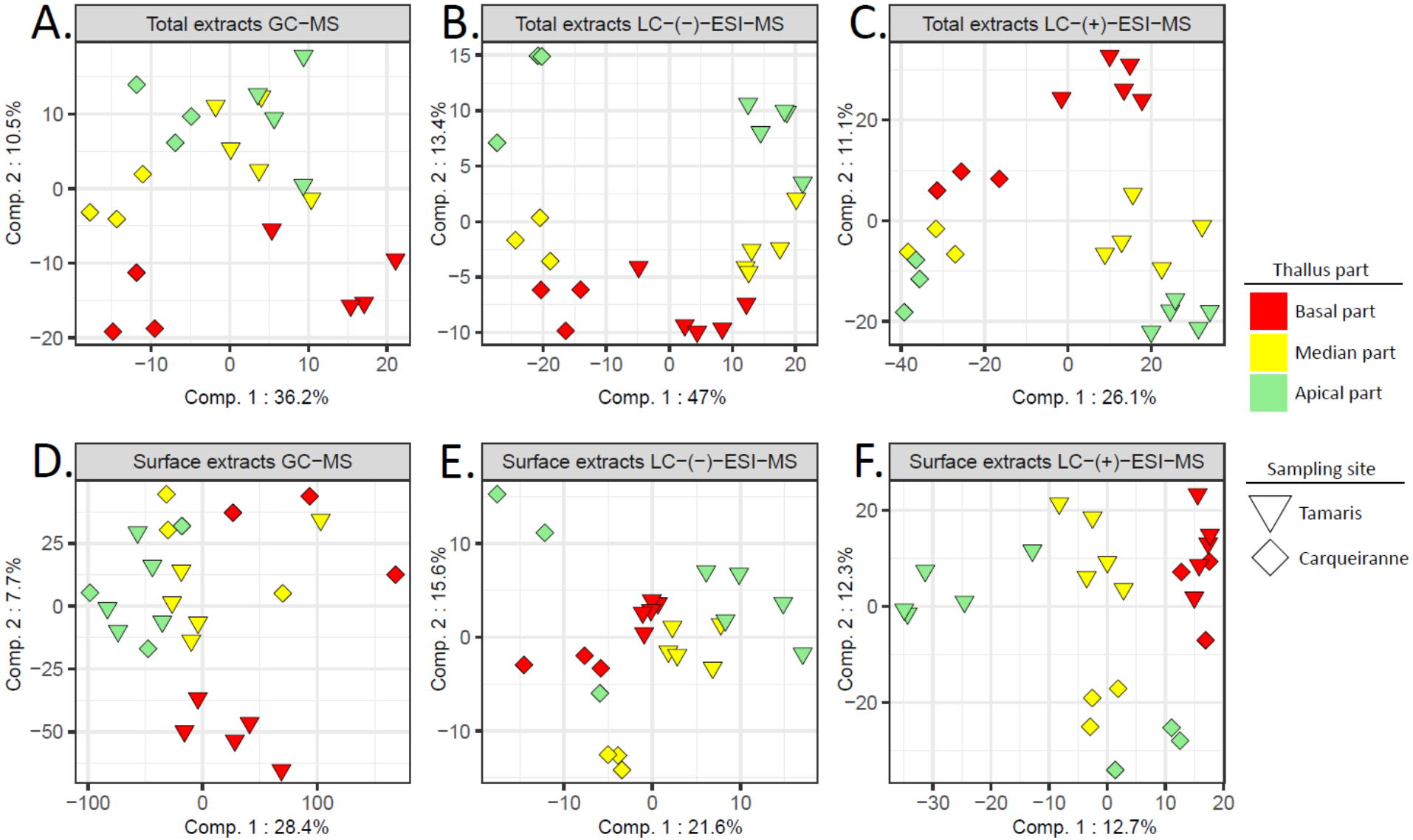

Figure SV.13. Molecular network for LC-(+)-ESI-MS dataset annotation.

Node colors were chosen according to their annotation. Node shapes were chosen according to their level of annotation (Schymanski et al., 2014; diamonds: level 1, squares: level 2, triangles: level 4 with a proposed molecular formula, circles: level 4 without molecular formula). Thickness and transparency of edge between two nodes was proportional to the cosine score (CS). Only clusters with at least three nodes were represented.

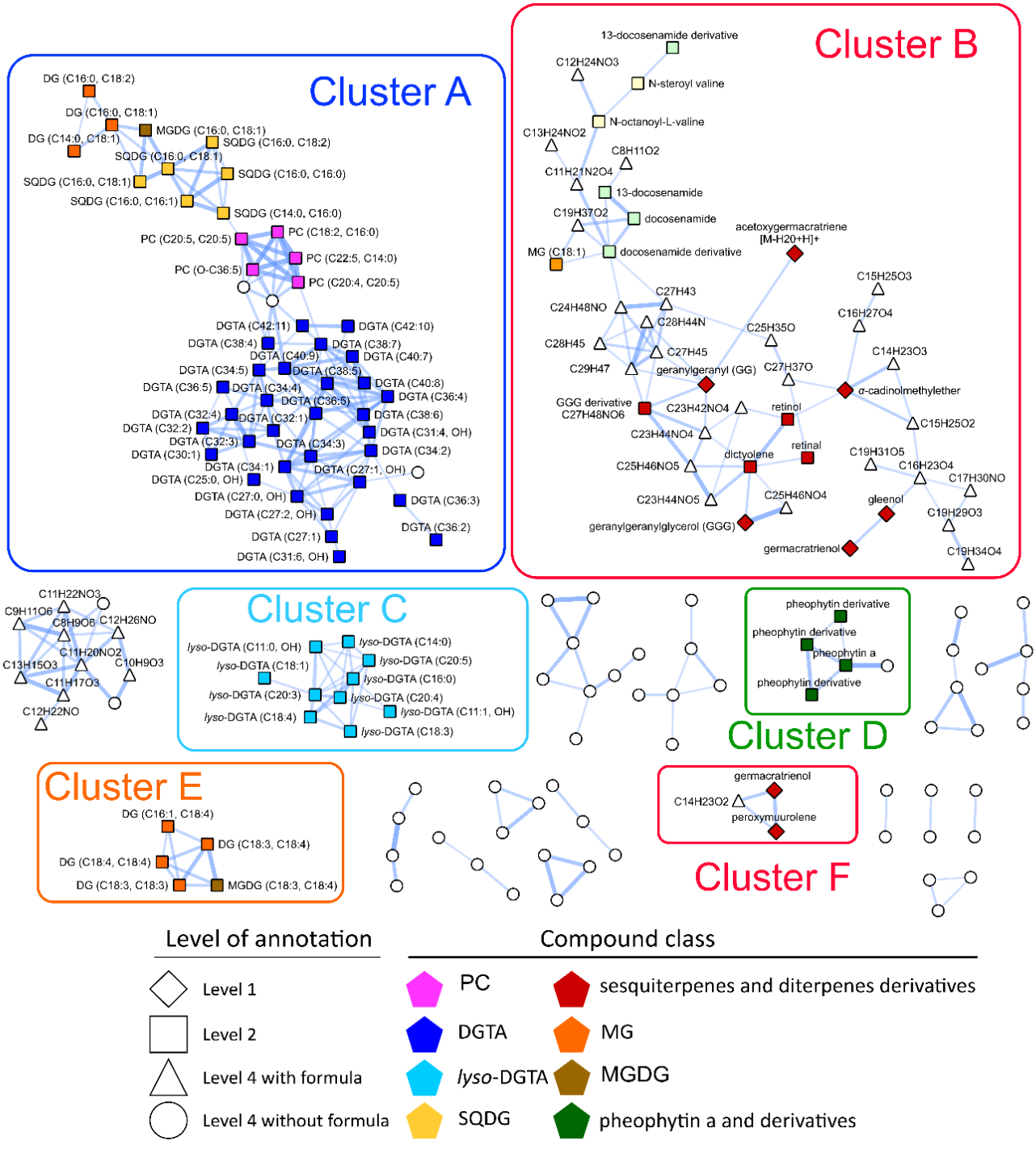

Figure SV.14. Molecular network for LC-(-)-ESI-MS dataset annotation.

Node colors were chosen according to their annotation. Node shapes were chosen according to their level of annotation (Schymanski et al., 2014; squares: level 2, circles: level 4). Thickness and transparency of edge between two nodes was proportional to the cosine score (CS). Only clusters with at least three nodes were represented.

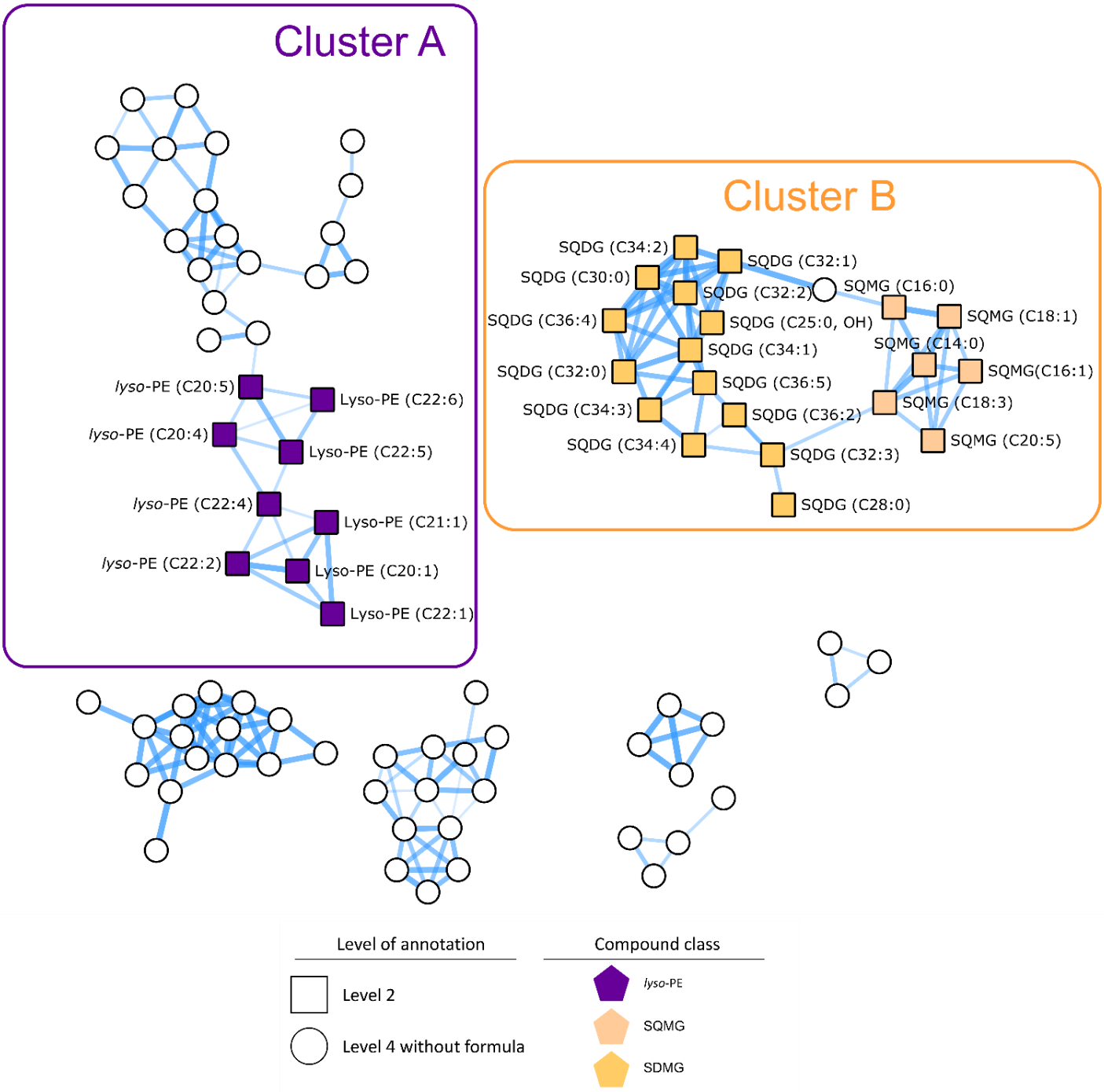

Figure SV.15. Heatmap of sesquiterpenes variations across samples identified in the GC-MS dataset.

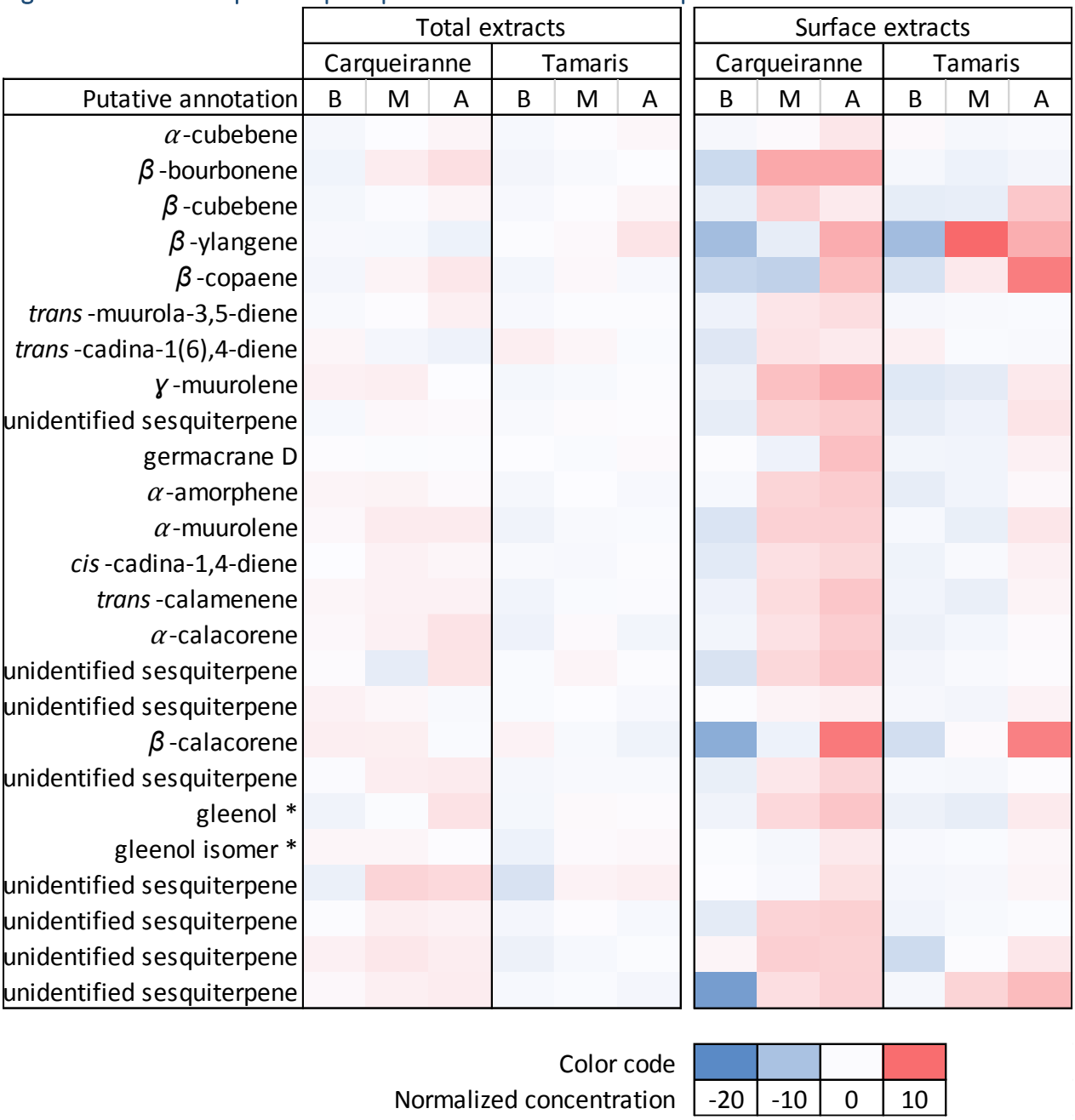

*Confirmed through purified standards.

Figure SV.16. Heatmap of annotated compounds variations identified in the LC-(+)-ESI-MS dataset (1/2).

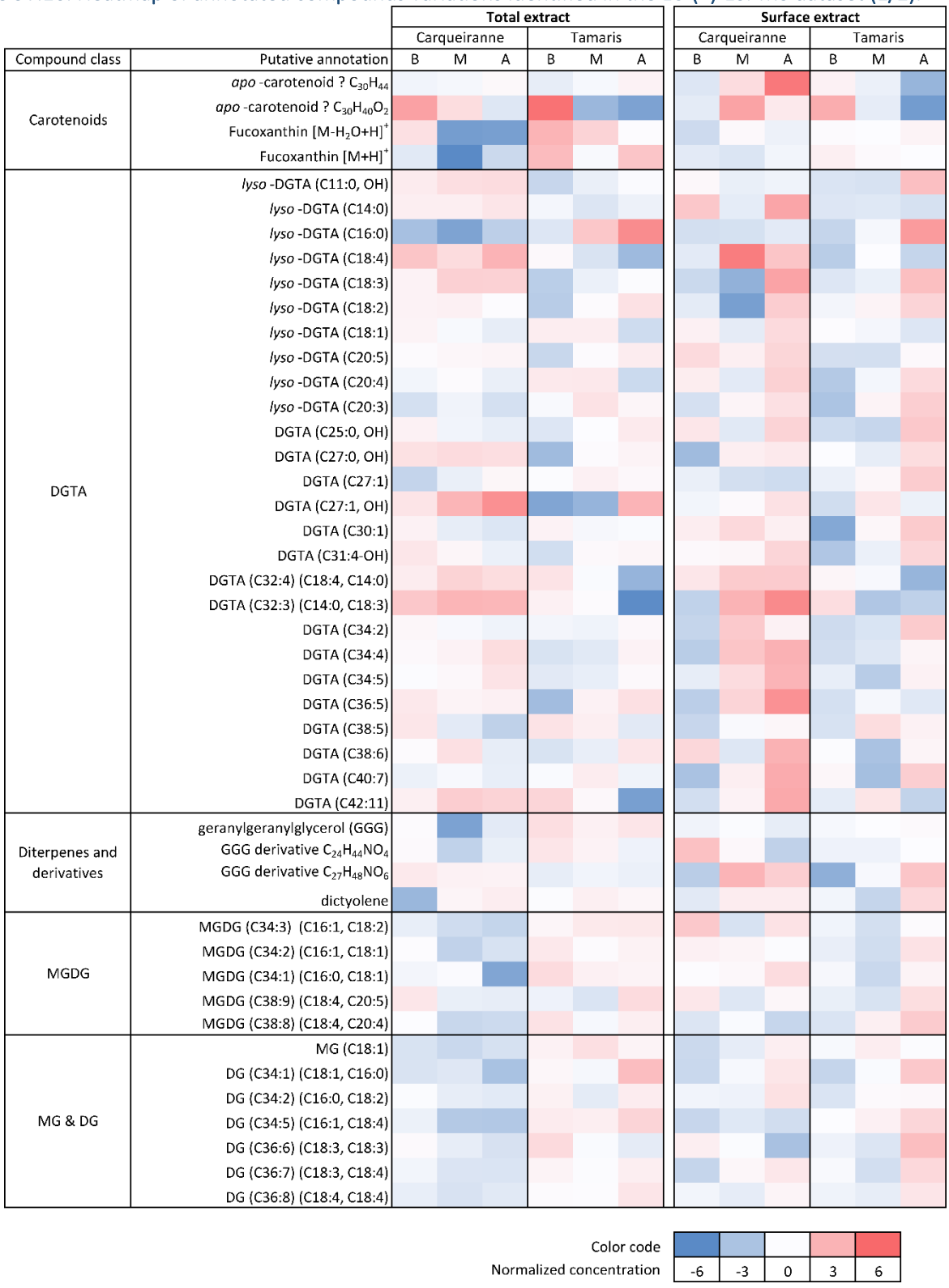

Figure SV.16. Heatmap of annotated compounds variations identified in the LC-(+)-ESI-MS dataset (2/2).

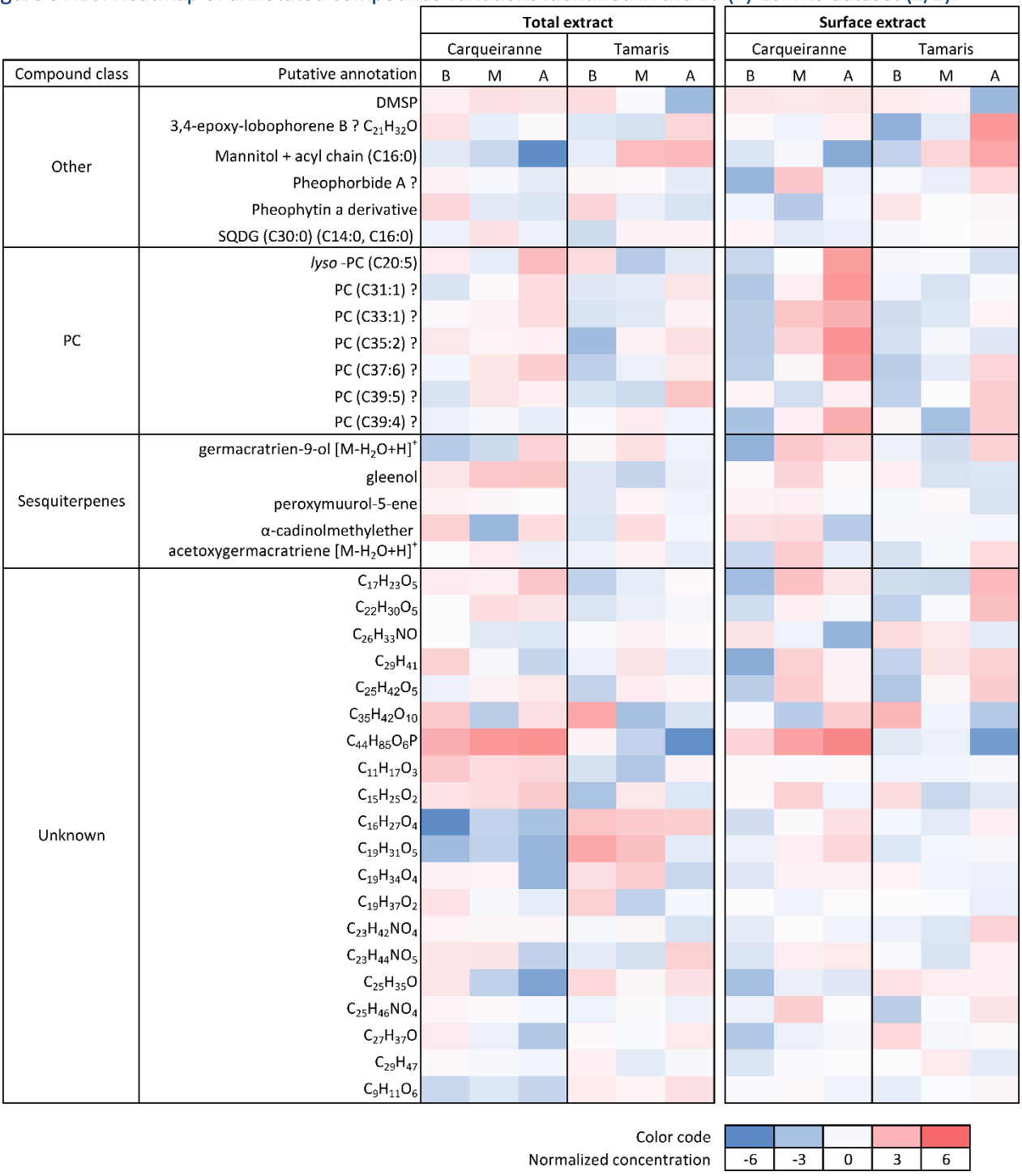

Figure SV.17. Heatmap of annotated compounds variations identified in the LC-(-)-ESI-MS dataset.

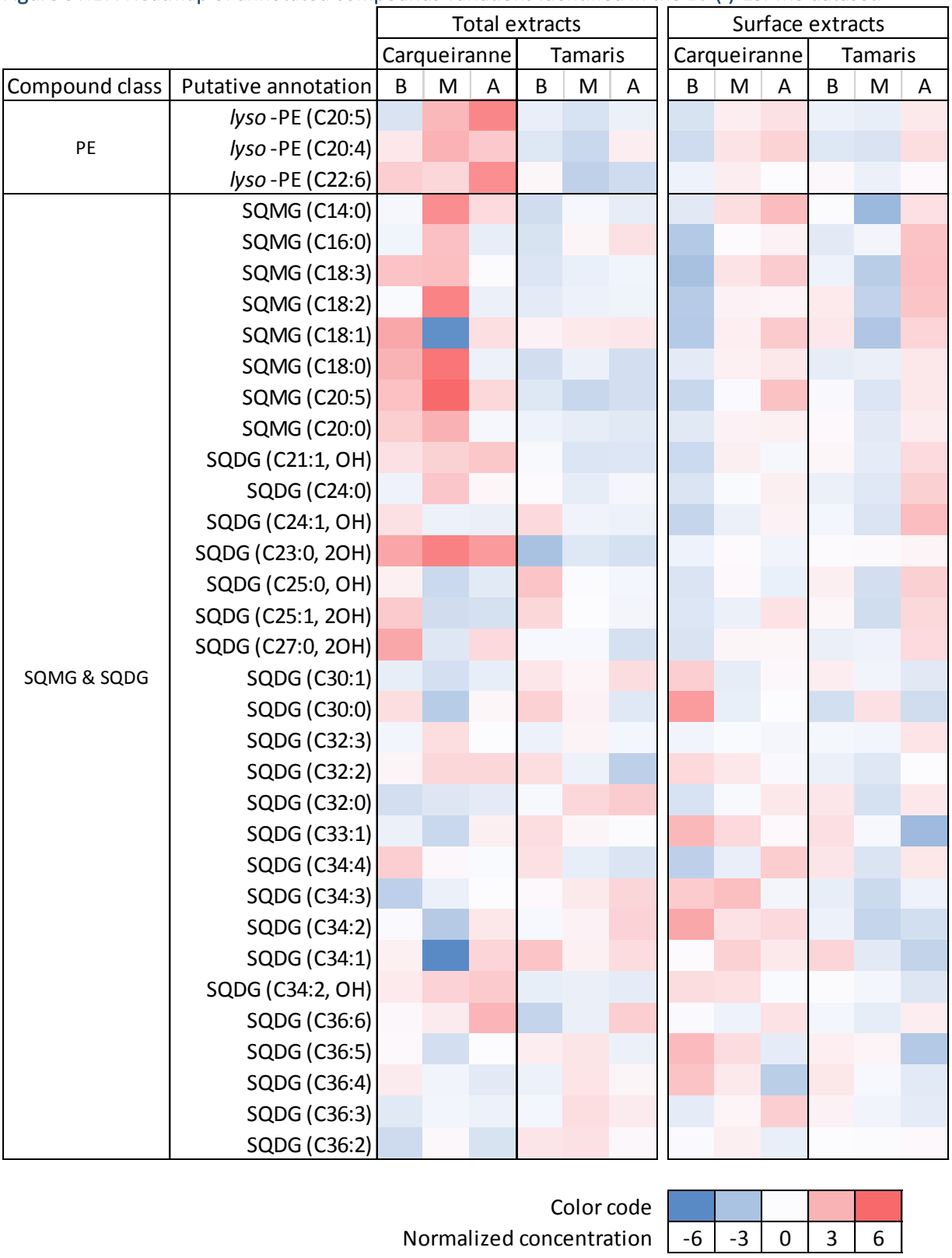

Annexe VI

Supporting information

for

A multi-omics approach deciphers how temperature and copper stress shape seaweed-microbiota interactions at the surface of *Taonia atomaria* on the NW Mediterranean coast

Benoit Paix[1], Nicolas Layglon[2], Christophe Le Poupon[2], Sébastien D'Onofrio[2], Benjamin Misson[2], Cédric Garnier[2], Gérald Culioli[1*] and Jean-François Briand[1*]

[1]*Université de Toulon, Laboratoire MAPIEM, EA 4323, Toulon, France*

[2]*Université de Toulon, Aix Marseille Université, CNRS, IRD, Mediterranean Institute of Oceanography (MIO), UM110, France*

*corresponding authors : briand@univ-tln.fr, culioli@univ-tln.fr

Supplementary information for Material and Methods

Supplementary information for sampling

Thalli of *Taonia atomaria* were collected by hand, by carefully detaching the holdfast from rocky substrates, using nitrile gloves to avoid DNA contaminations on algal surface. The GPS coordinates are 43°05'35.0"N 5°54'31.0"E for S1; 43°05'12.2"N 6°05'02.1"E for S2; 43°00'16.1"N 6°11'21.9"E for S3; 42°59'41.7"N 6°10'53.3"E for S4; and 43°07'13.7"N 6°16'00.3"E for S5. Sampling dates are detailed in Table S1. No thalli of *T. atomaria* were observed on the five sites after July. Rock and seawater (5L) samples were collected nearby algae samples. Rock samples were chosen haphazardly, and it resulted in various types of substrate.

In addition, surface seawater was collected in 1L fluorinated ethylene propylene (FEP) bottles (Nalgene) previously cleaned with 10% HNO_3 (Thermo Fisher Scientific, Illkirch, France), rinsed three times with Milli-Q water, filled with 0.1% HCl (TraceSelect, Fluka) and rinsed three times with seawater from the site. For each sampling, an aliquot of seawater was filtered in a 125 mL FEP bottle, over a 0.2 μm filter (pre-rinsed cellulose acetate syringe filter; Sartorius, Aubagne, France) in ordered to identify and quantify metals in the dissolved fraction, while a second aliquot was directly poured into a 125 mL FEP bottle for the total acid leachable fraction latter considered as the total fraction. All samples were then acidified with 0.2% HNO_3 (Suprapur; Merck) and UV-irradiated (150-W mercury lamp; Hanau, Germany) for at least 24h to degrade organic matter (Omanović et al., 2006) and to assess the concentration of metals by stripping voltammetry.

Supplementary information for dissolved organic carbon and total nitrogen analyses

Dissolved organic carbon (DOC) and total nitrogen (TN) analyses were performed using a TOC-VCSH analyzer. DOC and TN measurements are based on a high temperature catalytic oxidation followed by either an infrared (DOC) or a chemoluminescence detection (TN). The analyses were validated using certified reference materials (SUPER 05, Canada).

Supplementary information for dissolved and total concentrations trace metals analyses

Dissolved and total concentrations of trace metals were obtained by differential pulse anodic stripping voltammetry (DPASV). All measurements were performed using an Autolab III potentiostat (Metrohm, Courtaboeuf, France) equipped with an autosampler.

Supplementary information for flow cytometry analysis

Epiphytic cells were collected from algal samples by gently scraping the surface with sterile scalpels. Replicates of algal samples (n = 3) were fixed in 4 mL of 0.25% glutaraldehyde-sterile filtered seawater solution. Seawater samples (15 mL) were prefiltered using 40 μm cell strainers and fixed with 0.25% of glutaraldehyde. All samples were kept at -80°C until analysis. For algal samples, epiphytic cells potentially aggregated together were dissociated using a sonication step of 2 min. Heterotrophic prokaryotes were stained using SYBR green I (Invitrogen, Carlsbad, CA, USA) and enumerated using a BD Accuri C6 flow cytometer (BD Biosciences, San Jose, CA, USA) as previously described (Pollet et al., 2018). Heterotrophic prokaryotes were discriminated as described in Fig. S2. Results were expressed as densities of cells per cm^2 using the measured surface of each thallus estimated with the Mesurim pro software (v. 3.4).

Supplementary information for 16S rRNA gene metabarcoding analyses (FROGSS pipeline)

Sequences were filtered by removing those for which primers sequences were not present. The primer search accepts 10% of differences. Primers sequences were then removed in the remaining sequence using "cutadapt". Then, merged sequences with length below 300 pb and above 500 pb were removed. Clustering step was performed using SWARM with a clustering aggregation distance set to 3 (Mahé et al., 2014). Chimeric sequences were removed *de novo* using VSEARCH (Rognes et al., 2016). Rare OTUs representing less than 0.005% of all sequences were removed. OTUs were affiliated with the silva132 16S rRNA gene database. The final matrix was obtained by removing all sequences affiliated to 16S rRNA gene from chloroplasts and

mitochondria, and by performing a rarefaction to the minimum library size which correspond to 5 827 sequences, using the "phyloseq" R package (McMurdie and Holmes, 2013).
To investigate the effect of seawater abiotic parameters on the *β*-diversity of the algal epibacterial community, a db-RDA (Bray-Curtis distance) was performed using the rarefied OTU-table and the following seawater parameters: temperature, pH, salinity, [NO_3^-], [PO_4^-], [$Si(OH)_4$], DOC, TN, together with [Zn], [Pb], [Cd] and [Cu] (dissolved and total fractions). Oxygen measures were not used due to lacking values. As described in (Coclet et al., 2019), significant constraints were selected using "ordiR2step" constraints (999 permutations). High redundancy was observed between dissolved and total concentrations of trace metals, and only the dissolved ones were kept for the final analysis. Finally, only temperature, [PO_4^{3-}], [NO_3^-], [$Si(OH)_4$], DOC, TN, [Cu] and [Pb] were kept in the db-RDA final model. The overall significance of this model was then assessed using the *anova.cca()* function with 999 permutations using the "vegan" R package (Oksanen et al., 2019).

Supplementary information for Tax4Fun analysis

Predicted functions associated to the 16S rRNA gene dataset was performed using Tax4Fun with "themetagenomics" R package as described here: https://rdrr.io/cran/themetagenomics/man/t4f.html.
1-FTU scores were ranging from 10 to 60%. The data matrix resulted in a table of 3 610 KEGG orthologs (KO) analyzed using PCA. KEGG pathways were determined by summing respectively all affiliated KO using an in-house script. A total of 349 KEGG pathways were obtained. A focus was made on functions associated to pioneer colonization or metabolism of potential surface metabolites. 7 functions were related to pioneer colonization with the following pathways: KO02026 Biofilm formation (*E. coli*); KO0025 Biofilm formation (*P. aeruginosa*); KO05111 Biofilm formation (*V. cholerae*); KO02030 Bacterial chemotaxis; KO0240 Flagellar assembly; KO03070 Bacterial secretion system; KO00540 Lipopolysaccharide biosynthesis. Moreover, 6 pathways were focused according to the metabolism of potential surface metabolites: KO00480 Gluthathione metabolism; KO00071 Fatty acid degradation; KO00561 Glycerolipid metabolism; KO00330 Arginine and proline metabolism; KO00270 Cysteine and methionine metabolism; KO00531 Glycosaminoglycan degradation.

Supplementary information for metabolomics analyses

The surface extracts were concentrated to dryness under reduced pressure at a temperature lower than 35°C (Othmani et al., 2016a). Dried surface extracts were then transferred in 2-mL HPLC vials and stored under inert atmosphere (N_2) in the dark at -20°C until analysis. Before injection, samples were solubilized in 1mL of LC-MS grade methanol (Chromasolv, Sigma-Aldrich, St Louis, MO, USA). For all experiments, extraction and sample preparation were carried out by the same operator. Analytical blanks were prepared with exactly the same protocol as those used for surface extracts but without algal pieces. These blanks allowed the subsequent subtraction of contaminants or components coming from solvents and vials. In order to ensure quality control, a pool sample was prepared by combining 100 μL of each surface extract. The pool sample was divided into 18 2-ml HPLC vials (around 250 μL of solution in each vial) that were used as quality-control samples (QCs). To ensure analytical repeatability, a first QC was injected ten times at the beginning of the sequence in order to stabilize the chromatographic system. Then, the injection sequence consisted of the iterative injection of one QC and five samples (surface extracts and analytical blanks) randomly selected to avoid any possible time-dependent changes in LC–MS chromatographic fingerprints. Moreover, to assess sample carry-over of the analytical process, two solvent blanks (LC-MS grade methanol) were injected before the first QC and at the end of the injection sequence.
The UPLC-HRMS instrumentation consisted of a Dionex Ultimate 3000 Rapid Separation (Thermo Fisher Scientific, Waltham, MA, USA) chromatographic system equipped with a RS pump, a temperature-controlled autosampler, a thermostated column compartment and an UV-Vis diode array detector. This system was coupled to a QToF Impact II mass spectrometer (Bruker Daltonics, Bremen, Germany). The analyses were performed using an analytical core-shell reversed-phase column (150 × 2.1 mm, 1.7 μm, Kinetex Phenyl-Hexyl equipped with a SecurityGuard cartridge; Phenomenex, Le Pecq, France) with a column temperature of 40°C and a flow rate of 0.5 $mL.min^{-1}$. The autosampler temperature was set at 4°C and the injection volume was 5 μL. Mobile phases were: (A) water and (B) acetonitrile (Chromasolv; Sigma-Aldrich-Merck, Darmstadt,

Germany) containing each 0.1% (*v*/*v*) of formic acid (Ultra grade; Fluka, Fischer Scientific, Illkirch, France). The elution gradient started at 5% B and kept for 2 min, then to 100% B (linear ramp) in 8 min and kept for 4 min; then back to 5% B (linear ramp) over 0.01 min and maintained 1.99 min, for a total run time of 16 min.
The capillary voltage of the MS spectrometer was set at 4500V (positive mode), and the nebulizing parameters were set as follows: nebulizing gas (N_2) pressure at 0.4 bar, drying gas (N_2) flow at 4 $L.min^{-1}$, and drying temperature at 180°C. Mass spectra were recorded from *m/z* 50 to 1200 at a mass resolving power of 25 000 full width at half-maximum (FWHM, *m/z* = 200) and a frequency of 2 Hz. Tandem mass spectrometry analyses were performed thanks to a collision induced dissociation (CID) with a collision energy of 25 eV. A solution of formate/acetate forming clusters was automatically injected before each sample for internal mass calibration, and the mass spectrometer was calibrated with the same solution before each sequence of samples. Data handling was done using DataAnalysis software (version 4.3, Bruker Daltonics).
LC–MS raw data were automatically recalibrated using the calibration clusters found at the beginning of each chromatogram and converted into netCDF files (centroid mode) with a script developed within the DataAnalysis software. Converted files were preprocessed with the XCMS package (version 1.46.0) (Smith et al., 2006) in the R 3.2.3 environment: i) Peak picking was performed with the "centwave" method (peakwidth = c(2,20), ppm = 2) without threshold prefilter (Patti et al., 2012), ii) retention time correction was done with the "obiwarp" method (profstep = 0.1), iii) peaks were grouped using the following parameters bw = 10, minfrac = 0.5 and minsamp = 1, and iv) missing peaks were filled with default parameters.
To ensure data quality and remove redundant signals, three successive filtering steps were applied to preprocessed data using a R script described in (Favre et al., 2017). The first was based on the signal/noise (S/N) ratio to remove signals of QCs observed in analytical blanks (ratio set at 10 for features matching between QCs and analytical blanks). The second allowed suppression of signals based on the value of the coefficient of variation (CV) of the intensity of the variables in the QCs (cutoff set at 20%). A third filtering step was applied using the coefficient of the autocorrelation (with a cutoff set at 80%) between variables with a same retention time in the surface extract samples.

Supplementary information for the annotation procedure

In this study, three levels of annotation were applied for the identification of metabolites, following the same methodology described in (Paix et al., 2019, 2020).
The first approach, which corresponds to the level 1 of annotation according to (Schymanski et al., 2014), was based on the use of several commercial standards described in (Paix et al., 2019) including DMSP, proline betaine, proline and mannitol, as well as compounds previously purified from *T. atomaria* or *Dictyota* spp. by our team (Viano et al., 2009; Othmani et al., 2016b) including GGG, several sesquiterpenes and fucoxanthin. These standards were solubilized in MeOH at a concentration of 0.1 $mg.mL^{-1}$ and analyzed with the same experimental conditions used for the three metabolomics workflows. All commercial standards were purchased from Sigma-Aldrich or Cayman Chemicals.
The second strategy was to annotate putatively some *m/z* features by the comparison of their MS (and MS/MS for LC-MS analyses) data with reference databases. A match found with a MS (and MS/MS) library is considered with the level 2 of annotation (Schymanski et al., 2014). To facilitate the dereplication procedure, the molecular networking approach was used and allowed the clustering of metabolites with a similar chemical structure in a same sub-network (cluster) (Wang et al., 2016). Briefly, molecular networks were generated using GNPS platform (https://gnps.ucsd.edu/ProteoSAFe/static/gnps-splash.jsp) (Wang et al., 2016). MS/MS raw data (.mzxml files) were clustered using MS cluster with a tolerance of 0.02 Da for precursor ions and 0.02 Da for MS/MS fragment ions. Minimum cosine score (CS) value used for the clustering was set to 0.7. Data were exported and analyzed using Cytoscape (version 3.4.0). The resulting molecular network was analyzed and annotated based on MS/MS fragmentation pathways and comparison with in-house and public databases such as Metlin (https://metlin.scripps.edu/) or Lipidmaps (https://www.lipidmaps.org/).
When no characteristic fragmentation pathway was determined by comparison to the literature, the most probable chemical formula was proposed using the "Smart Formula" tool from DataAnalysis. This last step finally corresponded to the level 4 of annotation (Schymanski et al., 2014).

Supplementary information for multi-omics analysis

The MixOmics R package (Lê Cao et al., 2009) was used to perform the integration of environmental parameters together with 16S rRNA gene metabarcoding, functional predictions, and surface metabolomics datasets. For the metabolomics dataset, the matrix used was log_{10}-transformed and mean-centered. For the 16S rRNA gene metabarcoding dataset, the matrix used corresponded to the final rarefied OTU-table. The dataset of predicted functions was composed by all pathways listed in the supplementary information section for Tax4Fun analysis (a total of 13 KEGG pathways). For the environmental dataset, parameters kept in the data matrix were those selected in the final model db-RDA model as described in the supplementary section for 16S rRNA gene metabarcoding analysis.

The whole analysis was performed according to the DIABLO framework which is fully described with a case study here: http://mixomics.org/mixdiablo/case-study-tcga/. Briefly, the aim of this approach is to perform an optimal N-integration with a sparse method developed to reveal correlation between variables from heterogeneous datasets. The sparse PLS discriminant analysis allowed here to performs variable selection and classification in a one-step procedure with a PLS regression, and was used specifically here since each 'omic analysis performed corresponded to large data sets where Linear Discriminant Analysis faces collinearity issues. The analysis was performed by using a design matrix where all blocks were connected by the same link (0.1). The tuning to select the optimal number of components for each dataset was performed using the *perf()* function and resulted in 5 components for the metabarcoding and metabarcoding datasets, respectively, and 2 components for the Tax4Fun and environmental datasets, respectively. Then, the optimal number of variables per dataset was selected using the *tune.block.splsda()* function, allowing to obtain a sufficient number of variables for downstream validation/interpretation. The final model was then performed with the *block.splsda()* function. The *plotDiablo()* function allowed to determined correlations between each dataset. From this model, correlations were above 0.7 between all datasets. To visualize correlation between each variable of each dataset, the *network()* function was used with a correlation cutoff threshold set at 0.7. Subsequently, a total of 29 metabolites, 28 OTUs, 6 predicted pathways and 3 environmental parameters were selected for the network structuration with only positive correlations above 0.7 and negative correlations below -0.7. The resulting network was exported using "igraph" R package and analyzed using Cytoscape.

References

Coclet, C., Garnier, C., Durrieu, G., Omanović, D., D'Onofrio, S., Le Poupon, C., et al. (2019). Changes in bacterioplankton communities resulting from direct and indirect interactions with trace metal gradients in an urbanized marine coastal area. *Front. Microbiol.* 10, 257. doi:10.3389/fmicb.2019.00257.

Favre, L., Ortalo-Magné, A., Greff, S., Pérez, T., Thomas, O. P., Martin, J.-C., et al. (2017). Discrimination of four marine biofilm-forming bacteria by LC-MS metabolomics and influence of culture parameters. *J. Proteome Res.* 16, 1962–1975. doi:10.1021/acs.jproteome.6b01027.

Lê Cao, K.-A., González, I., and Déjean, S. (2009). integrOmics: an R package to unravel relationships between two omics datasets. *Bioinformatics* 25, 2855–2856. doi:10.1093/bioinformatics/btp515.

Mahé, F., Rognes, T., Quince, C., Vargas, C. de, and Dunthorn, M. (2014). Swarm: robust and fast clustering method for amplicon-based studies. *PeerJ* 2, e593. doi:10.7717/peerj.593.

McMurdie, P. J., and Holmes, S. (2013). phyloseq: an R package for reproducible interactive analysis and graphics of microbiome census data. *PLoS One* 8, e61217. doi:10.1371/journal.pone.0061217.

Oksanen, J., Blanchet, F. G., Friendly, M., Kindt, R., Legendre, P., McGlinn, D., et al. (2019). *vegan: Community ecology package*. Available at: https://CRAN.R-project.org/package=vegan [Accessed January 15, 2020].

Omanović, D., Kwokal, Ž., Goodwin, A., Lawrence, A., Banks, C. E., Compton, R. G., et al. (2006). Trace metal detection in Šibenik Bay, Croatia: Cadmium, lead and copper with anodic stripping voltammetry and manganese via sonoelectrochemistry. A case study. *J Iran Chem Soc* 3, 128–139. doi:10.1007/BF03245940.

Othmani, A., Briand, J.-F., Ayé, M., Molmeret, M., and Culioli, G. (2016a). Surface metabolites of the brown alga *Taonia atomaria* have the ability to regulate epibiosis. *Biofouling* 32, 801–813. doi:10.1080/08927014.2016.1198954.

Othmani, A., Bunet, R., Bonnefont, J.-L., Briand, J.-F., and Culioli, G. (2016b). Settlement inhibition of marine biofilm bacteria and barnacle larvae by compounds isolated from the Mediterranean brown alga *Taonia atomaria*. *J Appl Phycol* 28, 1975–1986. doi:10.1007/s10811-015-0668-4.

Paix, B., Carriot, N., Barry-Martinet, R., Greff, S., Misson, B., Briand, J.-F., et al. (2020). A multi-omics analysis suggests links between the differentiated surface metabolome and epiphytic microbiota along the thallus of a Mediterranean seaweed holobiont. *Front. Microbiol.* 11, 494. doi:10.3389/fmicb.2020.00494.

Paix, B., Othmani, A., Debroas, D., Culioli, G., and Briand, J.-F. (2019). Temporal covariation of epibacterial community and surface metabolome in the Mediterranean seaweed holobiont *Taonia atomaria*. *Environ. Microbiol.* 21, 3346–3363. doi:10.1111/1462-2920.14617.

Patti, G. J., Tautenhahn, R., and Siuzdak, G. (2012). Meta-analysis of untargeted metabolomic data from multiple profiling experiments. *Nat Protoc* 7, 508–516. doi:10.1038/nprot.2011.454.

Pollet, T., Berdjeb, L., Garnier, C., Durrieu, G., Le Poupon, C., Misson, B., et al. (2018). Prokaryotic community successions and interactions in marine biofilms: the key role of Flavobacteriia. *FEMS Microbiol. Ecol.* 94. doi:10.1093/femsec/fiy083.

Rognes, T., Flouri, T., Nichols, B., Quince, C., and Mahé, F. (2016). VSEARCH: a versatile open source tool for metagenomics. *PeerJ* 4, e2584. doi:10.7717/peerj.2584.

Schymanski, E. L., Jeon, J., Gulde, R., Fenner, K., Ruff, M., Singer, H. P., et al. (2014). Identifying small molecules via high resolution mass spectrometry: Communicating confidence. *Environ. Sci. Technol.* 48, 2097–2098. doi:10.1021/es5002105.

Smith, C. A., Want, E. J., O'Maille, G., Abagyan, R., and Siuzdak, G. (2006). XCMS: processing mass spectrometry data for metabolite profiling using nonlinear peak alignment, matching, and identification. *Anal. Chem.* 78, 779–787. doi:10.1021/ac051437y.

Viano, Y., Bonhomme, D., Camps, M., Briand, J.-F., Ortalo-Magné, A., Blache, Y., et al. (2009). Diterpenoids from the Mediterranean brown alga *Dictyota* sp. evaluated as antifouling substances against a marine bacterial biofilm. *J. Nat. Prod.* 72, 1299–1304. doi:10.1021/np900102f.

Wang, M., Carver, J. J., Phelan, V. V., Sanchez, L. M., Garg, N., Peng, Y., et al. (2016). Sharing and community curation of mass spectrometry data with Global Natural Products Social Molecular Networking. *Nat. Biotechnol.* 34, 828–837. doi:10.1038/nbt.3597.

Supplementary Tables

Table SVI.1. Environmental parameters and sampling dates (Part 1: from February to April 2017).
For trace metals, (d) and (t) indicates dissolved and total acid leachable fractions. n.d.: not determined.

Month	Site	Date	Temperature	O_2	pH	Salinity	$N\text{-}NO_3^-$	$SI(OH)_4$	PO_4^{3-}	DOC	TN	Zn (d)	Zn (t)	Pb (d)	Pb (t)	Cd (d)	Cd (t)	Cu (d)	Cu (t)
		(dd/mm)	(°C)	(%)	-	(ppt)	(μM)	(μM)	(μM)	(mg $C.L^{-1}$)	(mg $N.L^{-1}$)	(nM)	(nM)	(nM)	(nM)	(nM)	(nM)	(nM)	(nM)
M1 Feb.	S1	15/02	12.9	n.d.	8.2	37.8	0.38 ± 0.05	0.88 ± 0.04	0.33 ± 0.06	1.03 ± 0.01	0.10 ± 0.001	61.0	64.4	1.65	4.35	0.13	0.14	22.1	23.1
	S2	15/02	13.8	n.d.	8.2	38.1	0.38 ± 0.05	0.63 ± 0.03	0.23 ± 0.01	0.98 ± 0.01	0.07 ± 0.003	7.6	6.7	0.12	0.28	0.06	0.05	3.3	4.1
	S3	21/02	12.3	n.d.	8.4	38.6	0.51 ± 0.06	0.28 ± 0.04	0.27 ± 0.04	0.99 ± 0.01	0.07 ± 0.002	6.9	7.5	0.14	0.12	0.05	0.06	3.8	3.7
	S4	21/02	11.5	n.d.	8.4	38.6	0.51 ± 0.05	0.28 ± 0.04	0.26 ± 0.01	1.01 ± 0.02	0.09 ± 0.008	5.1	4.3	0.08	0.09	0.05	0.06	2.7	2.9
	S5	23/02	14.7	n.d.	8.2	38.4	0.38 ± 0.05	0.48 ± 0.07	0.22 ± 0.03	1.13 ± 0.01	0.09 ± 0.004	50.3	53.1	1.02	1.48	0.12	0.12	4.4	4.8
M2 Mar.	S1	27/03	15.8	103	7.8	36.5	0.44 ± 0.05	0.46 ± 0.04	0.23 ± 0.06	1.11 ± 0.01	0.11 ± 0.002	48.0	65.9	1.29	5.20	0.11	0.12	20.8	28.1
	S2	27/03	14.9	84	7.9	37.2	0.38 ± 0.05	0.59 ± 0.03	0.19 ± 0.07	1.03 ± 0.01	0.07 ± 0.002	7.4	7.9	0.14	0.34	0.07	0.04	3.7	4.3
	S3	23/03	15.5	83	8.3	38.3	0.35 ± 0.05	0.15 ± 0.16	0.18 ± 0.03	1.00 ± 0.01	0.07 ± 0.004	9.0	10.7	0.12	0.19	0.06	0.07	3.8	4.5
	S4	23/03	14.3	84	7.9	38.2	0.38 ± 0.05	0.40 ± 0.10	0.19 ± 0.05	1.02 ± 0.01	0.08 ± 0.004	6.8	7.5	0.09	0.25	0.07	0.07	3.1	3.7
	S5	27/03	14.4	94	8.0	37.1	0.35 ± 0.05	0.57 ± 0.05	0.18 ± 0.03	1.12 ± 0.01	0.18 ± 0.002	109.3	149.4	1.81	4.28	0.16	0.24	4.7	6.9
M3 Apr.	S1	18/04	16.9	119	8.1	36.8	0.35 ± 0.04	0.52 ± 0.09	0.34 ± 0.04	1.10 ± 0.02	0.09 ± 0.002	32.4	39.2	1.18	3.04	0.08	0.09	14.8	19.0
	S2	18/04	16.0	95	8.2	37.0	0.32 ± 0.04	0.57 ± 0.02	0.18 ± 0.01	1.07 ± 0.01	0.08 ± 0.002	6.1	8.2	0.14	0.44	0.05	0.05	4.1	5.4
	S3	27/04	14.6	88	7.7	37.2	0.28 ± 0.04	0.87 ± 0.01	0.36 ± 0.11	1.10 ± 0.01	0.26 ± 0.004	10.0	9.4	0.12	0.23	0.06	0.06	5.2	6.0
	S4	27/04	14.4	84	7.8	37.2	0.22 ± 0.04	0.22 ± 0.12	0.26 ± 0.06	1.07 ± 0.01	0.08 ± 0.001	10.6	10.4	0.07	0.23	0.07	0.06	2.8	3.7
	S5	18/04	15.2	86	8.0	37.3	0.28 ± 0.04	0.21 ± 0.01	0.28 ± 0.08	1.16 ± 0.01	0.10 ± 0.004	338.9	348.3	3.65	7.46	0.43	0.50	6.7	8.7

Table SVI.1. Environmental parameters and sampling dates (Part 2 from May to July 2017).

For trace metals, (d) and (t) indicates dissolved and total acid leachable fractions. n.d.: not determined.

Month	Site	Date	Temperature	O_2	pH	Salinity	$N\text{-}NO_3^-$	$SI(OH)_4$	PO_4^{3-}	DOC	TN	Zn (d)	Zn (t)	Pb (d)	Pb (t)	Cd (d)	Cd (t)	Cu (d)	Cu (t)
		(dd/mm)	(°C)	(%)	-	(ppt)	(μM)	(μM)	(μM)	(mg $C.L^{-1}$)	(mg $N.L^{-1}$)	(nM)	(nM)	(nM)	(nM)	(nM)	(nM)	(nM)	(nM)
M4 May	S1	29/05	22.1	90	8.1	36.6	0.28 ± 0.04	0.58 ± 0.09	0.18 ± 0.05	1.32 ± 0.01	0.09 ± 0.003	45.3	109.2	1.50	15.21	0.08	0.12	37.5	63.2
	S2	29/05	21.6	88	7.9	36.8	0.28 ± 0.04	0.34 (SD n.d.)	0.12 ± 0.02	1.34 ± 0.01	0.16 ± 0.001	14.0	15.9	0.74	0.28	0.06	0.06	6.2	6.5
	S3	18/05	18.4	93	8.2	36.8	0.25 ± 0.04	0.64 ± 0.21	0.10 ± 0.02	1.07 ± 0.01	0.08 ± 0.003	10.0	10.8	0.11	0.17	0.06	0.06	3.2	3.4
	S4	18/05	17.1	92	8.2	36.9	0.28 ± 0.04	0.40 ± 0.12	0.09 ± 0.01	1.10 ± 0.02	0.07 ± 0.001	7.1	5.8	0.10	0.24	0.06	0.06	2.7	3.0
	S5	29/05	19.9	85	8.0	36.8	0.28 ± 0.04	0.27 ± 0.08	0.06 ± 0.01	1.12 ± 0.01	0.08 ± 0.002	78.2	92.9	1.74	2.70	0.18	0.20	4.4	5.3
M5 Jun.	S1	27/06	24.3	82	8.0	36.9	0.29 ± 0.02	0.75 ± 0.02	0.10 ± 0.02	1.04 ± 0.01	0.11 ± 0.010	27.6	56.0	1.14	8.51	0.08	0.10	20.9	39.1
	S2	27/06	23.2	88	8.0	36.8	0.38 ± 0.02	0.75 ± 0.03	0.06 ± 0.01	1.06 ± 0.01	0.12 ± 0.010	8.8	11.0	0.17	0.41	0.06	0.06	6.1	6.5
	S3	21/06	23.6	94	7.9	36.9	0.35 ± 0.02	0.72 ± 0.07	0.16 ± 0.06	0.98 ± 0.02	0.08 ± 0.010	13.1	12.0	0.25	0.15	0.06	0.07	7.6	6.6
	S4	21/06	23.8	84	7.9	36.9	0.32 ± 0.02	0.5 ± 0.04	0.12 ± 0.06	1.16 ± 0.02	0.11 ± 0.010	7.5	7.9	0.10	0.17	0.08	0.10	4.0	3.8
M6 Jul.	S2	18/07	23.1	89	8.0	37.1	0.63 ± 0.05	0.58 ± 0.04	0.23 ± 0.02	1.15 ± 0.01	0.10 ± 0.001	6.8	15.4	0.11	0.18	0.07	0.06	6.3	6.4
	S4	12/07	21.3	80	8.0	37.0	0.65 ± 0.05	0.36 ± 0.02	0.26 ± 0.01	1.11 ± 0.02	0.08 ± 0.001	10.6	8.8	0.05	0.11	0.06	0.07	3.3	3.4

Table SVI.2. Multivariate pairwise results (*p* values) examining differences between "sample types" for the 16S rRNA gene dataset with all samples (999 permutations).

	Rocky biofilms	***T. atomaria***
T. atomaria	0.001	-
Seawater	0.001	0.001

Table SVI.3. Multivariate pairwise results (*p* values) examining differences between "months" and between "sites" for the 16S rRNA gene dataset with *Taonia atomaria* samples (999 permutations).

Comparison between months					
	M1	**M2**	**M3**	**M4**	**M5**
M2	0.001	-	-	-	-
M3	0.001	0.001	-	-	-
M4	0.001	0.001	0.003	-	-
M5	0.001	0.001	0.001	0.002	-
M6	0.001	0.001	0.001	0.001	0.031

Comparison between sites				
	S1	**S2**	**S3**	**S4**
S2	0.003	-	-	-
S3	0.003	0.023	-	-
S4	0.003	0.012	0.111	-
S5	0.003	0.023	0.039	0.012

Table SVI.4. Multivariate pairwise results (*p* values) examining differences between "months" and between "sites" for the 16S rRNA gene dataset with rocky biofilm samples (999 permutations).

Comparison between months					
	M1	**M2**	**M3**	**M4**	**M5**
M2	0.920	-	-	-	-
M3	0.110	0.230	-	-	-
M4	0.110	0.130	0.560	-	-
M5	0.110	0.230	0.230	0.630	-
M6	0.230	0.350	0.580	0.630	0.640

Comparison between sites				
	S1	**S2**	**S3**	**S4**
S2	0.072	-	-	-
S3	0.072	0.072	-	-
S4	0.072	0.235	0.903	-
S5	0.072	0.217	0.235	0.55

Table SVI.5. Multivariate pairwise results (*p* values) examining differences between "months" and between "sites" for the 16S rRNA gene dataset with seawater samples (999 permutations).

Comparison between months					
	M1	**M2**	**M3**	**M4**	**M5**
M2	0.224	-	-	-	-
M3	0.038	0.038	-	-	-
M4	0.038	0.038	0.038	-	-
M5	0.038	0.038	0.038	0.038	-
M6	0.057	0.056	0.056	0.119	0.900

Comparison between sites				
	S1	**S2**	**S3**	**S4**
S2	0.330	-	-	-
S3	0.330	0.820	-	-
S4	0.330	0.340	0.370	-
S5	0.240	0.750	0.920	0.240

Table SVI.6. SIMPER results of the most contributing genera to the dissimilarities between seawater and algal samples.

Only the first 50% of the cumulative contribution is shown. *p* values were calculated with a permutation test constructed with 999 permutations and corresponded to the probability of getting a larger or equal average contribution in random permutation of the group factor. Cum. sum corresponded to the ordered cumulative contribution.

Order	Family	Genus	Average contribution	SD	Av. water samples	Av. algal samples	Cum. sum	*p* value
Synechococcales	*Cyanobiaceae*	*Synechococcus*	6.8%	0.06	294	0	8.2%	0.020
Caulobacterales	*Hyphomonadaceae*	*Litorimonas*	3.6%	0.04	4	159	12.5%	0.216
Rhodobacterales	*Rhodobacteraceae*	*Litorimicrobium*	2.8%	0.04	123	0	19.8%	0.020
Thiohalorhabdales	*Thiohalorhabdaceae*	*Granulosicoccus*	2.8%	0.03	10	132	23.2%	0.137
Rhizobiales	*Rhizobiaceae*	*Nitratireductor*	2.5%	0.04	7	113	26.2%	0.647
Chitinophagales	*Saprospiraceae*	Unknown	2.5%	0.02	26	134	29.2%	0.020
Flavobacteriales	*Flavobacteriaceae*	*Algitalea*	2.4%	0.03	0	103	32.1%	0.490
Pirellulales	*Pirellulaceae*	Unknown	2.3%	0.02	102	0	34.9%	0.020
Flavobacteriales	*Flavobacteriaceae*	NS4 marine group	2.2%	0.04	97	0	37.6%	0.020
Flavobacteriales	*Flavobacteriaceae*	NS5 marine group	1.9%	0.04	84	0	40.0%	0.020
Rhodobacterales	*Rhodobacteraceae*	*Planktotalea*	1.5%	0.03	71	7	41.8%	0.020
Verrucomicrobiales	*Rubritaleaceae*	*Rubritalea*	1.3%	0.01	67	59	43.4%	0.20
Flavobacteriales	*Flavobacteriaceae*	*Formosa*	1.3%	0.02	56	0	45.0%	0.020
Rhodobacterales	*Rhodobacteraceae*	Unknown	1.2%	0.01	35	74	46.5%	0.863
Flavobacteriales	*Flavobacteriaceae*	*Croceitalea*	1.1%	0.01	10	57	47.8%	0.040
SAR11 clade	*Clade I*	Clade Ia	1.1%	0.03	46	0	49.1%	0.020

Table SVI.7. SIMPER results of the most contributing genera to the dissimilarities between rocky biofilm samples and algal samples.

Only the first 50% of the cumulative contribution is showed. *p* values were calculated with a permutation test constructed with 999 permutations and corresponded to the probability of getting a larger or equal average contribution in random permutation of the group factor. Cum. sum corresponded to the ordered cumulative contribution.

Order	Family	Genus	Average contribution	SD	Av. rocky biofilms	Av. algal samples	Cum. sum	*p* value
Caulobacterales	*Hyphomonadaceae*	*Litorimonas*	3.3%	0.04	17	159	4.8%	0.431
Rhizobiales	*Rhizobiaceae*	*Nitratireductor*	2.6%	0.04	2	113	13.0%	0.647
Thiohalorhabdales	*Thiohalorhabdaceae*	*Granulosicoccus*	2.6%	0.03	26	132	16.7%	0.255
Flavobacteriales	*Flavobacteriaceae*	*Algitalea*	2.3%	0.03	19	103	20.0%	0.490
Rhodobacterales	*Rhodobacteraceae*	*Loktanella*	1.9%	0.02	99	27	22.7%	0.020
Chitinophagales	*Saprospiraceae*	Unknown	1.5%	0.01	100	134	25.0%	0.941
Flavobacteriales	*Flavobacteriaceae*	*Maritimimonas*	1.5%	0.01	65	2	27.1%	0.020
Rhodobacterales	*Rhodobacteraceae*	Unknown	1.4%	0.01	95	74	29.0%	0.216
Chitinophagales	*Saprospiraceae*	*Lewinella*	1.2%	0.01	80	42	30.8%	0.020
Flavobacteriales	*Flavobacteriaceae*	*Aquimarina*	1.2%	0.02	52	22	32.6%	0.020
Verrucomicrobiales	*Rubritaleaceae*	*Rubritalea*	1.2%	0.01	12	59	34.3%	0.588
Flavobacteriales	*Flavobacteriaceae*	*Croceitalea*	1.1%	0.01	20	57	35.9%	0.118
Flavobacteriales	*Flavobacteriaceae*	*Winogradskyella*	0.9%	0.01	52	23	38.6%	0.020
Chitinophagales	*Saprospiraceae*	*Rubidimonas*	0.9%	0.01	19	51	39.9%	0.098
Thiotrichales	*Thiotrichaceae*	*Leucothrix*	0.9%	0.01	1	39	41.1%	0.118
Flavobacteriales	*Flavobacteriaceae*	*Maribacter*	0.9%	0.01	37	36	42.4%	0.510
Rhodobacterales	*Rhodobacteraceae*	*Litoreibacter*	0.8%	0.01	53	22	43.6%	0.020
Nostocales	*Xenococcaceae*	*Pleurocapsa*	0.8%	0.01	37	2	44.8%	0.020
Flavobacteriales	*Flavobacteriaceae*	*Tenacibaculum*	0.8%	0.01	12	38	45.9%	0.373
Microtrichales	*Microtrichaceae*	Sva0996 marine group	0.7%	0.01	9	34	47.0%	0.510
Rhodobacterales	*Rhodobacteraceae*	*Planktotalea*	0.7%	0.02	34	7	47.9%	0.686
Caulobacterales	*Hyphomonadaceae*	Unknown	0.7%	0.01	28	30	48.9%	0.373
Rhodobacterales	*Rhodobacteraceae*	*Ruegeria*	0.7%	0.01	35	12	49.9%	0.020

Table SVI.8. Multivariate pairwise results (*p* values) examining differences between "sample types" for the dataset of KO predicted by Tax4Fun analysis (999 permutations).

	Rocky biofilms	***T. atomaria***
T. atomaria	0.001	-
Seawater	0.001	0.001

Table SVI.9. Multivariate pairwise results (*p* values) examining differences between "months" and between "sites" for the dataset of KO predicted by Tax4Fun analysis (999 permutations).

Comparison between months					
	M1	**M2**	**M3**	**M4**	**M5**
M2	0.003	-	-	-	-
M3	0.003	0.004	-	-	-
M4	0.003	0.004	0.430	-	-
M5	0.003	0.013	0.242	0.443	-
M6	0.003	0.003	0.244	0.281	0.594

Comparison between sites				
	S1	**S2**	**S3**	**S4**
S2	0.280	-	-	-
S3	0.647	0.647	-	-
S4	0.280	0.647	0.647	-
S5	0.647	0.647	0.812	0.647

Table SVI.10. Multivariate pairwise results (*p* values) examining differences between "months" and between "sites" for the LC-(+)-ESI-MS metabolomics dataset (999 permutations).

Comparison between months					
	M1	**M2**	**M3**	**M4**	**M5**
M2	0.001	-	-	-	-
M3	0.001	0.009	-	-	-
M4	0.001	0.001	0.009	-	-
M5	0.001	0.001	0.001	0.001	-
M6	0.001	0.001	0.001	0.001	0.001

Comparison between sites				
	S1	**S2**	**S3**	**S4**
S2	0.009	-	-	-
S3	0.003	0.009	-	-
S4	0.003	0.053	0.005	-
S5	0.003	0.011	0.017	0.008

Table SVI.11. List of biomarkers (VIP score > 2) identified by LC-HRMS and involved in the discrimination between months within surface extracts of *T. atomaria* (Part 1).

P values corresponded to results of one-way ANOVA tests using "Month" as factor. Color codes corresponded to mean normalized concentrations (see Part2: Table S12).

m/z	Rt (s)	VIP score	Molecular formula	Adduct	Mass error (ppm)	mσ [a]	Putative identification [b]	MS/MS fragment ions	*p* values	M1	M2	M3	M4	M5	M6
704.5471	669	5.6	$C_{42}H_{74}NO_7$	$[M+H]^+$	-0.7	21.4	DGTA (C32:4) (C18:4/C14:0)	704.5473 $[M+H]^+$; 494.3488 $[C_{28}H_{48}NO_6]^+$; 476.3351 $[C_{28}H_{46}NO_5]^+$; 446.3483 $[C_{24}H_{48}NO_6]^+$; 428.3367 $[C_{24}H_{46}NO_5]^+$; 236.1494 $[C_{10}H_{22}NO_5]^+$	3.08E-14						
490.3743	519	5.4	$C_{26}H_{52}NO_7$	$[M+H]^+$	-0.2	9.2	*lyso*-DGCC (C16:0)	490.3744 $[M+H]^+$; 313.2748 $[C_{19}H_{37}O_3]^+$; 132.1019 $[C_6H_{14}NO_2]^+$; 104.1069 $[C_5H_{14}NO]^+$	2.67E-18						
706.5626	682	4.7	$C_{42}H_{76}NO_7$	$[M+H]^+$	-0.7	10.5	DGTA (C32:3) (C18:3/C14:0)	706.5621 $[M+H]^+$; 496.3635 $[C_{28}H_{50}NO_6]^+$; 446.3479 $[C_{24}H_{48}NO_6]^+$; 236.1492 $[C_{10}H_{22}NO_5]^+$	8.06E-14						
832.6098	688	4.0	$C_{52}H_{82}NO_7$	$[M+H]^+$	-4.2	-32.2	DGTA (C44:10) (C20:4/C22:6)	832.6121 $[M+H]^+$; 548.3946 $[C_{32}H_{54}NO_6]^+$; 548.3798 $[C_{32}H_{52}NO_6]^+$; 528.3683 $[C_{32}H_{50}NO_5]^+$; 522.3799 $[C_{30}H_{52}NO_6]^+$; 520.3658 $[C_{30}H_{50}NO_6]^+$; 236.194 $[C_{10}H_{22}NO_5]^+$	2.29E-20						
462.8933	475	3.3	$C_{16}H_{14}Br_2ClO_4$	$[M+H]^+$	1.4	?	Hemichrysophaentin D?	462.8933 $[C_{16}H_{14}Br_2ClO_4]^+$ $[M+H]^+$; 426.9164 $[C_{16}H_{13}Br_2O_4]^+$ $[M+H-HCl]^+$; 347.9987 $[C_{16}H_{13}BrO_4]^+$; 269.0807 $[C_{16}H_{13}O_4]^+$; 238.9708 $[C_{10}H_8BrO_2]^+$; 200.9553 $[C_7H_6BrO_2]^+$; 161.0599 $[C_{10}H_9O_2]^+$; 147.0446 $[C_9H_7O_2]^+$	2.31E-08						
542.3237	524	3.3	$C_{28}H_{49}NO_7P$	$[M+H]^+$	-0.2	12.7	*lyso*-PC (C20:5)	542.3242 $[M+H]^+$; 441.2975 $[C_{21}H_{46}O_7P]^+$; 184.0729 $[C_5H_{15}NO_4P]^+$; 104.1069 $[C_5H_{14}NO]^+$, 86.0964 $[C_5H_{12}N]^+$	1.08E-09						

[a] Constructor statistical match factor (comparison of theoretical and experimental isotopic patterns); [b] Abbreviations: DGTA: diacylglycerylhydroxymethyl-*N*,*N*,*N*-trimethyl-β-alanine, DGCC: monoacylglyceryl-3-O-carboxy-(hydroxymethyl)-choline, PC: diacylglycerophosphocholine.

Table SVI.11. List of biomarkers (VIP score > 2) identified by LC-HRMS and involved in the discrimination between months within surface extracts of *T. atomaria* (Part 2).

P values corresponded to results of one-way ANOVA tests using "Month" as factor. Color codes corresponded to mean normalized concentrations.

m/z	Rt (s)	VIP score	Molecular formula	Adduct	Mass error (ppm)	mσ [a]	Putative identification [b]	MS/MS fragment ions [c]	*p* values	M1	M2	M3	M4	M5	M6
718.5621	683	3.1	$C_{43}H_{76}NO_7$	$[M+H]^+$	0.5	50.3	DGTA (C33:3) ?	n.f.[e]	2.10E-09						
706.5628	691	2.9	$C_{42}H_{78}NO_7$	$[M+H]^+$	-1.4	13.9	DGTA (C32:2) (C18:2/C14:0) (C16:1/C16:1)	706.5633 $[M+H]^+$; 496.3638 $[C_{28}H_{50}NO_6]^+$; 446.3482 $[C_{24}H_{48}NO_6]^+$; 236.1493 $[C_{10}H_{22}NO_5]^+$	5.53E-14						
135.0476	54	2.9	$C_5H_{11}O_2S$	$[M+H]^+$	-1	6.1	DMSP [d]	135.0474 $[M+H]^+$; 73.0282 $[C_3H_5O_2]^+$; 63.0261 $[C_2H_7S]^+$; 61.0102 $[C_2H_5S]^+$; 55.0177 $[C_3H_3O]^+$	3.33E-06						
546.3790	504	2.8	$C_{32}H_{52}NO_6$	$[M+H]^+$	-1.5	-57.4	*lyso*-DGTA (C22:6)	546.3797 $[M+H]^+$; 236.1492 $[C_{10}H_{22}NO_5]^+$	2.71E-11						
536.3574	504	2.8	$C_{30}H_{46}NO_7$	$[M+H]^+$	0.5	14.9	$C_{30}H_{45}NO_7$	n.f.	8.75E-14						
696.5731	703	2.7	$C_{41}H_{78}NO_7$	$[M+H]^+$	0.3	31	DGTA (C31:1) ?	n.f.	1.51E-07						
417.3365	708	2.6	$C_{27}H_{45}O_3$	$[M+H]^+$	-0.4	287.3	Tocopherol derivative ?	207.1014 $[C_{12}H_{15}O_3]^+$; 193.0855 $[C_{11}H_{13}O_3]^+$; 153.0542 $[C_8H_9O_3]^+$; 137.0599 $[C_8H_9O_2]^+$	5.19E-08						
565.4034	696	2.4	$C_{40}H_{53}O_2$	$[M+H]^+$	1.1	44.5	Carotenoid ?	n.f.	2.72E-09						
219.1128	248	2.1	$C_{12}H_{15}N_2O_2$	$[M+NH_4]^+$	18.3	8.5	$C_{12}H_{15}N_2O_2$	219.1127 $[M+NH_4]^+$; 217.1030 $[C_{12}H_{13}N_2O_2]^+$; 202.0864 $[C_{12}H_{12}NO_2]^+$; 184.0753 $[C_{12}H_{10}NO]^+$; 174.0969 $[C_{11}H_{12}NO]^+$; 156.0805 $[C_{11}H_{10}N]^+$; 146.0600 $[C_9H_8NO]^+$; 132.0802 $[C_9H_{10}N]^+$	4.59E-06						

Color code					
-3	-1	1	3	5	7

[a] Constructor statistical match factor (comparison of theoretical and experimental isotopic patterns); [b] Abbreviations: DGTA: diacylglycerylhydroxymethyl-*N*,*N*,*N*-trimethyl-*β*-alanine; DMSP: Dimethylsulfoniopropionate. [c] not observed; [d] This identification was confirmed with a commercial standard; [e] Not fragmented.

Table SVI.12. List of biomarkers (VIP score > 2) identified by LC-HRMS and involved in the discrimination between sites within surface extracts of *T. atomaria*. *P* values corresponded to results of one-way ANOVA tests using "Sites" as factor. Color codes corresponded to mean normalized concentrations.

m/z	Rt (s)	VIP score	Molecular formula	Adduct	Mass error (ppm)	mσ[a]	Putative identification	MS/MS fragment ions	*p* values	S1	S2	S3	S4	S5
607.4362	662	7.0	$C_{38}H_{59}O_5$	$[M+H]^+$	-0.8	20	DG (C36:9) (C20:5/C16:4)	607.4349 $[M+H]^+$; 589.4270 $[C_{39}H_{57}O_4]^+$, 359.2584 $[C_{23}H_{35}O_3]^+$, 305.2110 $[C_{19}H_{29}O_3]^+$, 285.2212 $[C_{20}H_{29}O]^+$	1.44E-13					
903.5664	783	4.6	$C_{55}H_{75}N_4O_7$	$[M+H]^+$	-3.8	58.5	Pheophytin derivative (Pheo +2ox)	903.5681 $[M+H]^+$; 885.5552 $[C_{55}H_{73}N_4O_6]^+$; 625.2668 $[C_{35}H_{37}N_4O_7]^+$; 607.2532 $[C_{35}H_{35}N_4O_6]^+$; 581.2797 $[C_{34}H_{37}N_4O_5]^+$; 565.2464 $[C_{33}H_{33}N_4O_5]^+$; 503.2434 $[C_{32}H_{31}N_4O_2]^+$	7.30E-06					
490.3743	519	3.0	$C_{26}H_{52}NO_7$	$[M+H]^+$	-0.2	9.2	*lyso*-DGCC (C16:0)	490.3744 $[M+H]^+$; 313.2748 $[C_{19}H_{37}O_3]^+$; 132.1019 $[C_6H_{14}NO_2]^+$; 104.1069 $[C_5H_{14}NO]^+$	0.0017					
536.4361	773	2.6	$C_{40}H_{56}$	$[M^{\cdot}]+$	2.9	16.9	*β*-carotene	536.4391 $[M^{\cdot}]^+$; 457.0.3757 $[C_{34}H_{49}]^+$; 444,3754 $[C_{33}H_{47}]^+$; 429.3513 $[C_{32}H_{45}]^+$; 307.2419 $[C_{23}H_{31}]^+$; 267.2109 $[C_{20}H_{27}]^+$; 241.1950 $[C_{18}H_{25}]^+$; 177.646 $[C_{13}H_{21}]^+$; 133.1018 $[C_{10}H_{13}]^+$	2.64E-07					
659.4318	620	2.5	$C_{42}H_{59}O_6$	$[M+H]^+$	-1.8	35.1	Fucoxanthin [d]	659.4292 $[M+H]^+$; 411.1689 $[C_{20}H_{35}O]^+$; 355.2436 $[C_{27}H_{31}]^+$; 329.2255 $[C_{25}H_{29}]^+$; 263.1789 $[C_{20}H_{23}]^+$; 251.1799 $[C_{19}H_{23}]^+$, 213.1277 $[C_{15}H_{17}O]^+$; 109.1012 $[C_8H_{13}]^+$	9.30E-11					
482.3476	596	2.2	$C_{27}H_{48}NO_6$	$[M+H]^+$	-0.1	38.4	GGG derivative	482.3476 $[M+H]^+$; 271.2430 $[C_{20}H_{31}]^+$; 201.1638 $[C_{15}H_{21}]^+$; 175.1476 $[C_{13}H_{19}]^+$; 161.1323 $[C_{12}H_{17}]^+$; 135.1172 $[C_{10}H_{15}]^+$; 109.1007 $[C_8H_{13}]^+$	> 0.05					
563.4675	685	2.1	$C_{35}H_{63}O_5$	$[M+H]^+$	-0.9	44.1	$C_{35}H_{63}O_5$	563.4604 $[M+H]^+$; $[C_{31}H_{55}O_5]^+$; 293.1748 $[C_{17}H_{25}O_4]^+$; 237.1122 $[C_{13}H_{17}O_4]^+$; 209.1173 $[C_{12}H_{17}O_3]+$	4.20E-06					

Color code					
-2	-1	0	1	2	3

[a] Constructor statistical match factor (comparison of theoretical and experimental isotopic patterns); [b] Abbreviations: DG: diacylglycerol, DGCC : monoacylglyceryl-3-O-carboxy-(hydroxymethyl)-choline, GGG: geranylgeranylglycerol. [d] This identification was confirmed with a purified standard.

Supplementary Figures

Figure SVI.1. Map with the location of the sampling sites.
Dashed lines represented the limits of the preserved zone of the Porquerolles island within the Port-Cros National Park.

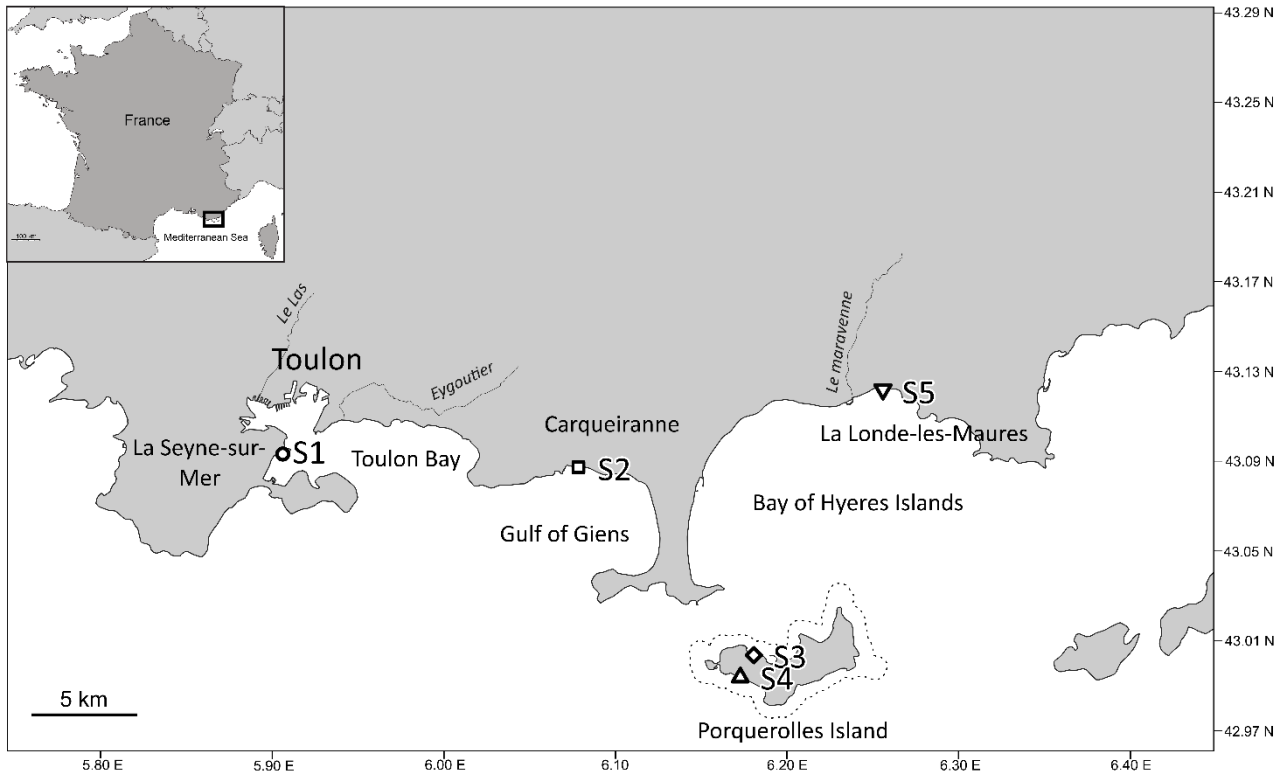

Figure SVI.2. Discrimination of heterotrophic prokaryotes by flow cytometry.

A successive 3-steps workflow was used. A: Samples were first screened for the presence of potential doublets or aggregates. Sample dilution was eventually adjusted in order to keep doublets below 5% of the total signal. B: Particles showing a red fluorescence (FL3) were excluded in order to keep only strict heterotrophs (*i.e.* presenting only the SYBR green-induced fluorescence). C: High side scatter signal harboring particles were excluded in order to enumerate only prokaryotes.

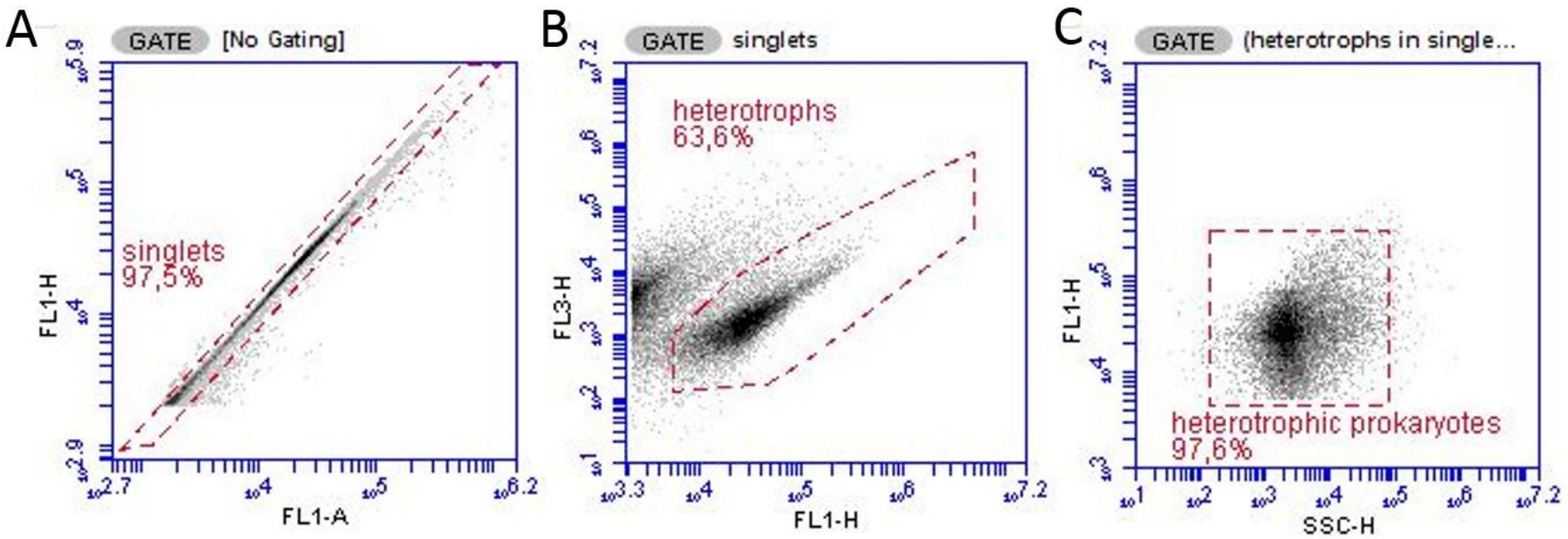

Figure SVI.3. Variations of thalli length (cm) conducted with all algal samples collected during the study and pictures of thalli collected at S1 (one replicate per month).

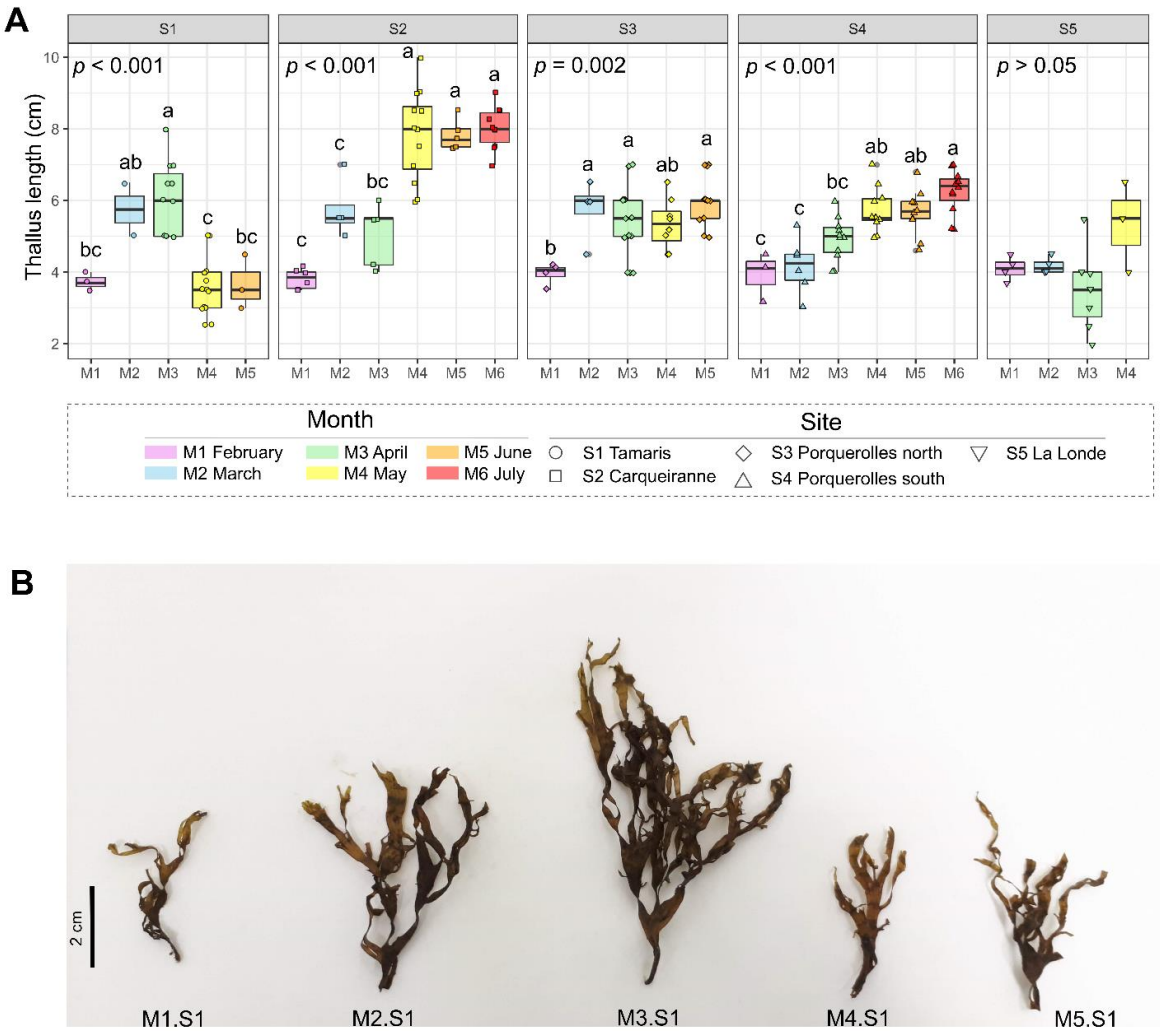

Figure SVI.4. Variations of cells densities at the surface of *T. atomaria* for each site (A) and heteroprokaryotic cell abundances in seawater samples (B).
p values corresponded to the results of a one-way ANOVA using "Month" as the factor.

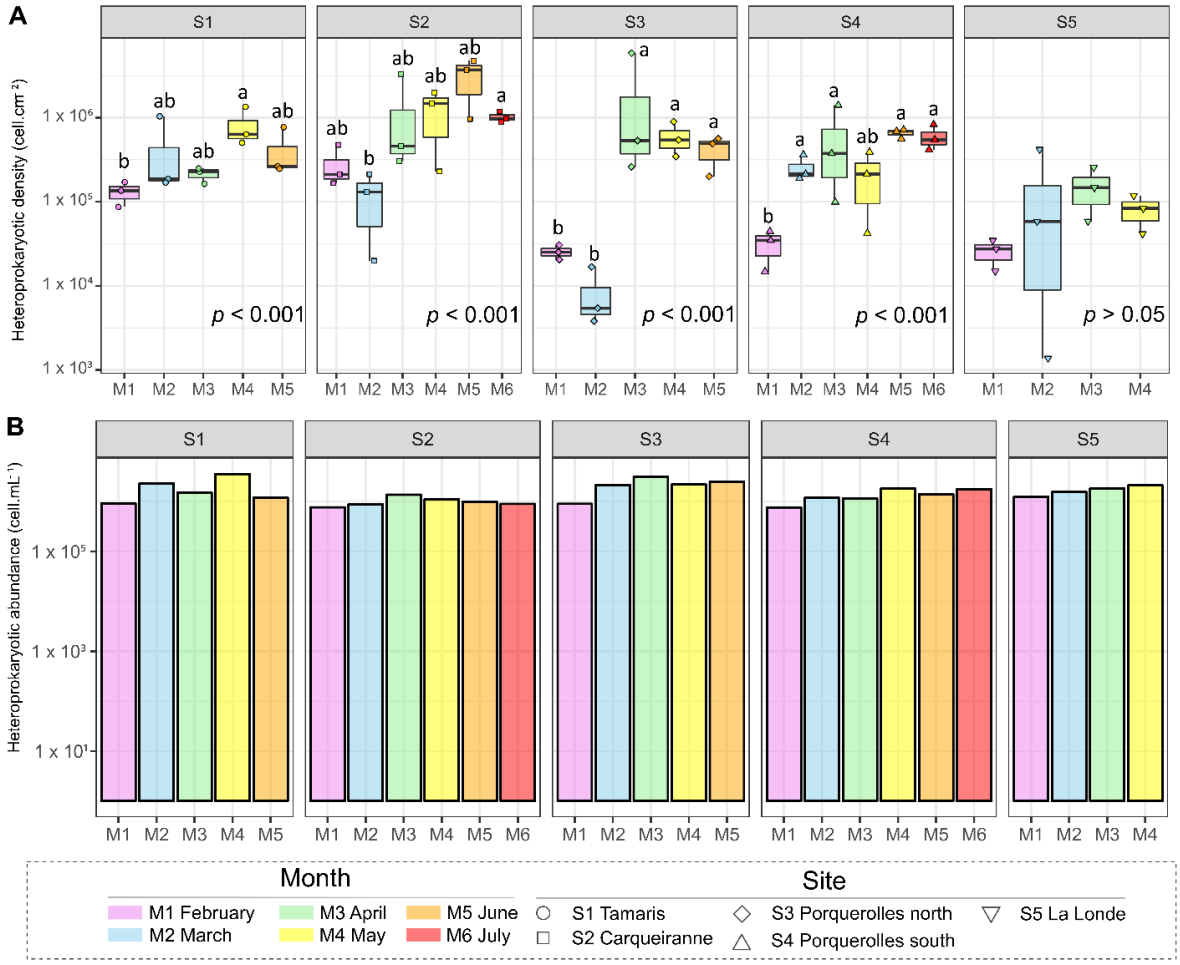

Figure SVI.5. Spatiotemporal dynamics of prokaryotic cell density (A), α-diversity (B), percentage of algal-core (C) and algal-enriched (D) taxa at the surface of *T. atomaria*.

p values correspond to the results of a one-way ANOVA using "Month" as factor.

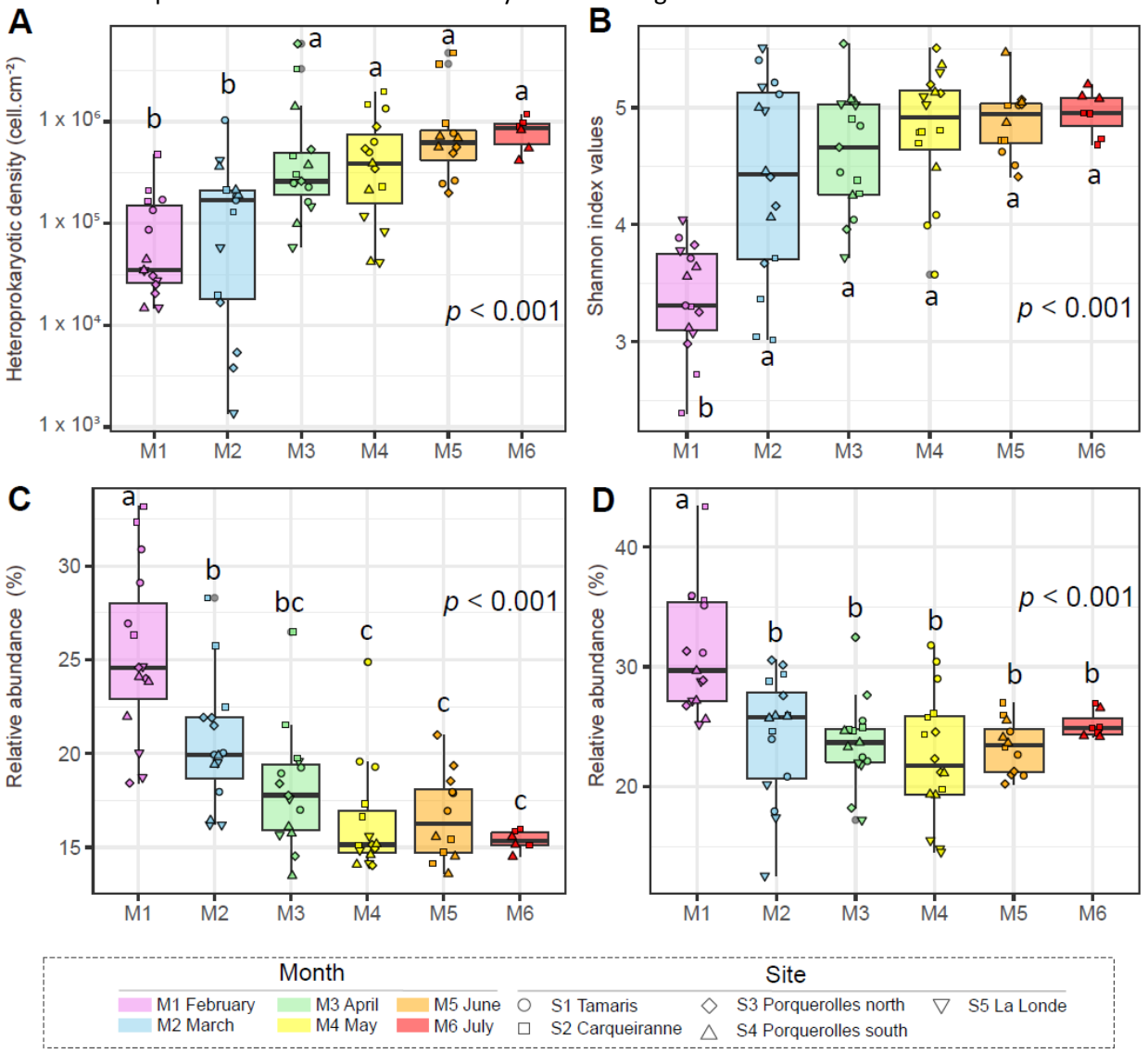

Figure SVI.6. NMDS (Bray-Curtis index) showing prokaryotic β-diversity of algal samples.
p values corresponded to results of the two-way PERMANOVA using "Month" and "Site" as factors.

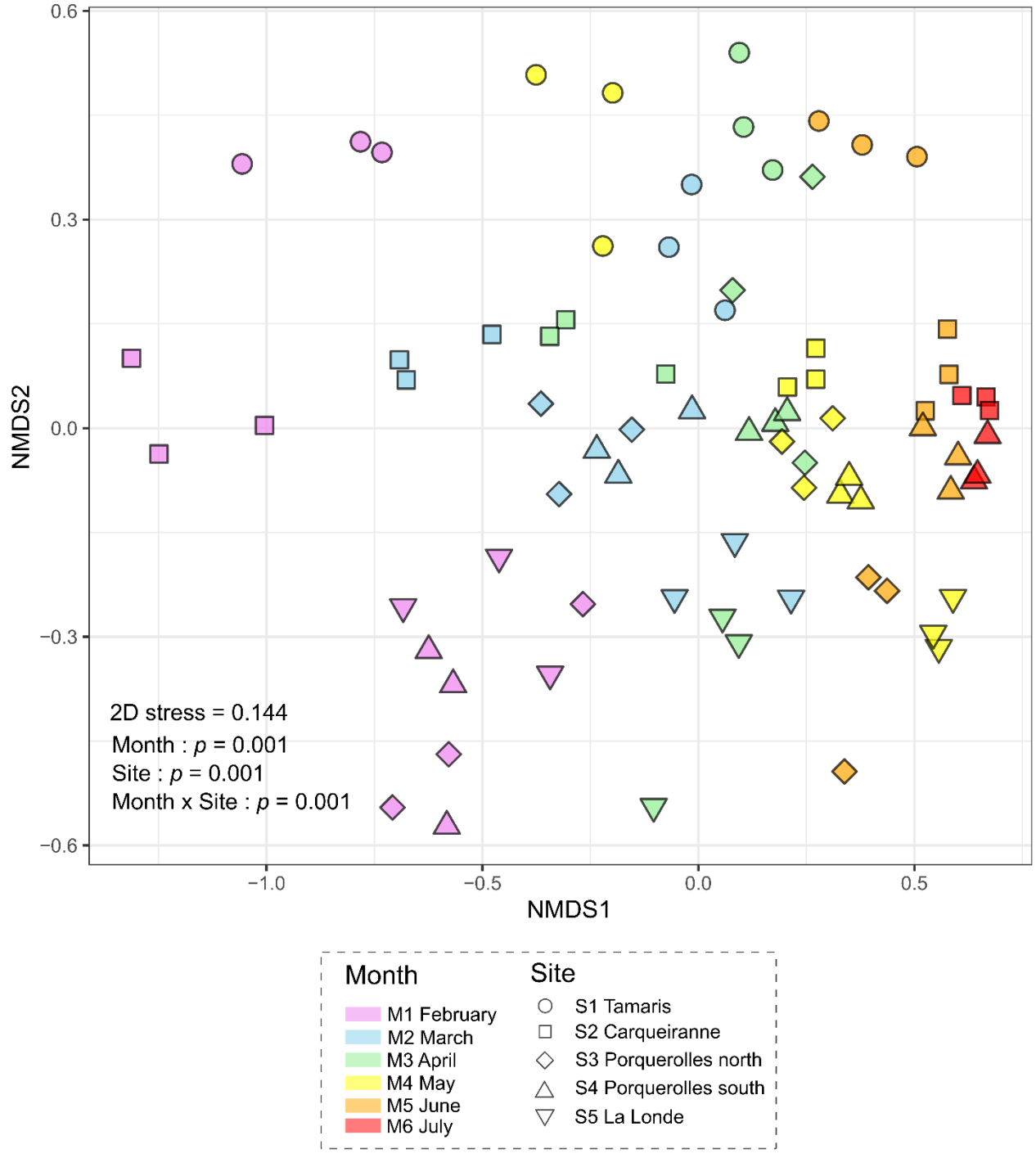

Figure SVI.7. NMDS (Bray-Curtis index) showing prokaryotic *β*-diversity of rocky biofilm (A) and seawater (B) samples.

p values corresponded to the results of a one-way PERMANOVA using whether "Month" or "Site" as factors.

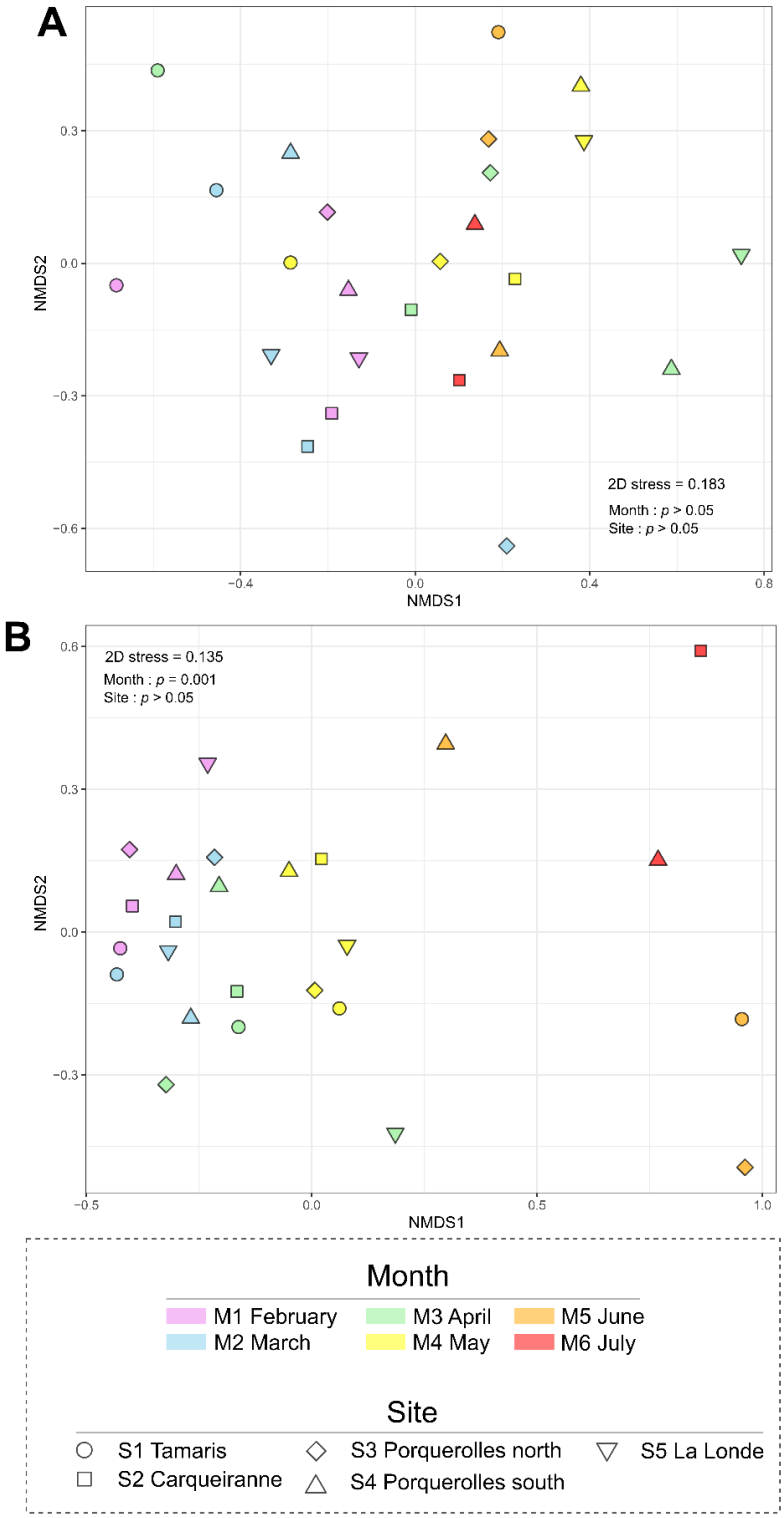

Figure SVI.8. Cladogram obtained from the LEfSe analysis built with the 16S rRNA gene dataset of all samples and revealing discriminant prokaryotic taxa specific to *T. atomaria*, to rocky biofilms and to seawater samples (LDA threshold set to 4).

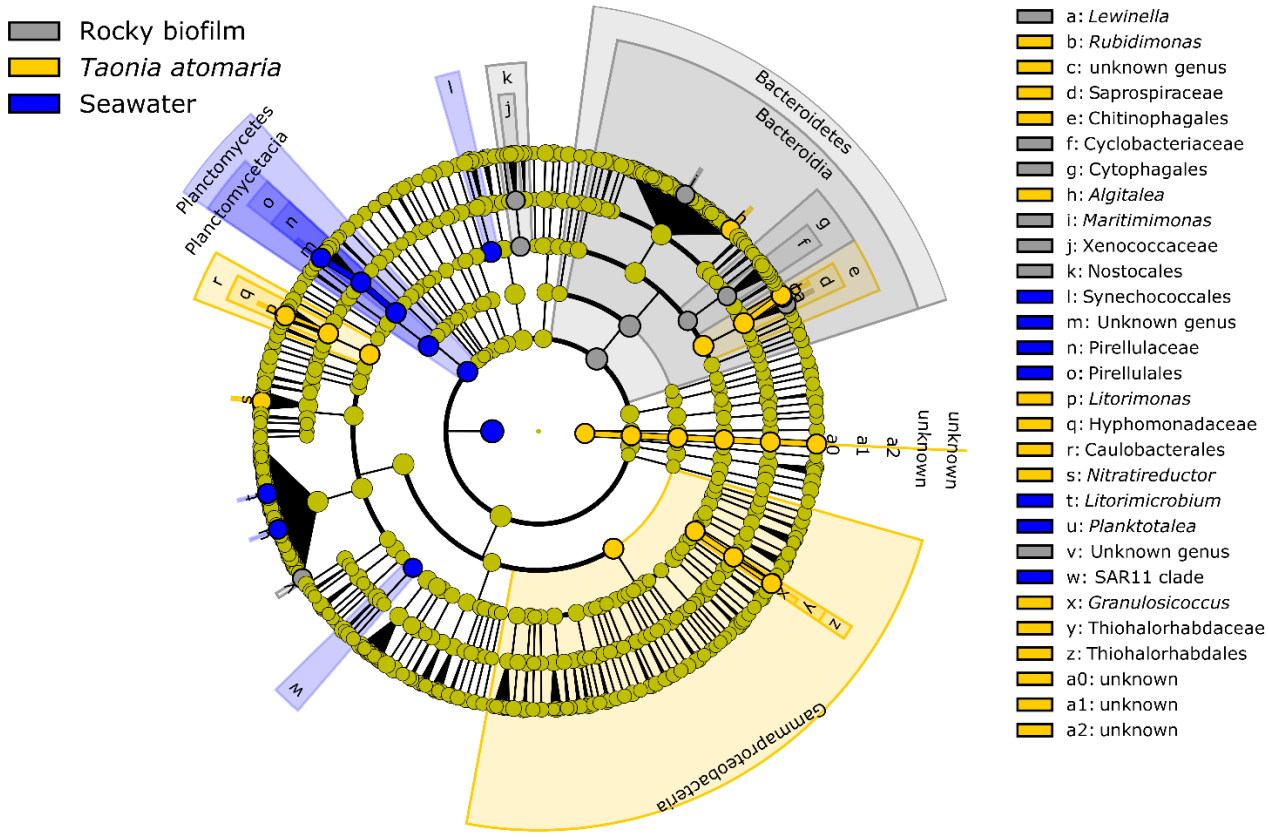

Figure SVI.9. Cladogram obtained from the LEfSe analysis built with the 16S rRNA gene dataset of *T. atomaria* samples and revealing discriminant epibacterial taxa specific to each sampling month (LDA threshold set to 4.5).

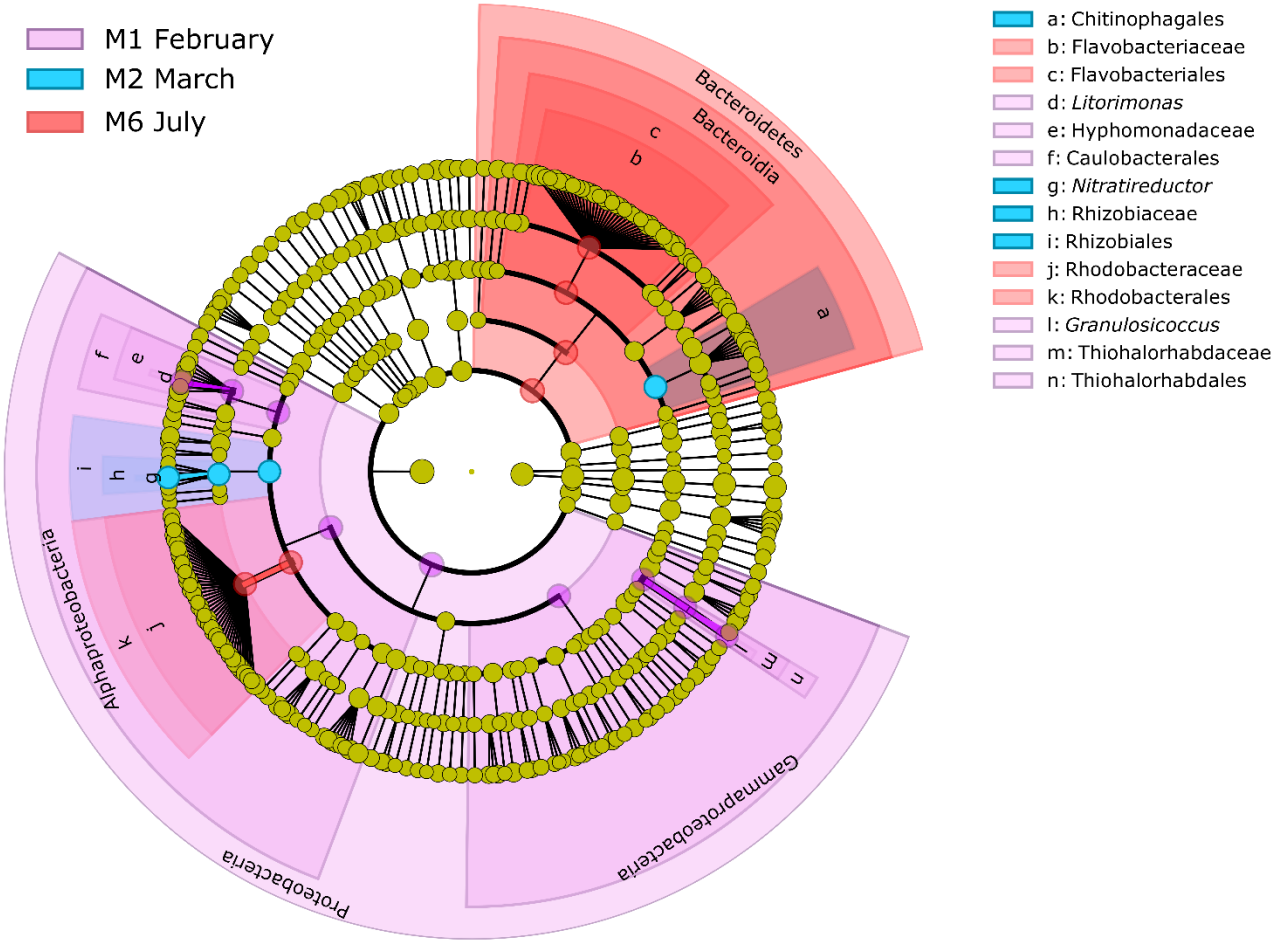

Figure SVI.10. Cladogram obtained from the LEfSe analysis built with the 16S rRNA gene dataset of *T. atomaria* samples and revealing discriminant epibacterial taxa specific to each sampling site (LDA threshold set to 3.5).

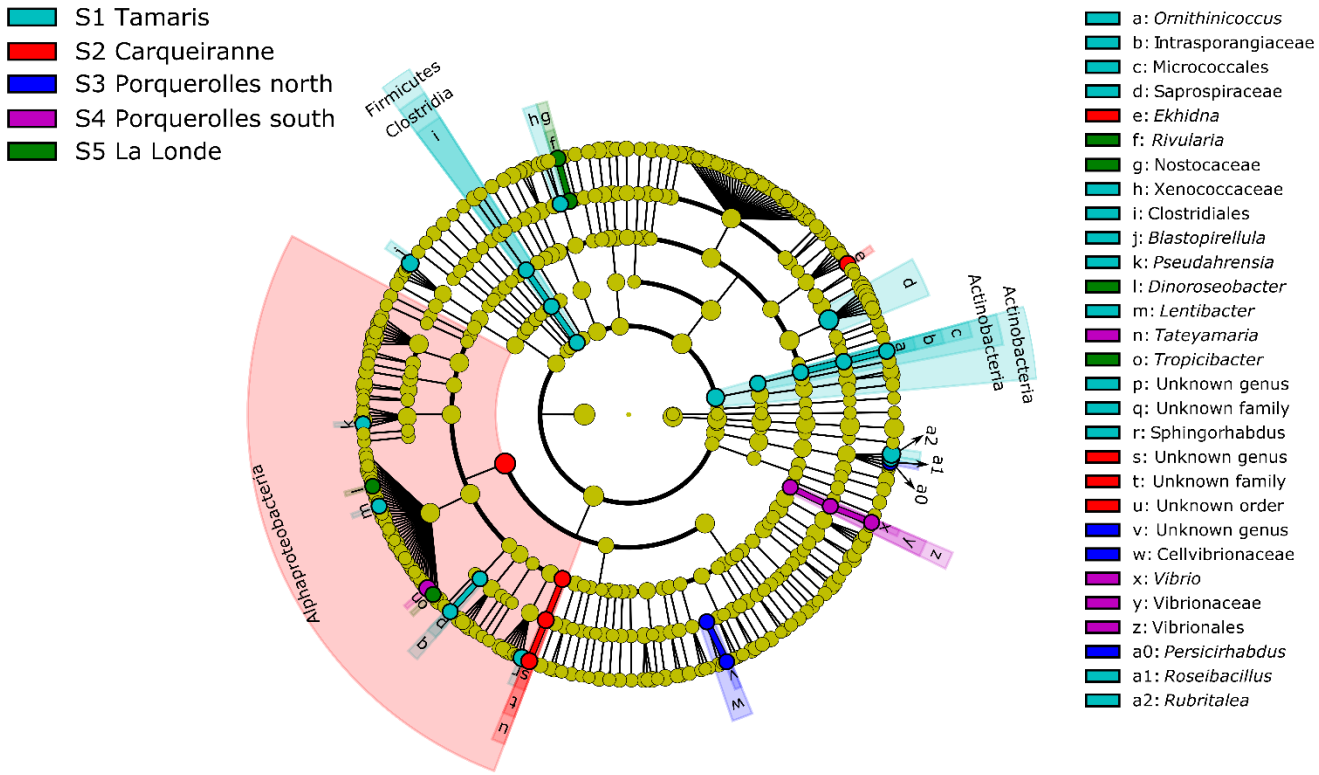

Figure SVI.11. Percentage of core community sequences (A) and algal-enriched community sequences (B).
*: "Other" corresponded to unaffiliated families and families below 1%.

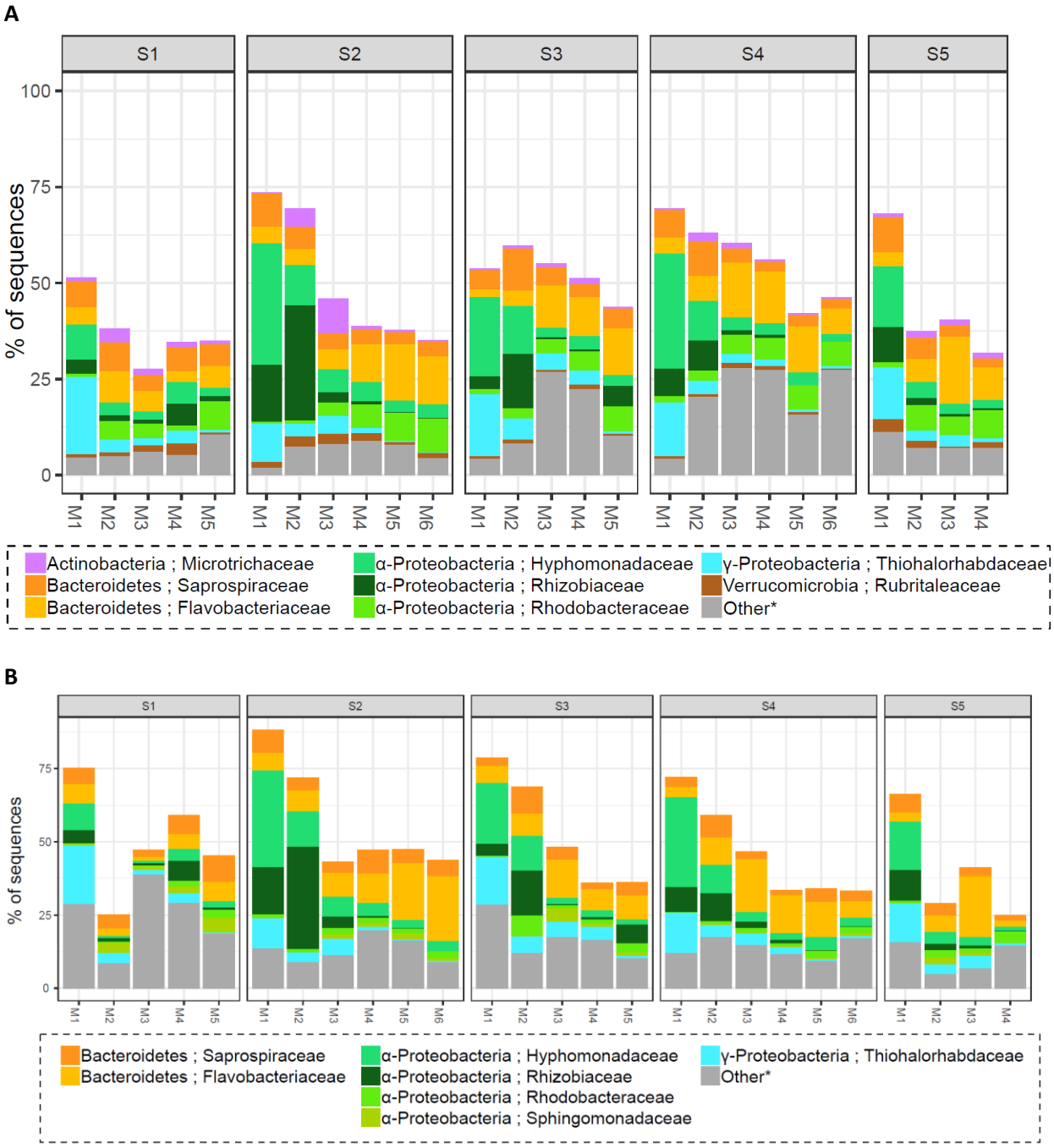

Figure SVI.12. PCA constructed with KEGG KO from Tax4Fun analysis with algal, rocky biofilm and seawater samples. *p* value corresponded to the results of the one-way PERMANOVA using "sample type" as the factor.

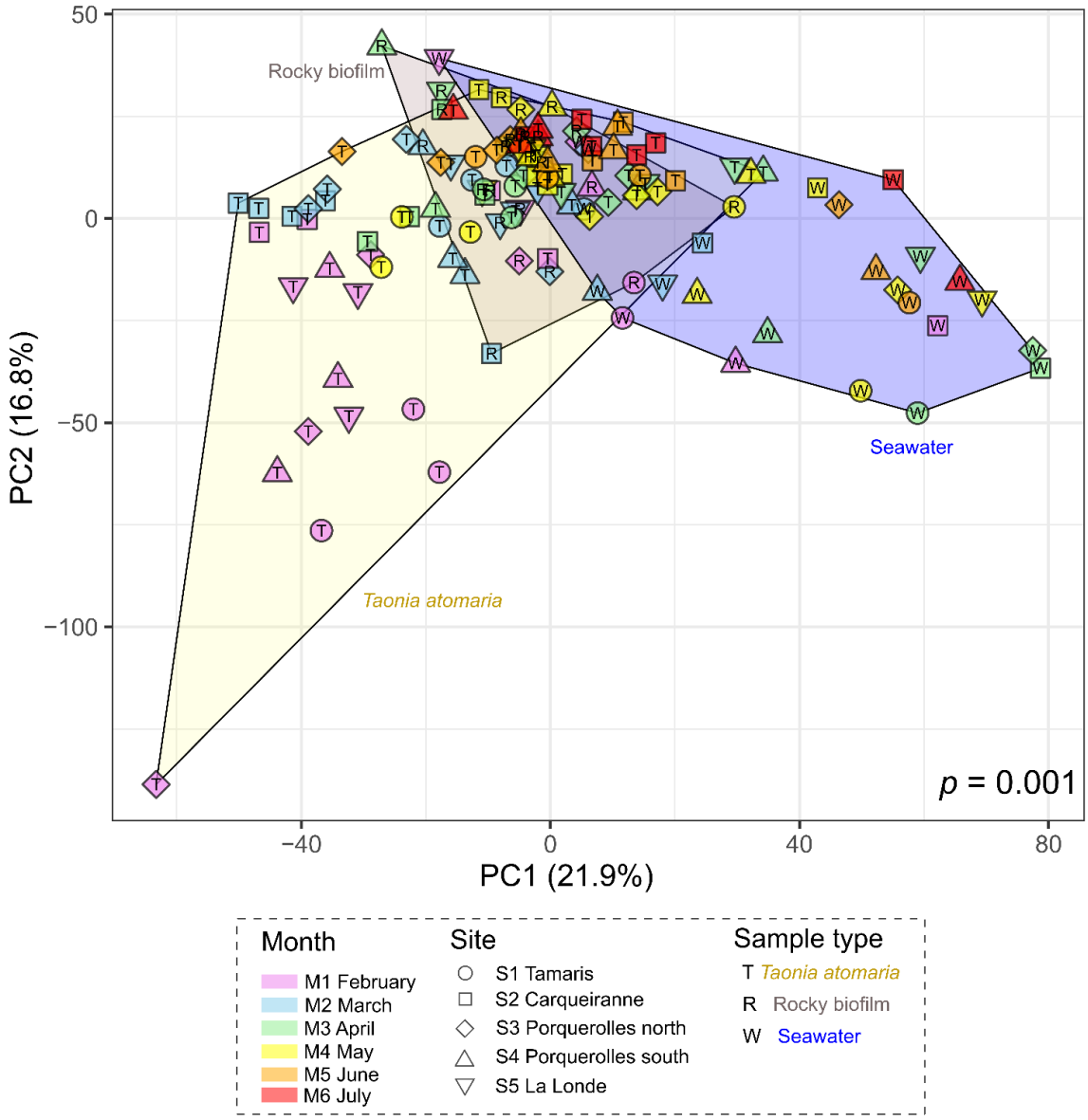

Figure SVI.13. PCA constructed with KEGG KO from Tax4Fun analysis with algal samples. *p* values corresponded to the results of the two-way PERMANOVA using "Month" and "Site" as factors.

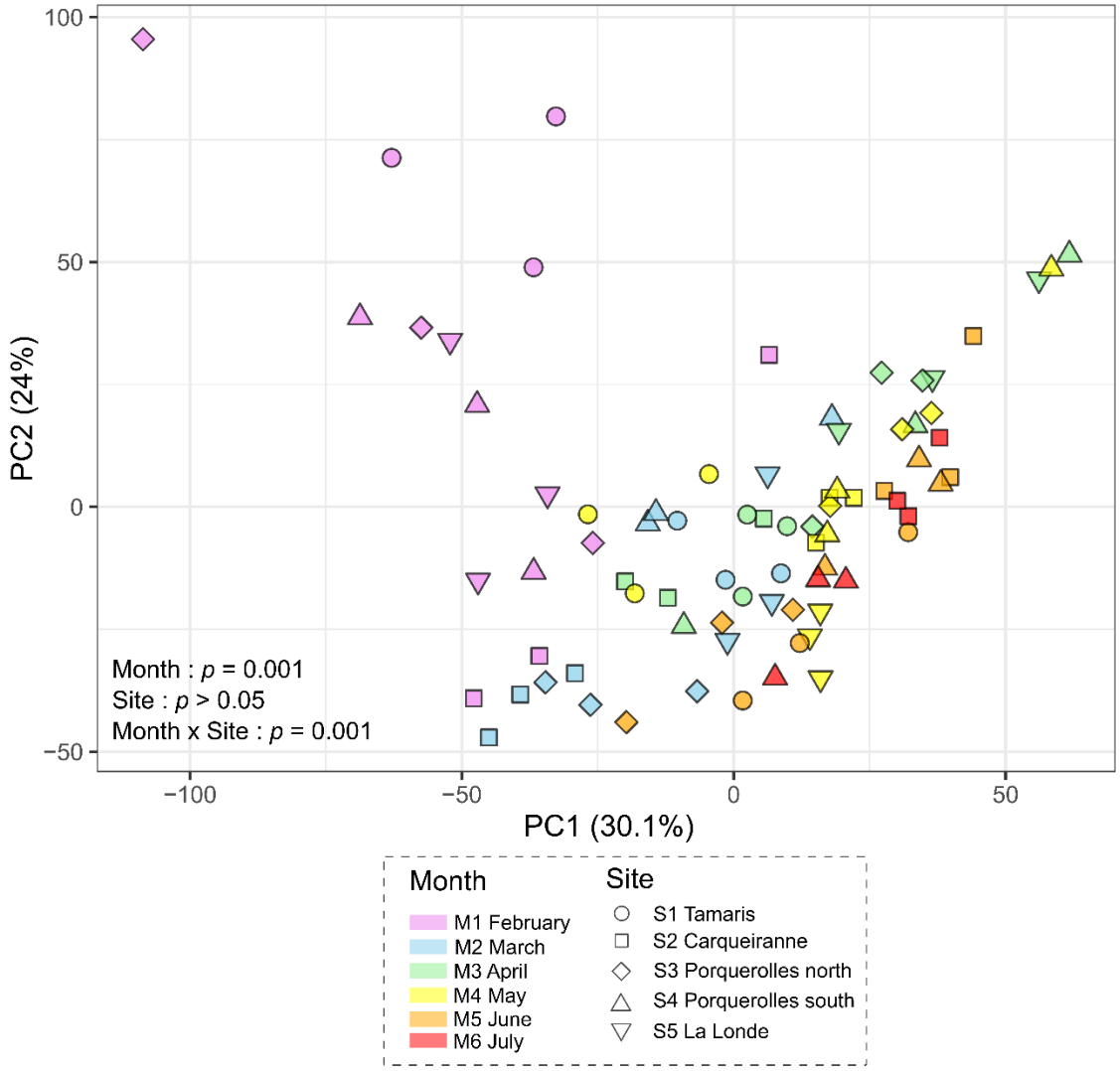

Figure SVI.14. Complementary KEGG pathways predicted by Tax4Fun analysis.

P values corresponded to the results of one-way ANOVA using "Month" as factor.

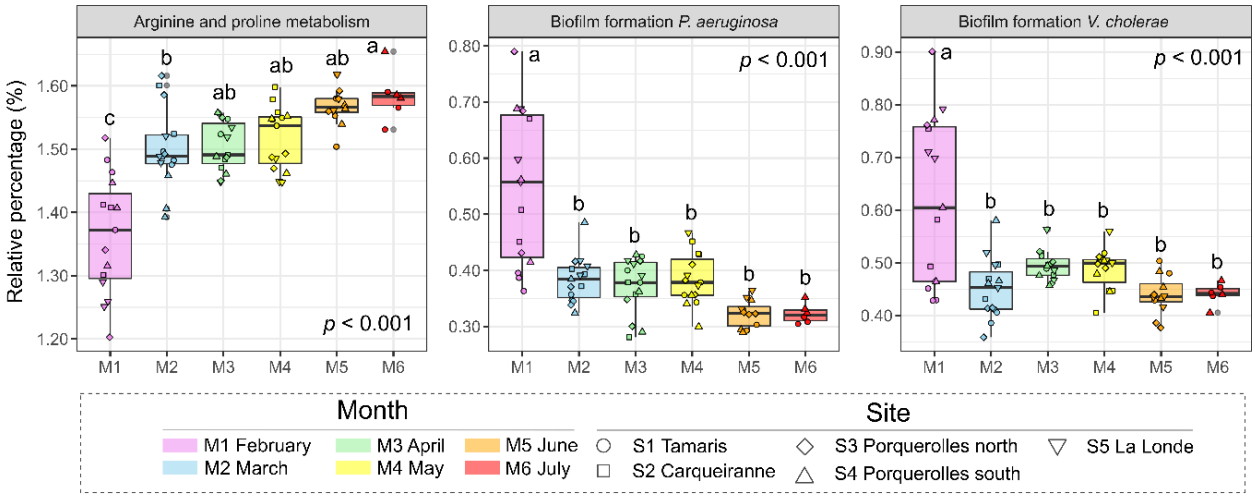

Figure SVI.15. GNPS molecular network built with LC-ESI-(+)-MS/MS data. Levels of annotations were attributed according to Schymanski et al., 2014.

Abbreviations: DGTA: diacylglycerylhydroxymethyl-*N*,*N*,*N*-trimethyl-β-alanine, DGCC: monoacylglyceryl-3-O-carboxy-(hydroxymethyl)-choline, DG: diacylglycerol, MG: monoacylglycerol, GGG: geranylgeranylglycerol, DGDG : digalactosyldiacylglycerol, MGDG : monogalactosyldiacylglycerol

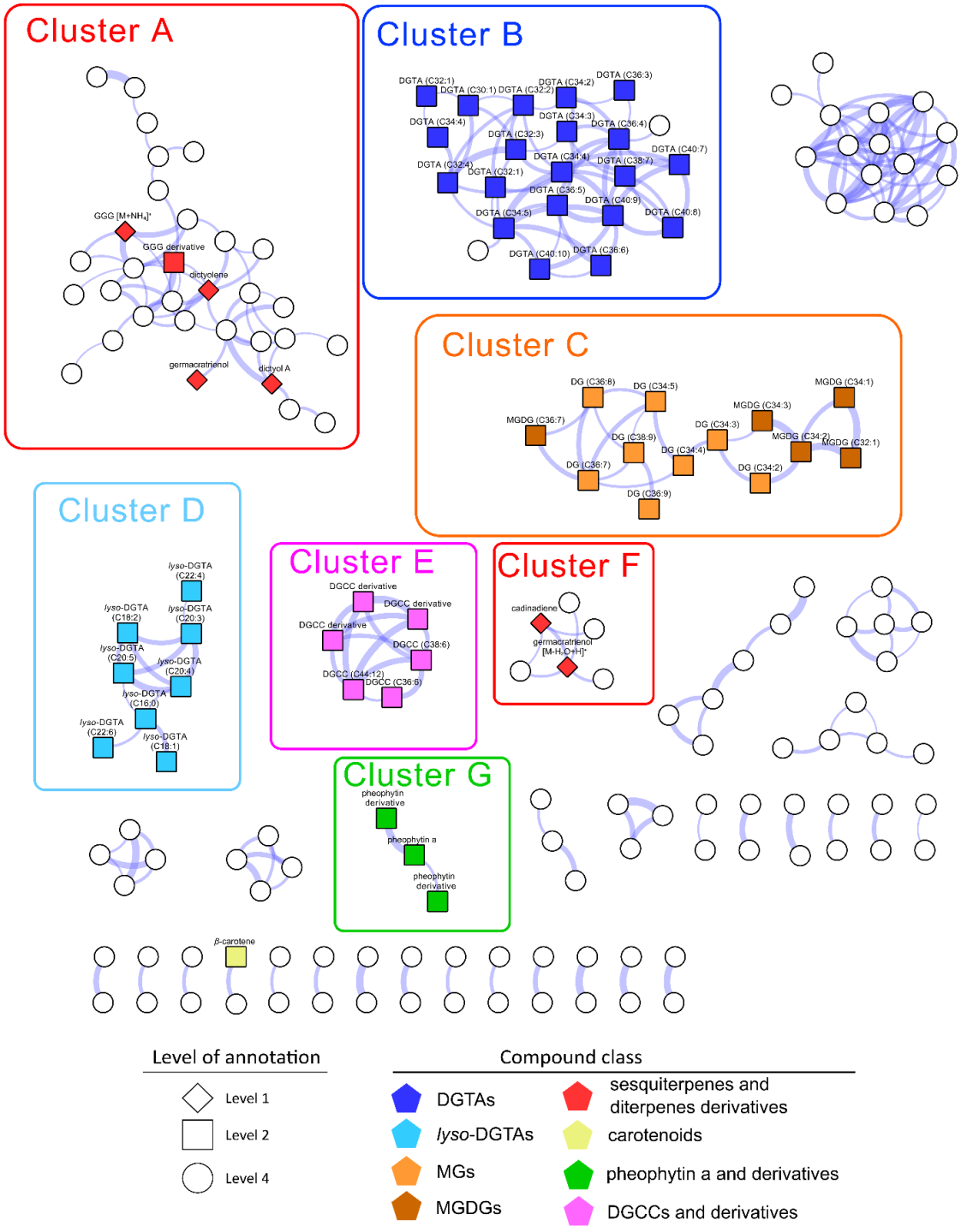

Annexe VII

Supporting information

for

Synergistic effects of temperature and light affect the relationship between *Taonia atomaria* and its epibacterial community: a mesocosm study

Benoit Paix[1], Philippe Potin[2], Nicolas Layglon[3], Christophe Le Poupon[3], Benjamin Misson[3], Catherine Leblanc[2], Gérald Culioli[1*] and Jean-François Briand[1*]

[1]*Université de Toulon, Laboratoire MAPIEM, EA 4323, Toulon, France*

[2]*Sorbonne Université, CNRS, Integrative Biology of Marine Models (LBI2M), UMR 8227, Station Biologique de Roscoff (SBR), Roscoff, France*

[3]*Université de Toulon, Aix Marseille Université, CNRS, IRD, Mediterranean Institute of Oceanography (MIO), UM110, France*

*corresponding authors : briand@univ-tln.fr, culioli@univ-tln.fr

Supplementary materials

Supplementary information concerning the pre-treatment of running seawater

Before its arrival to the experimental setup, the running seawater from Roscoff coast is conditioned in a pumping station of the CRBM – Roscoff Aquarium Services (see details here : http://www.sb-roscoff.fr/fr/station-biologique-de-roscoff/services/centre-de-ressources-biologiques-marines/roscoff-aquarium-services-ras/dispositifs-d-aquariologie). The seawater is then filtered upon AFM® 5 μm filters (Dryden Aqua, Edinburgh, United Kingdom) and then filtered upon cartridges equipped with 1 to 3 μm filters (Fisher scientific, Waltham, USA).

Supplementary information concerning the determination of the physico-chemical parameters of seawater

Temperature, irradiance, pH, O_2 and salinity were measured daily during the whole study and in all aquaria. For these measures, probes were directly immersed in the aquaria and rinsed with distilled water between each one. Seawater samples (60 mL) for nutrients ($[NO_3^-]$, $[PO_4^{3-}]$ and $[Si(OH)_4]$) were collected at each sampling time (field, t_0, t_1, t_2 and t_3) and for each condition. Percentage of dissolved oxygen was measured using an OXi 3310 equipped with a CellOX 325 probe (WTW^{TM}, Weilheim, Germany). Temperature, pH and salinity were measured using a YSI™ Professional Plus Multiparameter Instrument (YSI, Yellow Springs, USA). Irradiance was measured at the top of each aquarium using a RS PRO 180-7133 light-meter (RS PRO, Singapore). $[NO_3^-]$, $[PO_4^{3-}]$ and $[Si(OH)_4]$ were analyzed using standard colorimetric methods for seawater (Briand et al., 2017).

Supplementary information concerning the metabolomics analyses

The surface metabolome was extracted by dipping each frond in 5 mL of LC-MS grade methanol (Carlo Erba, Peypin, France) during 5s according to the protocol optimized by Othmani et al., 2016. The surface extracts were concentrated to dryness under reduced pressure at a temperature lower than 35°C (Othmani et al., 2016a). Dried surface extracts were then transferred in 2-mL HPLC vials and stored under inert atmosphere (N_2) in the dark at -20°C until analysis. Before injection, samples were solubilized in 1 mL of LC-MS grade methanol (Chromasolv, Sigma-Aldrich, St Louis, MO, USA). For all experiments, extraction and sample preparation were carried out by the same operator. Analytical blanks were prepared with exactly the same protocol as those used for surface extracts but without algal pieces. These blanks allowed the subsequent subtraction of contaminants or components coming from solvents and vials. In order to ensure quality control, a pool sample was prepared by combining 100 μL of each surface extract. The pool sample was divided into 18 2-ml HPLC vials (around 250 μL of solution in each vial) that were used as quality-control samples (QCs). To ensure analytical repeatability, a first QC was injected ten times at the beginning of the injection sequence in order to stabilize the chromatographic system. Then, the injection sequence consisted of the iterative injection of one QC and five samples (surface extracts and analytical blanks) randomly selected to avoid any possible time-dependent changes in LC–MS chromatographic fingerprints. Moreover, to assess sample carry-over of the analytical process, two solvent blanks (LC-MS grade methanol) were injected before the first QC and at the end of the injection sequence.

The UPLC-HRMS instrumentation consisted of a Dionex Ultimate 3000 Rapid Separation (Thermo Fisher Scientific, Waltham, MA, USA) chromatographic system equipped with a RS pump, a temperature-controlled autosampler, a thermostated column compartment and an UV-Vis diode array detector. This system was coupled to a QToF Impact II mass spectrometer (Bruker Daltonics, Bremen, Germany). The analyses were performed using an analytical core-shell reversed-phase column (150 × 2.1 mm, 1.7 μm, Kinetex Phenyl-Hexyl equipped with a SecurityGuard cartridge; Phenomenex, Le Pecq, France) with a column temperature of 40°C and a flow rate of 0.5 mL.min^{-1}. The autosampler temperature was set at 4°C and the injection volume was 5 μL. Mobile phases were: (A) water and (B) acetonitrile (Chromasolv; Sigma-

Aldrich-Merck, Darmstadt, Germany) containing each 0.1% (*v*/*v*) of formic acid (Ultra grade; Fluka, Fischer Scientific, Illkirch, France). The elution gradient started at 5% B and kept for 2 min, then to 100% B (linear ramp) in 8 min and kept for 4 min; then back to 5% B (linear ramp) over 0.01 min and maintained 1.99 min, for a total run time of 16 min. The capillary voltage of the MS spectrometer was set at 4500V (positive mode), and the nebulizing parameters were set as follows: nebulizing gas (N_2) pressure at 0.4 bar, drying gas (N_2) flow at 4 $L.min^{-1}$, and drying temperature at 180°C. Mass spectra were recorded from *m/z* 50 to 1200 at a mass resolving power of 25 000 full width at half-maximum (FWHM, *m/z* = 200) and a frequency of 2 Hz. Tandem mass spectrometry analyses were performed thanks to a collision induced dissociation (CID) with a collision energy of 25 eV. A solution of formate/acetate forming clusters was automatically injected before each sample for internal mass calibration, and the mass spectrometer was calibrated with the same solution before each sequence of samples. Data handling was done using DataAnalysis software (version 4.3, Bruker Daltonics).

In this study, three levels of annotation were applied for the identification of metabolites, following the same methodology described in Paix et al., 2019, 2020. The first approach, which corresponds to the level 1 of annotation according to Schymanski et al., 2014, was based on the use of several commercial standards described in Paix et al., 2019 including DMSP, proline betaine, proline and mannitol, as well as compounds previously purified from *T. atomaria* or *Dictyota* spp. by our team (Viano et al., 2009; Othmani et al., 2016a, 2016b) including GGG, several sesquiterpenes and fucoxanthin. These standards were solubilized in MeOH at a concentration of 0.1 $mg.mL^{-1}$ and analyzed with the same experimental conditions used for the metabolomics workflow. All commercial standards were purchased from Sigma-Aldrich or Cayman Chemicals. The second strategy was to annotate putatively some *m/z* features by the comparison of their MS and MS/MS data with reference databases. A match found with a MS (and MS/MS) library is considered with the level 2 of annotation (Schymanski et al., 2014). Data were analyzed and annotated based on MS/MS fragmentation pathways and comparison with in-house (Paix et al., 2019, 2020) and public databases such as Metlin (https://metlin.scripps.edu/) or Lipidmaps (https://www.lipidmaps.org/). When no characteristic fragmentation pathway was determined by comparison to the literature, the most probable chemical formula was proposed using the "Smart Formula" tool from DataAnalysis. This last step finally corresponded to the level 4 of annotation (Schymanski et al., 2014).

Data (.netCDF files) were processed for metabolomics analysis with MzMine 2.31 software (Katajamaa and Orešič, 2005; Pluskal et al., 2010). All data files including QC controls and MeOH blanks were examined to determine a minimum noise level threshold. The mass detection was performed using centroid algorithm with a noise level of 2000. The chromatogram building was established using a minimum time span of 0.03 min, minimum intensity of the highest data of 4000, *m/z* tolerance of 0.001. The peak deconvolution was performed using baseline cut-off algorithm with minimum acceptable peak height of 2500, and baseline level of 200. The chromatograms were deisotoped with *m/z* tolerance of 0.001, retention time tolerance of 0.1 min. The duplicate peaks were filtered with *m/z* tolerance of 0.001 and retention time tolerance of 0.1 min. All duplicate peaks were filtered by setting the *m/z* and retention time tolerances to 0.001 and 0.1 min respectively. In order to reduce the deviation of retention times between peak lists, the retention time normalizer algorithm was applied, with *m/z* tolerance of 0.001, Rt tolerance of 0.1 minutes and a minimum standard intensity set at 20000. The peak list was aligned using the join aligner algorithm with *m/z* tolerance of 0.001, retention time tolerance of 0.1 min. Then the gap-filling step was carried out by looking at the whole *m/z* and retention time range (*Intensity* tolerance of 0.5%, retention time tolerance of 0.1 min). The results were exported as a *.csv file containing all peaks observed and referenced by their mass to charge ratio (*m/z*) and retention times (Rt) together with their respective peak areas in each sample. The final matrix corresponded to a total of 101 features (*m/z*_Rt) and their respective areas in the 87 samples investigated.

References

Briand, J.-F., Barani, A., Garnier, C., Réhel, K., Urvois, F., LePoupon, C., et al. (2017). Spatio-temporal variations of marine biofilm communities colonizing artificial substrata including antifouling coatings in contrasted french coastal environments. *Microb. Ecol.* 74, 585–598. doi:10.1007/s00248-017-0966-2.

Katajamaa, M., and Orešič, M. (2005). Processing methods for differential analysis of LC/MS profile data. *BMC Bioinformatics* 6, 179. doi:10.1186/1471-2105-6-179.

Othmani, A., Briand, J.-F., Ayé, M., Molmeret, M., and Culioli, G. (2016a). Surface metabolites of the brown alga *Taonia atomaria* have the ability to regulate epibiosis. *Biofouling* 32, 801–813. doi:10.1080/08927014.2016.1198954.

Othmani, A., Bunet, R., Bonnefont, J.-L., Briand, J.-F., and Culioli, G. (2016b). Settlement inhibition of marine biofilm bacteria and barnacle larvae by compounds isolated from the Mediterranean brown alga *Taonia atomaria*. *J Appl Phycol* 28, 1975–1986. doi:10.1007/s10811-015-0668-4.

Paix, B., Carriot, N., Barry-Martinet, R., Greff, S., Misson, B., Briand, J.-F., et al. (2020). A multi-omics analysis suggests links between the differentiated surface metabolome and epiphytic microbiota along the thallus of a Mediterranean seaweed holobiont. *Front. Microbiol.* 11, 494. doi:10.3389/fmicb.2020.00494.

Paix, B., Othmani, A., Debroas, D., Culioli, G., and Briand, J.-F. (2019). Temporal covariation of epibacterial community and surface metabolome in the Mediterranean seaweed holobiont *Taonia atomaria*. *Environ. Microbiol.* 21, 3346–3363. doi:10.1111/1462-2920.14617.

Pluskal, T., Castillo, S., Villar-Briones, A., and Orešič, M. (2010). MZmine 2: Modular framework for processing, visualizing, and analyzing mass spectrometry-based molecular profile data. *BMC Bioinformatics* 11, 395. doi:10.1186/1471-2105-11-395.

Schymanski, E. L., Jeon, J., Gulde, R., Fenner, K., Ruff, M., Singer, H. P., et al. (2014). Identifying small molecules via high resolution mass spectrometry: Communicating confidence. *Environ. Sci. Technol.* 48, 2097–2098. doi:10.1021/es5002105.

Viano, Y., Bonhomme, D., Camps, M., Briand, J.-F., Ortalo-Magné, A., Blache, Y., et al. (2009). Diterpenoids from the Mediterranean brown alga *Dictyota* sp. evaluated as antifouling substances against a marine bacterial biofilm. *J. Nat. Prod.* 72, 1299–1304. doi:10.1021/np900102f.

Supplementary tables

Table SVII.1. Physico-chemical parameters (mean ± SD) measured *in situ* or in the aquaria.

		pH (pH unit)	O_2 (%)	Salinity (ppt)	$[NO_3^-]$ (μM)	$[PO_4^{3-}]$ (μM)	$[Si(OH)_4]$ (μM)
field		8.1	90.0	35.21	0.55 (± 0.28)	0.11	3.03 (± 0.01)
t_0		7.9 (± 0.23)	89.0 (± 0.6)	35.64 (± 0)	0.99 (± 0.47)	0.21	1.36 (± 0.01)
from t_0 to t_1	HT.HI	7.9 (± 0.06)	90.3 (± 1.5)	35.61 (± 0.02)	0.69 (± 0.11)	0.15	1.85 (± 0.06)
	AT.HI	7.8 (± 0.04)	90.0 (± 1.0)	35.65 (± 0.01)	0.89 (± 0.38)	0.05	1.69 (± 0.09)
	LT.HI	8.4 (± 0.05)	91.0 (± 1.0)	35.67 (± 0.01)	1.18 (± 0.05)	0.01	1.73 (± 0.01)
	HT.AI	8.3 (± 0.04)	89.0 (± 2.0)	35.65 (± 0.03)	0.33 (± 0.05)	0.09	1.83 (± 0.01)
	LT.AI	8.3 (± 0.10)	90.0 (± 2.6)	35.56 (± 0.02)	0.88 (± 0.32)	0.19	1.66 (± 0.06)
	LT.AI	8.0 (± 0.05)	89.7 (±1.2)	35.58 (± 0.02)	1.03 (± 0.06)	0.19	1.77 (± 0.01)
	HT.LI	8.1 (± 0.03)	90.3 (± 0.6)	35.6 (± 0.10)	0.66 (± 0.02)	0.19	1.89 (± 0.03)
	AT.LI	7.8 (± 0.09)	90.3 (± 1.2)	35.5 (± 0.02)	0.58 (± 0.06)	0.22	1.68 (± 0.01)
	LT.LI	7.9 (± 0.09)	90.3 (± 1.2)	35.54 (± 0.07)	1.07 (± 0.36)	0.28	1.94 (± 0.08)
from t_1 to t_2	HT.HI	7.9 (± 0.03)	90.3 (± 1.5)	35.92 (± 0.11)	1.04 (± 0.41)	0.10	2.46 (± 0.01)
	AT.HI	8.0 (± 0.06)	89.7 (± 1.2)	36.02 (± 0.04)	1.28 (± 0.28)	0.27	2.07 (± 0.01)
	LT.HI	7.9 (± 0.05)	91.3 (± 1.2)	36.09 (± 0.29)	1.08 (± 0.08)	0.27	2.19 (± 0.02)
	HT.AI	8.2 (± 0.01)	90.3 (± 1.5)	36.03 (± 0.17)	1.07 (± 0.36)	0.26	2.44 (± 0.04)
	LT.AI	8.2 (± 0.07)	90.3 (± 1.5)	36.10 (± 0.03)	1.06 (± 0.05)	0.32	2.09 (± 0.03)
	LT.AI	7.8 (± 0.06)	91.0 (± 1.7)	36.10 (± 0.02)	1.43 (± 0.43)	0.13	2.18 (± 0.01)
	HT.LI	8.5 (± 0.05)	90.3 (± 1.5)	36.21 (± 0.18)	0.75 (± 0.05)	0.17	2.48 (± 0.03)
	AT.LI	8.2 (± 0.06)	90.7 (± 0.6)	36.02 (± 0.01)	1.66 (± 0.03)	0.26	2.07 (± 0.01)
	LT.LI	8.4 (± 0.05)	89.7 (± 1.2)	36.03 (± 0.02)	1.39 (± 0.22)	0.08	2.19 (± 0.05)
from t_2 to t_3	HT.HI	7.8 (± 0.08)	90.3 (± 1.5)	35.87 (± 0.03)	1.18 (± 0.22)	0.12	1.77 (± 0.05)
	AT.HI	7.9 (± 0.09)	89.3 (± 1.2)	35.63 (± 0.06)	2.59 (± 0.04)	0.20	1.84 (± 0.01)
	LT.HI	8.2 (± 0.02)	90.3 (± 1.5)	35.59 (± 0.01)	1.96 (± 0.43)	0.34	1.42 (± 0.01)
	HT.AI	8.4 (± 0.08)	89.7 (± 2.5)	35.55 (± 0.07)	1.22 (± 0.36)	0.38	2.06 (± 0.01)
	LT.AI	8.4 (± 0.06)	90.3 (± 2.1)	35.86 (± 0.02)	2.57 (± 0.24)	0.22	1.86 (± 0.01)
	LT.AI	8.0 (± 0.04)	90.7 (± 1.5)	35.90 (± 0.01)	2.21 (± 0.04)	0.30	1.73 (± 0.01)
	HT.LI	8.1 (± 0.03)	90.3 (± 1.5)	35.77 (± 0.05)	0.95 (± 0.02)	0.38	2.15 (± 0.01)
	AT.LI	8.0 (± 0.03)	90.7 (± 1.5)	35.57 (± 0.02)	2.02 (± 0.02)	0.31	1.94 (± 0.01)
	LT.LI	8.1 (± 0.02)	90.2 (± 1.3)	38.81 (± 0.02)	1.89 (± 0.24)	0.17	1.83 (± 0.01)

Table SVII.2. Summary of three-way ANOVA tests examining the effect of sampling time, temperature and irradiance conditions for the cell densities at the algal surface, and the α-diversity indexes (Shannon and Chao1) of the epibacterial communities of *T. atomaria*.

	Cell densities		**Shannon index**		**Chao1 index**	
	F-value	*p*-value	F-value	*p*-value	F-value	*p*-value
Time	13.499	**9.92E-08**	39.253	**9.24E-16**	13.625	**7.40E-08**
Temperature	1.716	0.189	16.108	**2.85E-06**	32.439	**3.92E-10**
Irradiance	1.432	0.248	0.527	0.593	0.874	0.4228
Time x **Temperature**	0.33	0.856	1.109	0.361	3.342	0.0158
Time x **Irradiance**	0.553	0.697	0.559	0.694	0.464	0.7621
Temperature x **Irradiance**	0.241	0.914	0.203	0.936	0.373	0.8271
Time x **Temperature** x **Irradiance**	0.36	0.937	1.869	0.083	2.038	0.0578

Table SVII.3. Summary of three-way and two-way PERMANOVA results examining the effect of sampling time, temperature and irradiance conditions (for all samples, and for t_1, t_2, and t_3 samples, independently) for the 16S rRNA gene dataset obtained with the epibacterial communities of *T. atomaria*.

	All samples		
	F-value	R^2	*p*-value
Time	9.038	0.2589	**0.001**
Irradiance	2.305	0.0330	**0.002**
Temperature	8.785	0.1258	**0.001**
Time × Irradiance	0.995	0.0285	0.482
Time × Temperature	1.578	0.0452	0.012
Irradiance × Temperature	1.359	0.0389	0.051
Time x Irradiance × Temperature	1.073	0.0615	0.285
Residuals		0.4082	
Total		1	

	t_1			**t_2**			**t_3**		
	F-value	R^2	*p*-value	F-value	R^2	*p*-value	F-value	R^2	*p*-value
Irradiance	0.698	0.0487	0.985	1.515	0.0887	**0.019**	2.360	0.1183	**0.002**
Temperature	2.708	0.1891	**0.001**	4.198	0.2459	**0.001**	6.201	0.3108	**0.001**
Irradiance × Temperature	1.208	0.1687	0.064	1.181	0.1383	0.148	1.196	0.1199	0.166
Residuals		0.5935			0.5271			0.4511	
Total		1			1			1	

Table SVII.4. Multivariate pairwise results (*p*-values) examining differences between sampling times, temperature and irradiance conditions (for all samples, or for t_1, t_2, and t_3 samples, independently) for the 16S rRNA gene dataset (999 permutations) obtained with the epibacterial communities of *T. atomaria*.

All samples

	field	t_0	t_1	t_2
t_0	0.111	-	-	-
t_1	**0.0017**	0.111	-	-
t_2	**0.0017**	**0.0017**	**0.0017**	-
t_3	**0.0017**	**0.0029**	**0.0017**	**0.0037**

	AT	HT
HT	**0.001**	-
LT	**0.001**	**0.001**

	AI	HI
HI	**0.033**	-
LI	0.558	**0.033**

t_1 samples

	AT	HT
HT	**0.001**	-
LT	**0.001**	**0.001**

	AI	HI
HI	1	-
LI	1	1

t_2 samples

	AT	HT
HT	**0.001**	-
LT	**0.001**	**0.001**

	AI	HI
HI	0.54	-
LI	0.54	0.21

t_3 samples

	AT	HT
HT	**0.001**	-
LT	**0.001**	**0.001**

	AI	HI
HI	0.21	-
LI	0.308	**0.006**

Table SVII.5. Summary of taxa determined with LEfSe analysis (LDA > 4) corresponding to discriminating biomarkers of the epibacterial communities of *T. atomaria* for a specific sampling time (Part 1)

Phylum	Class	Order	Family	Genus	Species	Taxonomic rank	Discriminant sampling time	LDA	*p*-value
Proteobacteria	Gammaproteobacteria	Alteromonadales	**Alteromonadaceae**			Family	t_0	5.29	5.00E-13
Proteobacteria	Gammaproteobacteria	**Alteromonadales**				Order	t_0	5.28	5.74E-13
Proteobacteria	Gammaproteobacteria	Alteromonadales	Alteromonadaceae	***Alteromonas***		Genus	t_0	5.19	1.24E-13
Proteobacteria	**Gammaproteobacteria**					Class	t_0	5.18	2.61E-11
Proteobacteria	Gammaproteobacteria	Alteromonadales	Alteromonadaceae	*Alteromonas*	**unknown species**	Species	t_0	5.17	1.24E-13
Proteobacteria	Alphaproteobacteria	Caulobacterales	**Hyphomonadaceae**			Family	field	5.07	1.78E-10
Proteobacteria	Alphaproteobacteria	**Caulobacterales**				Order	field	5.04	1.46E-10
Proteobacteria	**Alphaproteobacteria**					Class	t_3	5.00	1.16E-08
Proteobacteria	Alphaproteobacteria	Caulobacterales	Hyphomonadaceae	*Litorimonas*	**unknown species**	Species	field	4.95	1.39E-09
Bacteroidetes	Bacteroidia					Class	field	4.73	4.39E-05
Bacteroidetes						Phylum	field	4.70	4.39E-05
Proteobacteria	Alphaproteobacteria	**Rhodovibrionales**				Order	field	4.69	8.84E-12
Proteobacteria	Alphaproteobacteria	Rhodovibrionales	Kiloniellaceae	*Kiloniella*	**Kiloniella laminariae**	Species	field	4.67	8.84E-12
Proteobacteria	Alphaproteobacteria	Rhodovibrionales	**Kiloniellaceae**			Genus	field	4.67	8.84E-12
Proteobacteria	Gammaproteobacteria	**Cellvibrionales**				Order	t_3	4.66	5.91E-12
Proteobacteria	Alphaproteobacteria	Rhodovibrionales	Kiloniellaceae	***Kiloniella***		Genus	field	4.65	8.84E-12
Proteobacteria	Gammaproteobacteria	Alteromonadales	Alteromonadaceae	***Aliiglaciecola***		Genus	t_1	4.49	6.64E-06
Proteobacteria	Gammaproteobacteria	Alteromonadales	Alteromonadaceae	*Aliiglaciecola*	**Aliiglaciecola aliphaticivorans**	Species	t_1	4.47	6.70E-10

Table SVII.5. Summary of taxa determined with LEfSe analysis (LDA > 4) corresponding to discriminating biomarkers of the epibacterial communities of *T. atomaria* for a specific sampling time (Part 2)

Phylum	Class	Order	Family	Genus	Species	Taxonomic rank	Discriminant sampling time	LDA	*p*-value
Proteobacteria	Gammaproteobacteria	Alteromonadales	Alteromonadaceae	*Paraglaciecola*	**unknown species**	Species	t_0	4.45	3.07E-10
Proteobacteria	Gammaproteobacteria	Alteromonadales	Alteromonadaceae	***Paraglaciecola***		Genus	t_0	4.43	2.98E-10
Proteobacteria	Alphaproteobacteria	**Rhizobiales**				Order	t_3	4.42	1.73E-06
Proteobacteria	Alphaproteobacteria	Caulobacterales	Hyphomonadaceae	unknown genus	**unknown species**	Species	t_3	4.41	1.22E-11
Proteobacteria	Alphaproteobacteria	Caulobacterales	Hyphomonadaceae	**unknown genus**		Genus	t_3	4.41	1.22E-11
Proteobacteria	Gammaproteobacteria	Cellvibrionales	**Spongiibacteraceae**			Family	t_3	4.40	6.09E-09
Proteobacteria	Alphaproteobacteria	Rhodobacterales	Rhodobacteraceae	*Primorskyibacter*	***Primorskyibacter aestuariivivens***	Species	t_3	4.32	5.50E-13
Proteobacteria	Alphaproteobacteria	Rhodobacterales	Rhodobacteraceae	***Primorskyibacter***		Genus	t_3	4.32	5.50E-13
Proteobacteria	Gammaproteobacteria	Cellvibrionales	Spongiibacteraceae	**unknown genus**		Genus	t_3	4.30	1.48E-11
Proteobacteria	Gammaproteobacteria	Cellvibrionales	Spongiibacteraceae	unknown genus	**unknown species**	Species	t_3	4.30	1.48E-11
Proteobacteria	Alphaproteobacteria	Rhodobacterales	Rhodobacteraceae	***Pseudophaeobacter***		Genus	t_1	4.23	1.12E-10
Proteobacteria	Gammaproteobacteria	**Oceanospirillales**				Order	t_1	4.23	1.71E-06
Proteobacteria	Alphaproteobacteria	Rhodobacterales	Rhodobacteraceae	*Pseudophaeobacter*	***Phaeobacter* sp.**	Species	t_0	4.22	6.50E-11
Proteobacteria	Gammaproteobacteria	Cellvibrionales	**Cellvibrionaceae**			Family	t_3	4.13	5.95E-09
Proteobacteria	Gammaproteobacteria	Oceanospirillales	**Nitrincolaceae**			Family	t_1	4.12	1.44E-06
Proteobacteria	Alphaproteobacteria	Rhizobiales	Rhizobiaceae	*Lentilitoribacter*	**unknown species**	Species	t_3	4.11	6.28E-06
Proteobacteria	Alphaproteobacteria	Rhizobiales	Rhizobiaceae	***Lentilitoribacter***		Genus	t_3	4.11	6.28E-06
Proteobacteria	Gammaproteobacteria	Oceanospirillales	Nitrincolaceae	***Neptuniibacter***		Genus	t_1	4.08	2.50E-08
Bacteroidetes	Bacteroidia	Chitinophagales	Saprospiraceae	*Rubidimonas*	**unknown species**	Species	field	4.04	1.45E-08
Bacteroidetes	Bacteroidia	Chitinophagales	Saprospiraceae	***Rubidimonas***		Genus	field	4.01	1.45E-08
Proteobacteria	Alphaproteobacteria	Rhizobiales	**Rhizobiaceae**			Family	t_3	4.00	6.49E-05

Table SVII.6. SIMPER results of the most contributing genera to the dissimilarities between field and t_0 samples of the epibacterial communities of *T. atomaria*.

Only the first 70% of the cumulative contribution is shown. *p*-values were calculated with a permutation test constructed with 999 permutations.

Order	Family	Genus	Average contribution	SD	Ratio	Av. field	Av. t_0	Cum. sum	*p* value
Alteromonadales	Alteromonadaceae	*Alteromonas*	13.1%	0.04	3.44	2592	8252	20%	0.006
Caulobacterales	Hyphomonadaceae	*Litorimonas*	7.7%	0.06	1.27	3509	160	32%	0.001
Thiohalorhabdales	Thiohalorhabdaceae	*Granulosicoccus*	5.7%	0.02	3.78	3163	687	40%	0.001
Rhodovibrionales	Kiloniellaceae	*Kiloniella*	4.2%	0.06	0.77	1869	40	47%	0.002
Chitinophagales	Saprospiraceae	*unknown genus*	3.6%	0.01	3.07	1967	426	52%	0.001
Alteromonadales	Alteromonadaceae	*Paraglaciecola*	2.8%	0.01	3.17	393	1612	56%	0.004
Caulobacterales	Hyphomonadaceae	*Hellea*	2.6%	0.03	1.02	1141	23	60%	0.001
Rhodobacterales	Rhodobacteraceae	*Sulfitobacter*	1.9%	0.01	3.11	460	1266	63%	0.213
Rhodobacterales	Rhodobacteraceae	*Pseudophaeobacter*	1.7%	0.01	2.35	51	796	66%	0.059
Alteromonadales	Alteromonadaceae	*Aliiglaciecola*	1.7%	0.01	2.00	67	807	68%	0.239
Flavobacteriales	Flavobacteriaceae	*Tenacibaculum*	1.7%	0.02	0.82	906	360	71%	0.161

Table SVII.7. Summary of affiliated genera determined through LEfSe analysis corresponding to discriminating biomarker taxa of the epibacterial communities of *T. atomaria* for a specific condition of temperature and irradiance at t_3 (LDA > 3.4).

Class	Order	Family	Genus	Discriminating condition	*p* value	LDA
Alphaproteobacteria	Rhodobacterales	Rhodobacteraceae	*Sulfitobacter*	HT.AI	0.039	4.510
Alphaproteobacteria	Rhodobacterales	Rhodobacteraceae	*Primorskyibacter*	HT.AI	0.008	4.668
Alphaproteobacteria	Rhizobiales	Rhizobiaceae	*Lentilitoribacter*	HT.HI	0.016	4.310
Gammaproteobacteria	Ectothiorhodospirales	Thioalkalispiraceae	*Thioprofundum*	AT.AI	0.012	4.312
Gammaproteobacteria	Oceanospirillales	Nitrincolaceae	*Neptuniibacter*	LT.LI	0.050	3.926
Bacteroidia	Flavobacteriales	Flavobacteriaceae	*Kordia*	LT.AI	0.007	3.953
Alphaproteobacteria	Caulobacterales	Parvularculaceae	*Parvularcula*	HT.HI	0.012	3.886
Alphaproteobacteria	Caulobacterales	Hyphomonadaceae	*Hirschia*	HT.LI	0.011	3.649
Gammaproteobacteria	Oceanospirillales	Oleiphilaceae	*Oleiphilus*	LT.LI	0.003	3.694
Gammaproteobacteria	Cellvibrionales	Halieaceae	*Congregibacter*	HT.HI	0.005	3.570
Bacteroidia	Flavobacteriales	Flavobacteriaceae	*Winogradskyella*	AT.AI	0.041	3.521
Alphaproteobacteria	Rhodobacterales	Rhodobacteraceae	*Jannaschia*	AT.HI	0.019	3.445
Alphaproteobacteria	Rhodobacterales	Rhodobacteraceae	*Silicimonas*	AT.AI	0.018	3.436

Table SVII.8. Summary of three-way and two-way PERMANOVA results examining the effect of sampling time, temperature and irradiance conditions (for all samples and for t_1, t_2, and t_3 samples, independently) for the LC-(+)-ESI-HRMS metabolomics dataset obtained with the surface extracts of *T. atomaria*.

	All samples		
	F value	R^2	*p* value
Time	4.6927	0.15094	**0.001**
Temperature	4.5275	0.07281	**0.001**
Irradiance	4.9263	0.07922	**0.001**
Time × Temperature	1.3779	0.04432	**0.035**
Time × Irradiance	1.3931	0.04481	**0.045**
Temperature × Irradiance	1.8541	0.05963	**0.001**
Time × Temperature × Irradiance	1.3978	0.08992	**0.009**
Residuals		0.45834	
Total		1	

	t_1			**t_2**			**t_3**		
	F value	R^2	*p* value	F value	R^2	*p* value	F value	R^2	*p* value
Temperature	1.44581	0.10222	0.082	4.1508	0.23109	**0.001**	3.795	0.19024	**0.001**
Luminosity	1.74058	0.12306	**0.028**	2.8607	0.15927	**0.001**	3.622	0.18157	**0.001**
Temperature × Luminosity	0.97872	0.1384	0.523	0.9751	0.10857	0.517	2.0155	0.20207	**0.001**
Residuals	0.63632			0.50107				0.42611	
Total								1	

Table SVII.9. Multivariate pairwise results (*p*-values) examining differences between sampling times, temperature and irradiance conditions (for all samples and for t_1, t_2, and t_3 samples, independently) for the LC-(+)-ESI-HRMS metabolomics dataset (999 permutations) obtained with the surface extracts of *T. atomaria*.

ALL samples

	field	t_0	t_1	t_2
t_0	0.1178	-	-	-
t_1	**0.005**	0.331	-	-
t_2	**0.0033**	**0.034**	**0.0033**	-
t_3	0.06166	0.11778	**0.0033**	0.06857

	LT	AT
AT	0.241	-
HT	**0.0015**	**0.0015**

	LI	AI
AI	**0.0015**	-
HI	**0.0015**	**0.047**

t_1 samples

	LT	AT
AT	0.198	-
HT	0.198	0.198

	LI	AI
AI	0.15	-
HI	**0.03**	0.12

t_2 samples

	LT	AT
AT	0.123	-
HT	**0.0015**	**0.0015**

	LI	AI
AI	**0.0285**	-
HI	**0.003**	0.3

t_3 samples

	LT	AT
AT	**0.03**	-
HT	**0.006**	**0.021**

	LI	AI
AI	**0.006**	-
HI	**0.003**	0.123

Table SVII.10. List of metabolites (VIP score > 0.6) identified by LC-(+)-ESI-HRMS and involved in the discrimination between each irradiance/temperature condition at t_3 within surface extracts of *T. atomaria* (Part 1).

VIP n°	*m/z*	Retention time (s)	VIP score (t_3)	Molecular formula	Type of ion	Mass error (ppm)	mσ[a]	Putative annotation	MS/MS fragment ions
1	203.1796	509	2.73	$C_{15}H_{23}$	$[M - H_2O + H]^+$	-1.0	27.6	Germacratrienol*	55.0545 $[C_4H_7]^+$, 69.0689 $[C_5H_9]^+$, 81.0701 $[C_6H_9]^+$, 95.0857 $[C_7H_{11}]^+$, 105.0698 $[C_8H_9]^+$, 119.0855 $[C_9H_{11}]^+$, 133.1010 $(C_{10}H_{13}]^{+\cdot}$ 147.1170 $[C_{11}H_{15}]^+$, 161.1318 $[C_{12}H_{17}]^+$
2	183.0865 205.068	48 48	2.16	$C_6H_{15}O_6$ $C_6H_{14}NaO_6$	$[M + H]^+$ $[M + Na]^+$	-1.2 1.1	3.5 3.6	Mannitol*	57.0333 $[C_3H_5O]^+$, 69.0333 $[C_4H_5O]^+$, 83.0490 $[C_5H_7O]^+$, 85.0283 $[C_4H_5O_2]^+$, 99.0442 $[C_5H_7O_2]^+$
3	411.3634	684	2.06	$C_{29}H_{47}O$	-	-0.4	35.3	-	57.070 $[C_4H_9]^+$, 83.0851 $[C_6H_{11}]^+$, 94.0650 $[C_6H_9O]^+$, 109.0648 $[C_7H_9O]^+$, 123.1171 $[C_9H_{15}]^+$, 203.1788 $[C_{15}H_{23}]^+$, 271.2072 $[C_{19}H_{27}O]^+$, 327.0765 $[C_{25}H_{11}O]^+$
4	613.4853	657	1.92	$C_{39}H_{65}O_5$	$[M + H]^+$	-4.3	63.9	DG (36:6) [C18:3/C18:3 & C18:4/C18:2]	81.0689 $[C_6H_9]^+$, 133.0865 $[C_6H_{13}O_3]^+$, 261.2219 $[C_{18}H_{29}O]^+$, 283.2613 $[C_{18}H_{35}O_2]^+$, 317.2472 $[C_{21}H_{33}O_2]^+$, 333.2414 $[C_{21}H_{33}O_3]^+$, 335.2574 $[C_{21}H_{35}O_3]^+$, 337.2738 $[C_{21}H_{37}O_3]^+$, 595.4699 $[C_{39}H_{63}O_4]^+$, 613.4853 $[C_{39}H_{65}O_5]^+$
5	409.1651	466	1.85	$C_{24}H_{25}O_6$	-	-1.4	19.3	-	239.1618 $[C_{14}H_{23}O_3]^+$, 309.1103 $[C_{19}H_{17}O_4]^+$, 317.1363 $[C_{18}H_{21}O_5]^+$, 327.1217 $[C_{19}H_{19}O_5]^+$, 355.1146 $[C_{20}H_{19}O_6]^+$, 409.1653 $[C_{24}H_{25}O_6]^+$
6	231.1380	686	1.83	$C_{15}H_{19}O_2$	$[M + H]^+$	-0.3	56.9	Unidentified sesquiterpene	91.0541 $[C_7H_7]^+$, 117.0697 $[C_9H_9]^+$, 131.0855 $[C_{10}H_{11}]^+$, 145.1012 $[C_{11}H_{13}]^+$, 157.0646 $[C_{11}H_9O]^+$, 175.0753 $[C_{11}H_{11}O_2]^+$, 189.0906 $[C_{12}H_{13}O_2]^+$
7	635.468	547	1.83	$C_{41}H_{63}O_5$	$[M + H]^+$	-1.5	25.3	DG (C38:9)	n.f.[b]
8	611.4687	650	1.38	$C_{39}H_{63}O_5$	$[M + H]^+$	-2.7	27.5	DG (C36:7)	n.f.
9	830.5953	621	1.52	$C_{52}H_{80}NO_7$	$[M + H]^+$	-3.2	47.7	DGTA (C42:11)	n.f.
10	808.6091	632	1.52	$C_{50}H_{82}NO_7$	$[M + H]^+$	-0.6	34.4	DGTA (C40:8) [C20:4/C20:4]	406.3300 $[C_{25}H_{44}NO_3]^+$, 504.3687 $[C_{30}H_{50}NO_5]^+$, 522.3795 $[C_{30}H_{52}NO_6]^+$
11	205.0845	119	1.34	$C_{11}H_{13}N_2O_2$	$[M + H]^+$	7.1	3.2	Tryptophan	n.f.
12	144.1019	48	1.28	$C_7H_{14}NO_2$	$[M + H]^+$	-0.2	20.9	Proline betaine*	58.0613 $[C_3H_8N]^+$, 84.0809 $[C_5H_{10}N]^+$, 102.0574 $[C_4H_8NO_2]^+$, 144.1018 $[M+H]^+$

[a] Constructor statistical match factor (comparison of theoretical and experimental isotopic patterns). [b] Not fragmented. * Annotation confirmed with a chemical standard.

Table SVII.10. List of metabolites (VIP score > 0.6) identified by LC-(+)-ESI-HRMS and involved in the discrimination between each irradiance/temperature condition at t_3 within surface extracts of *T. atomaria* (Part 2).

VIP n°	*m/z*	Retention time (s)	VIP score (t_3)	Molecular formula	Type of ion	Mass error (ppm)	mσ[a]	Putative annotation	MS/MS fragment ions
13	659.4343 681.4137	595 597	1.28	$C_{42}H_{59}O_6$ $C_{42}H_{58}NaO_6$	$[M + H]^+$ $[M + Na]^+$	-5.5 0.3	14.3 14.3	Fucoxanthin*	109.1016 $[C_8H_{13}]^+$, 119.0859 $[C_9H_{11}]^+$, 135.0812 $[C_9H_{11}O]^+$, 147.0813 $[C_{10}H_{11}O]^+$, 213.1284 $[C_{15}H_{17}O]^+$, 251.1799 $[C_{19}H_{23}]^+$, 263.1797 $[C_{20}H_{23}]^+$, 355.2418 $[C_{27}H_{31}]^+$, 411.2676 $[C_{30}H_{35}O]^+$, 581.3394 $[C_{40}H_{53}O_3]^+$
14	587.2406	621	1.20	$C_{38}H_{35}O_6$	-	3.7	5.7	-	n.f.[b]
15	135.05	46	1.11	$C_5H_{11}O_2S$	$[M + H]^+$	-2.3	10.7	DMSP*	n.f.
16	429.2969	606	1.10	$C_{27}H_{41}O_4$	$[M + H]^+$	7.1	5.5	MG (C24:7)	81.0628 $[C_6H_9]^+$, 95.0851 $[C_7H_{11}]^+$, 301.1429 $[C_{18}H_{21}O_4]^+$, 351.2213 $[C_{24}H_{31}O_2]^+$, 429.2960 $[C_{27}H_{41}O_4]^+$
17	205.1935	533	1.10	$C_{15}H_{25}$	$[M + H]^+$	7.8	2.4	δ-Cadinene*	69.0722 $[C_5H_9]^+$, 81.0713 $[C_6H_9]^+$, 93.0705 $[C_7H_9]^+$, 107.0857 $[C_8H_{11}]^+$, 121.1006 $[C_9H_{13}]^+$, 149.1312 $[C_{11}H_{17}]^+$, 205.1921 $[C_{15}H_{25}]^+$
18	166.0982	69	1.09	$C_9H_{12}NO_2$	$[M + H]^+$	8.0	1.1	Phenylalanine	93.0678 $[C_7H_9]^+$, 103.0557 $[C_8H_7]^+$, 120.0864 $[C_8H_{10}N]^+$, 132.0120 $[C_6H_2N_3O]^+$, 146.0401 $[C_7H_4N_3O]^+$
19	203.18	574	1.09	$C_{15}H_{23}$	$[M - H_2O + H]^+$	-2.3	51.8	Gleenol*	n.f.
20	82.5369	35	1.08	$C_6H_{15}NO_2S$	$[M + 2H]^{2+}$	16.8	59.5	Methylmethionine	n.f.
21	607.4366	632	1.03	$C_{39}H_{59}O_5$	$[M + H]^+$	-1.6	6.0	DG (C36:9)	n.f.

[a] Constructor statistical match factor (comparison of theoretical and experimental isotopic patterns). [b] Not fragmented. * Annotation confirmed with a chemical standard.

Table SVII.10. List of metabolites (VIP score > 0.6) identified by LC-(+)-ESI-HRMS and involved in the discrimination between each irradiance/temperature condition at t_3 within surface extracts of *T. atomaria* (Part 3).

VIP n°	*m/z*	Retention time (s)	VIP score (t_3)	Molecular formula	Type of ion	Mass error (ppm)	mσ[a]	Putative annotation	MS/MS fragment ions
22	557.299	569	1.02	$C_{25}H_{49}O_{11}S$	$[M + H]^+$	0.0	12.6	SQMG (C16:0)	313.2734 $[C_{19}H_{37}O_3]^+$, 239,2368 $[C_{16}H_{31}O]^+$
23	760.6093	652	0.95	$C_{46}H_{82}NO_7$	$[M + H]^+$	-1.0	n.d.[b]	DGTA (C36:4) [C16:0/C20:4]	456.3679 $[C_{26}H_{50}NO_5]^+$, 474.3797 $[C_{26}H_{52}NO_6]^+$, 504.3654 $[C_{30}H_{50}NO5]^+$, 522.3791 $[C_{30}H_{52}NO_6]^+$
24	734.5914	639	0.95	$C_{44}H_{80}NO_7$	$[M + H]^+$	-0.7	8.4	DGTA (C34:3) [C14:0/C20:3 & C16:0/C18:3]	393.2979 $[C_{24}H_{41}O_4]^+$, 428.3360 $[C_{24}H_{46}NO_5]^+$, 446.3491 $[C_{24}H_{48}NO_6]^+$, 456.3664 $[C_{26}H_{50}NO_5]^+$, 474.3809 $[C_{26}H_{52}NO_6]^+$, 478.3545 $[C_{28}H_{48}NO_5]^+$, 496.3605 $[C_{28}H_{50}NO_6]^+$, 506.3867 $[C_{30}H_{52}NO_5]^+$, 524.3970 $[C_{30}H_{54}NO_6]^+$
25	274.2769	434	0.89	$C_{16}H_{36}NO_2$	-	-2.8	10.9	-	n.f.[c]
26	756.5780	521	0.74	$C_{46}H_{78}NO_7$	$[M + H]^+$	-0.9	15.2	DGTA (C36:6) [C20:5/16:1 & C18:3/C18:3]	454.3515 $[C_{26}H_{48}NO_5]^+$, 472.3631 $[C_{26}H_{50}NO_6]^+$, 496.3629 $[C_{28}H_{50}NO_6]^+$, 520.3625 $[C_{30}H_{50}NO_6]^+$
27	487.3105	568	0.65	$C_{29}H_{43}O_6$	-	8.1	33.2	-	427.2831 $[C_{27}H_{39}O_4]^+$, 487.3581 $[C_{29}H_{43}O_6]^+$
28	806.5942	624	0.65	$C_{50}H_{80}NO_7$	$[M + H]^+$	-1.6	10.4	DGTA (C40:9) [C20:4/C20:5]	502.3524 $[C_{30}H_{48}NO_5]^+$, 504.3687 $[C_{30}H_{50}NO_5]^+$, 520.3625 $[C_{30}H_{50}NO_6]^+$, 522.3769 $[C_{30}H_{52}NO_6]^+$
29	395.3674	681	0.61	$C_{29}H_{47}$	$[M + H]^+$	-0.4	10.4	$C_{29}H_{46}$	n.f.

[a] Constructor statistical match factor (comparison of theoretical and experimental isotopic patterns). [b] Not determined. [c] Not fragmented.

Supplementary figures

Figure SVII.1. Representation of the experimental mesocosm systems used for the study.
The temperature-controlled room contained three shelves (one for each condition of temperature) of three floors (for each condition of irradiance). Each floor contained three aquaria (one for each replicate) containing each from 3 to 4 algal individuals (one for each sampling time). (**1**) The pre-treated seawater is firstly conditioned in a tank (50L) and UV-treated. (**2**) The seawater is then distributed in a chiller/heater system and pumped to be distributed to each aquarium. (**3**) Aquaria from the bottom floors are conditioned at "low irradiance" from t_0 to t_3 with a solar film on the LED system, (**4**) while those from the top floors are conditioned at "high irradiance" by adding a second LED system. (**5**) By overflowing, the water from the aquaria comes back to the tank, (**6**) through a micron bag. (**7**) The light:dark cycle is controlled by a 24h programmed timer.

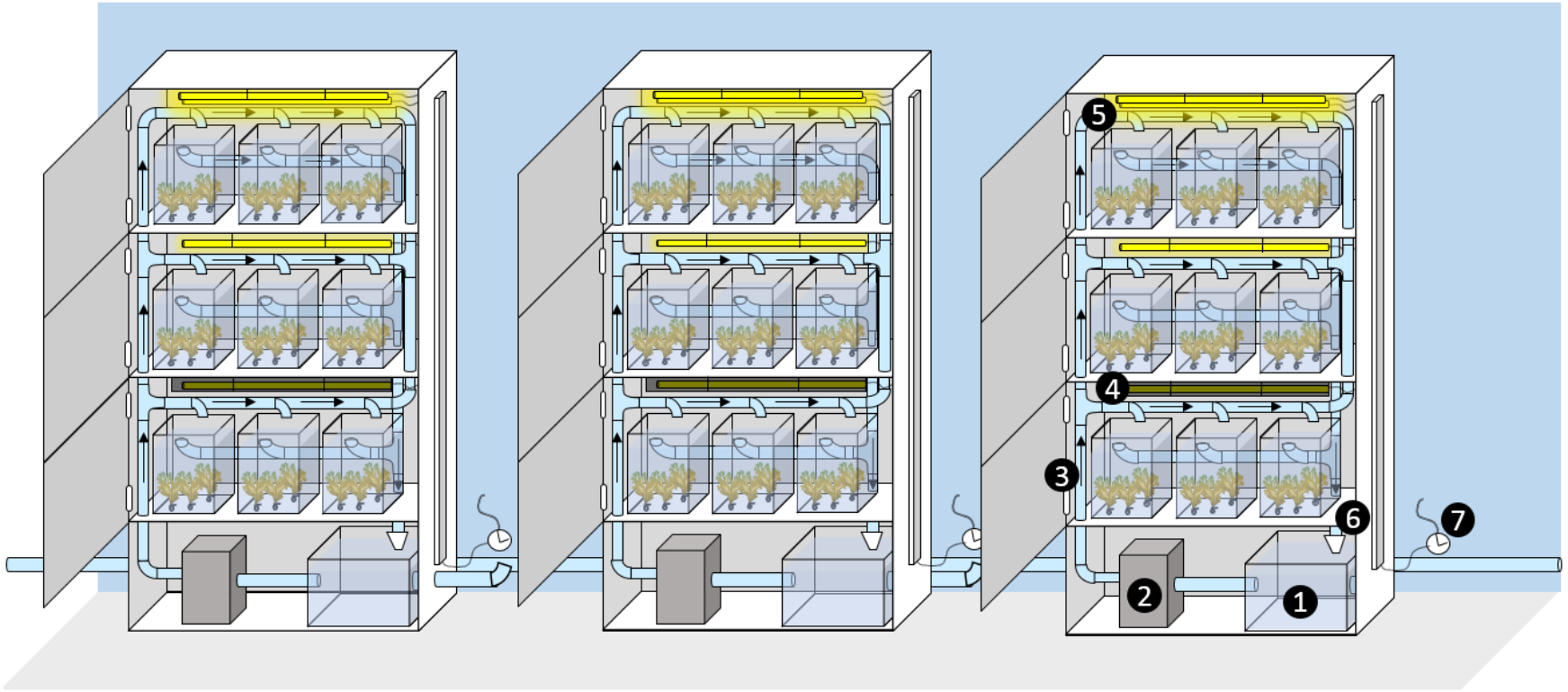

Figure SVII.2. Photographs of the experimental setup used to cultivate samples of *T. atomaria*.
(**A**) Two of the three shelves before algae were conditioned. (**B**) One of the three shelves, once algae were conditioned. (**C**) Single aquarium (15L) containing three algal specimens.

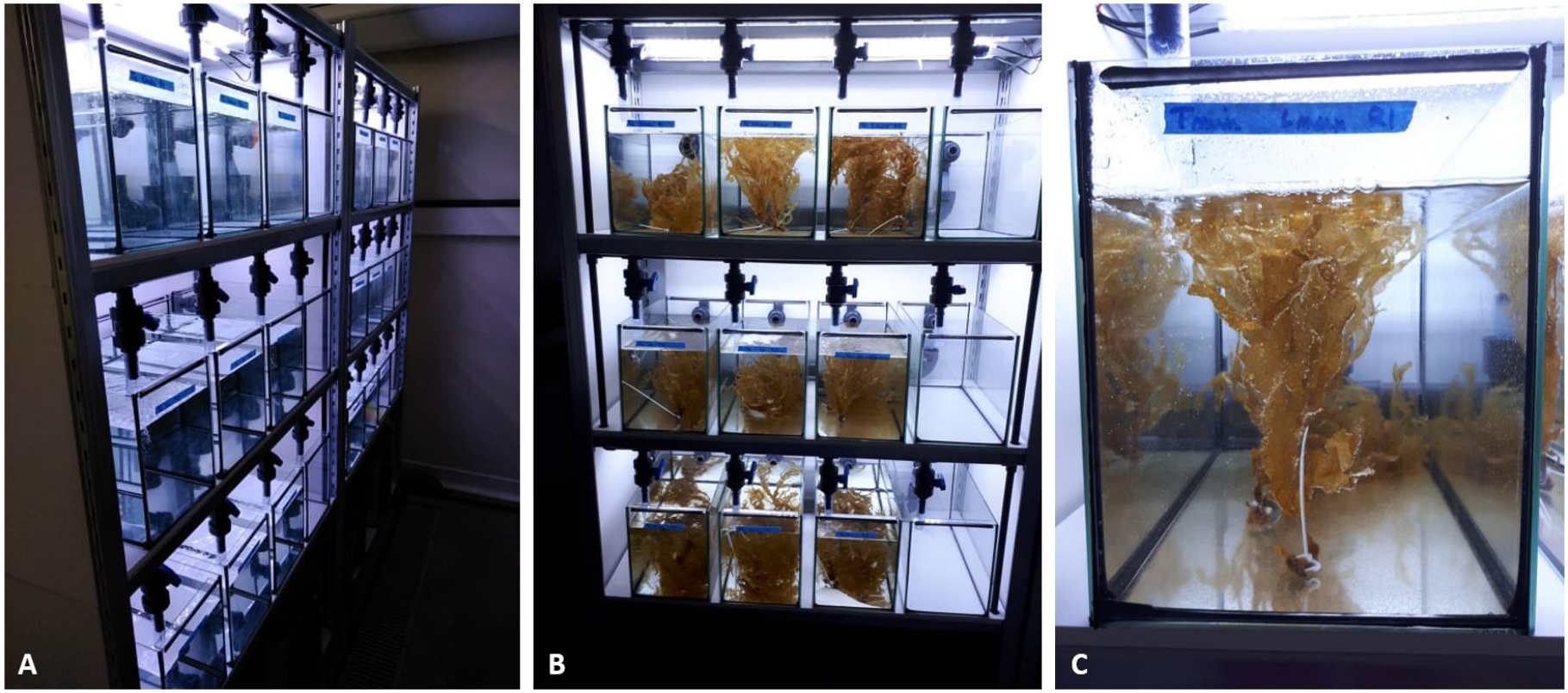

Figure SVII.3. Mean values (± SD) of maximum photosynthetic yield (F_v/F_m measures) of thalli of *T. atomaria* before extraction procedures.

Light blue, orange and red histograms represent samples at "low", "ambient" and "high" temperature conditions. Dark blue, green and yellow backgrounds represent samples at "low", "ambient" and "high" irradiance conditions.

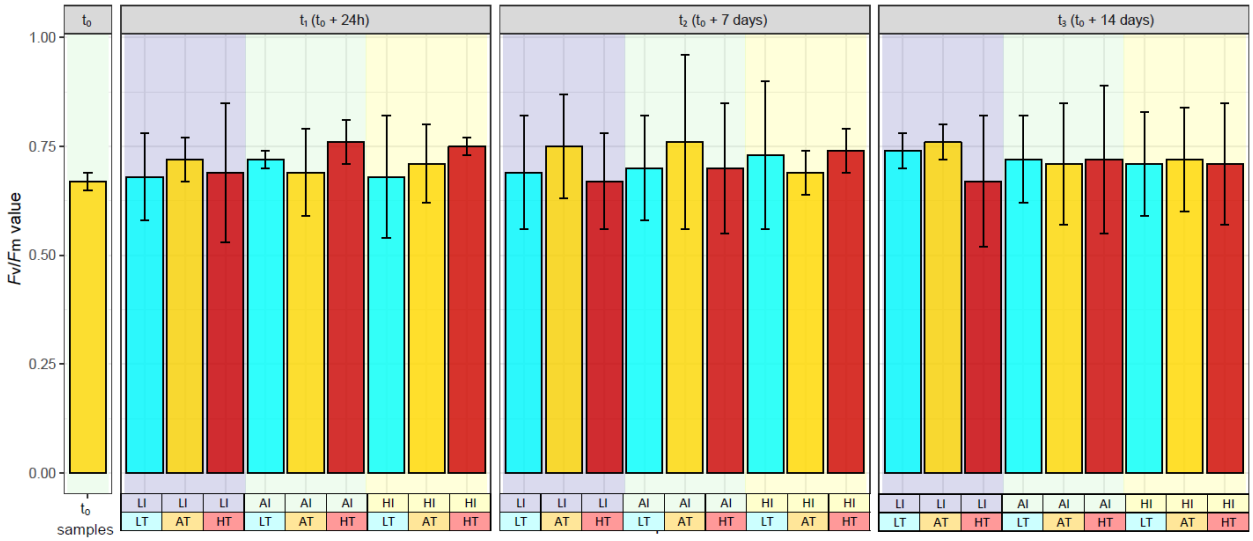

Figure SVII.4. Variations of cells densities at the surface of *T. atomaria*.

Light blue, orange and red boxplots represent samples at "low", "ambient" and "high" temperature conditions. Dark blue, green and yellow backgrounds represent samples at "low", "ambient" and "high" irradiance conditions. **A**, **B** and **C** represent results from Tukey's tests comparing sampling times.

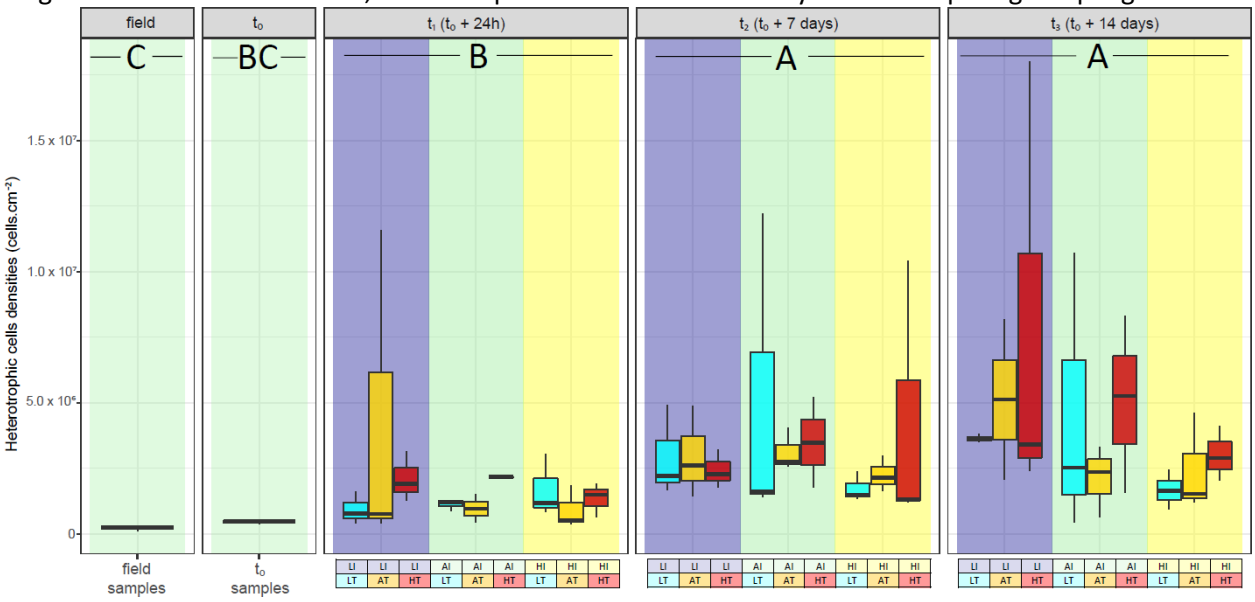

Figure SVII.5. Comparison of the epibacterial community structure of *T. atomaria* at the order level analyzed with 515F-Y / 926R and NOCHL primers for triplicates samples collected at t_0 and t_1 sampling times with ambient temperature (AT) and irradiance (AI) conditions.

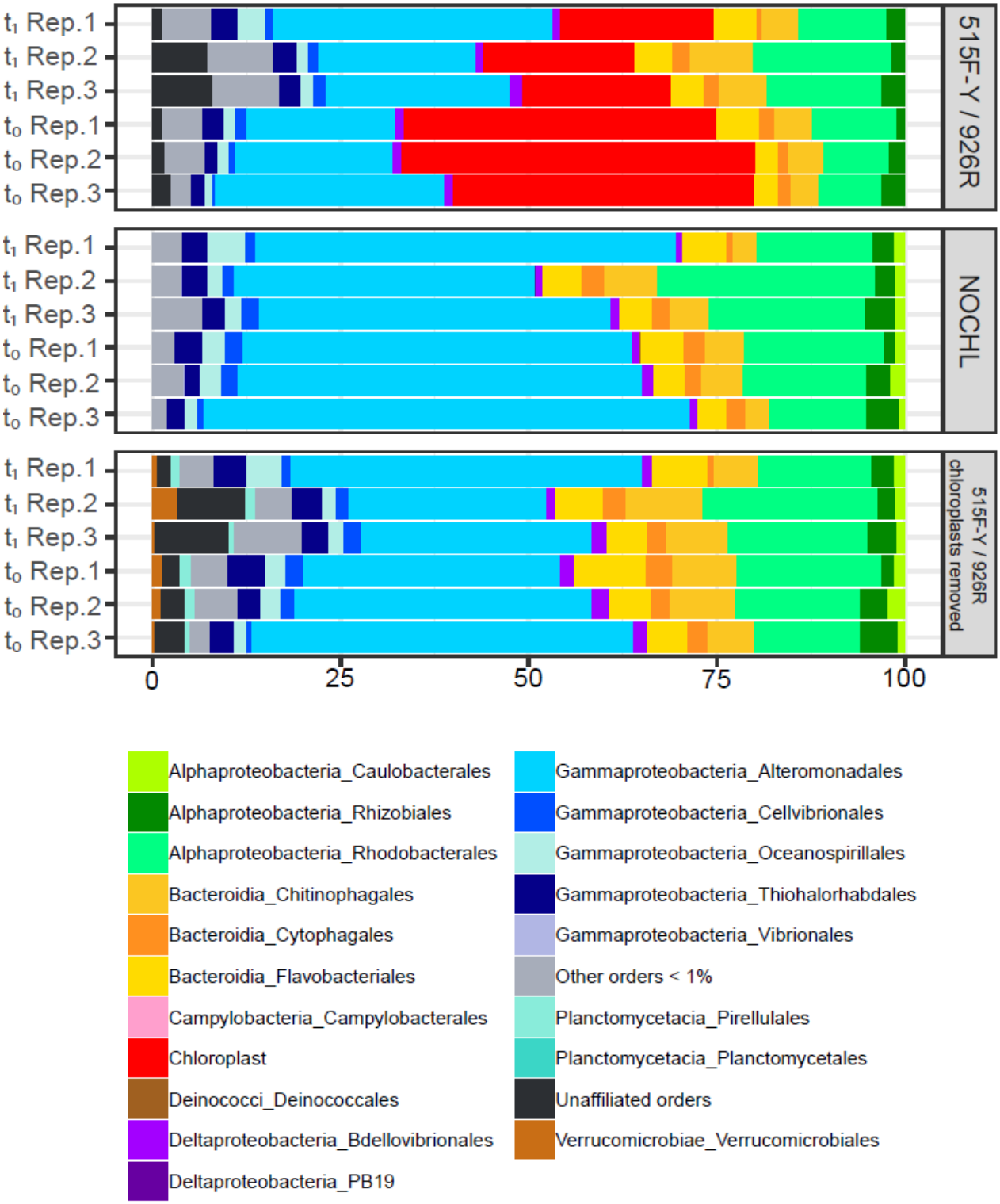

Figure SVII.6. Variations of *α*-diversity metrics (Shannon and Chao1 indexes) of the epibacterial communities of *T. atomaria*.

Light blue, orange and red boxplots represent samples at "low", "ambient" and "high" temperature conditions. Dark blue, green and yellow backgrounds represent samples at "low", "ambient" and "high" irradiance conditions. **a**, **b** and **c** represent results from Tukey's tests comparing each "temperature/irradiance" condition at t_3. For Chao1 index, significant differences are also observed between field and t_0 samples.

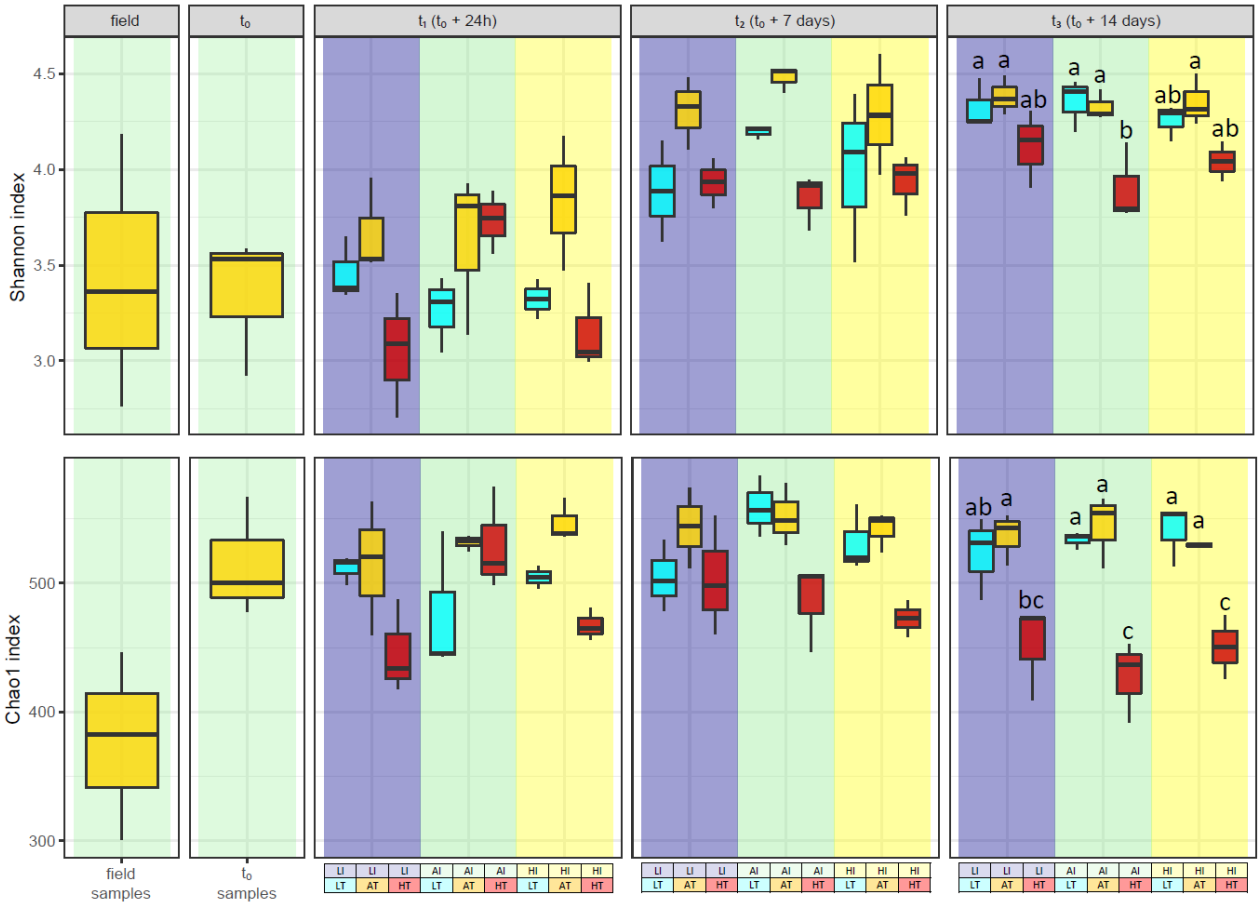

Figure SVII.7. Venn diagrams showing shared percentages of OTUs (A) and sequences (B) between samples of *T. atomaria* obtained at each sampling time.

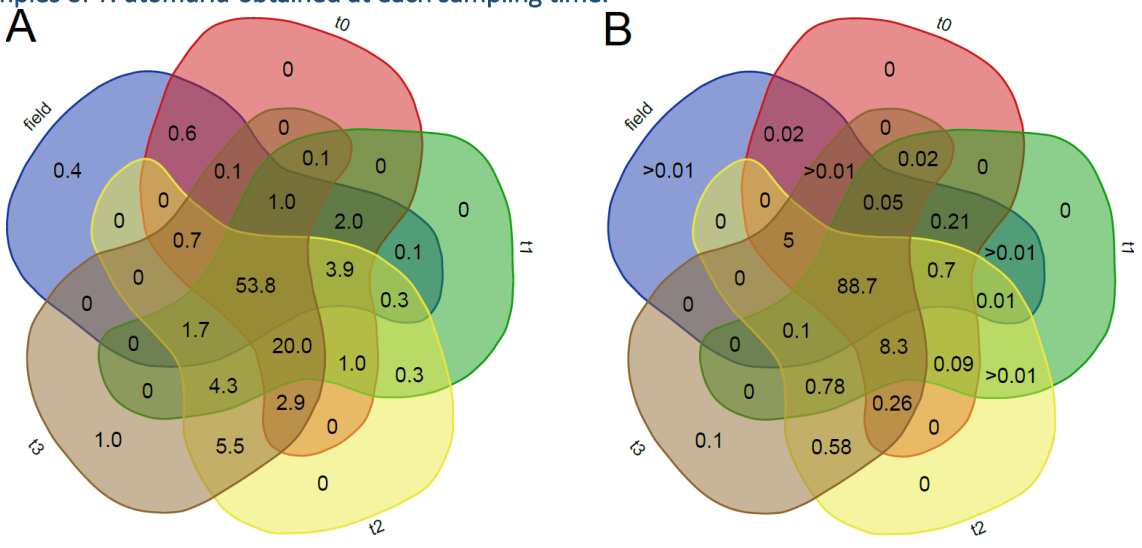

Figure SVII.8. Structure of epibacterial communities of *T. atomaria* at the family level.
Light blue, orange and red squares represent samples at “low”, “ambient” and “high” temperature conditions. Dark blue, green and yellow squares represent samples at “low”, “ambient” and “high” irradiance conditions.

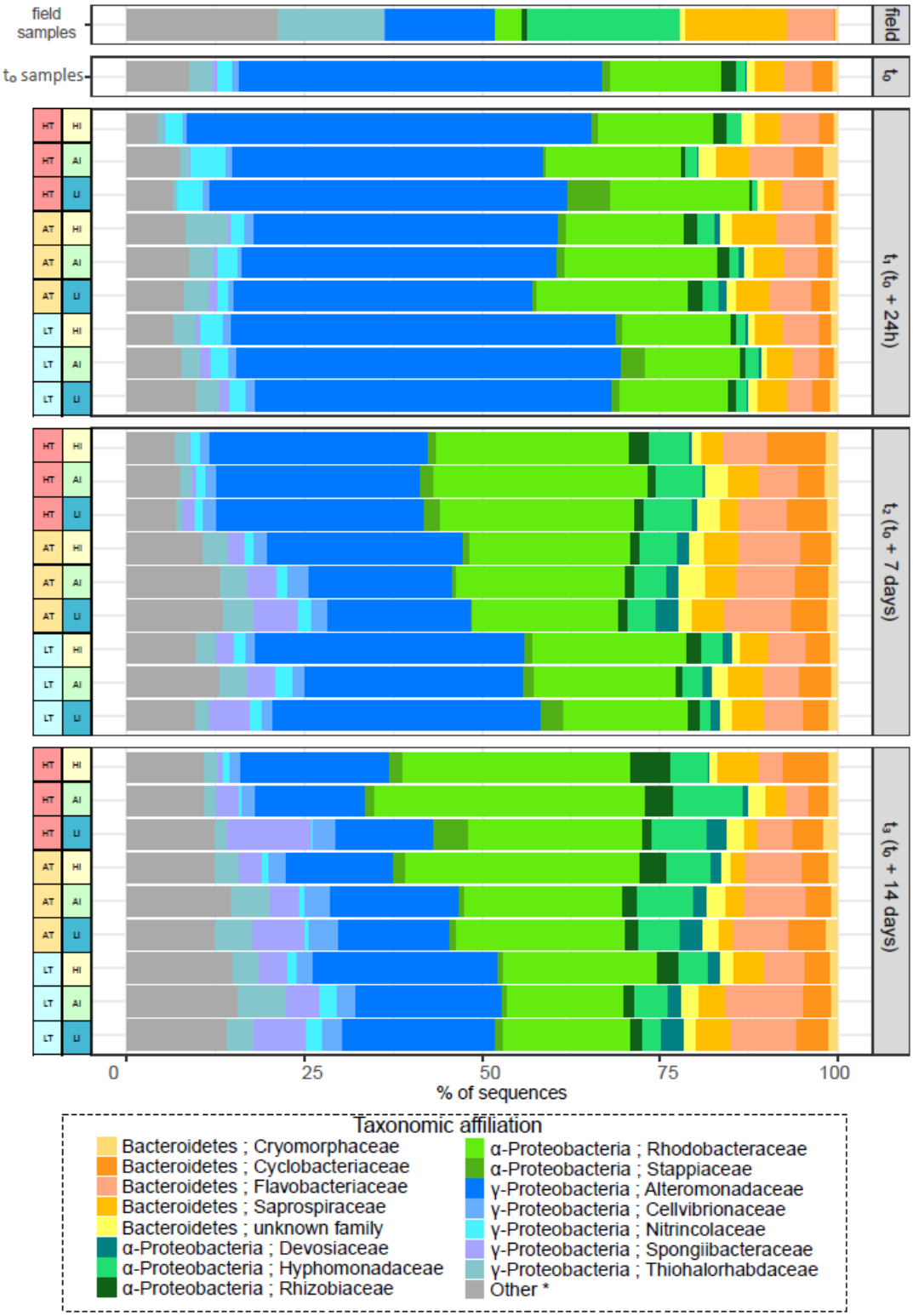

Figure SVII.9. Variation of biomarker genera identified through the LEfSe analysis conducted on t_3 samples (see Table SVII.7) (Part 1).

Light blue, orange and red boxplots represent samples at "low", "ambient" and "high" temperature conditions. Dark blue, green and yellow backgrounds represent samples at "low", "ambient" and "high" irradiance conditions. **a**, **b** and **c** represent results from Duncan's multiple tests comparing each "temperature/irradiance" condition at t_3.

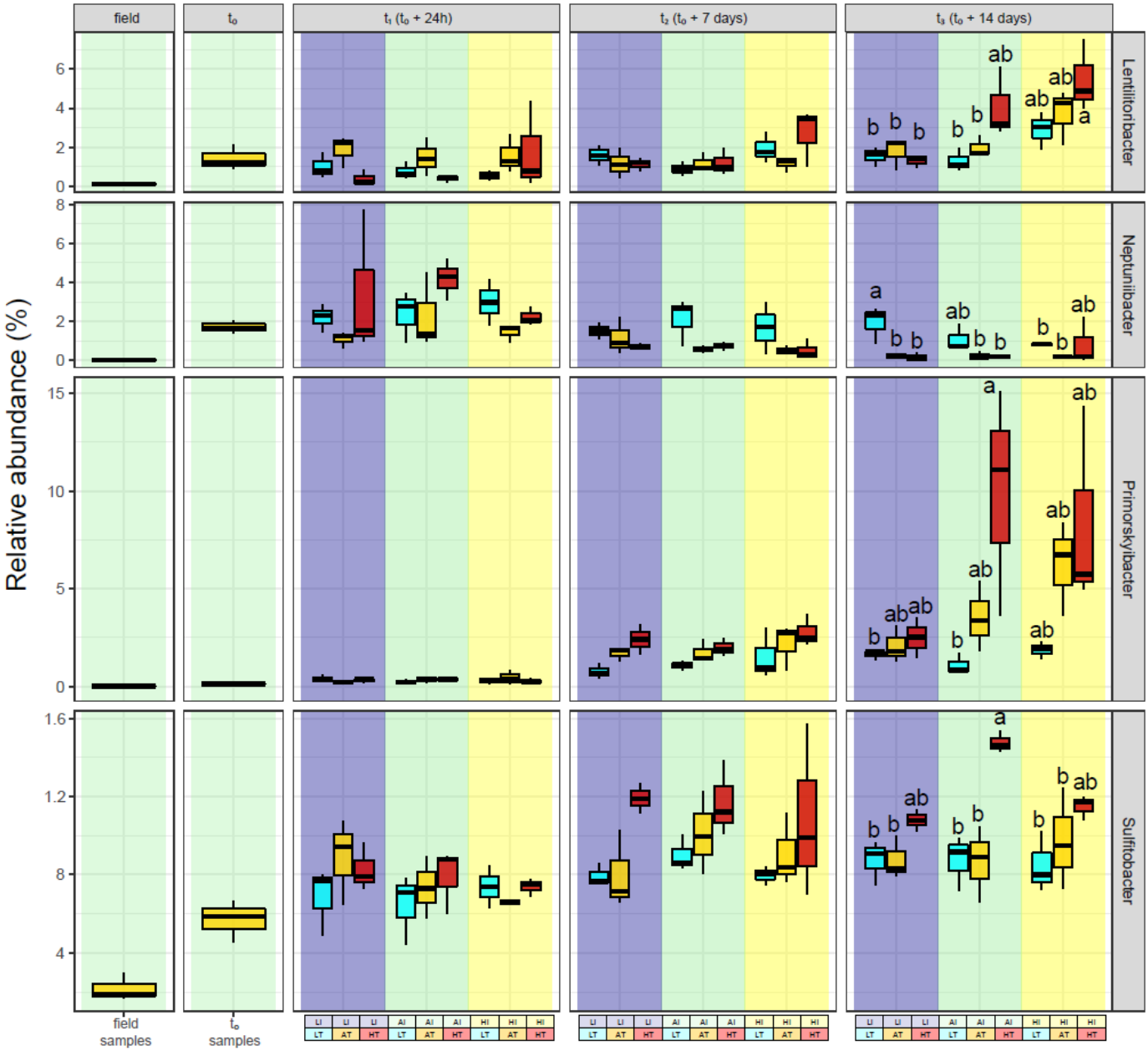

Figure SVII.9. Variation of biomarker genera identified through the LEfSe analysis conducted on t_3 samples (see Table SVII.7) (Part 2).

Light blue, orange and red boxplots represent samples at "low", "ambient" and "high" temperature conditions. Dark blue, green and yellow backgrounds represent samples at "low", "ambient" and "high" irradiance conditions. **a**, **b** and **c** represent results from Duncan's multiple tests comparing each "temperature/irradiance" condition at t_3.

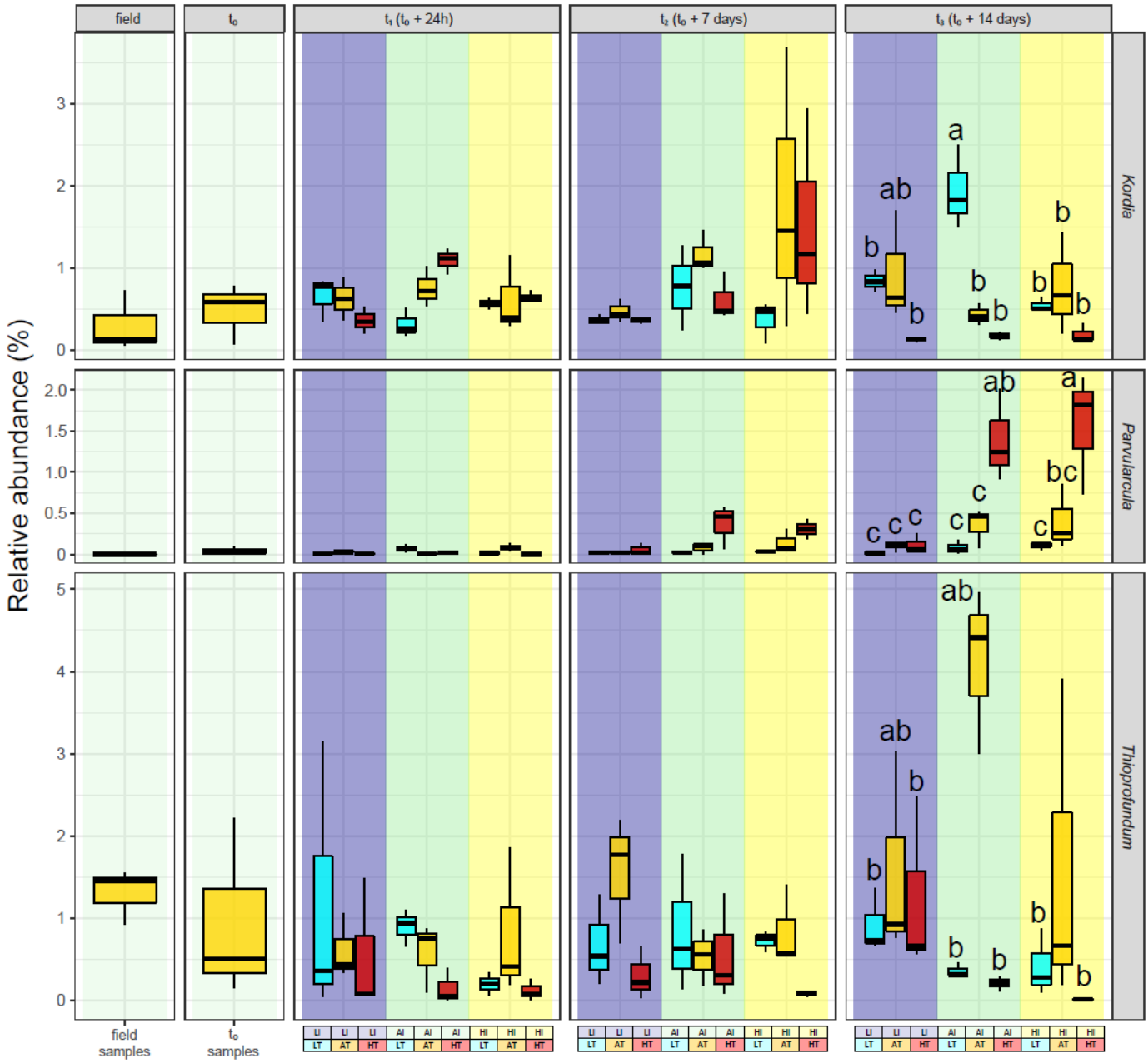

Figure SVII.9. Variation of biomarker genera identified through the LEfSe analysis conducted on t_3 samples (see Table SVII.7) (Part 3).

Light blue, orange and red boxplots represent samples at "low", "ambient" and "high" temperature conditions. Dark blue, green and yellow backgrounds represent samples at "low", "ambient" and "high" irradiance conditions. **a**, **b** and **c** represent results from Duncan's multiple tests comparing each "temperature/irradiance" condition at t_3.

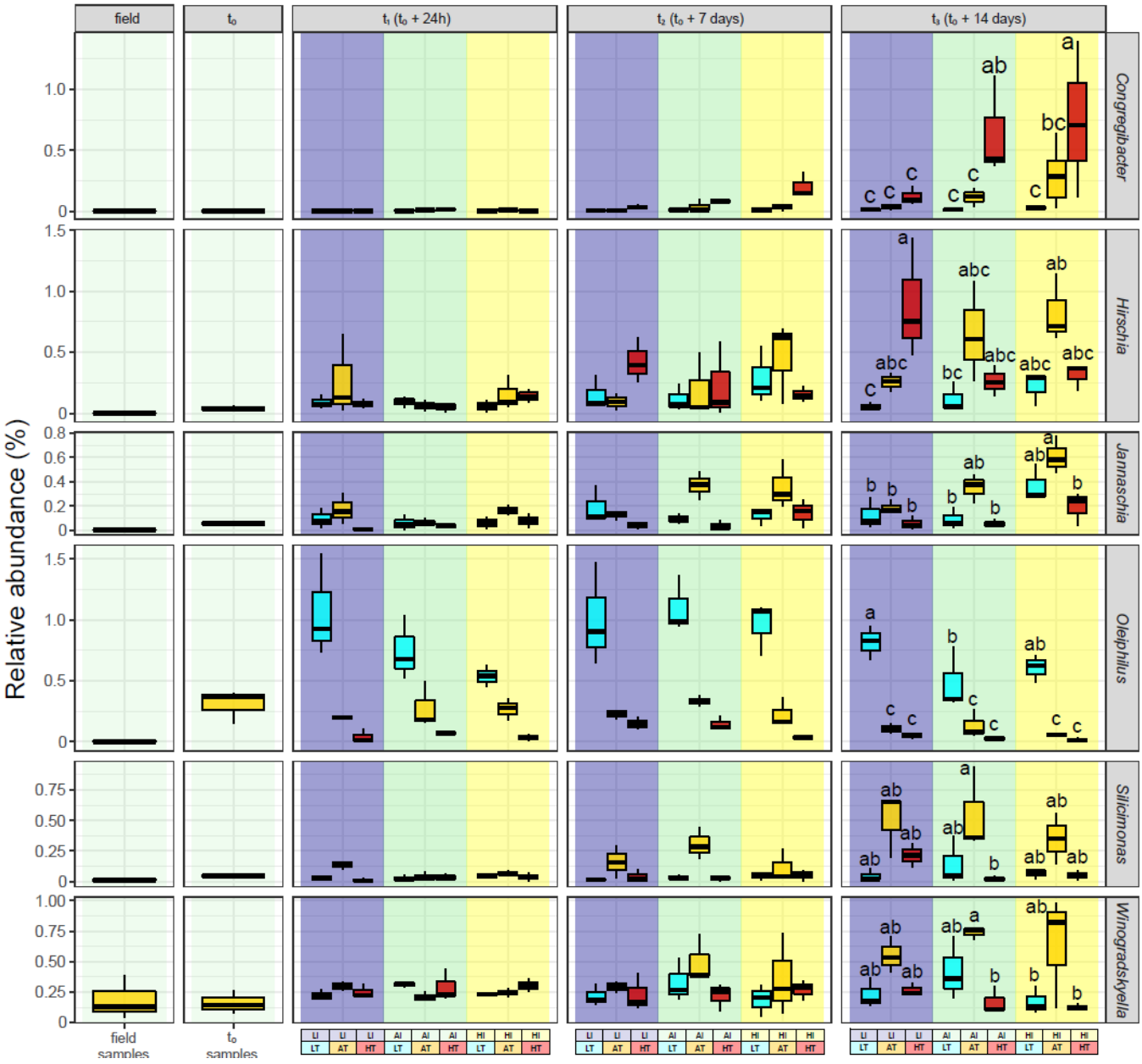

Figure SVII.10. Variation of annotated biomarker metabolites (VIPs, see Table SVII.10) involved in the discrimination between each condition at t_3 (Part 1)

Light blue, orange and red boxplots represent samples at “low”, “ambient” and “high” temperature conditions. Dark blue, green and yellow backgrounds represent samples at “low”, “ambient” and “high” irradiance conditions. **a**, **b** and **c** represent results from Tukey’s tests comparing each “temperature/irradiance” condition at t_3.

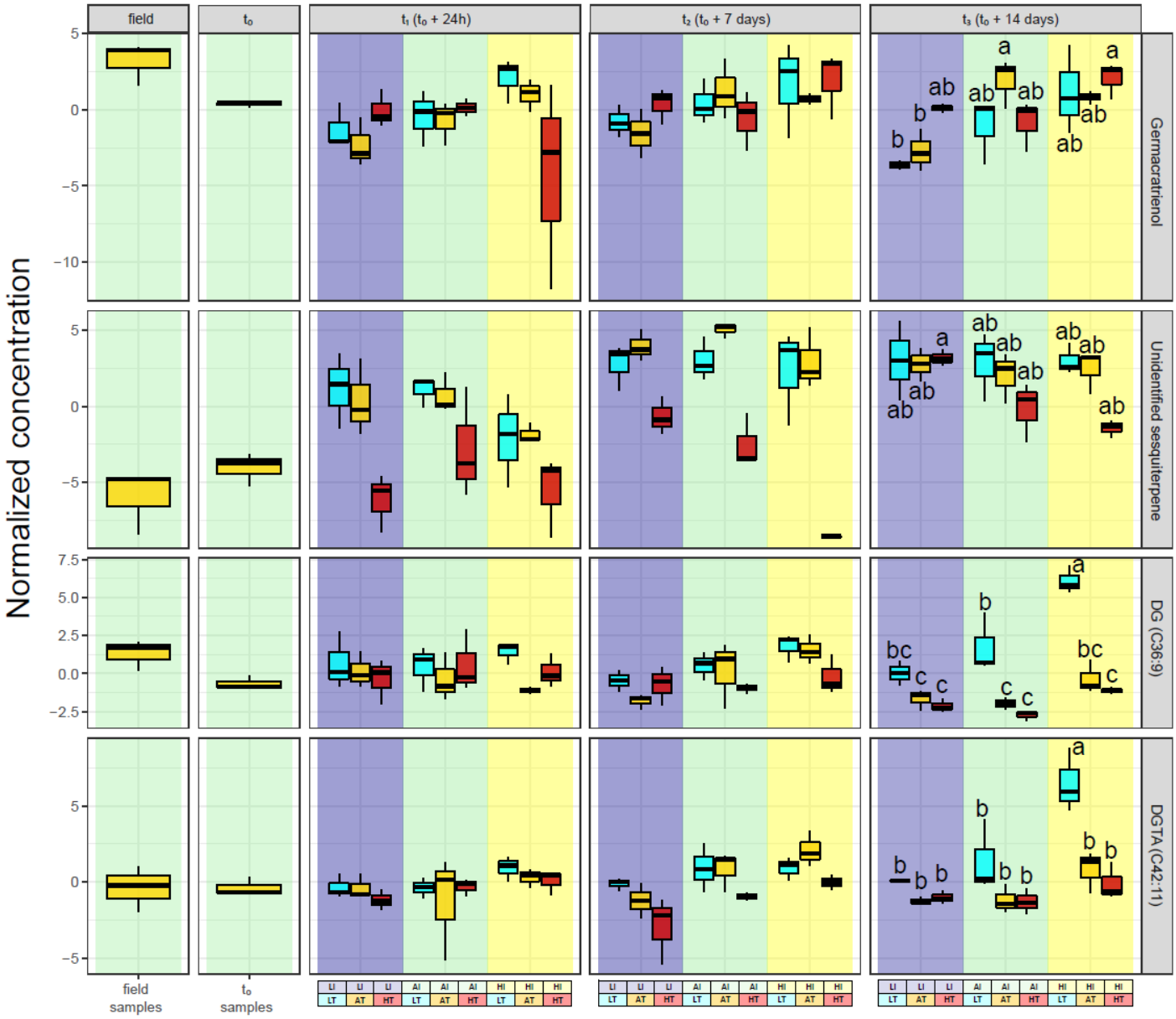

Figure SVII.10. Variation of annotated biomarker metabolites (VIPs, see Table SVII.10) involved in the discrimination between each condition at t_3 (Part 2)

Light blue, orange and red boxplots represent samples at "low", "ambient" and "high" temperature conditions. Dark blue, green and yellow backgrounds represent samples at "low", "ambient" and "high" irradiance conditions. **a**, **b** and **c** represent results from Tukey's tests comparing each "temperature/irradiance" condition at t_3.

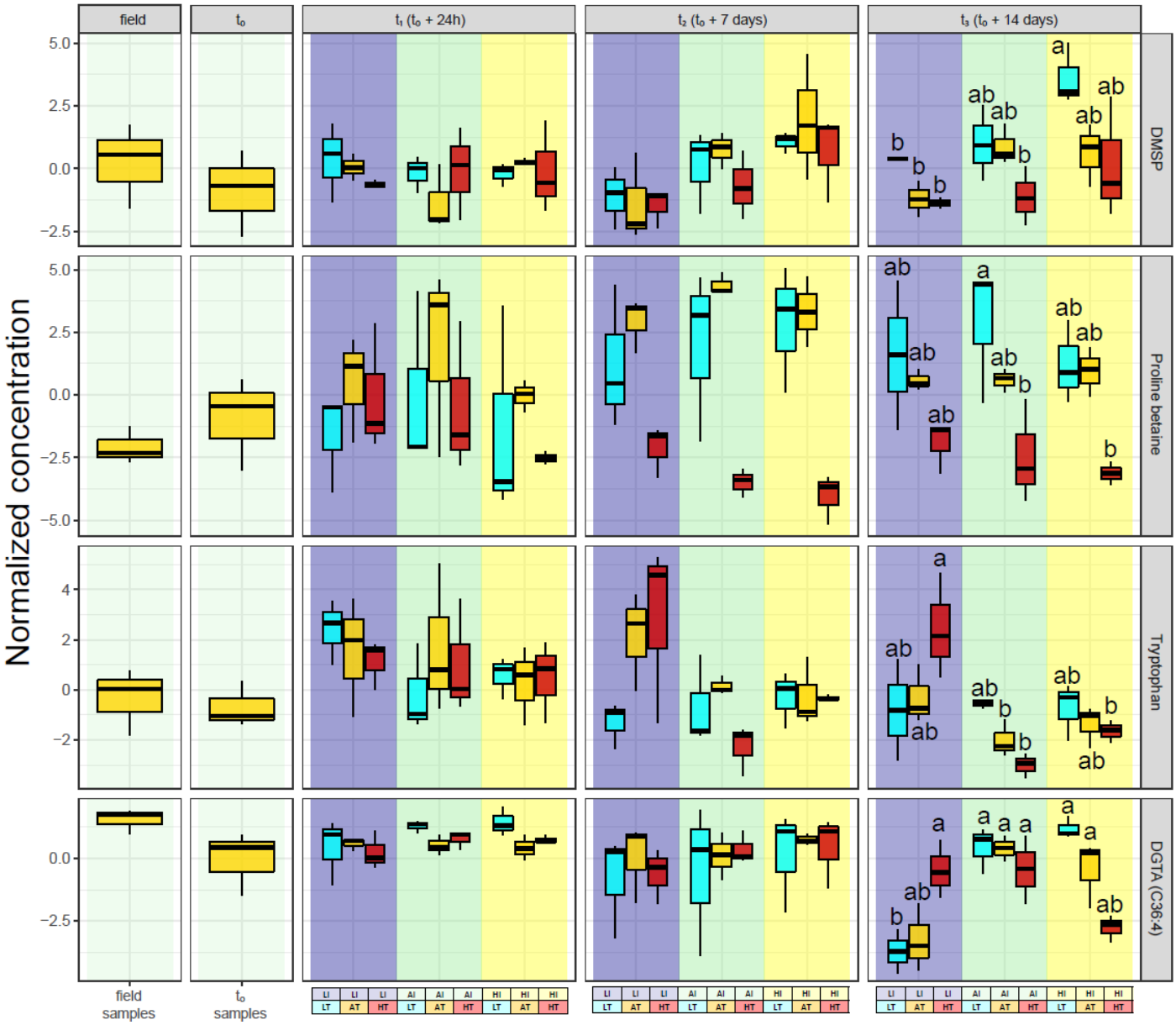

Figure SVII.10. Variation of annotated biomarker metabolites (VIPs, see Table SVII.10) involved in the discrimination between each condition at t_3 (Part 3)

Light blue, orange and red boxplots represent samples at "low", "ambient" and "high" temperature conditions. Dark blue, green and yellow backgrounds represent samples at "low", "ambient" and "high" irradiance conditions. **a**, **b** and **c** represent results from Tukey's tests comparing each "temperature/irradiance" condition at t_3.

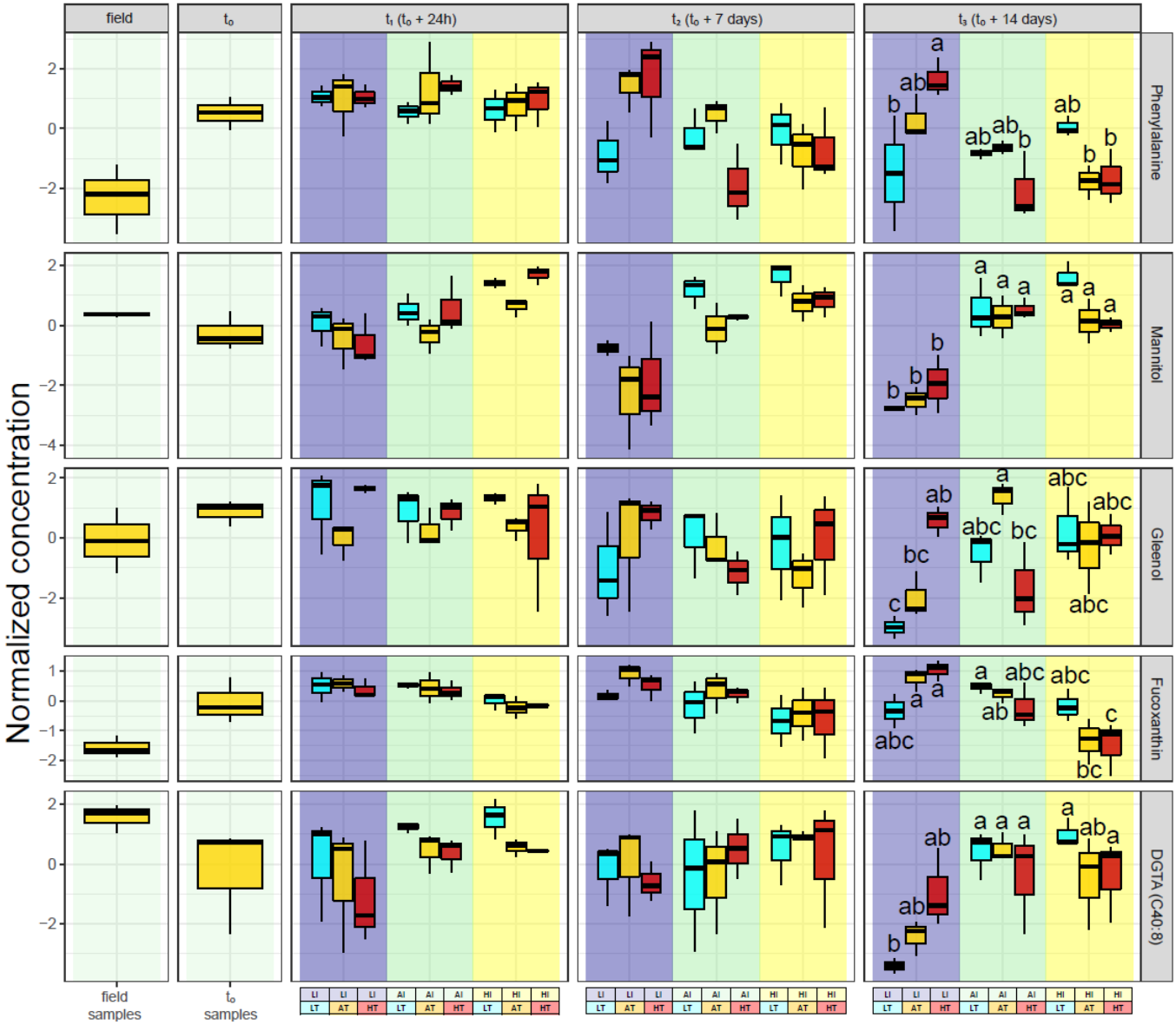

Annexe VIII

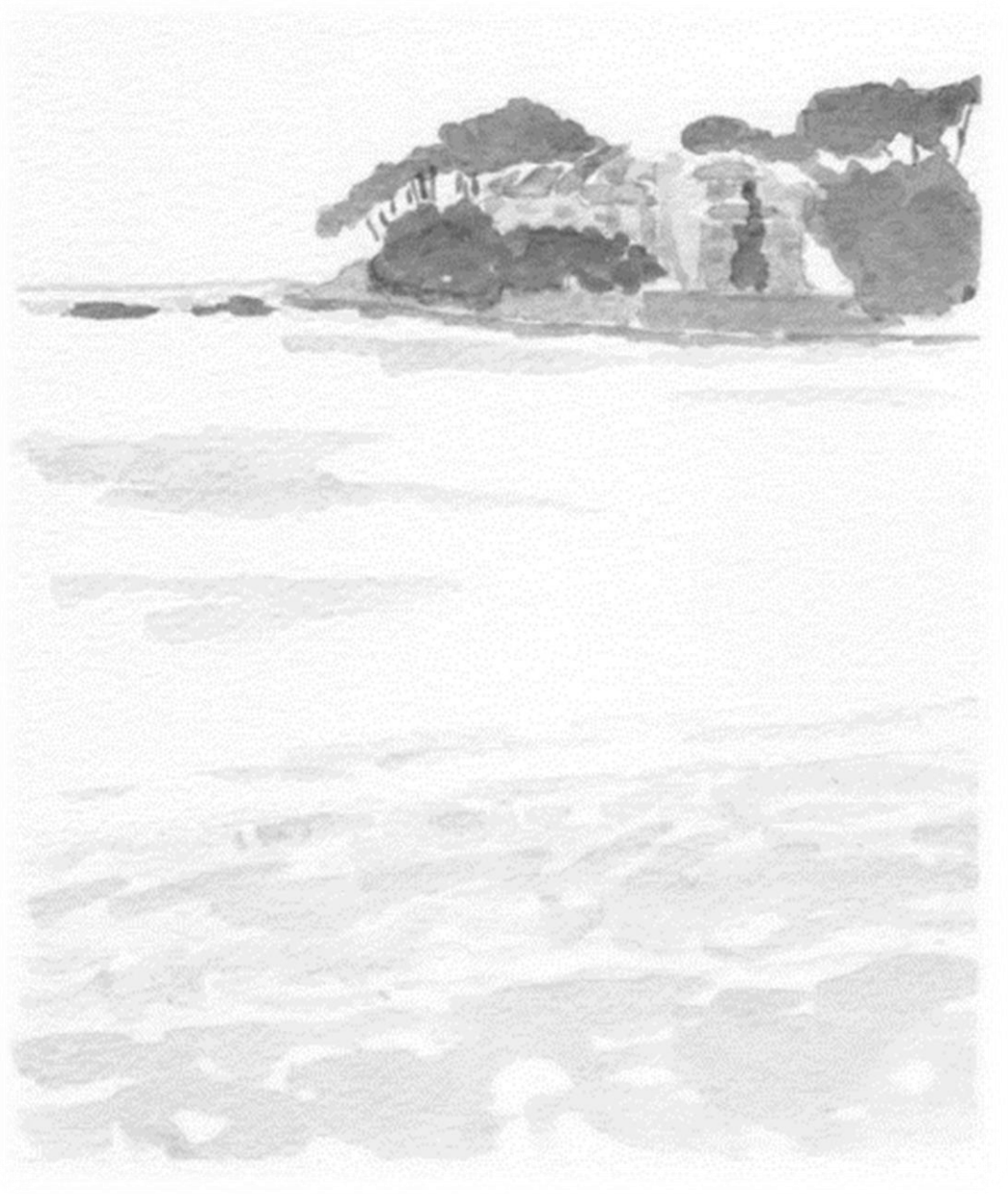

Supporting information
for
Exploring the role of macroalgal surface metabolites on the settlement of the benthic dinoflagellate *Ostreopsis* cf. *ovata*.

Eva Ternon[a,b,c *ǂ], Benoît Paix[d ǂ], Olivier P. Thomas[e], Jean-François Briand[d], Gérald Culioli [d*]

[ǂ] These authors contributed equally contributed to this work

a. Université Côte d'Azur, CNRS, OCA, IRD, Géoazur, 250 rue Albert Einstein, 06560 Valbonne, France, eva.ternon@imev-mer.fr (* corresponding author)

b. Sorbonne Universités, CNRS UMR7093, Laboratoire d'Océanographie de Villefranche, 06234 Villefranche-sur-Mer, France

c. Center for Marine Biotechnology and Biomedicine, Scripps Institution of Oceanography, University of California San Diego, La Jolla, CA, 92093, United States

d. Université de Toulon, Laboratoire MAPIEM, EA 4323, Toulon, France., paix@univ-tln.fr, briand@univ-tln.fr, culioli@univ-tln.fr (* corresponding author)

e. Marine Biodiscovery, School of Chemistry and Ryan Institute, National University of Ireland Galway (NUI Galway), University Road, H91 TK33 Galway, Ireland, olivier.thomas@nuigalway.ie

Figure SVIII.1. Eukaryotic communities' alpha-diversity obtained by 18S rRNA gene metabarcoding for the four macroalgae species and the surrounding seawater.

A: OTU number, B: Chao1 index. *p* values and a, b, c, d indexes correspond to results of the one-way ANOVA and Tukey's tests, respectively.

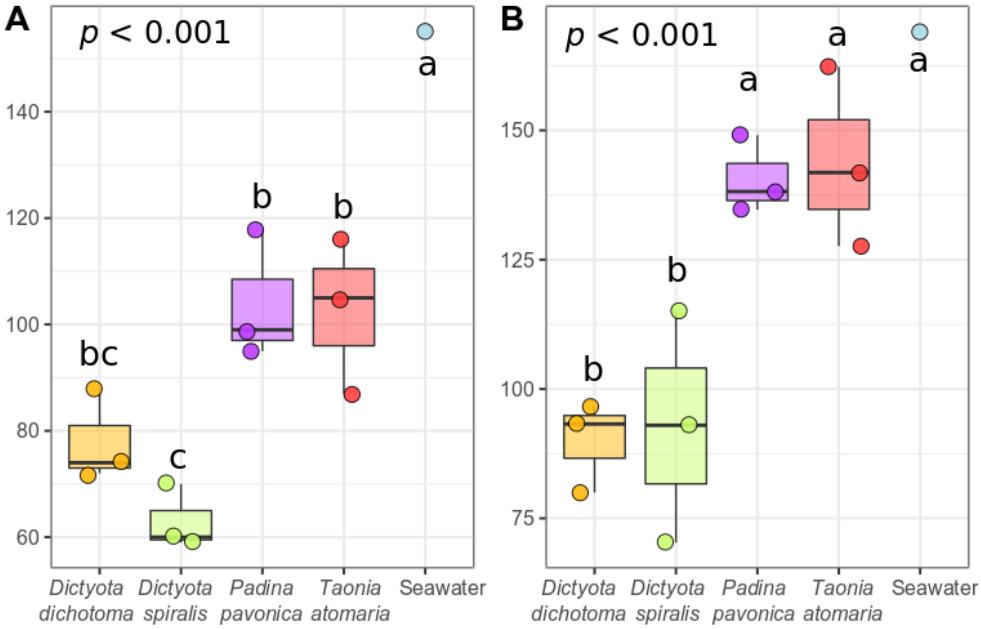

Figure SVIII.2. Eukaryotic communities' beta-diversity obtained by 18S rRNA gene metabarcoding for the four macroalgae species and the surrounding seawater: NMDS plot determined using the Jaccard index.

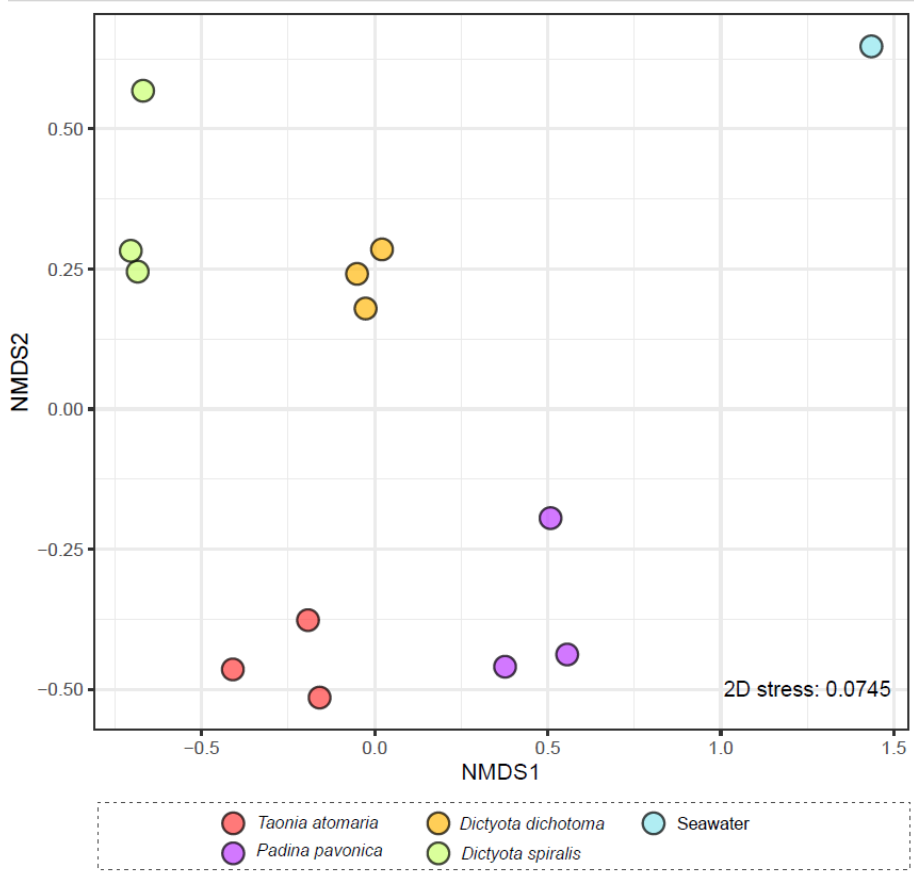

Figure SVIII.3. Relative abundance in the surface extracts (SE) of the four macroalgal species of (A) geranylgeranylglycerol, (B) DMSP, and the two unidentified biomarkers of *D. dichotoma*, (C) unknown compound and (D) carotenoid-like compound, based on their ion intensity in LC-MS analysis.
p values and a, b, c, d indexes correspond to results of the one-way ANOVA and Tukey's tests, respectively.

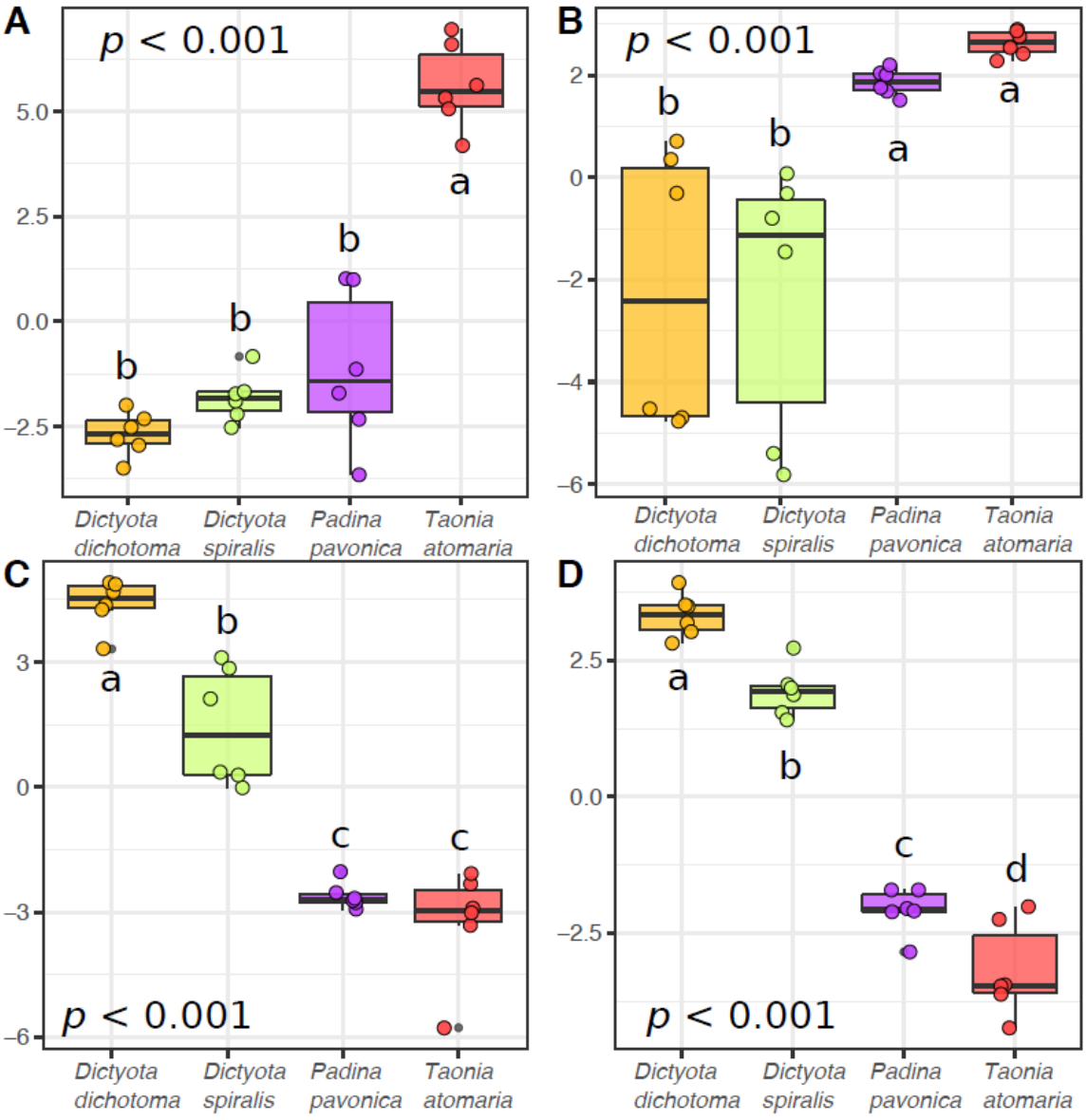

Table SVIII.1. Putative annotation of the first few biomarkers (VIP > 1.42) driving the distribution of the surface extracts (SEs) and the total extracts (TEs) obtained by PLS-DA analyses performed for each macroalgal species.

Identification of the compounds marked by * was confirmed with a chemical standard. nd: Not determined.

	VIP	Type of Extract	*m/z*	RT (min)	Putative annotation
Taonia atomaria	1	TE	316.2595	8.62	nd
	2	TE	420.1140	5.68	nd
	3	SE	135.0473	0.88	DMSP*
	4	TE	244.2059	8.93	nd
	5	SE	650.8684	10.02	nd
Padina pavonica	1	SE	490.3743	8.65	Lyso-DGCC (C16:0)*
	2	TE	599.4101	8.56	nd
	3	SE	316.7766	0.82	nd
	4	TE	425.2691	9.06	$C_{27}H_{37}O_4$ $[M+H]^+$
	5	SE	91.0544	10.06	nd
Dictyota dichotoma	1	SE	128.0192	0.70	acetyl-*L* cysteine $[M-2H_2O+H]^+$
	2	SE	95.5454	0.71	nd
	3	SE	132.9981	0.70	nd
	4	SE	350.7440	0.85	nd
	5	TE	933.5566	10.50	nd
	6	TE	728.5111	9.35	nd
Dicyota spiralis	1	SE	174.8704	0.85	nd
	2	SE	208.8910	0.79	nd
	3	SE	350.7440	0.85	nd
	4	TE	280.9793	0.86	nd